University of Glasgow | Institute of Infection, Immunity & Inflammation

Quantitative Proteomic responses of macrophages to *Leishmania mexicana* infection

Najad Zamirah Zaki

BSc (Hons), MSc (Research)

Submitted in fulfilment of the requirement for the Degree of Doctor of Philosophy

Institute of Infection, Immunity and Inflammation

College of Medical, Veterinary and Life Sciences

University of Glasgow

August 2017

Abstract

The dynamics of protein turnover is central to the regulation of protein expression. The steady-state level of a protein is the net outcome of the change in its rate of synthesis and degradation. Different biological states or perturbations cause changes in the expression of specific proteins, which can be assessed by proteomic analysis to reveal links between genotype and phenotype. Unlike other conventional proteomic methods, which measure the amount of proteins in the system at a specific point in time, pulse-chase stable isotope labelling by amino acids in cell culture (pcSILAC) can reveal changes in the rates of protein synthesis and degradation over time.

The causative agent of Leishmaniasis, *Leishmania,* has a digenetic lifestyle involving an extracellular flagellated promastigote living in the mid-gut of the sand fly vector and an aflagellated intracellular amastigote residing in the macrophage of the mammalian host. As they live in a different niche their protein expression could give insight into their adaptation and survival. The intricate interaction between the human host and the *Leishmania* parasite is key to pathology and may present new targets for chemotherapeutic development. Employing high-resolution mass spectrometry coupled with pulse-chase SILAC technique, we delved into the investigation of proteome changes in *L. mexicana*-infected macrophages.

The first part of the thesis discusses the quantitative proteomic analysis of *L. mexicana* promastigote and amastigote stage. In this work, stable isotope dimethyl labelling was employed to differentially labelled promastigotes and axenic amastigotes. Our results revealed transformation from promastigote to amastigote were accompanied by: i) reduced glycolytic and gluconeogenesis pathway, ii) increased fatty acid oxidation, iii) increased mitochondrial respiration, iv) reduced expression of proteins that may have flagellar role (e.g. flagellar connector protein, flagellum targeting protein KHARON1), v) reduced stress response proteins, vi) increased protein synthesis, and vii) increased proteolytic proteins. The findings reported here substantially advance our knowledge on the differences of protein expression in different life cycle stage of *L. mexicana* and could be useful in finding drug targets.

Another part of the thesis discusses the establishment and application of pulse-chase SILAC. In this work, a human macrophage-like cell line (THP-1) was grown in media containing L-Arg-$^{13}C_6$ and L-Lys-$^{13}C_6$ until isotope incorporation of >98% was achieved. Media was then replaced with light arginine and lysine so that light amino acids were pulsed into cells for 24 and 48 hours. In other words, protein synthesis is 'chased' with unlabelled amino acids. Synchronous with the switch from pulse to chase, the macrophages were infected with *L. mexicana*. This approach provides the ability to monitor the rates of heavy-label loss, hence determining protein degradation rates and half-lives.

At 24-hour post-infection, when compared to mock-infected cells, 2016 proteins were identified, 761 were quantified, and 51 were significantly modulated at p-value < 0.05. Interestingly, proteins involved in glycolysis were markedly downregulated in synthesis after infection while oxidative phosphorylation and fatty acid ß-oxidation had increased synthesis, suggesting a subversion of host cell metabolism by *Leishmania* which proposed to play a key role in microbial growth and persistence. Additionally, pro-apoptotic proteins such as apoptosis regulator BAX and caspase 3 had increased translation in cells infected for 24 hour. This was accompanied by the overexpression of STAT1 which could result in modulation of apoptotic pathways. These characteristics advocate that THP-1 cells most likely exhibit an M2 macrophage phenotype following 24-hour infection.

Temporal proteomic data revealed some striking changes in metabolisms of the host at 24 and 48-hour post-infection. After 48 hours of infection, 2104 proteins were identified, and 84 were significantly modulated post-infection at p-value < 0.05. After 48 hours of infection, relative to levels at 24 hours of infection, host cells increased the synthesis of glycolytic enzymes and reduced oxidative phosphorylation synthesis. Further, a total of 400 newly synthesized proteins were selected based on stringent criteria to measure synthesis rates, degradation rate constant (k_{deg}) and half-lives. These include several ribosomal proteins, pyruvate kinase, L-lactate dehydrogenase, moesin, several glycolytic enzymes such as glucose-6-phosphate isomerase and alpha enolase, gelsolin, galectin-9, catalase and lamin-B. We found that globally k_{deg} values in THP-1 were low ranging from 0.01 to 0.04 h^{-1}. Our degradation data indicated that proteins involved in mitochondrial related functions (TCA, oxidative phosphorylation) as well as other

energy production pathways were more stable and have longer half-lives. For the 400 proteins, the mean half-life for uninfected 24 h, 24 hpi, uninfected 48h and 48 hpi were 21.74 h, 20.51 h, 47.39 h and 47.33 h, respectively. Intriguingly, newly synthesized proteins involved in immune responses, including HLA complexes, were rapidly degraded in infected cells, despite having decreased synthesis rates after 48 hours of infection. Collectively, most proteins in the present study had decreased k_{deg} and longer half-lives following longer exposure of THP-1 to *L. mexicana*. Our data show the potential of pulse-chase SILAC to dissect the response of macrophages to *Leishmania* infection. To our knowledge, no studies have reported the proteome turnover of macrophage in response to *Leishmania* infection.

Table of Contents

List of Tables

Chapter 1

Chapter 2

Chapter 3

Chapter 4

Chapter 5

List of Figures

Chapter 1

Chapter 3

Chapter 4

Chapter 5

Chapter 6

List of Accompanying Material

- The full list of proteins identified in *L. mexicana* are provided in CD-ROM (in Excel spreadsheet).

- The proteomic data containing raw files, spectra, and identification profiles has been deposited to PRIDE archive (http://www.ebi.ac.uk/pride/archive/simpleSearch?q=&submit=Search) with title "Quantitative Proteomic responses of macrophages to *Leishmania mexicana* infection".

Conference proceedings

Parts of the following thesis have been presented at the following national and international conferences as well as various other local meetings:

- British Society of Proteome Research Conference, 2016, Glasgow

- British Society of Parasitology Conference, 2016, Ceske Budejovice (Czech Republic)

Acknowledgement

"It is by going down into the abyss that we recover the treasures of life. Where you stumble, there lies your treasure." ~Joseph Campbell

I am grateful to God for the perseverance that were necessary to complete this thesis. It has been a very difficult journey and yet the journey to gain knowledge is never ending. This journey has made me a different person.

Firstly, I would like to express my genuine gratitude to my supervisors Dr. Richard Burchmore and Prof. Jeremy Mottram for the continuous support of my PhD study, for their patience, understanding, motivation, and immense knowledge. Their guidance helped me in the time of research and writing of this thesis.

My assessors, Prof. Markus Meissner and Prof. James Brewer, thank you for their assessments, insightful comments and encouragement which helped widen my research from various perspectives. To Glasgow Polyomics people: Stefan Weidt, Christina Naula and Suzanne Edie who runs my samples on Mass Spec. To Dr. Sara Zanivan (Beatson Institute) for sharing expertise on MaxQuant and Perseus unreluctantly, and sincere and valuable guidance. To Phillip, for the much-needed 'R' advice and help, even when he was enjoying the Swiss Alp, he never missed replying to my emails. My viva examiners, Karl Burgess and Mary Doherty, thank you for the feedbacks and advice.

I acknowledged my fellow lab mates (Burchmore's group, Mottram's group, McCulloch's group, and Hammarton's group) for the technical supports in the lab and for the stimulating discussions during our lab meetings. I'm sorry I couldn't mention the names individually for it would be too long! Being a novice in Parasitology and being a foreigner here in the UK, getting help from them are much-needed and appreciated. To those who did not helped me when I desperately need their expert input, I'd still thanked them because it just made me stronger. I learned to think out of box and become independent. Special thanks also to the 3IIIs administrative staff, Graduate School staff, and especially to Jim Scott the technician in level 6. A warm gratitude also goes to ResearchGate community.

To Malaysia Ministry of Higher Education (MOHE) and National Defence University of Malaysia for providing the funding for the work for only 3 years.

Getting through my PhD project and thesis required more than academic support, and I have my husband, Mohd Firdaus Othman standing beside me over the past four years, listening to me patiently, encouraging me, providing for our family after the sponsorship 'ended' (until his knees wore out), and helping me with almost everything! He is my rock and my personal coach. He even helped me with R analysis! We bought R books and studied together until late at night. This thesis stands as a testament to your unconditional love and encouragement. Our two cheeky boys Nazhan Alfarisi and Nazrol Fahme, whom always happily greeted me at the door coming home from the lab, mommy love you guys to the moon and back! Special thanks to my family back in Malaysia: Mama, Ayah, my siblings, my family in-laws, Mak, Abah, for the spiritual encouragement from afar, not to mention the financial support during the 'dark' times (you know what I mean).

Perjalanan ini telah menjadikan diriku lebih matang, lebih mengenali erti kehidupan…Akan kusemat memori ini…

Thank you

Terima kasih

Author's Declaration

I hereby declare that this thesis has been written by myself. I declare that this thesis has not been submitted in any previous application for a higher degree. I declare that the research in this thesis is the result of my own original work, with exception of the LC-MS sample analysis and quantitation performed by Dr. Stefan Weidt, Dr Christina Naula and Suzanne Edie from Glasgow Polyomics. I declare that all sources of information have been specifically acknowledged by means of references.

Printed Name: NAJAD ZAMIRAH ZAKI

Signature: 

Definitions/Abbreviations

µl	Microlitre
µg	Microgram
µM	Micromolar
1,3-BPG	1,3-bisphosphoglycerate
1D-LCMS/2D-LCMS	1 Dimensional-liquid chromatography-mass spectrometry/ 2 Dimensional- liquid chromatography-mass spectrometry
2-DE	2-dimensional electrophoresis
2-PG	2-phosphoglycerate
3-PG	3-phosphoglycerate
ACN	Acetonitrile
ADP	Adenosine diphosphate
AHA	L-azidohomoalanine
AIDS	Acquired immune deficiency syndrome
ANOVA	Analysis of variance
AP-1	Activator protein-1
APCs	Antigen Presenting Cells
APEX	Absolute Protein Expression
AQUA	Absolute quantification
Arg	Arginine
Asl	Argininosuccinate lyase
Ass1	Argininosuccinate synthase
ATCC	American Type Culture Collection
ATP	Adenosine triphosphate
Bcl-2	B-cell lymphoma 2
BM2	Beta-2-microglobulin
BSA	Bovine serum albumin
C3b	Complement component 3 subunits
C3bi	Inactive complement subcomponent C3b
CALM1	Calmodulin
CALR	Calreticulin
CAT	Catalase
CDIT	Culture-derived isotope tags
CFL1	Cofilin-1
CL	Cutaneous leishmaniasis
CNS	Central nervous system
CO_2	Carbon dioxide
CoA	Coenzyme A
CTPS1	CTP synthase 1
CTSB	Cathepsin B
CTSD	Cathepsin D
Cy3, Cy5, Cy2	Cyanine dyes
Da/ kDa	Dalton/ kilodalton
DAPI	4',6' diamino-2-phenylindole-2HCl
DAVID	Database for Annotation, Visualization and Integrated Discovery
DB	Database
DCs	Dendritic cells

DDX3X	ATP-dependent RNA helicase
dFCS	Dialyzed serum
DiGE	Difference gel electrophoresis
DiMe	Stable isotope dimethyl labelling
DMSO	Dimethyl sulfoxide
DNA	Deoxyribonucleic acid
DTT	Dichloro-diphenyl-trichloroethane
e.g.	*exempli gratia*/ for example
ECL	Enhanced chemiluminescent
ECM	Extra-cellular matrix
EDTA	Ethylenediaminetetraacetic acid
EEF1A1	Elongation factor-1 alpha-1
EF	Elongation factor
ELISA	Enzyme-linked immunosorbent assay
ENO1	Alpha-enolase
Erk1/Erk2	Extracellular signal-regulated kinases 1 & 2
ERM	Ezrin-radixin-moesin family
ESI	Electrospray ionisation
Exp	Exponential
EZR	Ezrin
F6P	Fructose-6-phosphate
FABP4	Fatty acid-binding protein
FASP1	Filter-aided sample preparation
Fba1p	Fructose 1,6-bisphosphate aldolase
FC	Fold-change
Fc receptors	Fragment crystallisable receptors
FcγRs	Fc-gamma receptors
FDR	False discovery rate
FH	Fumarate hydratase
FSCN1	Fascin
g	gram
g	Gravity
G6P	Glucose-6-phosphate
G6PDH	Glucose-6-phosphate dehydrogenase
GALK1	Galactokinase 1
GAPDH	Glyceraldehyde-3-phosphate dehydrogenase
GFP	Green fluorescent protein
GIST	Global internal standard technology
GK	Glycerol kinase
GO	Gene Ontology
GOBP	Gene Ontology based on biological processes
GOMF	Gene Ontology based on molecular functions
gp46	Promastigote surface antigen protein 2
gp63	Glycoprotein-63/ leishmanolysin
GPCR	G-protein coupled receptor
GPI	Glucose 6-phosphate isomerase
GPIs	Glycosylinositol phospholipids
GSN	Gelsolin
GSTO1	Glutathione transferase omega
GUI	Graphical User Interphase
h	Hour

HCl	Hydrochloric acid
HI-FCS	Heat-inactivated foetal calf serum
HIST1 H2BL	Histone H2B type 1-L
HIV	Human Immunodeficiency Virus
HLA	Human Leukocyte Antigen
hnRNPs	Heterogeneous nuclear ribonucleoproteins
HOMEM	Haemoflagellate minimal essential medium
hpi	Hour post-infection
HSPs	Heat shock proteins
Hxk1p	Hexokinase
i.e.	*id est*/ that is
ICAT	Isotope-coded affinity tags
ID	Identifiers
IDH	Isocitrate dehydrogenase
IFI16	Gamma-interferon-inducible protein 16
IFN-γ	Interferon-gamma
IL	Interleukin
ILF	Interleukin-enhancer-binding factor
iNOS	Inducible Nitric Oxide Synthase
iTRAQ	Isotope tags for relative and absolute quantification
JAK	Janus tyrosine kinase
JNK	Jun N-terminal kinase
$_{k}$deg	Degradation rate constants
KEGG	Kyoto Encyclopaedia of Genes and Genomes
kh1	Flagellum targeting protein kharon1
KMP-11	Kinetoplastid membrane protein-11
L	Litre
L/H ratio	Light/Heavy ratio
LC-MS	Liquid chromatography mass spectrometry
LDHA	Lactate Dehydrogenase A
LFQ	Label-free quantification
Log	Logarithm
LPG	Lipophosphoglycan
LPL	Lipoprotein lipase
LPS	Lipopolysaccharide
Lys	Lysine
M	Molar
m/z	Mass to charge ratio
M1	Classically activated macrophages
M2	Alternatively activated macrophages
MALDI	Matrix-assisted laser desorption/ionization
MAPKs	Mitogen-activated protein kinases
Max	Maximum
MCL	Mucocutaneous leishmaniasis
MeCAT	Metal-coded affinity tag
mg	Milligram
MHC	Major histocompatibility complex
min	Minute
Min	Minimum
ml	Millilitre
mM	Millimolar

Moesin	Membrane-organizing extension spike protein
MRM	Multiple-reaction monitoring
mRNA	Messenger RNA
MS	Mass spectrometry
MSN	Moesin
MudPIT	Multidimensional Protein Identification Technology
MW	Molecular weight
MX1	Interferon-induced GTP-binding protein
NaCl	Natrium chloride
NADP/NADPH	Nicotinamide adenine dinucleotide phosphate
NaN	Non-Assigned Number, non-quantified values
NaOH	Natrium Hydroxide
NE	Neutrophil elastase
NETs	Neutrophil extracellular traps
NF-κB	Nuclear factor kappa-light-chain-enhancer of activated B cells
NH_3	Ammonia
NK	Natural Killer cells
nm	Nanometer
nM	Nanomolar
NO	Nitric oxide
No.	Number
NSUN2	tRNA (cytosine (34)-C (5))-methyltransferase
°C	Degrees Celsius
PACSIN2	Casein kinase substrate in neurons protein 2
PAMPs	Pathogen-associated molecular pattern molecules
PANTHER	Protein Analysis Through Evolutionary Relationships
PBMC	Primary human peripheral blood monocyte
PBS	Phosphate-buffered saline
PBS-T	PBS-Tween 20
PCA	Principal component analysis
PCR	Polymerase chain reaction
pcSILAC	Pulse-chase Stable isotope labelling with amino acids in cell culture
PEP	Posterior error probability
PEP	Phosphoenolpyruvate
PEPCK	Phosphoenolpyruvate carboxykinase
PEST sequence	Peptide sequence rich in proline (P), glutamic acid (E), serine (S), and threonine (T)
PFR	Paraflagellar rod protein
PGK1	Phosphoglycerate kinase 1
pI	Isoelectric point
PKC	Protein kinase C
PKM	Pyruvate kinase
PMA	Phorbol 12-myristate 13-acetate
PNP	Purine nucleoside phosphorylase
PPDK	Pyruvate phosphate dikinase
PPIs	Protein-protein interactions
ppm	Parts per million
PPP	Pentose phosphate pathway
PRDX2	Peroxiredoxin 2
PRDX6	Peroxiredoxin 6

Pro	Proline
PRRs	Pattern recognition receptors
PSMs	Peptide to Spectrum Matches
PTP	Protein tyrosine phosphatase
PTPLAD1	Very-long-chain (3R)-3-hydroxyacyl-CoA dehydratase 3
QUEST	Amidination-quantitation using enhanced signal tags
RAB1B	Ras-related protein
RFLP	Restriction fragment length polymorphism
RIA	Relative isotope abundance
ROS	Reactive oxygen species
RT-PCR	Reverse Transcriptase-Polymerase chain reaction
S/N ratio	Signal to noise ratio
SCX	Strong Cation exchange
sd	Standard deviation
SDS	Sodium dodecyl sulphate
SDS-PAGE	Sodium dodecyl sulphate polyacrylamide gel electrophoresis
SDT buffer	Buffer consist of SDS, Tris-HCl and DTT
sec	second
SHP-1	Src-homology 2 domain containing phosphatase-1
SILAC	Stable isotope labelling with amino acids in cell culture
SNARE	Soluble N-ethylmaleimide-sensitive factor attachment receptor
SOCS-1/ SOCS-3	Suppressor of Cytokine Signalling 1/ Suppressor of Cytokine Signalling 3
SOD	Superoxide dismutase
sp.	species
STAT	Signal transducer and activator of transcription factor
t	time
TAP	Tandem affinity purification
TCA cycle	Tricarboxylic acid cycle
TCPTP	T-cell protein tyrosine phosphatase
TeAB	Tetraethylammonium bromide
TFA	Trifluoroacetic acid
TFs	Transcription factors
TGF-β	Transforming growth factor-beta
Th1	T helper 1 type
Th2	T helper 2 type
THP-1	Human monocytic cell line derived from an acute monocytic leukaemia patient
TKT	Transketolase
TLRs	Toll-like receptors
TMT	Tandem mass tags
TNF-α	Tumour necrosis factor-alpha
TPI/ TIM	Triosephosphate isomerase
TRAP1	TNF receptor-associated protein 1
tRNA	Transfer ribonucleic acid
TTG buffer	Buffer consist of Tris-HCl, Triton X-100, and glycerol
TUBB4B	Tubulin beta
txt file	Tab delimited text file
UBE2N	Ubiquitin-conjugating enzyme E2 N
V	Volt

VL	Visceral leishmaniasis
VLCAD	Very long-chain acyl-CoA dehydrogenase
Vol	Volume
YARS	Tyrosine tRNA ligase

CHAPTER 1

1 Introduction

1.1 The *Leishmania* parasite

Trypanosomatids are ubiquitous unicellular protozoa that are ancient survivors on the Earth. They probably diverged from their evolutionary branch more than 500 million years ago (Stevens & Gibson 1999). Members of this group are flagellated and exclusively parasitic and found primarily dwelling in insects (Podlipaev 2001). Some of them have life-cycles involving a secondary host. The order kinetoplastids are characterized by several unique features that differ remarkably from their mammalian hosts. Paramount among these are the kinetoplast, which contains the mitochondrial DNA (Jensen & Englund 2012), compartmentalization of glycolysis within the glycosome (Michels et al. 2006) and the trans-splicing of a highly conserved short RNA leader sequence which participates in mRNA maturation in kinetoplastids (Simpson et al. 2000).

There is one family in this order, which is Trypanosomatidae. Three genera in this family are dixenous organisms that parasitize vertebrate (Trypanosome and *Leishmania*) and plant (*Phytomonas*) hosts (Wallace 1966; Vermelho et al. 2010). However, only two genera are found in humans and are etiologic agents of major human diseases; *Trypanosoma* and *Leishmania* (Maslov et al. 2013). The genus *Leishmania* is widely distributed in nature and one of the most species-rich groups of Trypanosomatidae (Figure 1.1). These species are nearly morphologically identical but they have different geographic distributions, different vectors and different manifestations of disease. Presently, approximately 30 different species of *Leishmania* are known to exist. At least 21 species of *Leishmania* are known to infect humans that threatened to decimate most parts of the world (Sharma & Singh 2009).

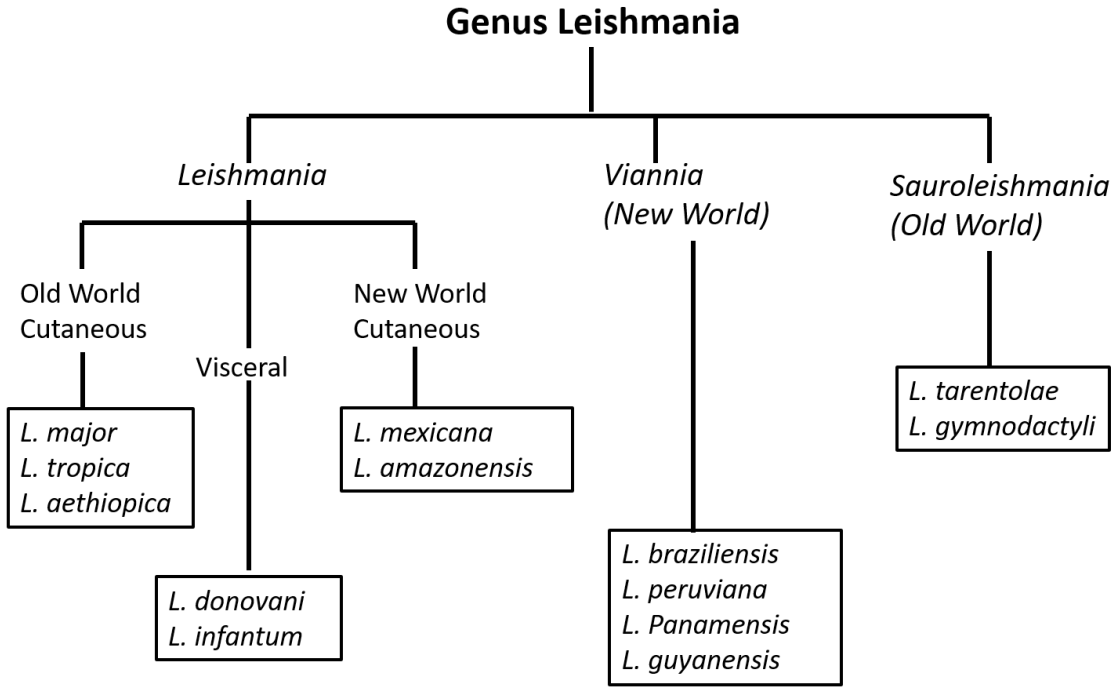

Figure 1.1: Outline classification of *Leishmania* illustrating the three subgenera.

Genus *Leishmania* are divide to three subgenera: *Leishmania*, *Viannia* and *Sauroleishmania*. Parasites in the subgenera *Leishmania* and *Viannia* infect mammals, whereas the *Sauroleishmania* infect reptiles as their vertebrate hosts. Over 30 species have been named in the genus including many that are non-pathogenic or of minor medical importance (of limited range or small numbers of recorded cases). The species named above are not comprehensive and only show some of the well-known species that are the focus of biomedical research. (Bates & Tetley 1993).

1.1.1 The *Leishmania* life cycle

Leishmania has a digenetic life cycle alternating between the motile, extracellular promastigote and non-flagellate, intracellular amastigote stages. Promastigotes have an elongated shape with long flagella. Fully developed promastigotes measure 10-20 µm in length and 1.5 - 3.5 µm in breadth. Promastigotes live in the digestive tract of the insect vector (sand flies). Amastigotes reside in the cells of reticuloendothelial system (macrophages, monocytes, polymorphonuclear leucocytes, or endothelial cells) of the vertebrate mammal host. Amastigote are non-motile, have a round or oval body measuring 3-7 µm in diameter along the longitudinal axis. As with promastigotes, amastigotes also have nucleus and kinetoplast (Awasthi et al. 2004). There are also two separate, consecutive growth phases during the development of *Leishmania* in sand flies involving four distinct life cycle stages. The first growth cycle is initiated by procyclic promastigotes, which divide in the bloodmeal in the abdominal midgut of the vectors. Procyclic promastigoes give rise to the non-dividing nectomonad promastigotes that will

migrate to the anterior abdomen and subsequently transform into leptomonad promastigotes. This will initiate a second growth cycle in the anterior midgut. Finally, leptomonad promastigotes differentiate into non-dividing metacyclic promastigote which is the mammal-infective stage (Figure 1.2) (Gossage et al. 2010). It has been shown that metacyclogenesis in *Leishmania* is induced *in vitro* by low pH and nutrient exhaustion (Bates 2007). Both the metacyclic and procyclic forms generated *in vitro* are morphologically similar to their insect counterparts (Sacks 1989; Debrabant et al. 2004). Morphologically, metacyclics are small, short and slender cells with a flagellum measuring at least twice the length of cell body (Gossage et al. 2010).

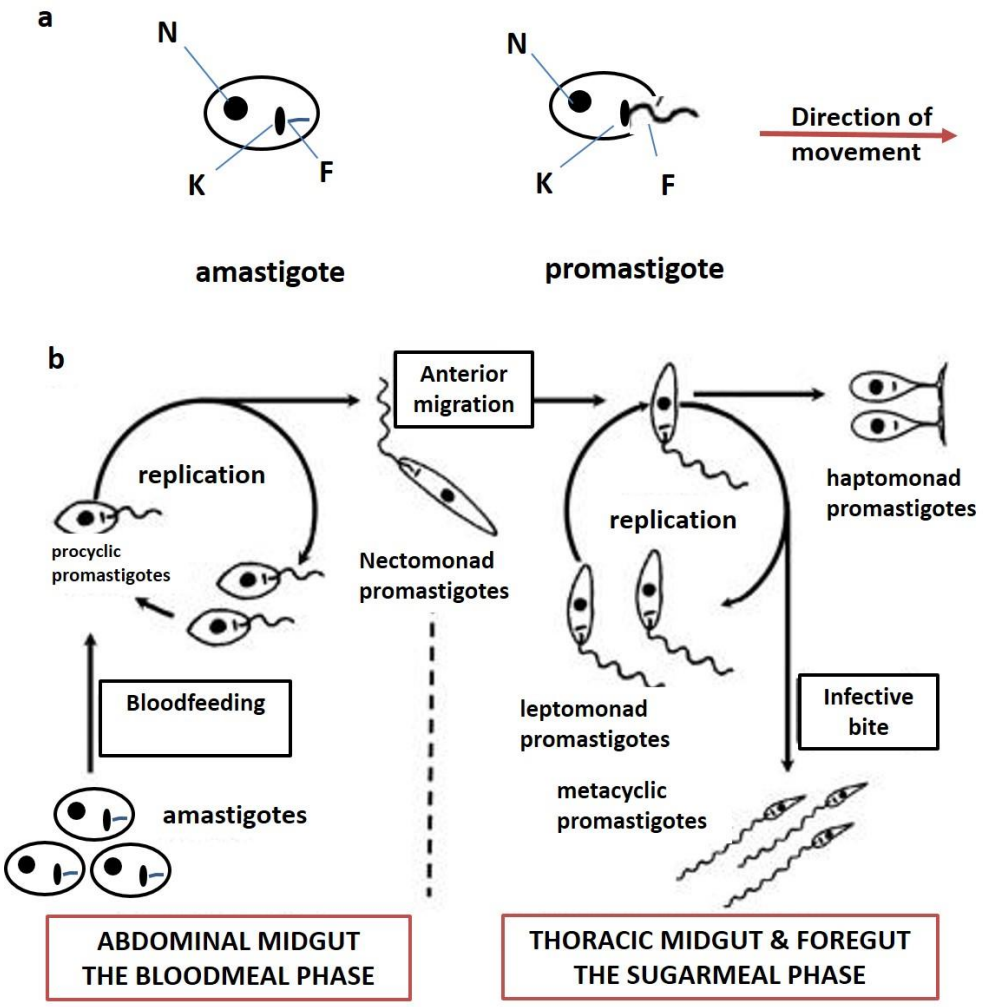

Figure 1.2: Development of *Leishmania* (*Leishmania*) species in the sand fly vector.

(a) The morphology of amastigotes and promastigotes. Each form has a nucleus (N), kinetoplast (K) and flagellum (F). The kinetoplast contains mitochondrial genome. The flagellum in amastigotes is internal and non-functional, whereas in promastigotes, the flagellum extends from the cell body, beats and pulls the organism in the direction shown, emerging from the anterior end of the cell. (b) The developmental sequence of the five major promastigote forms: procyclic promastigotes, nectomonad promastigotes, leptomonad promastigotes, haptomonad promastigotes and metacyclic promastigotes (Bates 1994).

When the sand fly is having a blood meal on the mammalian skin, metacyclic promastigotes are deposited into the mammalian skin through the proboscis. Macrophages will engulf and phagocytosed the promastigotes which will rapidly transformed into amastigotes (Walker et al. 2013). The macrophages become a host for amastigotes to replicate slowly by binary fission until it ruptures and releases the amastigotes to infect new macrophages (Figure 1.3). The parasites now are liberated into the circulation and can progress to other organs such as liver, spleen and bone marrow. When new sand fly takes blood meal from the infected host, it may take up infected macrophages and releases them into the midgut of the insect. The amastigotes will then transformed into promastigotes form and divide by binary fission before migrating to the insect's proboscis, where they are poised to infect a new human host through another blood meal (Awasthi et al. 2004). A recent work by Inbar et al. (2013) has demonstrated that *L. major* strains have sexual competency and that sex is a normal aspect of their reproductive strategy. Akopyants et al. (2009) discovered that *Leishmania* promastigotes can mate in the sand fly vector and the hybrids could be transmitted to the mammalian host by sand fly bite. The exchange of genetic materials is a significant factor as this allows the parasite to adapt to new ecological niches, vectors and hosts.

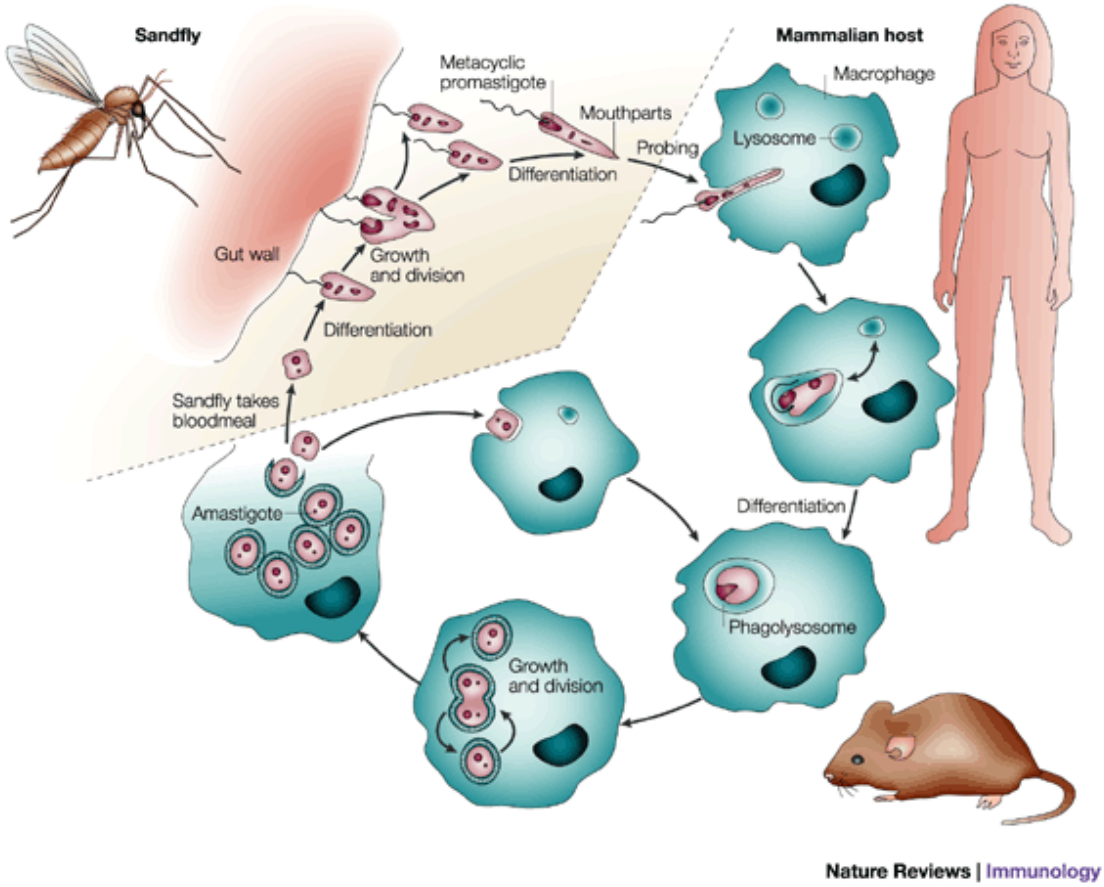

Figure 1.3: The lifecycle of *Leishmania*.

A small number of infectious metacyclic promastigotes are injected into host's skin through the bite of an infected sand flies. These promastigotes are then taken up by macrophages, where they reside in phagolysosomes and transform into replicating amastigotes. Infected macrophages are taken up by sand flies during blood feeding. These macrophages are lysed in the fly midgut, releasing parasites that transform into rapidly dividing, non-infectious-stage promastigotes. These forms undergo a process of differentiation to non-dividing, metacyclic promastigotes that can be transmitted when the sand fly takes another blood meal (Sacks & Noben-Trauth 2002). Permission to reproduce this image has been granted by Elsevier.

1.1.2 Transmitting vector

Like other kinetoplastids, *Leishmania spp*. are transmitted by phytophagous arthropods. Known collectively as Phlebotomines, there are over 500 species of sand flies have been described from numerous parts of the world, with most being assigned to three genera: *Phlebotomus* and *Sergentomyia* of the Old World, and *Lutzomyia* of the New World (Figure 1.4). The Old-World sand flies are habitually found in the Mediterranean, Southern Europe, Africa, the Middle East, Central Asia and South Asia. The *Lutzomyia spp*. are found throughout the Americas and North America.

There are three unique features that make them recognizable: when at rest, they characteristically hold their wings at an angle above the abdomen; they are hairy; and, they hop along the hosts' skin before settling down to bite. Unlike mosquitoes, their attack is silent and often unnoticed. Adult sand flies are small sized about 1.5-3 mm long. They are nocturnal and are weak flyers (Killick-Kendrick 1999).

As with all true Diptera flies, sand flies undergo complete metamorphosis and exhibit four complete life stages which are egg, larva, pupa and the adult. Dissimilar with mosquitoes, the immature stages do not require standing water to complete development, though they do require relatively warm, moist environments (Bates et al. 2015). Both female and male sand fly adults obtain carbohydrate nutrition from plant juices. In most species of sand fly only the female is responsible for biting and sucking the blood of mammals, reptiles and birds as she requires the protein in the blood to complete development of egg batches. Though some are autogenous (able to produce viable eggs without a blood meal). When a female bite, she injects saliva into the skin which not only gives rise to an allergic reaction in some individuals, but is believed to play a part in the successful establishment of *Leishmania* at the site of the bite (Bates et al. 2015).

Figure 1.4: The image of sand fly from genus Phlebotomines and *Lutzomyia*

(from http://www.infectionlandscapes.org/2011/05/leishmaniasis.html).
Sand flies are the vector responsible for transmitting *Leishmania spp*. Two of the genera are Phlebotomines (the Old World) and *Lutzomyia* (the New World).

1.2 Leishmaniasis: a global threat

1.2.1 Leishmaniasis, clinical manifestations and epidemiology

The World Health Organization (WHO) has designated leishmaniasis as a category 1 (emerging and uncontrolled) and neglected disease. Leishmaniasis is the ninth greatest global burden of disease among individual infectious diseases. It is a collection of diseases, each with its own clinical manifestations and epidemiology. Infection is initiated by the bite of an infected sand fly vector and parasites disseminate from the site of infection in the skin to reside and propagate within macrophages of the liver, spleen and bone marrow and in the skin of cutaneous leishmaniasis (McConville & Handman 2007). The nature and severity of the disease depends on the causative species, with spectrum of pathologies ranging from benign self-healing lesions of cutaneous leishmaniasis (CL) to metastasizing lesions of mucocutaneous leishmaniasis (MCL) and the severe visceral leishmaniasis (VL). *L. major, L. tropica* and *L. mexicana* causes CL which manifests as localised cutaneous lesions that generally self-heal. It can subsequently metastasise into MCL as it often does in the case of *L. braziliensis*. Whereas VL caused by *L. donovani* and *L. infantum* involves a chronic disseminating disease of the liver and spleen, which is often fatal if left untreated (Olliaro et al. 2013). Furthermore, the form and severity of the disease depends on the host immune system and the poorly understood interplay between host-parasite-vector.

Leishmaniasis is endemic in 88 countries, 72 of which are developing countries, and it has affected an estimated 12 million people each year with an annual mortality rate of 60,000 (Figure 1.5 and Figure 1.6) (Alvar et al. 2012). However, these numbers are not accurate as extensive numbers of cases are not recorded because notification of the incidence is compulsory in only 40 of the 88 affected countries. In addition, many leishmaniasis cases are either asymptomatic or misdiagnosed. On top of that, outbreaks often go unreported because they occur in zones of extreme conflict or in remote rural areas seldom visited by journalists or government officials. The disease primarily affects underprivileged population in Africa, Asia and Latin America, especially remote places that are not accessible to health facilities. Furthermore, there is limited investment in drugs and vaccines in those countries. The infection is also concomitant with socio-economic conditions such as lack of proper domestic sanitation and clean water, poor

housing and lack of resources. This combination of conditions is conducive to transmission of vector-borne diseases. Sand flies are attracted to crowded housing as these provide a good source of blood-meals. Infection can also increase due to environmental changes including urbanization and deforestation as well as climatic changes such as changes in temperature, rainfall and humidity that would bring about drought and global warming. Epidemics of both CL and VL are often associated with migration and the mobility of non-immune population into areas with existing transmission cycles. On top of that, the advent of the human immunodeficiency virus (HIV) is contributing to leishmaniasis becoming an opportunistic infection in AIDS patients (Diro et al. 2014). Leishmaniasis outbreaks have also become the new hallmark of late 20th or 21st century wars. CL in particular is a common scourge among civilian victims in the civil war in Syria, Iraq, Afghanistan and elsewhere in the Middle East and Central Asia (Hotez 2014). This disease has also affected military troops in Iraq and Afghanistan. When the infected patient succumbs to death they act as a reservoir of infection, passing on the parasite to other people through the bite of sand flies (Hailu et al. 2005). Animals such as dogs are also important reservoirs of human VL and most reported cases were in dogs that had originated in or travelled from areas where leishmaniasis is endemic (Reguera et al. 2016).

CL is more widely distributed, with about one-third of cases occurring in each of three epidemiological regions specifically the Americas, the Mediterranean basin, and western Asia from the Middle East to Central Asia. The ten countries with the highest estimated case counts are Afghanistan, Algeria, Brazil, Colombia, Costa Rica, Ethiopia, Iran, Peru, Sudan and Syria, and together account for 70 to 75% of global estimated CL incidence (WHO 2015).

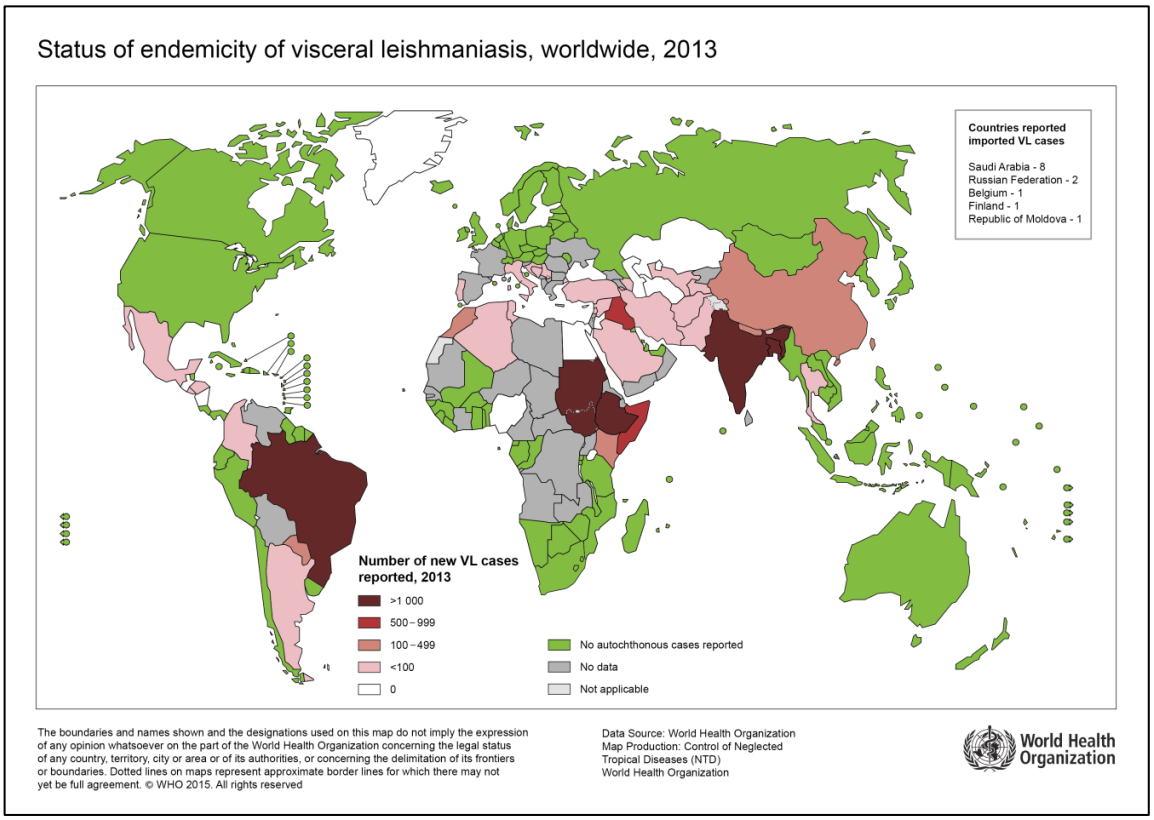

Figure 1.5: The distribution of visceral leishmaniasis in the world.

Source: WHO 2015.

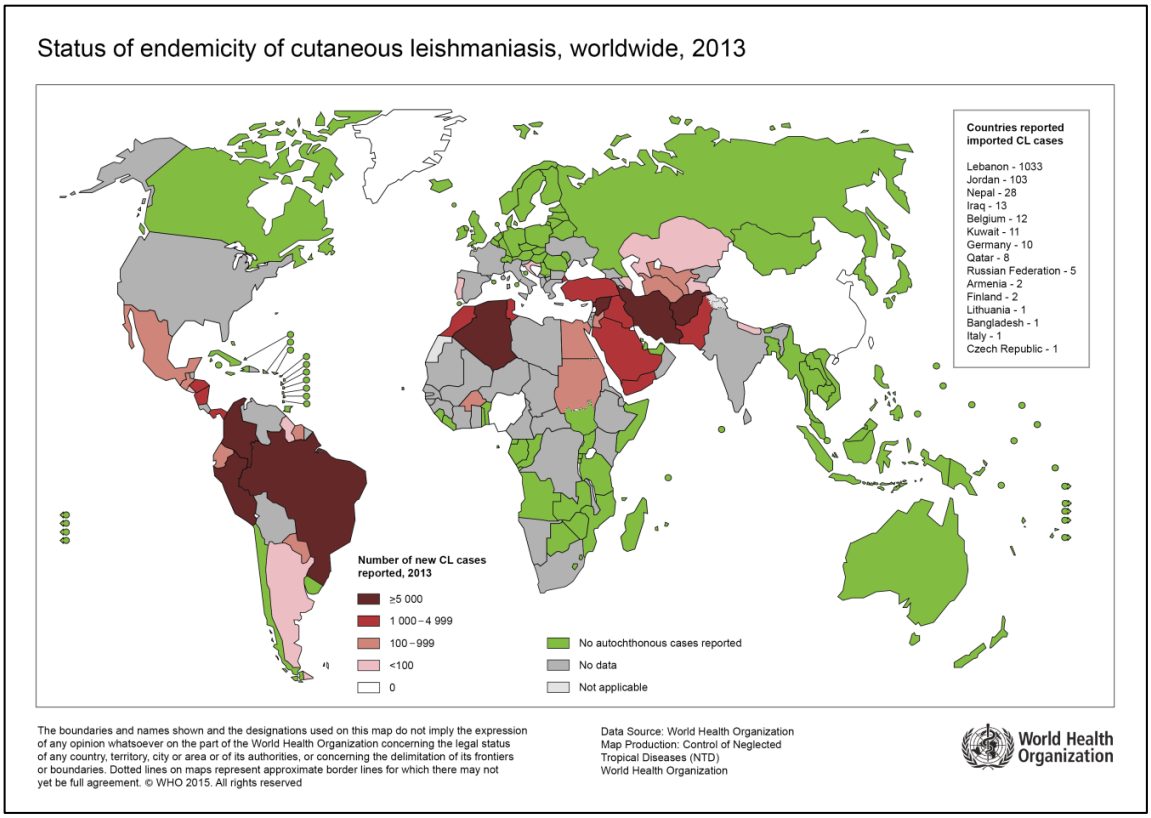

Figure 1.6: The distribution of cutaneous leishmaniasis worldwide.

Source: WHO 2015.

Table 1.1: *Leishmania* species causing human disease, reservoir hosts and vectors
(Oryan 2015)

Leishmania species	Infection	Geographical location	Reservoir	Vector
L. donovani	VL, PKDL	Old world, except Europe	Humans, rodents	*Phlebotomus argentipes, P. orinntalis, P. martini*
L. infantum	VL, CL, ML	New world for VL, old world for CL and ML	Rodents, dogs, foxes, jackals	*P. pcniciosufi, P. arias, Lutzomyia longipalpis*
L. chagasi	VL	New world	Foxes, dogs, opossums	*L. longipalpis*
L. major	CL, ML	Old world	Rodents, gerbils	*P. papatasi, P. duboscqi*
L. tropica	CL, ML, VL	Old world	Humans	*P. sergenti*
L. aethiopica	CL, DCL, MCL	Old world	Hyraxes	*P. longipes, P. pedifer*
L. mexicana	CL, DCL, MCL	New world	Forest rodents	*L. olmeca*
L. amazonensis	CL, DCL, MCL	New world	Forest rodents	*L. flaviscutellata*
L. braziliensis	CL, MCL	New world	Forest rodents, peri domestic anteaters	*Lutzomyia spp.*
L. guyanemis	CL, MCL	New world	Sloths arboreal anteaters	*L. umbratilis*
L. panamensis	CL, MCL	New world	Sloths	*L. trapidoictal*
L. peruviana	MCL	New world	Dogs	*L. verrucarun, L. pvmenis*

VL: Visceral leishmaniasis; PKDL: Post-kala azar dermal leishmaniasis; P: Phlebotomus; ML: Mucosal leishmaniasis; CL: Cutaneous leishmaniasis; L: *Lutzomyia*; DCL: Diffuse cutaneous leishmaniasis; MCL: Mucocutaneous leishmaniasis.

1.2.2 Diagnosis, treatment, vaccination and prevention

To date, a variety of diagnostic methods have been developed for diagnosis and identification of *Leishmania*. It has proven challenging to diagnose the symptoms of leishmaniasis in the early phase as the parasites could live inside the host for months asymptomatically. Furthermore, confirmation of diagnosis by laboratory methods is difficult in remote areas. Traditionally, *Leishmania* in clinical samples is detected microscopically but this method is not only insensitive but also laborious. Although the conventional molecular approaches such as PCR, RT-PCR and RFLP improve diagnosis and produce quantitative results, however, they are expensive and complex (Carson et al. 2010). Other techniques that use monoclonal antibodies such as ELISA, Southern, Dot, Spot, or Squash Blots are not feasible due to lack of specificity, sensitivity and rapidity for the isolates (Lockwood & Sundar 2006). Recently, Sattarahmady et al. (2016) have developed a new method of diagnosing leishmaniasis based on hybridization of gold nanoparticles linked to a

specific ssDNA probe from non-protein coding region of *L. major* minicircle kinetoplast DNA.

The current mainstay of treatment is based on chemotherapy, which relies on a handful of drugs. The gold standard against leishmaniasis that has been used for the last six decades is pentavalent antimonial. In some cases, other drugs such as amphotericin B, pentamidine, miltefosine, aminosidine, paromomycin, allopurinol, and sitamaquine can be used (Figure 1.7) (Monzote 2009). However, the therapeutic arsenal against leishmaniasis is currently limited due to low efficacy, emergence of resistant parasites, high toxicity of drugs that causes life threatening side-effects, high cost especially to the less developed countries, and difficulties of administration of the drugs (Mohapatra 2014). Therefore, there is a dire need for new chemotherapeutic agents against this perilous disease.

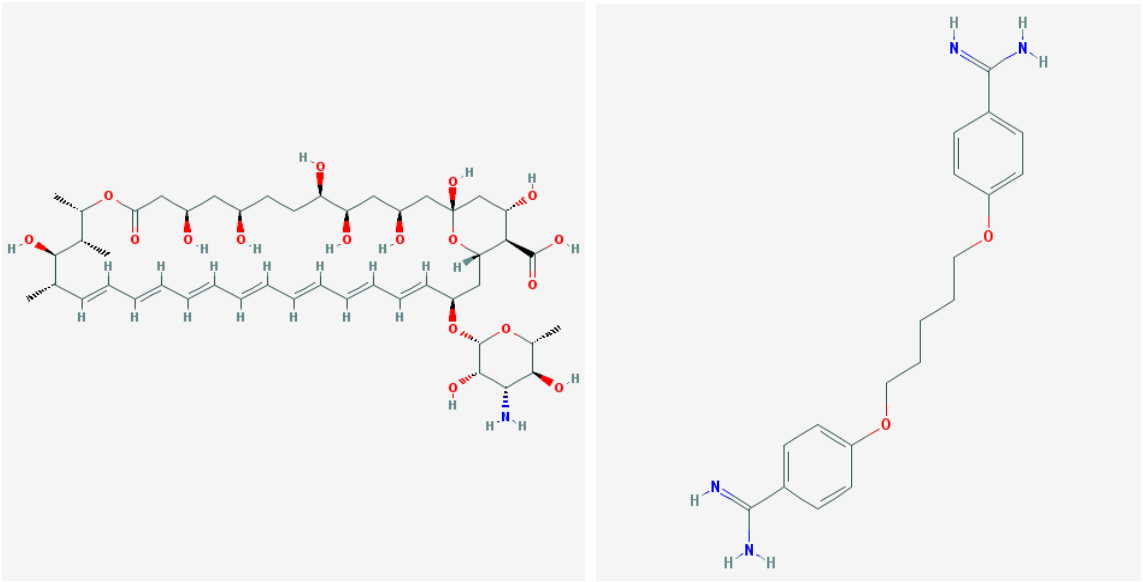

Figure 1.7: Chemical structure of antimonial drugs, amphotericin B and pentamidine.

Amphotericin B and pentamidine are among the most frequently used drugs in leishmanial infection. Amphotericin B binds to ergosterol, which is an essential component of the fungal cell membrane. This binding cause depolarization of the membrane and altering cell membrane permeability. This leads to leakage of important intracellular components, cell rupture, and eventually cell death. This agent may also induce oxidative damage in fungal cells and has been reported to stimulate host immune cells. Pentamidine is a synthetic derivative of amidine with antiprotozoal and antifungal activities. Although the precise mode of action of pentamidine is unclear, it appears to interact directly with the pathogen genome by binding to AT-rich regions of duplex DNA and the minor groove of DNA, thereby interfering with DNA replication.

Source: https://pubchem.ncbi.nlm.nih.gov/compound/

In recent years, there have been several promising compounds that show anti-leishmanial properties and are in different stages of drug development and clinical trials. These include 2-substituted quinolone, 8-aminoquinolines as well as drugs that targeting the metabolic pathways and biochemical structures of the parasite (Mohapatra 2014). As the key regulatory proteins, protein kinases have been targeted for the development of anti-leishmanial compounds. *L. mexicana* mitogen activated protein kinases-1 (LmxMPK-1) and mitogen activated protein kinases-2 (LmxMPK-2) were found to be essential for the survival of amastigotes in the host (Wiese 2007). There are also a growing interest in alternative natural products and plant compounds for the treatment of leishmaniasis (Oryan 2015).

On the other hand, vaccines have not been successful so far due to the complexity of the immune response caused by the parasite. To date there is still no effective vaccine available despite substantial efforts by many laboratories (Gillespie et al. 2016). Traditionally, leishmanization process which involves inoculation with live parasites has been given as vaccination in Asia, however in some cases this can lead to a chronic infection. Research has been carried out with heat-inactivated adjuvant-supplemented *Leishmania* or *Leishmania* fractions, genetically modified or live attenuated vaccines, as well as DNA vaccines (Rezvan & Moafi 2015). However, these researches are still undergoing clinical trials for safety, efficacy and immunogenicity. Another vaccine approach targets the parasite vector, i.e. selected sand fly salivary gland antigens, which can exacerbate *Leishmania* infection (Oliveira et al. 2015). One of the candidates that has succeed into phase I and II clinical trials is LEISH-F1 + MPL-SE fusion vaccine which is composed of the recombinant *Leishmania* polyprotein LEISH-F1 antigen that includes three proteins derived from *Leishmania* (elongation initiation factor, thiol-specific antioxidant, and stress-inducible protein 1) and the monophosphoryl lipid A-stable emulsion (MPL®-SE adjuvant) (Chakravarty et al. 2011). This vaccine has been shown to elicit a T helper 1 (Th1) immune response.

Besides trying to combat leishmaniasis, prevention steps are more important to circumvent spreading the infection. Measures to control transmission of infection vary according to local epidemiology. Some of the controlling strategies that have been used to combat leishmaniasis focussed on vector control, control of animal reservoirs and personal protection. Spraying houses with residual insecticide

containing DTT (dichloro-diphenyl-trichloroethane) has been an important measure to control the vector in the past. However, it has become inefficient because sand flies has become resistant (Coleman et al. 2015). Moreover, DTT was banned in the United States and many other developed countries. In areas where sand flies bite at night, the usage of insecticide-impregnated bed nets has decreased the incidence of leishmaniasis. However, one major problem limiting the use of conventional bed nets is the cost (Guerin et al. 2002).

Intense researches have been conducted on the vectors including identifying the location of metacyclic forms of *Leishmania* in specific parts of the sand fly gut, prevention of *Leishmania* attachment to the sand fly mid-gut (i.e. the role of lipophosphoglycan (LPG) and flagellar-specific protein), investigating the mechanics of sand fly biting as well as investigating the vector's saliva as mode of transmission (Bates et al. 2015).

Meanwhile in the Mediterranean basin and Brazil, as the principal reservoirs, the dog population has been targeted as preventative measures. It has been reported that the use of deltamethrin-impregnated dog collars gives up to 86% protection of dogs in seasons of high transmission (Maroli et al. 2001). Although this is a crucial epidemiological control, this approach presents logistical concerns. Recent reports revealed that domestic cats were infected with *Leishmania sp*. mainly *L. infantum* in urban areas of Brazil (Metzdorf et al. 2017).

Nevertheless, despite many efforts, disease control has proven very difficult to achieve given the myriad of epidemiological situations, the multiplicity of factors that influence disease transmission and continuing uncertainty about the biology of the parasite, its vector and its reservoir hosts.

Resistance to infection has been associated with a Th1-mediated immune response. However, cumulative evidence suggests that true protection from disease will require the involvement of both a Th1-mediated and a Th2-mediated immune response from vaccination (Nagill & Kaur 2011). Hence, understanding the drug resistance mechanism, the immune responses in host and the interaction between parasites, vectors and host, may provide ways to exploit many intracellular targets, which will provide clues for designing newer drugs.

1.3 Host-Parasite Interplay complexity

The host-parasite relationship is by far the most important factor in elucidating pathogenicity. It determines whether the host can control the infection or fail to resolve infection making parasite to progress and disseminate (de Morais et al. 2015). Three domains must be combined to fight against pathogens: (i) a comprehensive picture of the host immune response, (ii) comprehensive knowledge of the immune evasion mechanisms of the pathogens, and (iii) pathogen drug resistance mechanisms (Horvatić et al. 2016). Several mechanisms are involved in this complex interaction. Some pathogens including *Leishmania*, *Trypanosoma cruzi* and *Salmonella* have evolved evasive mechanism (Olivier et al. 2005; Walker et al. 2013; Eriksson et al. 2003).

1.3.1 Development of host immune response directed to *Leishmania*

The innate response of immune system is based on the recognition of pathogen-associated molecular pattern molecules (PAMPs) that serve as an exogenous signal that alerts the host of the presence of pathogens (Schenten & Medzhitov 2011). This initiate signalling cascade that leads to the activation of transcription factors in innate immune cells involving macrophages, dendritic cells (DCs), mast cells and neutrophils. The initial binding and internalization of promastigotes involves macrophage plasma membrane structures including complement component 3 subunits C3b and C3bi, Fc receptors, lectin receptors and integrin. At the same time, the major surface molecules of *Leishmania* that involves in this interaction include gp63, LPG and glycosylinositol phospholipids (GPIs) (de Morais et al. 2015).

Following entrance of *Leishmania* into the host skin, their first encounter will be resident cells such as dermal macrophages, keratinocytes and Langerhans cells (Liu & Uzonna 2012). It has been shown that keratinocytes play a critical role in the commencement of a protective immune response towards *Leishmania* by secreting immunomodulatory mediators such as interleukin-12 (IL-12), IL-1β, IL-4 and IL-6 (Ehrchen et al. 2010). Moreover, two-photon intravital imaging of mouse skin following inoculation of *L. major* has proved that dermal DCs take up parasites within the first few hours (Ng et al. 2008). As the number of dermal DCs are too limited to sustain parasite multiplication, the progression of infection requires the

recruitment of monocytes, which is facilitated by neutrophils (Kaye & Scott 2011). During a sand fly blood meal, haemorrhagic pool caused by the bite attracts neutrophils and monocytes to rush to the site of infection (de Menezes et al. 2016). Interestingly, while parasites used the monocytes as host, monocytes also upregulate the expression of major histocompatibility complex class II (MHC class II) molecules that act as antigen presenting cells (van Zandbergen et al. 2004; Ng et al. 2008).

Neutrophils are recruited to the site of infection due to the release of alarmins (signal for tissue damage), cytokines and chemokines (Kaye & Scott 2011). These cells then produce reactive oxygen species (ROS), neutrophil elastase (NE) and neutrophil extracellular traps (NETs) (de Morais et al. 2015). Neutrophils also secrete IL-8 to attract more neutrophils, while functioning as phagocytic cells ingesting *Leishmania* (Teixeira et al. 2006). However, if *Leishmania* can evade these mechanisms, they will stay in neutrophils until neutrophils undergo apoptosis and phagocytized by macrophages (de Morais et al. 2015). Engulfment by macrophages triggers anti-inflammatory signal pathways. Furthermore, by staying in neutrophils before being phagocytized by macrophages result in silent entry of the parasites inside macrophages, thereby hiding them from anti-inflammatory attacks.

Macrophages, together with DCs and Natural Killer cells (NK) are considered to play important roles in the immune response to *Leishmania* infection. The role of macrophages is to destroy foreign microorganisms, cellular debris, as well as senescent and damaged cells. Apart from phagocytized cells, macrophages also act as antigen presenting cell (APC), which is necessary for their efficient interaction with effector T cells and the delivery of cytokines to induce bactericidal activity through the involvement of Toll-like receptors (TLRs) molecule signalling (Meier et al. 2003). NK cells are recruited to the site of infection to produce interferon-gamma (IFN-γ) and $CD4^+$ cells that will restrict early parasite dissemination (Gupta et al. 2014). These cells also secrete IL-12 which is important for the induction of a host-protective T helper 1 (Th1) type response (Kaye & Scott 2011). TLR2 expressed on host macrophages recognize LPG from *Leishmania* resulted in the production of IL-12, nitric oxide (NO) and ROS

thereby inducing host protective immune response (Kavoosi et al. 2009; Bhattacharya et al. 2010).

Aside from innate response, adaptive response involving T and B lymphocytes also responsible in protecting host from harmful pathogens. Generally, IFN-γ-producing Th1 cells are required for resolution of infection. IFN-γ signals through JAK/STAT pathway is critical for the induction of NO (Jayakumar et al. 2008). While immune modulators such as IL-12, IFN-γ and tumour necrosis factor-alpha (TNF-α) mediate parasite clearance, others that dampen the immune response or activate immune response that will favour parasite persistence are associated with Th2 type response. These includes expression of IL-4, IL-10, IL-13 and transforming growth factor-ß (TGF-ß) (Gupta et al. 2014). Similar to TNF, IL-1ß can lead to either protective or pathogenic effects during *Leishmania* infection (Figure 1.8) (Scott & Novais 2016).

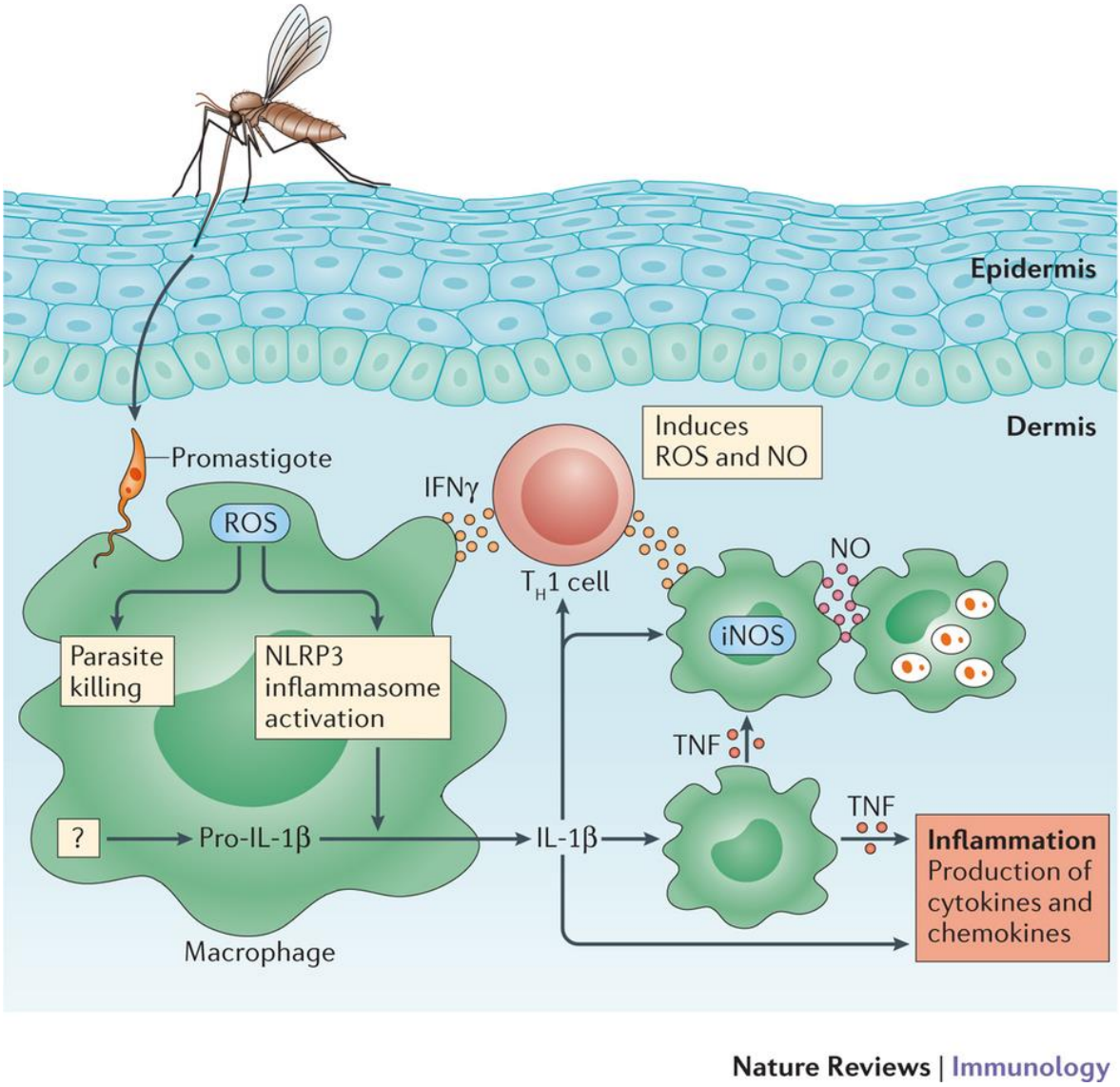

Figure 1.8: IL-1β and TNF can be protective or pathogenic in cutaneous leishmaniasis.

Reactive oxygen species (ROS) are induced following phagocytosis of *Leishmania* by innate cells. ROS can induce parasite elimination as well as activate the NLRP3 (NOD-, LRR- and pyrin domain-containing 3) inflammasome. Pro-IL-1β is processed by the inflammasome in the skin and its mature form can function in several ways during *Leishmania* infection. IL-1β is important in T helper 1 (Th1) cell expansion by promoting IL-12 production, thereby inducing nitric oxide (NO) activation either directly, by activating macrophages, or indirectly, by promoting Th1-type responses and interferon-γ (IFN-γ) production. IL-1β can also induce tumour necrosis factor (TNF), which can be protective when synergizing with IFN-γ and thus increasing inducible NO synthase (iNOS) production in innate cells. NO can promote parasite control in the iNOS-expressing cell, but it can also diffuse through tissue and act on neighbouring cells. In contrast to their protective roles, IL-1β and TNF can also enhance the production of several chemokines and cytokines therefore promote the expression of adhesion molecules, leading to the amplified recruitment of cells from the blood. This enhanced inflammation results in tissue destruction and disease severity. (adapted from Scott & Novais 2016).

1.3.2 Macrophage diversity

Macrophages are well known for their ability to respond to environmental stimuli and dramatically change their form and physiology. However, not all macrophage

activation responses are the same (Mosser & Edwards 2008). The innate immune response that is orchestrated by a series of signalling pathways involving TLR, IL and NF-κB will define the macrophages response towards pathogen infection. The flexibility of macrophages towards *in vivo* environments results in the induction of various types of macrophages during infections and differentially affects the course of disease. Because the macrophage activation states correspond to their functional phenotypes during infection with pathogens, it provides a useful framework to understand how the expressed proteome of these cells correspond to their physiological functions (Chawla 2010). Essentially, there are at least three distinct populations of macrophages that have been extensively studied: classically activated macrophages (M1), alternatively activated macrophages (M2) and type II-activated macrophage (Figure 1.9). Each cell type appears to have different biological roles. The metabolic screening of cell extracts done by Lamour et al. (2012) has revealed clear metabolic differences between M1 and M2 macrophages in *L. major* infected and uninfected state.

M1 macrophages have been comprehensively characterized and well described among macrophage population (Gordon 2007; Martinez et al. 2009). These cells are important in host defence by propagating inflammatory responses. They are formed in response to IFN-γ and TNF, also referred as Th1 cytokines (Mosser & Zhang 2010). The activation process involves two steps. The first step occurs when IFN-γ induces macrophage to exhibit enhanced MHC class II expression and antigen presentation. The second step involves the activation of TLRs by stimulus such as lipopolysaccharide (LPS). The activation of TLRs induces the production of TNF and this cytokine acts in an autocrine manner to stimulate macrophages (Mosser & Zhang 2010). M1 macrophages are essential for rapid clearance of invading pathogens by producing NO and its derivatives. In addition to secreting NO, they also upregulate MHC-II and co-stimulatory molecules such as CD40, and produce many other inflammatory cytokines and mediators (Lamour et al. 2012). The immunoregulatory cytokines TGF-ß and IL-10 play an important role in dampening macrophage activation (Mosser 2003).

In contrast with M1 macrophages, macrophage exposure to IL-4, IL-13, and IL-21 (representing Th2 cytokines) stimulates the transcription of arginase and polyamines which are used as substrates for parasite growth and replication.

These macrophages are known as M2 macrophages (Kropf et al. 2005). M2 macrophages do not require a priming stage as opposed to M1. They do not produce NO that is responsible for microbial killing. Although they upregulate some MHC class II molecules, they are not efficient at antigen presentation, and may inhibit T cell proliferation (Mosser 2003). Arginase 1 is responsible for the hydrolysis of L-arginine into ornithine which is the building block for polyamines production. High level of polyamines contributes to the inefficient host defence by inhibiting the secretion of proinflammatory cytokines in host (Kropf et al. 2005).

Like the M1 macrophages described above, the type II activation phenotype required two signals. The first signal is the ligation of Fc-gamma receptors (FcγRs). Second signal comes from macrophage stimulatory signal (CD40 or CD44) through TLRs (Mosser 2003). Ligation of FcγRs on these macrophages turned off IL-12 synthesis and induced the secretion of large amounts of IL-10 (Sutterwala et al. 1997; Sutterwala et al. 1998). Additionally, the production of other M1-associated cytokines, such as TNF, IL-1 and IL-6, remains intact (Gerber & Mosser 2001). Furthermore, the dramatic induction of IL-10 by these macrophages suggested that they would have anti-inflammatory properties (Sutterwala et al. 1998). The ligation of FcγR on activated macrophages by antigen-IgG complexes induced T cells to produce IL-4, which in turn induced B cells which produced Th2-like responses (Anderson & Mosser 2002).

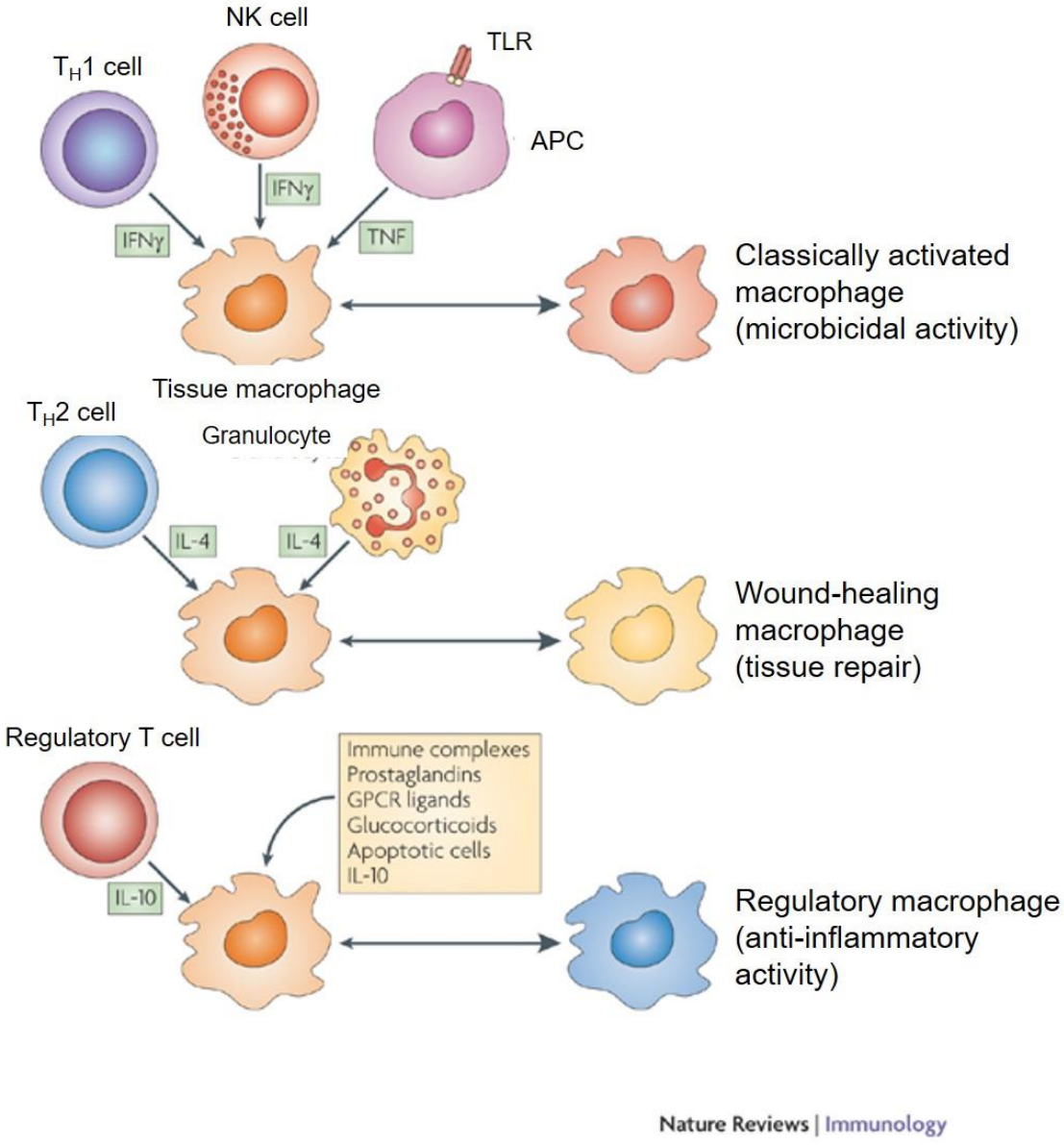

Figure 1.9: Cytokines produced by immune cells can give rise to macrophages with distinct physiologies.

Classically activated macrophages arise in response to interferon-γ (IFN-γ), which can be produced during an adaptive immune response by T helper 1 (Th1) cells or CD8+ T cells (not shown) or during an innate immune response by natural killer (NK) cells, and tumour-necrosis factor (TNF), which is produced by antigen-presenting cells (APCs). Wound-healing (alternatively activated) macrophages arise in response to interleukin-4 (IL-4), which can be produced during an adaptive immune response by Th2 cells or during an innate immune response by granulocytes. Regulatory macrophages are generated in response to various stimuli, including immune complexes, prostaglandins, G-protein coupled receptor (GPCR) ligands, glucocorticoids, apoptotic cells or IL-10. Each of these three populations has a distinct physiology. Classically activated macrophages have microbicidal activity, whereas regulatory macrophages produce high levels of IL-10 to suppress immune responses. Wound-healing macrophages are similar to the previously described alternatively activated macrophages and have a role in tissue repair (adapted from Mosser & Edwards 2008).

1.3.3 Metabolic reprogramming in macrophages

Moreira et al. (2015) demonstrated that *Leishmania* can hijack mitochondrial pathways required for glucose metabolism. Early during infection, *L. infantum* was found to augment aerobic glycolysis, which was followed by a switch to mitochondrial metabolism and oxidative phosphorylation later during infection (Moreira et al. 2015). Of note, neutrophils depend on aerobic glycolysis for ATP production (Rossi & Zatti 1964). LPS produced by Gram-negative bacteria activates TLR4 in neutrophils and increases glucose consumption as well as oxygen consumption which is used to produce ROS (Guthrie et al. 1984). Pro-inflammatory stimuli induced by LPS activates macrophages and DCs that causes them to utilise more glycolysis and reduce oxidative phosphorylation (Kelly & O'Neill 2015a). Infection with *Mycobacterium bovis* BCG showed continual generation of NO following stimulation by LPS and IFN-γ (Qualls et al. 2013). NO expression induced by inducible nitric oxide synthase (iNOS) inhibit mitochondrial respiration through nitrosylation of iron-sulfur proteins present in electron transport chain complexes (Kelly & O'Neill 2015a). In macrophages activated by LPS and IFN-γ or infection, arginine is metabolized to NO and citrulline by iNOS. When arginine is scarce, citrulline is recycled to arginine via argininosuccinate synthase (Ass1) and argininosuccinate lyase (Asl) (Qualls et al. 2013). This is important to control infection. Therefore, some pathogens including *Leishmania* have mechanisms for depleting arginine by expressing arginase to inhibit NO production (Boitz et al. 2017). In fact, many metabolic enzymes involved in glycolysis, TCA cycle and fatty acid metabolism are S-nitrosylated on cysteine residues by NO (Doulias et al. 2014). For example, when very long-chain acyl-CoA dehydrogenase (VLCAD) was nitrosylated, its activity was increased thereby boosting fatty acid metabolism in ß-oxidation of fatty acids pathway (Doulias et al. 2014).

However, another type of macrophages which is the M2 (alternatively activated macrophages) have different metabolic profile than M1 (classically activated macrophages) macrophages (Mosser & Edwards 2008). It has been reported that M2 macrophages exhibit increased oxidative phosphorylation but have decreased production of NO and TNF-α (Doyle et al. 1994). While M1 macrophages are fuelled by glycolysis, M2 macrophages are fuelled by fatty acid uptake and oxidation in the mitochondria which are induced by IL-4 and IL-13 via signal transducer and activator of transcription 6 (STAT6) (Szanto et al. 2010).

1.3.4 Mechanisms of immune evasion by *Leishmania*

The balance between Th1 and Th2 type response could be exploited by pathogens to evade host immune responses. *Leishmania* have found ways to escape the innate immune response, permitting its persistence within the mammalian host. A significant number of virulence factors have been discovered in *Leishmania* (Gupta et al. 2013).

Leishmania are most vulnerable when they have just entered a mammalian host. Therefore, in this stage promastigote requires an array of strategies to evade the host immune system. The surface-bound display or secretion of virulence factors are important for the parasite to enter the host cell undetected. Promastigotes secrete proteases such as glycoprotein 63 (GP63) and cysteine proteases to breakdown host extracellular matrix to facilitate internalization into host (de Menezes et al. 2016). GP63 is also pivotal for resisting complement lysis by cleaving the host C3b to an inactive form C3bi, thereby hindering the complement system (Yao et al. 2003; Laurenti et al. 2004). The complement system is part of the immune system that enhances the ability to clear pathogens by triggering phagocytosis, inflammation and attacking membranes of foreign cells (Kenneth et al. 2017).

On the other hand, the intracellular amastigote stage is more resistant to the hostile environment when they are engulfed by phagocytes. After internalization into phagosomes, metacyclic promastigotes rapidly transform into amastigotes, shedding the promastigote LPG. LPG migrates to the surface of the infected macrophages and inhibited the respiratory burst occurs by phagocytosis (Awasthi et al. 2004). Once inside the phagolysosome of the host, amastigotes not only can survive the acidic pH, they also relies on the host cells for nutrients such as sugars, amino acids, lipids and phosphate (Burchmore & Barrett 2001).

Leishmania are able to hijack the microbicidal function of macrophages, mainly by interfering with intracellular signalling initiated by IFN-γ and TLR. As TLR2 induce immune responses, *L. major* recruit suppressors for the cytokines, namely SOCS-1 and SOCS-3 (Flandin et al. 2006). *L. amazonensis* subvert TLR2 signalling pathway by increasing the expression of IFN-β that increase superoxide dismutase 1 (SOD1) levels. Consequently, this inhibit superoxide-dependent parasite killing

(Vivarini et al. 2011). Besides TLR2, *Leishmania* could also alter TLR4 signalling pathways to favour establishment of infection. For example, *L. mexicana* capitalizes on TLR4 signalling to inhibit the production of IL-12 by infected macrophages and thereby promotes infection (Shweash et al. 2011). One of the main signalling molecules involve is Src-homology 2 domain containing phosphatase-1 (SHP1) (Shio et al. 2012). SHP1 has a central role in the regulation of iNOS and NO by inactivating JAK2 and Erk1/Erk2. Studies with SHP1-deficient infected macrophages confirmed the role of this phosphatase in the regulation of Erk1/2 signalling (Blanchette et al. 2009). Interestingly, *L. mexicana* amastigote block LPS induced IL-12 production by degrading the Erk1/2 and Jun N-terminal kinase (JNK) using their cysteine proteinases (Cameron et al. 2004). Next, protein kinase C (PKC) signalling is important to drive the expression of NO and oxidative burst (Shio et al. 2012). However, *Leishmania* LPG can block PKC activity by binding to the regulatory domain of PKC (Turco & Descoteaux 1992). JAK activation plays an important role in apoptosis and immune activation through the activation of STAT1 and transcription factors (TFs) (Rawlings et al. 2004). More importantly, the gene promoter on iNOS has binding sites for several TFs including STAT1. *Leishmania* has developed several strategies to interfere with these TFs including NF-κB, STAT-1α and AP-1 (Shio et al. 2012). One study reported that cysteine proteinases of *L. mexicana* degrade NF-κB and resulted in failure to bind to its DNA consensus on iNOS gene (Cameron et al. 2004). In addition, GP63 is responsible to degrade AP-1 subunits and block its downstream functions such as NO production (Contreras et al. 2010).

Collectively, it is very clear that *Leishmania* have the ability to evade host immune responses as well as modulating most of the key immune regulator molecules and signalling pathways produced by the host. Therefore, critical macrophage functions that were meant to threaten parasites were interfered, making them to persist in the host.

1.4 Proteomics

Recent advances in next-generation DNA sequencing and proteomics provide an unprecedented ability to survey mRNA and protein abundances. Such proteome-wide surveys are illuminating the extent to which different aspects of gene expression help to regulate cellular protein abundances. Proteomics is an

emerging field of research facilitated by the advancements in protein separation, mass spectrometry, genome sequencing, and protein search databases. The most applied approaches to proteomics research can be generally classified as having one of two major objectives: (1) protein or peptide separation, and (2) identification and characterization of proteins or peptides.

Proteins are essential players in all cellular processes, with numerous functions as enzymes and structure-forming or signal-transducing molecules. Their enormous characteristics enable a myriad of necessary tasks to ensure proper function of each cell. Changes in biological events such as disease, drug effect, or physiological activity will be reflected in abundancies or processing of the proteins. Therefore, proteins have always been, and presumably will always be, the target of all types of studies in biological sciences.

Unlike the genome, the proteome is dynamic, responding to any change in genetic and environmental factors. Furthermore, the proteome is more complex than a genome due to post-translational modification events. Moreover, the dynamic range of the protein abundance makes protein studies even more difficult. In order to decipher the constituents of a proteome, the dynamics and complexity of proteins could be analysed quantitatively. Gel-based proteomics have always used by many scientists. However, limitations such as reduced reproducibility and time-consuming make scientists to seek for other alternatives. Thus, methods such as in-solution digestions, liquid chromatography, and Multidimensional Protein Identification Technology (MudPIT), which are gel-free, are favoured when dealing with complex proteins samples.

1.4.1 Gel-based protein separation and detection

Currently, there are three preferred methods for separation of complex protein samples: SDS-PAGE, 2-DE, and DiGE. Each of these has its own merits and drawbacks.

First reported by Laemmli in 1970, sodium dodecyl sulphate polyacrylamide gel electrophoresis (SDS-PAGE) is a very common method for separating proteins by electrophoresis using a discontinuous polyacrylamide gel as a support medium and sodium dodecyl sulphate (SDS) to denature the proteins. Proteins were separated

according to size. Although SDS-PAGE is relatively easy to use and have low cost, it has low resolution, low accuracy and samples of high complexity are unable to be separated.

As an alternative, researchers moved to 2-dimensional gel electrophoresis (2-DE). 2-DE was pioneered by O'Farrell (1975). This technique separate proteins from complex samples based on their isoelectric points and molecular weights. In the first dimension, proteins are separated by their isoelectric point (isoelectric focusing; IEF) and in the second dimension by their molecular weight. After separation, proteins can be visualized, cut out of the gel, and identified by mass spectrometry. For comparative purposes, samples are loaded on separate gels and protein spot patterns are compared visually using 2D gel analysis software. Despite its powerful resolving capabilities, 2-DE technique lack reproducibility and laborious (Delahunty & Yates 2005). Additionally, there are several challenges for automatic software-based analysis such as incompletely separated (overlapping) spots, weak spots/ noise, running differences between gels (e.g., protein migrates to different positions on different gels) as well as unmatched or undetected spots. Nevertheless, many researchers employ 2-DE coupled with mass spectrometry (MS) as a standard protocol of proteomics, where automated in-gel digestion of protein spots will be subjected to subsequent identification of the proteins by MS.

In a variation of 2-DE technique, difference gel electrophoresis (DiGE), proteins from up to three different samples are labelled with different size-matched, charge-matched spectrally resolvable fluorescent dyes (e.g. Cy3, Cy5, Cy2) and then mixed, making it possible to directly compare different samples on a single gel. Interesting spots with differential fluorescent intensity between the dyes are removed from the preparative gel after post-staining with Coomassie Blue in order to allow proteins identification by MS analysis. Limitations of this method include time-consuming technique, and limited sensitivity, which, as a consequence, proteins with a low concentration may be failed to be selected (Unlu et al. 1997).

Another method that combines gel-based separation with MS is called OFFGEL. This separation is based on immobilized pH gradient (IPG) strips to separate peptides and proteins according to their isoelectric point (pI), that will be captured in solution, thus making recovery for LCMS much easier than traditional gels (Chenau et al. 2008).

The first comparative proteomic analyses utilising 2-DE on *Leishmania spp.* were done by El Fakhry et al. (2002), Bente et al. (2003), and Nugent et al. (2004). These studies were done on promastigotes and axenic amastigotes of *L. infantum*, *L. donovani* and *L. mexicana* where 2000 protein spots were detected. Of these spots, 3-5% were differentially expressed including proteins involved in carbohydrate metabolism, proteolysis, and response to stress.

1.4.2 Gel-free proteomics

The greatest step forward in the last decade has been the application of the physical sciences to cell biology. The behaviour of a cell emerges from the collective property of the millions of molecules in a cell could be elucidated. However, knowledge of molecules does not tell us how a cell is organized. Thus, the physical sciences provide us with the tools and techniques to answer such problems. Hence, MS-based proteomics approaches are essential in this regard.

One of the example of gel-free proteomics is the use of multi-dimensional capillary liquid chromatography coupled to tandem mass spectrometry to separate and identify the peptides obtained from the enzymatic digest of an entire protein extract. Proteins are cleaved into peptides using proteolytic enzymes and, subsequently separated and subjected to tandem mass spectrometric analysis. Mass spectrometric identification of these peptides allows the determination of the protein content of the initial sample. Since peptides can be more easily separated by liquid chromatography than proteins, a peptide based proteomic analysis can be performed much faster than a complete gel-based analysis.

In a typical shotgun proteomics experiment using MS, a complex protein sample is enzymatically digested into peptides which are then separated by HPLC, introduced into a mass spectrometer, fragmented, sequenced and used to identify the parent protein via database searching (Matallana-Surget et al. 2010). MS is currently the driving force to generate massive amount of proteomics data due to the ability to detect and identify proteins in large scale. Another benefit of this technique is its sensitivity. Most importantly, the ground-breaking development of specific ionization techniques (particularly ESI and MALDI) awarded with the Nobel Prize in 2002, ultimately rendered biological molecules amenable to MS and

made instruments to become widespread in research laboratories (Cox & Mann 2011).

In ESI, high voltage is applied to a flowing solution containing the analyte as it passes through a narrow needle. As the solution of charged molecules evaporates, the emitted droplets shrink into smaller droplets and shortly thereafter enter the gas phase (Thelen 2007). ESI produces multiple charge ions compared to singly charged ions as produced in MALDI. MS-MS spectra reveal fragmentation patterns. In MALDI, a laser is fired at a stainless-steel plate under vacuum. The analyte will be dried on the plate, co-crystallized with "matrix", which is a small organic molecule that absorbs the pulsed UV laser light. The laser light pulsed on the co-crystallized matrix-analyte layer resulting in the vaporization of matrix and the associated analyte. Spectra indicate masses of the peptide ions and protein identification is achieved by peptide mass fingerprinting. Although MALDI-MS has high sensitivity, quick and not expensive, some of the disadvantages of MALDI include low reproducibility and repeatability of single shot spectra.

Nevertheless, MS-based proteomics are costly and requires highly-skill person. At present, MS-based proteomics has become the method of preference to study differences in global protein compositions, for detection of post-translational modifications (PTMs) and protein-protein interactions (PPIs) as well as for protein biomarker discovery (Cox & Mann 2011).

1.5 Quantitative approaches in MS-based Proteomics

LC-MS/MS is one of the most powerful techniques in proteomics allowing high throughput identifications of proteins out of complex protein mixtures. MS has both qualitative and quantitative uses. Quantitative proteomic experiments usually aim at detecting differentially regulated proteins between different sample groups, e.g., tumour tissue samples versus healthy control samples. In MS approach, quantification of proteins is based on the peak height or area of the proteolytic peptide peaks in the mass spectrum and/or chromatogram. However, peak intensity differences of the same analyte within one LC-MS run often cannot be distinguished. One way to distinguish the same analyte from different sample sources within one LC-MS experiment is by using labelling technique. Coupled with labelling techniques (chemical and metabolic labelling), the relative amounts of

proteins can be measured at any given time and therefore provide more insight into the dynamics of biological system.

There are two types of quantification: relative quantification and absolute quantification. In relative quantification, samples are differentially labelled with stable isotopes, combined, and subjected to quantitative MS. Peak intensity ratio between unlabelled and labelled peptides is measured to learn relative change in protein abundance (Kito & Ito 2008). These approaches are often used in discovery proteomics, where many proteins are identified across a broad dynamic range using different-sized labels. In MS-based absolute quantification, a known amount of isotope-labelled authentic standard is spiked with the analyte before introducing the mixture into mass spectrometer. The absolute amount of the analyte is calculated from the ratio of ion intensity between the analyte and its standard (Kito & Ito 2008). Absolute quantitation is performed in targeted proteomic experiments and increases the sensitivity of detection for a limited number of target analytes.

LC-MS protein quantification strategies fall into two broad categories: label free and protein/peptide labelling (also known as differential mass tagging or isotopic labelling). Label-free quantification is the simplest and most economical approach. Label-free quantitation methods involve comparison of peptide ion currents between samples or the comparison of spectral counts for peptide ions from particular proteins across the samples. This approach is suitable to any kind of samples including samples that cannot be directly metabolically labelled (Cox et al. 2014). In contrast, labelling strategies allow the mixing of samples prior to LC-MS, thereby reducing error. Thus, multiple samples can be run simultaneously with the same peptides (or proteins) being identically separated and co-eluted into the mass spectrometer with ion intensities being directly compared in the same MS or MS/MS scans.

Many MS-based approaches that utilize stable isotopes have been explored and implemented for the routine quantitation of proteins (Figure 1.10) (Ong & Mann 2005). Till date, several approaches have been developed for comprehensively assessing proteomes. They include Isotope-coded affinity tags (ICAT), Isotope tags for relative and absolute quantification (iTRAQ), stable isotope dimethyl labelling (DiMe) and stable isotope labelling with amino acids in cell culture (SILAC)

(Bantscheff et al. 2007). Owing to the natural occurrence of certain stable heavy isotopes (e.g., ^{13}C, ^{15}N, ^{18}O, ^{2}H) each peptide/protein contains a certain proportion of these; the isotope pattern seen in the mass spectrometer thus reflects the natural abundances of these heavy isotopes within the peptide. Artificial incorporation of heavy isotopes produces a mass shift of the peptide's peaks in the mass spectrum. Thus, intensity ratios of peaks corresponding to different isotopic compositions of the same molecular species reflect quantitatively the isotopic abundance ratios. Due to the different mass introduced during labelling process, peptides derived from the various samples can be directly compared and this reflects the relative quantities of the particular peptide and proteins.

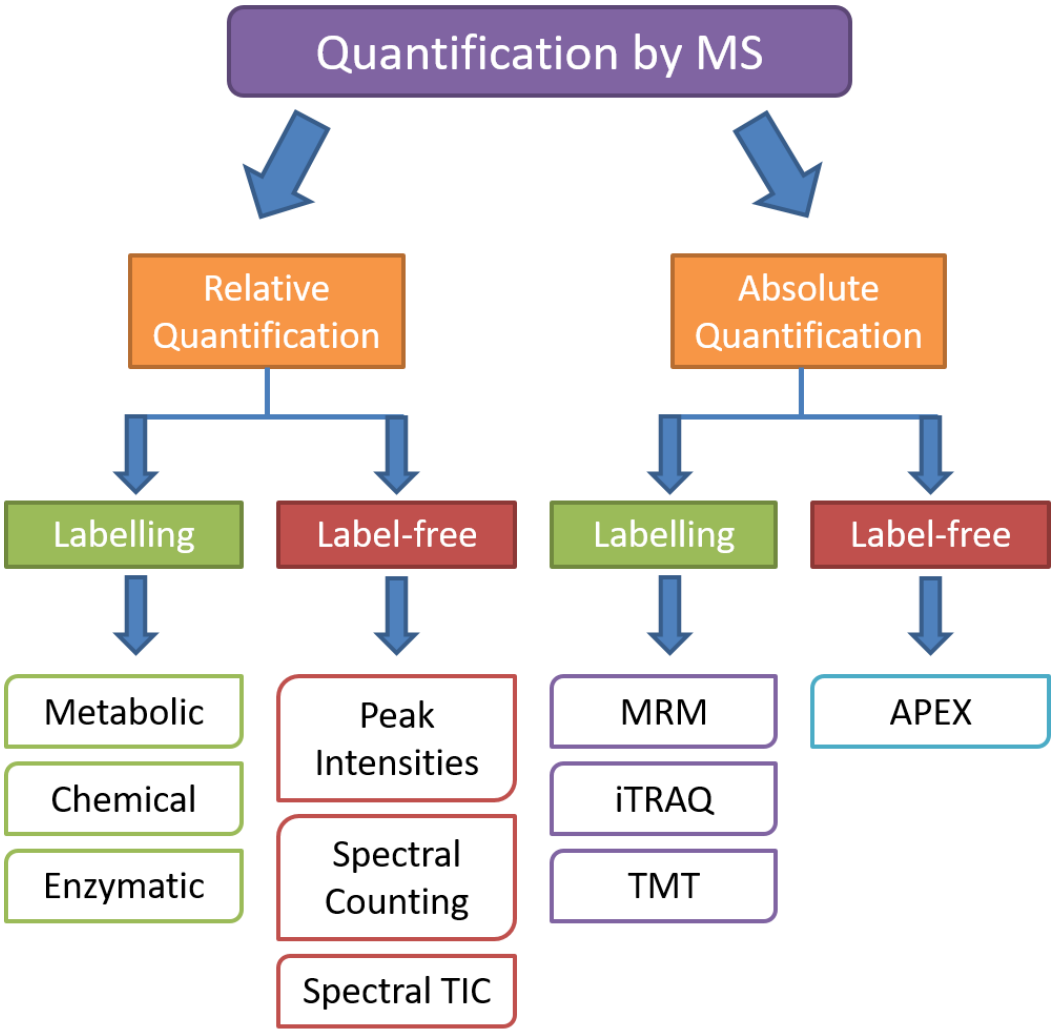

Figure 1.10: An overview of mass spectrometry-based quantitative proteomics.

Mass spectrometry (MS)-based quantification can be achieved either by relative or absolute quantification (AQUA). Both relative and AQUA can be further classified into labelled and label-free quantification, each of which can be performed by several approaches. Abbreviations: MRM - Multiple-reaction monitoring, TMT - Tandem mass tags, APEX - Absolute Protein Expression (Lill 2003; Mirza 2012).

Despite the phenomenal impact of MS and peptide separation techniques on proteomics, the identification and quantification of all the proteins in a biological system is still an unmet technical challenge (Figure 1.11). Several factors affect quantitative capabilities of MS including factors related to instrument as well as sample-related (Urban 2016). As the quality and reproducibility of sample preparation significantly impact results from MS instruments, proper sample preparation is critical for MS analysis.

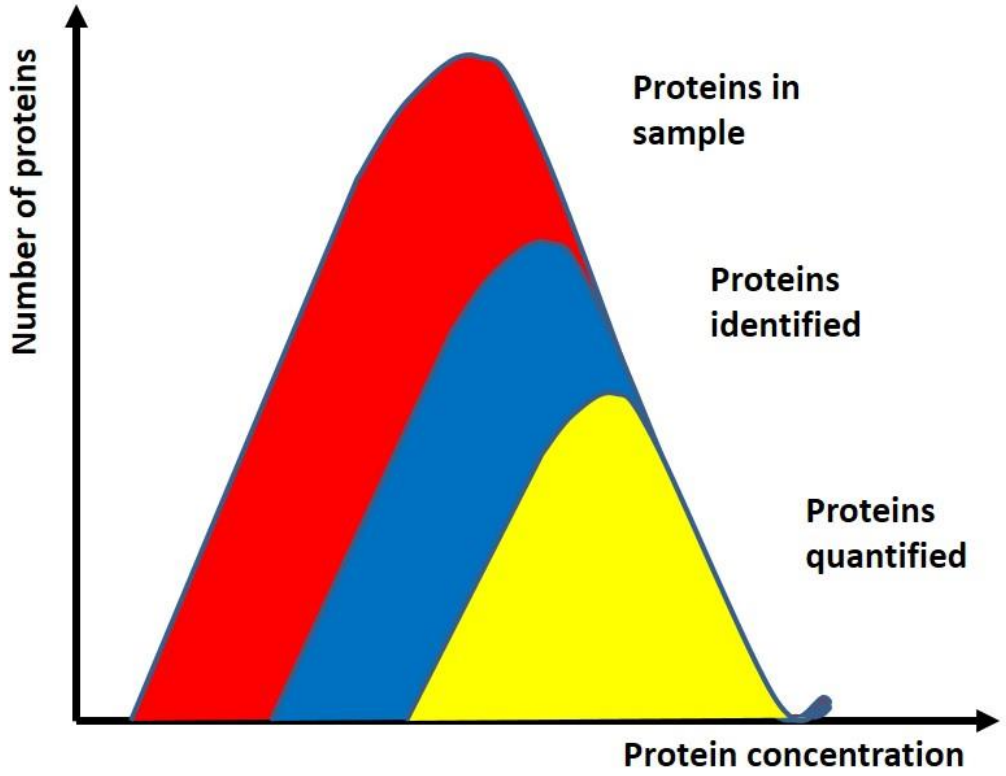

Figure 1.11: Quantification bias.

Schematic representation of the fraction of a proteome that can by identified or quantified by mass-spectrometry-based proteomics. Cellular proteins span a wide range of expression and current mass spectrometric technologies typically sample only a fraction of all the proteins present in a sample. Due to limited data quality, only a fraction of all identified proteins can also be reliably quantified (Bantscheff et al. 2007).

In the *Leishmania* research field, proteomic studies have provided valuable insights into the identification of molecules and pathways involved in the parasite (El Fakhry et al. 2002; Bente et al. 2003; Biyani & Madhubala 2012). However, only very few studies used proteomics to identify proteins expressed by the host cell in response to *Leishmania*. MS-based proteomic was used to identify markers of resistance and susceptibility in CBA mouse macrophages during *L. major* and *L. amazonensis* infection in vitro (Menezes et al. 2013). A total of 1352 proteins were found expressed in both infected and uninfected CBA macrophages. Of these, only 62 proteins were predominantly expressed in infected macrophages. Most of these proteins were involved in cell metabolism, cell signalling, cellular detoxification and cell immune response. Interesting, only 10 out of the 62 proteins were exclusively identified in *L. major* infection: ribosomal protein S13, glutamate receptor ionotropic, guanine nucleotide binding protein (G protein, γ8 subunit),

myosin, proteasome ß3 subunit, ras homolog gene family member B, cytochrome c-1, N-acetylglucosamine kinase, TNF receptor-associated protein 1 (TRAP1), and translin. By contrast, the unique protein found expressed in *L. amazonensis* infection was succinate dehydrogenase which is an enzyme involved in cell metabolism (Menezes et al. 2013).

Another study that evaluated the host cell response to *Leishmania* infection using proteomics was done by Singh et al. (2015). In this study, the authors employed iTRAQ and LC-MS/MS to compare the expression profiles of non-infected and *L. donovani*-infected THP-1 cells. They found that proteins involved in major metabolic pathways, including glycolysis and fatty acid oxidation, are highly expressed following *L. donovani* infection, suggesting a parasite-induced global reprogramming of cell metabolism. Furthermore, proteins involved in gene transcription, RNA splicing (heterogeneous nuclear ribonucleoproteins (hnRNPs)), histones, DNA repair and replication was also found to be increased in response to infection.

1.5.1 Stable isotope labelling technique

Stable isotope labelled analogues of substances have been used as standards for quantitative measurements with MS for a long time. Several methods have been developed to quantify proteins by MS. Stable isotope labelling is by far the most accurate type of quantitative proteomics (Ong & Mann 2005). As mentioned before, these approaches exploited the identical physicochemical properties of labelled and native peptides (e.g., in stable isotope labelling with amino acids in cell culture, SILAC) or of peptides labelled with physicochemically identical reagents (e.g., in iTRAQ) for relative comparison of intensities of mass-shifted peaks within the same mass spectrum (Kito & Ito 2008; Urban 2016). Stable isotopes can be introduced at the protein or peptide level either chemically (e.g. ICAT, iTRAQ, DiMe), enzymatically (^{18}O) or metabolically (SILAC) (Ong & Mann 2005).

The chemical labelling approaches make use of tags with the same (isobaric labelling) or different masses (isotopic labelling). Isobaric labelling (e.g., iTRAQ, TMT) consists of peptide tags which generate specific fragment ions by MS/MS whereby relative quantitation is performed by comparison of intensities of the

'reporter' fragments in the MS/MS spectra. In contrast, isotopic labelling methods (e.g., ICATs or proteolytic ^{18}O labelling) generate pairs (or more) of peptides with a mass difference introduced by the label. Chemical labelling is essentially based on similar mechanisms as metabolic labelling, except that the label is introduced into proteins or peptides by a chemical reaction, e.g., with sulfhydryl groups or amine groups, or through acetylation or esterification of amino acid residues (Chahrour et al. 2015). In general, the advantage of chemical labelling over metabolic labelling is the possibility to label a wide range of different sample types, since incorporation of the label is performed only after harvesting cells and subsequent purification of proteins.

When using any labelling approach for LC-MS, the labels are best introduced at the earliest point in the workflow to minimise differences introduced into the samples between LC-MS runs. This could be achieved by metabolic labelling during cell growth and division. Metabolic labelling involves the *in vivo* incorporation of stable isotopes into the protein sequence, supplied through the growth medium during protein biosynthesis. Historically, this been done with unstable isotopes of amino acids of which the radioactive decay could be measured in time. Figure 1.12 depicted some of the type of stable isotope labelling for quantitative proteomics. Of all these approaches, SILAC is the mode popular and has enormous potential (Ong & Mann 2005).

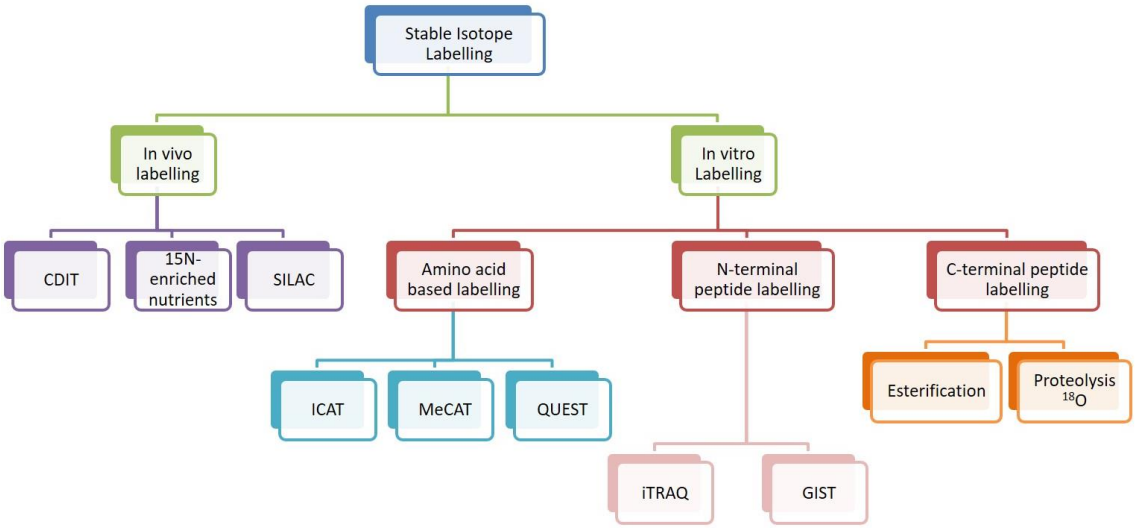

Figure 1.12: Stable-isotope tagging techniques on in vivo and in vitro labelling for differential proteomic.

Abbreviations: CDIT - Culture-derived isotope tags, SILAC - Stable isotope labelling with amino acids in cell culture, ICAT - Isotope-coded affinity tags, MeCAT - Metal-coded affinity tag, QUEST - Amidination-quantitation using enhanced signal tags, iTRAQ - Isotope tags for relative and absolute quantification, GIST - Global internal standard technology (Lill 2003; Chakraborty & Regnier 2002; Rauniyar & Yates 2014).

SILAC was originally developed in the lab of Matthias Mann in 2002. Typical SILAC experiment involves the growth of cells in culture medium supplemented with heavy stable isotope versions of essential amino acids (Ong & Mann 2006). SILAC replaces natural amino acids with a stable isotope-labelled version. For example, it might substitute C-13 for C-12 in particular amino acids, normally $^{13}C_6$-arginine and $^{13}C_6$-lysine. Other isotopes widely used include $^{15}N_2$, D_3-leucine, and D_{10}-leucine. The labelled amino acids are added to the growth medium, taken up by the cells during cell divisions, and subsequently incorporated into newly synthesized proteins. The two versions of the proteins (labelled and not labelled) can be processed together (mixed, digest) and differentiate on MS (Mann 2014). This implies that errors introduced by the aforementioned sample preparation steps are overcome. As trypsin predominantly cleaves proteins at the carboxyl side (or 'C-terminal side') of the amino acids lysine and arginine, all tryptic cleavage products of a protein (except for the very C-terminal peptide) carry at least one labelled amino acid resulting in a constant mass increment over the non-labelled counterpart. Depending on the label used in SILAC, light and heavy peptide peaks differ in mass from at least four up to ten Dalton. This allows researchers to look at the relative quantity of proteins in two different samples.

The application of SILAC is enormous. SILAC has been successfully used in studying differential protein expression to identify disease biomarkers. Gronborg (2005) have used this strategy to do differential secretome proteomics in case of pancreatic cancer. Similar approach has been undertaken by Hoedt et al. (2014) to do differential proteomics on proteins associated with antitumoral activities in breast cancer cells. SILAC has also been used for cells signalling dynamics studies. For example, Olsen et al. (2006) employed SILAC to study temporal dynamics of signalling pathways by exploiting phosphorylation based enrichment methods coupled to MS. SILAC was used in *Trypanosoma brucei* to compare the proteome of two different life cycle stages to better understand the sophisticated life cycle of this parasite (Butter et al. 2013). The application of SILAC in PTMs studies has been widely used (Pimienta et al. 2009; Zhang & Neubert 2009; Zanivan et al. 2013; Ibarrola et al. 2003). In the past few years, the applicability of SILAC has been revolutionized to label entire organisms such as mouse and bacteria (e.g., Zanivan et al. 2012; Soufi et al. 2010). Application of SILAC to whole organisms is valuable when *in vivo* experiments are performed that analyse whole tissues rather than cultured cells. As an alternative to the classical SILAC approach, heavy-labelled samples can be used as an internal standard for quantification. This approach is termed as Spike-in SILAC (Geiger et al. 2011). Use of SILAC-labelled cells as a 'spike-in' standard overcomes the labelling problem as the quantification of each of the tissue samples can be performed relative to a standard. Furthermore, when the samples of interest are diverse, several SILAC-labelled cell lines that together serve as the spike-in standard can be mixed, creating a super-set of SILAC labelled cells, termed 'super-SILAC' mix (Geiger et al. 2011; Geiger et al. 2012).

While SILAC is very powerful, however, since steady-state protein levels reflect the net outcome of antagonizing protein synthesis and protein degradation processes, the typical SILAC method was not useful to explicitly measure differences in protein translation. Hence, different variants of SILAC such as pulse-chase SILAC (pcSILAC) were invented that enable quantification of different aspects of proteome dynamics on a global scale (Bunner & Williamson 2009). In pcSILAC, differentially treated cell populations are simultaneously transferred to culture medium supplemented with different versions of stable-isotope labelled amino acids after certain time. After extraction, digestion, and identification of

proteins by tandem MS, the heavy/light ratios determined for peptides provide the level of label incorporation during the time frame considered. This is advantageous over the classic SILAC strategy as MS-based relative quantification is exclusively based on the newly synthesized protein amounts. This enables the specific detection of differences in protein translation resulting from the differential treatment. pcSILAC is powerful enough to be use on its own (Fierro-Monti et al. 2013; Bunner & Williamson 2009; Kristensen et al. 2012; Schmidt et al. 2010). However, some researchers employed pcSILAC along with pulsed AHA labelling to try to enrich the number of newly synthesized proteins they could capture (Debarba et al. 2015).

1.6 Protein dynamics

For any cell or tissue, protein balance reflects the net protein synthesis and protein degradation that differ significantly among tissues and organs and between cell compartments (Poortmans et al. 2012). Thus, protein turnover is the balance between protein synthesis and protein degradation (Figure 1.13). When older proteins are broken down in the body, they must be replaced. Whereas, protein synthesis occurs during the process of translation on ribosomes. Protein turnover has a substantial metabolic demand due to high energy needs for both biosynthesis and degradation of proteins. For example, in the young rat, the rate of synthesis of liver proteins is about 50% per day, and in the young mouse, it may be as high as 100% per day (Claydon & Beynon 2012). A primary function of this energetically expensive constant turnover is to alter the levels of specific proteins in response to physiological changes, hormonal status, or diet (Claydon & Beynon 2012). How rapid the proteins being replaced correspond to its turnover rate. Different types of proteins have different turnover rates (Pratt et al. 2002; Beynon 2005). For a protein with high turnover rates, the change in abundance can be rapid. Changes in the abundance of proteins in response to different stimuli or environment is control by the rate of turnover. A protein that has a high rate of turnover can be increased in abundance, or removed from the protein pool, very rapidly.

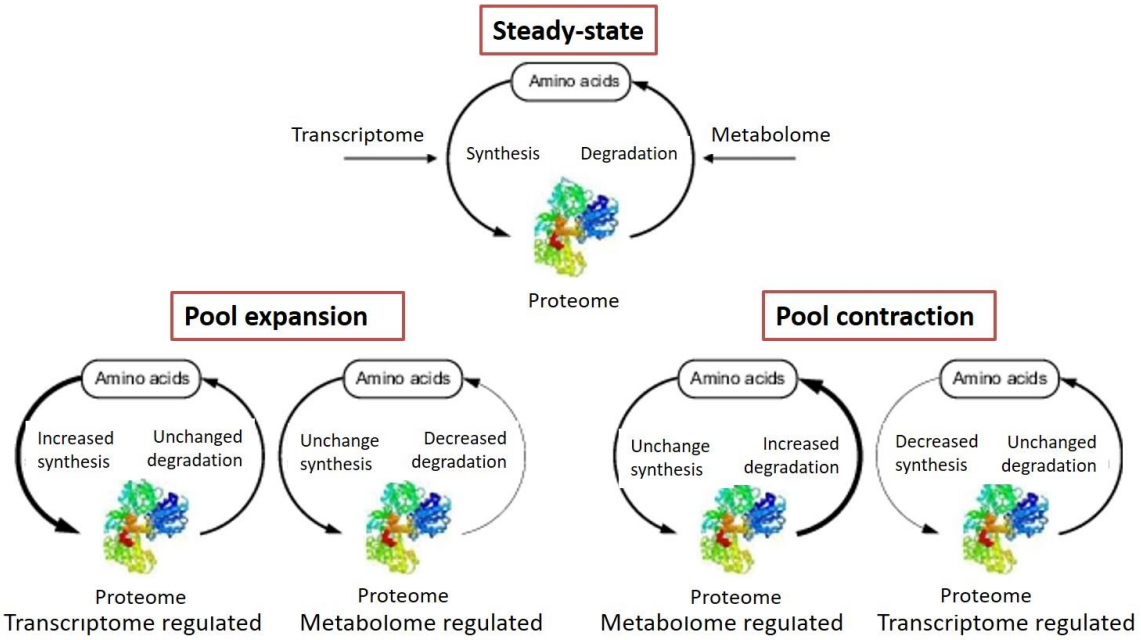

Figure 1.13: States of protein turnover.

During steady state, protein synthesis equal to degradation with neither the related transcriptome nor the metabolome affected. When protein pool expands, there is increased synthesis or decreased degradation with the related transcriptome or metabolome being modulated, respectively. During protein pool contraction, there is decreased synthesis (transcriptome changed) or increased degradation (metabolome changed). Adapted from (Chou et al. 2012).

In steady-state systems, where the concentration of all proteins is assumed to be constant, incorporation ratios allow to measure protein turnover and half-life. Our scientific heritage in the study of protein metabolism started with Black (1756) and Rutherford (1772) who observed the release of CO_2 and NH_3 in animal tissues. Since then, the metabolic changes produced by an intake of protein have been widely studied. Before the advent of proteomic MS, protein turnover was studied using radiolabel pulse-chase experiments that are similar to the modern MS-based turnover studies. MS-based pulse-chase labelling was later used for targeted analyses to measure the flux of ribosomal proteins in nucleoli (Lam et al. 2007; Bunner & Williamson 2009) and to determine turnover for bacteria (Pförtner et al. 2013; Schmidt et al. 2010), yeast (Christiano et al. 2014; Helbig et al. 2011a; Belle et al. 2006; Martin-Perez & Villén 2015), as well as several human cell lines (Kristensen et al. 2012; Eichelbaum & Krijgsveld 2014). Although most turnover studies relied on isotope labelling and MS, GFP-tagging and other classical biochemical approaches have also been used to determine turnover (Bojkowska et al. 2011; Lam et al. 2007). However, SILAC based strategies are nevertheless preferred for the large-scale analysis of protein levels and protein turnover.

To determine the rate of protein synthesis using mass spectrometry, the incorporation of a stable isotope-labelled tracer into newly synthesized proteins can be monitored. Similarly, to assess rates of degradation, loss of the tracer is followed (Claydon & Beynon 2012).

Direct measurement of protein synthesis can provide relevant information regarding the metabolic state of individual tissues. Protein turnover is an important aspect of the regulation of cellular processes for organisms when responding to developmental or environmental cues. Notably, the measurement of protein turnover in mammalian cells, in contrast to that of rapidly growing unicellular organismal cultures, is more complicated by the high degree of amino acid recycling. Therefore, the data analysis part will be very critical to translate them into meaningful inferences related to the biology of organisms.

1.7 Aims

There were two important motivations that drive this research. First, *Leishmania* cause life-threatening diseases that significantly affect global health and present an economic burden. New treatments against these infections are urgently needed since the current treatments are limited by emerging drug resistance, poor efficacy, and insufferable side effects. In addition, the development of effective vaccines has remained elusive. Second, the intricate relationship between *Leishmania* and host that could unravel potential candidates for chemotherapeutic development. As *Leishmania* have evolved unique strategies to successfully co-exist with their hosts, it is important to understand the responses of host towards this parasite. Therefore, the aims of this project are to:

1. Employ discovery and quantitative proteomics approaches on human host macrophages infected with parasite *L. mexicana*.

2. Establish the method of pulse-chase stable isotope labelling with amino acids in cell culture on human host macrophages infected with *L. mexicana* for 24 hours.

3. Extend the approach of pulse-chase stable isotope labelling with amino acids in cell culture to investigate the proteome dynamic in terms of synthesis, degradation, half-lives and turnover upon 24 and 48 hours infection.

As proteome dynamics is an essential aspect of biological processes, understanding the differences of protein expressions in *Leishmania*-infected macrophages could give insights into host metabolic processes, immune responses, and signalling pathways.

CHAPTER 2

2 Materials and Methods

2.1 Parasites and cell lines used

The parasite used in this work is *Leishmania mexicana* strain MNYC/BZ/62/M379. For infection experiments, THP-1 (ATCC TIB-202TM), which is a human monocytic cell line derived from an acute monocytic leukaemia patient was used.

2.2 Tissue culture

2.2.1 L. mexicana

Promastigotes of *L. mexicana* were cultivated in complete haemoflagellate minimal essential medium (HOMEM) (Life Technologies) supplemented with 10% (vol/vol) heat-inactivated foetal calf serum (HI-FCS) (Life Technologies) and 100 U/ml penicillin-streptomycin (Life Technologies) and incubated at 27°C. Promastigotes were transformed into axenic amastigotes by cultivation in Schneider's Drosophilla Medium (SDM) (Life Technologies) (pH 5.5) supplemented with 20% (vol/vol) HI-FCS (Life Technologies) and Hemin (2.5 mg/ ml in 50 mM NaOH) (Sigma Aldrich) and incubated at 32°C with 5% CO_2 (Bates et al., 1992). A typical starting density of 10^5 cells per ml was used and counted with Neubauer haemocytometer. Growth curve was made using Microsoft Excel and doubling time was calculated using the formula below:

$$T\ (d) = (t3 - t1) \times [\log(2) \div \log(Q3 \div Q1)]$$

T_3-t_1 = two time intervals in log phase,
Q_3 = No. of cells at T_3,
Q_1 = No. of cells at T_1,
Log (2) = 0.30103

2.2.2 THP-1

The THP-1 cell line, an acute monocytic leukemia-derived human cell line (ATCC TIB-202TM), was cultured at a density of 0.5-8 x 10^5 cells/ml in RPMI 1640 (Thermo

Scientific) supplemented with 10% HI-FCS, 2 mM L-glutamine, 10 mM HEPES and 100 U/ml penicillin-streptomycin. The number of cells per ml should not be higher than 10^6 and were seeded every 3 days. The cultures were maintained at 37°C in a humidified atmosphere (95% air/5% CO_2) and assessments with trypan blue exclusion were done regularly to check viability. To assess the cells viability, cells were mix with 0.4% trypan blue solution (in PBS) in 1:1 ratio and incubated at room temperature for several min. After that, cells were counted. The viable cells will exclude trypan blue whereas dead cells will be stained blue. Growth curve was made and doubling time was calculated using the formula below:

$$T\ (d) = (t3 - t1) \times [\log(2) \div \log(Q3 \div Q1)]$$

T_3-t_1 = two time intervals in log phase,
Q_3 = No. of cells at T_3,
Q_1 = No. of cells at T_1,
Log (2) = 0.30103

2.3 Sample collection for stabilates and storage

To make stabilates, cell cultures were centrifuged at 1000 x g for 10 min. Supernatant was discarded but a total of 5 ml of supernatant were left to resuspend. 500 µl of cultures were transferred into a cryovial and added with 500 µl of cryoprotectant (in 1:1 ratio). The tubes were vortex, wrapped in cotton wool and frozen at -80°C before storing them in the liquid nitrogen tank. A cryoprotectant for parasites consists of 70% of HI-FCS and 30% glycerol whereas for THP-1 it was consisted of 95% Hi-FCS and 5% DMSO (Sigma Aldrich) or glycerol. THP-1 was grown to a confluent of 10^6 cells/ml.

To recover stabilates, they were thawed by warming them using hand and then poured into new media and incubated.

2.4 Generation of proteomics samples

2.4.1 Proteomics samples from promastigotes and amastigotes

Cells were cultivated to a log phase ($5x10^8$ cells/ml) and harvested by centrifuge at 1000 x g for 10 min. Pellets were rinsed 3 times with PBS before lysis. Cells were then lysed in SDT lysis buffer (4% SDS, 100mM Tris/HCl pH 7.6, 0.1 M DTT,

and protease inhibitor cocktails (100 µg/ml of Leupeptin, 500 µg/ml of Pefabloc, 2 mM of 1,10-Phenanthroline, 5 µg/ml of Pepstatin A and 50 µg/ml of E-64) (Sigma Aldrich), pH 7.4). Protease inhibitors were prepared according to the manufacturer protocol (Sigma Aldrich). DTT and protease inhibitors were added fresh to the buffer. Apart from SDT lysis buffer, we also tried using a different lysis buffer (TTG lysis buffer) consisting of 500 mM Tris-HCl pH 8, 0.25% Triton X-100, 20% glycerol and protease inhibitors cocktail. The compositions in extraction buffers used in this work were described in Table 2.1. Samples were heated at 95°C for 5 min. Samples were briefly sonicated (3 sec, repeated 3x with 1 min interval in between) with Soniprep 150 (MSE) before doing acetone precipitation. (Probe sonication times were optimised in this work). Four volumes of 100% cold acetone was added to each sample and left overnight in -20°C. Samples were centrifuged at 14, 000 x g for 15 min and supernatants containing protein lysates were collected for proteomics analysis. Subsequently, the protein pellet was washed once with 80% cold acetone and dried briefly. Subsequently, the protein pellet was resuspended in lysis buffer containing the protease inhibitor cocktails. Lysates can be stored at -80°C.The protein concentration was assayed in triplicate for each sample by the Bradford assay (Biorad).

Table 2.1: Compositions of Extraction Buffers.

Two types of extraction buffers were used to extract proteins from *L. mexicana* and THP-1.

Extraction buffers	Chaotrope/detergent	Reductant
SDT	4% SDS, 100mM Tris/HCl pH 7.6	0.1 M DTT
TTG	500 mM Tris-HCl pH 8, 0.25% Triton X-100, 20% glycerol	0.1 M DTT

Following whole cell extraction, 50-100 µg of lysates were digested with sequencing grade trypsin (Promega) using the Filter Aided Sample Preparation 1 (FASP 1) method (as described in 2.4.1.2.). Peptides were then dried using the speed vacuum Concentrator 5301 (Eppendorf) for 30 min at room temperature. If there were salts present in the peptide mixtures, solid phase extraction clean-up (desalting) using SepPak C18 cartridges (Sigma Aldrich) should be carried out followed by drying the samples and resuspended in 10% (v/v) acetonitrile for LC-MS/ MS analysis.

2.4.1.1 Optimisation of protein extraction with different protease inhibitors

Cells harvested from growth medium were rinsed 3 times with PBS before lysis. Cells were then lysed in lysis buffer (as described in Table 2.1) supplemented with protease inhibitors. Different protease inhibitors (as listed below) were used and assessed to get better result. The optimisations were assessed by 1D-SDS-PAGE.

1. cOmplete™, Mini, EDTA-free protease inhibitors cocktail tablet (Roche, UK).

2. 100 µg/ml of Leupeptin, 500 µg/ml of Pefabloc, 1 mM of 1,10-Phenanthroline, 5 µg/ml of Pepstatin A (Sigma Aldrich) and 1 mM EDTA (Nugent et al. 2004).

3. 100 µg/ml of Leupeptin, 500 µg/ml of Pefabloc, 2 mM of 1,10-Phenanthroline, 5 µg/ml of Pepstatin A (Sigma Aldrich) and 1 mM EDTA.

4. 100 µg/ml of Leupeptin, 500 µg/ml of Pefabloc, 2 mM of 1,10-Phenanthroline, 5 µg/ml of Pepstatin A and 25 µg/ml of E-64 (Sigma Aldrich)

5. 100 µg/ml of Leupeptin, 500 µg/ml of Pefabloc, 2 mM of 1,10-Phenanthroline, 10 µg/ml of Pepstatin A and 50 µg/ml of E-64 (Sigma Aldrich)

As described in 2.4.1, samples were briefly sonicated before doing acetone precipitation. Subsequently, the protein pellet was resolubilized in lysis buffer containing the protease inhibitor cocktails. The protein concentration was assayed by the Bradford assay (Biorad).

2.4.1.2 SDS-PAGE

Mini-PROTEAN precast polyacrylamide gels TGX 4 – 20% (Biorad or Invitrogen) was used in this work. Before placing the gel cassettes into the electrode assembly, the comb and tape on the gel was removed. The assembly was done according to the manual by Biorad or Invitrogen. The electrophoresis module was placed into the tank and filled up with 1x running buffer (25 mM Tris, 192 mM glycine, 0.1% SDS). Samples with approximately 10 µg of concentration was diluted with 2x

sample buffer (62.5 mM Tris-HCl, pH 6.8, 2% SDS, 25% (v/v) glycerol, 0.01% bromophenol blue) with added reducing agent (5% ß-mercaptoethanol, freshly added). The diluted samples along with Protein Marker Broad range (New England Biolab) were vortex and heated at 95°C for 5 min before loading the samples into the gel well. The proteins were allowed to separate using the running conditions suggested by the manufacturer which is 1 hour at 200 V. After that, the gel was removed, fixed with fixing solution (40% methanol, 10% acetic acid) for 30 min, stained with stain solution (0.025% (w/v) Coomassie Blue G-250, 50% methanol, 10% acetic acid) for 2 – 4 hour and destained with destaining solution (40% methanol, 10% acetic acid) overnight. The gel was then documented using GelDoc instrument (BioRad).

2.4.1.3 Filter aided sample filtration (FASP)

Protein lysates were subjected to proteolysis by FASP 1 (Wisniewski et al. 2009) (Figure 3.11) to generate peptides for mass spectrometry. In this protocol, protein lysates were mix with 200 µl of 8M urea in 0.1 M Tris/HCl pH 8.5 (freshly prepared) and transfer into Microcon YM-30 (Millipore) filter unit for centrifugation at 14, 000 x g for 40 min. This process was repeated twice and the flow through was discarded, followed by the addition of 100 µl of 0.05 M iodoacetamide in urea buffer (freshly prepared). Samples were mix at 600 rpm in a thermomixer for 1 min before further incubation without mixing for 10 min. The filter units were centrifuged at 14, 000 x g for 30 min. 100 µl of urea buffer was added to the filter unit and centrifuge at 14, 000 x g for 15 min. This step was repeated twice. Then, a total of 100 µl of 0.05M ammonium bicarbonate was added to the filter units and centrifuge at 14, 000 x g for 10 min. Again, this step was repeated twice. 40 µl of ammonium bicarbonate with trypsin was added and mix at 600 rpm in thermomixer for 1 min before incubating the units in a wet chamber at 37°C for 4 - 18 h. After incubation, the filter units that contains the digested peptides were transferred to new collection tubes and spin at 14, 000 x g for 10 min. Finally, 40 µl of ammonium bicarbonate was added and centrifuge at 14, 000 x g for 10 min, acidify with Trifluoroacetic acid (TFA) and proceed with desalting process.

This original protocol was modified and optimised to suit our samples and to get better resolution on mass spectrometry. We have tried using both trypsin and endoproteinase Lys-C enzyme (Promega) for proteolysis. The ratios of

enzyme:protein were also optimised from 1:100 to 1:50. Furthermore, instead of using ammonium bicarbonate for completing elution, 10% acetonitrile was used to avoid performing desalting process.

2.4.1.4 Desalting

This protocol involves placing 3 ml EMPORE SPE Extraction disk cartridges (C18-SD) (Sigma Aldrich) in 15 ml tubes, adding 1 ml of methanol and centrifuge at 1,500 x g for 1 min, followed with addition of 0.5 ml of 70% of acetonitrile in water, 0.1% of TFA and centrifuge at 1,500 x g for 1 min. Next, 0.5 ml of 0.1% TFA in water was added and centrifuge at 1,500 x g for 1 min. The filtrates collected after FASP were added to the SPE cartridges and centrifuge at 150 x g for 3 min. After this, 0.5 ml of 0.1% TFA was added and centrifuge at 150 x g for 3 min. Lastly, the eluates were washed with 0.5 ml of 70% acetonitrile and centrifuge at 150 x g for 3 min in new tubes. Different volumes of conditioning or washing buffer may be applied based on the size of C18 cartridge used in the experiments. Samples were dried in a speedVac before subjecting to mass spectrometry.

2.4.2 Proteomics samples from THP-1

For THP-1 proteolysis, a modified FASP-1 adapted from Zanivan et al. (2012) was used. According to this protocol, 100 µg of lysate was mix with 200 µl of 8M Urea buffer on a Microcon 10 kDa filter followed by centrifugation at 14, 000 x g for 15 min. This step was repeated before adding 100 µl of alkylation buffer containing iodoacetamide, mix at 600 rpm in thermomixer and incubation for 20 min at room temperature in the dark. Filter units were then centrifuged at 14, 000 x g for 15 min. 100 µl of 8M Urea buffer was added, centrifuged at 14, 000 x g for 15 min and repeated 3 times. Flow-through was removed after this step. Next, 100 µl of 50 mM ammonium bicarbonate was added, centrifuged at 14, 000 x g for 15 min and repeated 3 times. However, after this step the flow-through was kept in the collection tubes to retain humidity. 40 µl of 50 mM ammonium bicarbonate with Trypsin (1 mg every 50 mg of lysate) was added, mix for 1 min at 600 rpm in thermo-mixer and incubate overnight at 37°C in a wet chamber. The digested peptides were collected by centrifugation at 14, 000 x g for 10 min in a new collection tubes. Finally, the elution was completed by adding 50 µl of 10%

acetonitrile and centrifuge before acidifying the peptides with 10% TFA to stop digestion and samples drying in Concentrator 5301.

2.5 Protein concentration determination

To determine protein concentration in samples, the Bio-Rad protein assay was used. It is based on the colour change of Coomassie brilliant blue G-250 dye in response to various concentrations of protein. The dye binds to primarily basic (especially arginine) and aromatic amino acid residues. This assay is useful for measuring proteins and polypeptides with molecular weights >3,000–5,000.

A diluted Protein Assay Dye-reagent (BioRad) was prepared by diluting it with water in 1:5 ratios. BSA standards with concentration of 0.1 mg/ml, 0.2 mg/ml, 0.3 mg/ml, 0.4 mg/ml and 0.5 mg/ml were prepared in order to make a standard curve. 10 µl of the same buffer as in the samples was used as blank whereas samples were diluted 10-fold and pipetted onto microplate well. A total of 200 µl of diluted dye-reagent were added to each well. The plate was incubated for 5 min on a shaker before reading the absorbance at 595 nm. The concentration of the samples was determined by plotting a standard curve on Excel.

2.6 Labelling for quantitation

In this work, stable isotope dimethyl labelling method was used to label different growth stages of *L. mexicana* which are promastigotes and amastigotes whereas SILAC was performed on THP-1. Label free quantitation was also done on promastigotes and amastigotes.

2.6.1 Stable Isotope Dimethyl labelling (DiMe)

DiMe was employed to promastigotes and axenic amastigotes following FASP and desalting (Figure 3.2). In this work, two different DiMe protocols were chosen to get better result. The first protocol (Hsu et al. 2003) started with the reconstitution of peptides in 90 µl of 100 mM sodium acetate to all samples. Next, 10 µl of 4% H_2 formaldehyde (Sigma Aldrich) was added to the 'light' samples (or in this case, promastigotes) while 10 µl of 4% D_2 formaldehyde (Sigma Aldrich) was added to the 'heavy' (or amastigotes) samples. After this, 10 µl of 1M sodium cyanoborohydride was added to all samples, vortex and incubated for 5 min. A

total of 10 µl of 4% ammonium hydroxide was added to all samples to stop the labelling reaction. Finally, both promastigotes and amastigotes samples were mix together and desalting protocol was repeated. The labelled peptides were then dried in Concentrator 5301.

Another protocol for DiMe chosen was adapted from Boersema et al. (2009). The dried peptides were reconstituted in 100 µl of 100 mM Triethyl Ammonium Bicarbonate (TeAB). 4ul of 4% CH_2O or CD_2O (Formaldehyde) were added to samples accordingly. Samples were mix and pulse centrifuged. Then, 4 µl of freshly prepared 0.6 M Sodium cyanoborohydride was added to the samples and mix in fume hood for 1 h at room temperature. Labelling reaction was quenched by adding 16 µl of 1% ammonia hydroxide. Samples were mix and pulsed centrifuged, followed by addition of 8 µl of 5% formic acid in water to acidify samples. This step needs to be done on ice. Finally, the differentially labelled samples were mix thoroughly and dried in Concentrator 5301 at room temperature and analysed on mass spectrometry.

2.6.2 SILAC

Before starting SILAC experiment, growth rate of THP-1 in dialyzed serum was tested to ensure it does not affect the cells. Specially formulated media for SILAC were from Dundee Cell Products Ltd (Dundee). RPMI 1640 medium with heavy L-[$^{13}C_6$] Arg and L-[$^{13}C_6$] Lys isotopes (R_6K_6) supplemented with 10% (v/v) dialyzed FCS (Invitrogen) and 100 U/ml penicillin-streptomycin was used alongside RPMI 1640 with naturally occurring isotopes (R_0K_0). 2 mM of L-glutamine (Life Technologies) and 25 mM of HEPES (Life Technologies) were also added to make it identical to the normal media used for culturing THP-1. They were grown for at least 8 cell doublings to ensure complete incorporation of the isotopes into proteins (Ong et al. 2002). In order to check the labelling efficiency, small amount of protein lysates from the THP-1 grown in SILAC medium were run on SDS PAGE and several random bands were excised from the gel. The gel pieces were then subjected to tryptic digestion and mass spectrometry. R script was used to generate a density plot of the heavy to light ratio of the peptides. The labelling efficiency was calculated using the formula:

$$\left\{1-(1\ \div ratio\frac{H}{L})\right\}\times 100\%$$

where 'ratio H/L' = median of the ratio H/L (log_2 normalized) of the quantified peptides in the 'peptide.txt' output file of MaxQuant, after removal of reverse and contaminant peptides.

2.6.2.1 Pulse-chase SILAC

The work-flow of a pcSILAC experiment is depicted in Figure 4.1. In the pcSILAC labelling scheme, unstimulated THP-1 was cultured in R_6K_6 (^{13}C-Arg, ^{13}C-Lys) medium until the level of heavy isotopes incorporation achieved more than 95%. There are four groups of samples in this experiment which are uninfected THP-1 (control), 24 hour infected THP-1, 48 hour uninfected THP-1 and 48 hour infected THP-1. The mock-infected cells were grown in parallel with the perturbed cells. Each group were performed in at least triplicate. NUNC flasks (Thermo Scientific) were used for large scale experiment. Cells were then allowed to undergo differentiation with PMA (explain in 2.8.1). The cells adhere to the surface of the flask when they have differentiated into macrophage-like cells. Medium was removed and rinsed with warm RPMI by gently rocking the flask. The heavy medium was exchanged to R_0K_0 (^{12}C-Arg, ^{12}C-Lys) medium before infection. To harvest the cells upon infection, cells were rinsed with warm media, cold PBS was pipetted into the flask and incubate at 4°C for 15 min. After that, the cells were scraped gently using a cell scraper and collected in a tube before centrifuge at 1000 x g for 10 min and proceeds to protein extraction (as described in 2.4.2), FASP and mass spectrometry.

2.6.3 Label free

Promastigotes and axenic amastigotes were cultivated in their normal respective media. Cells were harvested followed by protein extraction (as described in 2.4.1) and Bradford assay (as described in 2.5). Equal concentrations of lysates were digested individually by FASP (as described in 2.5.1.2) and subjected to individual LC-MS/MS analysis on MaxQuant. Quantification is based on the comparison of peak intensity of the same peptide or the spectral count of the same protein.

2.7 Infections

2.7.1 THP-1 differentiation

The desired amount of monocytes ($1.0x10^6$ cells/ml) was collected by centrifugation at 700 x g for 10 min and supernatant was discarded. Activation of monocytic THP-1 cell line was obtained by incubation with fresh RPMI 1640 medium containing phorbol 12-myristate 13-acetate (PMA) (Sigma Aldrich) dissolved in DMSO (Sigma Aldrich). Several methods have been tried and optimised in terms of the concentration of PMA and period of incubation:

1. PMA concentration of 300 ng/ml (0.5 µM), incubate for 24 h.

2. PMA concentration of 60 ng/ml (0.1 µM), incubate for 24 h.

3. PMA concentration of 60 ng/ml (0.1 µM), incubate for 48 h.

At this point, some of the cells were plated on LabTek 16-well chamber slides (Thermo Scientific) at a density of $0.15x10^6$ cells/ml to assess the rate of infection, while the remaining cells were left in the pre-treated flask (NUNC) for large scale experiment (Table 2.2). Cells were incubated at 37°C, 5% CO_2. Cell adhesion and spreading, which are the hallmarks of macrophages, were then examined under a microscope. The unattached cells were centrifuged, resuspended in 200 µl of media, and counted in order to determine the adherence percentages. Cells were rinsed with warm media to remove excess PMA and infection experiments were carried out.

Table 2.2: Number of cells needed to be plated in tissue culture dishes.
THP-1 cells were counted as depicted in this table for infection studies.

Plate	Volume per well	Cells/well
6 well	3 ml	$1 X 10^6$
24 well	1 ml	$0.4 X 10^6$
96 well	200 µl	$0.15 X 10^6$

2.7.2 Determination of infectivity rates

After PMA stimulation, cells were rinsed with warm RPMI 1640 media and changed with the same volume of fresh media. THP-1 cells were incubated with promastigotes, metaclyclic promastigotes and axenic amastigotes, respectively, at 32°C, 5% CO_2, after which they were washed to remove extracellular parasites. Different ratios of macrophage to parasites and several incubation times were used to get the best result:

Macrophage: parasites	Incubation period
1:5	6 hour
1:8	24 hour
1:10	48 hour

Cells on the chamber slides were stained with Giemsa and DAPI (Vector Laboratories, USA). The percentage of infected macrophages and number of amastigotes per infected macrophage were determined by examination of 100 macrophages per well under confocal microscope and fluorescence microscopy using a Zeiss Axioskop 2 mot plus (Zeiss Ltd, Cambridge, UK). To harvest the cells upon infection, cells were rinsed with warm media, cold PBS was pipetted into the flask and incubate at 4°C for 15 min. After that, the cells were scraped gently using a cell scraper and collected in a tube before centrifuge at 1000 x g for 10 min.

2.7.3 Isolation of metacyclic promastigotes

Metacyclic promastigotes were isolated by using a Ficoll PM 400 (Sigma Aldrich) based on density gradient (Serafim et al. 2012). 20% Ficoll PM 400 was prepared in Milli-Q water and heated at 60°C to dissolve it then filter sterilized. Approximately 10 ml of early stationary phase *L. mexicana* grown in HOMEM was centrifuged at 1000 x g for 10 min. Pellet was washed twice with PBS. 2 ml of 10% Ficoll solution in PBS was added slowly at the bottom of the tube and centrifuged at 107 x g with slow acceleration and deceleration for 15 min. Supernatant containing metacyclics was collected in a new tube and washed with PBS to

remove Ficoll. Morphology and motility of the metacyclics was assessed under microscope.

2.8 Microscopy

Cells on the chamber slides were stained with Giemsa and DAPI (Vector Laboratories, USA). The percentage of infected macrophages and number of amastigotes per infected macrophage were determined by examination of 100 macrophages per well under confocal microscope and fluorescence microscopy using a Zeiss Axioskop 2 mot plus (Zeiss Ltd, Cambridge, UK).

For differential counting of THP-1 cells nuclei and parasite nuclei, ImageJ (http://rsb.info.nih.gov/ij/download.html) was used. Cell counter was found in Analyse option in plugin of the Software. The image was initialized and cell counter type 1 was selected for THP-1 cell nuclei and cell counter type 2 was selected for parasite nuclei.

2.8.1 Giemsa staining

Cells were fixed with methanol for 1 min followed and air dried. This followed by staining the slide with 10% Giemsa (filtered) for 20 min and lastly, washed with water.

2.8.2 DAPI (4',6' diamino-2-phenylindole-2HCl) staining

Cells on the slide were washed once with 100 µl of filtered PBS. Then, it was fixed with 2% formaldehyde in PBS for 10 to 20 min at 4°C. 10 µl of 1% Triton X-100 in PBS was added to the slide to permeabilize the cells. Cells were washed twice with PBS and air dried. A few drops of Vectashield-DAPI were laid on top of the cells and cover with coverslip before sealing it with nail varnish on the edge to prevent from drying.

2.9 Mass spectrometry

Mass spectrometry was conducted by MS Technologist, Dr Stefan Weidt, Dr Cristina Naula and Suzanne Edie from Glasgow Polyomics Facility.

Peptides were routinely run through Amazon Speed ion trap MS/MS (Bruker Daltonics) for quality control before using the higher resolution mass spectrometer. For this step, peptides were solubilized in 0.5 % formic acid and fractionated on a nanoflow uHPLC system (Thermo RSLCnano) before online analysis by electrospray ionisation (ESI) mass spectrometry on an Amazon Speed ion trap MS/MS. Peptide separation was performed on a Pepmap C18 reversed phase column (LC Packings), using a 5 - 85% (v/v) acetonitrile gradient (in 0.5% formic acid) run over 45 min at a flow rate of 0.2 µl/min. Mass spectrometric (MS) analysis was performed using a continuous duty cycle of survey MS scan followed by up to ten MS/MS analyses of the most abundant peptides, choosing the most intense multiply charged ions with dynamic exclusion for 120s.

2.9.1 High-Resolution 1D-LC-MS/MS and 2D-LC-MS/MS

For 1D-LC-MS/MS, peptide samples were analysed by LC-MS using an Orbitrap Elite MS (Thermo Scientific), using the same gradient as previously stated. The Orbitrap Elite acquires a continuous duty cycle of a high-resolution precursor scan at 60,000 RP (at 400 m/z), while simultaneously acquiring the top 20 precursors subjected to CID fragmentation in the linear ion trap. Singly charged ions are excluded from selection, while selected precursors are added to a dynamic exclusion list for 120s.

Peptides were solubilized in 2% acetonitrile with 0.1% TFA and fractionated on a nanoflow uHPLC system (Thermo Scientific RSLCnano) before online analysis by electrospray ionisation (ESI) mass spectrometry on an Amazon Speed ion trap MS/MS for quality control. Peptide separations were performed on a Pepmap C18 reversed phase column (Thermo Scientific). Peptides are desalted and concentrated for 4 min on trap column followed by an acetonitrile gradient (in 0.1% v/v formic acid) (3.2 - 32% v/v 4 - 27 min, 32% to 80% v/v 27 - 36 min, held at 80% v/v 36- 41 min and re-equilibrium at 3.2%) for a total time of 45 min. A fixed solvent flow rate of 0.3 µl/min is used for the analytical column. The trap column solvent flows at a fixed at 25 µl/min using 2% acetonitrile with 0.1% (v/v) TFA. Mass spectrometric (MS) analysis were performed using a continuous duty cycle of survey MS scan followed by up to ten MS/MS analyses of the most abundant peptides, choosing the most intense multiply charged ions with dynamic exclusion for 120s.

For 2D-LC-MS/MS, the desired peptide digest was loaded onto the cation exchange (SCX) column and the column was eluted using as series of salt steps ranging from 0 to 2000 mM natrium chloride, pH 3.5 containing 10% acetonitrile (ACN).

The effluent of the SCX column in each case was directed onto the reversed phase (RP) column through the automated valve. The valve was programmed to direct liquid flow from the pumps through a flow split (1:1000) to the RP column. Following a 2-min pulse at the desired salt concentration at flow rate of approximately 600 nL/min, the SCX column was washed for 10 min with buffer. 0.02% TFA was added to load the eluted sample onto the RP column in an automatic fashion. The RP column was eluted with a linear acetonitrile gradient elution from buffer A (H_2O + 0.02% TFA) to 50% buffer A + 50% buffer B (ACN+ 0.02% TFA) in 100 min using the Voyager pumps at a flow rate of approximately 400 nL/min. Nanospray ionization was accomplished through an 8-µm fused silica tip with a spray voltage of 1.65 kV and heated capillary temperature of 230 °C. Data dependent MS scans were performed and the four strongest ions in each MS spectrum (with threshold intensity set at 1×10^5) were subjected to MS/MS analysis with collision energy set at 35%.

2.10 Bioinformatics analysis

This work has generated proteomics data from DiMe-labelled-*L. mexicana* promastigotes and axenic amastigotes, label-free *L. mexicana* promastigotes and axenic amastigotes and THP-1-pcSILAC experiments. Proteomics data from the parasite were mainly analysed on Mascot Distiller whereas data from THP-1 were analysed on different tools including MaxQuant and Perseus.

2.10.1 Mascot Distiller and Daemon

The yep/buf files generated by the Amazon ion Speed and/or Xcalibur files generated by Orbitrap Velos were processed with Mascot Distiller, Data Analysis software (Bruker) and the automated Matrix Science Mascot Daemon server (v2.4.1). The default processing options were applied for MS data processing according to the type of instrument. Protein identifications were assigned using the Mascot search engine to interrogate protein sequences in the NCBI Genebank database (taxanomy: *Leishmania*/*Homo sapiens*), allowing a mass tolerance of 10

ppm for both MS and MS/MS analyses. Peptide tolerance was set to 0.3 Da and peptide charge was 2+, 3+, 4+. Search settings allowed two missed cleavages with trypsin, one fixed modifications (carbamidomethylation of cysteine) and one variable modification (oxidation of methionine). A quantification setting was set as Dimethylation for DiMe-labelled peptides and 13C-K(6) + 13C-R(6) for SILAC-labelled peptides with a coefficient of 1.0. Signal to noise ratio (S/N) was set using the default setting which is 2. Protein significance was calculated by Mascot Distiller via the following comparison equation:

$$|x - \mu| \leq t * \frac{s}{\sqrt{N}}$$

where N = number of peptide ratios,
s = standard deviation,
x = mean of the peptide ratios (s and x calculated in log space),
μ = ratio with a true value of 0 in log space,
t = Student's t test for N-1 degrees of freedom and a two-sided confidence level of 95%.
Significantly modulated are the proteins that are different from unit which is 1.

Statistical confidence limits of 95% were applied for protein identification. Where matches were obtained to predicted proteins annotated as hypothetical and unspecified product, the protein ID was manually validated on http://tritrypdb.org/tritrypdb/ (for *Leishmania*) and http://www.uniprot.org (for human THP-1). The database was also used to get information on gene ontology and metabolic pathway by uploading the gene ID into the database.

To predict potentially secreted proteins, sequences were analysed with SignalP 4.1 Server (http://www.cbs.dtu.dk/services/SignalP/) with default parameters. Transmembrane domains were predicted with TMHMM 2.0 (http://www.cbs.dtu.dk/services/TMHMM/).

2.10.2 MaxQuant and Perseus

MaxQuant and Perseus are available to download on http://www.coxdocs.org/doku.php?id=maxquant:start and http://www.coxdocs.org/doku.php?id=perseus:start, respectively. To run MaxQuant, several programs were installed on the local computer including .NET

framework 4.5 as well as the MSFileReader for Thermo data. Local storage was used for all raw files belonging to a project, and about half of this size were needed for intermediate results. The raw files were stored in the same directory to avoid crashes.

The raw files generated by the LTQ-Orbitrap were processed and analysed using MaxQuant (Cox et al. 2009; Tyanova et al. 2016), Version 1.5.2.8 and 1.5.5.1 using the UniProt (www.uniprot.org/) protein FASTA database (2015, April version; 2016, Aug version), including commonly observed contaminants. The following settings were applied: cysteine carbamidomethylation was selected as fixed modification; methionine oxidation and protein N-terminal acetylation were set as variable modification; and enzyme specificity was set to trypsin. Up to two missed cleavages of trypsin were allowed. Precursor ion mass tolerances were 7 ppm, and fragment ion mass tolerance was 10 ppm for MS/MS spectra. If the identified peptide sequences from one protein were equal to or contained within another protein's peptide set, then the proteins were grouped together and reported as one protein group. Protein and peptide identifications were filtered at 1% false discovery rate (FDR) established by MaxQuant against a database of reversed sequences and a minimum length of seven amino acids was used for peptides identification. MaxQuant used a posterior error probability (PEP) based on the peptide P-score distribution to set the cutoff of FDR (Cox & Mann 2008). A threshold PEP of 1 was applied. Quantification was performed using median normalized log2 L/H ratio. Protein ratio was calculated on unique and razor peptides (Occam's razor principle). Minimum ratio count for SILAC quantification was set to two. Computation times vary with sample complexity, richness of spectra and LC gradient length. Typical values for 72 LC/MS runs are 10 – 72 h.

The MaxQuant output was further analysed for quantification on Perseus Version 1.5.1.6 by first uploading the 'ProteinGroups.txt' file generated by MaxQuant. Common contaminants, reversed sequences and sequence only identified by site were omitted. All data was inverted to L/H ratio, $\log_2$ transformed and median normalized before further analysed.

2.10.3 Functional analyses

Several tools were used for further functional analysis including Gene Ontology Enrichment, subcellular localisation, functional domains and motifs, pathways, and protein-protein interactions. Among the tools used in this work are The Database for Annotation, Visualization and Integrated Discovery, DAVID (https://david.ncifcrf.gov) (Huang et al. 2009), Kyoto Encyclopaedia of Genes and Genomes, KEGG (http://www.genome.jp/kegg/), and functional protein association networks, STRING10 (http://string-db.org).

2.10.4 Identification of newly synthesized proteins and protein synthesis rate calculation

Evidence tab delimited (txt) file generated as output from MaxQuant were used to identify newly synthesized proteins following THP-1 infection based on the L intensity of the proteins. The L and H spectra were validated using SeeMS and Skyline. The criteria for assessing relative isotope abundance (RIA) are: 1) RIA was calculated at each time point and in triplicate, 2) Minimum peptide is 7, 3) Minimum individual peptide is 2.

A script written in R (https://www.r-project.org) was used to determine rate of protein synthesis. Non-normalized data of control_24h, 24hpi, control_48h and 48hpi THP-1 (pcSILAC data) was used for this purpose to avoid introducing a transformative distortion. Calculation of protein synthesis rates were based on abundance ratios of new (partly labelled) to old proteins (fully labelled). RIA was calculated using formula (Pratt et al. 2002):

$$RIA\ (syn) = \frac{newProtein}{oldProtein + newProtein} = \frac{L}{H + L}$$

2.10.5 Skyline

Raw data were imported into Skyline (https://skyline.ms/project/home/begin.view?). The monoisotopic peak of each precursor ion extracted using the software's defined settings for MS1 quantification, peak picking manually checked and correlated in terms of

retention time with the identifications from Andromeda generated from MaxQuant (Schilling et al. 2012).

2.10.6 Protein degradation rate and half-life calculation

A script written in R (https://www.r-project.org) was used to determine rate of protein degradation. Non-normalized data of control_24h, 24hpi, control_48h and 48hpi THP-1 (pcSILAC data) was used for this purpose. Relative isotope abundance (RIA) was calculated using formula (Pratt et al. 2002):

$$RIA\ (\mathrm{deg}) = \frac{oldProtein}{oldProtein + newProtein} = \frac{H}{H + L}$$

The RIA data were fitted to a single exponential decay curve. The degradation rate constants (k_{deg}) was calculated using formula:

$$RIA\ = \ln(kdeg) \times t$$

$$\ln(kdeg) = \frac{RIA}{t}$$

True degradation rate constant was calculated by subtracting dilution rate (D) (0.006 h^{-1}) derived from doubling time.

Half-life of a proteins ($t_{½}$) (in h) were calculated by using formula (Helbig et al. 2011):

$$t\ 1/2 = \frac{\ln 2}{kdeg}$$

$$= \frac{0.693}{kdeg}$$

2.11 Protein Validation

Two significant proteins found from pcSILAC data were validated via non-quantitative Western blot.

2.11.1 Immunoblot Analysis

Immunoblot analyses were performed using standard SDS-PAGE chemiluminescent procedures. Protein lysates from uninfected THP-1, 24 h infected THP-1 and 48 h infected THP-1 was separated on a RunBlue pre-cast polyacrylamide gel 4-20% (Expedeon, UK). 10 µg of protein lysates were solubilized in 4 x sample loading buffer (Expedeon) and boiled at 95°C for 10 min, together with RunBlue prestained tri-color marker (5 – 180 kDa) (Expedeon). Gels were subsequently transferred onto PVDF membranes (Thermo Fisher) in XCell II Blot Module (Invitrogen) filled with transfer buffer (Tris-SDS-Glycine and 20% methanol) at 30 V for 1.5 h. Following transfer, membranes were stained with Ponceau S reagent for 5 min and then were destained with water. After that, the membranes were blocked overnight in 5% (w/v) milk in PBS-T (0.5% (v/v) Tween 20 in PBS) at 4°C. The membranes were washed with PBS-T for 5 min and repeated 3 times before incubation with primary antibody diluted in 5% (w/v) milk in PBS-T for 1 h at room temperature. Rabbit polyclonal anti-gelsolin (1 µg/ml or 500x dilutions) (Abcam, UK) and rabbit polyclonal anti-galectin-9 (500x dilutions) (Thermo Fisher) were used as primary antibodies in this work. Anti-alpha tubulin (rabbit) (Cell Signaling Technology) was used as loading control. Blots were washed with PBS-T for 5 min, repeated 3 times and incubated for 45 min with horseradish peroxidase-conjugated goat anti-rabbit IgG (Thermo Fisher) diluted 1:1000 in blocking buffer. The membranes were washed as above, incubated with ECL Pico chemiluminescent substrate (Expedeon) for 1 min and exposed to X-ray film.

CHAPTER 3

3 A quantitative proteomic approach to identify developmentally regulated proteins in *L. mexicana*

3.1 Introduction

In order to continue through their life cycle, *Leishmania* oscillate between the motile, extracellular promastigote that lives in sand fly vector and non-flagellated, intracellular amastigote stages that proliferate inside the acidified phagolysosomes of host macrophages. Following transmission, promastigotes gain entry into mammalian cells when they are rapidly taken up by phagocytes where they transformed into amastigotes. This change in environment brings about dramatic morphological and molecular changes to the parasites. Both environments have different pH and temperature (Zilberstein & Shapira 1994) as well as different nutrient availability (Burchmore & Barrett 2001). In addition, they are being confronted by different types of hostile host defence mechanisms including cytotoxic activities. *Leishmania* respond to the challenging changes they encounter by differentiating into highly adapted forms that enable them to be transmitted, survive and proliferate. It has been reported by Bente et al. (2003) that *Leishmania* encounter three environmental shifts as they move between their hosts: they switch (i) from a poikilothermic to a homeothermic host; (ii) from an insect to a mammal; and (iii) from an extracellular to an intracellular lifestyle. These transformations are vital for the parasite's transmission. Yet, the molecular basis underlying this transformation is poorly understood. The complex differentiation process involves different expression and regulation of numerous sets of proteins (Rochette et al. 2008). Proteins differentially expressed in both stages of the parasites are thought to be important to give insight on intracellular survival and subsequently pathogenicity.

Although both promastigote and amastigote form can initiate infections, the infections are maintained by amastigotes. They reside within the acid

phagolysomal vacuole of the host macrophages and can persist in cells for many days. This is when clinical symptoms start to develop.

Several reports have suggested that stage-specific gene expression is associated with and required for transformation, as well as for intracellular survival. For example, several proteins or protein families were reported to be promastigote- or amastigote-specific in *L. donovani* including LdARL-3A and GP63 which are promastigote-specific (Bente et al. 2003). LdARL-3A is a G-protein involved in flagellum biosynthesis (Cuvillier et al. 2000) while GP63 is a virulence factor that plays a major role in protection against complement-mediated lysis and is needed by promastigotes prior to entry into the mammalian host cell (Joshi et al. 1998). Stage specific differences in protein abundance were also detected in *L. panamensis*, where 75 proteins were found upregulated in axenic amastigotes and 45 were solely detected in promastigotes (Walker et al. 2006). 2-DE and gel-free analysis of *L. mexicana* promastigotes and lesion-derived amastigotes revealed a set of proteins identified solely in amastigotes including HSPs, ß-tubulin, and the EF-1α subunit (Paape et al. 2008; Zilberstein & Shapira 1994; Paape et al. 2010; Brotherton et al. 2010).

In contrast to higher eukaryotes, trypanosomatid genomes are constitutively expressed and they regulate their protein expression and abundance post-transcriptionally (Papadopoulou et al. 2003). Therefore, proteomics is the method of choice to investigate gene expression patterns in different stages of *Leishmania*.

L. mexicana is an excellent model of *Leishmania* species. The genome has been sequenced and annotated (*Leishmania mexicana* Genome Project, http://www.sanger.ac.uk/sequencing/Leishmania/mexicana/). Both major life cycle stages, the promastigote and the amastigote, can be cultivated and differentiated *in vitro* (Bates 1994; Antoine et al. 2004; Gossage et al. 2010). *In vitro* induced axenic amastigotes closely resemble animal-derived amastigotes (Bates 1993; Saar et al. 1998; Gupta et al. 2001; Burchmore & Landfear 1998).

3.1.1 Promastigotes

The promastigote form occurs in the alimentary tract of the insect vector. They are very well adapted to survive and multiply within the intestine of the sand fly before being transmitted to the mammalian host. Promastigotes are able to break down the peritrophic matrix during blood feeding and protect themselves from proteolytic enzymes secreted by the midgut of the sand fly. Quantitative transcriptomic analysis of midgut tissues from the sand fly *P. perniciosus,* infected with *L. infantum* showed a slight decrease in the abundance of the tryptic protease that is induced by blood feeding, suggesting the parasites were able to modulate the expression of the vector's proteases (Dostálová et al. 2011). Another factor that aids in promastigote transmission is the glycoconjugate Lipophosphoglycan (LPG). LPG is a surface coat composed of glycosylphosphatidylinositol (GPI)-anchored phosphoglycosylated glycans that are found on parasite's membrane. They form a highly hydrophobic barrier that acts to protect against host immune responses (Forestier et al. 2014). LPG helps parasites to bind to the midgut epithelium of the sand fly. This attachment prevents the parasites from being excreted. Furthermore, this binding is stage-dependent as it is only a property of nectomonad and leptomonad forms (Dostálová et al. 2011). The LPG-enriched glycocalyx of *Leishmania* also constitutes the primary encounter when parasites inoculated into mammalian host by the sand fly vector (Forestier et al. 2014). Furthermore, promastigotes secrete chitinase that can damage the stomodaeal valve which controls the junction between midgut and foregut, allowing them to pass through this barrier (Rogers et al. 2008). Promastigotes proliferate optimally at ambient temperatures (around 25°C) in a mildly basic environment (pH > 8), reflecting conditions within the sand fly gut.

Several proteomic studies have been undertaken to elucidate the proteins and metabolic pathways involved when procyclic promastigotes differentiate to metacyclic promastigotes. In *L. mexicana*, cysteine proteinase b and trypanoredoxin were upregulated during the differentiation (Nugent et al. 2004). During metacyclogenesis, expression of promastigote virulence factors increases significantly. These include major surface protease GP63 and gp46 (also called promastigote surface antigen protein 2) (Yao et al. 2010). In addition, metabolic enzymes were reported to be decreased in *L. chagasi* (Yao et al. 2010).

3.1.2 Amastigotes

Amastigotes are the intracellular lifecycle stage of *Leishmania* in a mammalian host. They are normally found in mononuclear phagocytes. All *Leishmania* have an amastigote stage of their lifecycle. Amastigotes are oval and smaller than promastigotes, with 3-6 μm in length and 1–3 μm in breadth. The flagellum is very short, so it does not emerge from the flagellar pocket and does not confer motility on the parasite. The kinetoplast and basal body situated towards the anterior end.

During the differentiation from metacyclic promastigotes to amastigotes, a series of changes on the morphology, cell surface properties and metabolism occur. The promastigote LPG coat is lost during the transformation while amastin surface proteins are upregulated (Wu et al. 2000). Importantly, a change in metabolism allows amastigotes to increase ß-oxidation of fatty acids and catabolism of amino acids to replace glucose and proline as their main carbon sources (Opperdoes & Coombs 2007; McConville & Naderer 2011). In *L. donovani, L. mexicana* and *L. infantum*, differentiation from promastigotes to amastigotes were accompanied by reduced glycolytic pathway, increased fatty acid oxidation, increased gluconeogenesis, and increased mitochondrial respiration (Bente et al. 2003; Nugent et al. 2004; Rosenzweig et al. 2008; Brotherton et al. 2010; Paape et al. 2010). Several virulence factors have been reported to be expressed in amastigote forms including superoxide dismutase (SOD) (Paramchuk et al. 1997), the major surface protease GP63 (leishmanolysin) (Isnard et al. 2012), cysteine peptidases (Mottram et al. 2004), the iron transporter LIT1 (Huynh et al. 2006), and A2 proteins (Zhang & Matlashewski 2001). Early research on *L. mexicana* found that cysteine protease activity was considerably greater in the amastigote form than the promastigote forms, suggesting that the cysteine proteases might be important for survival of the parasite in the mammalian host (North & Coombs 1982).

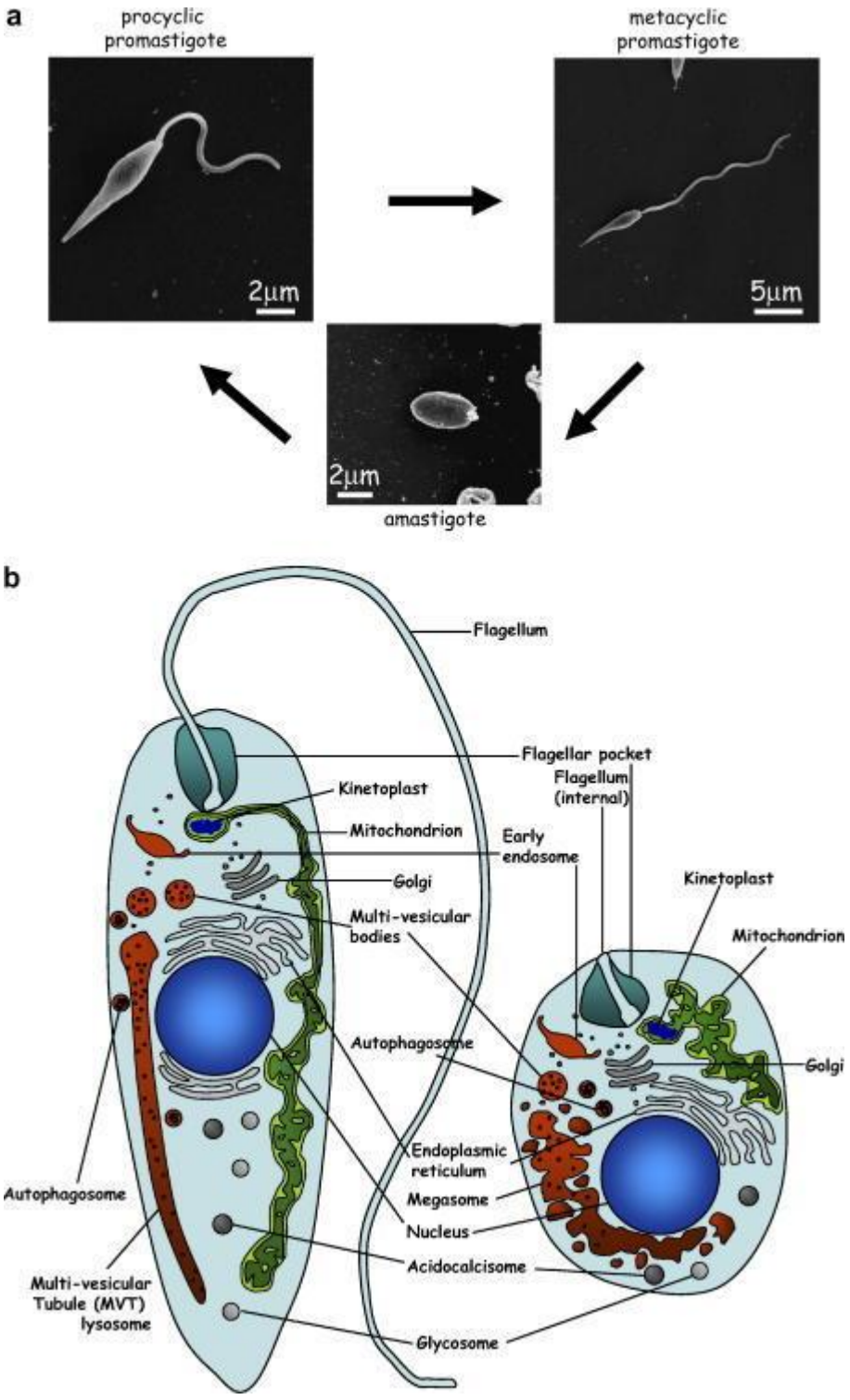

Figure 3.1: Changes in cell shape during the *Leishmania* life-cycle.

(a) Scanning electron microscope images of the main *Leishmania major* life-cycle stages, the procyclic and metacyclic promastigotes were grown in culture, the amastigote was isolated from an infected mouse macrophage. (b) Schematic representation of the main intracellular organelles from *Leishmania* promastigote (left) or amastigote (right) forms. The flagellar pocket marks the anterior end of the cell (adapted from Besteiro et al. 2007).

3.1.3 Host-free *in vitro* differentiation (axenic system)

To study the biology of amastigotes, parasites have been isolated from infected animals or in vitro infected macrophages or alternatively, generated from promastigotes in host-free medium. These cells are called “axenic amastigote”. Amastigotes that are differentiated from promastigotes *in vitro* are an attractive model for biochemical analyses, including proteomics, because axenic culture avoids the inclusion of heterologous biological material. Although axenic amastigotes generated *in vitro* may not precisely represent the phenotype of intracellular amastigotes, it is not possible to obtain these cells without disrupting the niche to which they are adapted and triggering a phenotypic response. Furthermore, for similar reasons, analysis of promastigotes is focused on a similar axenic culture system. *In vitro* cultivation offers an indefinite source of viable, homogenous amastigotes and promastigotes that can be compared by quantitative proteomic approaches.

Several laboratories have succeeded in axenic culture of *Leishmania* amastigotes by combining both acidic pH and elevated temperature. Axenic amastigotes have been considered to mimic animal-derived amastigotes based on their morphology, molecular and biochemical characteristics (Bates et al. 1992; Pral et al. 1993; Saar et al. 1998; Gupta et al. 2001; Burchmore & Landfear 1998). Transmission electron microscopy of axenic amastigotes showed that the cells have amastigotes-specific features including the shape, flagellum and megasomes (Bates et al. 1992; Pral et al. 1993). Although they are grown without a host, they are virulent as they can infect hamsters and macrophage cell lines (Jain et al. 2012; Pescher et al. 2011). However, a study from Pescher et al. (2011) argues that the virulence of *L. infantum* axenic amastigotes were attenuated compared to splenic amastigotes. Thus, the advantages of using axenic amastigotes are the ability to get higher number of cells as opposed from purification of amastigotes from macrophages and the cells are free from contaminating host cell material. Nevertheless, the extent to which axenically-generated *Leishmania* promastigotes or amastigotes recapitulate the phenotype of these stages in their natural niche.

In this work, we employed differential peptide labelling, together with mass spectrometry, to compare the proteomes of axenically-maintained promastigotes and amastigotes of *L. mexicana*. This study will be extremely useful for additional

biological, biochemical and molecular studies of the developmental stages in *Leishmania* in the aid of identifying suitable novel target proteins for therapeutic development.

3.1.4 Stable isotope dimethyl labelling (DiMe)

Stable isotope dimethyl labelling (DiMe) using reductive amination for MS-based quantitative proteomics was first reported in 2003 by Hsu et al. (2003). DiMe is a method used to quantify protein abundance by introducing "light" or "heavy" isotopic tags (normally formaldehyde) to generate chemically similar peptides that will be separated by a known m/z shift in subsequent LC-MS analysis. The relative ion intensity of each isotopic peak provides an estimate of the relative abundance of the peptide in the two samples (Hsu et al. 2003). Labelling is achieved through the α- and ε-amino group of lysine residues via reductive amination (Hsu et al. 2003). Formaldehyde forms Schiff base with the N-terminus or ϵ-amino group of Lys residue of a peptide/protein; the aldimine intermediate is then reduced by sodium cyanoborohydride ($NaBH_3CN$) to form a secondary amine. This secondary amine is more nucleophilic than the primary amine. The secondary amine immediately reacts with another formaldehyde molecule to form dimethylamino group. Reductive amination is a global labelling method for all peptides with one labelling site for peptides without Lys residue or 1 + N labelling sites for peptides with N Lys residues. All amino groups are dimethylated except the N-termini of Pro residue, which is a secondary amino group and is monomethylated by the reaction (Hsu et al. 2016). In MS/MS analysis, this labelling strategy provides a signal enhancement for the a_1 and y_{n-1} ions, which are not detectable from most of the non-derivatized fragments (Hsu et al. 2003). Because formaldehyde (CH_2O) is small and water-soluble, the labelling reaction is quick, specific and complete (Hsu et al. 2016). A multiplex labelling strategy using isotopic reagents of formaldehyde ($H_{12}CHO$, $D_{13}CDO$) and cyanoborohydride ($NaBH_3CN$, $NaBD_3CN$) may be also applied for comparison of up to four samples (Boersema et al. 2009). This method is convenient, robust and relatively cheap compared with other labelling techniques. It has been widely used in quantitative proteomics for global expression profiling, post-translational modifications (PTMs) and protein interaction (reviewed in Hsu et al. (2016).

In this work, two DiMe protocols were employed in order to get higher protein recovery. Figure 3.2 illustrate the workflow of DiMe in this study.

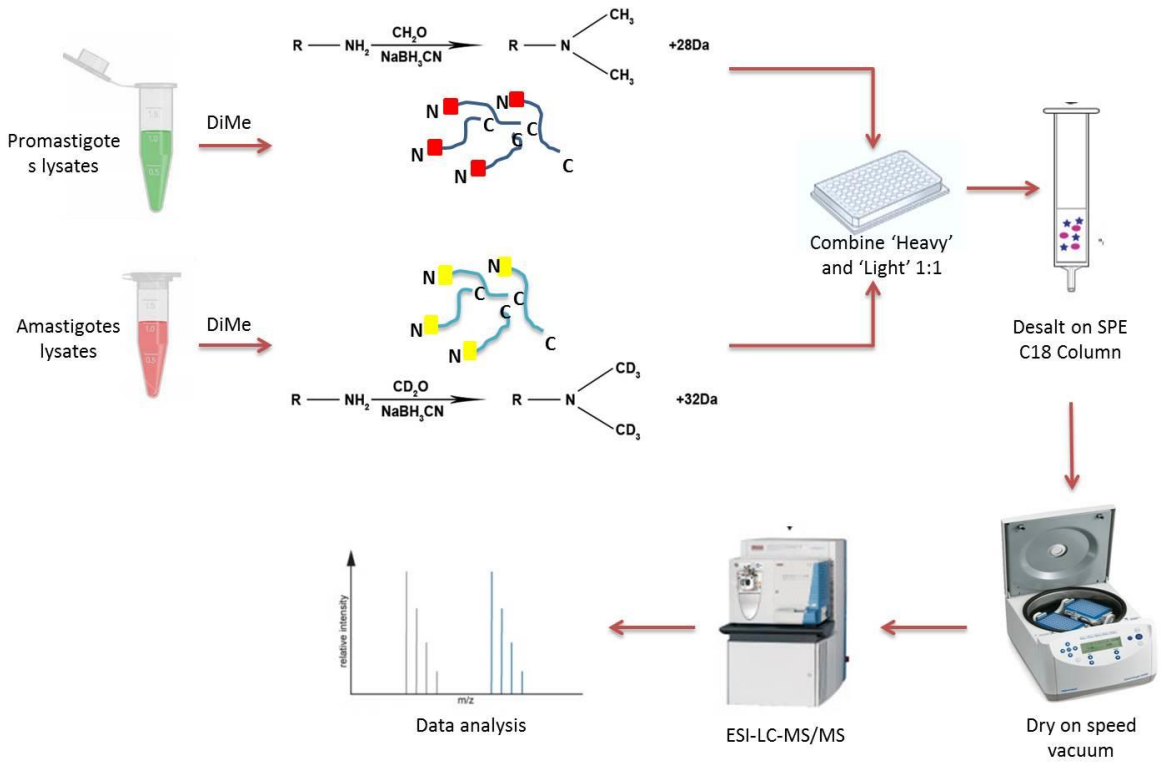

Figure 3.2: Schematic illustration of stable isotope dimethyl labelling for relative quantitation of protein.

Reductive N-dimethylation of aliphatic amines in a peptide is carried out by using $H_{12}CHO$ (light) or $D_{13}CDO$ (heavy) and sodium cyanoborohydride. The isotopic mass shift between the light and heavy labelled peptides is Δ = 4 Da. Labelled peptides were combined and processed through sample clean-up, drying and MS.

Originally we followed the protocol from Hsu et al. (2003) as described in section 2.6.1. We then tried the protocol adapted from Boersema et al. (2009) to circumvent the desalting step as this seemed to result in significant protein loss.

3.2 Aims

In this chapter, the various optimisations for proteomics and labelling will be explored and discussed. There are several important aims in this chapter, which were to:

- Optimise protein extraction method from promastigotes and amastigotes
- Enhance proteolysis of the samples to increase proteome coverage on MS
- Employ stable isotope dimethyl labelling method to differentially label promastigote and amastigote
- Assess label-free approach on promastigotes and amastigotes.

Ultimately, we used a comparative proteomic approach based on a stable isotope dimethyl labelling method to identify proteins that were differentially expressed in different stages of the parasite *L. mexicana*.

3.3 Results

3.3.1 Growth and differentiation

L. mexicana promastigote was maintained in HOMEM supplemented with 10% FCS and 1% penicillin/streptomycin. A typical growth curve was done by counting the cells every day for 7 consecutive days and shown in Figure 3.3. Doubling time for promastigotes during the peak of log phase is 7.5 h.

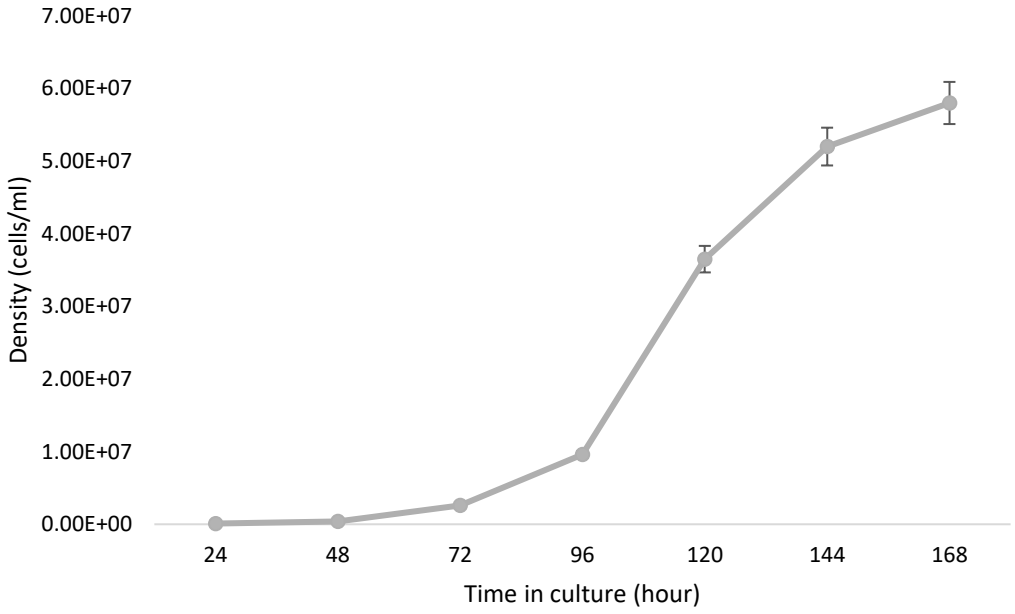

Figure 3.3: Growth curve of *L. mexicana* promastigote in HOMEM.

A culture was initiated at 1 x 10^5 cells/ml and samples taken on 7 consecutive days for cell counting. Cells were fixed in 2% formaldehyde/PBS and counted on Neubauer haemocytometer. Doubling time taken at the peak of log phase for promastigote is 7.5 h.

Amastigote was transformed from stationary phase promastigotes in Schneider's Drosophila Media supplemented with 20% FCS and 1% penicillin/ streptomycin at a lower pH (pH 5.5) and higher temperature (32ºC). Promastigotes were transformed into amastigote morphology after about 5 days. Cultures were subpassaged every 6-7 days by passing them through a syringe needle gauge (22G) as the cells tend to clump with each other. After transformation, cells were counted every day for 5 consecutive days to determine the doubling time which is 10.68 h (Figure 3.4). Following this, all experiments subsequently described in this thesis were performed on promastigotes and amastigotes which had been in culture for no more than 10 subpassages.

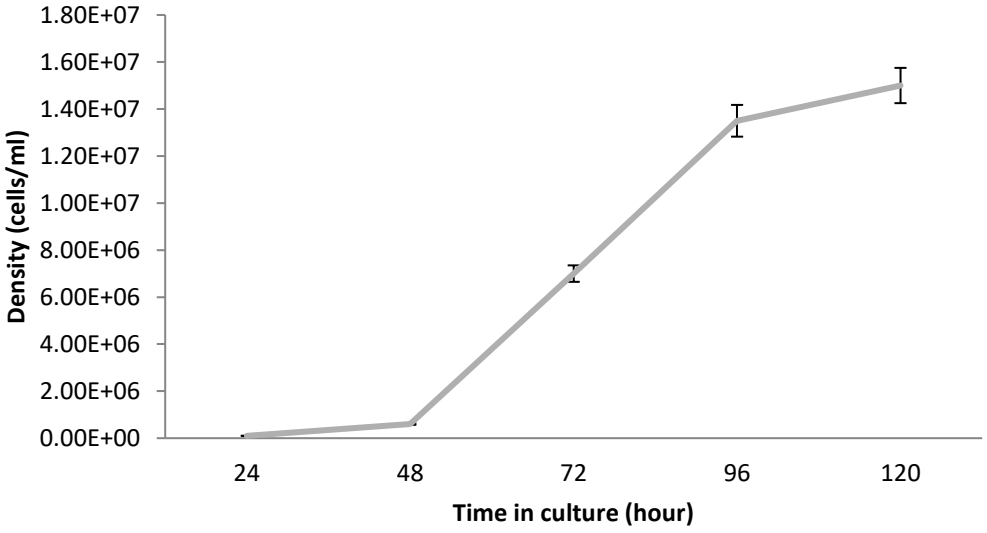

Figure 3.4: Growth curve of *L. mexicana* axenic amastigote in Schneider's Drosophila Media.

After first passage, cells were passed through a needle gauge, fixed in 2% formaldehyde/PBS and counted on Neubauer haemocytometer. Cells were taken for 5 consecutive days and the number of cells was plotted against time. Doubling time for axenic amastigotes was 10.68 h.

Promastigote and amastigote cells were stained with DAPI and observed on a Zeiss Axioskop microscope, as shown in Figure 3.5.

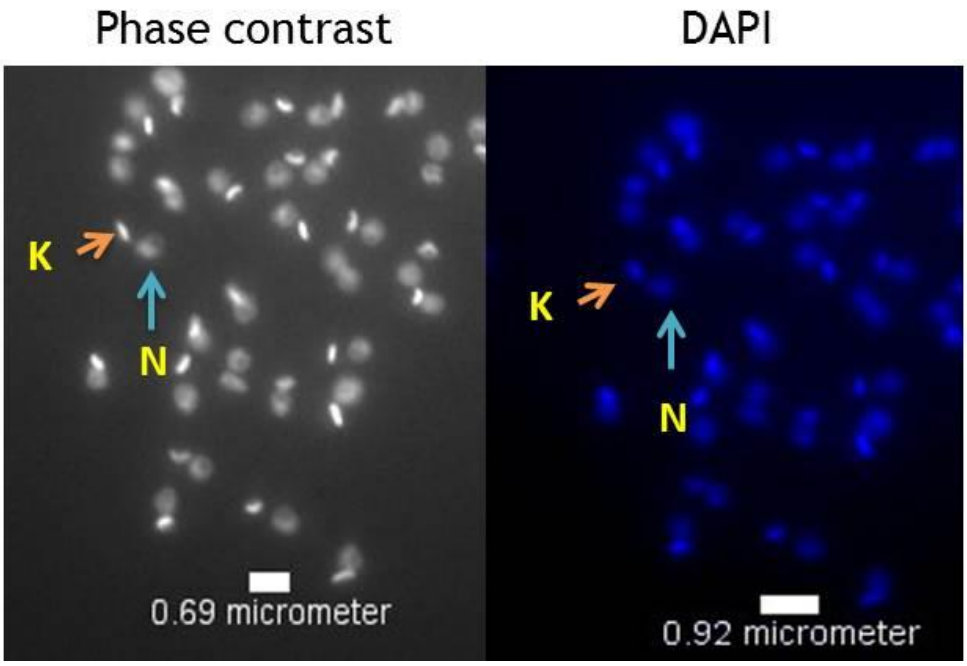

Figure 3.5: DAPI-stained of *L. mexicana* promastigotes in exponential growth.

It was observed that all cells contained one kinetoplast (K) and one nucleus (N).

3.3.2 Protein concentration determination

Following protein extraction, lysates were subjected to Bradford assay to determine the concentration. Firstly, a standard curve with a known concentration of BSA was plotted in order to determine the concentration of unknown samples. In this work, BSA with concentration of 0.1, 0.2, 0.3, 0.4 and 0.5 mg/ml were measured by spectrometer at 595 nm wavelength. They were plotted on Microsoft Excel (Figure 3.6) and the concentration of an unknown protein samples were determined using formula $y = mx + c$. Standard curve assay was plotted every time Bradford assay was done to ensure accuracy. The concentrations obtained will be used for SDS PAGE and FASP.

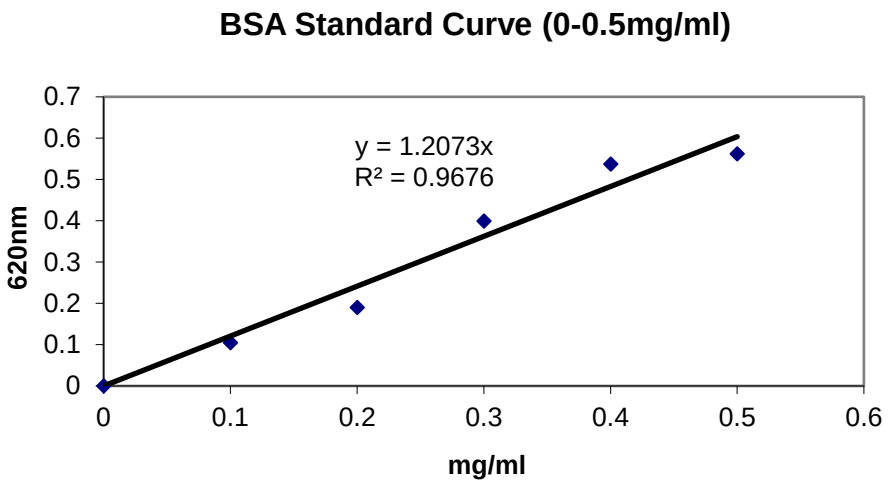

Figure 3.6: Standard curve assay to determine protein concentration.

BSA with different concentrations was used to make a standard curve for protein concentration determination.

3.3.3 Sample preparation optimisations

3.3.3.1 Protein extraction

Several optimisations for protein extraction method were considered in this research, prior to finalising the method as described in section 2.4.1. The variables that were tested include the constituent of the lysis buffer, the type of protease inhibitors, the probe sonication time and heating the samples at 95°C.

Two types of lysis buffer were tested on promastigotes and amastigotes to improve protein extraction (Table 2.1). The lysis buffers tested were:

1. SDT buffer (4% SDS, 100mM Tris-HCl pH 7.6, 0.1 M DTT)

2. TTG buffer (500 mM Tris-HCl pH 8, 0.25% Triton X-100, 20% glycerol).

Protein lysates were run on a 1D sodium dodecyl sulphate polyacrylamide gel electrophoresis (SDS-PAGE) to get a general overview of the protein distribution. Both lysis buffers were tested and evaluated on SDS-PAGE (Figure 3.7 and 3.8, respectively).

In addition, different cocktails of protease inhibitors were also optimised. Originally, cOmplete™, Mini, EDTA-free protease inhibitors cocktail tablet from Roche was routinely added fresh to lysis buffer (Figure 3.7 and 3.8). The figures clearly showed that the protein separation was not good as no distinct bands could be seen. Since it is known that amastigotes have more proteases activity (North & Coombs 1982), we decided to try different protease inhibitors in order to get more proteins in the lysates. We started with mixture of 100 µg/ml of Leupeptin, 500 µg/ml of Pefabloc, 1 mM of 1,10-Phenanthroline, 5 µg/ml of Pepstatin A and 1 mM EDTA (Figure 3.9).

Several techniques in the original protocol were modified too. Initially, the samples were not heated at 95°C prior to sonication. Figure 3.7 showed protein lysates that were extracted without and with prior heating. When the samples were heated at 95°C, there seems to be more protein bands on the gel (b).

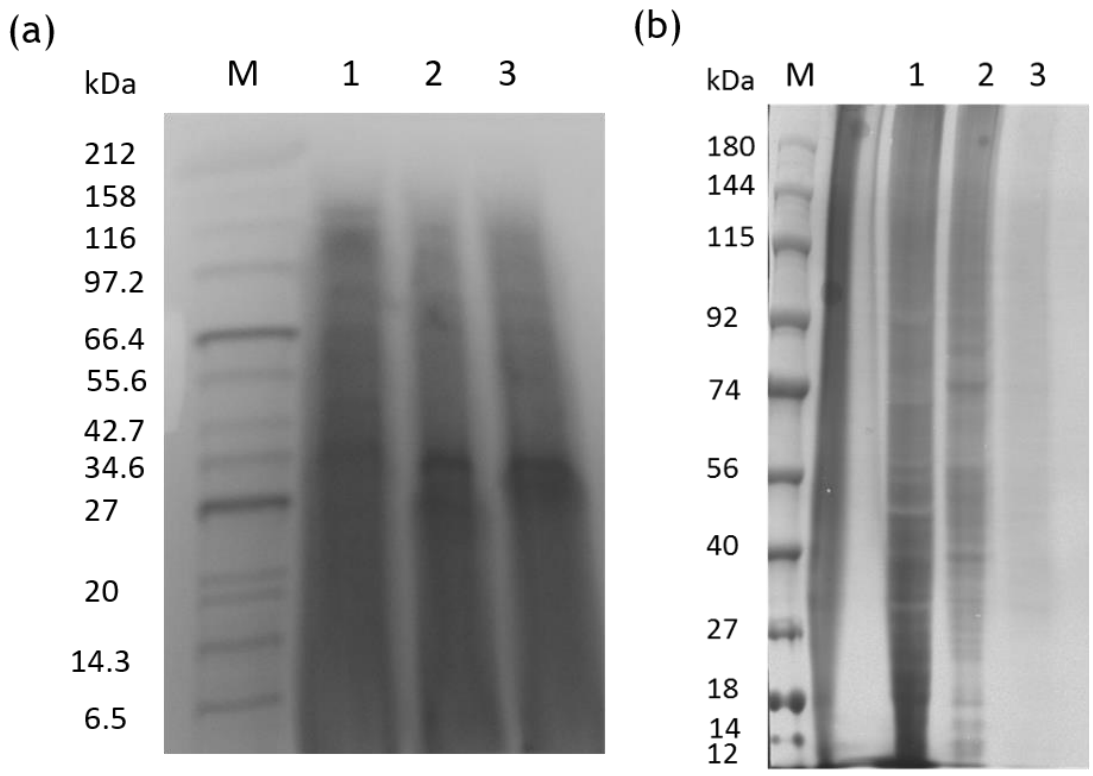

Figure 3.7: SDS PAGE profile of promastigotes and amastigotes lysates with and without heat treatment.

(a) All samples were sonicated for 1 min without prior heating at 95°C. 10 µg of lysates was analysed on SDS PAGE. Lane M: Broad range marker (NEB); lane 1: amastigote in SDT lysis buffer with cOmplete™, Mini, EDTA-free protease inhibitors cocktail tablet; lane 2-3: promastigote in SDT lysis buffer with cOmplete™, Mini, EDTA-free protease inhibitors cocktail tablet. (b) All samples were heated at 95°C followed by 1 min on sonicator. 10 µg of lysates was analysed on SDS PAGE. Lane M: Prestained marker (Expedeon); lane 1: promastigote in SDT lysis buffer with cOmplete™, Mini, EDTA-free protease inhibitors cocktail tablet; lane 2: promastigote in SDT lysis buffer with cOmplete™, Mini, EDTA-free protease inhibitors cocktail tablet; lane 3: amastigote in SDT lysis buffer with cOmplete™, Mini, EDTA-free protease inhibitors cocktail tablet.

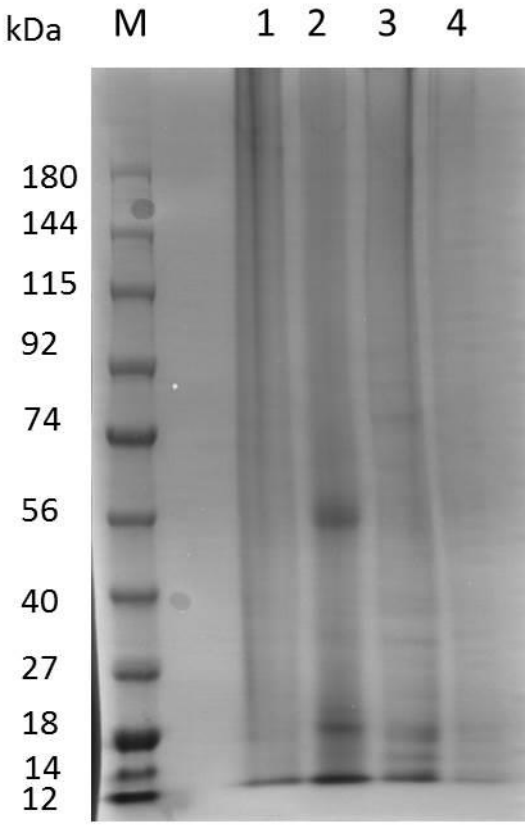

Figure 3.8: SDS PAGE profile of promastigotes and amastigotes lysates showing the effect of TTG lysis buffer.

All samples were sonicated for 1 min without prior heating at 95°C. 10 µg of lysates was analysed on SDS PAGE. Lane M: Prestained marker (Expedeon); lane 1: promastigotes in TTG lysis buffer with cOmplete™, Mini, EDTA-free protease inhibitors cocktail tablet; lane 2: promastigotes in TTG lysis buffer with 100 µg/ml of Leupeptin, 500 µg/ml of Pefabloc, 2 mM of 1,10-Phenanthroline, 5 µg/ml of Pepstatin A and 1 mM EDTA; lane 3: amastigote in TTG lysis buffer with cOmplete™, Mini, EDTA-free protease inhibitors cocktail tablet; lane 4: amastigote in TTG lysis buffer with 100 µg/ml of Leupeptin, 500 µg/ml of Pefabloc, 2 mM of 1,10-Phenanthroline, 5 µg/ml of Pepstatin A and 1 mM EDTA.

However, when the protein lysates were trypsin digested and subjected to mass spectrometry, the number of peptides identified was only 200. As long sonic burst may cause proteins to overheat and denature we experimented with multiple short sonic bursts. Daneshvar et al. (2012) suggested modifying the probe sonication timing from 1 min on the probe to only 3 secs, repeated 3 times with 1 min interval in between. The process was done on ice to minimize heating. As shown in Figure 3.9 and 3.10, the protein lysates that were obtained with heating at 95°C followed by shorter bursts of sonication have better proteins separation.

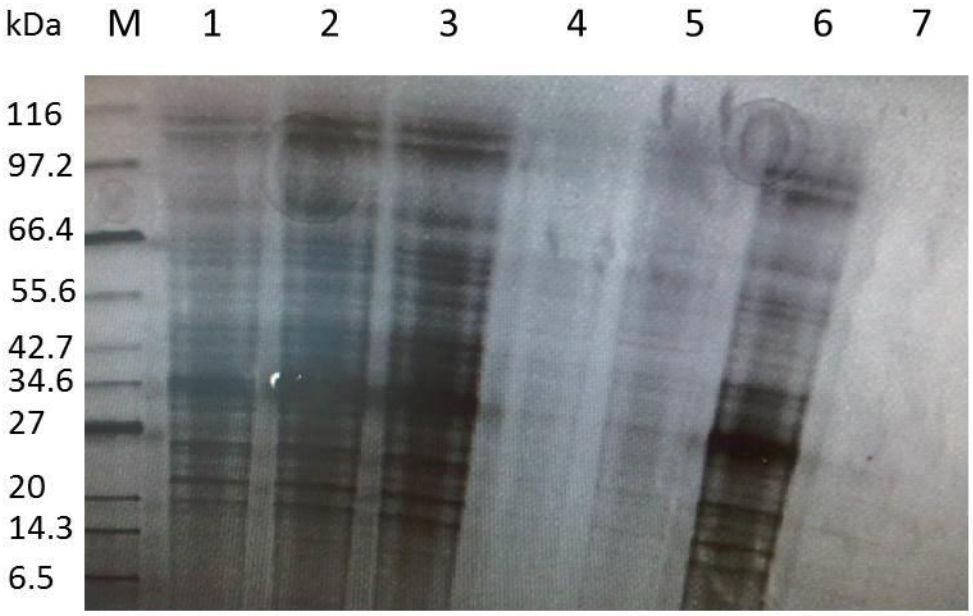

Figure 3.9: SDS PAGE profile of promastigotes and amastigotes lysates showing the effects of protease inhibitors.

All samples were heated at 95°C for 5 min and sonicated for 3 sec, repeated 3x. 10 µg of lysates was analysed on SDS PAGE. Lane M: Broad range marker (NEB); lane 1-3: promastigote in SDT lysis buffer with 100 µg/ml of Leupeptin, 500 µg/ml of Pefabloc, 2 mM of 1,10-Phenanthroline, 5 µg/ml of Pepstatin A and 1 mM EDTA; lane 4-5: amastigote in SDT lysis buffer with 100 µg/ml of Leupeptin, 500 µg/ml of Pefabloc, 2 mM of 1,10-Phenanthroline, 5 µg/ml of Pepstatin A and 1 mM EDTA; lane 6: promastigote in TTG lysis buffer with 100 µg/ml of Leupeptin, 500 µg/ml of Pefabloc, 2 mM of 1,10-Phenanthroline, 5 µg/ml of Pepstatin A and 1 mM EDTA; lane 7: amastigote in TTG buffer with 100 µg/ml of Leupeptin, 500 µg/ml of Pefabloc, 2 mM of 1,10-Phenanthroline, 5 µg/ml of Pepstatin A and 1 mM EDTA.

Since we still could not get good MS data, different concentrations of protease inhibitors were tested (as described in 2.4.1.1) to improve peptides identification with LCMS. After several repeats, it was observed that increasing the concentration of Pepstatin A and E-64 gave more bands on SDS PAGE (Figure 3.10). Extraction in SDT buffer with 100 µg/ml of Leupeptin, 500 µg/ml of Pefabloc, 2 mM of 1,10-Phenanthroline, 10 µg/ml of Pepstatin A and 50 µg/ml of E-64 showed high extraction and solubilisation efficiency across a broad MW range.

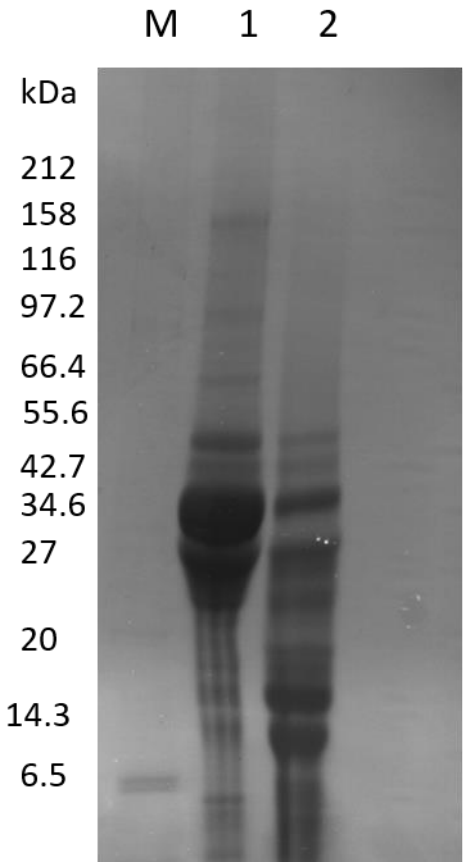

Figure 3.10: SDS PAGE profile of promastigotes and amastigotes lysates showing the effects of increased Pepstatin A and E-64 concentrations.

All samples were heated at 95°C and sonicated for 3 secs, repeated 3 times. 10 µg of lysates was analysed on SDS PAGE. Lane M: Broad range marker (NEB) (marker was not clear on this gel); lane 1: promastigote in SDT lysis buffer with 100 µg/ml of Leupeptin, 500 µg/ml of Pefabloc, 2 mM of 1,10-Phenanthroline, 10 µg/ml of Pepstatin A and 50 µg/ml of E-64; lane 2: amastigote in SDT lysis buffer with 100 µg/ml of Leupeptin, 500 µg/ml of Pefabloc, 2 mM of 1,10-Phenanthroline, 10 µg/ml of Pepstatin A and 50 µg/ml of E-64.

There were also small but rather critical adjustments made such as using freshly prepared DTT and protease inhibitors, keeping the buffer in -20°C and keeping the samples on ice all the time to prevent protein degradation.

3.3.3.2 Proteolysis and labelling

Digestion of proteins is a critical step in proteomic workflows, especially for quantitative experiments. It is also the most time-consuming step in the sample preparation workflow. The protocol adapted from Wisniewski et al. (2009) was employed for protein digestion prior to LC-MS/MS. In general, the workflow of FASP is depicted in Figure 3.11. The filter acts like a proteomic reactor where protein lysates were reduced, alkylated and digested. *L. mexicana* promastigote

and amastigote whole cell protein lysates were digested with trypsin before labelled with DiMe and separated by LCMS. In this study, several optimisations were done on proteolysis and all digests were examined through Amazon Speed ion trap MS/MS.

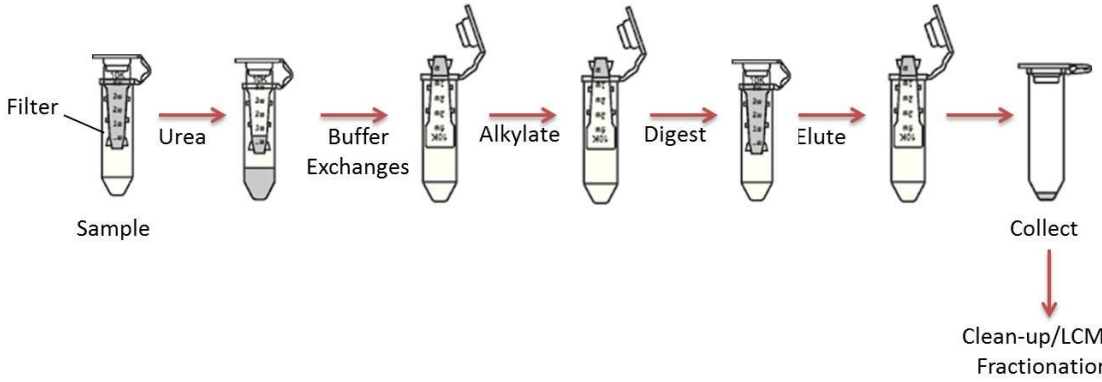

Figure 3.11: General workflow of FASP.

Samples that were prepared in 4% SDS were diluted with 8 M urea to dissociate SDS from proteins. Diluted samples were then applied to Microcon filters for buffer exchanges, eliminating SDS and contaminants. Proteins are reduced and alkylated followed by successive buffer exchanges. Proteins were digested in the column overnight before centrifuge and elution in the collection tube. Peptides could be processed through sample clean-up, for fractionation or directly analysis by LC–MS.

We initially employed the protocol from Wisniewski et al. (2009) starting with as little as 10 µg lysates and 1:100 enzyme to protein ratio. The elution buffer chosen was NaCl and desalting with SPE cartridges was required for sample clean-up. However, when the digested peptides were analysed on 1D- LC-MS/MS on Amazon Speed ion trap MS/MS less than 100 proteins were identified. Upon further investigation, it emerged that the starting concentration of protein lysates used for FASP was very low and that significant proportions of peptides were being lost during the workflow. Processing small quantities of sample led to proportionally larger losses. Lysate concentration was increased up to 100 µg to increase peptide recovery following FASP. We also tried different ratios of digestion enzyme to protein's concentration as the recommended 1:100 enzymes to protein ratio was not found satisfactory. Furthermore, proteolysis using endoproteinase LysC together with trypsin did not give higher protein identification in our experiments. This might be due to increased competition for trypsin cleavage sites. Additionally, it was observed that desalting process greatly reduced peptide identification, leading to lower peptide ion abundances thereby reducing signal intensity from the peptides. Therefore, we modified the original FASP protocol to

replace the salt elution step with elution with 50% acetonitrile. Adding ACN has been shown to improve sequence coverage and enhance solubility of tryptic peptides (Hervey IV et al. 2007). Without desalting, we manage to increase peptide yield by 30%. Table 3.1 describe the different parameters that were optimised on FASP in order to give higher peptide yield.

Table 3.1: **Analysis of promastigotes and amastigotes lysate processed by FASP with different parameters.**

Lysates (n=1) were prepared using SDT buffer with 100 µg/ml of Leupeptin, 500 µg/ml of Pefabloc, 2 mM of 1,10-Phenanthroline, 10 µg/ml of Pepstatin A and 50 µg/ml of E-64. Then, the lysates were subjected to FASP for protein digestion. Peptides were run on Amazon Speed ion trap MS/MS.

Digestion enzyme	Enzyme:Protein ratio	Elution buffer	Lysates quantity (µg)	Clean-up method	Proteins identified
Trypsin	1:100	NaCl	10	*Desalt	39
Trypsin	1:100	NaCl	25	*Desalt	77
Trypsin	1:100	NaCl	50	*Desalt	207
Trypsin	1:100	NaCl	100	*Desalt	522
Trypsin and LysC	1:100	NaCl	50	*Desalt	195
Trypsin	1:100	ACN	50	None	464
Trypsin	1:100	ACN	100	None	769
Trypsin	1:50	ACN	100	None	1119

*Desalting was done on SPE cartridge

Following proteolytic digestion, peptides were chemically labelled with DiMe. Preliminary protocol that was employed was adapted from Hsu et al. (2003) where peptides were reconstituted in sodium acetate followed by labelling with formaldehyde, quenching with sodium cyanoborohydride and the reaction was stop with ammonium hydroxide. Then, we tried another protocol for DiMe from Boersema et al. (2009). In this method, TeAB was used for peptides reconstitution before they were labelled with L and H formaldehyde. Peptides were incubated with sodium cyanoborohydride before quenching with ammonium hydroxide and acidifying with formic acid.

3.3.4 Proteome analysis and quantification of stage-regulated proteins

To perform a global quantitative proteome analysis of stage-regulated proteins, we subjected the same amount of digested peptides from promastigotes and amastigotes to stable isotope DiMe followed by analysis on 1D high performance liquid chromatography (HPLC) using Amazon Speed ion trap MS/MS. The promastigotes were light labelled whereas amastigotes were heavy labelled. In

this work, several bioinformatics tools were used for peptide identification (Figure 3.12).

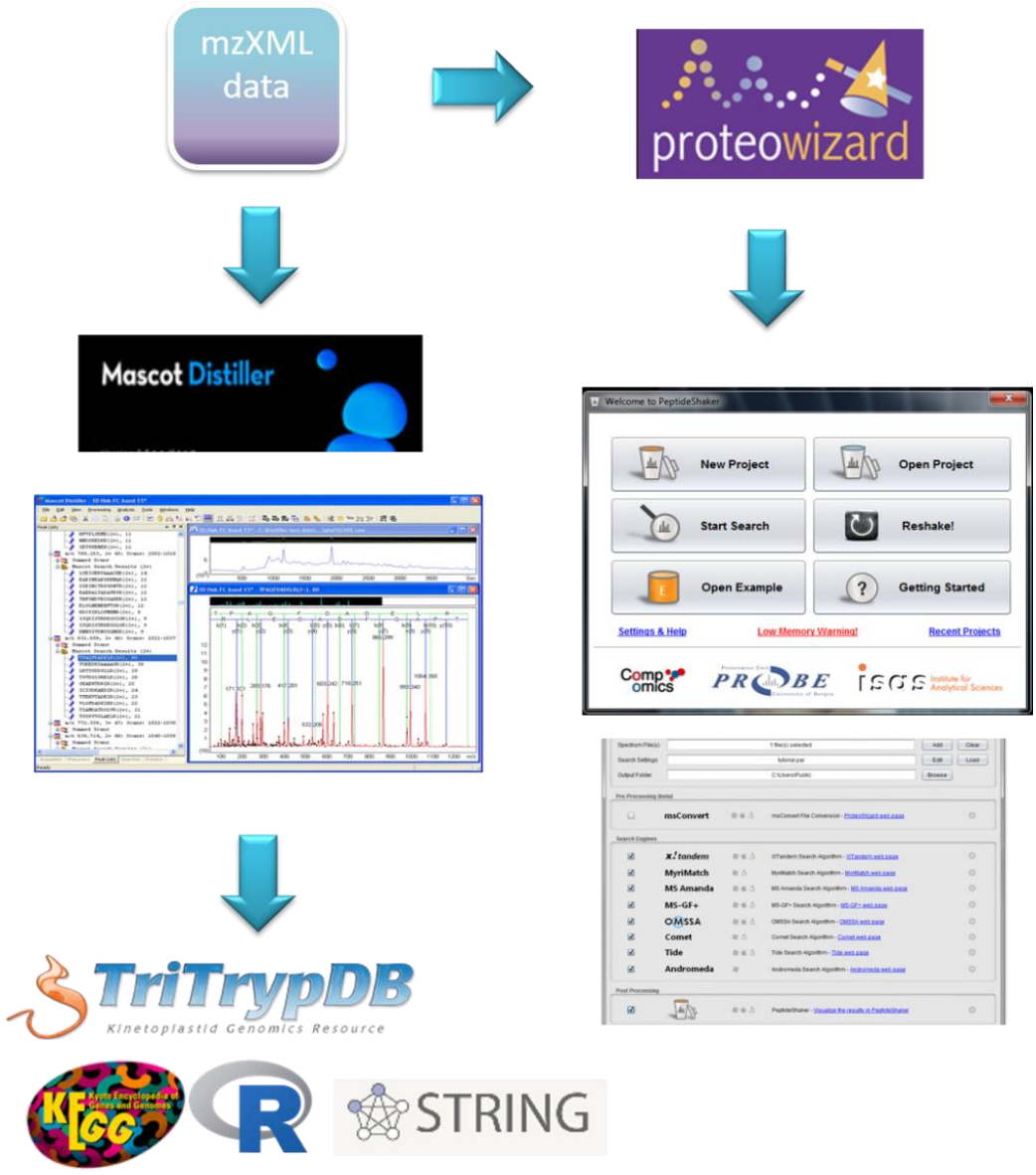

Figure 3.12: A schematic overview of bioinformatic tools used for analysing *Leishmania* proteomic data.

Amazon Ion Speed Mass spectrometer gives mzML data format as output which can be process with Mascot Distiller for peptide quantification and Mascot Daemon for protein identification. After that, various tools can be used for functional analysis and statistical analysis including Kinetoplastid Genomics Resource TriTrypDB, Kyoto Encyclopaedia of Genes and Genomes (KEGG), R and Functional Protein Associations Network (STRING). On the other hand, mzmL format needs to be converted to mgf format using ProteoWizard and process with PeptideShaker for protein identification and quantification.

The Mascot search showed that virtually all peptides were DiMe-labelled with 99% labelling efficiency (Figure 3.13). A minimum of 2 matched peptides and Mascot report parameter set as maximum number of hits: AUTO which means only

statistically significant ($p<0.05$) proteins were reported. To ensure the quality of our quantitation result, a default S/N ratio cut-off for all peptide peaks was set at 2. With Mascot search, total protein identified in all combined replicates was 1411. Out of this, the functions of 710 proteins are known while the remaining 678 proteins were hypothetical proteins with unknown functions and 23 unspecified products. Hypothetical proteins and unspecified products were manually validated on TriTrypDB and UniProt databases. Hypothetical proteins are predicted by bioinformatical genome analysis but with no known homologs. Whereas, unspecific products are predicted and proven to exist experimentally but are not characterized. Of the 1411 total proteins identified, 203 proteins were predicted by SignalP to have a signal peptide which could potentially target a protein for translocation across the membrane. 190 proteins predicted to have at least one transmembrane domain. 94 of the hypothetical proteins were predicted to have transmembrane while 109 have signal peptide.

Among the 710 genes which encode proteins with putative function, 91 proteins were membrane related proteins containing transmembrane region, of which the important proteins being amastin-like surface protein, amino acid transporter, cathepsin, cysteine peptidases, GP63 and 3-ketoacyl-CoA reductase. In addition, 94 proteins with putative function were predicted to have signal peptide. These includes amastin-like surface protein, GP63, cathepsin, cysteine peptidases, 3-ketoacyl-CoA reductase, ABC transporter, adenylate kinase and cyclophilin. Cathepsin and cysteine peptidases are involved in proteolysis which may assist in evading the host immune system (Mottram et al. 2004; Vermelho et al. 2010). The *Leishmania* surface proteinase leishmanolysin GP63 has been postulated to be a virulence factor involved in the promastigote and host receptor interaction (Isnard et al. 2015; Joshi et al. 1998). Interestingly, there was one protein involve in pathogenesis (based on GO) which is flagellum targeting protein kharon1. This novel protein has been reported to be important for the flagellar trafficking of a glucose transporter (Tran et al. 2013). *Kh1* null mutants were shown to attenuate amastigotes growth within host macrophages, suggesting it may be important for pathogenesis (Tran et al. 2013).

The application of Mascot Distiller enabled relative quantitation of matched peptides. The presence of L and H pair spectra were analysed using SeeMS tool

that is included in ProteoWizard 3.0.9 package (Figure 3.14). Of the identified proteins, only 38% of them were quantified, equivalent to 542 proteins.

1. LmxM.08.1171 Mass: 50319 Score: 75 Matches: 19(1) Sequences: 8(1) emPAI: 0.09
| organism=Leishmania mexicana | product=unspecified product | location=LmxM.08:1668001-1669332(-) | length=443

Query	Score	Expect	Rank	U	Peptide
3133	24	0.91	1	U	R.INVYFDESAGGR.Y [Dimethyl] + Dimethyl (N-term)
3165	26	0.76	1	U	R.INVYFDESAGGR.Y [Dimethyl:2H(4)] + Dimethyl:2H(4) (N-term)
3166	10	29	1	U	R.INVYFDESAGGR.Y [Dimethyl:2H(4)] + Dimethyl:2H(4) (N-term)
2290	20	3.6	1	U	R.INVYFDESAGGRYVPR.A [Dimethyl] + Dimethyl (N-term)
4700	45	0.0089	1	U	R.AVLMDLEPGTMDSVR.A [Dimethyl] + Dimethyl (N-term)
4703	30	0.27	1	U	R.AVLMDLEPGTMDSVR.A [Dimethyl] + Dimethyl (N-term)
4749	11	17	1	U	R.AVLMDLEPGTMDSVR.A [Dimethyl] + Oxidation (M); Dimethyl (N-term)
1320	1	3e+02	9	U	R.AVLMDLEPGTMDSVR.A [Dimethyl:2H(4)] + 2 Oxidation (M); Dimethyl:2H(4) (N-term)
1670	6	92	4	U	R.FPGQLNSDLR.K [Dimethyl] + Dimethyl (N-term)
807	19	4	1	U	K.NMMQAADPR.H [Dimethyl] + Dimethyl (N-term)
1030	2	1.3e+02	4	U	K.NMMQAADPR.H [Dimethyl] + 2 Oxidation (M); Dimethyl (N-term)
1031	15	7.9	3	U	K.NMMQAADPR.H [Dimethyl] + 2 Oxidation (M); Dimethyl (N-term)
889	15	10	1	U	R.YLTASALFR.G [Dimethyl:2H(4)] + Dimethyl:2H(4) (N-term)
892	18	5.5	1	U	R.YLTASALFR.G [Dimethyl:2H(4)] + Dimethyl:2H(4) (N-term)
3455	1	2.7e+02	3	U	K.MSVTFIGNNTCIQEMFR.R [Dimethyl:2H(6)13C(2)] + Oxidation (M); Dimethyl:2H(6)13C(2) (N-ter
1893	7	63	1	U	R.VGEQFTGMFR.R [Dimethyl] + Dimethyl (N-term)
2044	7	55	1	U	R.VGEQFTGMFR.R [Dimethyl] + Oxidation (M); Dimethyl (N-term)
2056	2	1.9e+02	3	U	R.VGEQFTGMFR.R [Dimethyl:2H(4)] + Oxidation (M); Dimethyl:2H(4) (N-term)
2058	0	3e+02	1	U	R.VGEQFTGMFR.R [Dimethyl:2H(4)] + Oxidation (M); Dimethyl:2H(4) (N-term)

Figure 3.13: Partial peptide summary of unspecified product (*L. mexicana*) identified as protein hit #1 in promastigote sample.

The peptide sequences showed the modifications occurred, in this case, labelling with heavy dimethyl, indicating efficient DiMe labelling into the peptides.

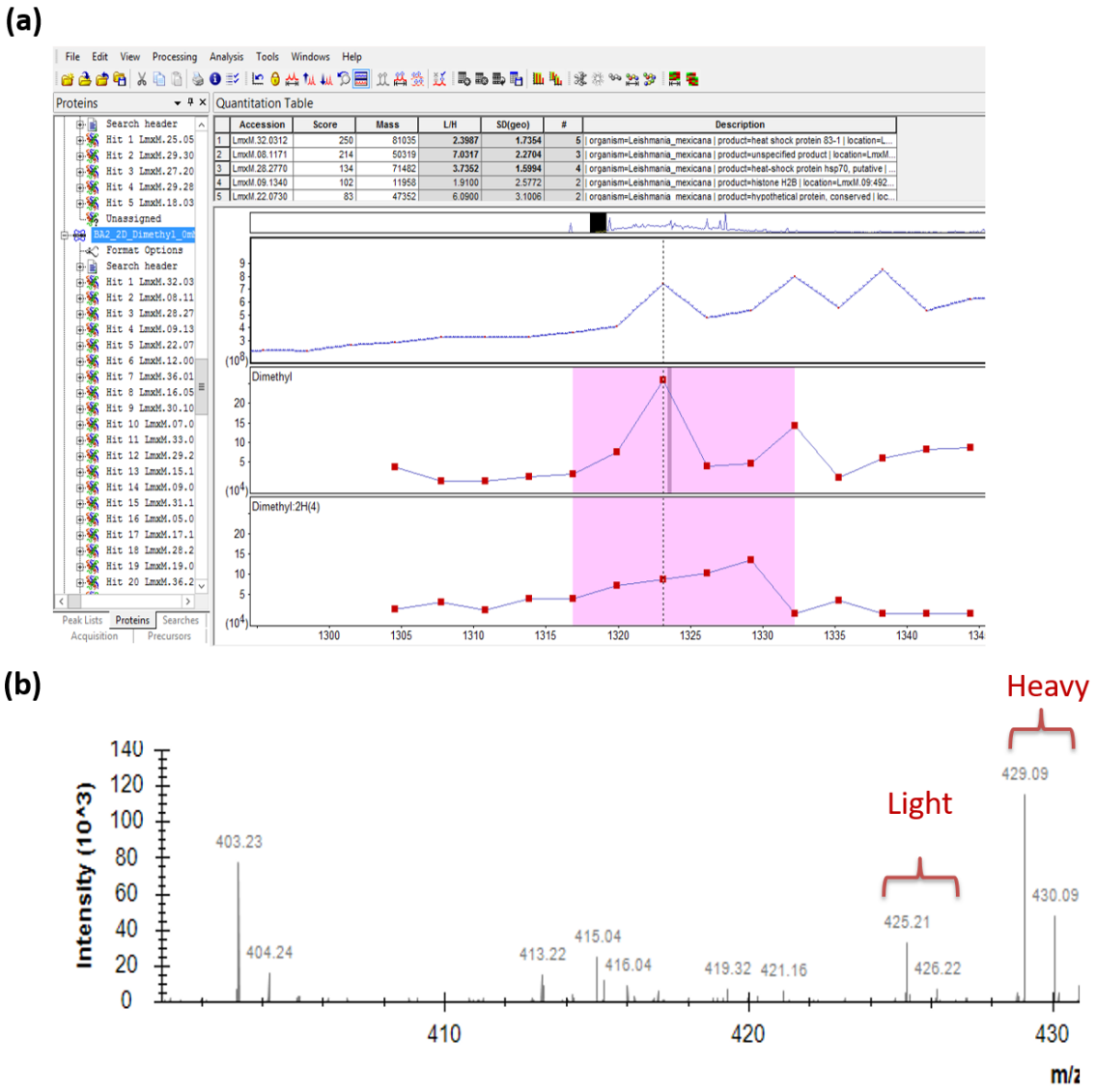

Figure 3.14: MS/MS spectra of tryptic peptides showing DiMe pair of heavy and light.

(a) An example of protein quantification using Mascot Distiller (Matrix Science). (b) mgf data generated by Amazon Speed ion trap MS/MS was analysed by SeeMS tool (included in ProteoWizard 3.0.9 package) to verify spectra that has been labelled with heavy and light formaldehyde.

The high abundance proteins spotted in every biological replicate (n=6) included actin, tubulin, heat shock proteins, ribosomal proteins (40S and 60S), enolase, ABC transporter, protein kinases, elongation factor proteins, and several types of peptidases. Gene ID of all 1411 proteins identified were uploaded on TriTrypDB for functional analysis. *Leishmania mexicana* MHOM/GT/2001/U1103 strain was used as reference. Gene Ontology (GO) Enrichment tool was chosen with p-value cutoff 0.05. Figure 3.15 show GO with molecular function of the proteins. Notably, 60% of the proteome involves in metabolic processes such as carbohydrate, lipid,

and nucleic acid metabolism, followed by biosynthetic process and cellular process. These includes fumarate hydratase, ribonuclease mar1 and long-chain-fatty-acid-CoA ligase. Biosynthetic process is the chemical reactions and pathways resulting in the formation of substances. From our data, proteins involves in this process include alanine aminotransferase, adenylosuccinate synthetase and myo-inositol-1-phosphate synthase. For instance, alanine aminotransferase catalyzes the reversible transamination between alanine and 2-oxoglutarate to form pyruvate and glutamate in gluconeogenesis pathway. Most hypothetical proteins predicted on TriTrypDB in our data involves in cellular processes such as cell cycle, autophagy, endocytosis and DNA repair.

Figure 3.16 shows the significant pathways in *L. mexicana*. Most altered pathways involves within the parasite are glycolysis and gluconeogenesis for energy production. Example of proteins that we found in our data involves in this pathway are glucose-6-phosphate isomerase, enolase, glycosomal malate dehydrogenase, phosphoglycerate kinase C and 6-phospho-1-fructokinase.

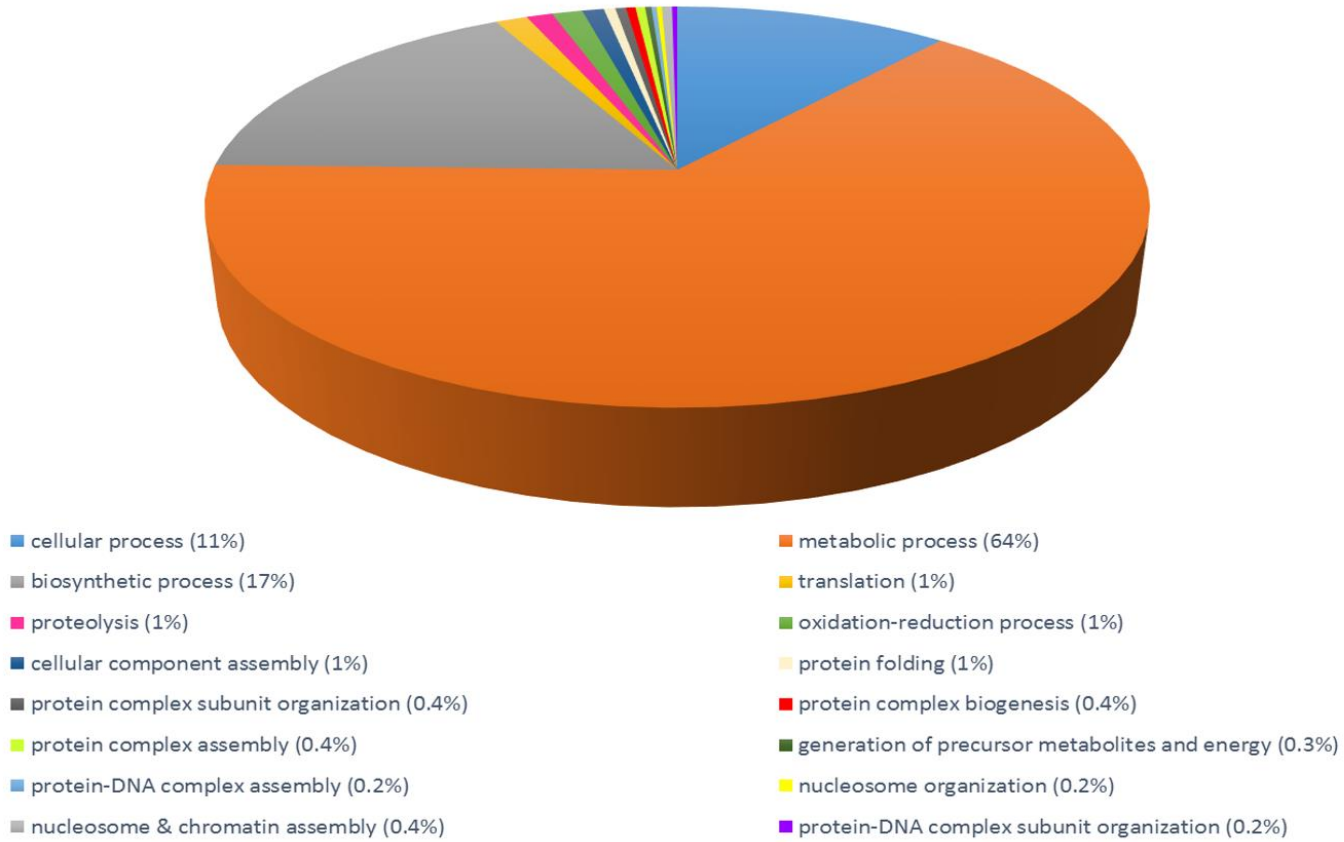

Figure 3.15: Clustering of Gene Ontology based on biological processes (GOBP) of all proteins detected in *L. mexicana*.

The total number of proteins identified in *L. mexicana* was analysed on TriTrypDB based on molecular function they involve in.

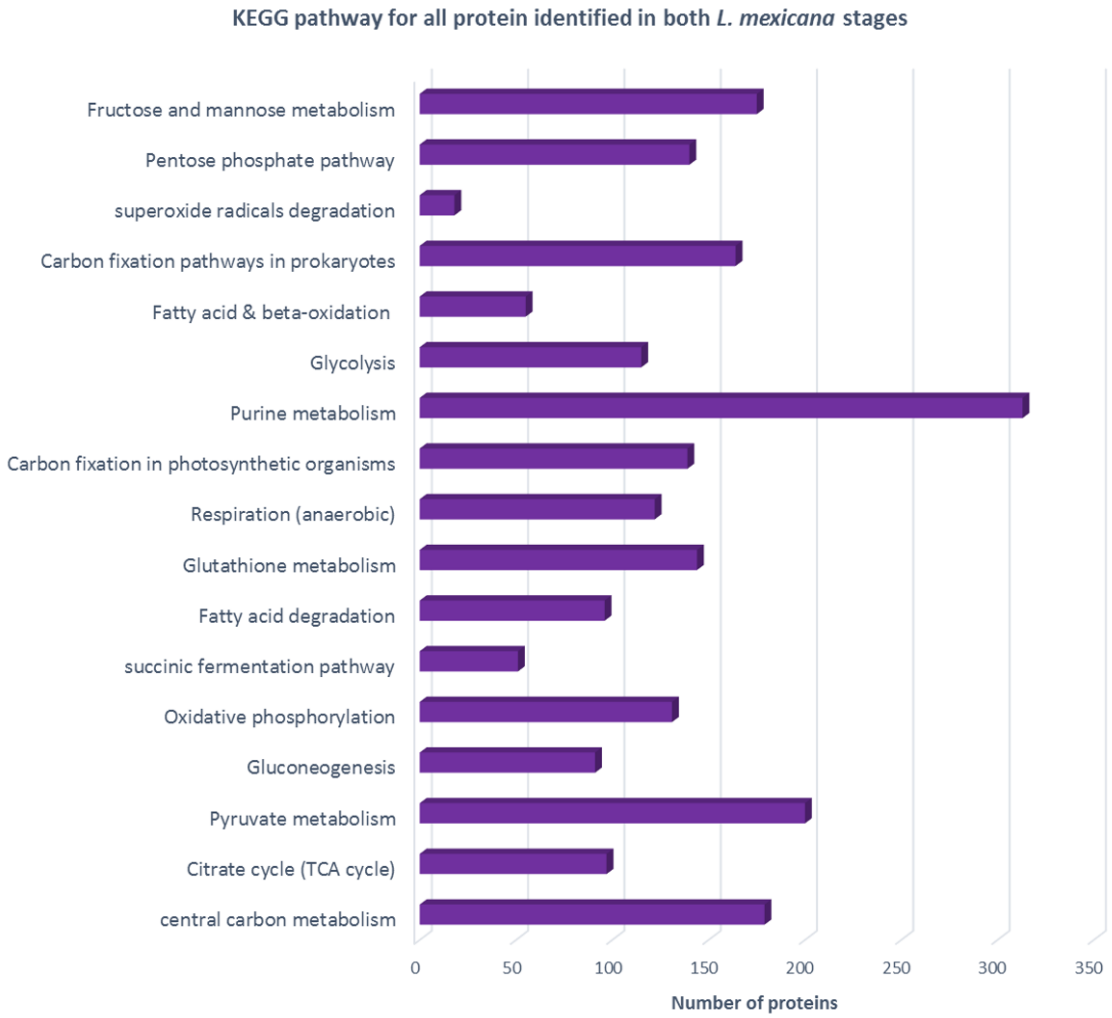

Figure 3.16: Pathway analysis on KEGG showing most enriched pathways in *L. mexicana*.

The total number of proteins identified in *L. mexicana* was analysed on TriTrypDB with links to KEGG in order to identify the pathways they are involved in.

Comparative analysis of ESI-LC-MS/MS of *L. mexicana* promastigotes and amastigotes revealed several (542 proteins) differentially expressed proteins. The values of L/H ratio give information about stage-regulated proteins. In this case, L/H>1 indicates that a protein is upregulated in promastigotes, compared with amastigotes. Likewise, L/H<1 suggests that the protein is upregulated in amastigotes. 542 proteins were identified as both L and H labelled pairs, enabling this ratio to be calculated. Of these, 317 proteins showed a L/H ratio greater than 1, while 225 proteins showed a ratio less than 1 (Figure 3.18). Supplementary table 8.1 and 8.2 (in Appendix) lists proteins modulation in promastigote and amastigote respectively. Distribution of the quantified proteins based on L/H ratio obtained

by Distiller showed most L/H ratios were in range of 2-10 for promastigote life stage and 0.1-0.5 for amastigote life stage (Figure 3.17).

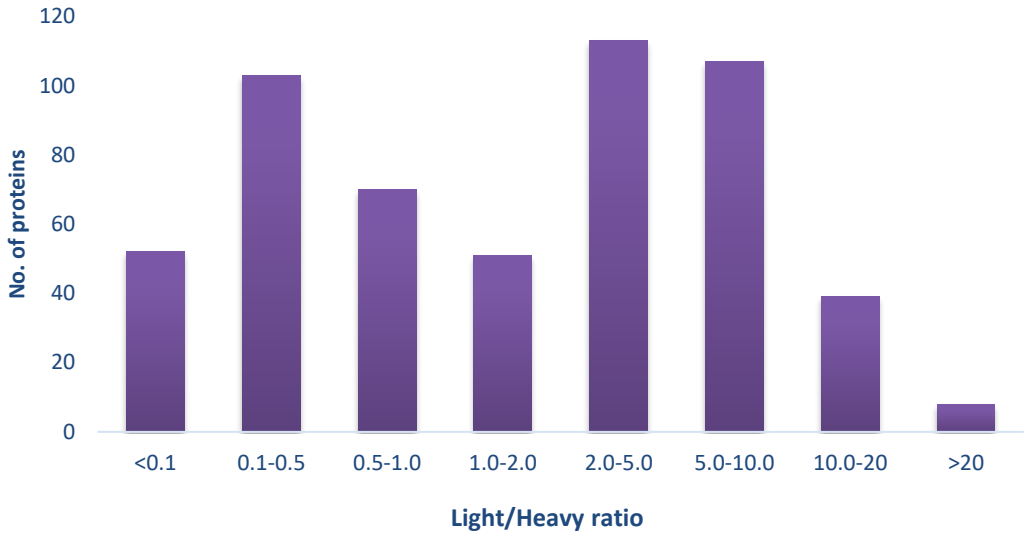

Figure 3.17: Distribution of the significantly modulated proteins in *L. mexicana* based on L/H ratio.

Peptide quantifications were performed in Mascot Distiller where DiMe-labelled pair will be given an L/H ratio. These ratios were grouped within certain range to see the overall distributions. Most peptides were in the range of 2-10 and 0.1-0.5.

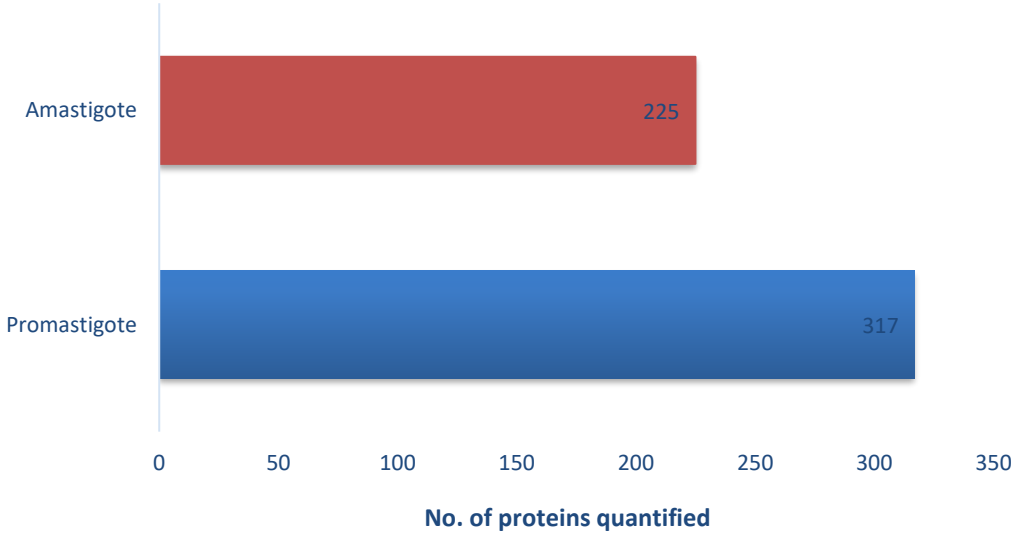

Figure 3.18: Differential protein expressions in promastigote and amastigote.

Protein quantification was performed using Mascot Distiller to give rise of L/H ratios (total of 542).

We found several well-documented promastigote stage specific proteins including kinetoplastid membrane protein-11 (KMP-11) (Stebeck et al. 1995; Bhaumik et al. 2009), SNF2/RAD54 related DNA helicase putative (Alcolea et al. 2016), elongation factor 1-alpha (Brotherton et al. 2010), heat shock protein (Brotherton et al. 2010), ß-tubulin (Leifso et al. 2007) and paraflagellar rod proteins (Moore et al. 1996; Brotherton et al. 2010). The most strongly modulated protein was KMP-11 with L/H ratio of 55 and Mascot score of 53. The 317 promastigote specific proteins detected were divided into the following putative functional classification categories based on GO annotations: metabolic process, oxidoreductase, transportation, translation, catalytic activities, cellular process and microtubule based movement (Figure 3.19). Examples of proteins from our data that involves in metabolic process are glyceraldehyde 3-phosphate dehydrogenase with L/H ratio of 16.81, glycosomal phosphoenolpyruvate carboxykinase with L/H ratio of 16.68 and 6-phosphogluconate dehydrogenase with L/H ratio of 15.03. Fascinatingly, there were 66 hypothetical proteins and 10 unspecific products in our data with L/H>1. Pathway analysis showed glycolysis, gluconeogenesis, amino acid metabolism, sugar metabolism, tricarboxylic acid (TCA) cycle, fatty acid degradation and many more were modulated between promastigotes and amastigotes (Figure 3.20).

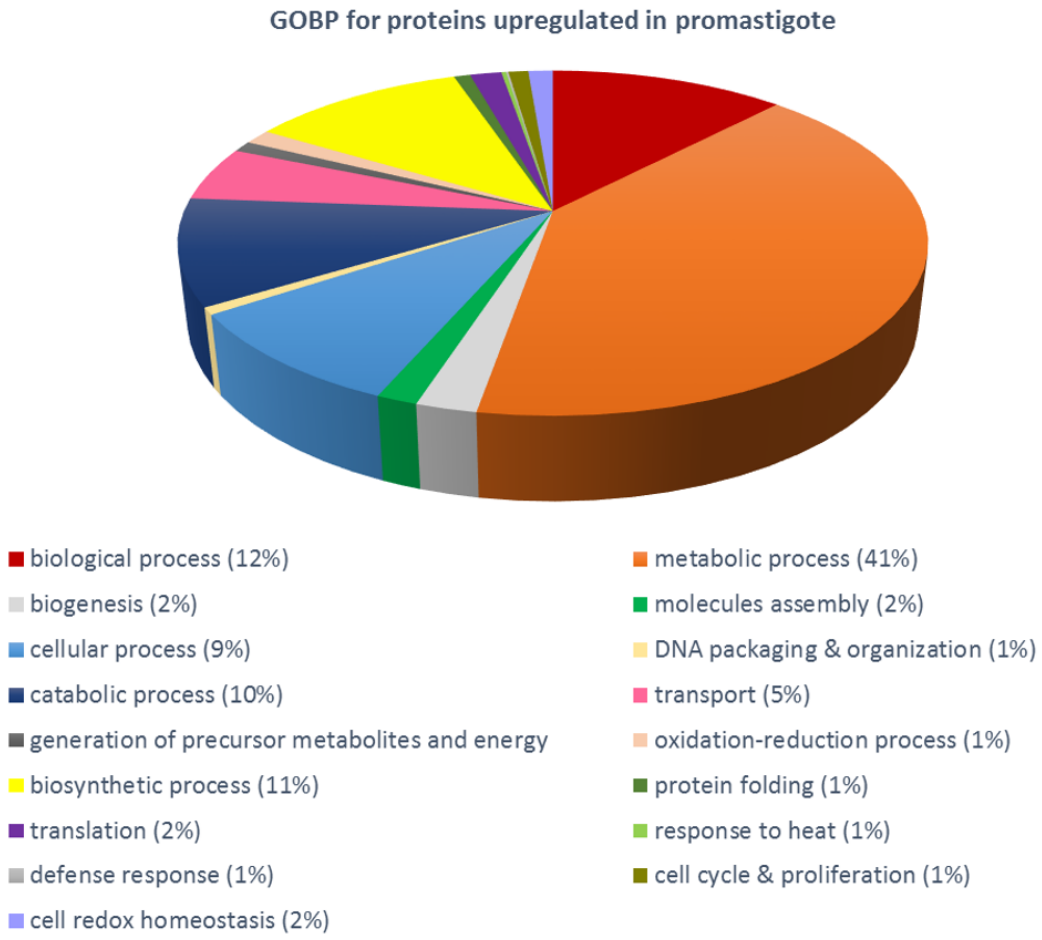

Figure 3.19: Clustering of Gene Ontology based on biological process (GOBP) of proteins detected in *L. mexicana* promastigote stage.

The proteins that were considerably upregulated in promastigote stage was analysed on TriTrypDB based on the biological processes they are involved in.

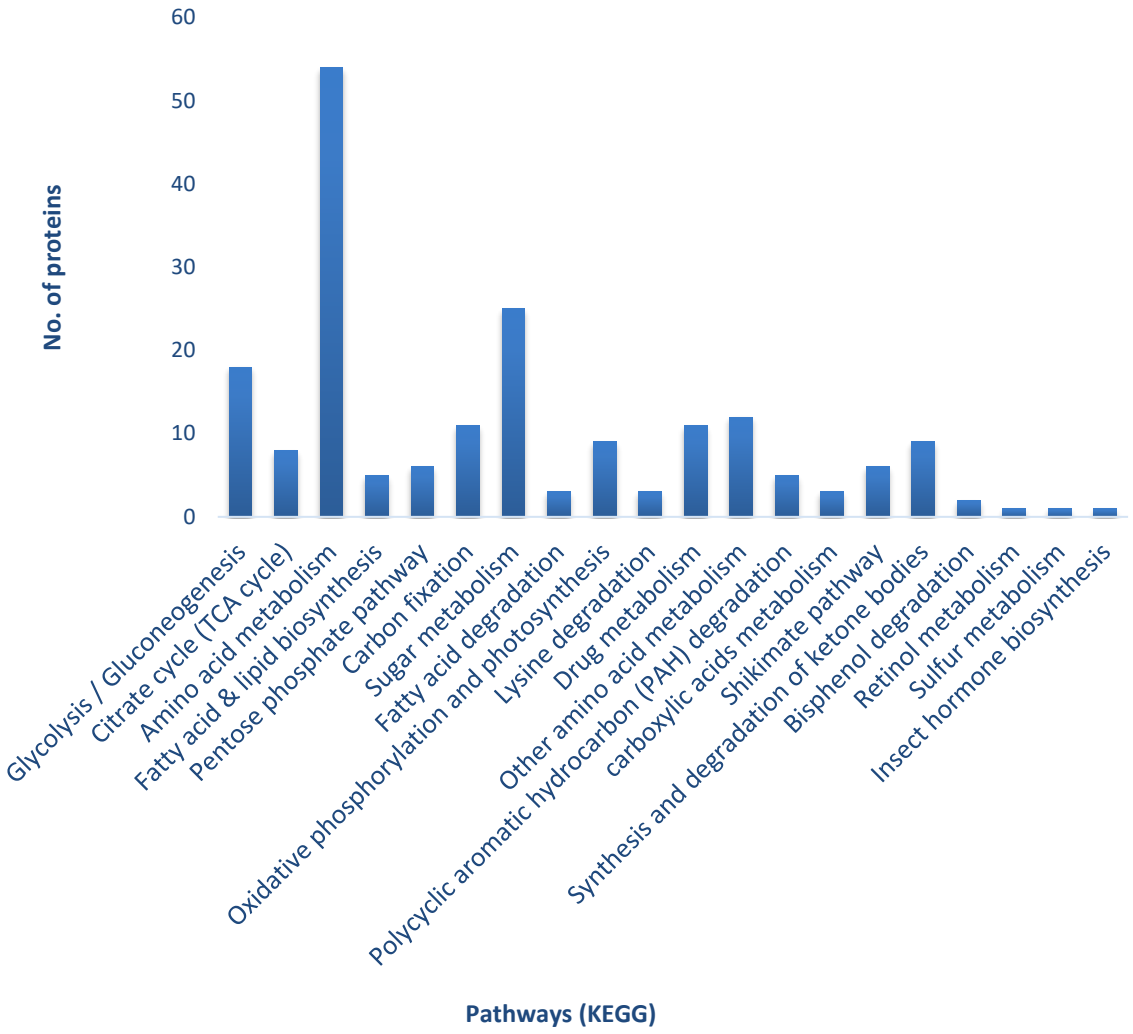

Figure 3.20: Pathway analysis on KEGG showing most altered pathways in *L. mexicana* promastigote stage.

The proteins that were considerably upregulated in promastigote stage was analysed on TriTrypDB with links to KEGG to identify the pathways they are involved in.

Upregulated amastigote proteins included ribosomal proteins, calpain-like cysteine peptidase, GP63/leishmanolysin, aminopeptidase putative, histone, cathepsin L-like protease putative and carboxypeptidase. Notably, peptidases were found more in amastigote compared to promastigote. Of the 225 proteins, 64 were predicted to be hypothetical proteins while 4 predicted as unspecific product. The proteins that were detected in amastigote stage were grouped into classification categories based on GO annotation: metabolic process, proteolysis, translation, oxidation-reduction process, biosynthetic process, cellular process and microtubule-based process (Figure 3.21). The majority of the proteins that were observed to be upregulated in amastigotes were implicated in amino acid

metabolism, fatty acid metabolism and vitamin metabolism (Figure 3.22). Several differentially expressed proteins in amino acid metabolism were upregulated in amastigote such as aldehyde dehydrogenase, arginase, ribose-phosphate pyrophosphokinase and dihydrolipoamide dehydrogenase.

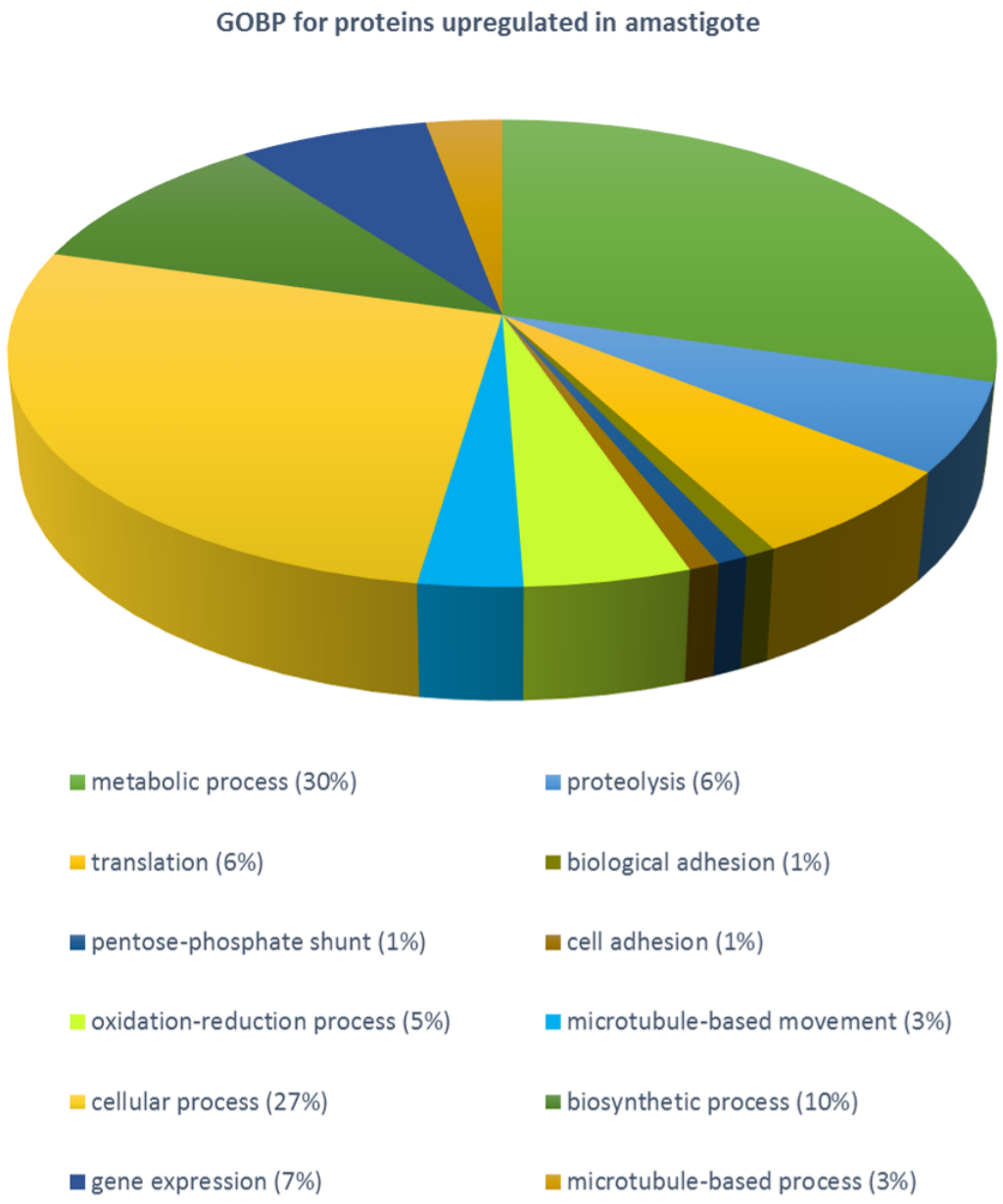

Figure 3.21: Clustering of Gene Ontology based on biological process (GOBP) of proteins detected in *L. mexicana* amastigote stage.

The proteins that were considerably upregulated in amastigote stage was analysed on TriTrypDB based on biological processes they involve in.

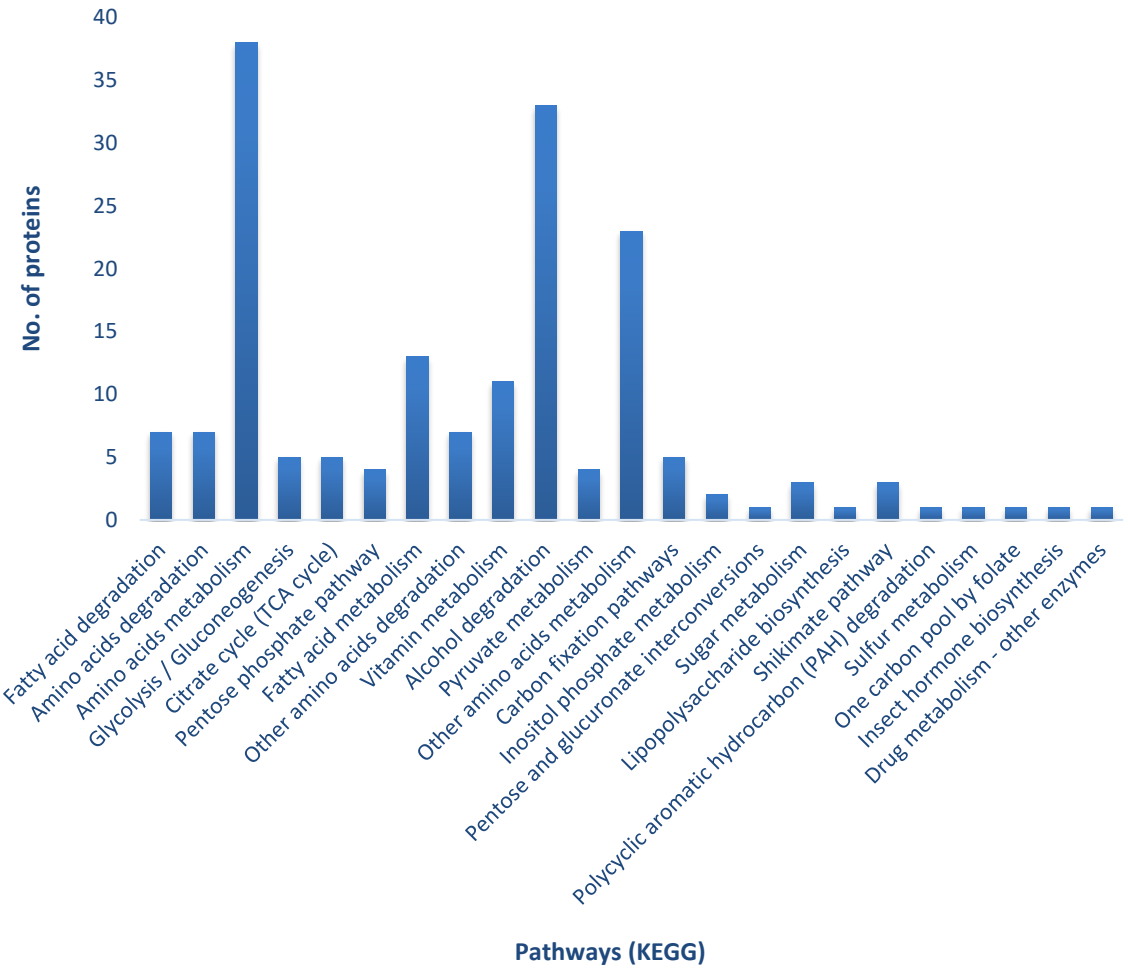

Figure 3.22: Pathway analysis on KEGG showing most altered pathways in *L. mexicana* amastigote stage.

The proteins that were considerably upregulated in amastigote stage was analysed on TriTrypDB with links to KEGG to identify the pathways they are involved in.

Further analysis on the presence of signal peptide revealed a total of 28 proteins predicted to have signal peptides were upregulated in amastigote stage (Table 3.2). Most mitochondrial proteins are synthesized as cytosolic precursors containing uptake peptide signals and post-translationally targeted to the mitochondria (Lithgow 2000). Some of the proteins listed in Table 3.2 have a mitochondrial role including aldehyde dehydrogenase, cytochrome c oxidase and malate dehydrogenase.

Table 3.2**: Proteins upregulated in amastigote stage with predicted signal peptide.**

The protein sequence of amastigote proteins was analysed on SignalP for detection of predictive signal peptide.

Accession ID	L/H	Protein name
LmxM.23.0690	0.26	3-ketoacyl-CoA thiolase-like protein
LmxM.19.0995	0.63	4-coumarate:coa ligase-like protein
LmxM.15.1203	0.99	60S acidic ribosomal protein P2
LmxM.29.2900	0.47	aldehyde dehydrogenase, putative
LmxM.21.0895	0.4	aspartyl-tRNA synthetase, putative
LmxM.08.1070	0.54	cathepsin L-like protease, putative
LmxM.19.1420	0.18	cysteine peptidase A (CBA)
LmxM.26.1710	0.96	cytochrome c oxidase subunit V, putative
LmxM.21.0550	0.27	dihydrolipoamide acetyltransferase precursor like protein
LmxM.07.0600	0.11	electron transfer flavoprotein-ubiquinone oxidoreductase, putative
LmxM.10.0610	0.06	endonuclease G, putative
LmxM.10.0390	0.03	GP63, leishmanolysin
LmxM.16.0670	0.64	hypothetical protein, conserved
LmxM.17.0910	0.59	hypothetical protein, conserved
LmxM.03.0530	0.41	hypothetical protein, conserved
LmxM.02.0470	0.85	hypothetical protein, unknown function
LmxM.27.0930	0.5	isovaleryl-coA dehydrogenase, putative
LmxM.09.0800	0.01	kinetoplast-associated protein-like protein
LmxM.33.0140	0.34	malate dehydrogenase
LmxM.13.0870	0.77	mitochondrial processing peptidase alpha subunit, putative,metallo-peptidase, Clan ME, Family M16
LmxM.13.1060	0.95	NADH-cytochrome b5 reductase, putative
LmxM.28.1240	0.59	p450 reductase, putative
LmxM.26.1610	0.74	proline oxidase, mitochondrial precursor-like protein
LmxM.06.1050	0.63	protein disulfide isomerase
LmxM.15.0275	0.77	ribonucleoprotein p18, mitochondrial precursor, putative
LmxM.34.1120	0.02	Selenoprotein T, putative
LmxM.08.1030a	0.41	unspecified product

Figure 3.23 shows differences in how many promastigote and amastigote proteins are involve in each pathway. It is apparent from the figure that more proteins upregulated in promastigote have been associated with metabolic pathway, carbon metabolism, biosynthesis of secondary metabolites, TCA cycle and amino acid metabolism. On the other hand, more ribosomal proteins are upregulated in the amastigote, compared to the promastigote stage.

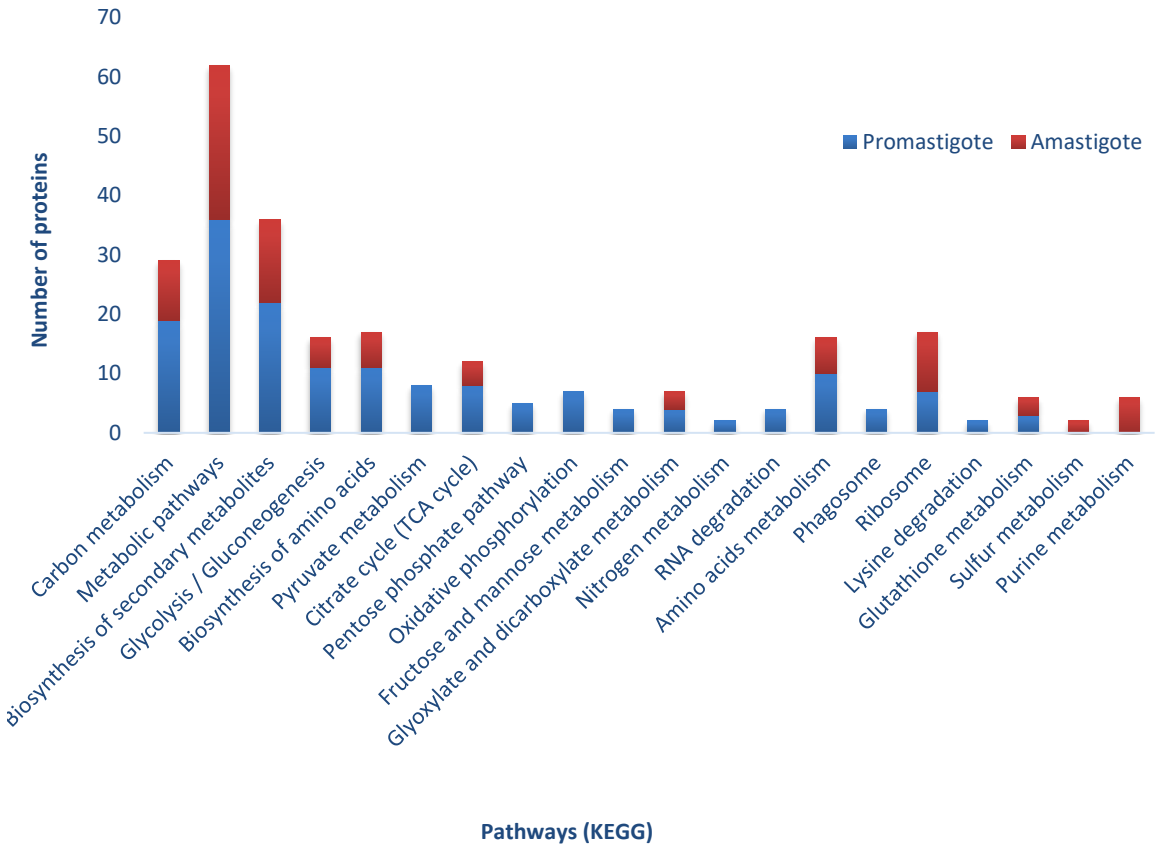

Figure 3.23: Pathway analysis on KEGG showing most altered pathways in *L. mexicana* promastigote and amastigote stage.

Both promastigote and amastigote proteins stage were analysed on StringDB with links to KEGG to identify the pathways they involve in. The chart shows pathway differences in both stages.

We analysed the proteins enriched in promastigote (Figure 3.24) and amastigote (Figure 3.25) on StringDB to know the protein-protein interactions highlighting proteins involved in metabolic pathway. There were several ATPase synthases found in promastigotes. Arginase was found in amastigotes and it has been reported to be critical for parasite replication (Kropf et al. 2005).

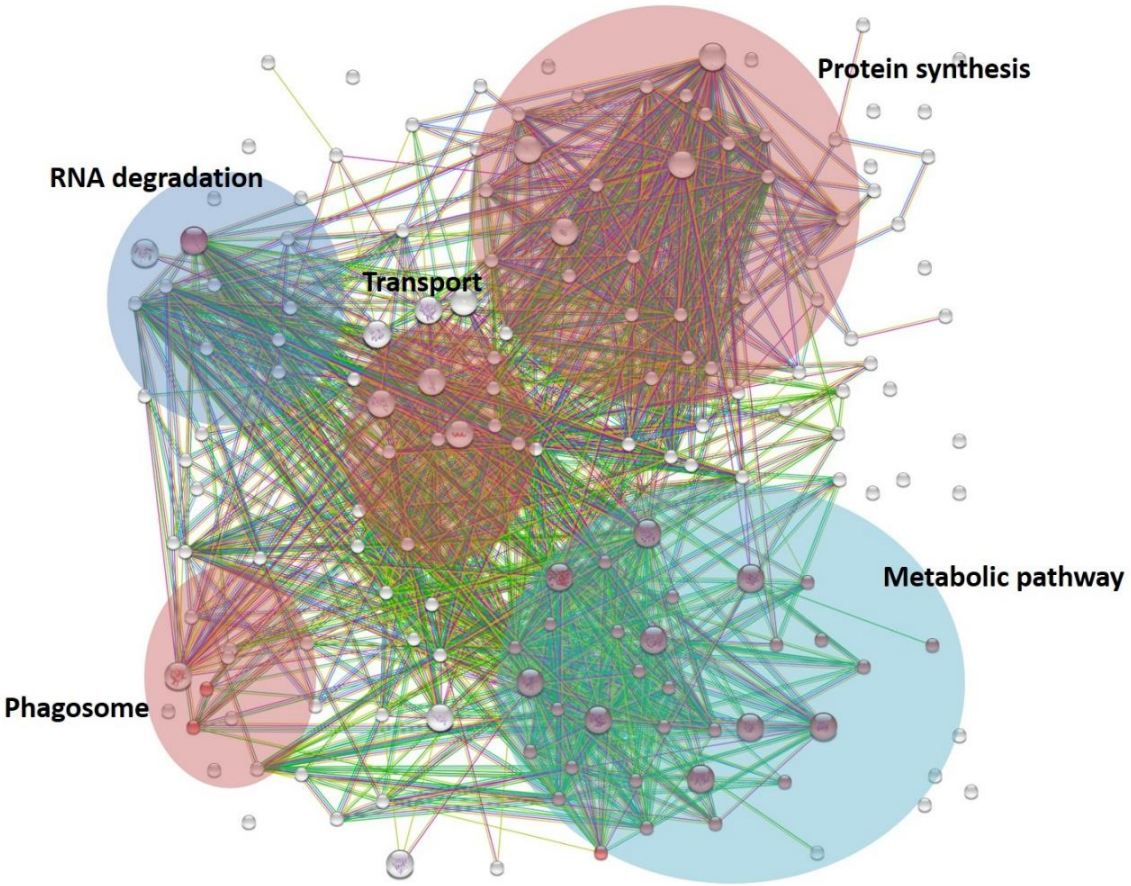

Figure 3.24: Protein network between identified proteins in promastigote.

Protein ID of proteins identified in promastigote were uploaded on STRING database to show the complex protein network and protein-protein interactions.

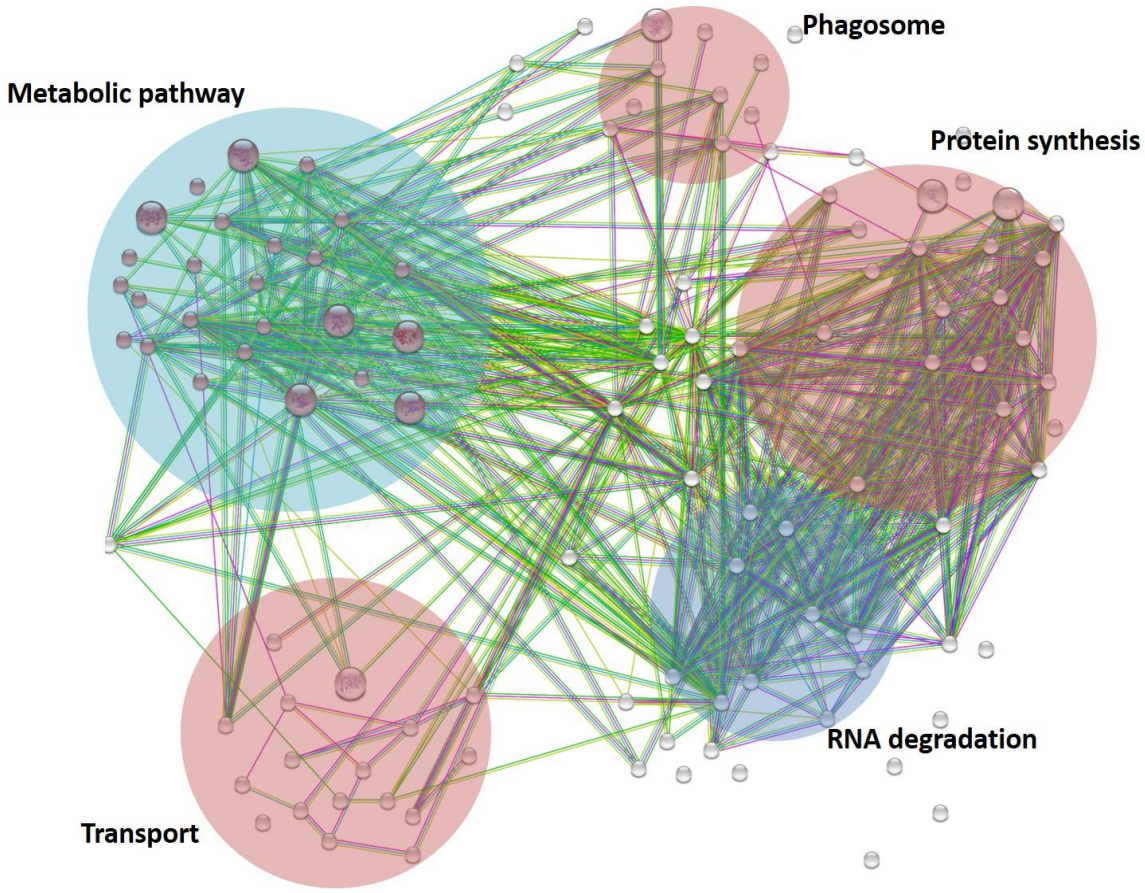

Figure 3.25: Protein network between identified proteins in amastigote.

Protein ID of proteins identified in amastigote were uploaded on STRING database to show the complex protein network and protein-protein interactions.

Label-free proteomics was attempted to analyse total proteins found in *L. mexicana* with the hope of getting higher number of identified proteins and higher coverage. Analysis was performed using MaxQuant with LFQ intensity. There were 6 biological replicates for promastigote and amastigote. Applying the default setting on MaxQuant we only managed to discover 117 proteins. Multiscatter plot analysis was performed on all replicates with Pearson correlation close to 1 suggesting good reproducibility (Figure 3.26). Comparing with DiMe-labelled proteins, 7 proteins found exclusively in label-free sample: carboxypeptidase B2, Complement C3 precursor, Heat shock protein 83, Cysteine proteinase B, Probable quinone oxidoreductase, Triosephosphate isomerase and Multidrug resistance protein 1. We could not detect these 7 proteins using DiMe probably due to incomplete labelling or the low intensity of H or L isotope which prevented the detection of one of the isotopes by MS. Figure 3.27 showed analysis of label-free proteins performed on Perseus. Histogram below showed the distribution in

triplicates of promastigote and amastigote with the red colour indicates proteins involved in glycolytic process (Figure 3.27 b). Promastigote appeared to have greater number of glycolytic enzymes, in accordance with previous results from DiMe-labelled proteins described earlier. However, we note that this experiment was done once and was not optimised. The number of proteins detected using label-free approach was too low compared to DiMe. This could be due to sample preparation problem. Hence, the results were preliminary.

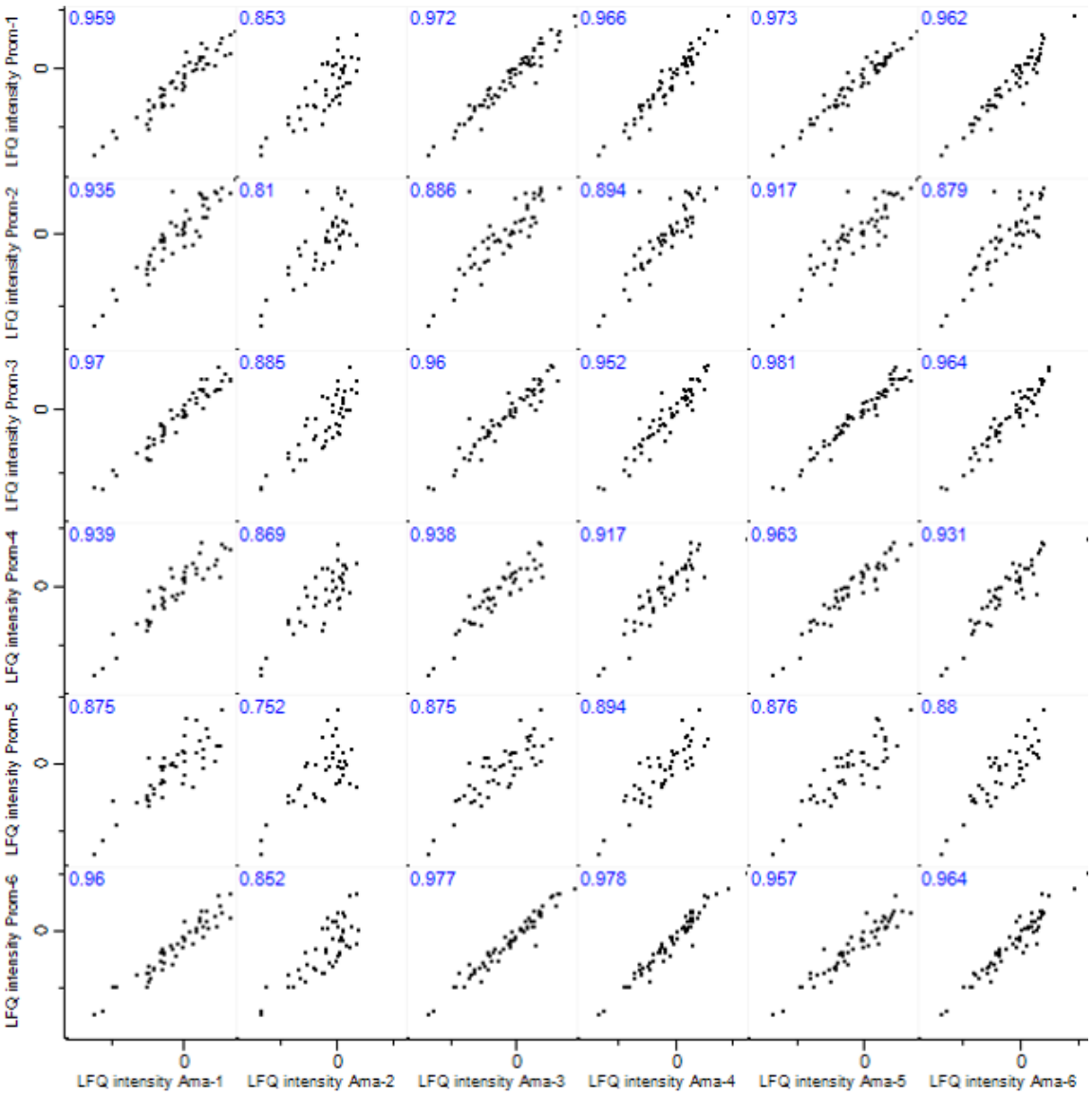

Figure 3.26: Label-free proteomics of replicates of promastigote and amastigote.

6 biological replicates of each promastigote and amastigote were subjected to FASP and 1D-LCMS/MS on Orbitrap Velos. Multiscatter plot with Pearson correlation close to 1 showed good reproducibility between each replicate.

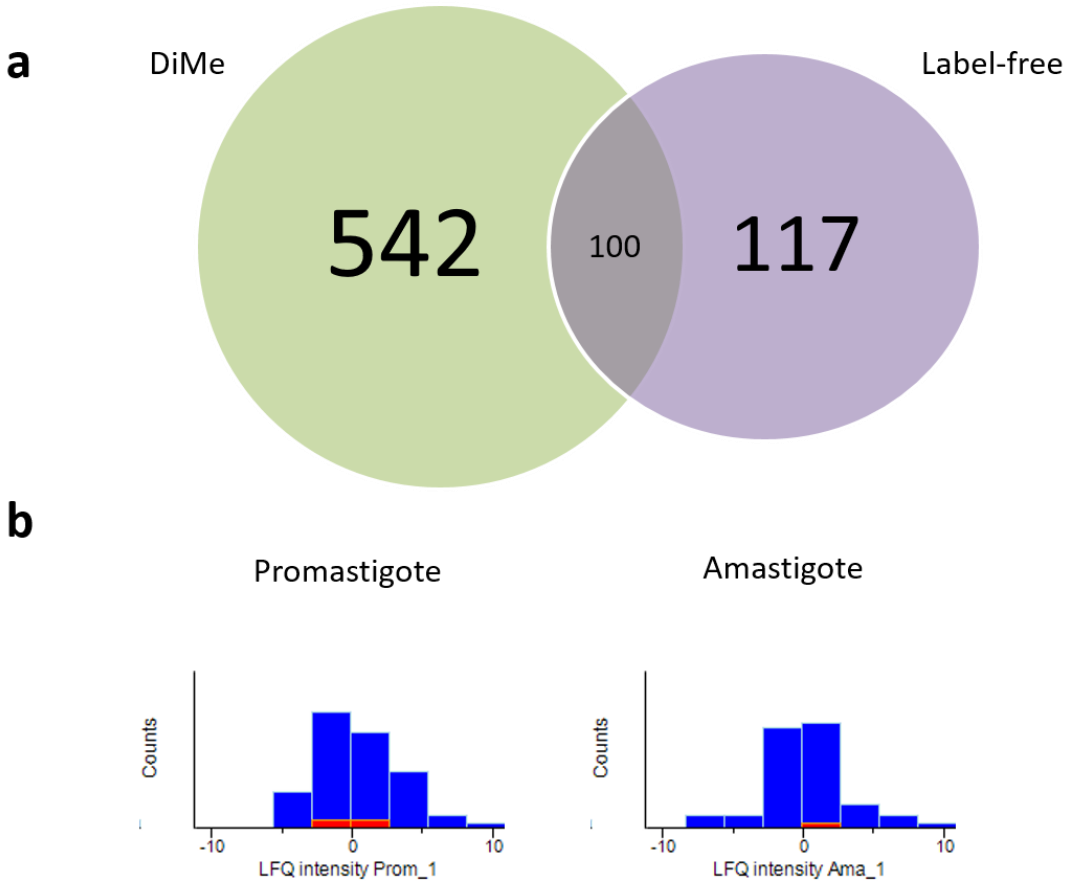

Figure 3.27: Label-free proteins distribution in *L. mexicana*.

Protein lysates from both promastigote and amastigote were subjected to FASP and 1D-LCMS/MS on Orbitrap Velos (biological replicates, n=3). The raw data was analysed on MaxQuant and Perseus. (a) Venn diagram showed total proteins identified by DiMe and label-free (b) Histogram showed the distribution of fold changes of label-free peptides between promastigote and amastigote, red colour indicates proteins involves in glycolytic process.

3.4 Discussion

Many investigations on stage-regulated proteins in *Leishmania* have been done over the years (Lynn et al. 2013; Leifso et al. 2007; Pescher et al. 2011; Walker et al. 2006; Bente et al. 2003; El Fakhry et al. 2002; Nugent et al. 2004; Zilberstein & Shapira 1994; Paape et al. 2010; Zilberstein 2015). Since the *Leishmania* genome is, in general, constitutively expressed with regulation occurring via post-transcriptional mechanisms (Leifso et al. 2007), proteomic studies that are focused on profiling global differences in life-stage specific expression have enhanced value, compared with systems where transcriptional regulation is significant (Lynn et al. 2013). Previous studies utilised 2D gel techniques as well as MS-based proteomics. In the present studies, we exploited stable isotope

labelling as means of comparative quantitation of the proteins in the main *L. mexicana* life stages: promastigote and amastigote.

The reliability of quantitative proteomic experiments depends on the consistency and the robustness of the protein extraction and digestion methods utilized. With this in mind, we employed a relatively new method for proteomic sample proteolysis, namely filter-aided sample preparation (FASP) that was invented by Wisniewski et al. (2009). FASP has been shown to be able to circumvent many of the challenges associated with other proteomic sample preparation methods, particularly elimination of contaminants that will affect downstream processes. This is achieved using a filter unit. In a single filter, a total of 0.2-200 µg of total protein can be processed at a time. However, despite the advantages, one major drawback of FASP is it causes a significant sample loss.

Sample preparation factors influencing proteomic results, aside from enzymatic digestion, include protein concentration, detergents used and the efficiency of the clean-up process. Protein extraction was initially found to be a problem during the preparation of protein samples especially on amastigote lysates. This could possibly due to the large amount of proteolysis enzymes presence in amastigote stage (Mottram et al. 2004). To overcome this problem, lysates were routinely prepared in the presence of an extensive inhibitor cocktail of protease inhibitors. This cocktail dramatically improved the number of gel bands when analysed on SDS-PAGE. In accordance with a report by Nugent et al. (2004), we also found that when testing the inhibitors individually, leupeptin was revealed to be the most effective component, nonetheless the entire cocktail was necessary to avoid detectable proteolysis. Furthermore, omitting elution with salt, thus obviating the need for subsequent desalting, improved protein coverage by 30%.

The total number of proteins identified in *L. mexicana* was 1411 with 50.3% proteins with known function, while the remaining were hypothetical proteins with no known homologs and unspecified products that are not yet characterized. The set of the regulated proteins reported here includes characterized *L. mexicana* proteins such as KHARON1 (KH1) which is the first protein identified in kinetoplastid protozoa that functions to selectively target an integral membrane protein to the flagellar compartment (Tran et al. 2013). KH1 mediates flagellar targeting of a glucose transporter in *L. mexicana* and is critical for viability of

infectious intracellular amastigotes (Tran et al. 2013). Also included are amastin-like surface protein and lypophosphoglycan (LPG). Amastin is a surface glycoprotein and highly expressed in the intracellular amastigote stages of *Trypanosoma cruzi* and *Leishmania spp* (de Paiva et al. 2015). To date, the function of amastin is still unknown. However, work by de Paiva et al. (2015) documented that amastin knockdown parasites had growth attenuation after *in vitro* infection of mouse macrophages and completely failed to produce infection when inoculated in BALB/c mice. This implied that amastin has significant role in pathogenesis. LPG is the most abundant major surface glycoconjugate that present in all *Leishmania* species. LPG help promastigote to attach on the lining of sand fly gut as well as protecting them from degradation by proteolytic enzymes (Diniz Atayde et al. 2016). Furthermore, Argueta-donohué et al. (2015) reported that LPG impairs nuclear translocation of NF-κB in monocytes with the subsequent decrease in IL-12 production, thereby advancing the progression of infection in host.

Of the proteins identified, 118 proteins were predicted to have multiple putative transmembrane domains which could be associated with membrane. These include protein kinase, protein tyrosine phosphatase, protein disulphide isomerase, Qc-SNARE protein, ABC transporter, cathepsin L-like protease, hsp-90, GP63, NADH-cytochrome b5 reductase, fatty acid elongase, cysteine peptidase A, and 3-ketoacyl-CoA reductase. Most studies involving *Leishmania* membrane-bound or secreted molecules have been done with the promastigote where they are known to synthesize and traffic most surface molecules such as LPG, GP63 and acid phosphatases (Mcconville et al. 2002). Analysis of these proteins on SignalP confirmed the presence of signal peptides. LPG and GP63 were postulated to be transported out to flagellar pocket in large translucent vacuoles for adaptations to parasitic lifestyles (Mullin et al. 2001; Mcconville et al. 2002). Phosphatases have been identified as virulence factors in many pathogenic microorganisms such as virus, fungi and parasites by deregulating the signalling pathways of the host cell (Shibata et al. 1994; Escalona-Montaño et al. 2016). Phosphatases are enzymes that remove phosphate groups from molecules such as amino acid residues of proteins. Escalona-Montaño et al. (2016) has shown that *L. mexicana* promastigotes and amastigotes secrete proteins with phosphatase activity to the culture medium. They also showed that phosphatases were located in the flagellar

pocket. We found several phosphatases in our data such as phosphatase 2C. However, only one (vacuolar-type proton translocating pyrophosphatase 1) had a predicted signal peptide. As secreted proteins could be potential vaccine candidates, we believe this data offer a useful resource even though signal peptide independent secretory pathways exist in *Leishmania*. It is known that the vast majority of the characterized *Leishmania* secreted proteins have no secretion signal sequence which suggests the existence of important non-classical pathways of secretion (Mcconville et al. 2002).

To define the molecular mechanism of leishmanial differentiation, we used the DiMe to identify and quantify the proteins preferentially expressed in promastigotes and amastigotes of *L. mexicana*. Similar quantities of protein lysate from promastigote and amastigote were mixed and subjected to LC-MS analysis. When promastigote transforms to amastigote, *Leishmania* undergo significant changes in metabolism, cell morphology, motility, cell division and infectivity for adaptation to different microenvironment. These changes are reflected in the proteome differences between promastigote and amastigote. Thus, we observed many identified putative proteins that were differentially regulated covered a diversity of functions, mainly metabolism, redox process, proteolysis and protein synthesis. Proteins that have yet to be assigned a function are also important as they could give more insight on the molecular adaptation of *Leishmania*.

We observed that many metabolic enzymes were upregulated in promastigotes, compared to amastigotes. This is consistent with an increased growth rate and motility in the promastigote stage (Holzer et al. 2006), and also with the stringent response that is reportedly induced in amastigotes. Additionally, increased expression in the promastigote of proteins involved in carbon metabolism, TCA cycle, amino acid metabolism, glycolysis and gluconeogenesis, are consistent with a higher energy requirement by the promastigote. Promastigotes expressed higher levels of mitochondrial proteins such as pyruvate dehydrogenase E1. This enzyme generates acetyl-CoA that enters TCA cycle. This is in corroboration with our findings where glycolytic pathway and TCA pathway were elevated in promastigote. Other mitochondria proteins upregulated in promastigotes include isocitrate dehydrogenase (NADP), ATP synthase and aldehyde dehydrogenase.

Fewer mitochondrial proteins were upregulated in amastigotes, including proline oxidase, trifunctional enzyme alpha subunit and DNA topoisomerase II.

The promastigotes can import sugar from the extracellular environment when available, and they are able to synthesize sugar de novo, via gluconeogenesis, under sugar starvation (Burchmore & Landfear 1998; Rodriguez-Contreras & Hamilton 2014). Our data support the hypothesis that promastigotes can utilize glucose and amino acids such as lysine as energy source. The catabolism of these substrates involves glycolysis and the TCA cycle. There is also evidence that other sugars could be used by promastigotes. These include fructose and mannose. Glycerol kinase (GK), phosphoenolpyruvate carboxykinase (PEPCK), and pyruvate phosphate dikinase (PPDK) play important role in gluconeogenesis (Rodriguez-Contreras & Hamilton 2014). As illustrated in figure 3.20, promastigotes upregulate expression of sugar metabolism proteins. This is important as promastigotes living in the midgut of the primarily phytophagous sand fly will encounter abundant plant sugars (Cameron et al. 1995). From our data, PEPCK and PPDK were found to be upregulated in promastigotes. PEPCK catalyses the conversion of oxaloacetate into phosphoenolpyruvate (PEP) while PPDK catalyses the conversion of pyruvate into PEP. GK, which catalyses the conversion of glycerol into glycerol 3-phosphate, was not found in our data. As *L. mexicana* is able to use glycerol, aspartate, and alanine to synthesize their storage carbohydrate mannogen, glycerol enters the gluconeogenesis pathway through GK, whereas aspartate and alanine enter through PEPCK and PPDK, respectively (Rodriguez-Contreras & Hamilton 2014). Furthermore, Rodriguez-Contreras & Hamilton (2014) showed that PEPCK was constitutively expressed in promastigotes, suggesting the importance of this enzyme in promastigote stage.

Compared with promastigotes, amastigotes have been previously shown to increase fatty acid β-oxidation and reduce glycolysis. This notion is in agreement with a previous report showing that amastigotes exhibit low rates of glucose uptake (Burchmore & Hart 1995). These metabolic adaptations are also in good agreement with previous reports (Opperdoes & Coombs 2007; Paape et al. 2008; Rosenzweig et al. 2008; McConville & Naderer 2011; Saunders et al. 2014; McConville et al. 2015). Fatty acid β-oxidation enzymes are reported to be highly expressed in amastigotes (Saunders et al. 2014). The increased of fatty acid

metabolism in amastigote suggest more efficient utilization of fatty acids as alternative carbon source. Contrary to promastigote, amastigote stage in the phagosome most probably feeds on fatty acids and amino acids as there are limited availability of glucose and other sugars in the phagosome (McConville et al. 2007). Additionally, our data showed amino acids metabolism was decreased in amastigote, which could affect protein and lipid biosynthesis. It is well established that *Leishmania* species are auxotrophic for several amino acids, thereby necessitating them to scavenge amino acids from the phagolysosome (McConville et al. 2007; Opperdoes & Coombs 2007). This could suggest the increase of amino acids degradation in amastigote. Recently, Saunders et al. (2014) reported that lesion-derived amastigotes have a similar metabolic profile to axenic amastigotes, thus indicating that the differences between axenic amastigotes and promastigotes should also reflect the parasite in their natural environment. Specifically, promastigotes exhibited high metabolic activity, with high rates of glucose and amino acid consumption and secretion of metabolic end-products, while amastigotes exhibited lower levels of catabolism of glucose and other potential carbon sources such as amino acid uptake as well as increased catabolism of fatty acids (Figure 3.28). This switch to a more economical metabolism in amastigotes has been termed the stringent response (Saunders et al. 2014; McConville et al. 2015).

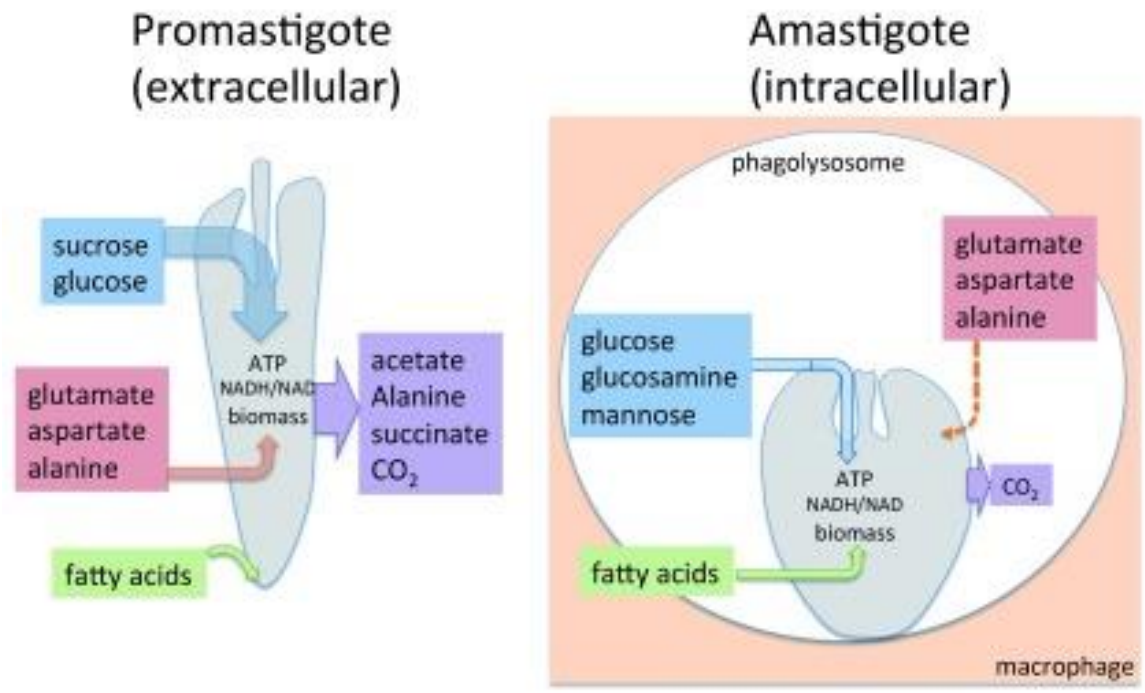

Figure 3.28: Intracellular amastigotes exhibit a stringent metabolic response.

The differentiation of *Leishmania* promastigotes to amastigotes is accompanied with major changes in central carbon metabolism. Promastigotes exhibit high rates of glucose and (non-essential) amino acid uptake as well as uptake of fatty acids (downward arrow). Amastigotes also preferentially use glucose as a carbon source. However, they exhibit much lower rates of sugar and amino acid uptake. Although amastigotes continue to take up essential amino acids but these amino acids were used mainly for protein synthesis. Amastigotes also actively catabolize fatty acids in the tricarboxylic acid (TCA) cycle, because of reduced glucose uptake. The downregulation of hexose/ amino acid uptake in amastigotes (stringent response) is due to differentiation and is associated with a reduced growth rate (adapted from McConville et al. 2015).

The pathway of glycolysis/ gluconeogenesis in figure 3.29 displayed a conspicuous presence of proteins identified in our data (bright green box). Figure 3.29 showed the glycolytic proteins that were upregulated in promastigote and amastigote stage.

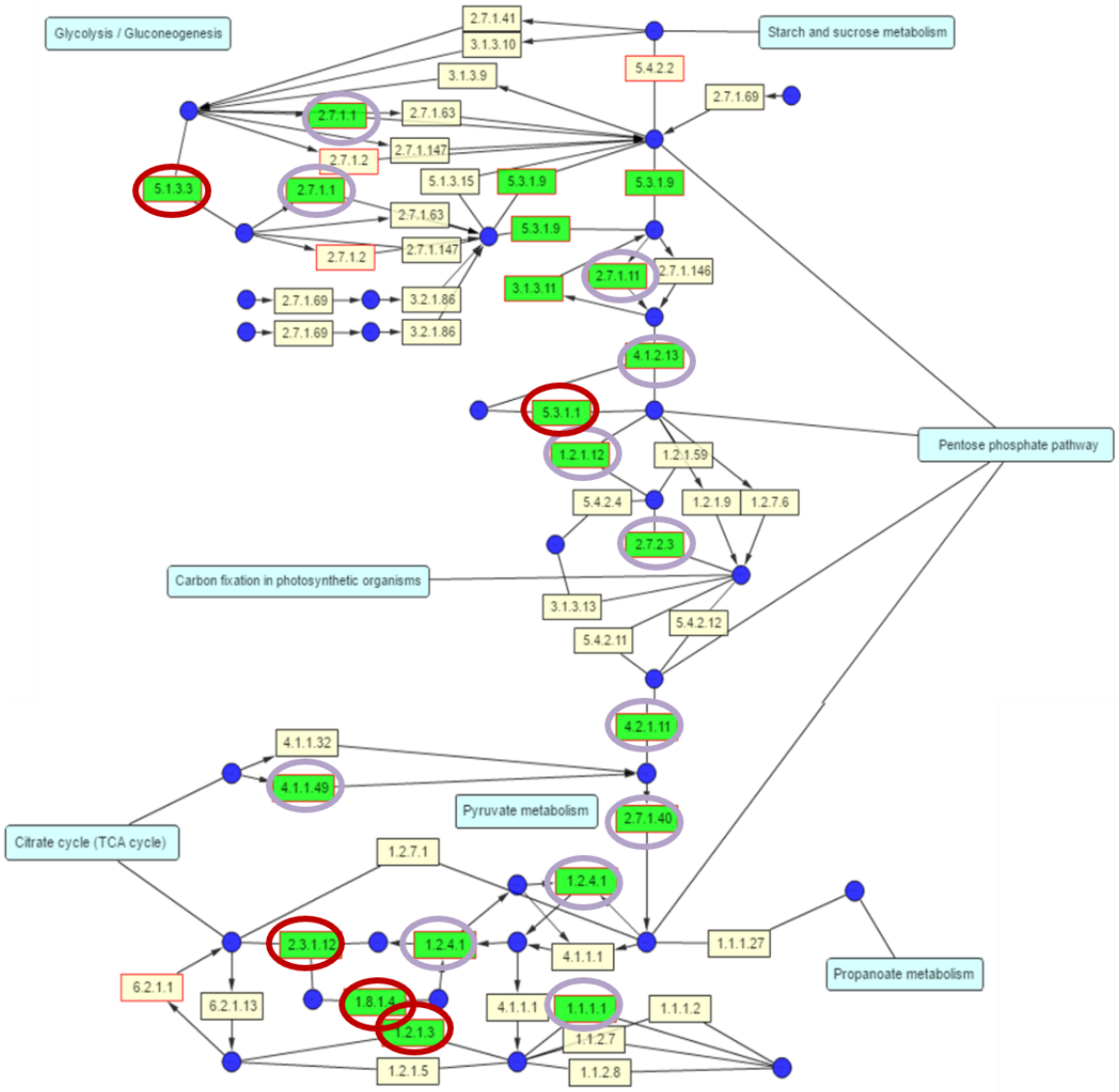

Figure 3.29: Diagram of glycolysis and gluconeogenesis pathway in *L. mexicana*.

The total proteins identified by Mascot were uploaded on TriTrypDB for functional analysis. The gene ID were transformed to pathways given an output of the list of pathways involve in *L. mexicana*. The diagram showed pathway of glycolysis/ gluconeogenesis involving starch and sucrose metabolism, pentose phosphate pathway, carbon fixation in photosynthetic organisms, TCA cycle, pyruvate metabolism and propanoate metabolism. The boxes with bright green colour represent proteins identified in our data. The red circles indicated proteins upregulated in promastigote, whereas the purple circles represented proteins upregulated in amastigote. Abbreviations: 5.1.3.3 – aldose 1-epimerase, 5.3.1.1 – triose-phosphate isomerase, 2.3.1.12 – dihydrolipoyllysine-residue acetyltransferase, 1.8.1.4 – dihydrolipoyldehydrogenase, 1.2.1.3 – aldehyde dehydrogenase, 2.7.1.1 – hexokinase, 2.7.1.11 – 6-phosphofructokinase, 4.1.1.13 – fructose-bisphosphate aldolase, 1.2.1.12 – glyceraldehyde-3-phosphate dehydrogenase, 2.7.2.3 – phosphoglycerate kinase, 4.2.1.11 – phosphopyruvate hydratase, 2.7.1.40 – pyruvate kinase, 4.1.1.49 – phosphoenolpyruvate carboxykinase, 1.2.4.1 – pyruvate dehydrogenase, 1.1.1.1 – alcohol dehydrogenase.

Figure 3.30 illustrated purine metabolism in *Leishmania* (KEGG) with proteins found in this study (bright green boxes). Specifically, we found proteins involved in alanine, aspartate, glutamate metabolism, histidine metabolism, riboflavin metabolism, arginine and proline metabolism and folate biosynthesis.

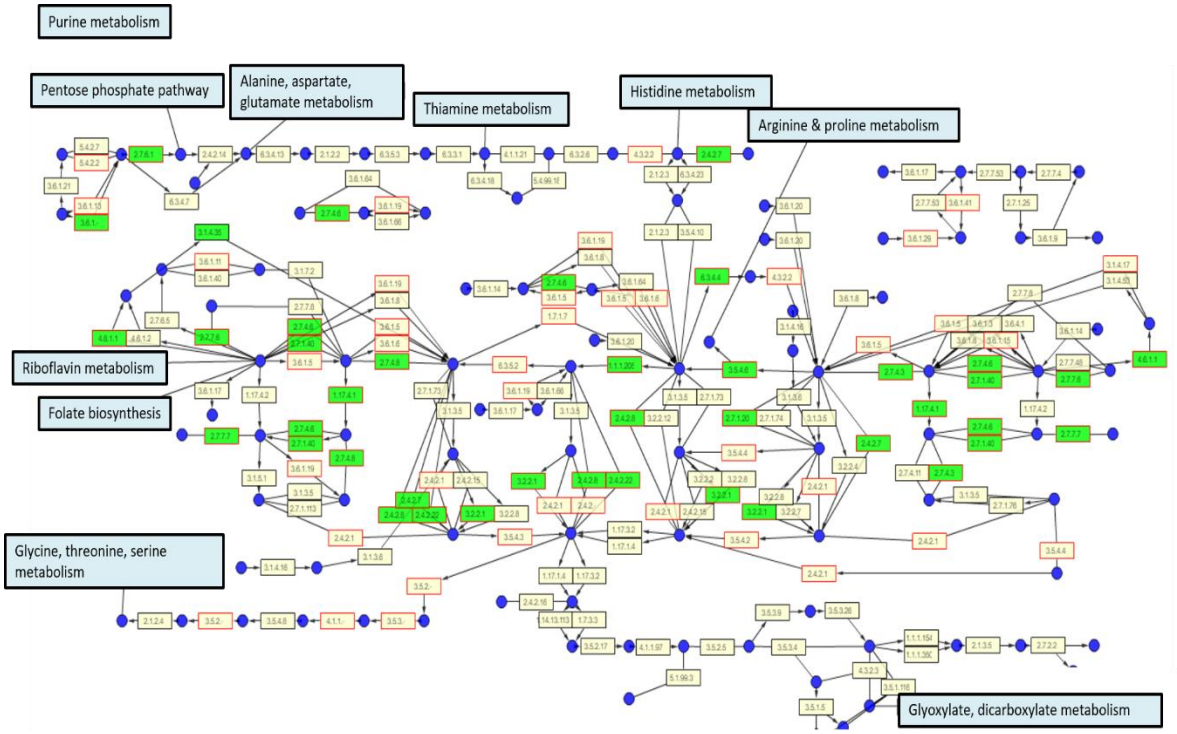

Figure 3.30: Diagram of purine metabolism pathway in *L. mexicana.*

The proteins identified by Mascot were uploaded on TriTrypDB for functional analysis. The gene ID were transformed to pathways given an output of the list of pathways involve in *L. mexicana*. The diagram showed pathway of purine metabolism. The boxes with bright green color represent proteins found in our data.

We also identified several proteins correlated with oxidative phosphorylation in promastigote including 2,4-dienoyl-coa reductase fadh1, 2-hydroxy-3-oxopropionate reductase, 6-phosphogluconate dehydrogenase and aldehyde dehydrogenase. In this pathway, cells use enzymes to oxidize nutrients in the mitochondria, thereby releasing energy which is used to reform ATP.

Several of the promastigote-enriched proteins in this study may have a role in flagellar function. Among the proteins are paraflagellar rod protein (PFR), dynein heavy chain protein, dynein light chain, beta-tubulin, centrin, kinesin, flagella connector protein, flagellar pocket cytoskeletal protein Bilbo 1 and flagellum targeting protein KHARON 1. The promastigote flagellum is important for motility and attachment within the sand fly gut (Cuvillier et al. 2003). Although many literatures reported that amastigotes are aflagellate, in fact they retain a short flagellum that extends to the neck of the flagellar pocket (Gluenz et al. 2010).

Various reports documented that *Leishmania* contain high abundance of cysteine proteases of the papain family (C1) and that the cysteine proteases show a high level of stage-regulated expression (Brooks et al. 2000; Alves et al. 2001; Denise et al. 2006). In *L. mexicana*, it was found that cysteine protease activity was considerably greater in the mammalian amastigote form than the promastigote forms that live in the sand fly vector (North & Coombs 1982). Several other proteins involved in proteolysis were also detected in our data including aminopeptidase and cathepsin L-like protease. The fact that amastigotes express more proteolytic proteins suggests that they might be important for survival of the parasite in the mammalian host.

3.5 Summary

Comparative analysis of proteins across *L. mexicana* promastigote and amastigote forms revealed that 542 are differentially expressed between promastigotes and axenic amastigotes. There were variations in the function of stage-regulated proteins that could reflect the differing challenges that they face in their habitat (Figure 3.31). The promastigote relies mostly on glycolysis and amino acid metabolism for energy production. A large proportion of proteins that were downregulated during differentiation to amastigotes were associated with glycolysis, gluconeogenesis and amino acid biosynthesis. Instead, amastigote use fatty acid ß-oxidation metabolism as carbon source, and this is reflected in our data. Proteins related to a motile flagellum are also down-regulated in amastigote. In contrast, proteins that were upregulated in amastigotes included cell surface proteins, peptidases, amino acids degradation proteins, and many uncharacterized genes. This study could complement present information on the differences of protein expression in different life cycle stage of *L. mexicana*.

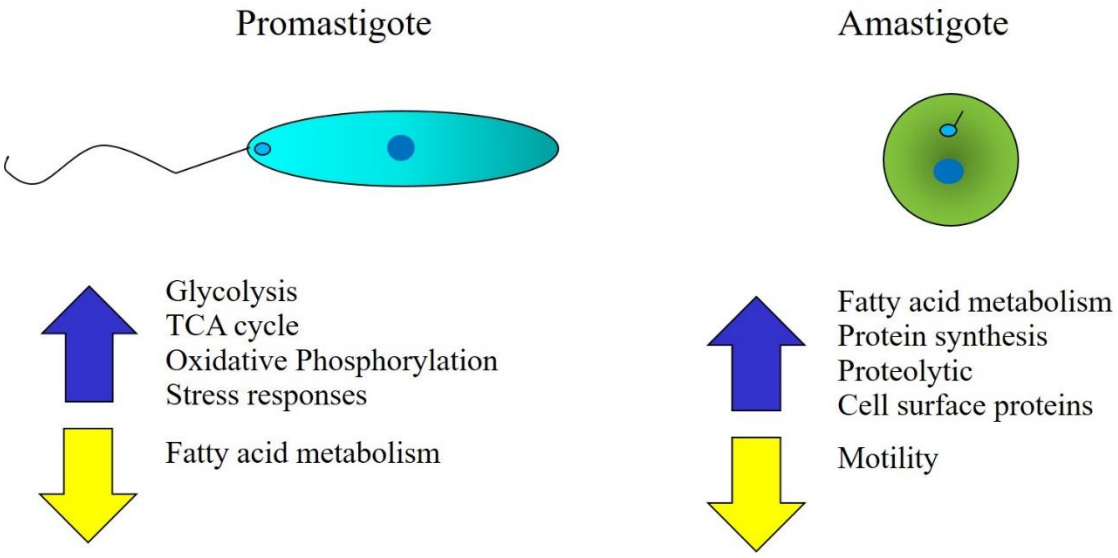

Figure 3.31: Summary of differentially regulated proteins between promastigote and amastigote.

Diagram showed the differences in proteins regulation between promastigote and amastigote.

CHAPTER 4

4 A quantitative proteome dynamic analysis of the macrophage in response to *L. mexicana*: Determination of newly synthesized proteins

4.1 Introduction

Infectious diseases such as leishmaniasis are one of the principal challenges in the world. The limitations with current treatments and the lack of vaccines mean that new treatments for leishmaniasis are urgently needed. However, the development of new chemotherapies requires a thorough understanding of the pathophysiology of infectious diseases, especially of the intricate interplay between the pathogen and the host during the progression of disease. *Leishmania* has developed a complex relationship with its host, where it exploits and subverts the host immune system to ensure its survival. The parasites are able to seek refuge in the host macrophages, utilizing available resources from the host and hiding from the host immune system for an indefinite period of time.

4.1.1 SILAC

In this post-genomic era, rapid developments in proteomics technologies have empowered researchers to obtain a wealth of information that relates the genomic blueprint to specific phenotypes. Moreover, the development of quantitative methods makes it possible to acquire information about differences between samples and to monitor temporal changes in the proteome by mass spectrometry. In this regard, SILAC is considered as a gold standard of quantitative proteomics. Cells are differentially labelled by cultivating them in the presence of normal or heavy isotope-substituted amino acids. As labelling does not affect chromatographic characteristics, co-eluting pairs of chemically equivalent peptides emerge in the same mass spectrum but can still be distinguished from each other due to the constant mass increment conferred by heavy isotopes. Hence, the ratio of intensities for such peptide pairs accurately reflects the

abundance ratio for the corresponding proteins (Mann 2014), particularly in steady-state protein levels (Figure 4.1 a).

4.1.2 Pulse-chase SILAC (pcSILAC) measures changes in protein production

Although standard quantitative proteomics techniques are essential to identify and measure variations in protein abundances, they are not adapted to determine if such variations are due to changes in synthesis rates, decay rates, or a combination of both. Nor are these techniques able to quantitate other properties such as turnover, which may give an indication of the intrinsic stability and half-life of proteins (Fierro-Monti et al. 2013). Pulse-chase SILAC (pcSILAC), a variant of the standard SILAC workflow, involves cultivating cells in media with either light or heavy-labelled amino acids, prior to perturbation accompanied by medium exchange (Figure 4.1 b). This can provide information on how proteins that are expressed under specific conditions affect the phenotype on a global scale. The advantage of pcSILAC over standard SILAC is that the quantitation is exclusively based on the newly synthesized protein amounts in a given time and consequently, in this project, allows delineation of a subset of proteins that show modulated expression upon infection. Understanding the changes in host macrophage protein expression that accompany *Leishmania* infection could shed light on the interactions between host and parasite and will present an additional research tool to investigate the pathways that determine the outcome of infection.

Dynamic proteome analysis has been pioneered by the Beynon group (Pratt et al. 2002; Beynon 2005; Doherty et al. 2005). The technique that they used consists of exchanging specific amino acid sources in media at a particular time point from light to heavy (or vice versa). As the cells grow in labelled medium, the original pool of unlabelled amino acids is diluted. Several doubling times (6-8) ensures that all proteins have been turned-over intracellularly and labelled. From the point of media exchange, all exogenously-acquired amino acids will be distinguishable from those acquired prior to media exchange. Providing the biological system under study is auxotrophic for the labelled amino acids employed, newly synthesized proteins will be distinct from those that were expressed prior to media exchange. Therefore, in principle, it is straightforward to determine protein turnover by looking at the changes of the precursor relative isotope abundance

(RIA) in the mass spectra over time, as all 'heavy' will gradually transition to all 'light' as protein turnover progresses (Claydon & Beynon 2012).

Protein biosynthesis consumes a high amount of energy during cellular proliferation. Translation by ribosomes is estimated to account for ~50% of the energy consumption of a rapidly growing bacterial cell, and ~30% of that for a differentiating mammalian cell (Russell & Cook 1995). The huge cost associated with protein synthesis makes it a key step for regulating diverse cellular functions (Li et al. 2015). Hence, understanding and determining how a cell allocates its synthesis capacity for each protein offers foundational information for systems biology. Methods to monitor protein synthesis rates at the global level have mainly relied on pulsed metabolic labelling followed by two-dimensional gel electrophoresis, or more recently by mass spectrometry (Schwanhäusser et al. 2009; Schwanhäusser et al. 2008).

SILAC has been extensively used in mammalian cells including the human monocytic leukaemia cell line THP-1 (Klegeris et al. 2008), human lymph node carcinoma of prostate LNCaP cell line (Piechura et al. 2012; Geiger et al. 2012), cervical carcinoma HeLa cells (Thiede et al. 2013; Geiger et al. 2012), embryonic kidney cells HEK293 (Geiger et al. 2012) and so on. On the other hand, pcSILAC labelling scheme has been applied in HeLa cells (Andersen et al. 2005), Jurkat T-lymphocytes (Fierro-Monti et al. 2013), bacteria Staphylococcus aureus (Schmidt et al. 2010) and human adenocarcinoma A549 cells (Doherty et al. 2009) for protein dynamic studies. In this work, we have applied pcSILAC strategy on THP-1. To date, there is no application of pcSILAC to investigate host responses towards *Leishmania* infection. Therefore, this is a very novel research. However, because of the large amount of data involved, interpretation of results is still a limiting factor. These includes the processing power to analyse the huge datasets that are generated using relevant bioinformatic tools, time acquired to analyse the data, and the requirement for skills in specific bioinformatic tools and approaches.

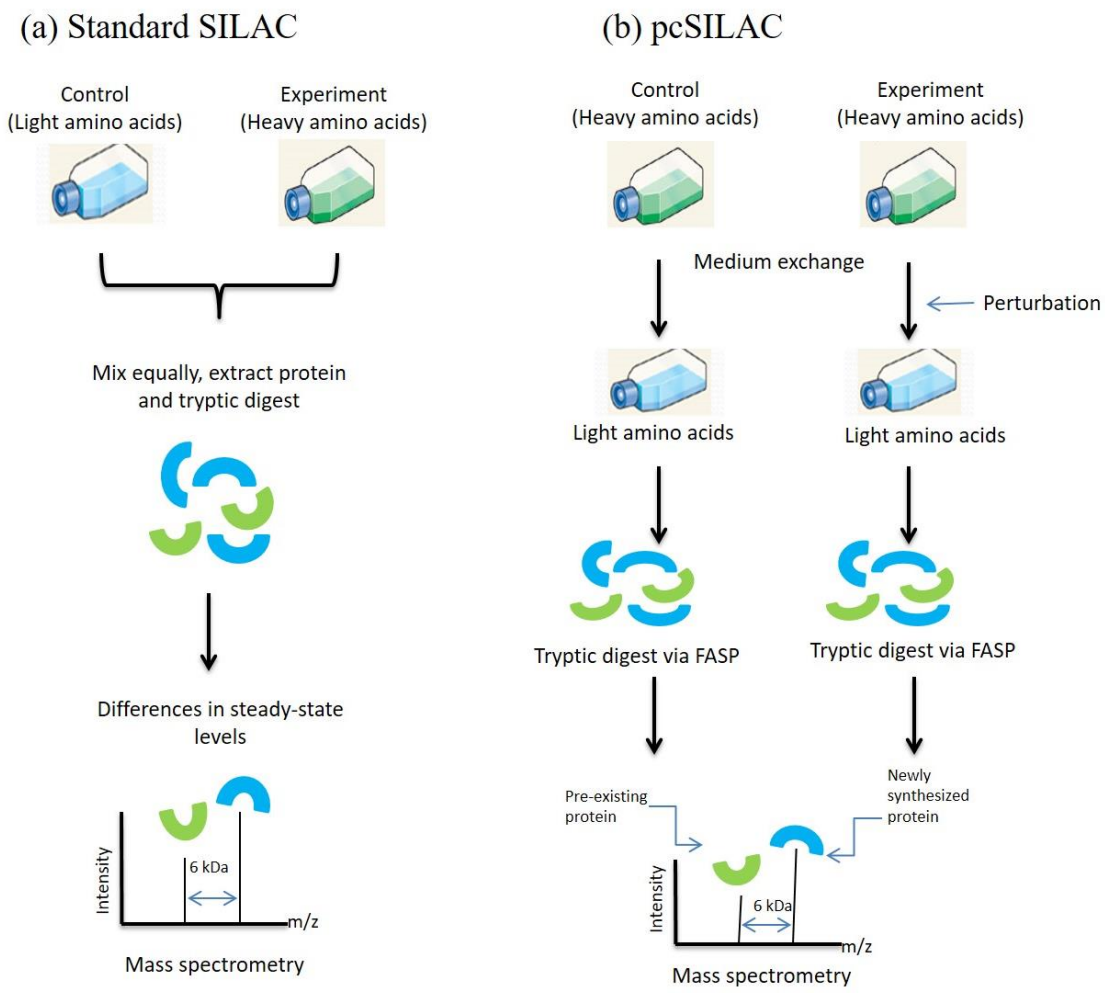

Figure 4.1: Workflow of standard SILAC and pulse-chase SILAC.

(a) Cells are grown in culture media that are identical with exception of certain amino acids. The "light" culture (L) contains all the amino acids in unlabelled form and the "heavy" culture (H) contains one or two amino acids in labelled form only. Cells from both cultures are mixed in a 1:1 ratio. The proteins of interest are extracted and digested with trypsin or LysC. The proteolytic cleavage creates pairs of peptides deriving from protein synthesised during culture in "light" and "heavy" media, differing by a molecular weight of 6 Da. The ratio of the amount of light and heavy peptides is determined by mass spectrometry. (b) In the pcSILAC method, cells are first cultivated in standard growth medium with "heavy" (H) amino acids. Concomitantly with differential treatment, cells are transferred to culture medium containing "light" (L) isotope-coded amino acids. Therefore, cells are 'chased' with L amino acids, thus all newly synthesized proteins will incorporate the L amino acids. Two cell populations are further processed separately and analysed by MS.

Substantial effort has focused on elucidating host gene expression profiling using different (murine and/or human) cell types and different species of *Leishmania* (Rodriguez et al. 2004; Menezes et al. 2013; Paape & Aebischer 2011; Li et al. 2012; Singh et al. 2015). This information provides key insights into an extensive modulation of protein function and contributes to a better understanding of the dynamics of protein expression following infection. It has been noted that transcriptome-based analysis has major limitations as it does not represent the

true effectors of cellular functions. In the present study, we have adopted a quantitative proteomics-based approach to gain insight into the reprogramming of the THP-1 cell line, an acute monocytic leukaemia-derived human cell line, infected with *L. mexicana* for 24 hours.

Several considerations have been undertaken for pcSILAC to determine protein turnover (Hinkson & Elias 2011):

1) Cells are auxotrophic for the amino acid used. This would minimise any dilution of the label by *de novo* synthesis.

2) The amino acids are highly abundant

3) The mass difference between the heavy and light labels must be at least 4 Da for optimal distinction between isotopic envelopes.

4) Minimal amino acid recycling. We ensure this by using dialyzed serum in the media and considered the dilution rates through cell growth.

5) Use compatible proteases for amino acid pair. For example, lysine and arginine pair are most suited to use trypsin, while lysine is compatible with endoproteinase Lys-C.

While chapter 3 elaborated on the differential stage-regulated proteomes of the parasite *Leishmania*, this chapter focuses on the establishment of pcSILAC as a tool to monitor protein expression with time, and to reveal host proteome changes in response to infection with *Leishmania*.

4.2 Aims

This study has produced a large volume of data. Therefore, we will divide the study into two chapters (chapter 4 and 5). The first part of the chapter describes the establishment of pcSILAC, a modified version of the classic SILAC approach, to investigate changes in protein expression in a macrophage cell line upon infection with *L. mexicana* as well as to derive protein synthesis rate. The workflow was developed by comparing protein expression in uninfected macrophages with expression in macrophages 24 h after *Leishmania* infection. Following this, mock-infected, 24 h infection data and 48 h infection data were used to analyse newly synthesized proteins. Another chapter (Chapter 5) extends this study to investigate protein degradation and turnover in response to *Leishmania* infection.

The aims of this study were to:

- Isolate metacyclic promastigotes for THP-1 infection
- Optimise THP-1 differentiation
- Enhance proteolysis of the samples in order to increase proteome coverage on MS.
- Establish pulse-chased SILAC approach as a new quantitative technique to investigate the proteome changes of THP-1 when infected with *L. mexicana* for 24 h, comparing with mock-infected THP-1.
- Extend the application of pulse-chase SILAC to investigate the proteome changes in the THP-1 macrophage cell line when infected with *L. mexicana* with additional time-course infection of 48 h.
- Undertake a statistical analysis of the protein modulations observed.
- Investigate newly synthesized proteins and calculate relative protein synthesis rate.

Investigation of this parasite's interaction with the host macrophage may lead to a better understanding of how the macrophage proteome changes in response to

Leishmania infection, thus, assisting in the development of new chemotherapeutic strategies against leishmaniasis.

4.3 Results

4.3.1 THP-1 differentiation and infection assays

The human monocytic cell line, THP-1, has been used as a model host macrophage for *Leishmania* for over two decades (Gebre-Hiwot et al. 1992; Tsuchiya et al. 1982). *In vitro* cultured THP-1 monocytes must be induced into adherent macrophage-like cells with chemical agents such as PMA, 1,25-dihydroxyvitamin D3, retinoic acid or DMSO (Tsuchiya et al. 1982; Daigneault et al. 2010).

PMA has been used at concentrations of 10 – 400 ng/ml, regardless of whether this will affect the regulation of some genes (Daigneault et al. 2010). At the outset of this study, we tested various concentrations of PMA. We first tried using PMA at 60 ng/ml (0.1 μM) and 300 ng/ml (0.5 μM) incubated for 24 h. However, cell attachment after 24 h incubation proved to be unstable as the cells were easily detached during washing. We then tried incubating the cells with PMA at the same concentration but for 48 h. Under these conditions, we observed approximately 98% of THP-1 cells adhered strongly to tissue culture flask/dish even after 3 washes with PBS, indicating complete differentiation, as illustrated in Figure 4.2. Cells attachment for each optimisation was determined by counting the unattached cells after washing (Figure 4.3). A lower concentration of PMA is preferable to limit the effect on gene regulation (Daigneault et al. 2010), so we selected 0.1 μM PMA for induction over a 48 h period. Cell viability was determined to be >97% by the Trypan blue dye exclusion method. For large scale experiments, we compared non-treated Corning flask and Nuclon Delta treated-surface flasks, determining that the latter was the best option (by observation), as it enhance cell attachment and differentiation.

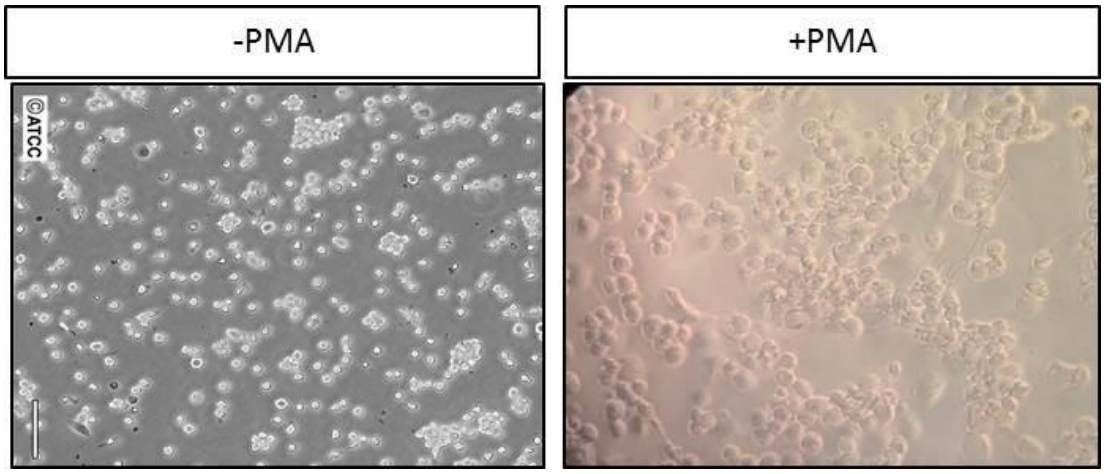

Figure 4.2: Differentiation of THP-1 cells with PMA.

THP-1 cells were cultured in media containing 60 ng/ml of PMA and incubated at 37°C for 48 hours. After that, cells were washed with PBS three times. At this point, 98% of the cells were differentiated and adhered to the flask. Picture without PMA (on the right) was taken from ATCC website.

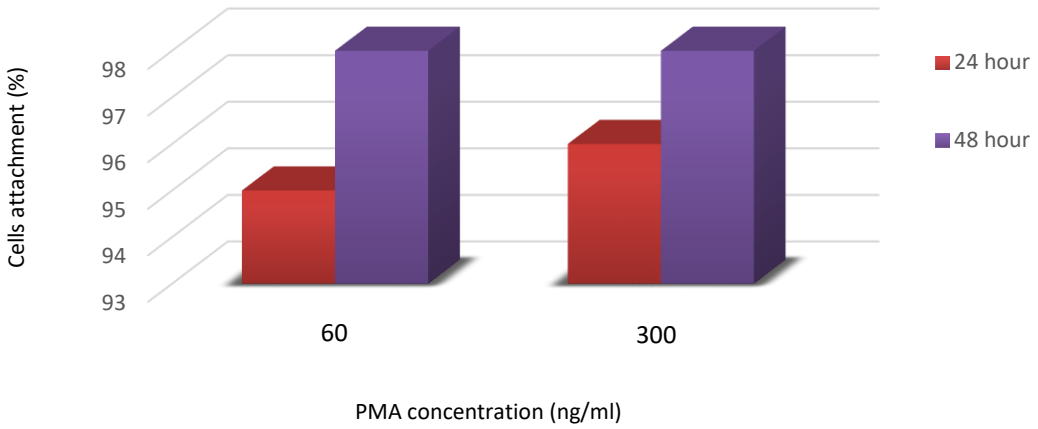

Figure 4.3: Optimisations of THP-1 activation by PMA.

THP-1 cells were induced with PMA with different concentrations of PMA (60 and 300 ng/ml) and different incubation time (24 and 48 hour) to obtain better differentiation.

Following differentiation, the cells stop dividing and adhere to the base of the tissue culture with a macrophage-like morphology. Induced-THP-1 were infected with *L. mexicana* and observed by microscopy. Figure 4.4 depicts a microscopic view of the THP-1 infected with *L. mexicana*. Figure 4.5 shows an example of a fluorescent image of infected THP-1, counted using ImageJ software (http://rsb.info.nih.gov/ij/download.html). Infections were tested several times using both axenic amastigotes and metacyclic promastigotes. Several conditions (macrophage:parasites ratios and period of incubations) were tested to find the

optimal and most reproducible infection protocol. We tested 1:5, 1:8 and 1:10 ratios incubated at 37°C for 6 h, 24 h and 48 h. Cells were washed several times to ensure complete removal of non-internalized parasites before staining the cells with DAPI or Giemsa. Both macrophage nuclei and intracellular *Leishmania* nuclei with kinetoplast DNA were observed under the fluorescent microscope. Uninfected THP-1 was used as a control. The ImageJ software was used to analyse these images.

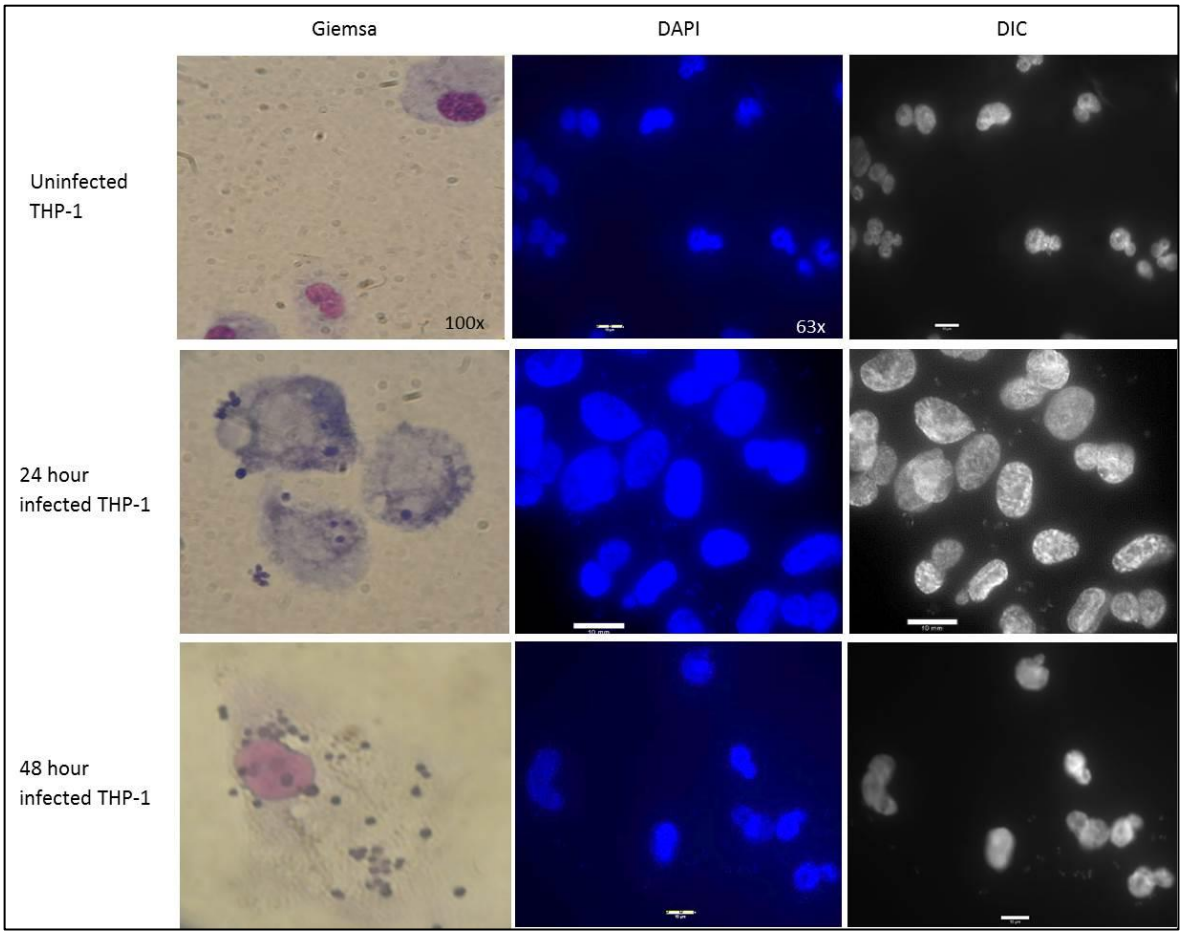

Figure 4.4: Microscopic view of PMA-differentiated THP-1 macrophages uninfected and infected with *L. mexicana*.

Differentiated THP-1 were incubated with parasites at a ratio of 1:8 for 24 h and 48 h. Giemsa and DAPI staining were performed to determine the infectivity. Cells were imaged at 63×, scale bar shows 20 µm.

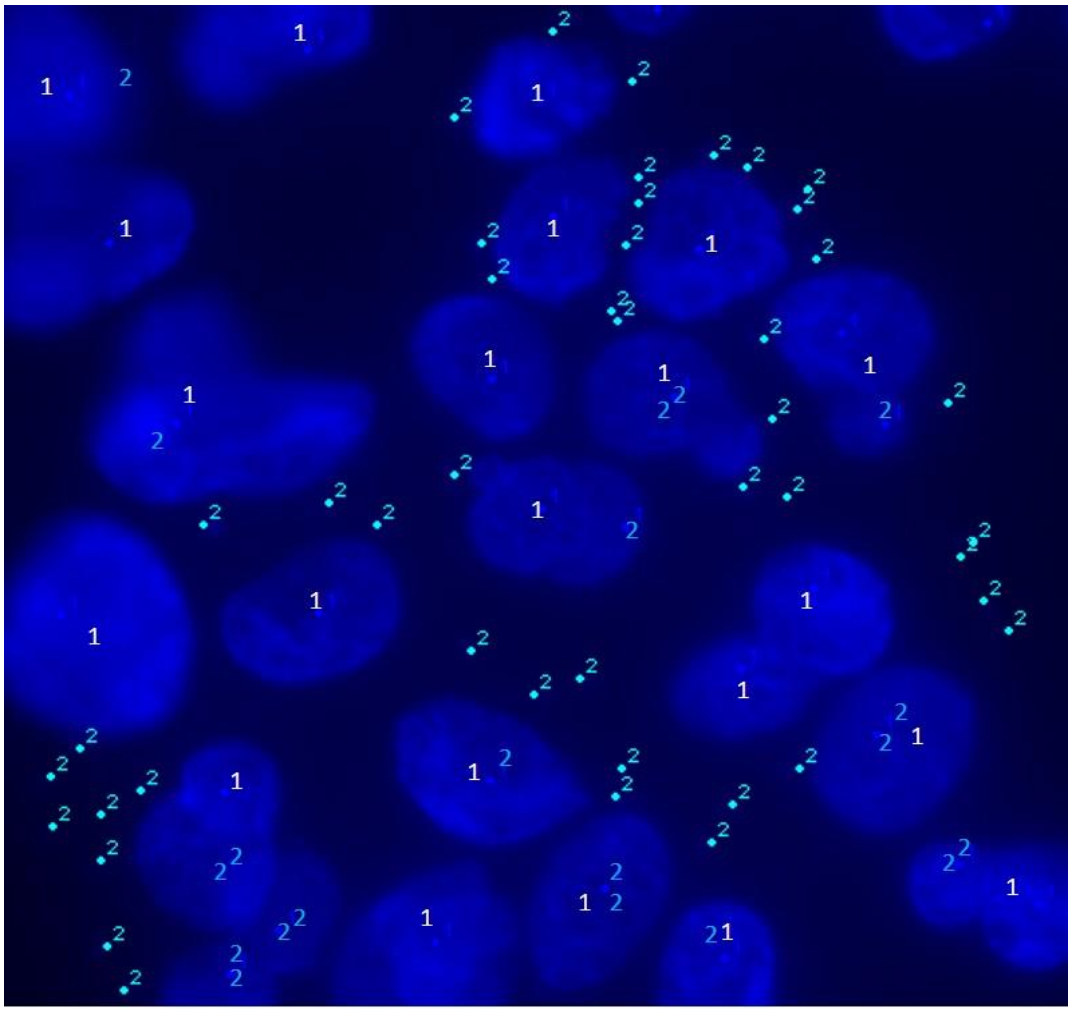

Figure 4.5: Fluorescent (DAPI) image of a differentiated THP-1 cell infected in vitro with *L. mexicana* amastigotes.

Differential counting of THP-1 cell nuclei and parasite nuclei was performed by ImageJ. Cell counter type 1 was selected for THP-1 cell nuclei and cell counter type 2 was selected for parasite nuclei. Differential counting was done for at least 200 THP-1 cell nuclei. Cells were imaged at 63x. Legend: 1 – THP-1 nuclei, 2 – parasite nuclei.

Figure 4.6 shows the differential infectivity in THP-1 cells at different macrophage:parasites ratios and different period of incubations. Results were quantified as percentage of infected THP-1 cells and were mean of triplicates. We examined the effect of axenic amastigotes and metacyclic promastigotes, that were enriched from a mixed culture of procyclic and metacyclic promastigotes by Ficoll density gradient centrifugation. For both axenic amastigotes and metacyclic promastigotes, a ratio of 10:1 and incubation for 24 h yielded optimum and reproducible infection rate at approximately 90% (89.7% for axenic amastigotes and 91.7% for metacyclic promastigotes). The average number of amastigotes in each infected macrophage was 17±6 (on 100 macrophages). The infectivity rate for THP-1 infected with *L. mexicana* for 48 h was 93% (Figure 4.7). Based on these

results, subsequent experiments were done using metacyclic promastigotes instead of amastigotes, as we elected to investigate the response of the macrophage to infection by promastigotes. In addition, we observed infected THP-1 cultures for 7 days. After 7 days, the parasite burden increased markedly and lysis of the host cells occurred progressively (by observation, result not shown).

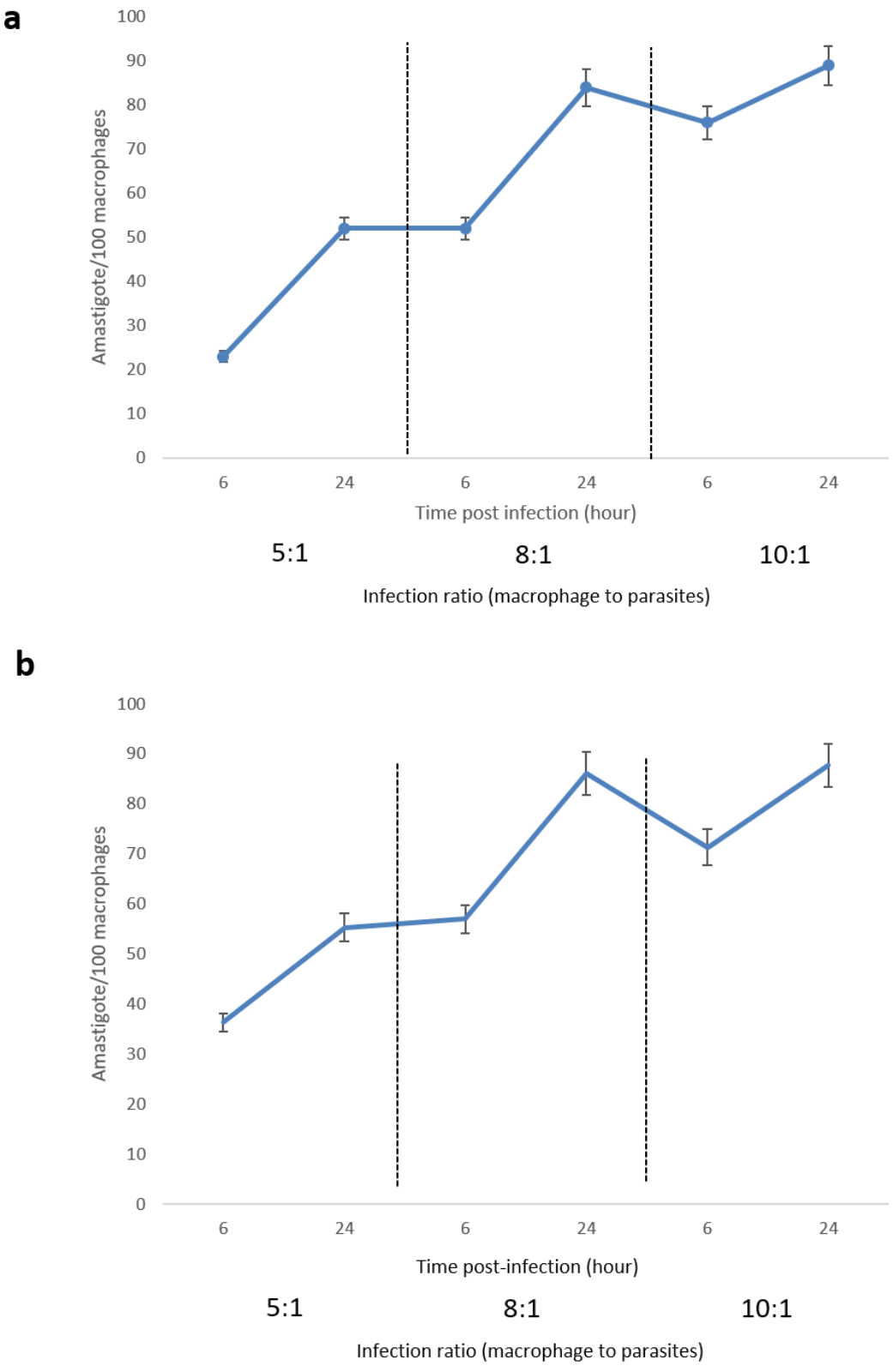

Figure 4.6: Time kinetics of phorbol 12-myristate 7-acetate (PMA)-treated adherent THP-1 cell infection by *L. mexicana*.

Differentiated THP-1 were incubated on LabTek slides with parasites at a ratio of 5:1, 8:1 and 10:1 for 6 h and 24 h. Infected macrophages were counted for every 100 macrophages to obtain infection rate. (a) Infection with axenic amastigotes obtained from transformed promastigotes in Schneider Drosophilla medium. (b) Infection with metacyclic promastigotes obtained from stationary phase of parasites culture and separated through Ficoll gradient.

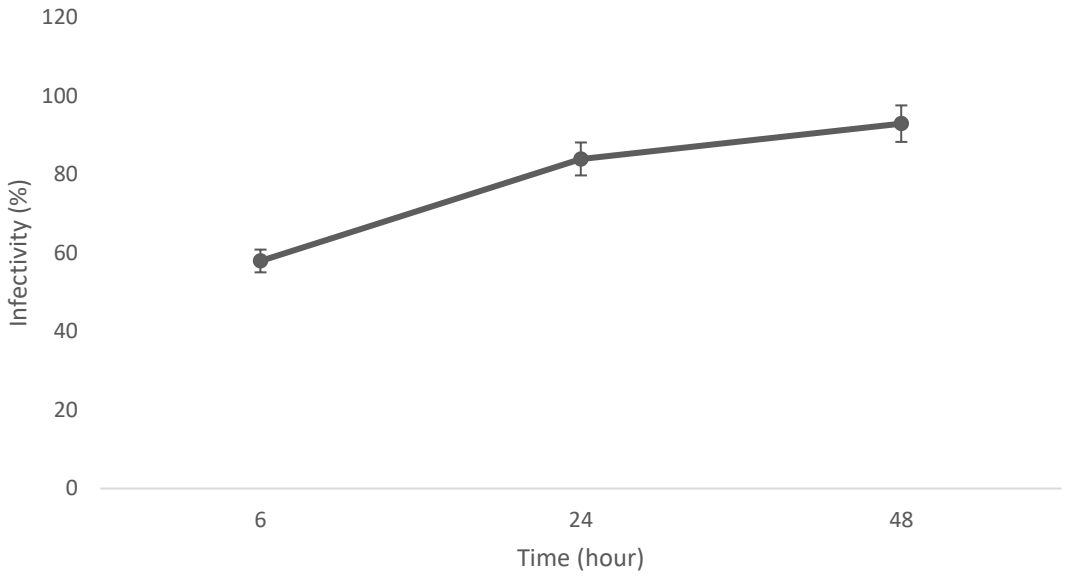

Figure 4.7: Time kinetics of PMA-treated adherent THP-1 cell infection by *L. mexicana*.

Differentiated THP-1 were incubated on LabTek slides with parasites at a ratio of 1:8 for 6 h, 24 h and 48 h. Non-internalized parasites were washed away with PBS after 6 h. Cell were fixed and stained with Giemsa at each time point. The proportion of infected macrophages was assessed by microscopy. Error bar represented mean ± standard error from triplicates.

Additionally, the method for releasing adhered and infected THP-1 cells into the medium was important for the integrity of the cells. Thus, we experimented with different approaches such as the use of syringe, cell scraper and the addition of EDTA. It was observed that the use of cell scraper after cells were kept in 4°C for 15 min was the best approach to harvest high volume of cells.

4.3.2 Establishment of pulse-chase SILAC for global assessment of infection-regulated proteins

There are several prerequisites to a SILAC approach. First, the cells to be labelled must be auxotrophic for the labelled amino acids. In this case, we used arginine and lysine. Second, cells need to be able to grow in SILAC-compatible media, which must lack unlabelled sources of these amino acids. To ensure that cells only incorporate the labelled amino acids into their proteome, cells to be heavy labelled are grown with dialyzed serum (dFCS) since standard FCS contains unlabelled (light) amino acids. Some cell types require low molecular mass growth factors that are not present in dialyzed serum (Mann 2006). It is therefore imperative to do a preliminary test to monitor the growth of the cells in the SILAC media for certain amount of time. Figure 4.8, shows that THP-1 cells cultivated

in SILAC media grow at approximately the same rate as in normal RPMI media. Doubling time for THP-1 grown in RPMI 1640 media containing standard FCS is 19 h whereas for THP-I grown with dFCS it is 20.4 h.

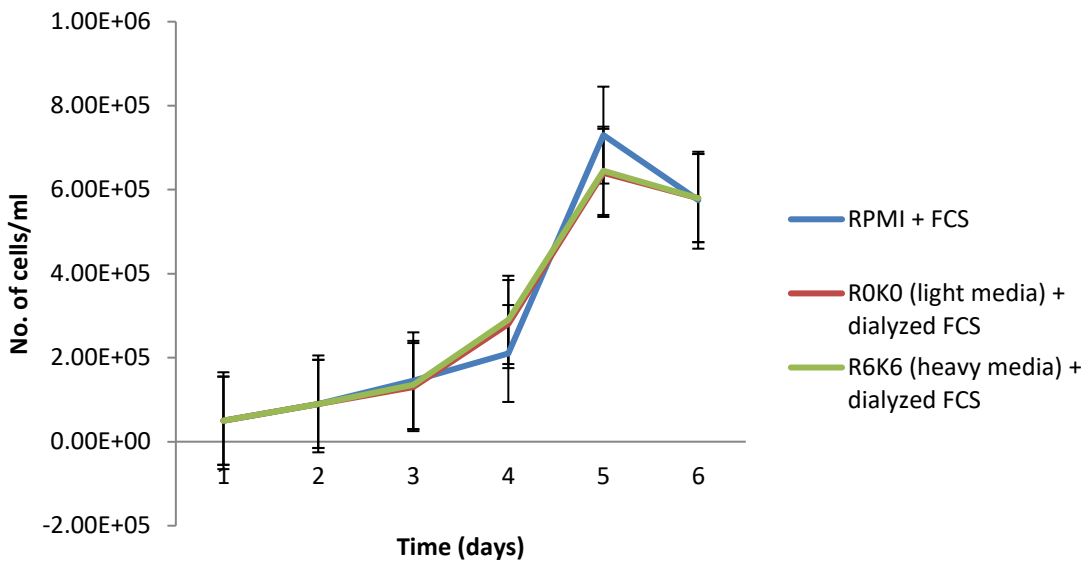

Figure 4.8: Growth curve analysis of THP-1 grown in normal RPMI media and SILAC media.

A culture was initiated at 1 x 10^5 cells/ml for all conditions and samples taken on 6 consecutive days for cell counting. Cells were fixed in 2% formaldehyde/PBS and counted on Neubauer haemocytometer.

Third, the incorporation of isotopically labelled amino acids should approach 100%, meaning that the isotopes are almost fully incorporated into the cells. This is to obtain clear discrimination of the signal originating from each sample. Thus, cultivating the cells in SILAC media for at least 6 doubling time (in our case, 8 doubling times) is obligatory. The level of incorporation of stable isotope-labelled amino acids in the cells was assessed by fractionating using SDS–PAGE followed by tryptic digestion. Proteomic analyses were performed using LTQ-Velos Orbitrap mass spectrometer and the data were processed by MaxQuant. MS data showed that the level of incorporation of stable isotope labelled amino acids in the THP-1 cells was high enough to proceed with SILAC experiments (Figure 4.9). We did not detect any significant arginine to proline transition in THP-1 cells. Labelling efficiency was calculated using formula given in 2.6.2 and it was over 99%. Moreover, we analysed the spectra by the SeeMS tool from ProteoWizard 3.0.9

package, to confirm presence of heavy and light-labelled SILAC pairs (example in Figure 4.10).

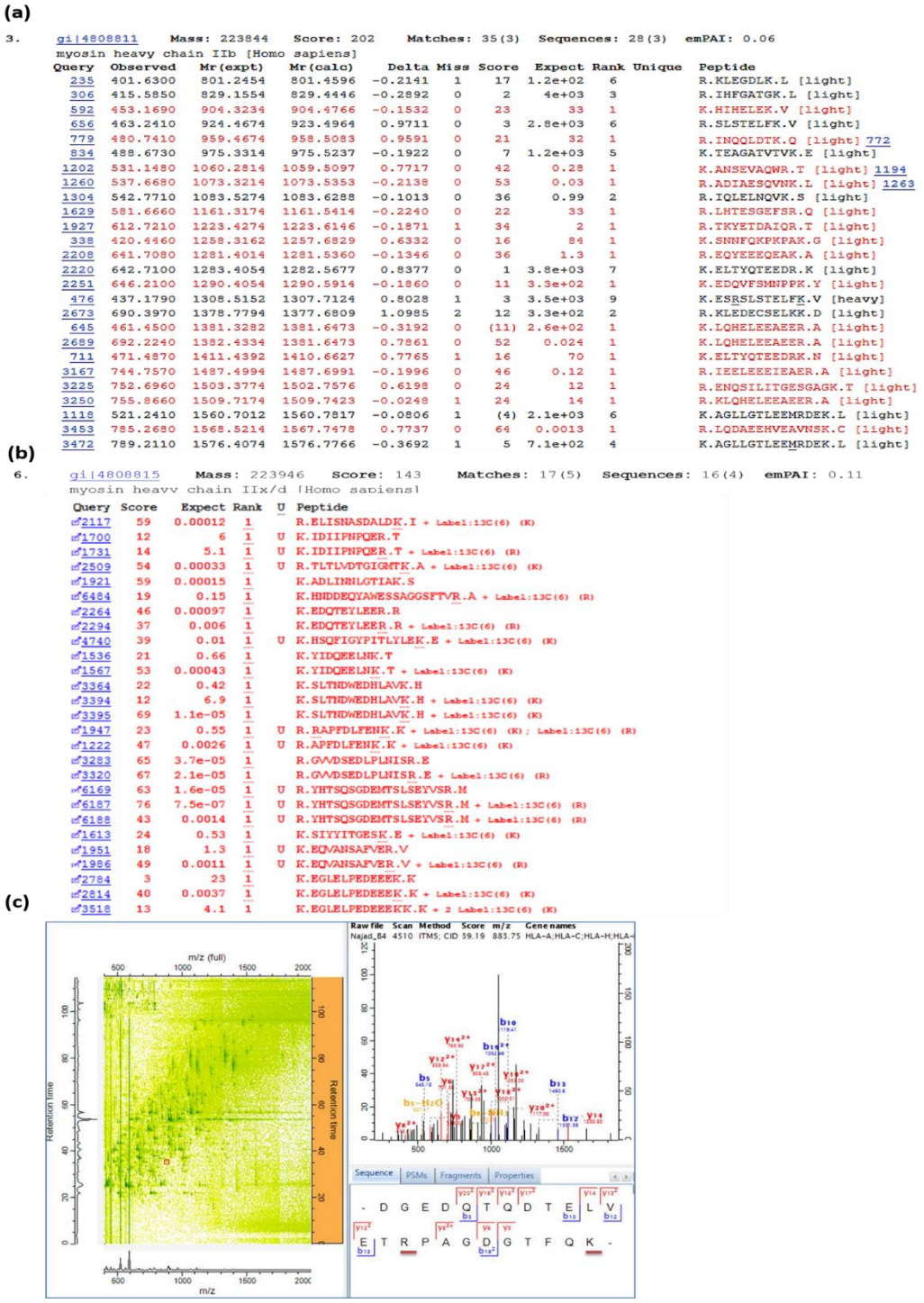

Figure 4.9: Partial peptide summary of myosin heavy chain (*Homo sapiens*) identified as protein hit #3 and #6 in THP-1 uninfected sample.

(a) The peptide sequences from samples that was cultivated in heavy SILAC medium for 1 cell doubling showed all peptides were still labelled with ^{12}C-R and ^{12}C-K. (b) After 8 cell doublings, cells were fractionated on SDS-PAGE, gel-digested and subjected to MS. The peptide sequences showed the modifications occurred, in this case, labelling with heavy ^{13}C-R and ^{13}C-K, indicating high heavy amino acids incorporation into the cells. (c) MaxQuant viewer output showing the MS/MS spectrum with labelling of K and R.

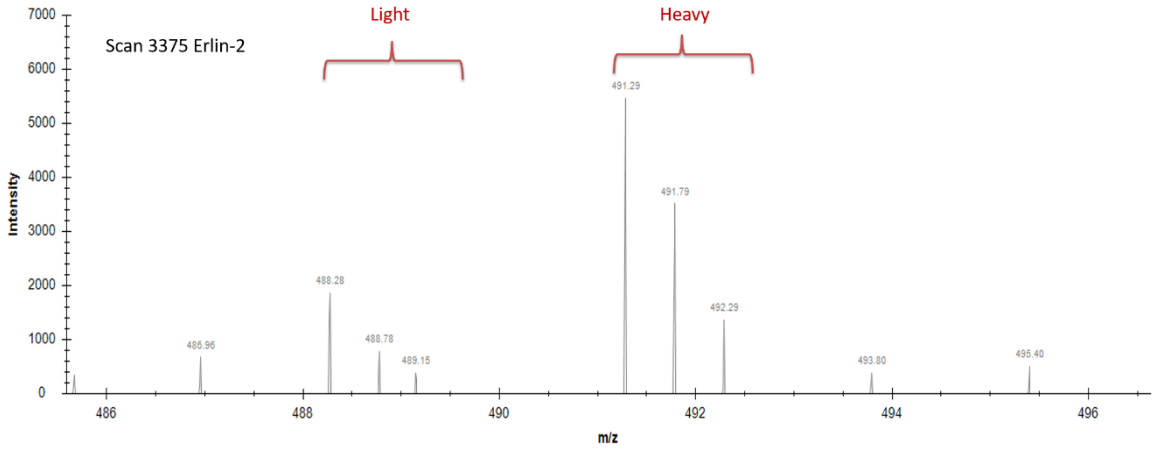

Figure 4.10: MS/MS spectra of tryptic peptides showing SILAC pair of heavy and light.

Raw file generated by Orbitrap Velos MS was analysed by SeeMS tool (included in ProteoWizard 3.0.9 package). Scan 3375 belonging to Erlin-2 showed SILAC pair containing light and heavy spectra.

After maintenance in SILAC culture media for at least the period required to achieve better than 99% labelling, THP-1 were induced with PMA to become macrophage-like cells. At this stage, heavy SILAC medium was exchanged to light SILAC medium (RPMI 1640 containing ^{12}C-Arg and ^{12}C-Lys isotope) and the cells were infected with metacyclic promastigotes (1:8) for 24 h and 48 h. In parallel, mock-infected THP-1 were also treated the same way but without infection, to serve as a control. Sample preparation optimisations were also applied as described in chapter 3 (section 3.3.3). During this incubation phase, all newly-synthesized proteins should incorporate light-labelled lysine and arginine. Subsequently, the uninfected and infected cells were harvested by scraping the adhered cells and cell lysis was performed followed by MS. This project produced 72 LC/MS raw files from at least 6 SILAC experiments consisting of 2 sample groups (uninfected and 24 h-infected). Each experiment included 3 biological replicates. For quality control, the protein lysates were analysed on Amazon Speed ion trap 1D-LCMS/MS. We tested different parameters for Filter-Assisted Sample Preparation (described in Table 4.1) and found that a trypsin to protein ratio of 1:50 and elution with ACN without desalting gave the best protein identification. For 2-D LC/MS, each replicate has 12 fractions. These files were analysed separately and/or together by the MaxQuant software using the Andromeda search engine.

Table 4.1: Analysis of uninfected THP-1 lysate processed by FASP with different parameters.

Lysates (n=1) were prepared using SDT buffer with 100 µg/ml of Leupeptin, 500 µg/ml of Pefabloc, 2 mM of 1,10-Phenanthroline, 10 µg/ml of Pepstatin A and 50 µg/ml of E-64. Then, the lysates were subjected to FASP for protein digestion. Peptides were run on Amazon Speed ion trap MS/MS.

Digestion enzyme	*Enzyme:Protein ratio*	*Elution buffer*	*Lysates quantity (µg)*	*Clean-up method*	*Proteins identified*
Trypsin	1:100	NaCl	50	*Desalt	240
Trypsin	1:100	NaCl	100	*Desalt	595
Trypsin and Lys-C	1:100	NaCl	50	*Desalt	203
Trypsin	1:100	ACN	100	None	947
Trypsin	1:50	ACN	100	None	1206

*Desalting was done on SPE cartridge

Three biological replicates for both uninfected and 24 hpi THP-1 were run on 1-D LC/MS and analysed together on MaxQuant before being evaluated in Perseus for quantification. As the range of the expression values can vary more than 10-fold, the expression values were Log transformed to facilitate the calculation of the protein expression fold change. The Log transformation of the expression values create a pool of "NaN" (Non-Assigned Number, non-quantified values) values, which correspond to expression values originally equal to zero, when one of the SILAC pairs were not detected by the mass spectrometer. Non-quantified values also arise when the SILAC pairs ratio does not met the minimum ratio for quantification threshold (in this case it is set at 2) or the peak intensities are below the instrument detection level. Figure 4.11 (a and b) shows a total of 732 proteins that were identified in uninfected cells (in all three replicates) and different numbers of proteins were quantified (having L/H ratios) in each replicate (80 proteins in Control-1, 213 proteins in Control-2, 90 proteins in Control-3). Only 47 proteins were quantified in all three replicates. Whereas, 695 proteins were identified in infected samples but only 7, 20 and 558 proteins were quantified in each biological replicate, respectively (Figure 4.11 d and e). Again, for this analysis, the median-normalized data of all quantified proteins were considered. We first inspected the reproducibility of the SILAC protein quantification between these replicates and found an average Pearson correlation coefficient of 0.76 for uninfected and 0.5 for 24 hpi THP-1. From these data, it is evident that 1-D LC/MS did not yield high reproducibility between replicates. Furthermore, the reproducibility of quantified protein in 24 hpi was low in two of the replicates.

This might be due to the low intensity of H or L label that could not be detected by MS.

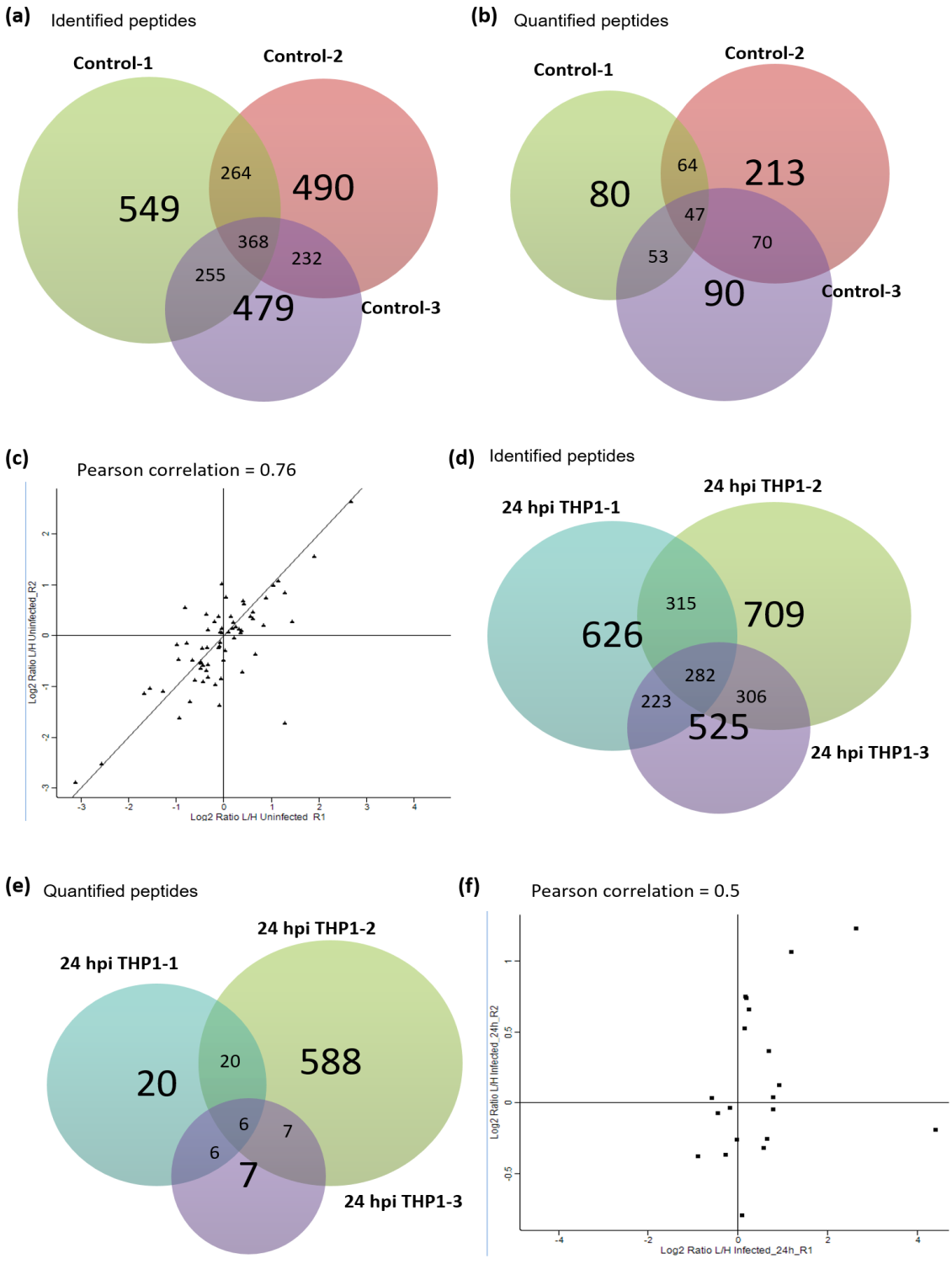

Figure 4.11: 1D-LCMS/MS data analysis from biological replicates of uninfected and 24 hpi THP-1.

Digested peptides were run on the Orbitrap Velos instrument. Thermo raw files of uninfected and 24 h infection (n=3, biological replicates) were analysed on MaxQuant and Perseus for quantitative analysis. (a) A total of 778 proteins were found in uninfected sample. (b) Venn Diagram shows that out of 778 proteins found in uninfected sample, 213 proteins were quantified in replicate_1, 80 in replicate_2 and 90 in replicate_3. (c) Pearson correlation of 3 biological replicates was 0.76,

indicating good reproducibility between replicates (close to 1). (d) A total of 724 proteins were found 24 h infected sample. (e) Venn Diagram shows that out of 724 proteins found in 24 h infected sample, 558 proteins were quantified in replicate_1, 20 in replicate_2 and 7 in replicate_3. (f) Pearson correlation of 3 biological replicates was 0.5, indicating the reproducibility between replicates was not good.

Subsequently, we moved on to 2-D LC/MS in order to increase proteome coverage as this method enhances the identification of lower abundance proteins by increasing the separation of peptides. Combined analysis of the triplicates of uninfected THP-1 together, using a peptide and protein FDR of 1%, yielded 1472 identified proteins and 650 proteins quantified in one of the replicates. The highest Andromeda score of identified proteins were 323, the average number of peptides per protein was 13 (the highest number of peptides per protein was 62, giving to 80% sequence coverage). Andromeda is a novel peptide search engine using a probabilistic scoring model of peptide−spectrum matches. This score measures how well an acquired spectrum matches the theoretical fragment masses. High Andromeda score cutoff of 100 indicates very high spectral quality (Cox et al. 2011). Depicted in Figure 4.12 are the proteins detected in each biological replicate of uninfected group (a) as well as scatter plot (b), heat map (c) and profile plot (d) analysis. Protein expression was comparable between replicates, as shown in the heat map and profile plot. A similar analysis on 24 hpi THP-1 was performed to assess the reproducibility of the replicates. Biological replicates of 24 hpi THP-1 were analysed together on MaxQuant. The total number of proteins detected was 1653 with 739 proteins quantified in one of them. In Figure 4.13, the Venn diagram depicts the number of proteins detected in each replicate (a), the multiscatter plot shows Pearson correlation coefficient for all replicates (b), and the heat map (c) and the profile plot (d) show that expression between replicates was similar. These two figures clearly show that the proteomic profiles of biological replicates of uninfected and 24 hpi THP-1 were quantitatively similar. More than 50% of the proteins were identified by 2D-LC/MS compared to 1D-LC/MS. These data clearly showed that 2D-LC/MS gave better proteome coverage and yielded a higher number of identified and quantified proteins compared to 1-D LC/MS as it allows the separation and characterisation of peptides derived from less abundant proteins.

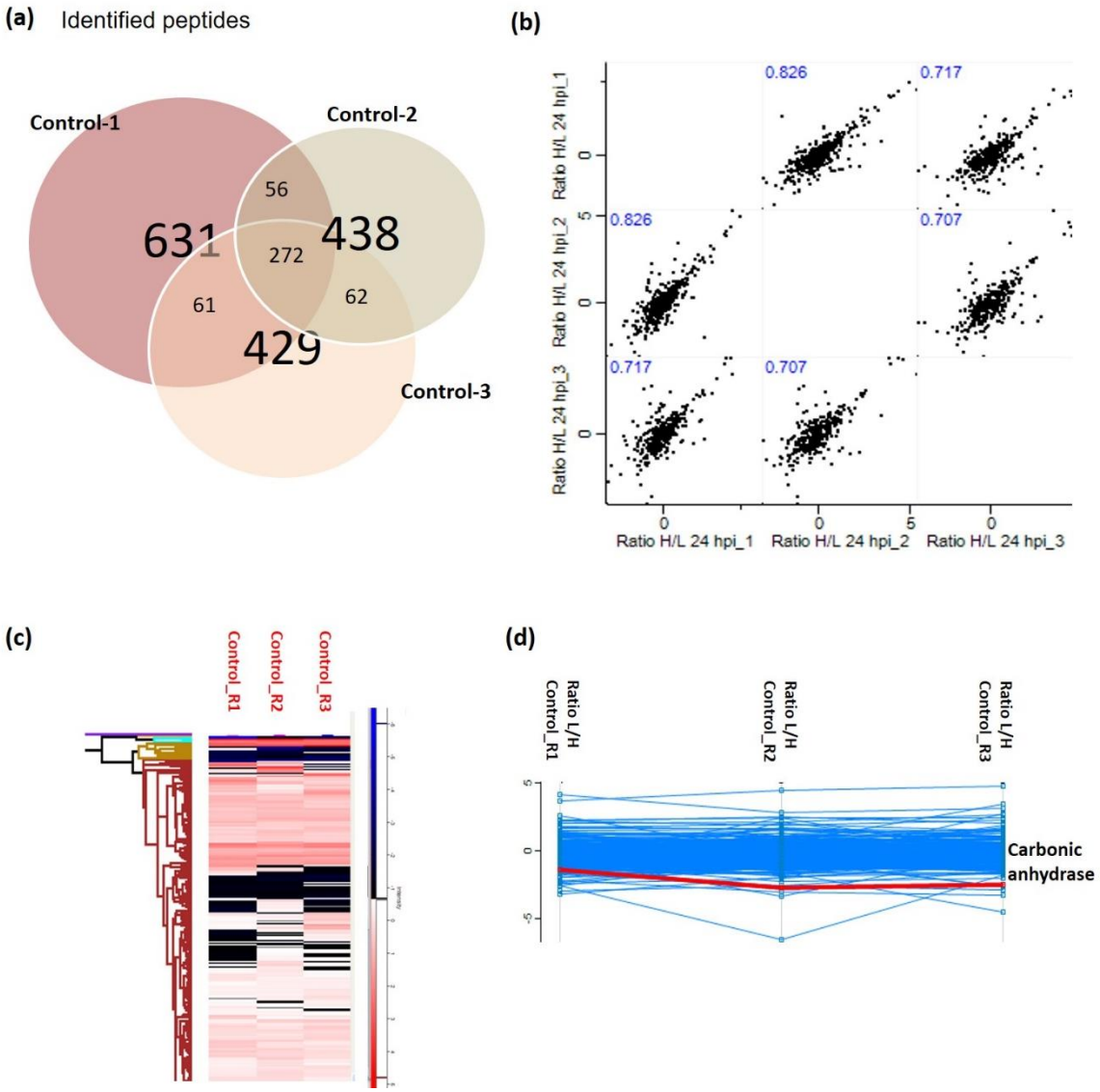

Figure 4.12: 2D-LCMS/MS profiles from biological replicates of uninfected THP-1.

Digested peptides were subjected to SCX and RP separation on the Orbitrap Velos MS instrument. Thermo raw files of uninfected (n=3, biological replicates) were analysed on MaxQuant and Perseus for quantitative analysis. (a) Venn diagram showing the number of proteins detected in each replicate. (b) Multiscatter plot with Pearson correlation values (blue font) of near 1 indicates good correlation between replicates. (c) Heat map distribution of protein expressions in all replicates shows similar pattern. (d) Profile plot of protein expression with carbonic anhydrase (red) as example shows similar pattern.

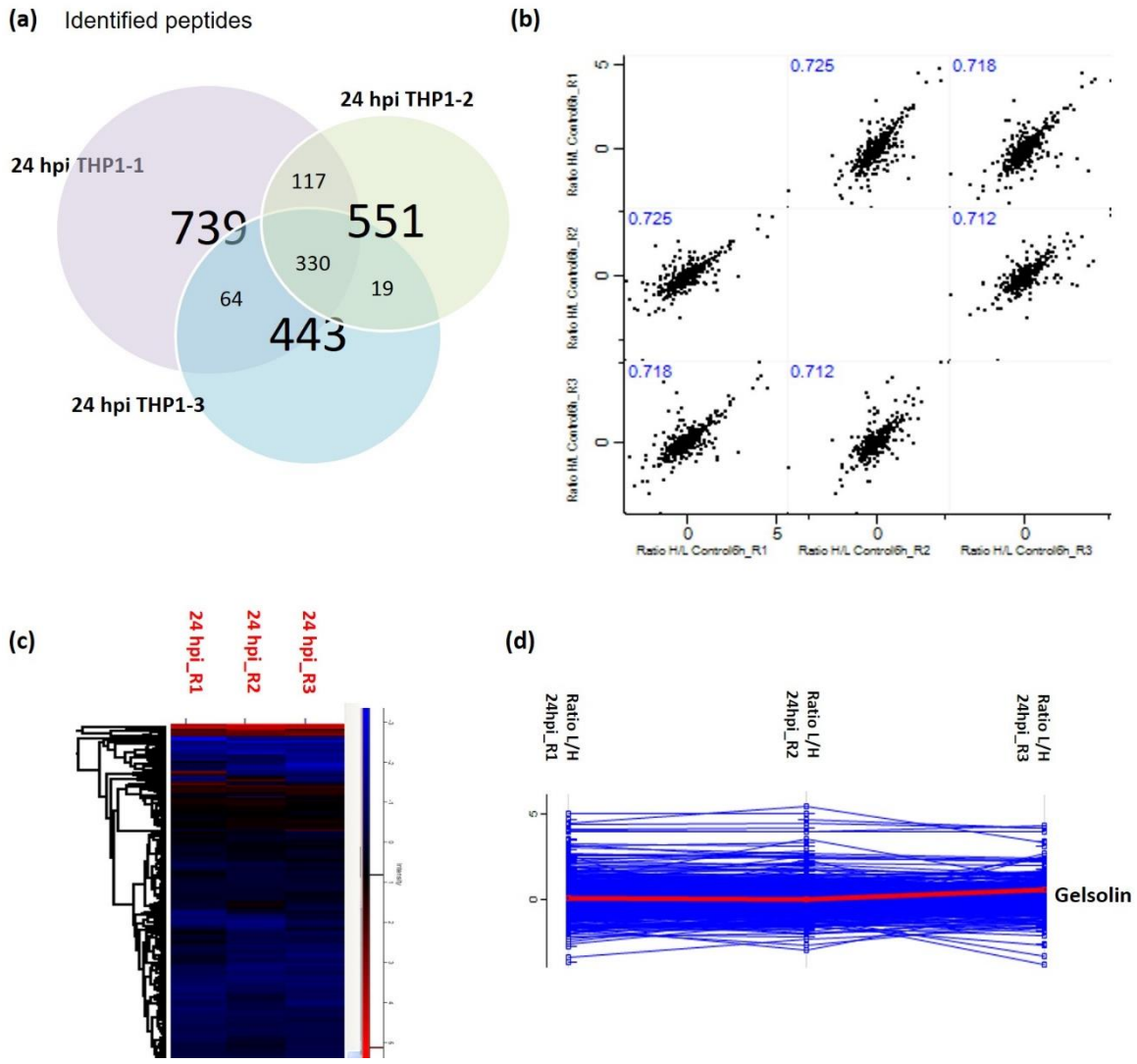

Figure 4.13: 2-D LCMS/MS profiles from biological replicates of 24 hpi THP-1.

Digested peptides were subjected to SCX and RP separation on the Orbitrap Velos MS instrument. Thermo raw files of uninfected (n=3, biological replicates) were analysed on MaxQuant and Perseus for quantitative analysis. (a) Venn diagram showing the number of proteins detected in each replicate. (b) Multiscatter plot with Pearson correlation values (blue font) of near 1 indicates good correlation between replicates. (c) Heat map distribution of protein expressions in all replicates shows similar pattern. (d) Profile plot of protein expression with gelsolin (red) as example shows similar pattern.

After inspecting the reproducibility between replicates, we then combined raw data from uninfected and 24 hpi THP-1, each contain 12 fractions, and analysed them together on MaxQuant and Perseus for comparative analysis. This yielded 2016 identified protein and 761 quantified proteins in at least one of the group (summarized in Figure 4.14 and in Table 4.4).

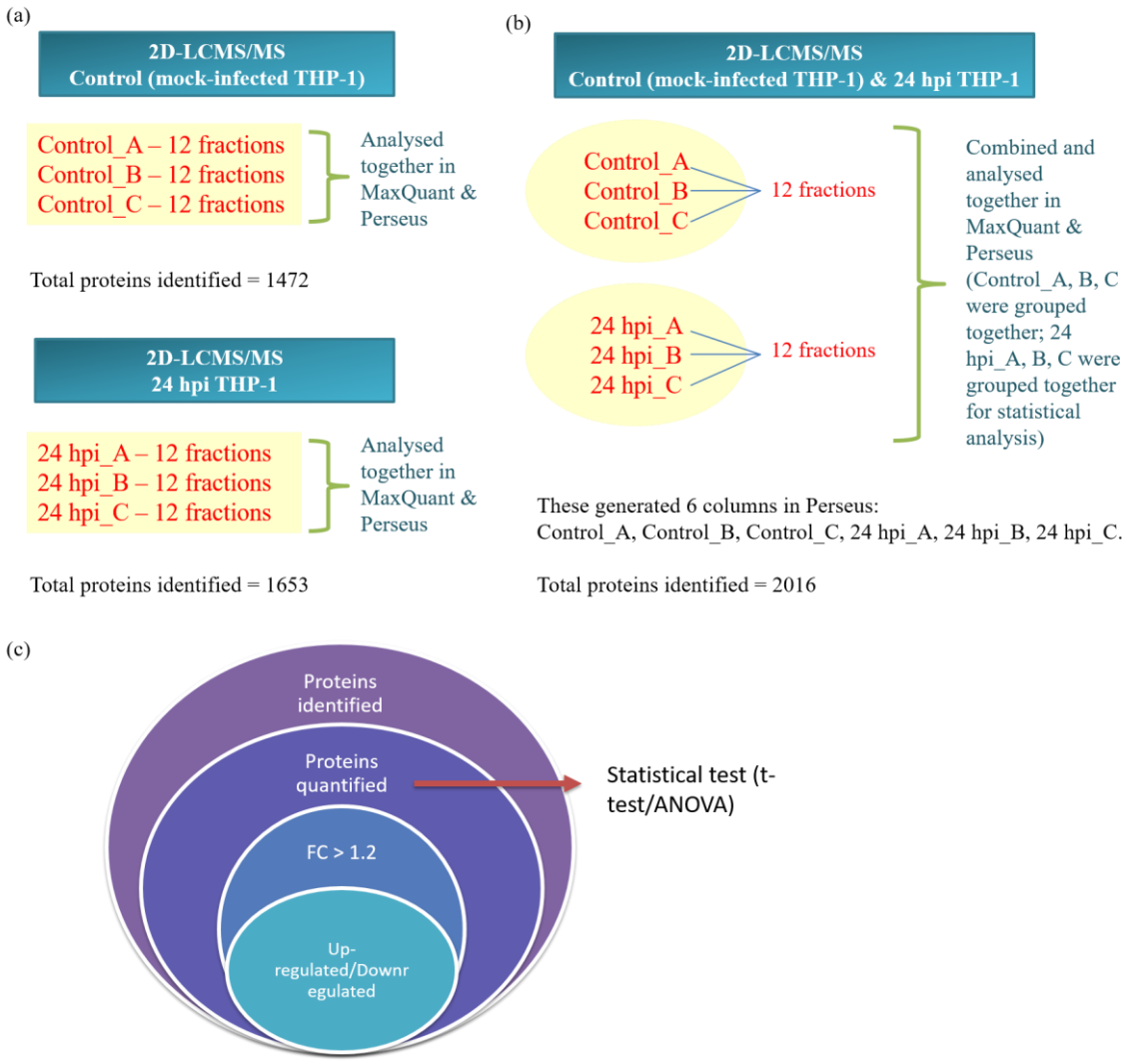

Figure 4.14: Strategy for analysing raw data using MaxQuant and Perseus.

This diagram explains how we analyse raw data from Orbitrap Velos MS. For statistical purpose, we only use protein lysates from biological replicates that were prepared and processed on the same day. (a) Each uninfected and 24 hpi biological replicates (with 12 fractions each) were analysed separately on MaxQuant and Perseus. The number of proteins quantified were varies in all replicates. (b) 3 biological replicates of uninfected and 24 hpi were combined and analysed together on MaxQuant and Perseus. These generated 6 columns in Perseus: control_A, control_B, control_C, 24 hpi_A, 24 hpi_B, 24 hpi_C. For 2 samples t-test analysis, control_A, _B and _C were grouped as control, whereas 24 hpi_A, _B and _C were grouped as 24 hpi. (c) Of the total proteins identified, they were filtered to proteins with quantification in all replicates. This subset of data was used for statistical analysis. Of these, the quantified proteins were narrowed down to fold-change (FC) greater than 1.2 to determine the modulations. Data for 48 hpi was analysed using the same strategy.

After filtering missing values from the data (in Perseus), 521 proteins were quantified in all replicates. The proteins identified include neutrophil cytosol factor 1, galectin-9, galectin-1, actin, tubulin, Dynamin-1-like protein, Tripeptidyl-peptidase 1 and Thioredoxin-like protein. We predicted that the proteomes measured here are not complete and there is a likely bias toward proteins with high expression levels.

Functional analyses were performed on the proteins identified. Gene Ontology analysis based on biological process using DAVID showed that proteins involved in metabolic processes were most highly represented, followed by proteins involved in transport and apoptosis (Figure 4.15 a). Metabolic processes were then narrowed down to specific aspects of metabolism (Figure 4.15 b). Meanwhile, pathway analysis revealed that the majority proteins involve in metabolic, ribosome, oxidative phosphorylation, regulation of actin cytoskeleton and lysosome pathways (Figure 4.16). DAVID version 6.7 is designed around the "DAVID Gene Concept", a graph theory evidence-based method to agglomerate species-specific gene/protein identifiers from a variety of public genomic resources including NCBI, PIR and Uniprot/SwissProt (Huang et al. 2009). We also analysed the proteins identified on Reactome (http://www.reactome.org) for curated human pathways as well as how they relate with each pathway (Figure 4.17). Reactome is an open source, expert-curated and peer-reviewed database of biological reactions and pathways with cross-references to major molecular databases. The basic information in the Reactome database is provided by either publications or sequence similarity-based inference (Matthews et al. 2009). The yellow line shows all proteins found in our data. For example, gelsolin was found in programmed cell death pathway. Furthermore, programmed cell death pathway seems to connect with cellular responses to stress.

(a)

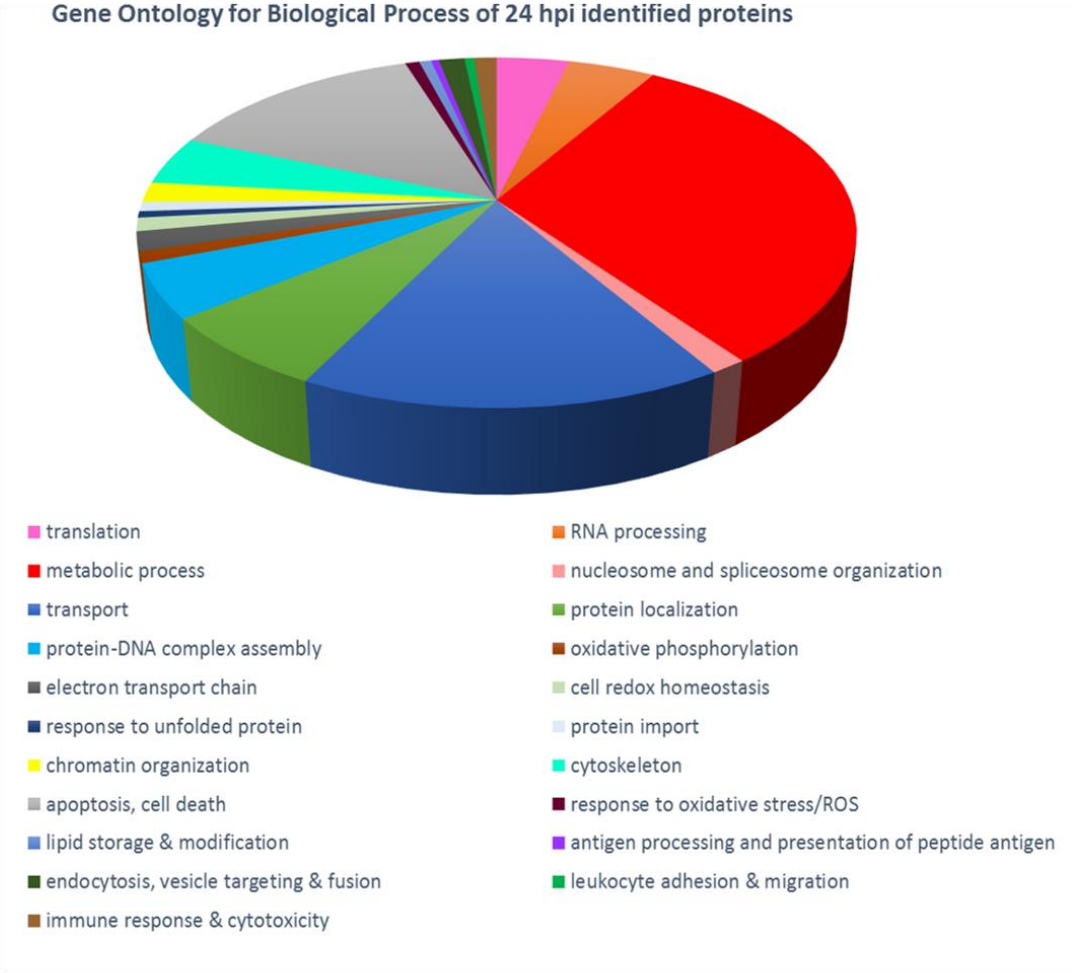

(b)

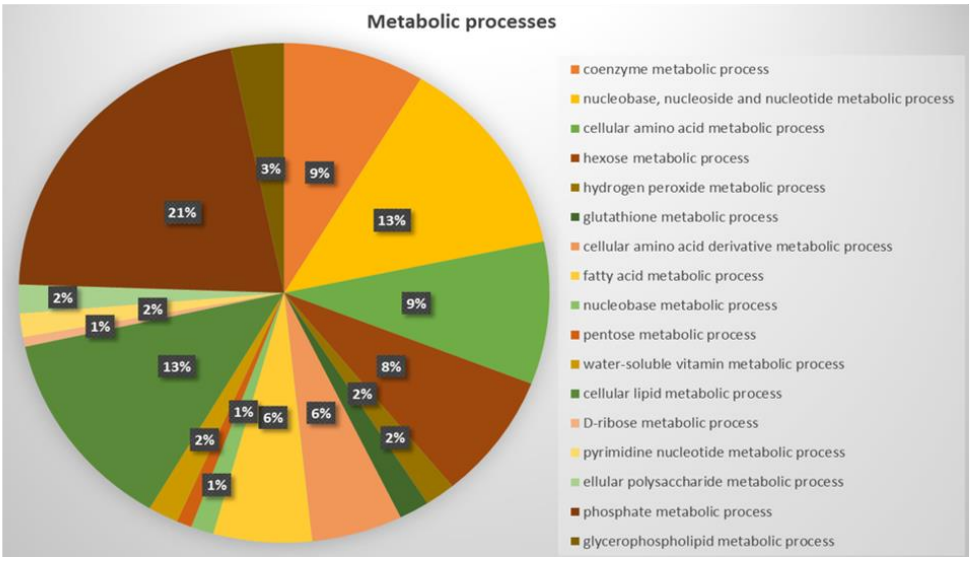

Figure 4.15: Clustering of Gene Ontology based on biological process (GOBP) of all proteins detected after infection (24 hpi).

The total number of proteins (UniProt identifiers) identified in uninfected and 24 hpi were analysed on DAVID based on biological processes they involve in**.** (a) GOBP of all proteins detected in 24 hpi THP-1. (b) GOBP partitions on metabolic processes.

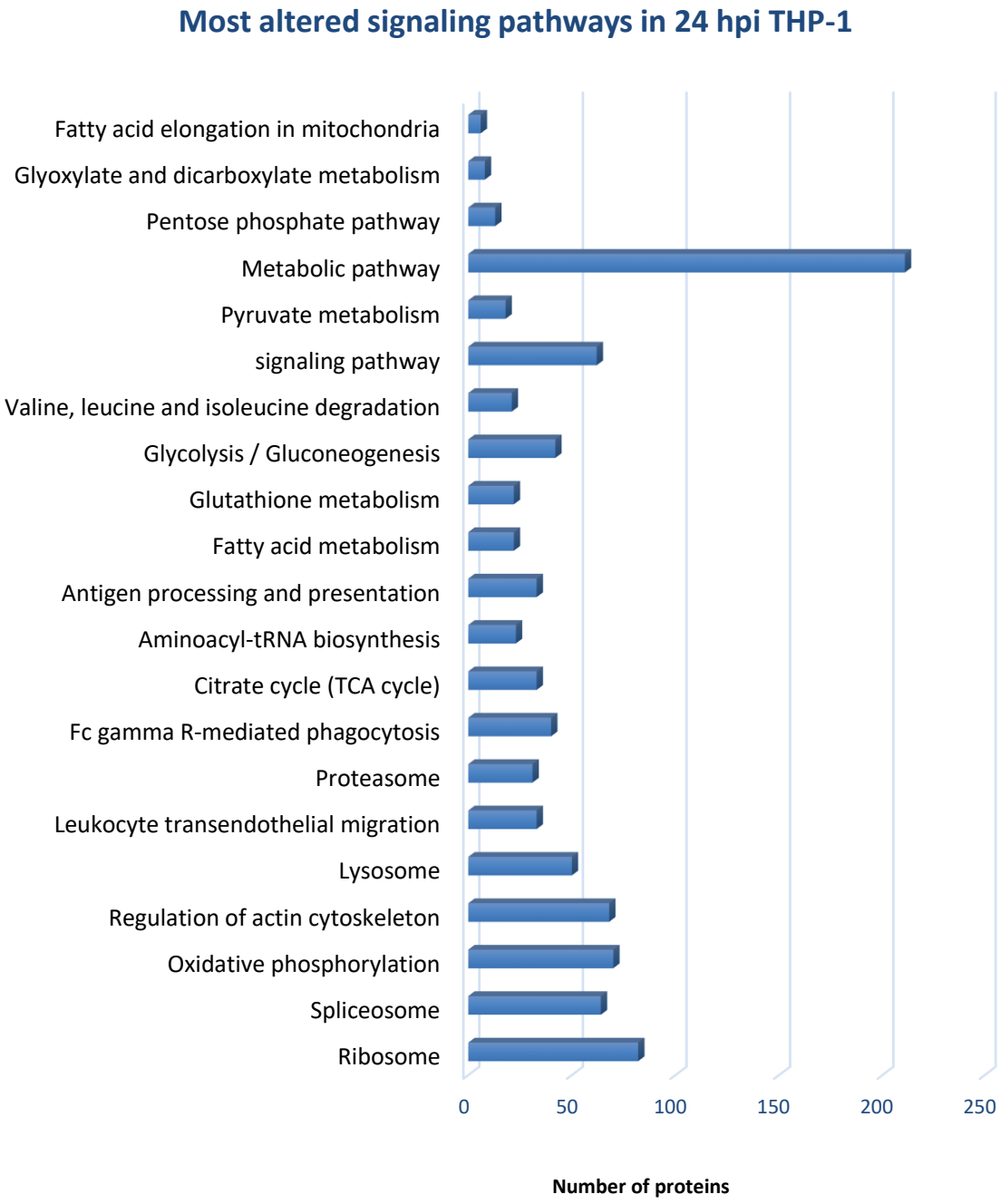

Figure 4.16: Canonical pathway analysis on KEGG showing most altered pathways in uninfected and infected THP-1.

The total number of proteins identified in uninfected and 24 hpi were analysed on DAVID with links to KEGG to identify the pathways they involve in ($p \leq 0.01$; Fisher's exact test).

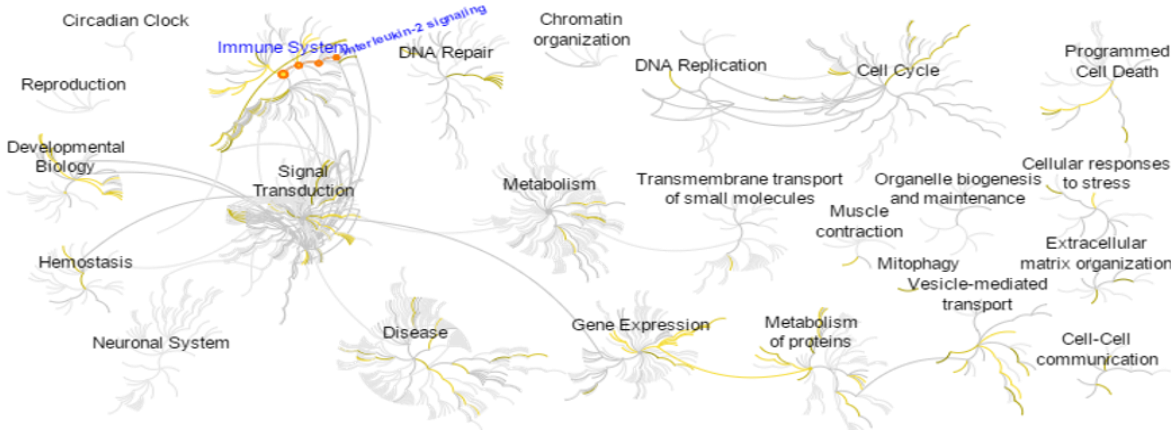

Figure 4.17: Overview of Reactome pathways involve in this study.

All proteins identified were analysed on Reactome to know the overview of biological pathways involve in our data. The yellow line represents proteins found in our data. The 'Immune system' pathway was highlighted in blue when we click on it.

Data analysis using Mascot Distiller on the same data set revealed a total of 1642 proteins identified with 135 proteins with no known function (proteins that are unclear to encode actual proteins) and 200 hypothetical proteins (proteins with no known homologs). Note that the reason of using Mascot Distiller in this regard was to identify hypothetical proteins as we did not detect these proteins using MaxQuant. We did not further analyse these data due to insignificant number of quantified proteins.

We then analysed raw files of 48 h uninfected and infected samples alone to evaluate the reproducibility and to identify proteins that were only present at this time point. Three biological replicates were run on 2-D LC/MS and analysed together on MaxQuant generating 25,455 MS scans and 143,735 MS/MS scans equivalent to 1929 proteins identified in all replicates of uninfected group. Whereas, 9583 MS scans and 167,600 MS/MS scans corresponding to 1183 proteins were generated in 48 hpi groups (FDR of 1%, minimum ratio count of 2). Protein groups containing matches to proteins from the inverted database or contaminants were discarded. The number of quantified proteins with L/H ratios varies between replicates, ranging from 634 - 859 in uninfected and 454 - 484 in 48 hpi, as depicted in Venn diagram in Figure 4.18. Multiscatter plot analyses were applied to all replicates with Pearson correlation coefficient values ranges from 0.7 – 0.9. This indicated a good reproducibility across all replicates.

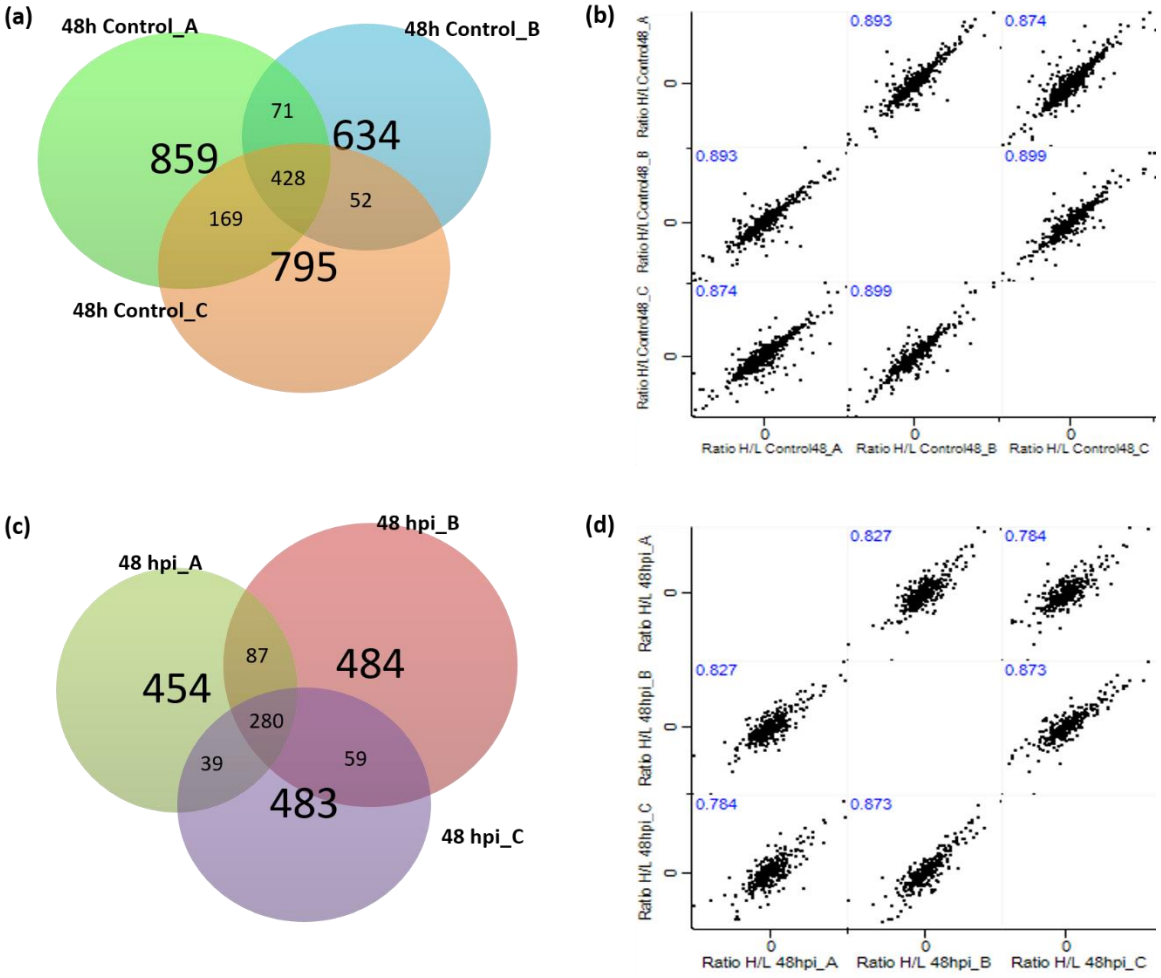

Figure 4.18: 2D-LCMS/MS data analysis from biological replicates of uninfected and 48 hpi THP-1.

Digested peptides were run on the Orbitrap Velos instrument. Thermo raw files of control and 48 h infection (n=3, biological replicates) were analysed separately on MaxQuant and Perseus for quantitative analysis. (a) Venn Diagram shows that 859 proteins were quantified in Control_A, 634 in Control_B and 795 in Control_C. (b) Multiscatter plot analysis were performed on all replicates of control. Blue font indicates a Pearson correlation value. Pearson correlation value near 1 showed high reproducibility (c) Venn Diagram shows that 454 proteins were quantified in 48 hpi_A, 484 in 48 hpi_B and 483 in 48 hpi_C (d) Multiscatter plot analysis were performed on all replicates of 48 hpi. Blue font indicates a Pearson correlation value. Pearson correlation value near 1 showed high reproducibility.

Expression profiles, displayed as a heat map between replicates for both uninfected and 48 hpi THP-1, showed similar patterns (Figure 4.19 a and c). Profile plots were performed on both uninfected and 48 hpi THP-1 using Perseus. Several proteins including SOD1, SOD2, GAPDH, PNP, prelamin A/C and galectin-9 were chosen as examples to show similar patterns across all replicates (Figure 4.19 b and d).

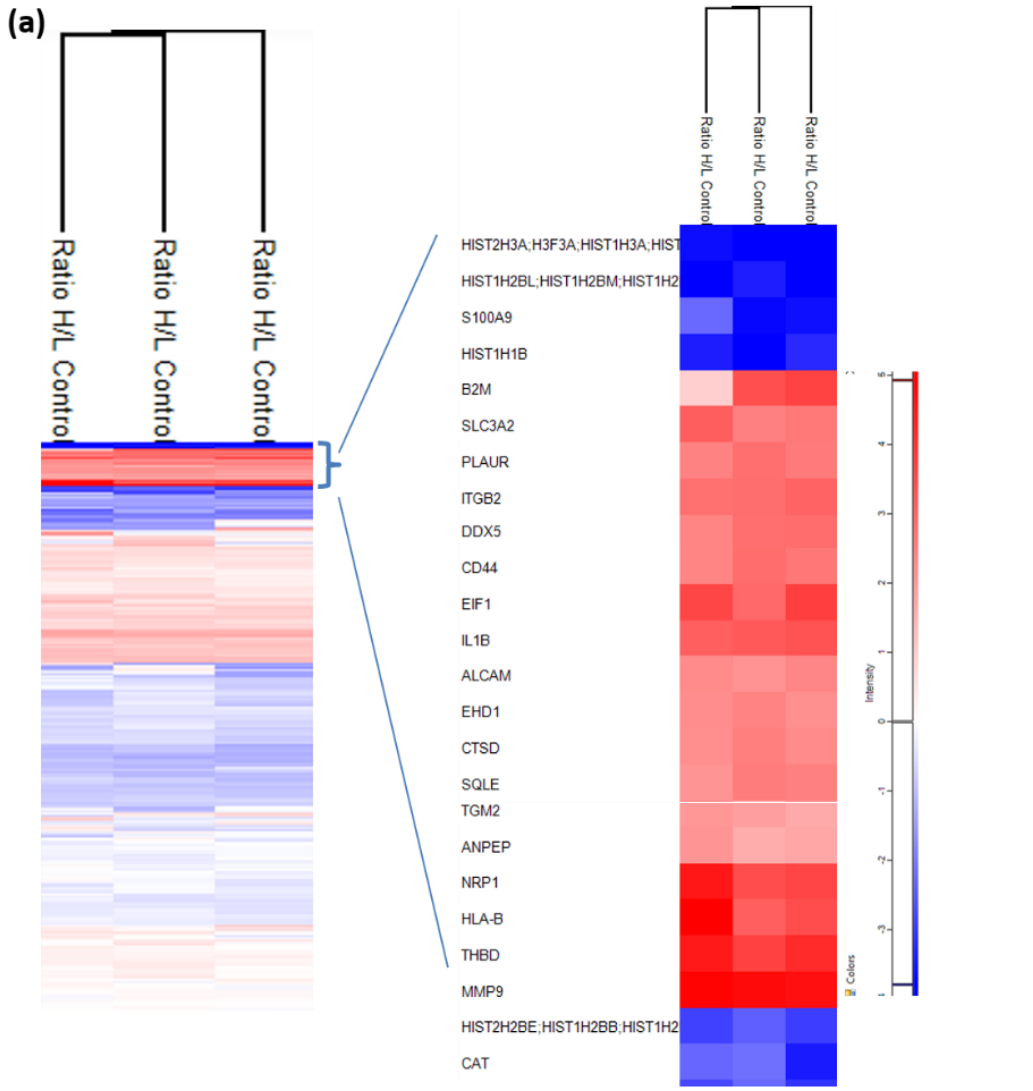
(a)
Ratio H/L Control
Ratio H/L Control
Ratio H/L Control
HIST2H3A;H3F3A;HIST1H3A;HIST
HIST1H2BL;HIST1H2BM;HIST1H2
S100A9
HIST1H1B
B2M
SLC3A2
PLAUR
ITGB2
DDX5
CD44
EIF1
IL1B
ALCAM
EHD1
CTSD
SQLE
TGM2
ANPEP
NRP1
HLA-B
THBD
MMP9
HIST2H2BE;HIST1H2BB;HIST1H2
CAT
Intensity
Color
(b)
Ratio H/L Contro
Ratio H/L Contro
Ratio H/L Contro
5
0
SOD2
Prelamin A/C
GAPDH
PNP
SOD1

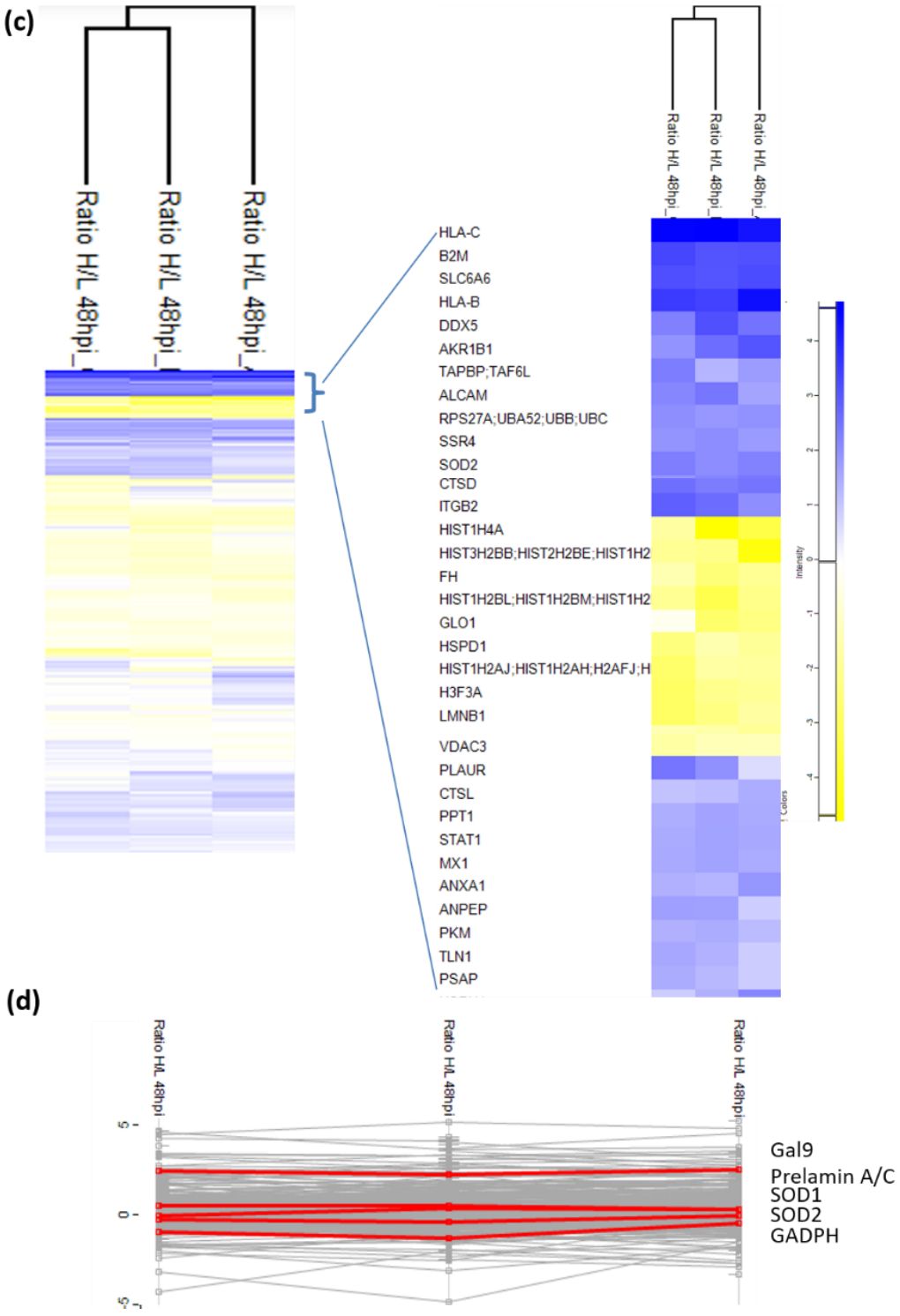

Figure 4.19: Expression profiles of uninfected and 48 hpi THP-1.

Triplicates of uninfected and 48 hpi THP-1 were analysed separately on MaxQuant and Perseus. (a) Heat map distribution of protein expressions in all replicates of uninfected THP-1 showed similar patterns (b) Profile plot of protein expression in uninfected THP-1 with several proteins as example shows similar pattern (c) Heat map distribution of protein expressions in all replicates of 48 hpi THP-1 shows similar pattern (d) Profile plot of protein expression 48 hpi THP-1 with several proteins as example shows similar pattern.

After examining the reproducibility between replicates, raw data from uninfected and 48 hpi THP-1 were combined (n = 3, each contain 12 SCX fractions) and analysed together on MaxQuant and Perseus for comparative analysis. Example of the strategy to analyse these data was illustrated in Figure 4.13. Using stringent parameters as described earlier, a total of 2280 proteins were detected in both groups (Figure 4.20). Each replicate of uninfected and 48 hpi were grouped together in Perseus for statistical analysis. For subsequent data analysis, we only considered protein with quantification in all 6 groups (Control_A, Control_B, Control_C, 48 hpi_A, 48 hpi_B and 48 hpi_C), leading to a total of 233 proteins (11%). Our 48 hpi datasets contains more proteins with NaN (missing values). This could be due to the greater reduction in the labelled protein that is expected over a longer chase period, resulting in the labelled population of certain proteins falling below the limit of detection. Furthermore, minimum ratio count for quantification was set to 2.

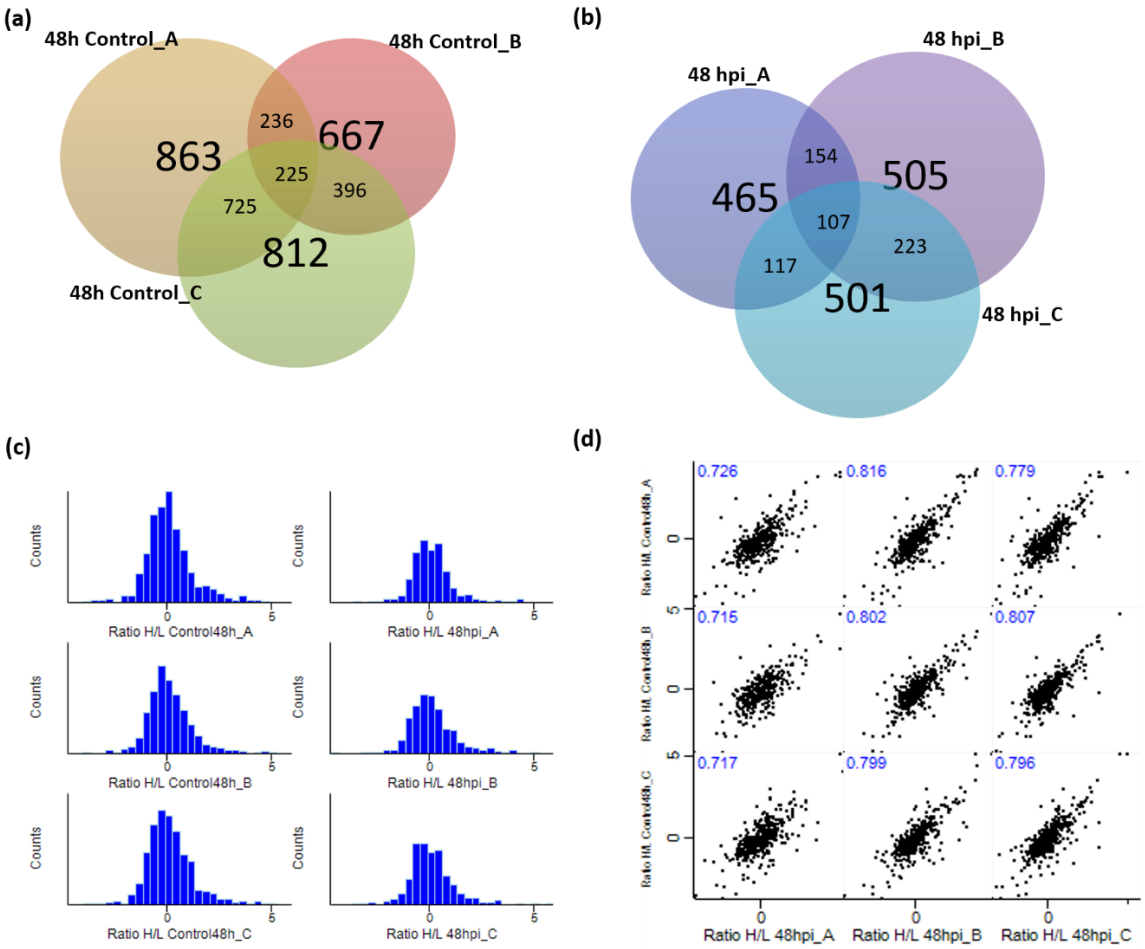

Figure 4.20: 2D-LCMS/MS data analysis of uninfected and 48 hpi THP-1.

Digested peptides were run on the Orbitrap Velos instrument. Thermo raw files of uninfected and 48 h infection (n=3, biological replicates) were analysed together on MaxQuant and Perseus for quantitative analysis. (a) Venn Diagram shows that 863 proteins were quantified in Control_A, 667 in Control_B and 812 in Control_C. (b) Venn Diagram shows that 465 proteins were quantified in 48 hpi_A, 505 in 48 hpi_B and 501 in 48 hpi_C (c) Histogram of uninfected and 48 hpi groups displayed a normal distribution (d) Multiscatter plot analysis were performed on all replicates of uninfected and 48 hpi. Blue font indicates a Pearson correlation value.

Protein ID (from Uniprot) for the proteins identified (2104 proteins) were uploaded to Database for Annotation, Visualization and Integrated Discovery (DAVID) as well as the Protein Analysis Through Evolutionary Relationships (PANTHER) classification system for global functional analysis. Gene Ontology analysis by biological process showed that metabolic processes were most highly represented, followed by localisation and response to stress/stimulus (Figure 4.21).

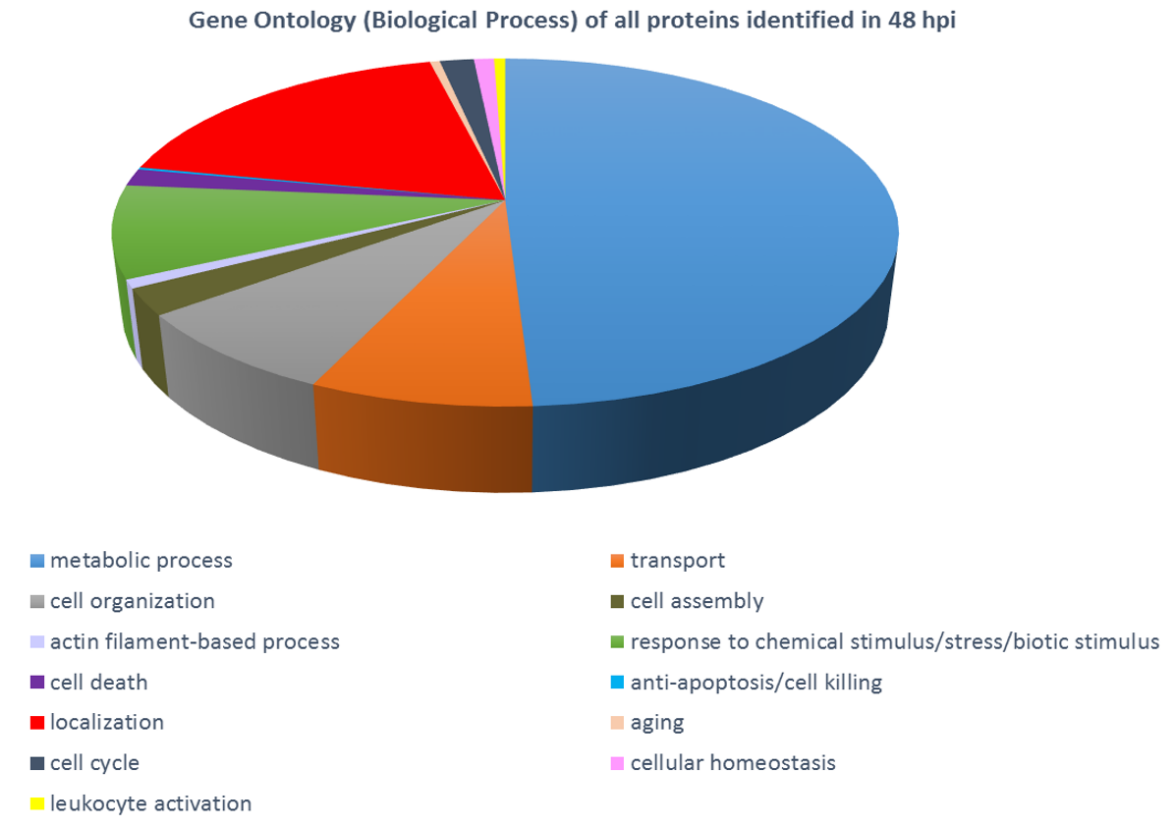

Figure 4.21: Clustering of Gene Ontology based on biological process (GOBP) of all proteins detected after infection (48 hpi).

The total number of proteins (UniProt identifiers) identified in uninfected and 48 hpi were analysed on DAVID based on biological processes they involve in. Pie chart showed that most proteins involved in metabolic process, localisation and response to stress/stimulus.

From DAVID, a link to KEGG pathways could also be retrieved. Pathway analysis on uninfected and 48 hpi THP-1 revealed that the top pathways associated with the proteins detected were ribosome, spliceosome, regulation of actin cytoskeleton, oxidative phosphorylation and lysosome (Figure 4.22).

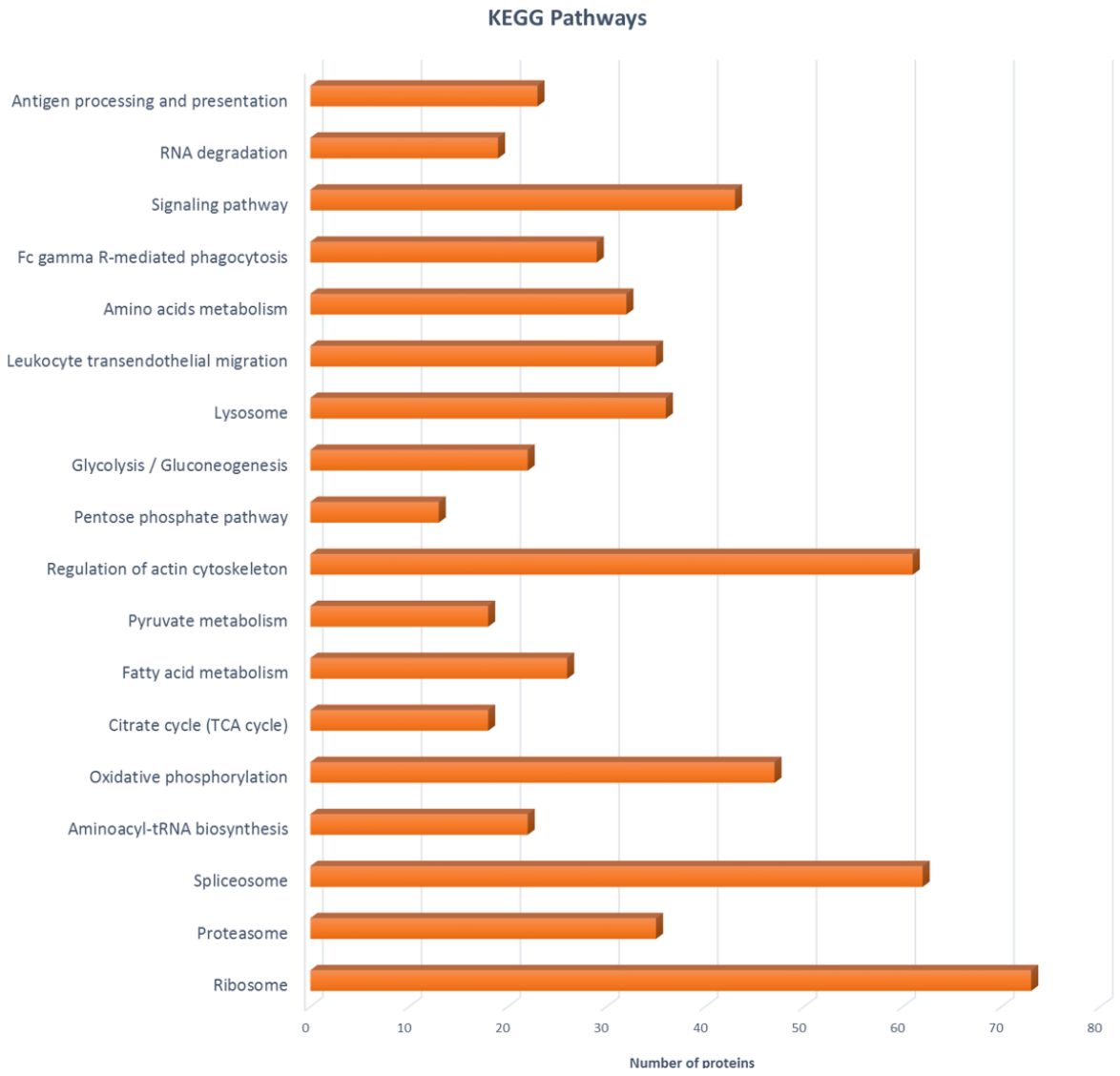

Figure 4.22: Canonical pathway analysis on KEGG showing most altered pathways in uninfected and 48 hpi THP-1.

The total number of proteins identified in uninfected and 48 hpi were analysed on DAVID with links to KEGG to identify the pathways they involve in ($p \leq 0.01$; Fisher's exact test).

4.3.3 Determination of protein synthesis rate

THP-1 cells were pre-labelled with heavy Arg and heavy Lys for approximately 160 h, equivalent to 8 doubling times. After sufficient labelling had been achieved, light-labelled Arg and Lys were added in the medium-exchange process. Cells were exposed to metacyclic promastigote of *L. mexicana* at the start of the chase period and the cells were harvested at 24 and 48 h, and proteins were extracted. Uninfected cells were treated in the same way in parallel except without infection. During the chase period following infection, all newly synthesized proteins should only incorporate light-labelled Arg and Lys. The ratio of the H

versus the L intensity reflects the extent to which proteins have been turned over since the start of the chase and differences in this ratio reflect differences in the turnover of specific proteins between uninfected and infected macrophages. Protein populations that have persisted since before the chase remain in the H form, so the ratio of L:H reflects both the rate of synthesis and the rate of degradation.

Replicates from both uninfected, 24 hpi and 48 hpi THP-1 (from MaxQuant and Perseus) were grouped and light (L) and heavy (H) intensities were averaged. To determine the synthesis rate, averaged intensities L/(L+H) were calculated (section 2.10.4) and plotted against time to monitor incorporation of heavy label. Only proteins with valid values with minimum individual peptides of 2 were considered for this purpose, leaving 400 proteins in total. Note that the doubling time for THP-1 in SILAC media was used to determine the dilution rate (k_{dil}) over 160 h of cultivation which is 0.006 h^{-1}. Therefore, the dilution rate is negligible since over 99% of the arginine and leucine in the cells would be the stable isotope-labelled form. Several of the proposed newly synthesized proteins were accessed on SeeMS and Skyline to look at the H and L spectra (Figure 4.23 and 4.24).

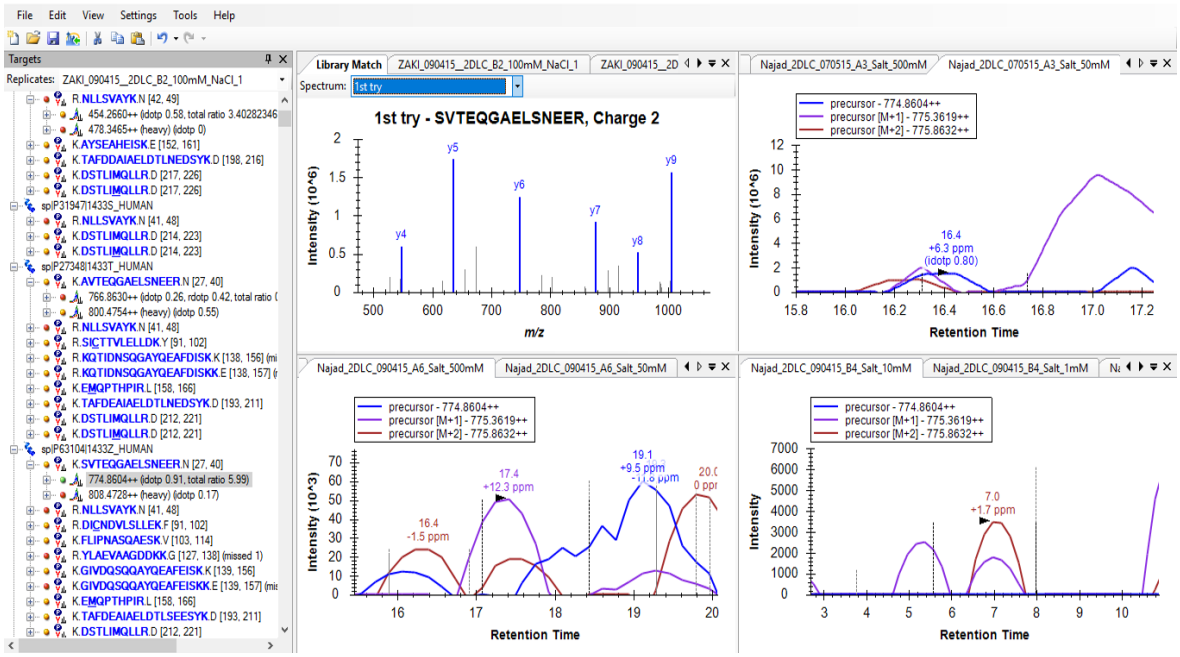

Figure 4.23: Example of MS spectra and chromatogram in Skyline.

Skyline was used to analyse the MS1 spectra by building a spectral library containing all spectra from raw files generated from Orbitrap Velos MS. Quantification of heavy Arg and Lys were applied on the setting.

t = 24 h

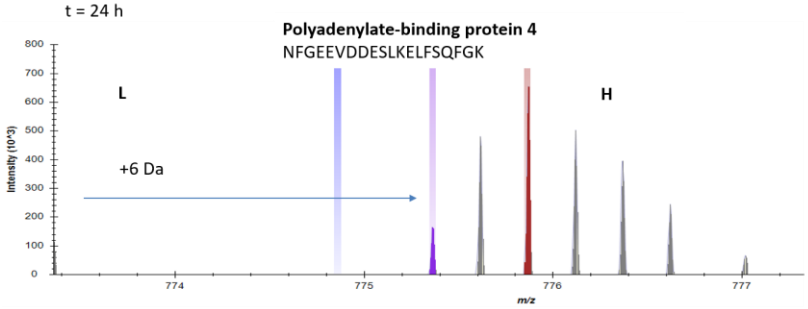

t = 48 h

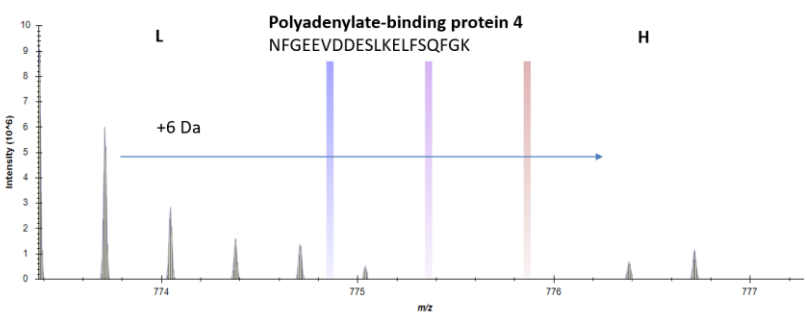

t = 24 h

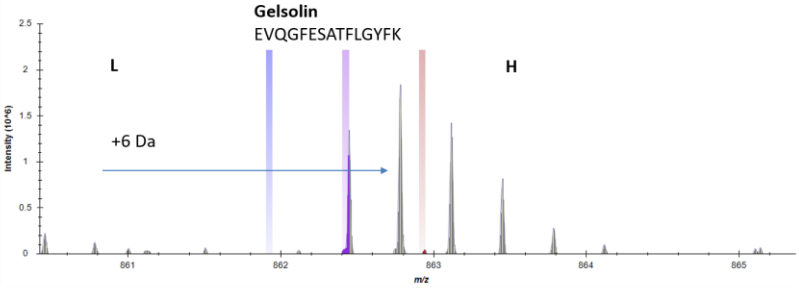

t = 48 h

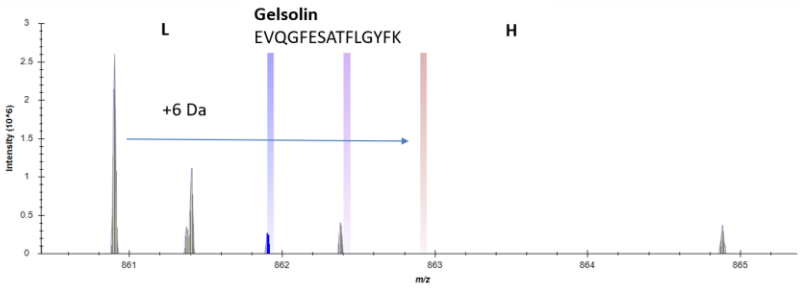

t = 24 h

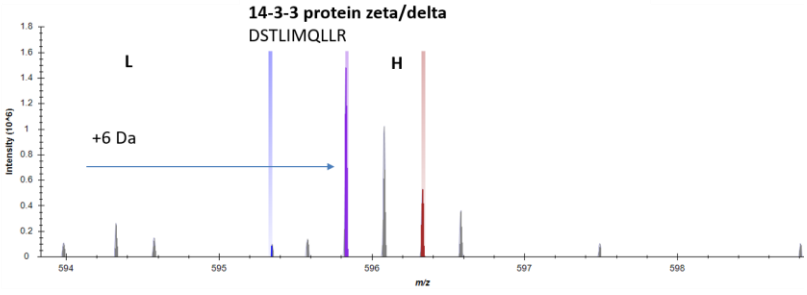

t = 48 h

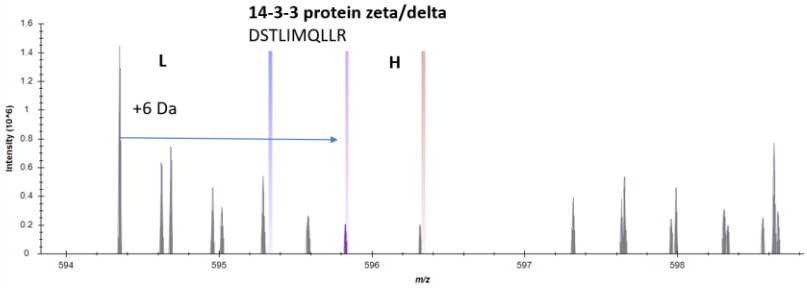

Figure 4.24: Generation of labelled isotopologues of newly synthesized proteins.

Mass spectra showing the appearance of the heavy isotopologue of polyadenylate-binding protein 4, gelsolin and 14-3-3 protein zeta/delta at 24 h. After 48 h, the light isotopologues were incorporated into newly synthesized protein molecules, showing an increase of L intensity.

A two-sample t-test was performed on the filtered data and gave rise to a subset of 51 proteins showed significant changes in synthesis rate for 24 hpi (Figure 4.25) and 84 proteins for 48 hpi (p-value < 0.05, FDR = 0.05). Table 4.2 and 4.3 list the significantly synthesized proteins in 24 hpi and 48 hpi, respectively.

They were analysed in DAVID for functional annotation based on biological process, as shown in Figure 4.26. It is evident from the pie chart that these proteins are involved in various types of biological processes. However, in order to determine significant annotations between groups and to elucidate the common cluster of annotations in the group, we performed a Fisher Exact test (Benjamini-Hochberg FDR < 0.02) for enrichment of proteins that showed significant modulation of expression (Subramanian et al. 2005). The most highly differentially expressed proteins were involved in metabolic process, translational processes, apoptosis, and RNA/mRNA processing. Also, we found multiple metabolic pathways, including fatty acid metabolism, amino acid metabolism and pyruvate metabolism. This demonstrates the diversity of energy production and biosynthetic pathways that are employed by the cells in response to infection.

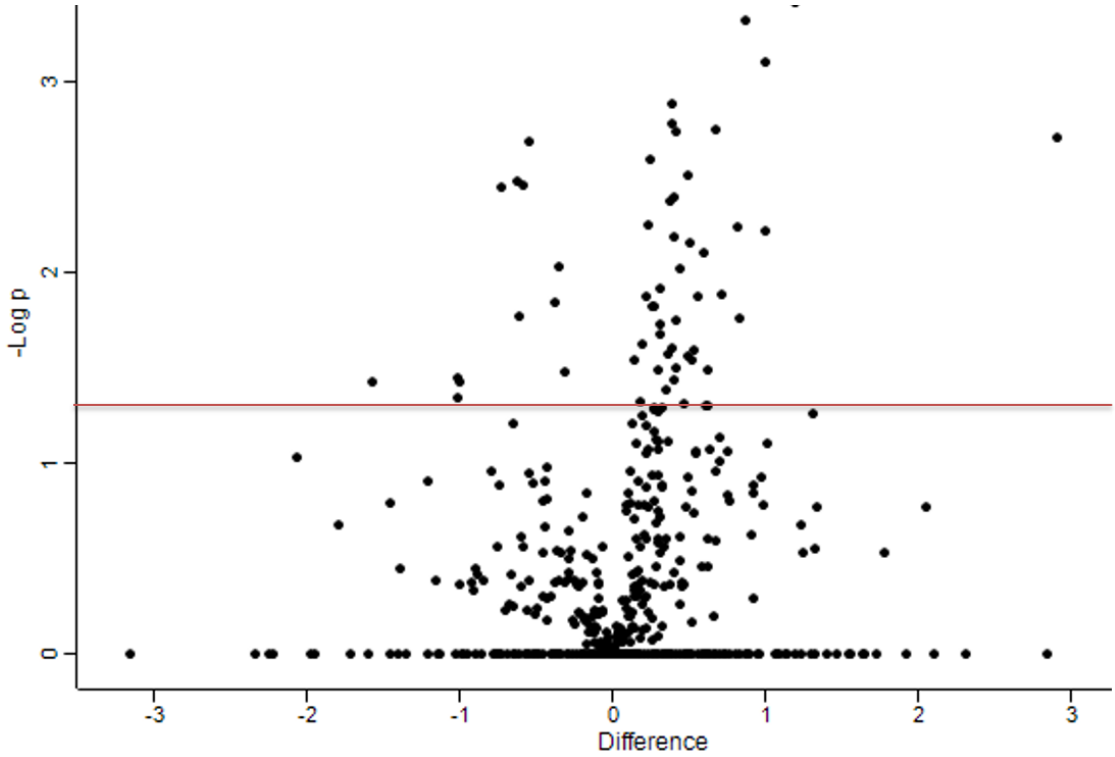

Figure 4.25: Volcano plot showing proteins with different synthesis rate in uninfected and 24 h infected THP-1 with FDR = 0.05.

Conventional data were normalized and proteins with no quantification report were removed from all samples. t-test was performed on the remaining data to produce statistically significant proteins with p-value < 0.05 (above black line). The proteins were assigned with gene names. FDR of 0.05 was applied on the data producing 51 proteins with differential synthesis rate.

Result from functional analyses also revealed that most of the proteins significantly synthesized in 24 hpi were involved in spliceosome, oxidative stress response, JAK/STAT signalling pathway, amino acids metabolism and translation (Figure 4.27).

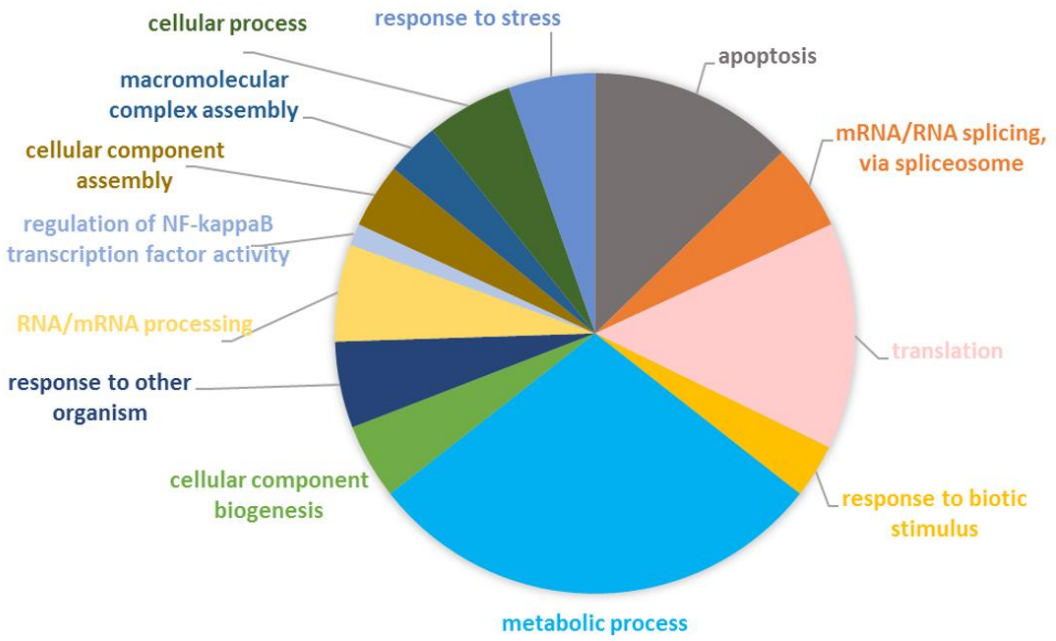

Figure 4.26: Pie chart illustrating the types of biological processes involves in the 51 significantly synthesized proteins in 24 hpi.

RIA synthesis was determined for proteins identified in uninfected and 24 hpi. Proteins with no quantification report were removed from all samples. t-test was performed on the remaining data to produce 51 statistically significant proteins with p-value < 0.05. These proteins were assigned on Gene Ontology based on biological processes they involve in.

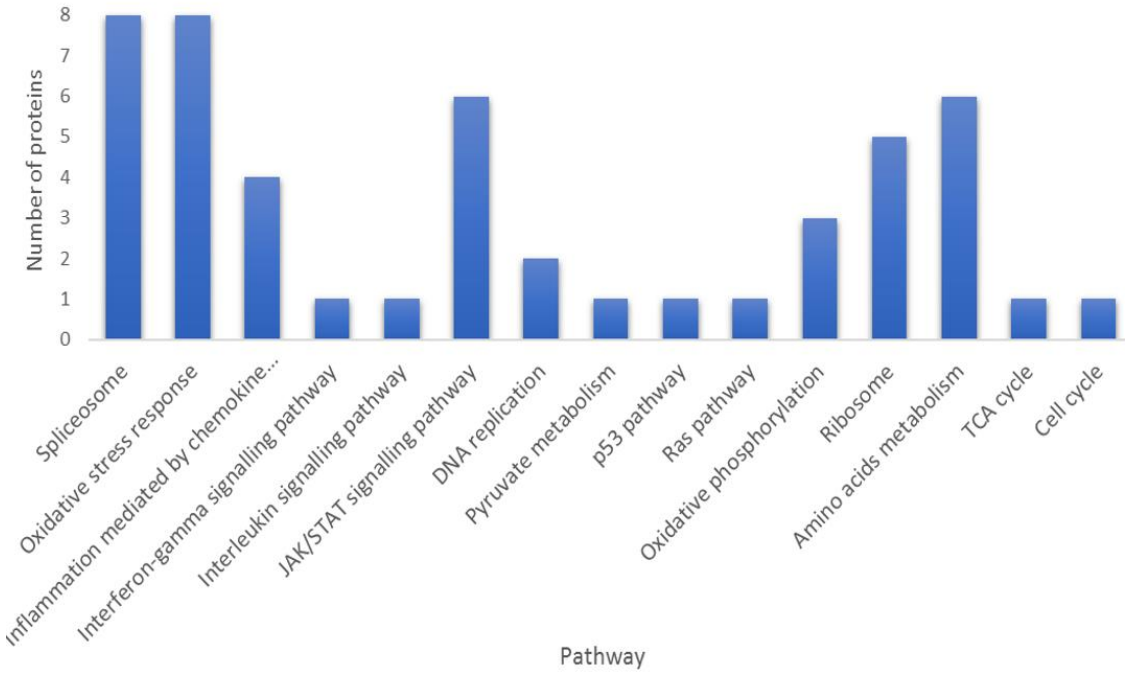

Figure 4.27: Canonical pathway analysis on KEGG showing most altered pathways in the 51 significantly synthesized proteins in 24 hpi THP-1.

The highly synthesized proteins identified in uninfected and 24 hpi were analysed on DAVID with links to KEGG to identify the pathways they involve in ($p \leq 0.01$; Fisher's exact test).

Additionally, GO analysis on proteins significantly synthesized in 48 hpi showed that most proteins involved in metabolic process, response to stimulus, and nucleosome, chromatin, protein-DNA assembly (Figure 4.28). The group was also enriched in proteins involved in metabolic pathways and antigen processing and presentation (Figure 4.29).

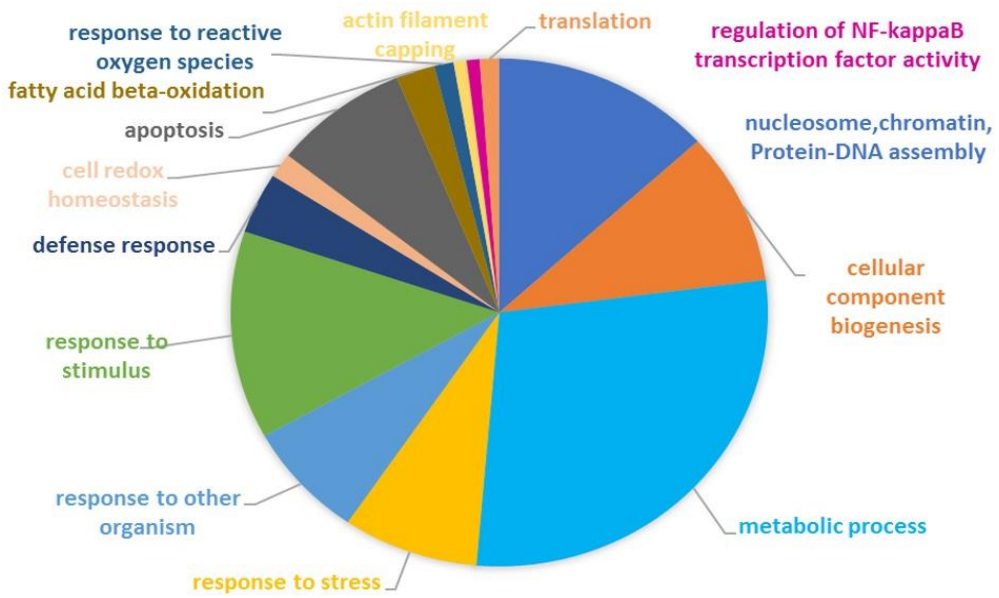

Figure 4.28: Pie chart illustrating the types of biological processes involves in the 84 significantly synthesized proteins in 48 hpi.

RIA synthesis was determined for proteins identified in uninfected and 48 hpi. Proteins with no quantification report were removed from all samples. t-test was performed on the remaining data to produce 84 statistically significant proteins with p-value < 0.05. These proteins were assigned on Gene Ontology based on biological processes they involve in.

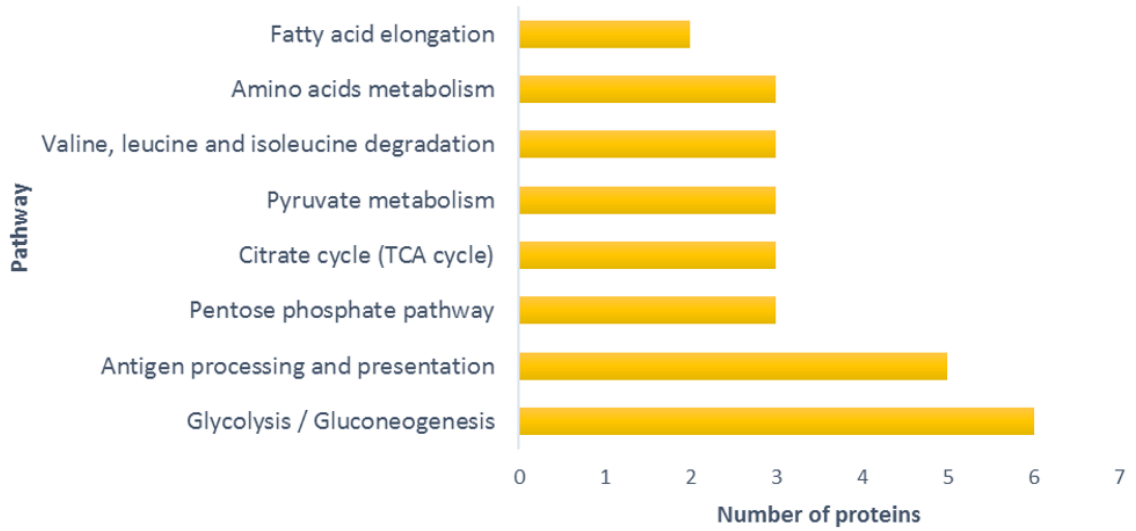

Figure 4.29: Canonical pathway analysis on KEGG showing most altered pathways in the 51 significantly synthesized proteins in 24 hpi THP-1.

The highly synthesized proteins identified in uninfected and 48 hpi were analysed on DAVID with links to KEGG to identify the pathways they involve in ($p \leq 0.01$; Fisher's exact test).

Gamma-interferon-inducible protein 16 was on top of the list with the biggest fold change of RIA synthesis in 24 hpi (RIA = 0.06) as compared to uninfected cells (RIA = 0.31). Carbonic anhydrase 2 showed high synthesis rate in 24 hpi (RIA synthesis = 0.05) compared to uninfected cell (RIA synthesis = 0.21). Galectin-9 showed RIA synthesis value of 0.18 in uninfected cell while 0.36 in 24 hpi. Another interesting protein showed increased turnover in infected cells was interferon-induced GTP-binding protein Mx1 which is involved in the innate immune response and apoptotic processes and has been shown to have antiviral activities (Andersson et al. 2004). Hypoxia up-regulated protein 1 and Signal transducer and activator of transcription 1-alpha/beta (STAT1) also showed increased synthesis rate in 24 hpi compared to control with 2.3 and 1.5-fold change, respectively. 14-3-3 protein beta/ alpha, also known as protein kinase C inhibitor protein 1, has increased synthesis p.i. As the name suggests, it is involve in the MAP kinase cascade by interacting with a variety of Akt substrates, thereby regulating diverse biological processes including signal transduction, cell cycle uninfected, and apoptosis (Fu et al. 2000; Jang et al. 2009).

On the other hand, 84 proteins were significantly showed increased synthesis in 48 hpi THP-1 (Table 4.3). These included histone H1.5 that had increased synthesis rate p.i by more than 3-fold, catalase (2.8-fold), gelsolin (1.6-fold), L-lactate

dehydrogenase A (2.1-fold) and Interferon-induced GTP-binding protein Mx1 (2-fold).

Table 4.2: Proteins significantly synthesized in 24 hpi groups.

Replicates from both uninfected and 24 hpi THP-1 were grouped. Light (L) and heavy (H) monoisotopic intensities were averaged. RIA synthesis was calculated using formula in section 2.10.4. Only proteins that have been quantified in all biological replicates were considered for this statistical test. Two-sample t-test was performed on the filtered data and gave rise to 51 differentially synthesized proteins (FDR value = 0.05).

Protein names	Gene names	RIA (synthesis) Uninfected24h	RIA (synthesis) 24hpi	RIA (synthesis) Uninfected48h	RIA (synthesis) 48hpi	Peptides	Unique peptides	Mol. weight [kDa]	Score
Gamma-interferon-inducible protein 16	IFI16	0.06	0.31	0.35	0.37	6	6	88.255	53
Carbonic anhydrase 2	CA2	0.05	0.21	0.11	0.17	16	16	29.246	233
Proliferation-associated protein 2G4	PA2G4	0.05	0.17	0.20	0.22	9	9	43.786	189
Calcium-binding protein 39	CAB39	0.13	0.32	0.38	0.35	4	4	39.869	13
Elongation factor Tu, mitochondrial	TUFM	0.12	0.29	0.16	0.16	15	15	49.541	323
Hypoxia up-regulated protein 1	HYOU1	0.13	0.30	0.21	0.21	27	27	111.33	323
Serine/arginine-rich splicing factor 1	SRSF1	0.13	0.30	0.30	0.41	6	6	27.744	51
Hippocalcin-like protein 1; Neuron-specific calcium-binding protein hippocalcin	HPCAL1; HPCA	0.15	0.32	0.55	0.41	7	7	22.313	68
Inorganic pyrophosphatase 2, mitochondrial	PPA2	0.05	0.11	0.14	0.13	10	10	37.92	175
Galectin-9	LGALS9	0.18	0.36	0.41	0.37	4	4	26.152	165
Ras-related protein Rab-1b	RAB1B	0.14	0.27	0.38	0.44	7	7	23.897	89
Brain acid soluble protein 1	BASP1	0.22	0.39	0.32	0.30	15	15	22.693	190
Interferon-induced GTP-binding protein Mx1, N-terminally processed	MX1	0.14	0.24	0.24	0.49	7	4	75.519	58
116 kDa U5 small nuclear ribonucleoprotein component	EFTUD2	0.28	0.26	0.40	0.31	12	12	109.43	180
Phosphate carrier protein, mitochondrial	SLC25A3	0.16	0.27	0.22	0.24	8	8	40.094	41

Protein names	Gene names	RIA (synthesis) Uninfected24h	RIA (synthesis) 24hpi	RIA (synthesis) Uninfected48h	RIA (synthesis) 48hpi	Peptides	Unique peptides	Mol. weight [kDa]	Score
Heterogeneous nuclear ribonucleoprotein U-like protein 1	HNRNPUL1	0.21	0.35	0.36	0.39	7	7	95.737	51
Small nuclear ribonucleoprotein Sm D1	SNRPD1	0.03	0.04	0.14	0.15	4	4	13.281	45
ATP-citrate synthase	ACLY	0.13	0.22	0.22	0.28	16	16	120.84	251
Glutathione S-transferase P	GSTP1	0.13	0.21	0.22	0.24	7	7	23.356	114
Histone H3.3	H3F3A	0.05	0.08	0.04	0.03	6	1	15.328	37
40S ribosomal protein S3	RPS3	0.17	0.27	0.31	0.23	10	10	26.688	88
Signal transducer and activator of transcription 1-alpha/beta	STAT1	0.25	0.38	0.43	0.53	8	8	87.334	21
Cytosol aminopeptidase	LAP3	0.18	0.27	0.33	0.35	9	9	56.166	278
Isoleucine--tRNA ligase, mitochondrial	IARS2	0.12	0.18	0.23	0.30	14	14	113.79	126
Prostaglandin E synthase 3	PTGES3	0.16	0.23	0.24	0.21	3	3	18.697	60
Splicing factor U2AF 65 kDa subunit	U2AF2	0.23	0.33	0.34	0.56	8	8	53.5	80
Heat shock 70 kDa protein 1B; Heat shock 70 kDa protein 1A	HSPA1B; HSPA1A	0.25	0.36	0.22	0.38	10	4	70.051	30
Bifunctional glutamate/proline--tRNA ligase; Glutamate--tRNA ligase; Proline--tRNA ligase	EPRS	0.13	0.18	0.35	0.22	28	28	170.59	213
F-actin-capping protein subunit beta	CAPZB	0.16	0.22	0.35	0.29	7	7	31.35	211
Catalase	CAT	0.06	0.08	0.05	0.14	14	14	59.755	182
RNA-binding motif protein, X chromosome; RNA-binding motif protein, N-terminally processed; RNA binding motif protein, X-linked-like-1	RBMX; RBMXL1	0.18	0.24	0.27	0.23	8	7	42.331	50
14-3-3 protein beta/alpha;14-3-3 protein beta/alpha, N-terminally processed	YWHAB	0.15	0.21	0.25	0.28	11	8	28.082	323
T-complex protein 1 subunit delta	CCT4	0.14	0.19	0.23	0.19	9	9	57.924	81

Protein names	Gene names	RIA (synthesis) Uninfected24h	RIA (synthesis) 24hpi	RIA (synthesis) Uninfected48h	RIA (synthesis) 48hpi	Peptides	Unique peptides	Mol. weight [kDa]	Score
Endoplasmic reticulum metallopeptidase 1	ERMP1	0.16	0.21	0.17	0.33	7	7	100.23	23
40S ribosomal protein S12	RPS12	0.18	0.24	0.21	0.32	6	6	14.515	189
Prohibitin	PHB	0.15	0.19	0.12	0.22	8	8	29.804	186
60S ribosomal protein L3	RPL3	0.14	0.18	0.33	0.31	12	12	46.108	57
Multifunctional protein ADE2; Phosphoribosylaminoimidazole-succinocarboxamide synthase;Phosphoribosylaminoimidazole carboxylase	PAICS	0.25	0.32	0.20	0.21	6	6	47.079	10
Vesicle-fusing ATPase	NSF	0.20	0.26	0.27	0.44	8	8	82.593	82
Inorganic pyrophosphatase	PPA1	0.11	0.14	0.17	0.12	9	9	32.66	43
Adenylate kinase 2, mitochondrial;Adenylate kinase 2, mitochondrial, N-terminally processed	AK2	0.07	0.09	0.14	0.09	10	10	26.477	323
Sulfide:quinone oxidoreductase, mitochondrial	SQRDL	0.30	0.38	0.46	0.36	24	24	49.96	323
Serpin H1	SERPINH1	0.12	0.15	0.21	0.10	7	7	46.44	47
Phosphoglucomutase-2	PGM2	0.11	0.14	0.10	0.22	11	11	68.283	323
Cytochrome c oxidase subunit 6A1, mitochondrial	COX6A1	0.22	0.27	0.32	0.32	1	1	12.155	79
60S ribosomal protein L5	RPL5	0.15	0.19	0.21	0.43	8	8	34.362	68
Transitional endoplasmic reticulum ATPase	VCP	0.25	0.30	0.44	0.39	20	20	89.321	271
Ras-related protein Rab-2A; Ras-related protein Rab-2B	RAB2A; RAB2B	0.25	0.31	0.43	0.41	9	9	23.545	372
Calumenin	CALU	0.16	0.20	0.43	0.40	8	8	37.106	73
Stress-induced-phosphoprotein 1	STIP1	0.21	0.26	0.37	0.30	17	17	62.639	133

Protein names	Gene names	RIA (synthesis) Uninfected24h	RIA (synthesis) 24hpi	RIA (synthesis) Uninfected48h	RIA (synthesis) 48hpi	Peptides	Unique peptides	Mol. weight [kDa]	Score
Extended synaptotagmin-1	ESYT1	0.17	0.20	0.11	0.24	16	16	122.85	196

Table 4.3: Proteins significantly synthesized in 48 hpi groups.

Replicates from both uninfected and 48 hpi THP-1 were grouped. Light (L) and heavy (H) monoisotopic intensities were averaged. RIA synthesis was calculated using formula in section 2.10.4. Only proteins that have been quantified in all biological replicates were considered for this statistical test. Two-sample t-test was performed on the filtered data and gave rise to 84 differentially synthesized proteins (FDR value = 0.05).

Protein names	Gene names	RIA (synthesis) Uninfected24h	RIA (synthesis) 24hpi	RIA (synthesis) Uninfected48h	RIA (synthesis) 48hpi	Peptides	Unique peptides	Mol. weight [kDa]	Score
Histone H1.5	HIST1H1B	0.09	0.03	0.03	0.11	6	6	23	85
Electron transfer flavoprotein subunit beta	ETFB	0.37	0.11	0.10	0.29	6	6	28	70
Leukotriene A-4 hydrolase	LTA4H	0.13	0.12	0.21	0.61	9	9	69	55
Catalase	CAT	0.06	0.08	0.05	0.14	14	14	60	183
Annexin A6	ANXA6	0.08	0.06	0.06	0.15	16	16	76	225
Histone H4	HIST1H4A	0.10	0.04	0.03	0.08	12	12	11	185
Dolichyl-diphosphooligosaccharide--protein glycosyltransferase subunit 1	RPN1	0.12	0.13	0.16	0.40	25	25	69	323
Dolichyl-diphosphooligosaccharide--protein glycosyltransferase 48 kDa subunit	DDOST	0.16	0.12	0.19	0.45	10	10	51	182
Dihydropyrimidinase-related protein 2	DPYSL2	0.25	0.20	0.19	0.45	10	10	62	174
Extended synaptotagmin-1	ESYT1	0.17	0.20	0.11	0.24	16	16	123	196

Protein names	Gene names	RIA (synthesis) Uninfected24h	RIA (synthesis) 24hpi	RIA (synthesis) Uninfected48h	RIA (synthesis) 48hpi	Peptides	Unique peptides	Mol. weight [kDa]	Score
Protein S100-A4	S100A4	0.18	0.15	0.13	0.30	5	5	12	19
L-lactate dehydrogenase A chain	LDHA	0.21	0.15	0.17	0.37	24	23	37	323
Acyl-CoA-binding protein	DBI	0.16	0.12	0.13	0.27	5	5	10	17
Phosphoglucomutase-2	PGM2	0.11	0.14	0.10	0.22	11	11	68	323
Endoplasmic reticulum resident protein 29	ERP29	0.10	0.07	0.07	0.14	8	8	29	56
60S ribosomal protein L5	RPL5	0.15	0.19	0.21	0.43	8	8	34	68
Liver carboxylesterase 1	CES1	0.13	0.05	0.05	0.11	20	20	63	323
Interferon-induced GTP-binding protein Mx1, N-terminally processed	MX1	0.14	0.24	0.24	0.49	7	4	76	58
T-complex protein 1 subunit epsilon	CCT5	0.17	0.14	0.24	0.49	16	16	60	193
Ezrin	EZR	0.14	0.17	0.21	0.40	17	9	69	245
Endoplasmic reticulum metallopeptidase 1	ERMP1	0.16	0.21	0.17	0.33	7	7	100	23
Dihydrolipoyl dehydrogenase, mitochondrial	DLD	0.15	0.14	0.20	0.39	7	7	54	54
Prohibitin	PHB	0.15	0.19	0.12	0.22	8	8	30	186
Trifunctional enzyme subunit beta, mitochondrial;3-ketoacyl-CoA thiolase	HADHB	0.26	0.12	0.18	0.32	8	8	51	173
Ubiquitin-conjugating enzyme E2 L3	UBE2L3	0.39	0.19	0.27	0.46	5	5	18	53
Heat shock 70 kDa protein 1B; Heat shock 70 kDa protein 1A	HSPA1B; HSPA1A	0.25	0.36	0.22	0.38	10	4	70	30
Lysosome-associated membrane glycoprotein 2	LAMP2	0.21	0.13	0.27	0.46	3	3	45	36
60S acidic ribosomal protein P0;60S acidic ribosomal protein P0-like	RPLP0; RPLP0P6	0.19	0.15	0.23	0.40	8	8	34	146
Histone H2B type 1-L; Histone H2B type 1-M;Histone H2B type 1-N;Histone H2B type 1-H;Histone H2B type 2-F;Histone H2B type 1-C/E/F/G/I	HIST1H2BL; HIST1H2B	0.06	0.03	0.03	0.06	7	2	14	168

Protein names	Gene names	RIA (synthesis) Uninfected24h	RIA (synthesis) 24hpi	RIA (synthesis) Uninfected48h	RIA (synthesis) 48hpi	Peptides	Unique peptides	Mol. weight [kDa]	Score
	M;HIST1H2BN;HIST1H2BH;HIST2H2BF								
Heat shock protein 105 kDa	HSPH1	0.15	0.16	0.34	0.56	12	12	97	128
Heat shock 70 kDa protein 4	HSPA4	0.20	0.13	0.29	0.48	15	15	94	323
Histone H2B type 2-E; Histone H2B type 1-B;Histone H2B type 1-O;Histone H2B type 1-J;Histone H2B type 3-B	HIST2H2BE;HIST1H2BB;HIST1H2BO;HIST1H2BJ;HIST3H2BB	0.06	0.03	0.04	0.06	7	2	14	30
Heat shock 70 kDa protein 6; Putative heat shock 70 kDa protein 7	HSPA6; HSPA7	0.28	0.24	0.26	0.42	8	1	71	11
Splicing factor U2AF 65 kDa subunit	U2AF2	0.23	0.33	0.34	0.56	8	8	54	80
Vesicle-fusing ATPase	NSF	0.20	0.26	0.27	0.44	8	8	83	83
Gelsolin	GSN	0.33	0.24	0.31	0.49	26	10	86	323
Triosephosphate isomerase	TPI1	0.11	0.11	0.25	0.39	13	13	31	262
Lactoylglutathione lyase	GLO1	0.17	0.08	0.15	0.24	14	14	21	244
78 kDa glucose-regulated protein	HSPA5	0.15	0.15	0.24	0.38	30	29	72	323
Prostaglandin G/H synthase 1	PTGS1	0.24	0.21	0.19	0.29	6	6	69	76
Macrophage-capping protein	CAPG	0.20	0.10	0.14	0.22	7	7	38	258
Glucose-6-phosphate isomerase	GPI	0.18	0.15	0.21	0.32	15	11	63	302
Beta-actin-like protein 2	ACTBL2	0.22	0.18	0.23	0.34	8	1	42	3
Protein disulfide-isomerase A4	PDIA4	0.12	0.07	0.15	0.22	24	23	73	303

Protein names	Gene names	RIA (synthesis) Uninfected24h	RIA (synthesis) 24hpi	RIA (synthesis) Uninfected48h	RIA (synthesis) 48hpi	Peptides	Unique peptides	Mol. weight [kDa]	Score
Carbonic anhydrase 2	CA2	0.05	0.21	0.11	0.17	16	16	29	233
40S ribosomal protein S12	RPS12	0.18	0.24	0.21	0.32	6	6	15	190
Peroxiredoxin-5, mitochondrial	PRDX5	0.17	0.09	0.17	0.26	7	7	22	139
Deoxynucleoside triphosphate triphosphohydrolase SAMHD1	SAMHD1	0.10	0.11	0.14	0.20	21	21	72	323
Procollagen galactosyltransferase 1	COLGALT1	0.21	0.13	0.17	0.25	10	10	72	60
Peroxisomal multifunctional enzyme type 2;(3R)-hydroxyacyl-CoA dehydrogenase;Enoyl-CoA hydratase 2	HSD17B4	0.10	0.10	0.15	0.21	17	17	80	195
UTP--glucose-1-phosphate uridylyltransferase	UGP2	0.13	0.08	0.14	0.20	3	3	57	235
Endoplasmin	HSP90B1	0.15	0.09	0.12	0.16	37	33	92	323
Fructose-bisphosphate aldolase A	ALDOA	0.20	0.16	0.26	0.37	27	22	39	323
Trifunctional enzyme subunit alpha, mitochondrial;Long-chain enoyl-CoA hydratase;Long chain 3-hydroxyacyl-CoA dehydrogenase	HADHA	0.17	0.11	0.19	0.27	22	22	83	323
Peroxiredoxin-2	PRDX2	0.13	0.07	0.12	0.17	7	6	22	69
Serine/arginine-rich splicing factor 1	SRSF1	0.13	0.30	0.30	0.41	6	6	28	51
Puromycin-sensitive aminopeptidase	NPEPPS	0.21	0.12	0.20	0.27	10	10	103	58
Pyruvate kinase PKM	PKM	0.31	0.22	0.39	0.52	33	32	58	323
Isoleucine--tRNA ligase, mitochondrial	IARS2	0.12	0.18	0.23	0.30	14	14	114	127
Heat shock protein HSP 90-alpha	HSP90AA1	0.15	0.16	0.24	0.32	38	24	85	323
Isocitrate dehydrogenase [NADP], mitochondrial	IDH2	0.15	0.07	0.16	0.21	14	14	51	169
ATP-citrate synthase	ACLY	0.13	0.22	0.22	0.28	16	16	121	251
Alpha-enolase	ENO1	0.20	0.13	0.21	0.28	27	27	47	323

Protein names	Gene names	RIA (synthesis) Uninfected24h	RIA (synthesis) 24hpi	RIA (synthesis) Uninfected48h	RIA (synthesis) 48hpi	Peptides	Unique peptides	Mol. weight [kDa]	Score
Very-long-chain 3-oxoacyl-CoA reductase	HSD17B12	0.17	0.11	0.15	0.20	7	7	34	151
ATP-dependent RNA helicase DDX39A	DDX39A	0.15	0.10	0.19	0.25	13	6	49	45
Actin, cytoplasmic 1;Actin, cytoplasmic 1, N-terminally processed	ACTB	0.25	0.17	0.24	0.30	27	2	42	323
Histone H1.4	HIST1H1E	0.16	0.09	0.14	0.18	6	2	22	26
Ras-related protein Rab-7a	RAB7A	0.31	0.22	0.42	0.53	11	11	23	312
Alpha-soluble NSF attachment protein	NAPA	0.22	0.23	0.36	0.46	5	5	33	80
Thymosin beta-4; Hematopoietic system regulatory peptide	TMSB4X	0.38	0.18	0.33	0.41	9	7	5	140
Programmed cell death 6-interacting protein	PDCD6IP	0.42	0.22	0.42	0.53	14	14	96	72
Peroxiredoxin-6	PRDX6	0.27	0.15	0.22	0.28	12	12	25	177
40S ribosomal protein S20	RPS20	0.16	0.17	0.24	0.30	3	3	13	57
Fatty acid synthase; [Acyl-carrier-protein] S-acetyltransferase;[Acyl-carrier-protein] S-malonyltransferase;3-oxoacyl-[acyl-carrier-protein] synthase;3-oxoacyl-[acyl-carrier-protein] reductase;3-hydroxyacyl-[acyl-carrier-protein] dehydratase;Enoyl-[acyl-carrier-protein] reductase;Oleoyl-[acyl-carrier-protein] hydrolase	FASN	0.21	0.15	0.22	0.27	36	36	273	323
Phosphoglycerate kinase 1	PGK1	0.17	0.13	0.25	0.31	22	22	45	323
Signal transducer and activator of transcription 1-alpha/beta	STAT1	0.25	0.38	0.43	0.53	8	8	87	21
Endoplasmic reticulum resident protein 44	ERP44	0.18	0.15	0.24	0.30	8	8	47	65
ERO1-like protein alpha	ERO1L	0.17	0.11	0.22	0.27	9	9	54	44
Tripeptidyl-peptidase 1	TPP1	0.29	0.21	0.31	0.37	4	4	61	31

Protein names	Gene names	RIA (synthesis) Uninfected24h	RIA (synthesis) 24hpi	RIA (synthesis) Uninfected48h	RIA (synthesis) 48hpi	Peptides	Unique peptides	Mol. weight [kDa]	Score
L-lactate dehydrogenase B chain	LDHB	0.15	0.07	0.14	0.17	11	10	37	280
Cytochrome b-c1 complex subunit 1, mitochondrial	UQCRC1	0.26	0.22	0.28	0.34	9	9	53	80
60 kDa heat shock protein, mitochondrial	HSPD1	0.10	0.07	0.10	0.12	32	32	61	323
Protein disulfide-isomerase A6	PDIA6	0.12	0.08	0.14	0.17	19	19	48	323
Succinate dehydrogenase [ubiquinone] flavoprotein subunit, mitochondrial	SDHA	0.21	0.14	0.23	0.28	8	8	73	109

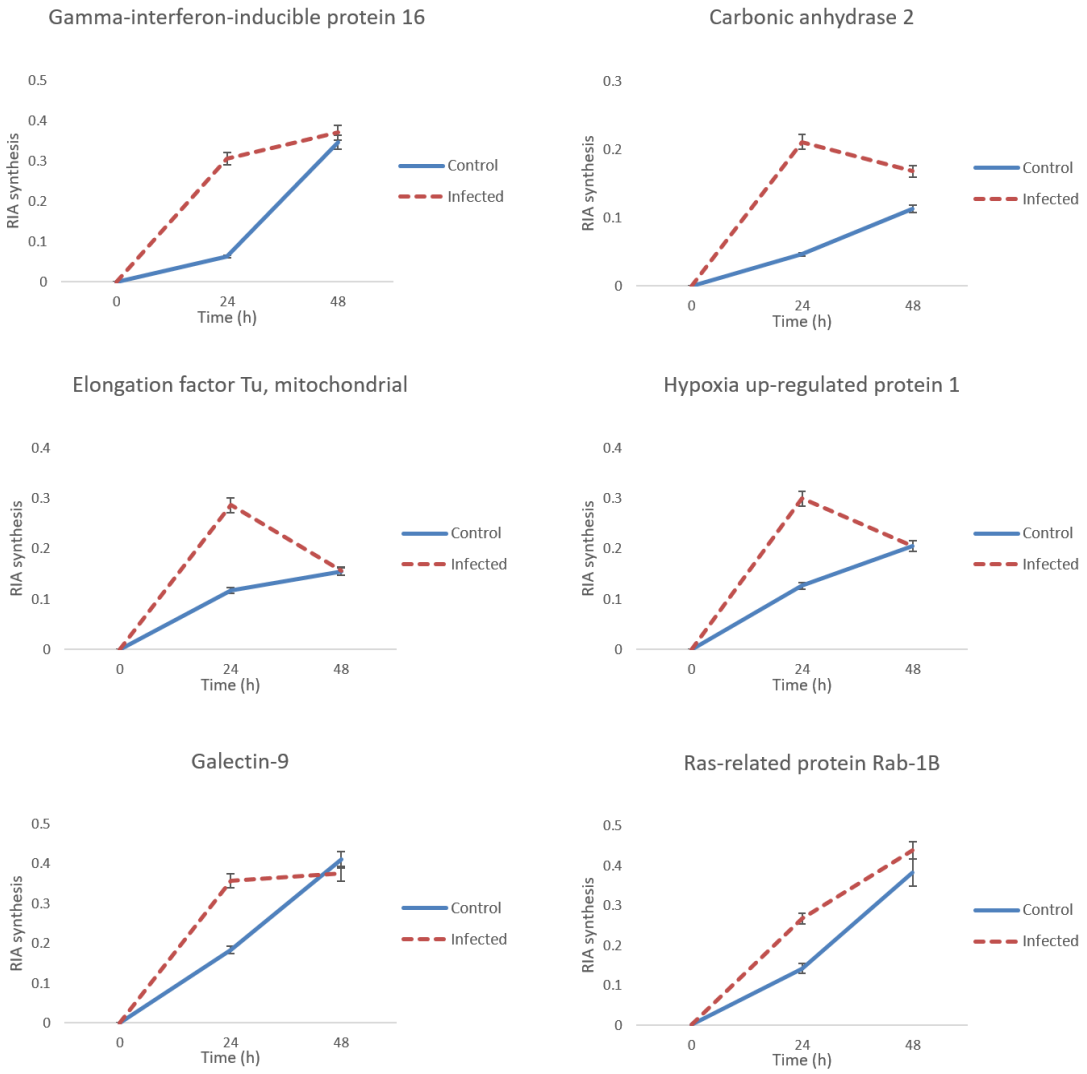

Figure 4.30: Determination of protein synthesis rate of proteins identified in uninfected and infected THP-1.

RIA synthesis was calculated for several proteins and plotted against time (n = 3). Values represent mean ± SD of three replicates.

Figures 4.30 and 4.31 showed RIA synthesis for several proteins with significant change in synthesis rate between uninfected, 24 h and 48 h infected cells. It was evident from the graphs that these proteins were synthesized more in infected cell compared to uninfected. For example, interferon-induced GTP-binding protein Mx1 had an increase of synthesis after 48 hpi by 2.5-fold. Although carbonic anhydrase 2, elongation factor Tu and hypoxia upregulated protein 1 had reduced synthesis from 24 to 48 hpi, the rate of synthesis were still higher than the uninfected cell.

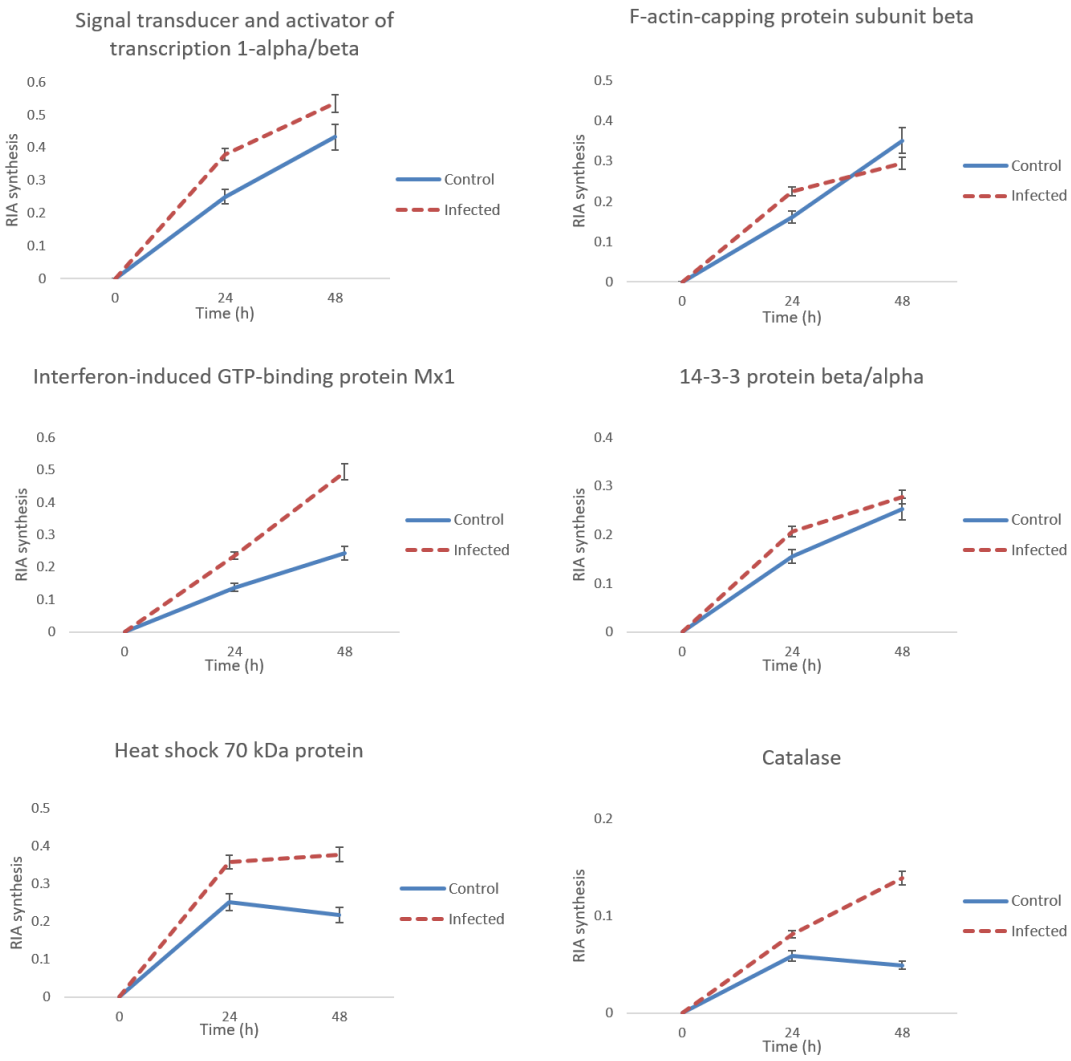

Figure 4.31: Determination of protein synthesis rate of proteins identified in uninfected and infected THP-1.

RIA synthesis was calculated for several proteins and plotted against time (n = 3). Values represent mean ± SD of three replicates.

Some of the proteins showed reduced synthesis following infection as compared to uninfected THP-1, including moesin, purine nucleoside phosphorylase, CD44, and gelsolin (Figure 4.32).

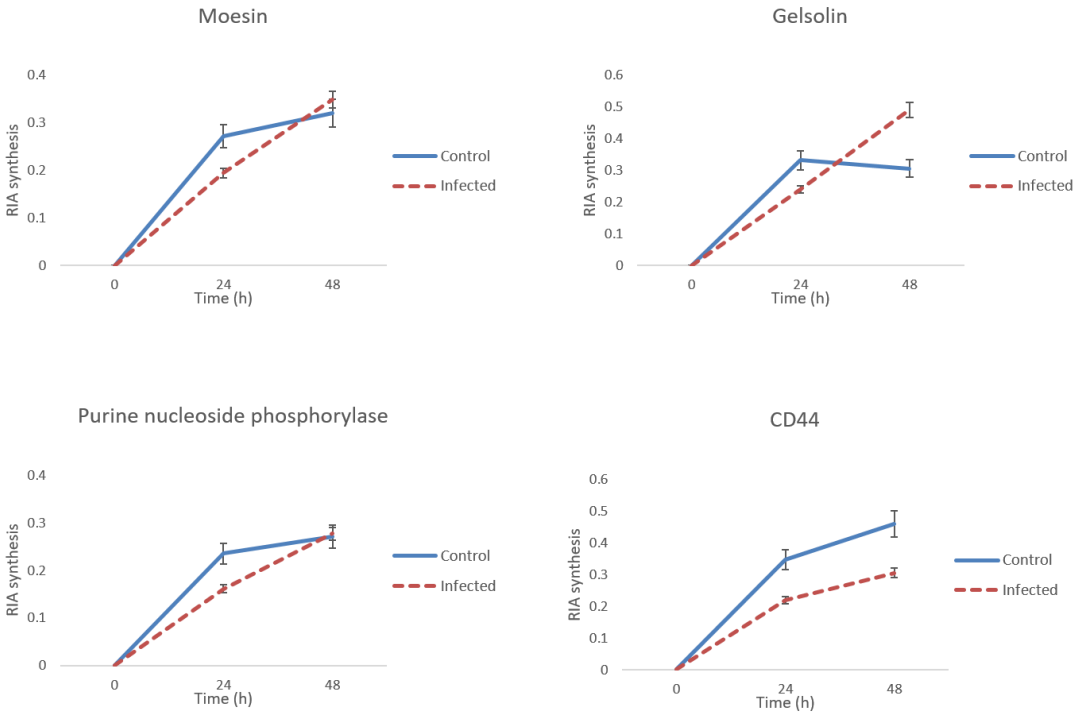

Figure 4.32: Determination of protein synthesis rate of proteins identified in uninfected and infected THP-1.

RIA synthesis was calculated for several proteins and plotted against time (n = 3). Values represent mean ± SD of three replicates.

We also investigate the synthesis rate of several metabolic enzymes involve in glycolysis, oxidative phosphorylation, and others. It appears that some of the enzymes had decreased synthesis during 24 h of infection but increased their synthesis rate after 48 h of infection. These include alpha-enolase, fatty acid synthase, fructose-bisphosphate aldolase A, isocitrate dehydrogenase, L-lactate dehydrogenases, glucose-6-phosphate isomerase, and phosphoglycerate kinase 1 (Figure 4.33).

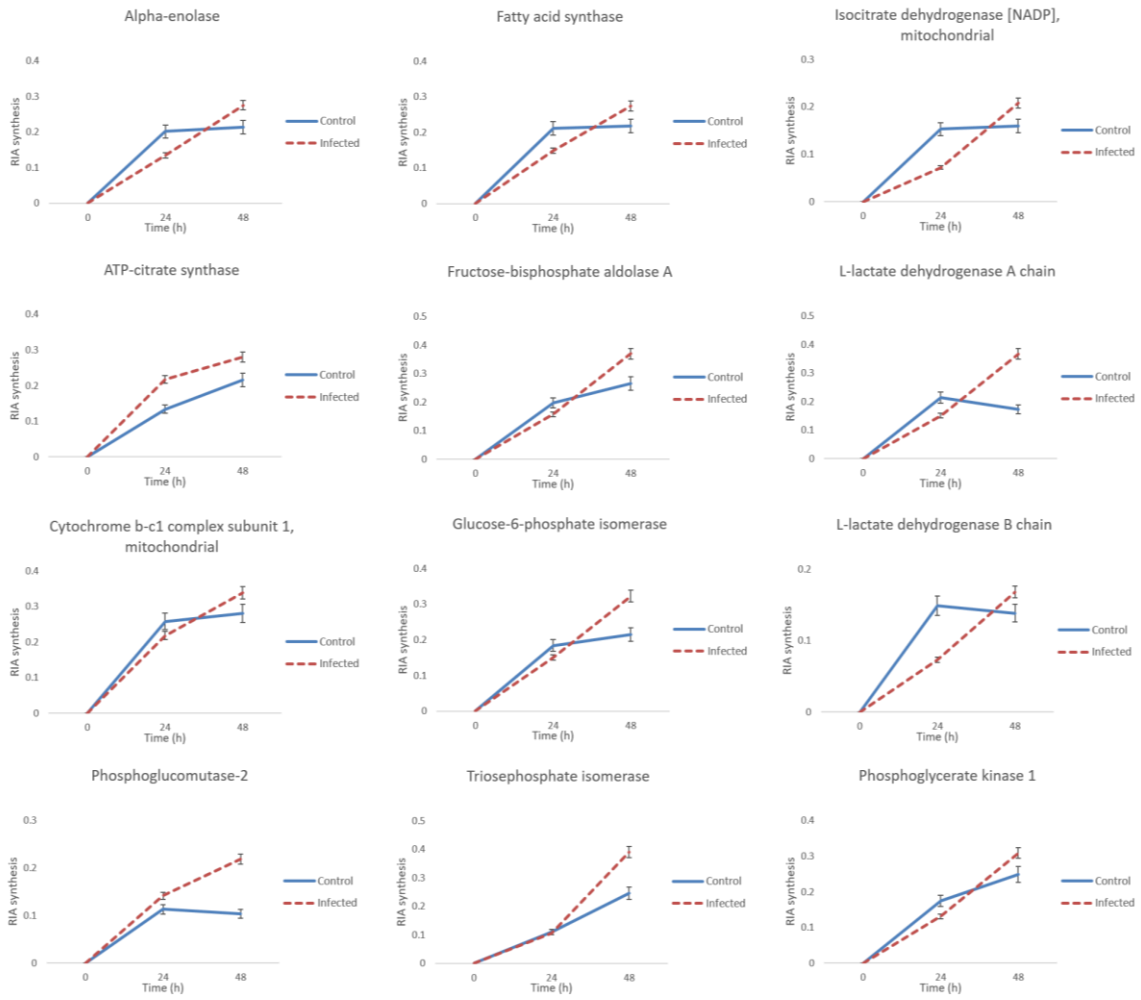

Figure 4.33: Determination of protein synthesis rate of metabolic proteins identified in uninfected and infected THP-1.

RIA synthesis was calculated for several metabolic proteins and plotted against time (n = 3). Values represent mean ± SD of three replicates.

Several ribosomal proteins such as 40S ribosomal protein S12, 40S ribosomal protein S20 and 60S ribosomal protein L5 had increased synthesis following infection (compared to uninfected), except 60S acidic ribosomal protein P0 which had decreased synthesis after 24 h of infection then increased its synthesis after 48 h of infection (Figure 4.34). Furthermore, we looked at several proteins involve in stress response and found that proteins including peroxiredoxin-2, peroxiredoxin-5 and peroxiredoxin-6 had decreased synthesis rate after 24 h of infection but later increased their synthesis after 48 h of infection (Figure 4.35).

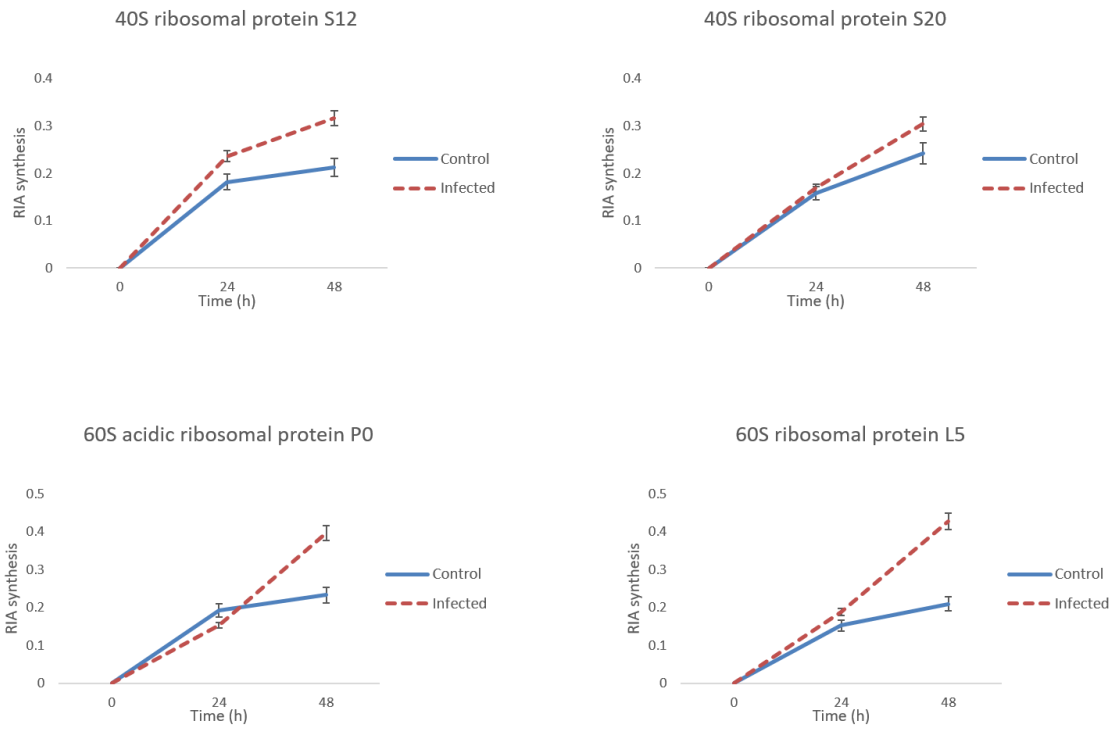

Figure 4.34: Determination of protein synthesis rate of ribosomal proteins identified in uninfected and infected THP-1.

RIA synthesis was calculated for several ribosomal proteins and plotted against time (n = 3). Values represent mean ± SD of three replicates.

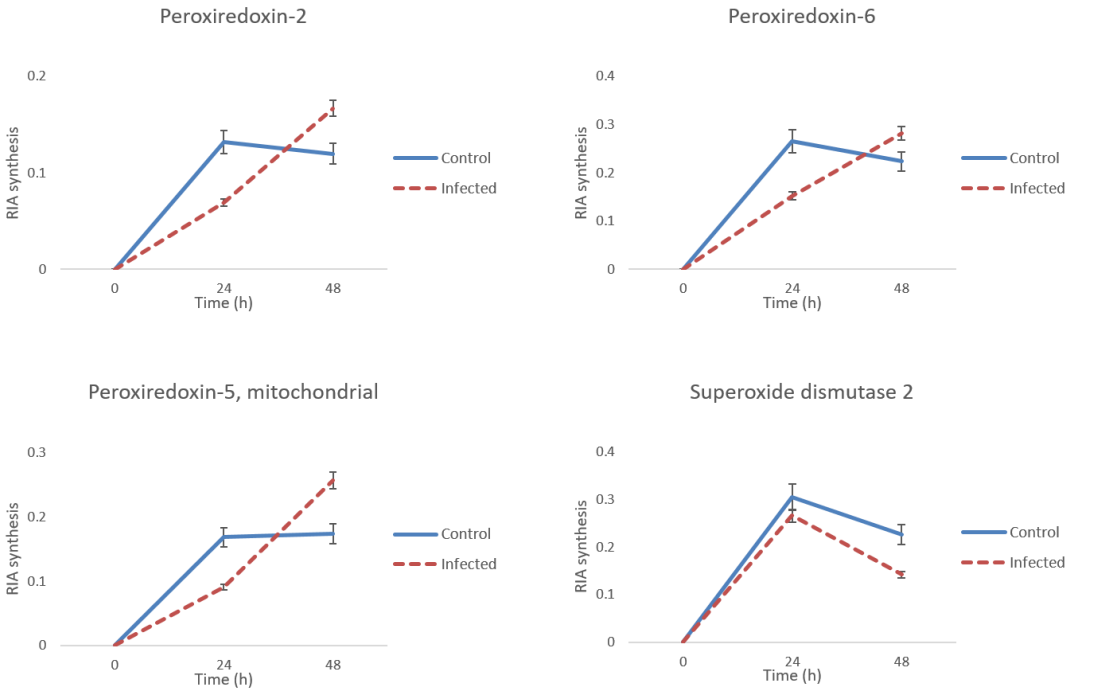

Figure 4.35: Determination of protein synthesis rate of stress response proteins identified in uninfected and infected THP-1.

RIA synthesis was calculated for several proteins involve in stress response and plotted against time (n = 3). Values represent mean ± SD of three replicates.

Gelsolin was one of the proteins that showed significant decreased of synthesis in infected cells. Gelsolin is well recognised for its involvement in the actin cytoskeleton dynamics by interacting with actin filaments and membrane during a variety of forms of cell motility (Kwiatkowski 1999). As expected, when we mapped the proteins found in our data onto KEGG pathways, gelsolin was found in two important pathways: regulation of actin cytoskeleton and $Fc_{\gamma}R$-mediated phagocytosis (Figure 4.36 and 4.37). Gelsolin works with other proteins in the protein network to regulate actin cytoskeleton and phagocytosis. In one of the pathways, gelsolin also interacts with actin that was similarly significantly decreased p.i.

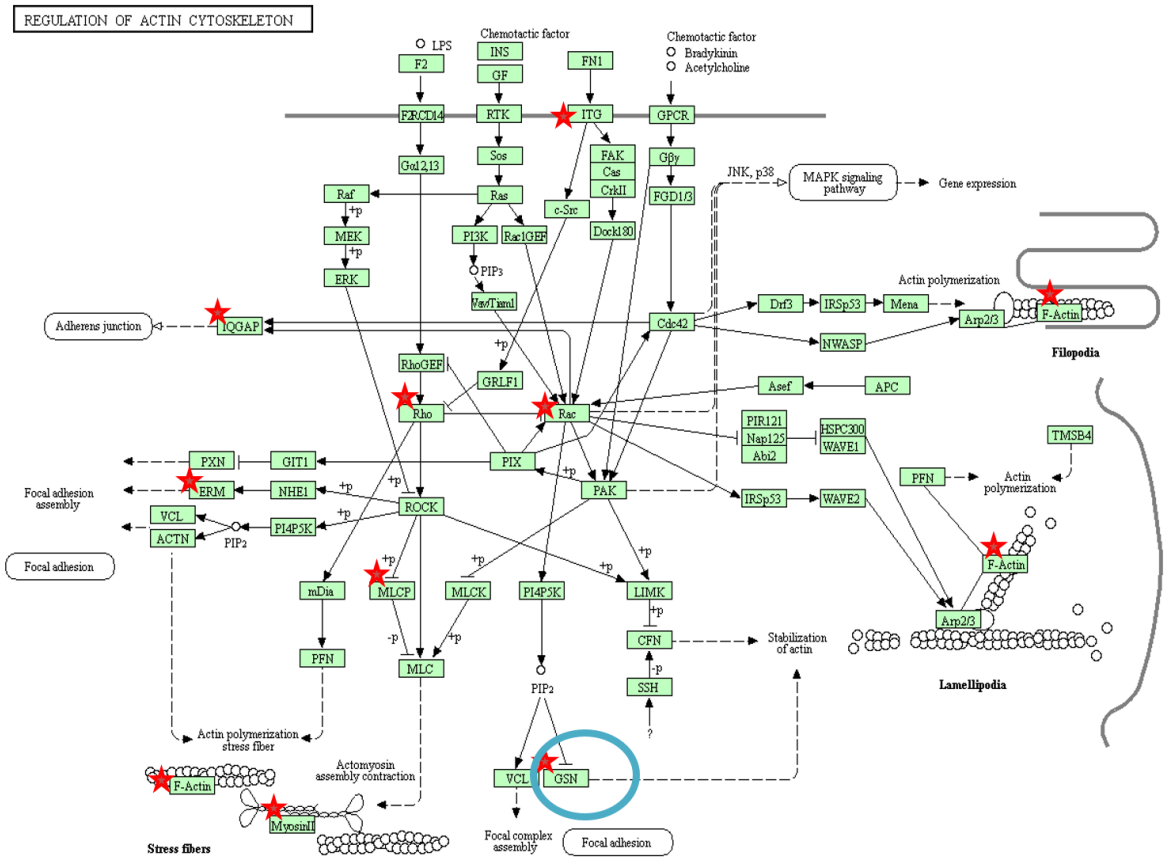

Figure 4.36: Regulation of actin cytoskeleton KEGG pathway.

All proteins identified in this study were analysed on DAVID. The pathways linked to KEGG were chosen and gelsolin was found in actin cytoskeleton pathway (blue circle). The red stars represent the proteins found in our data.

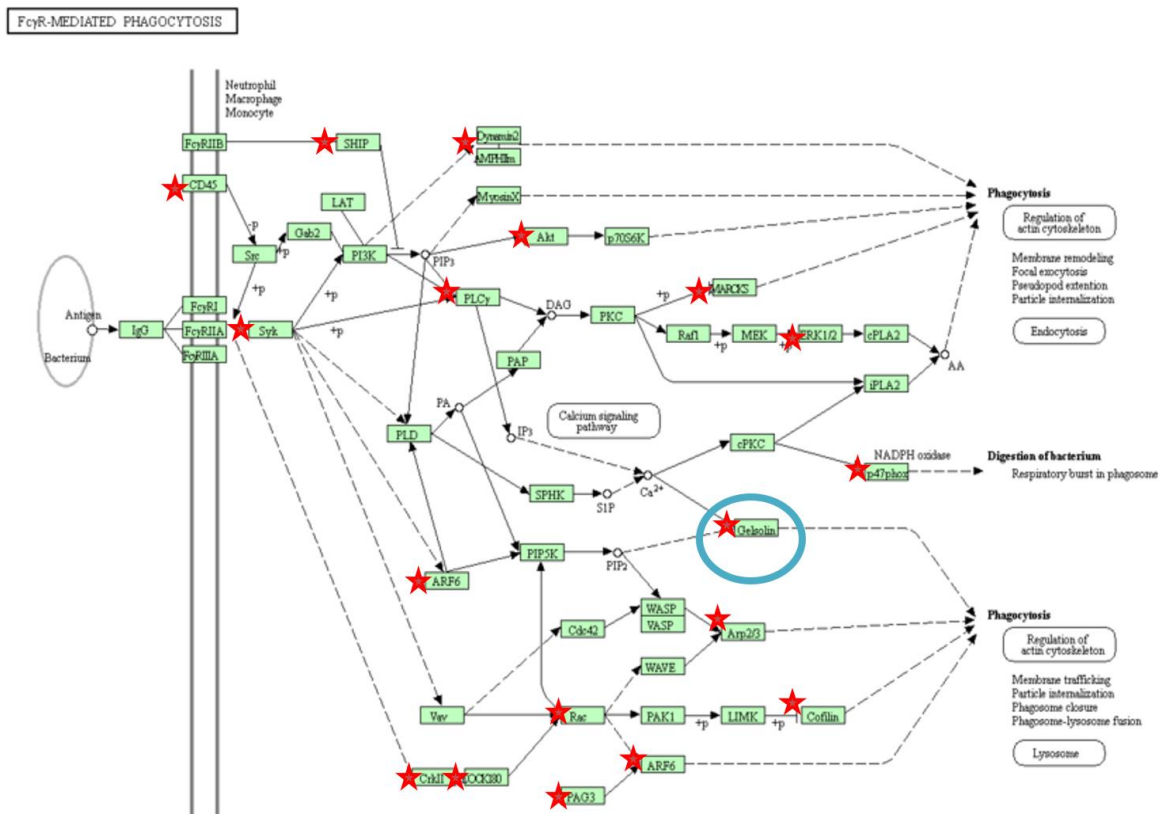

Figure 4.37: $Fc_{\gamma}R$-mediated phagocytosis KEGG pathway.

All proteins identified in this study were analysed on DAVID. The pathways linked to KEGG were chosen and gelsolin was found in $Fc_{\gamma}R$-mediated phagocytosis (blue circle). The red stars represent the proteins found in our data.

Table 4.4**: Summary of identified and quantified proteins in uninfected, 24 hpi and 48 hpi THP-1.**

Following 2-D LCMS/MS, raw data were analysed on MaxQuant and Perseus.

	Proteins identified	*Proteins quantified*	*Proteins with significant increased synthesis 24 hpi*	*Proteins with significant increased synthesis 48 hpi*
*Uninfected THP-1***	1472	652		
*24 hpi THP-1***	1653	739		
*Uninfected 48h THP-1***	1929			
*48 hpi THP-1***	1183			
Uninfected, 24 hpi & 48 hpi THP-1#	2280	761	51	84

*Analysed separately on MaxQuant.

Combined on MaxQuant.

In addition, KEGG analysis reveals that we found quite a lot of proteins in essential subunits of complex I, III, IV and V of oxidative phosphorylation pathway (represented by red star in Figure 4.38). Amongst them are NADH dehydrogenase,

succinate dehydrogenase, cytochrome c oxidase, cytochrome c reductase and ATPase. However, some of these proteins were not quantified (have missing values).

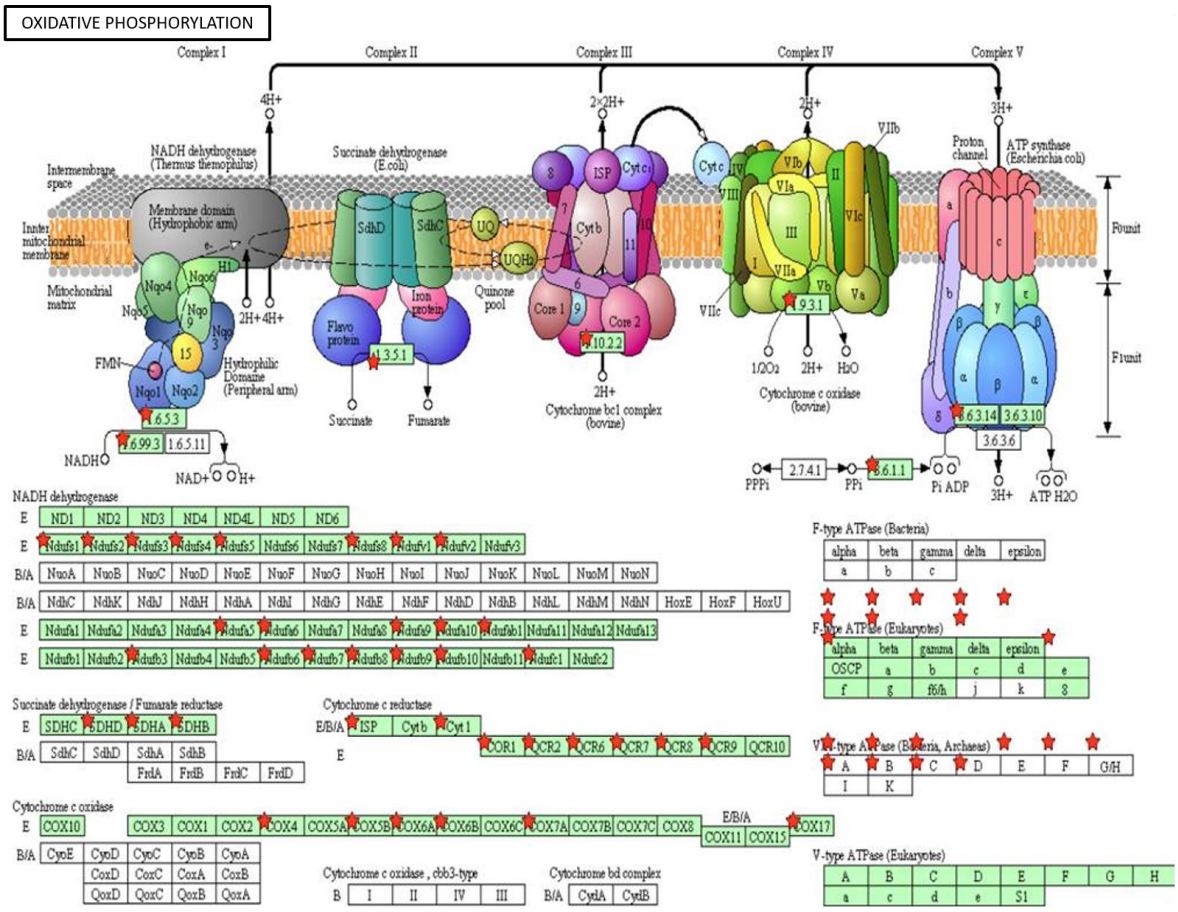

Figure 4.38: Oxidative phosphorylation KEGG pathway.

In the upper part are shown the five respiratory chain complexes with the corresponding E.C. numbers. In the bottom part are the subunits of each respiratory chain complex. All proteins identified in this study were mapped onto KEGG pathway. Several proteins were found in this pathway are represented by the red star.

To better understand how biological pathways were modulated in infected cells, we performed protein-protein interaction (PPI) network analysis on these proteins using the STRING database and visualizing results with Cytoscape. Highly modulated proteins showed very complex interactions among each other, although there are several proteins with no interaction within the network such as CD109, though it may interact with other proteins not in this list (figure not shown). They also demonstrate a more centralized and tightly connected interaction with each other. A subset of 84 statistical significant proteins (from 48 hpi data) showed high protein-protein interaction (Figure 4.39). For example, proteins involve in

cytoskeleton such as ß-tubulin (TUBB4B), actin (ACTB), gelsolin (GSN) and meosin (MSN) appeared to be interacting with each other. Recent data from Mazur et al. (2016) showed gelsolin interacts with several components of the cytoskeleton including actin and ß-tubulin.

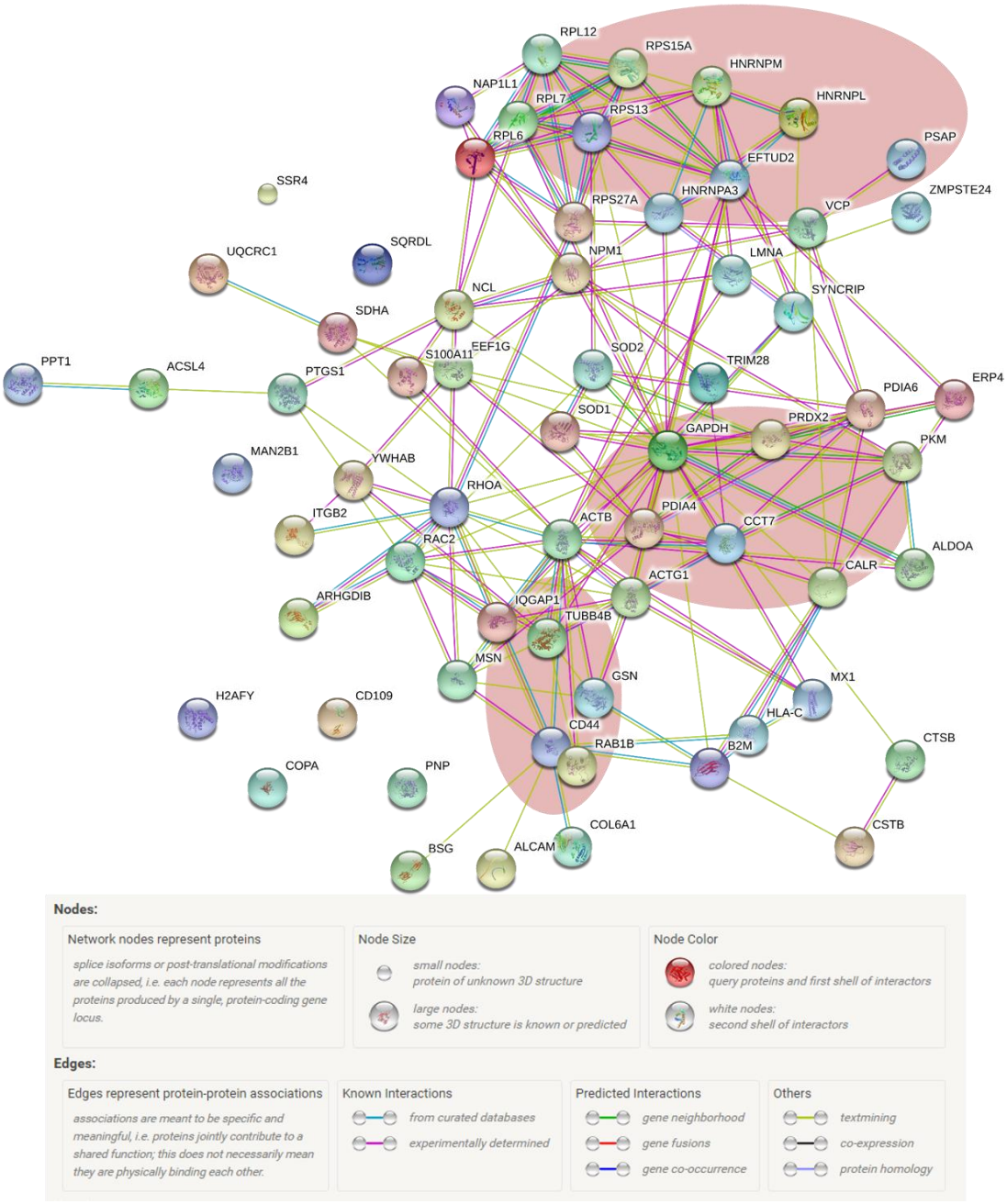

Figure 4.39: Protein network of 84 significant proteins (p=0.05).

A total of 84 proteins were statistically significant upon t-test analysis. These proteins were analysed on the STRING database to determine the protein-protein interactions between them. Proteins in red circles represented those involve in metabolic processes.

Of those 84 statistically significant proteins, 40 are implicated in metabolic processes. These include glyceraldehyde-3-phosphate dehydrogenase (GAPDH), peroxiredoxin 2 (PRDX2) and beta-2-microglobulin (BM2). GADPH is also involved in the immune response, together with MHC class I, C (HLA-C), cathepsin B (CTSB), CD44 and CD109. GADPH seems to have interactions with several other proteins such as CCT7 and superoxide dismutase 2 (SOD2). This observation suggests that in many metabolic enzymes interact with each other to produce small compounds or other macromolecules.

4.3.4 Validation of proteomic data

Proteomic data was validated by immunoblotting (Western blot) technique performed according to section 2.11.1. Following two sample t-test analysis, proteins that were shown to be differentially synthesized significantly at p-value of 0.05 including galectin-9 and gelsolin were chosen to be validated by Western blot to represent proteins with significant changes in infected cells. Gelsolin showed an intense band at the expected molecular weight of 86 kDa while galectin-9 showed two bands at the molecular weight of 38 and ~36 kDa (Figure 4.40). The presence of two bands on galectin-9 was probably due to alternate splicing variants that has been reported in Spitzenberger et al. (2001). Anti-alpha tubulin (52 kDa) was used as loading control.

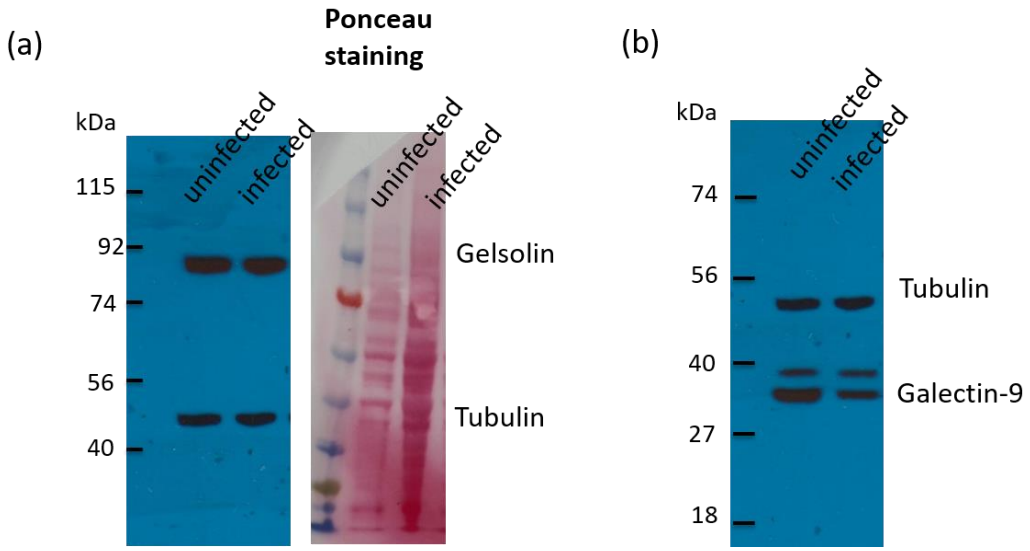

Figure 4.40: Immunoblot profile of gelsolin and galectin-9.

Protein lysates from uninfected and infected samples were separated on polyacrylamide gel and blotted onto membrane and analysed using specific antibodies against gelsolin and galectin-9. The position of molecular mass standards is indicated at the left.

4.4 Discussions

In this work, a comprehensive SILAC-based proteome analysis of the response of THP-1 cell to infection with *L. mexicana* is presented. The effect of parasite infection on the cellular proteome was investigated to gain insights into regulatory modulations associated with a productive infection cycle. Inarguably, analysing the data generated using multiple bioinformatics tools could unravel numerous important players in the complex molecular interplay of host and parasite.

Central to the host-*Leishmania* relationship is the macrophage. Some of the major functions of macrophages include maintaining tissue homeostasis, recognising and destroying pathogens through phagocytosis, alerting the immune system to foreign invasion through various signalling pathways, as well as apoptotic roles (Teo & Hughes 2003). Macrophages mediate innate immune responses and contribute to adaptive immunity to the host. There are three distinct populations of macrophages recognised to date: classical activated macrophages (M1), alternatively activated macrophages (M2) and type-2 activated macrophages. When macrophages are exposed to IFN-γ and TNF, along with exposure to microbial product such as LPS, T-cell induces Th1 responses that will induce IL-12 and upregulate MHC class II. This in turn upregulate the production of NO via inducible nitric oxide synthase (iNOS) gene. Together with toxic oxygen species, these will kill intracellular pathogen (Mosser 2003). These describe the characteristic of M1 macrophages. In M2 macrophages, exposure to IL-4 induced Th2 responses that will upregulate IL-10 and arginase production instead of NO. Arginase lead to polyamine biosynthesis that promotes cell growth and tissue repair (Hesse et al. 2001; Mosser 2003). Type-2 activated macrophages occur when they expose to FCγRs that will unexpectedly turned off IL-12 synthesis and induce IL-10. However, ligation of FCγR requires a macrophage stimulatory signal through any TLRs such as CD44 (Sutterwala et al. 1997; Sutterwala et al. 1998; Mosser 2003). Many pathogens such as *Leishmania* and *Mycobacterium spp* have been reported to evade host and have the ability to interfere with host signalling pathways to prevent macrophage activation in order to favour their survival (Nandan et al. 2000). Therefore, the macrophage response to infection will determine the susceptibility or resistance of *Leishmania* in host.

While there are numerous sources of macrophages from animals and from immortalized cell lines available for *in vitro* studies, we chose the monocytic THP-1 cell line as it provides a homogeneous population of macrophages, in comparison to those isolated from animals or humans, e.g. primary human peripheral blood monocyte (PBMC) derived macrophages (Auwerx 1991; Tsuchiya et al. 1982; Mehta et al. 2011). Numerous earlier studies on THP-1 cells have indicated that the cells resemble primary monocytes and macrophages in terms of macrophage differentiation, regulation of macrophage-specific genes as well as morphological and functional properties of macrophages (Kramer & Wray 2002; Tsuchiya et al. 1982; Chanput et al. 2014; Daigneault et al. 2010). Furthermore, THP-1 has been shown to respond well to infection by several intracellular pathogens including some *Leishmania* species such as *L. donovani, L. infantum* and *L. braziliensis* (Ogunkolade et al. 1990; Kang et al. 2006; Jain et al. 2012; Oveland et al. 2009; Millar et al. 2015). Inarguably, it is easier to perform SILAC approach on cell-lines as they can grow indefinitely in *in vitro* culture.

Quantitative proteomics techniques have been extensively used to define changes between control and experimental groups. Despite the labelling techniques straightforwardly available, interpretation of datasets derived from these experiments is challenging. Nevertheless, in this study, we established a pulse-chase SILAC approach (pcSILAC), in an attempt to shed some light on the dynamics of protein expression in macrophages infected with *Leishmania*. This chapter focuses on the establishment of pcSILAC in THP-1, comparing uninfected with 24 hour- and 48 hour-infected cells, as well as determination of synthesis rate, before expanding the set up for protein degradation rate in order to define turnover (chapter 5).

pcSILAC has the power to measure changes in protein production between conditions integrated over time after the pulse. At the beginning of chase starting point, all proteins are universally labelled, in this case with heavy Lys and Arg. During the chase period, exogenous amino acids are exclusively light labelled, so that newly synthesized proteins will contain light Lys and Arg, while proteins that persist from the pulse period will be heavy labelled. The rate at which heavy labelled proteins are replaced by light labelled equivalents is a reflection of the proteins turnover rate under the conditions employed. This rate can be measured

by MS analysis of tryptic peptides, in a workflow that infers the relative abundance of light and heavy labelled peptides.

As it is crucial that the growth rate of THP-1 in heavy and light-labelled SILAC media be as similar as possible to minimise dilution rate, we adapted THP-1 in SILAC media with dFCS and assessed the growth profiles over time. Moreover, we used pcSILAC approach to specifically investigate the proteome dynamics when host's cells were infected with *L. mexicana*. Since we did not use another heavy isotope (heavy, medium and light isotope) in SILAC media, the infected samples are compared with mock-uninfected.

Employing high-resolution 2-D LC/MS coupled with pcSILAC technique, we have successfully identified 2016 proteins in uninfected THP-1 (control) and *L. mexicana*-infected THP-1. Our study was conducted at 24 hpi to assess cellular proteomics modulations associated with the establishment of infection. All biological replicates gave Pearson coefficient values of greater than 0.5, meaning that they are highly reproducible. Consistently, heat map and profile plot reflect this reproducibility.

Here, we report protein expression changes in several GO annotation terms and cellular pathways. Overall, the majority of the proteins in our dataset were primarily associated with metabolic process, transport, apoptosis and cell death, protein regulation, biosynthetic process, catabolic process and protein localisation. Global pathways modulated are metabolic pathway, constituent of ribosome, spliceosome, lysosome, regulation of actin cytoskeleton, leukocyte transendothelial migration, proteasome, Fcγ-R-mediated phagocytosis, TCA cycle, antigen processing and presentation, glycolysis/ gluconeogenesis and several signalling pathways.

Of those 2016 proteins, 761 were quantified in at least one replicate. Stringent filtering of the dataset to have at least values in all replicates with minimum quantification ratio at 2 yielded only 521 quantified proteins. This is a common issue in SILAC studies as one of the labelled pairs might not be detected by MS. Of those, 400 were considered for determination of protein synthesis rates that were selected based on stringent criteria as described earlier. These include PKM, L-lactate dehydrogenase, moesin, several glycolytic enzymes such as glucose-6-

phosphate isomerase and alpha enolase, gelsolin, galectin-9, catalase and lamin-B. Remarkably, several proteins involved in immune response such as HLA complexes, interleukins, CD44 antigen and Toll-like receptor were observed to have higher synthesis rates. This observation was to be expected as macrophages increased the expression of proteins involved in immune response when they sense intruders (Giudice et al. 2012).

Interestingly, there was a striking contrast in GO functional annotation terms between the proteins with increased synthesis in 24 and 48 hpi. While both 24 and 48 hpi harbours more metabolic enzymes, proteins with increased synthesis in 24 hpi were most highly associated to apoptosis and translation while proteins with increased synthesis in 48 hpi were mostly involved in response to stimulus and nucleosome, chromatin and protein-DNA assembly. This observation clearly showed that during early infection, macrophages upregulate expression of proteins involved in cellular processes that are fundamental to cells, involving complex cascades of biochemical reactions and signalling pathways. These include communication between a cell and the environment, cell recognition in which a cell interprets its surrounding, cell cycle, cell growth, cell proliferation to increase population size, DNA repair, protein targeting and apoptosis or programmed cell death. This is not surprising as the host presumably increases these proteins when they sense intruders at the early stage of infection. Following infection, *Leishmania* induce IL-8, a known chemotactic factor, from the host neutrophils to upsurge neutrophil recruitment to the site of infection (Van Zandbergen et al. 2002). IL-8 induces phagocytosis and a series of signalling pathway that causes oxidative burst that is lethal to the pathogen (Dixit & Simon 2012). Our dataset included several other interleukins such as IL-1β, IL-10 and interleukin-enhancer-binding factor (ILF). IL-1β, also known as leukocytic endogenous mediator, produced by macrophages as a mediator of the inflammatory responses. It is also involved in various cellular activities namely cell proliferation, differentiation and apoptosis (Dinarello 2009; Dinarello 2011). Th2 activation stimulates the production of IL-10 that downregulates the expression of Th1 cytokines such as IL-12 while inhibiting NF-κB activity (Aste-Amezaga et al. 1998). Notably, IL-10 has been shown to be produced by an M2 type (Mosser 2003). However, the function of IL-10 in tumour cells remains controversial as it has both tumour-suppressive and oncogenic roles (Fujii et al. 2001).

In addition, several anti- and pro-apoptosis proteins were found in this study including TNF-α-induced protein, cofilin, Bcl-2-associated transcription factor, programmed cell death protein, apoptosis-inducing factor-1, mitochondria, apoptosis regulator BAX and caspase 3. There are increased apoptosis activities in neutrophils and macrophages where the host eliminate infected cells. Various intracellular pathogens modulate apoptosis that favours their survival (Koziel et al. 2009). Of note, certain pathogens such as *Staphylococcus aureus* and *Chlamydia spp* appeared to repress apoptosis to allow them to replicate while silently persist in the host (Fischer & Häcker 2003). Apoptosis, a form of programmed cell death, is implemented by a series of signal transduction pathways and is employed as part of host defence mechanism against environmental stimuli which threatens the organism's integrity. Central in this pathway are Bcl-2 family members and caspase family. Bcl-2 is an intracellular protein that interfere with apoptosis and prolong survival of the cell (Hockenbery et al. 1990). Karsan et al. (1996) found that Bcl-2 is specifically induced by proinflammatory cytokines. Increase in Bcl-2 was orchestrated through TLR2-MEK-ERK signalling, and changes in TLR-2 levels affected parasite uptake (Pandey et al. 2016). Recent work by Pandey et al. (2016) demonstrated that *L. donovani* infection increased Bcl-2 expression in macrophage and more importantly, the inhibition of Bcl-2 accelerated the clearance of parasite, suggesting potential anti-leishmanial agents. In contrast to Bcl-2, apoptosis regulator BAX accelerates apoptosis (Noble et al. 1999). TNF-α is a cytokine that have a myriad of functions in the inflammatory responses. Stimulation of TNF in monocytes causes induction of IL-10 which reduce the overexpression of Bcl-2 homolog (Noble et al. 1999). The release of cytochrome c from mitochondria also stimulates apoptosis via the activation of caspase-9 which in turn activate caspase-3 (Rolland & Conradt 2006). Enhanced expression of caspase-9 and caspase-3 in CL patients suggested mechanisms associated with the progression of tissue damage observed in lesions (Santos et al. 2015). Bcl-2 family members exert anti-apoptotic activity by preventing the release of cytochrome c from mitochondria while Bak1 stimulates cell death (Cory & Adams 2002). Furthermore, overexpression of this anti-apoptotic proteins has been experimentally verified to abrogate the function of pro-apoptotic proteins, thereby eliciting a protective outcome on host cells (Koziel et al. 2009; Hockenbery et al. 1990).

Even though apoptosis is indispensable for host's defence against intracellular pathogens, several pathogens are known to modulate apoptotic machinery in order for them to replicate inside macrophages (Bruchhaus et al. 2007). Studies on several *Leishmania* species suggested that they manage to prevent host cell from undergoing apoptosis. This allow parasites to invade the host silently without triggering immune response from host (Getti et al. 2008). Apoptosis cells have been reported to recruit macrophages to the site of infection (Lauber et al. 2003) and this was taken advantage by *Leishmania* to recruit uninfected macrophages, allowing them to spread and establish infection (Getti et al. 2008). A study by Getti et al. (2008) confirmed that the induction of apoptosis after infection increased the number of infected macrophages thereby intensify infection. Likewise, it has been shown that phagocytosis of apoptotic neutrophils by *L. major*-infected BALB/c mice leads to an increase in parasite burden (Ribeiro-Gomes et al. 2004).

Other protein with increased synthesis p.i. in our dataset involving in cellular process specifically cell-cell communication is STAT1. STAT1 is a latent cytoplasmic TFs that mediate various biological responses, including cell proliferation, survival, apoptosis, and differentiation (Kim & Lee 2007). Activation of STAT1 by different cytokines resulted in modulation of broad spectrum of cell death, comprising both apoptotic and non-apoptotic pathways (Kim & Lee 2007). This activation is dependent upon phosphorylation of conserved tyrosine and serine residues in their C-terminal transactivation domain through JAK/STAT pathway and mitogen-activated protein kinases (MAPKs) (Rawlings et al. 2004). Interestingly, STAT1 may play an important role in the regulation of the cell death response through caspase-mediated cleavages (Kim & Lee 2007). Moreover, dephosphorylation of STAT1 abrogates IL-12 expression (de Morais et al. 2015). Particularly, STAT1 was upregulated/has increased turnover following infection by up to 10-fold. Taken together, proteins involve in cellular processes including apoptosis, cell communication and cell recognition were highly produced by THP-1 after infection with *L. mexicana*. Similar findings were also reported by Singh et al. (2015) where proteins involved in cell survival and signal transduction were more abundant in response to *L. donovani* infection.

In contrast, most of the proteins with reduced synthesis during early infection (24 h) were mostly involves in metabolic process. Subversion of host cell metabolism by intracellular pathogens has been proposed to play a key role in microbial growth and persistence by accessing essential nutrients (McConville & Naderer 2011; McConville et al. 2007; Liévin-Le Moal & Loiseau 2016).

Glycolysis, a major route of carbohydrate breakdown in eukaryotes, metabolizes glucose to pyruvate which enters the mitochondria where it is converted to acetyl-coA. Acetyl-coA also used in fatty acid biosynthesis and cholesterol synthesis. Glucose 6-phosphate isomerase (GPI), GAPDH, triosephosphate isomerase (TPI or TIM) (EC 5.3.1.1), isocitrate dehydrogenase (IDH) and pyruvate kinase (PKM) are some of the isoenzymes essential to glycolysis. In glycolysis and gluconeogenesis, GPI (E.C. 5.3.1.9) interconverts glucose-6-phosphate (G6P) and fructose-6-phosphate (F6P). However, this protein has different roles as well, including neuroleukin, autocrine motility factor, maturation factor and major surface antigen in sperm agglutination (Read et al. 2001; Yakirevich & Naot 2000). G6PDH (EC 1.1.1.49) is a housekeeping enzyme that catalyzes the chemical reaction between G6P and 6-phospho-D-glucono-1,5-lactone in pentose phosphate pathway (PPP). This pathway supplies reducing energy to cells by maintaining the level of the NADPH which provides pentoses for nucleic acid synthesis. NADPH not only important in protecting cells from oxidative damage, it is also essential for tissues actively engaged in biosynthesis of fatty acids such as liver (Kotaka et al. 2005; Liaud et al. 2000). Rabhi et al. (2012) reported that GPI and GADPH transcripts were upregulated in mice macrophage infected with *L. major* at 12 hpi but were downregulated at 24 hpi. PKM enzyme catalyzes the final step of glycolysis, in which pyruvate and ATP are formed. Pyruvate then enters TCA cycle to produce more ATP. Exposure of A549 human lung cancer cells to sources of ROS resulted in decreased in PKM activity (Anastasiou et al. 2012). Consequently, glucose flux is no longer converted into pyruvate, but is instead utilized in the PPP, resulting in the detoxification of ROS. They concluded that the regulatory mechanisms in PKM may be responsible for aiding cancer cell resistance to oxidative stress and enhanced tumorigenesis (Anastasiou et al. 2012). The reduced synthesis of PKM in THP-1 infected with *L. mexicana* may be due to the increased production of ROS by macrophages to kill the parasites. Our data showed that several of glycolysis and TCA cycle proteins had decreased synthesis rate in 24 hpi. This notion is in

agreement with several reported data such as Kelly & O'Neill (2015) and Singh et al. (2015).

Mitochondria are vital eukaryotic cell organelles involved in several metabolic pathways, calcium and iron homeostasis, ROS production and programmed cell death (Newmeyer & Ferguson-Miller 2003). Oxidative phosphorylation takes place inside mitochondria in most eukaryotes. Although both glycolysis and oxidative phosphorylation produce ATP, the latter is much more efficient in releasing more energy (Rich 2003). While oxidative phosphorylation is a vital part of metabolism, it also produces ROS that causes oxidative damage to the cells (Figure 4.41). We found several important respiratory enzymes in our dataset including NADH dehydrogenase, succinate dehydrogenase, cytochrome c oxidase, cytochrome c reductase and ATP synthase. Of these, only one of the ATP synthases showed increased synthesis in infected cells while the rest were not quantified in this work.

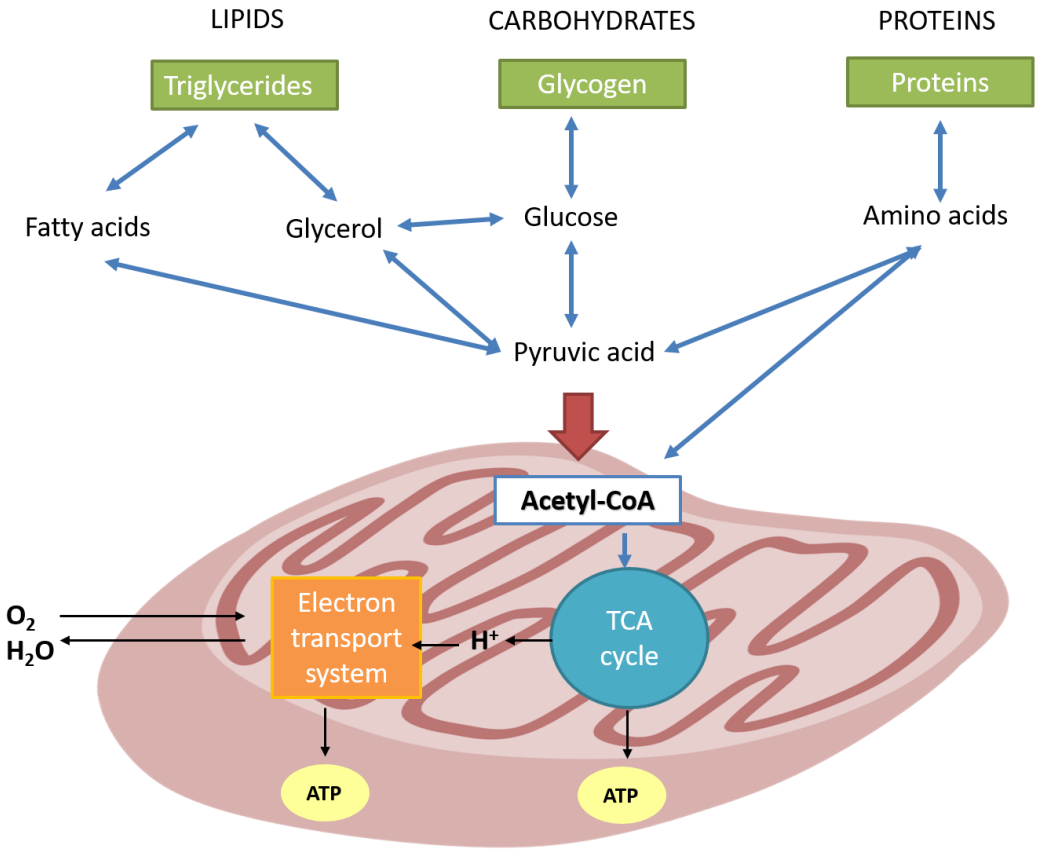

Figure 4.41: Representative scheme of metabolic processes in mitochondria.

Lipid, carbohydrates and amino acids metabolisms takes place in the cyrosol while TCA cycle and oxidative phosphorylation occurs in mitochondria.

To detect differentially expressed proteins between groups, two-sample t-test of uninfected and infected groups were applied. Among the 394 quantified proteins, 135 proteins achieved nominal significance at a 5% level. Of these, 51 proteins showed increased synthesis in 24 hpi. They were galectin-9, interferon-induced GTP-binding protein Mx1, 14-3-3 protein beta/alpha, ras-related protein Rab-1B and many more. On the other hand, 84 proteins have increased synthesis in 48 hpi including STAT-1, ras-related protein Rab-1B, catalase, gelsolin and moesin.

Pattern recognition receptors (PRRs) on the surfaces of these macrophages can recognize pathogen-associated molecular patterns (PAMPs) present in the invaders to activate intracellular signalling cascades for pro-inflammatory response (Kelly & O'Neill 2015a). Galectin-9 can bind to *L. major* in a species-specific manner through *L. major*-specific poly-ß-galactose and promote macrophage interaction (Pelletier et al. 2003). Galectins are a family of mammalian lectins and are released under stress condition such as infection. It has been overexpressed in many types of immune cells, such as Th cells, cytotoxic T lymphocytes, DCs, macrophages and NK cells (Vasta 2009). Galectin-9 has been reported to be induced in HIV infection, hepatitis B infection as well as in *M. tuberculosis*-infected macrophage to inhibit pathogen growth (Liu et al. 2016; T et al. 2016).

Apart from that, few of proteins involved in amino acid pathway, nucleotides pathway and cell redox pathway showed significant decreased synthesis p.i. These include PNP, calreticulin and CD44. PNP is an enzyme involved in purine metabolism where it metabolizes inosine into hypoxanthine and guanosine into guanine, in each case creating ribose phosphate (Freitas et al. 2015). Interestingly, *Leishmania* are purine auxotroph that obtain their purines from exogenous sources through purine salvage pathways (Freitas et al. 2015). Millar et al. (2015) reported that several genes involving in purine biosynthesis or salvage pathways were significantly overexpressed in *L. mexicana* infected THP-1 cells. The decreased production of PNP p.i. in our data might be a way for the host to prevent *Leishmania* from using purine for their purine metabolism.

The oxidative stress response pathway elicited in response to infection primarily involved proteins with antioxidant properties. The core response proteins associated with these annotation terms include SOD, thioredoxin, peroxiredoxin and cathepsin. SOD, which is crucial in the breakdown of ROS (Bresciani et al.

2015), had decreased in production by 1.3-fold in infected cells. We hypothesized that *Leishmania* modulated the expression of SOD to protect them from microbicidal ROS produced in macrophages. This is in accordance with the decreased activity of PKM when high level of ROS were present (Anastasiou et al. 2012).

14-3-3 proteins are a family of conserved regulatory molecules ubiquitously expressed in eukaryotic cells (Fu et al. 2000). They have a distinct feature which is the ability to bind to a multitude of signalling proteins, from kinases, phosphatases to transmembrane receptors. They have multifunctional properties such as modulating various cellular proteins, modulating signal transduction activities and regulating biochemical processes (Obsil & Obsilova 2011a). The general accepted classification of 14-3-3 is based on the following modes of action: (i) direct conformational change of the target protein; (ii) physical occlusion of sequence-specific or structural features; and (iii) scaffolding that anchors proteins within close proximity of one another (Figure 4.42) (Jang et al. 2009; Tzivion & Avruch 2002; Aitken et al. 2002; Obsil & Obsilova 2011b). 14-3-3 protein also involves in cell cycle control, survival signalling, cell adhesion and several microorganism pathogenesis (Fu et al. 2000). Given the plethora of functions and broad participation of 14-3-3 in diverse processes, it is no surprise that this protein has increased synthesis during infection. 14-3-3 has been found to interact with a pro-apoptotic member of the Bcl-2 family, Bad, by antagonizing its function to promote cell death (Zha et al. 1996). 14-3-3s are present in the central nervous system (CSF) of patients with HIV and could be a potential biomarkers for HIV-related neurodegeneration (Morales et al. 2012). Monroy (2012) speculated that infection of intestinal epithelial cells may result *in T. gondii*-induced regulation of 14-3-3 proteins expression leading to increased cell survival and proliferation, and suppression of apoptosis of parasitized cells.

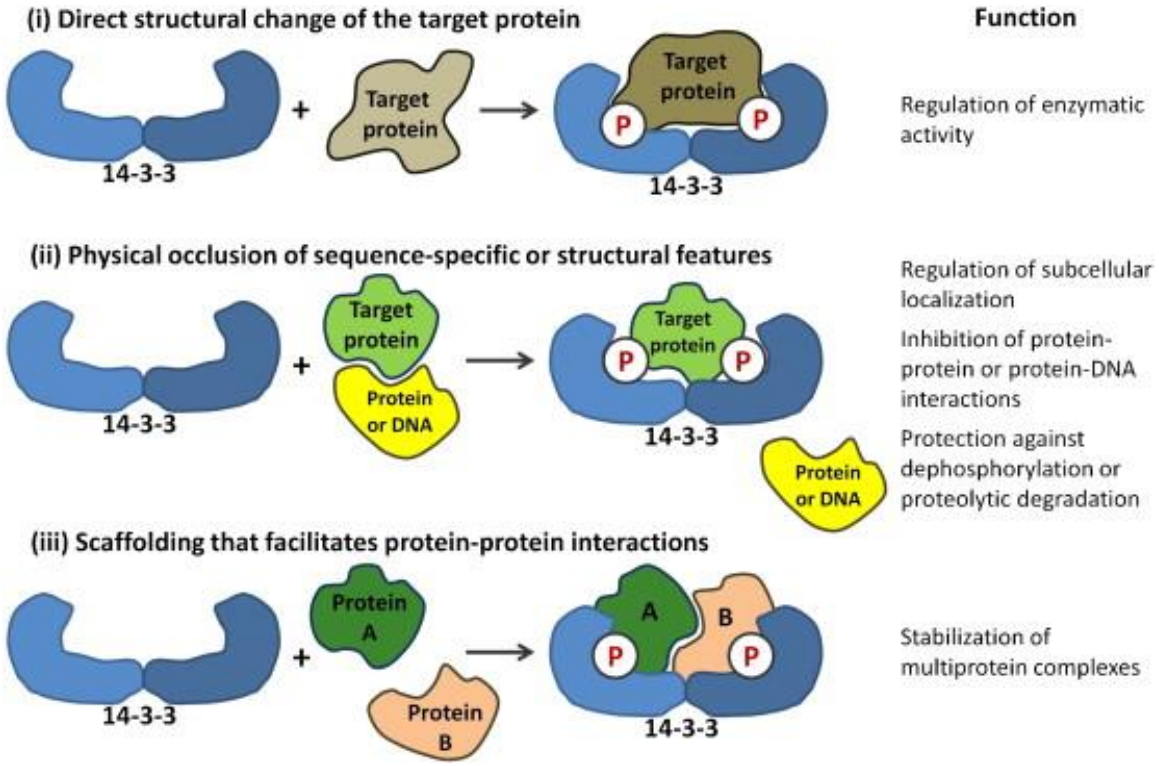

Figure 4.42: Modes of 14-3-3 protein action.

The 14-3-3 protein binding can: (i) induce a conformational change of the target protein; (ii) mask a specific region in the target protein; or (iii) facilitate the interaction between two other proteins. (adapted from Jain et al. 2012; Obsil & Obsilova 2011).

Gelsolin is an actin-binding protein that is a key regulator of actin filament assembly and disassembly (capping protein) that plays a role in podosome (actin-rich structures found on the outer surface of the plasma membrane of animal cells) formation (Koya et al. 2000; Kwiatkowski 1999). Not only It involves in cytoskeletal remodelling, gelsolin also involves in phagocytosis and ion channel regulation (Nag et al. 2009; Koya et al. 2000). Interestingly, gelsolin has both anti- and pro-apoptotic functions depending on the cell types, tissues and pathological conditions involved (Koya et al. 2000). Guerfali et al. (2008) has reported that mRNA expression level of gelsolin was downregulated in macrophage infected with *L. major*. Increased in gelsolin may contributes to fight Group B *Streptococcus* (GBS) induction in macrophages (Fettucciari et al. 2015). We postulated that the decreased of gelsolin in *L. mexicana* 24 h-infection might be a way of modulation by this parasite to survive during early infection.

Another significant protein that we found had decreased synthesis in 24 hpi is moesin (membrane-organizing extension spike protein) which belongs to ezrin-

radixin-moesin (ERM) family of cytoskeletal proteins that is essential for actin assembly by phagosomes (Defacque et al. 2000; Hirata et al. 2012). ERM proteins are key elements linking actin filaments with plasma membrane. They are important for maintenance of cell morphology, cell migration, tissue structure and invasion of intracellular pathogens (Defacque et al. 2000). More importantly, moesin have been implicated in signalling pathways which incorporate extracellular signals into intracellular mechanisms (Zawawi et al. 2010). Previous publications suggested a role for moesin in LPS-induced immune responses (Iontcheva et al. 2004; Zawawi et al. 2010) in which moesin is expressed on the surface of monocytes/macrophages and surface expression is increased after LPS stimulation. As LPS is associated with M1 macrophages, this means that moesin is downregulated in M2 type of macrophages, possibly subverted by pathogens to their advantage. To date, there was no report on infection with *Leishmania*.

One of the challenges we faced in data analysis is the occurrence of missing values in the data (no L/H ratio values in either uninfected or 24 hpi or both). This genuine phenomenon is rather frequent in global discovery proteomic studies. There are several approaches reported in dealing with missing values when applying statistical data for better interpretation of proteomic datasets (Donders et al. 2006; Zhang et al. 2011; Karpievitch et al. 2012; Wiberg et al. 2016). Some of the options are (i) ignoring the missing value proteins, (ii) impute missing values with a constant (i.e. zero), (iii) impute missing values from normal distribution, (iv) replace missing values based on transcript data or GO terms (Lazar et al. 2016; Zhang et al. 2011). Perseus offers several imputation techniques including a method that draws random values from a distribution meant to simulate expression below the detection limit. The width and the down shift of the distribution can be set to closely represent the missing population (Tyanova et al. 2016). Using Perseus, we imputed the missing values from Gaussian normal distribution using default parameters (width relative to the sd of measured values = 0.3, the amount by which the distribution used for the random numbers is shifted downwards = 1.8). However, we only performed imputation on proteins with missing values in all replicates (other than the 521 proteins).

Of interest, we discovered that proteins involved in oxidative phosphorylation in which we were previously not able to quantify namely NADH dehydrogenases (e.g.

NDUFB6, NDUFB8), succinate dehydrogenase, cytochrome c oxidase, acyl carrier protein, fumarate hydratase and several subunits of ATP synthases were all have increased synthesis within 24 h of infection. This suggests that following infection, glycolysis and TCA cycle were reduced while oxidative phosphorylation increased. Activation of macrophage by LPS were reported to have increased glycolysis, high ROS production by the electron transport chain and reduced oxidative phosphorylation (Kelly & O'Neill 2015b). In this cascade, LPS induced iNOS to produce more NO (Figure 4.43). This causes nitrosylation of electron transport chain complexes which resulted in reduced oxidative phosphorylation (Kelly & O'Neill 2015b). Arginine is the substrate for iNOS. Recycling of arginine is achieved via argininosuccinate synthase which is important for controlling mycobacterial infection (Qualls et al. 2013). Some pathogens have mechanisms to deplete arginine. *Helicobacter pylori* and *Leishmania* express arginase that inhibit NO production by activated macrophage (Gobert et al. 2001; Kropf et al. 2005). The imputed data revealed that argininosuccinate synthase was decreased upon early infection with *L. mexicana*. Moreover, TNF-α-induced protein 8 that inhibit iNOS was increased p.i. Cumulatively, the downregulation of argininosuccinate synthase and the upregulation of TNFα-induced protein 8 may be modulated by *L. mexicana* to establish infection. This is accompanied by the decreased of glycolysis and increased of oxidative phosphorylation. Similarly, *L. infantum*-infected macrophage demonstrated to induced a switch towards mitochondrial oxidation phosphorylation favouring its own growth (Moreira et al. 2015).

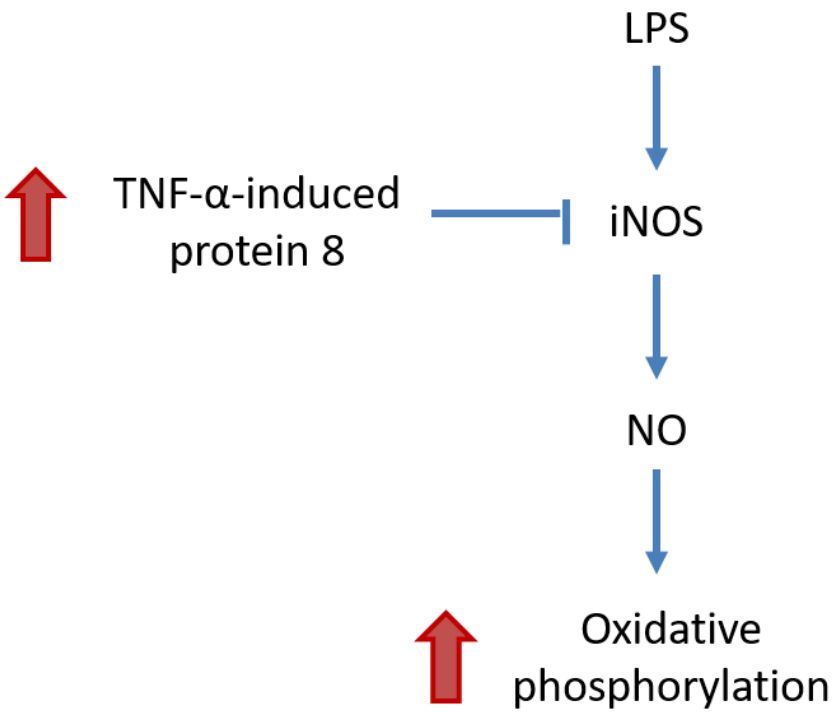

Figure 4.43: Cascade involving in oxidative phosphorylation affected by LPS.

LPS induced iNOS (inducible nitric oxide synthase) to produce more nitric oxide (NO). This causes nitrosylation of electron transport chain complexes which resulted in reduced oxidative phosphorylation. iNOS can be abrogated by TNFAIP8 which impairs NO production, thereby increasing oxidative phosphorylation.

Another intriguing finding derived from the imputed data was that proteins involved in lipid or fatty acids metabolism such as long chain fatty acid CoA ligase, 3-hydroxyacyl-CoA dehydrogenase, 3-oxoacyl-CoA reductase, acetyl-CoA acetyl transferase and prostaglandin E synthase had increased synthesis in 24 hpi THP-1. It is known that M2 macrophages are fuelled by fatty acid ß-oxidation in the mitochondria (Kelly & O'Neill 2015b). Macrophages secrete lipoprotein lipase (LPL), the key enzyme responsible for extracellular release of fatty acids from triglyceride-rich lipoproteins (Zhu et al. 2015; Dinasarapu et al. 2013). IL-4-activated mouse M2 macrophages showed a significant upregulation of fatty acids uptake and fatty acid oxidation (Odegaard & Chawla 2012).

4.5 Conclusion

In general, global proteomics is challenging due to the complexity and dynamic range of the proteome. In practise, we are trying to identify and characterise as many of the proteins as we can. In order to detect more proteins, global coverage need to be increased, for instance, using better MS instruments and applying different data acquisition as well as improve data analysis using different bioinformatics tool. Of note, these will increase cost substantially. Given with what we have, results generated in the present work enabled us to use it to infer the biological response of human macrophage when interacting with parasite. Notably, we were able to employ pcSILAC in THP-1 infected with *L. mexicana*.

The mechanisms employed by *Leishmania* to survive in host are highly complex. They rely on both pathogen effector molecules and distinct functional activities in host cells. The nature of the changes in metabolic pathways suggested changes in the cellular requirement for energy metabolism, nucleic acid synthesis and anti-oxidants when facing threat from pathogens. Although there is considerable amount of data available on the mechanisms deployed by *Leishmania* to survive in the host, to our knowledge, this study is the first study employing proteomics with SILAC labelling on *L. mexicana*-infected macrophage.

Collectively, we observed that THP-1 have general suppression of gene expression during *L. mexicana* infection. Of particular interest, infection switches the host metabolism from glycolysis to oxidative phosphorylation and fatty acid oxidation, contrary to the Warburg effect (Warburg et al. 1926; Kelly & O'Neill 2015). Most of the proteins significantly modulated in the present study have been associated with M2 macrophages. Although, there are some conflicting results from what have been reported in literatures as it has been noted that different species of *Leishmania* react differently in the human host (Singh et al. 2015; DaMata et al. 2015; Menezes et al. 2013). Nevertheless, these observations contribute a foundation for future studies to define the mechanisms involved in host-parasite interaction.

CHAPTER 5

5 Turnover of the proteome in macrophages after infection with *L. mexicana*

5.1 Introduction

The proteome is a dynamic system in which proteins are interacting to contribute the phenotype of a cell. Protein properties including protein abundance, protein expression, protein synthesis and degradation, subcellular localisation, posttranslational modifications and protein-protein interactions are highly complex. Presently, most global quantitative proteomics investigations are focused on the changes in protein abundance or steady-state protein expression differences between samples. However, such approaches are unable to give any information on protein dynamics which is vital to understanding physiological changes and processes. Advances in MS-based proteomics have enabled the measurement of these properties. Understanding proteome dynamics contributes in deciphering how cells deploy regulatory processes to accomplish physiological changes in different conditions.

Protein turnover refers to the balance between protein synthesis and protein degradation processes (net changes) that are continually occurring in cells. It is the rate at which the proteins are replaced. When the rate of protein synthesis is equal to the rate of protein degradation, the cells are said to be in steady-state. However, when the cells are growing, the rate of protein synthesis is greater than the rate of protein degradation (anabolism), while the opposite is called catabolism. This balancing act allows a cell to regulate its function to quickly respond to challenges (Doherty & Whitfield 2011). Various factors influence the rates of protein synthesis including mRNA transcript concentration and ribosomal activity. Of note, most proteins do not exist for extended periods of time. Instead, they will be renewed, and existing protein recycled or degraded. Although, there are some proteins that live for as long as the organism itself, example being human collagen (Verzijl et al. 2000). Half-life relates to the time it takes to replace half of the molecules (in this case, proteins). The half-life of proteins within cells

varies from minutes to several days. The differences in synthesis and degradation rates are important for cell regulation. Most regulatory molecules such as transcription factors are rapidly degraded. This is to allow them to change accordingly in response to external stimuli (Pratt et al. 2002).

Protein degradation is one of the fundamental cellular processes involved in gene expression. In eukaryotic cells, there are two major pathways that mediate protein degradation: the ubiquitin-proteasome system and lysosomal proteolysis. The ubiquitin-proteasome system selects proteins that have been tagged by a polyubiquitin chain and directs them to the 26S proteasome to be degraded (Ciechanover 2005). Lysosomes contains a huge number of proteases used for degrading proteins including cathepsins and aspartic proteases (Xu & Ren 2015). Protein degradation is important in the regulation of some physiological and cellular processes to prevent the accumulation of unwanted or damaged proteins in cells thus ensuring a functional proteome throughout the cell's lifetime. Most cellular proteins are rapidly degraded and replaced with newly synthesized copies. More importantly, degradation is also triggered by stress such as starvation (Doherty & Whitfield 2011). Consequently, a better understanding of degradation rates of specific proteins particularly in different conditions would facilitate drug development for various diseases (Bedford et al. 2011).

Many studies have attempted to address protein degradation, synthesis and ultimately protein turnover rates in cells. The application of pulse-chase experiments has begun more than 30 years ago. In essence, isotopic tracers were introduced in cells to measure the level of the tracers incorporated in tissues of interest. Early studies measured the half-life of a specific protein by pulse labelling cells with radioisotope (e.g., 35S-methionine, 59Fe-transferrin), followed by immunoprecipitation with a specific antibody during a chase period, to reveal the rate at which labelled protein was depleted (Roberts & Bomford 1988; Rotundo et al. 1989). Radioactive labelling while sensitive, it is not suitable for high-throughput studies (Fierro-Monti et al. 2013). Later, the technique was progressed by the use of tags with cycloheximide treatment to block protein translation (Belle et al. 2006; Bojkowska et al. 2011) and imaging-based approaches combined with photobleaching (Eden et al. 2011; Geva-Zatorsky et al. 2012). In a study conducted by Belle et al. (2006), the half-life of several thousand

yeast proteins was measured by utilising an epitope-tagged fusion protein with tandem affinity purification (TAP) tag and cycloheximide. The degradation rates of the TAP-tagged proteins were quantified by Western blotting at 0, 15 and 45 min after cyclohexamide treatment. They reported that proteins that are stable are mainly involved in protein production including ribosomal proteins, as well as enzymes involved in amino acid metabolism and biosynthesis. In contrast, proteins that have regulatory flexibility (i.e. rapidly degrading) are proteins associated with cell cycle and transcriptional regulation. However, despite these remarkable studies, the use of tags can potentially impair protein stability and interfere with protein function (Christiano et al. 2014). Moreover, blocking translation can induce stress response (MacGurn et al. 2011). Besides that, due to cellular toxicity of the applied drugs, turnover is measured when overall protein synthesis is abrogated and thus may not reflect the actual turnover rate under physiological growth conditions.

In this regard, MS-based proteomics approaches are promising as researchers can investigate global protein turnover of an organism at the level of individual gene products. Recently, variants of these approaches utilizing non-radioactive tracers have been developed that allow for global analysis of protein turnover (Pratt et al. 2002; Beynon & Pratt 2005). Motivated by the lack of methods to explicitly explore changes in protein dynamics in different cellular conditions, a modified version of the classic SILAC approach was established, namely pulse-chase SILAC (pcSILAC) (Gustavsson et al. 2005; Fierro-Monti et al. 2013; Schmidt et al. 2010). In contrast with the classic SILAC, the labelling in pcSILAC is conducted for a selected period of time where all proteins will be labelled with heavy (H) amino acids, hence the word ‘pulse’. The medium is exchanged with light (L) amino acids following perturbation where the L amino acids will be ‘chased’ into the cells. During this phase, all newly synthesized proteins will appear in the L form. As the strategy exclusively labels newly synthesized proteins, relative changes in protein translation rates between two cellular conditions can be accurately quantified. Nevertheless, as this is both pulse and chase experiments, linking these two parameters together is very complex.

In the simplest experimental design, there are two strategies that could be employed using stable isotope to determine protein turnover. Cells are exposed

to a stable isotope precursor where it could be incorporated into proteins and the rate of incorporation is determined. This is called “labelling” experiment. The other way is called “unlabelling” experiment where the cells are pre-labelled with stable isotope-labelled precursor before being transferred to an unlabelled condition, and the rate of loss of label is determined (Figure 5.1).

Although the ratio of H to L peptides indicates the turnover rate of the respective protein, it does not directly provide information on the translation rate. This is due to the fact that protein turnover is affected by both synthesis and degradation. To illustrate, a high H/L ratio could either indicate a high translation rate of a stable protein or a low translation rate of a protein that is rapidly degraded (Schwanhäusser et al. 2009).

Protein degradation rates by MS has been widely applied on several cell lines or organisms including yeast model, mouse, chicken and human A549 adenocarcinoma cell line (Pratt et al. 2002; Doherty et al. 2005; Doherty et al. 2009; Belle et al. 2006; Price et al. 2010; Christiano et al. 2014). Schwanhäusser et al. (2009) applied the method with HeLa cells to investigate a model of iron homeostasis. Bunner & Williamson (2009) also used pcSILAC to explore *E. coli* 30S ribosome assembly dynamics.

To understand the underlying mechanisms of cellular functions it is critical to monitor protein abundance and their changes over time. This will allow us to investigate the intrinsic dynamic processes governing life that causes physiological responses, including regulatory networks. Given that proteins exhibit vastly different turnover rates, changes in gene expression induced by different treatment will affect steady-state protein levels with different kinetics and by different magnitudes. Incidentally, we are using pcSILAC on THP-1 where the cells were prelabelled with heavy isotopes until full incorporation before changing the media to light label media (unlabelling experiment) and infected with *L. mexicana* for 24 and 48 h. This media change will deplete the labelled pool, thus decreasing the precursor relative isotope abundance (RIA) so that the loss of RIA can be monitored to dictate degradation. Pre-labelled proteins could have two fates: to be degraded or to be diluted into daughter cells through cell growth. In this work, we assume that amino acids derived from protein degradation will not be used for

protein synthesis. Cell were then subjected to protein extraction, proteolysis and MS analysis. The strategy employed was illustrated in detail in Figure 5.2.

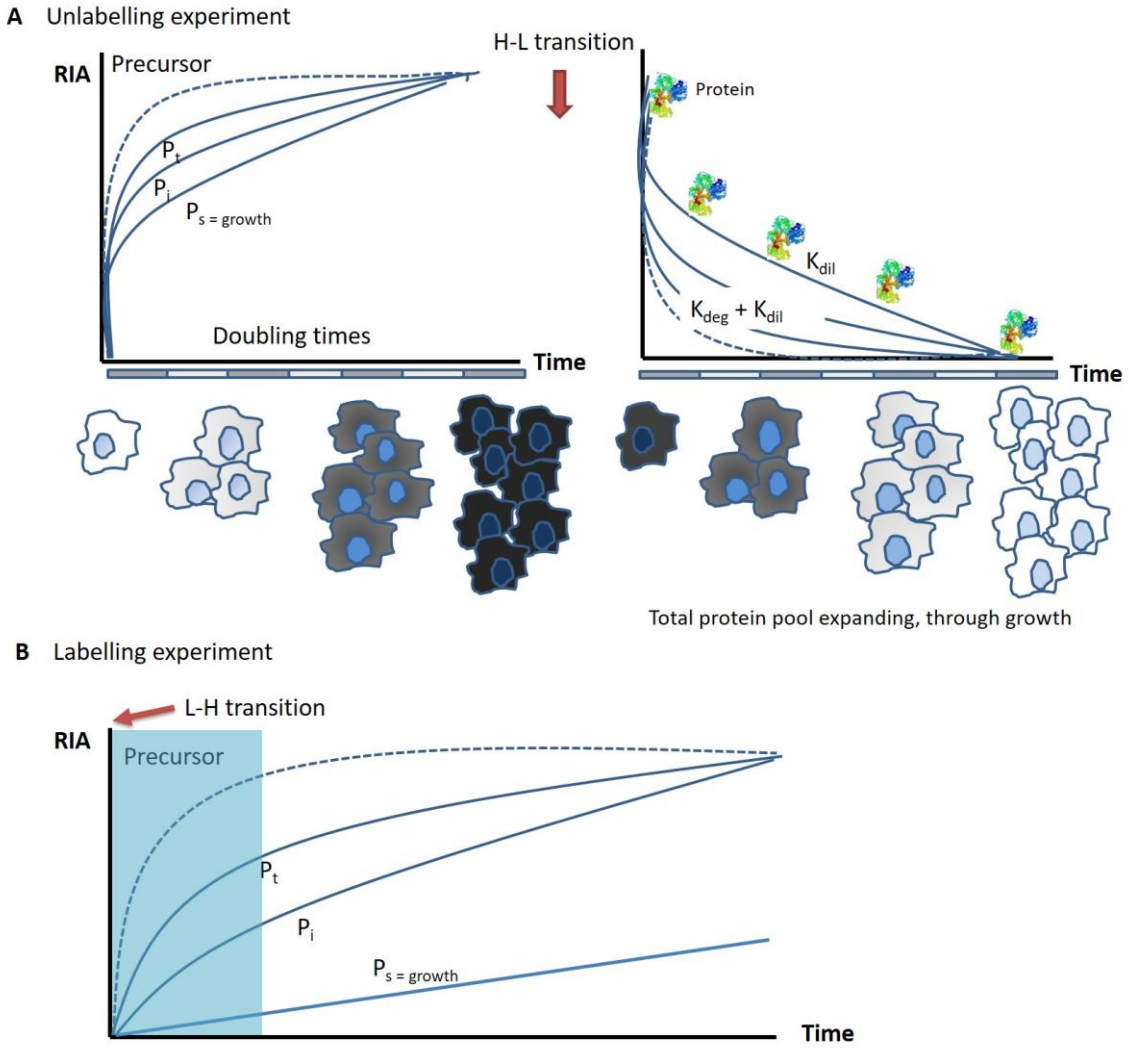

Figure 5.1: Strategies for turnover analysis.

Turnover studies using stable isotopes measures either the rate of entry of precursor into the protein pool ("labelling" experiment) (B) or the rate of exit of label from previously labelled proteins ("unlabelling" experiment) (A). (A) In "unlabelling" experiment, proteins (Pf, Pi, Ps: fast, intermediate, and slow turnover proteins, respectively) are pre-labelled through a combination of turnover and pool expansion through growth, as the cells are usually undergoing exponential growth. Irrespective of the turnover rate, all proteins will be fully labelled after several doubling times. Subsequently, the medium is changed to medium containing no label, and the rate of loss of label from proteins is assessed by means of mass spectrometry. Because the cells continue to divide, label is lost from proteins through a combination of growth and intracellular degradation. (B) Labelling experiments are more common in animal studies, in which tissue growth might be much lower. Here the stable isotope label is administered at the start of the experiment, and mass spectrometry is used to monitor the rate of label incorporation into proteins. These experiments are often conducted in the absence of significant tissue growth, and the exponential rise to plateau yields a reliable measure of the turnover rate. In both experimental modalities, the extent and rate of labelling of the precursor amino acid pool (dotted lines) is critical (adapted from (Claydon & Beynon 2012).

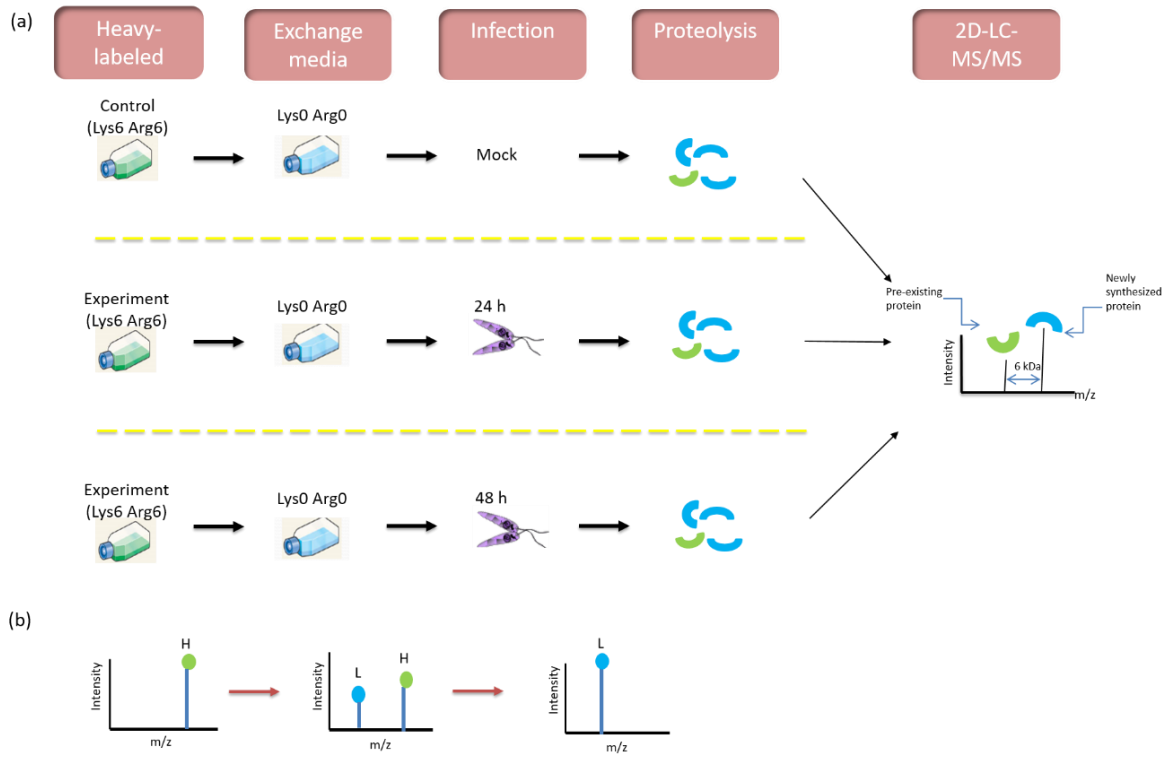

Figure 5.2: Schematic outline of pulse-chase SILAC approach for 24 and 48 hpi THP-1.

(a) Uninfected and infected THP-1 were cultivated in heavy (H) SILAC medium until full incorporation was achieved (the pulse-labelling phase). Concomitantly with differential treatment (infection), cells are transferred to culture medium containing light (L) isotope-coded amino acids. Therefore, cells are 'chased' with L amino acids, thus all newly synthesized proteins will incorporate the L amino acids. The cell populations are further processed separately and analysed by MS. (b) The mass spectrum shows a gradual shift from fully H labelled to towards fully L labelled over 48 h period. At the pulse-chase starting point, only H peptides are present. During time, the intensities of L peptides continuously increase until H peptides are not detected against the vast majority of L peptides.

5.2 Aims

The aims of this work were to:

- Extend the application of pulse-chase SILAC to investigate the dynamic proteome degradation in human macrophage cell line THP-1 infected with *L. mexicana* for 24 and 48 hours, compared with uninfected THP-1.

- Determine protein half-life and turnover in human macrophage cell line THP-1 infected with *L. mexicana* for 24 and 48 hours, compared with uninfected THP-1.

- Undertake a statistical analysis of the protein modulations observed.

By quantifying protein half-lives, turnover times, and the degradation rate constant of proteins in large scale, we hope to get insights to the physiological nature of these parameters thereby deepen our understanding of cellular processes occurring during parasite infection.

5.3 Results

5.3.1 Global characterisation of protein degradation using pulse-chase SILAC, in response to *L. mexicana* infection.

Following complete incorporation of heavy isotope labelled amino acids into the THP-1 proteome (RIA ~ 1) (as described in section 4.3.2), THP-1 were activated with PMA to become macrophage-like cells. Next, heavy SILAC medium was exchanged for light SILAC medium (RPMI 1640 containing ^{12}C-Arg and ^{12}C-Lys isotope) and the macrophages were exposed to metacyclic promastigotes, at the ratio of 8 parasites/macrophage that we have previously shown (Figure 4.6 and 4.7) to result in a high prevalence of infection. In parallel, similar labelled but uninfected THP-1 cultures were chased with light SILAC media, as control. Both infected and uninfected cultures were washed at 6 h to remove extracellular parasites from infected cultures. At 24 and 48 h post-infection, uninfected and infected cells were harvested by scraping the adhered cells into cold PBS and cell lysis was performed followed by trypsinization and 2D LC-MS/MS analysis on an Orbitrap Velos instrument. All raw LC/MS files of a time series experiment were then processed on MaxQuant, generating proteinGroup.txt output file which was further analysed on Perseus.

Triplicates of uninfected THP-1, 24 hpi and 48 hpi THP-1 were grouped and analysed together on MaxQuant and Perseus. Using the same parameters as describe in previous chapter, a total of 2280 proteins were identified in all groups. To identify rapidly degraded proteins, we measure the rate of loss of heavy Arg and Lys at 24 and 48 hours after infection with the parasites. For this purpose, all proteins with no L/H ratio in either one of the replicates were omitted, leaving 400 proteins. The value of relative isotope abundance (RIA) of the proteins changes over the 48 h period. Average RIA values from the three replicates in control, 24 hpi and 48 hpi were calculated for each peptide at each time-point. These data were then processed using an R script and RIA equation as described in section 2.10.6 (Pratt et al. 2002). The dilution rate (k_{dil}) over 160 h of cultivation of THP-1 in SILAC media was calculated from the doubling time of THP-1, which is 0.006 h^{-1}. Therefore, the dilution rate is negligible since over 99% of the arginine and leucine in the cells would be the stable isotope-labelled form.

We minimised the dilution rate by using dialyzed serum and auxotrophic amino acids during cultivation.

To identify rapidly degraded proteins with high statistical significance, *p* values were calculated using *t* test analysis. A significance cutoff value of $p < 0.05$ ($-Log_{10}(p) > 1.2$) was used, producing 50 proteins in 24 hpi (Figure 5.3, Table 5.1) and 38 proteins in 48 hpi THP-1 (Figure 5.6, Table 5.2).

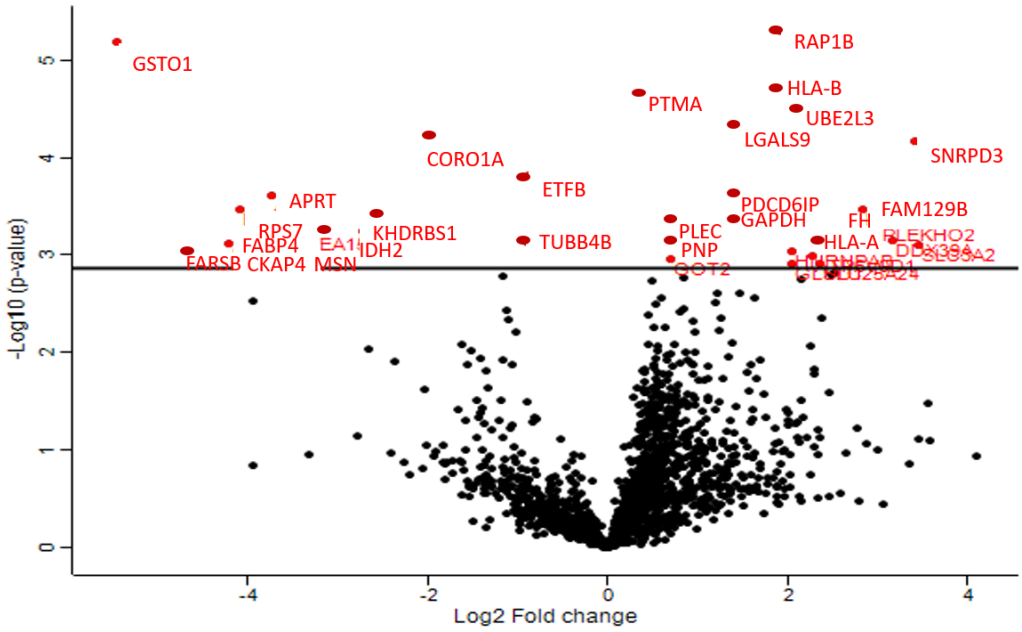

Figure 5.3: Volcano plot showing proteins with different degradation rate in uninfected and 24 h infected THP-1 with FDR = 0.05.

Conventional data were normalized and proteins with no quantification report were removed from all samples. t-test was performed on the remaining data to produce statistically significant proteins with p-value < 0.05 (red circle). The proteins were assigned with gene names. FDR of 0.05 was applied on the data producing 50 proteins with differential degradation rate.

The protein Uniprot ID of significant proteins in 24 hpi and 48 hpi were uploaded on DAVID database and PANTHER for functional analysis. PANTHER was used when DAVID could not give more annotation. A Fisher Exact test (Benjamini-Hochberg FDR < 0.02) was applied to highlight significant enrichment in ontology (Benjamini & Hochberg 1995). It was observed that most of the proteins with different degradation rates p.i. were involved in cellular process, metabolic, localisation, and antigen processing and presentation (Figure 5.4). Pathway analysis based on KEGG showed that proteins associated with apoptosis, followed by the antigen

processing and presentation, and aminoacyl-tRNA biosynthesis predominated (Figure 5.5). Many proteins with significant degradation rates in 48 hpi were also involved in metabolic processes, but also in oxidation reduction and immune system process (Figure 5.7). Additionally, pathway analysis revealed that most rapidly degraded proteins involve in ribosomal pathway, glycolysis, TCA cycle, and oxidative stress response (Figure 5.8).

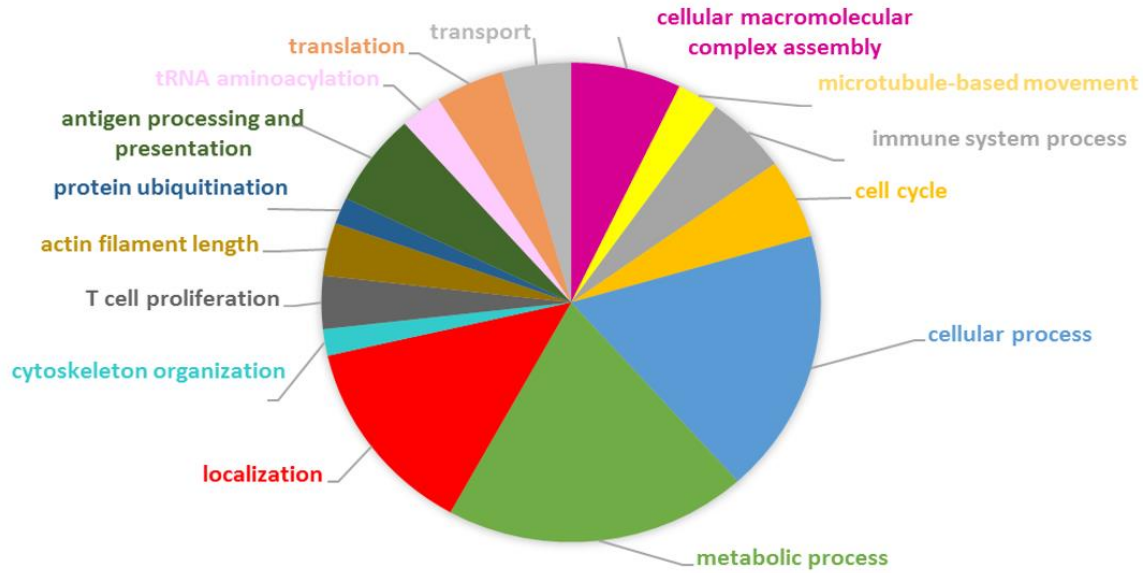

Figure 5.4: Gene Ontology of proteins with significantly changing degradation rates post 24 h infection.

The total number of proteins (UniProt identifiers) identified in the uninfected and 24 hpi were ranked according to fold changes and analysed on DAVID based on biological processes they involve in. Pie chart showed that most proteins involved in cellular process, metabolic process, localisation, and antigen processing and presentation.

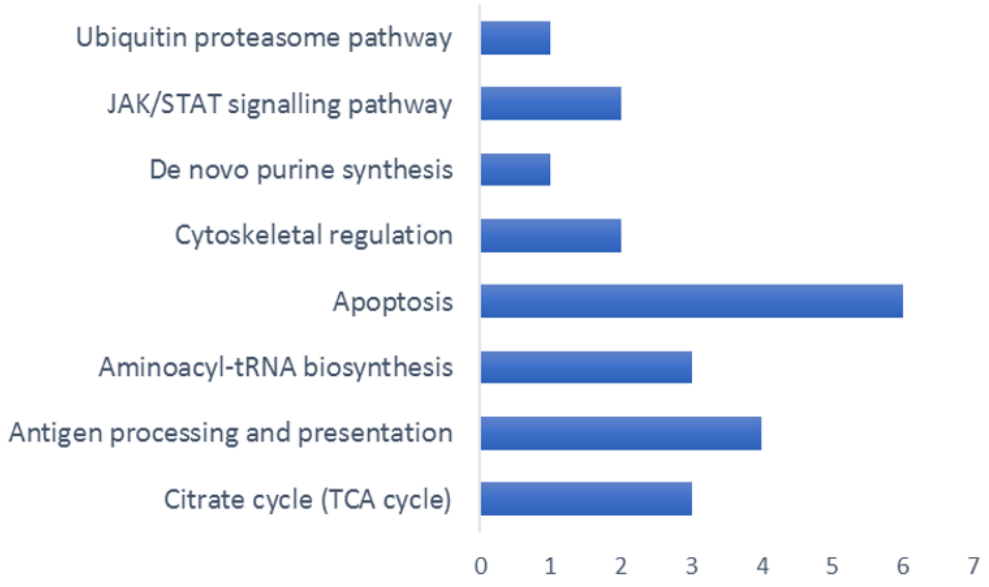

Figure 5.5: Canonical pathway analysis on KEGG showing most altered pathways in the 50 significantly degraded proteins in 24 hpi THP-1.

The highly degraded proteins identified in uninfected and 24 hpi were analysed on DAVID with links to KEGG to identify the pathways they involve in ($p \leq 0.01$; Fisher's exact test).

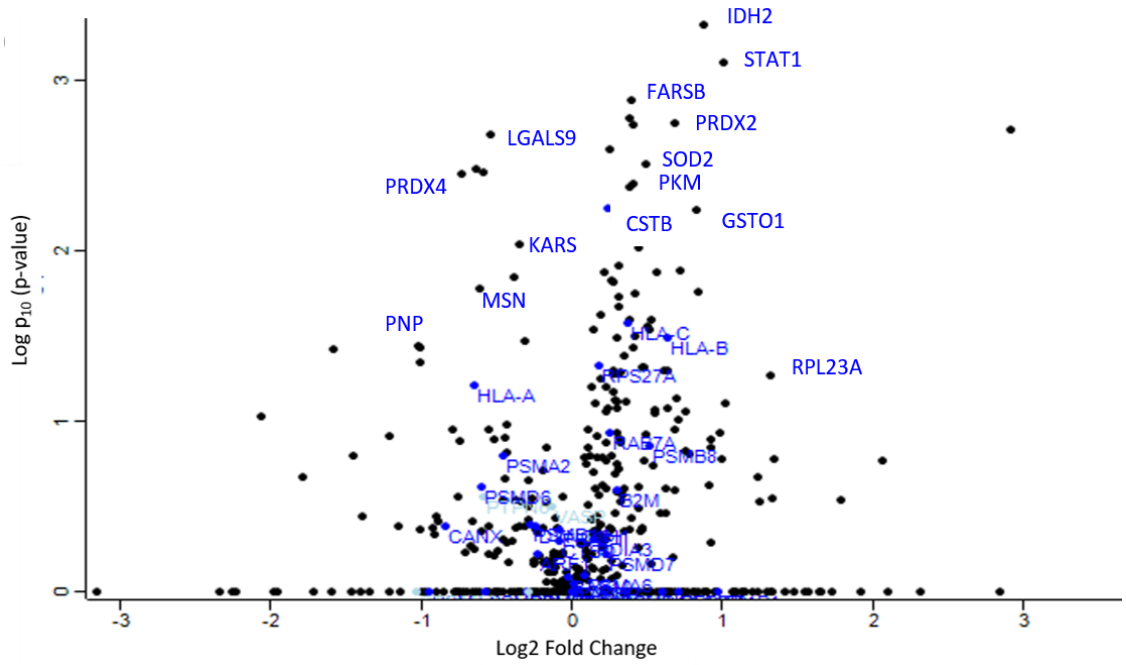

Figure 5.6: Volcano plot showing proteins with different degradation rate in uninfected and 48 h infected THP-1 with FDR = 0.05.

Conventional data were normalized and proteins with no quantification report were removed from all samples. t-test was performed on the remaining data to produce statistically significant proteins with p-value < 0.05 (blue font). The proteins were assigned with gene names. FDR of 0.05 was applied on the data producing 38 proteins with differential degradation rate.

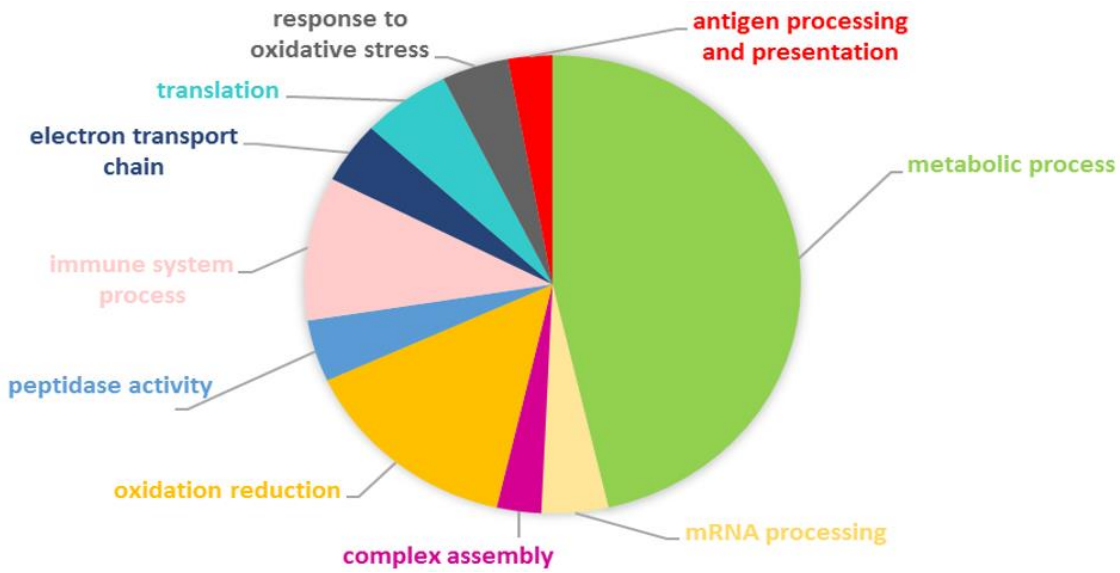

Figure 5.7: Gene Ontology of proteins with significantly changing degradation rates post 48 h infection.

The total number of proteins (UniProt identifiers) identified in the uninfected and 48 hpi were ranked according to fold changes and analysed on DAVID based on biological processes they involve in. Pie chart showed that most proteins involved in metabolic processes, oxidation reduction and immune system process.

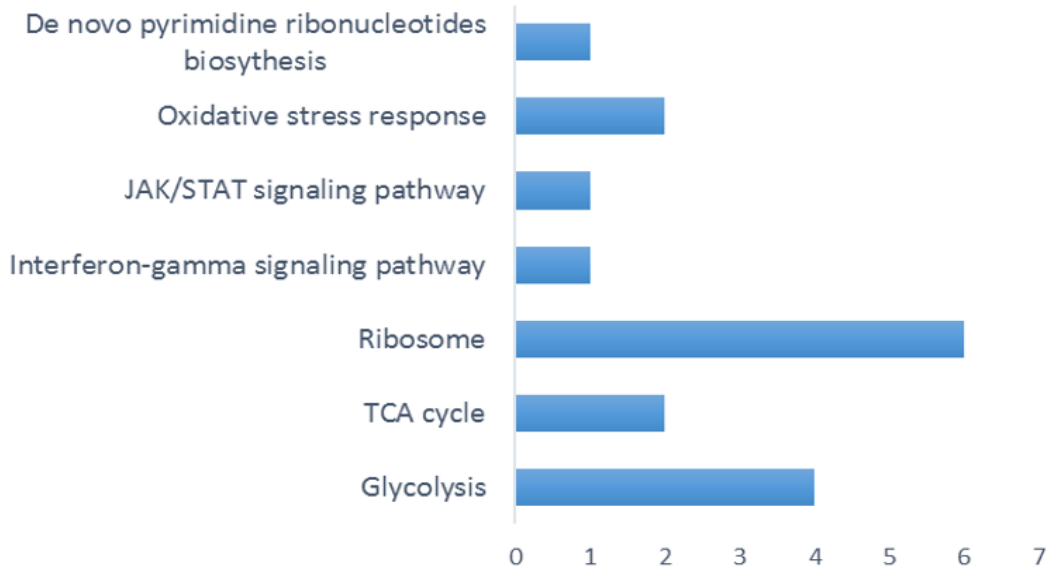

Figure 5.8: Canonical pathway analysis on KEGG showing most altered pathways in the 38 significantly degraded proteins in 48 hpi THP-1.

The highly degraded proteins identified in uninfected and 48 hpi were analysed on DAVID with links to KEGG to identify the pathways they involve in ($p \leq 0.01$; Fisher's exact test).

We choose several pathways that appear to be highly degradable p.i. to overlay onto KEGG pathway diagrams: the ribosome pathway (Figure 5.9), aminoacyl-tRNA biosynthesis (Figure 5.10), and antigen processing and presentation (Figure 5.11). Of note, the remaining proteins represented by red star found in this data have missing values in either the uninfected, 24 hpi or 48 hpi group, hence we could not determine the modulation on these proteins between uninfected, 24 hpi and 48 hpi.

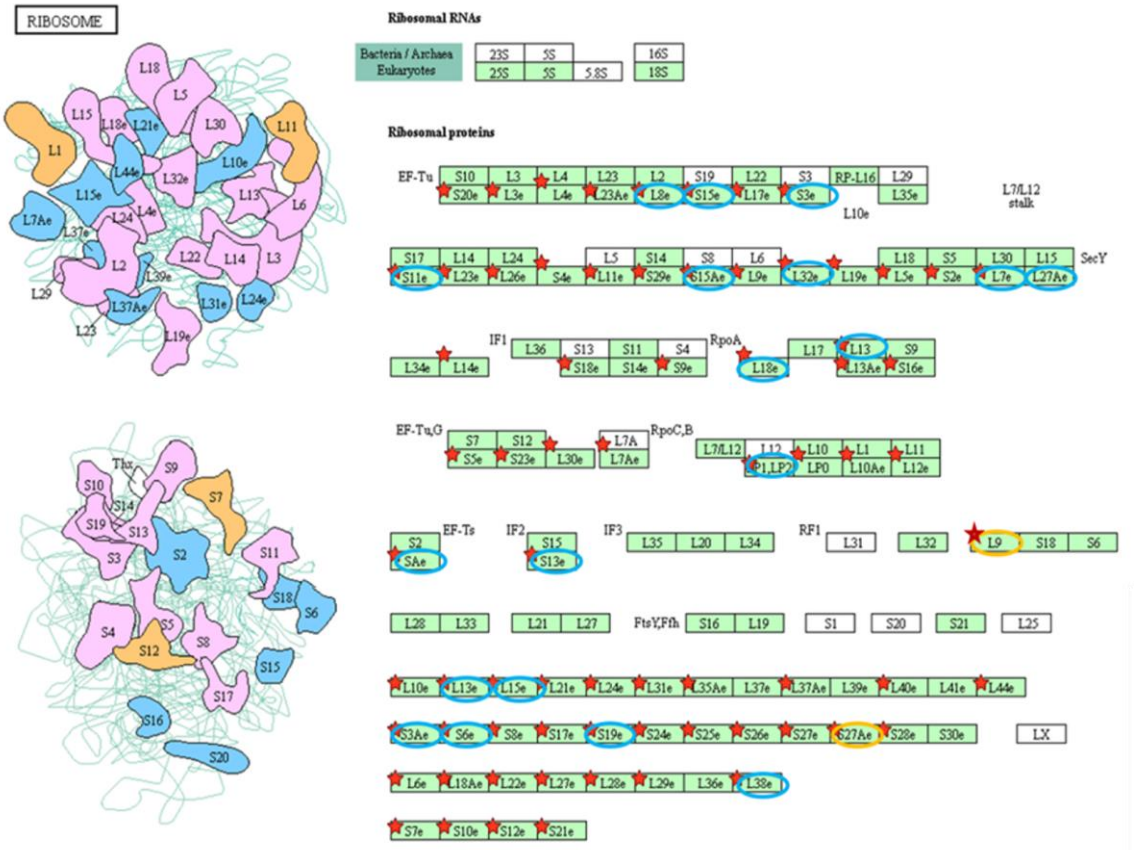

Figure 5.9: Ribosome pathway derived from KEGG with the proteins found in this work.

All proteins identified in this study were analysed on DAVID. The pathways linked to KEGG was chosen with *Homo sapiens* as the reference organism and most proteins found were involved in ribosome pathway. Red star represented the proteins found in this data. Blue circle represented the significantly degraded proteins in 24 hpi while orange circle represented the significantly degraded proteins in 48 hpi.

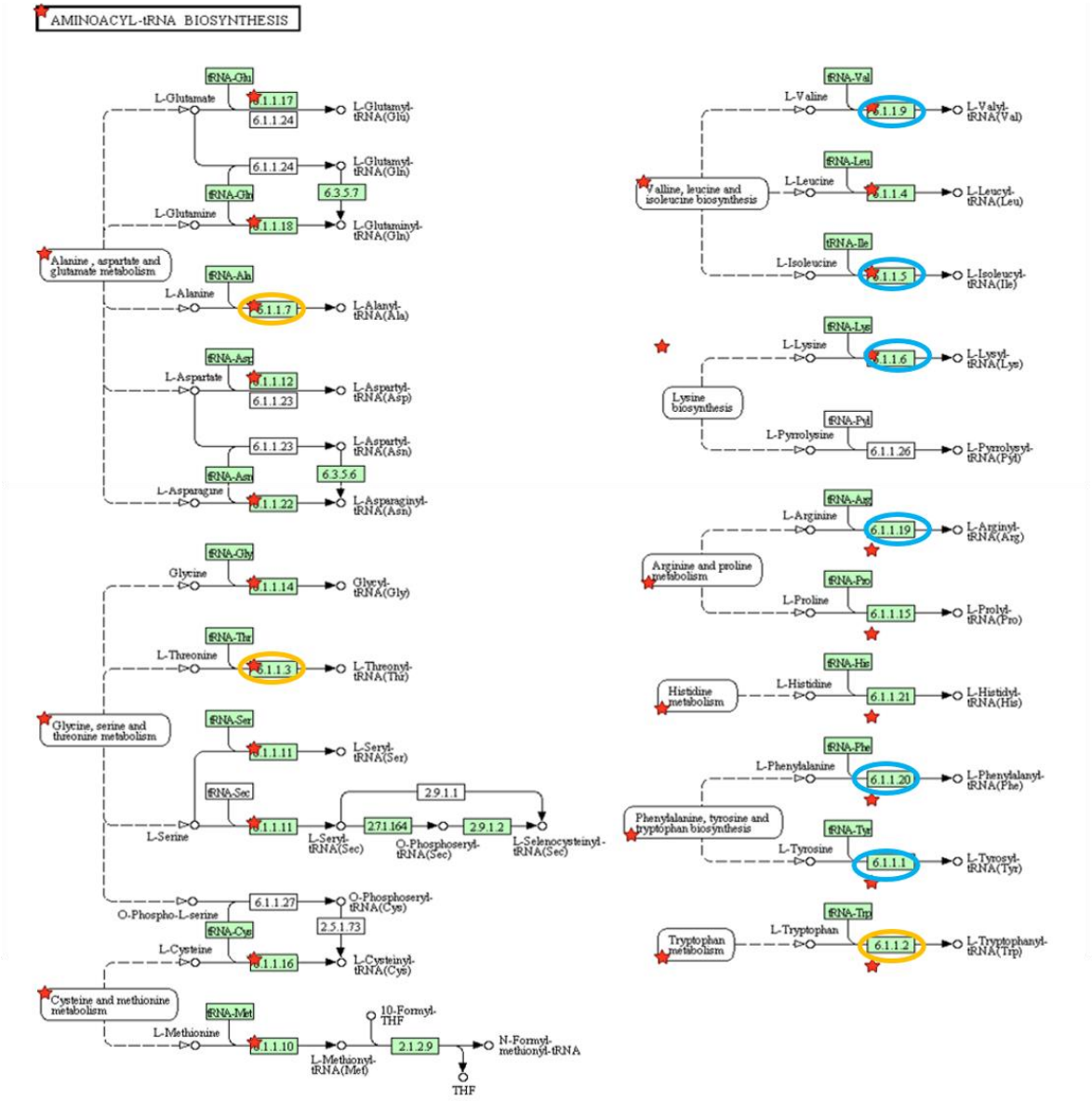

Figure 5.10: Aminoacyl tRNA biosynthesis pathway derived from KEGG contains proteins found in this data.

All proteins identified in this study were analysed on DAVID. The pathways linked to KEGG was chosen. Red star represented the proteins found in this data. Blue circle represented the significantly degraded proteins in 24 hpi while orange circle represented the significantly degraded proteins in 48 hpi. Abbreviations: 6.1.1.17 – glutamate-tRNA ligase, 6.1.1.18 – glutamine-tRNA ligase, 6.1.1.7 – alanine-tRNA ligase, 6.1.1.12 – aspartate-tRNA ligase, 6.1.1.22 – asparagine-tRNA ligase, 6.1.1.14 – glycine-tRNA ligase, 6.1.1.3 – threonine-tRNA ligase, 6.1.1.16 – cysteine-tRNA ligase, 6.1.1.10 – methionine-tRNA ligase, 6.1.1.9 – valine-tRNA ligase, 6.1.1.4 – leucine-tRNA ligase, 6.1.1.5 – isoleucyl-tRNA synthetase, 6.1.1.6 – lysine-tRNA ligase, 6.1.1.19 – arginine-tRNA ligase, 6.1.1.15 – proline-tRNA ligase, 6.1.1.21 – histidine-tRNA ligase, 6.1.1.20 – phenylalanine-tRNA ligase, 6.1.1.1 – tyrosine-tRNA ligase, 6.1.1.2 – tryptophan-tRNA ligase.

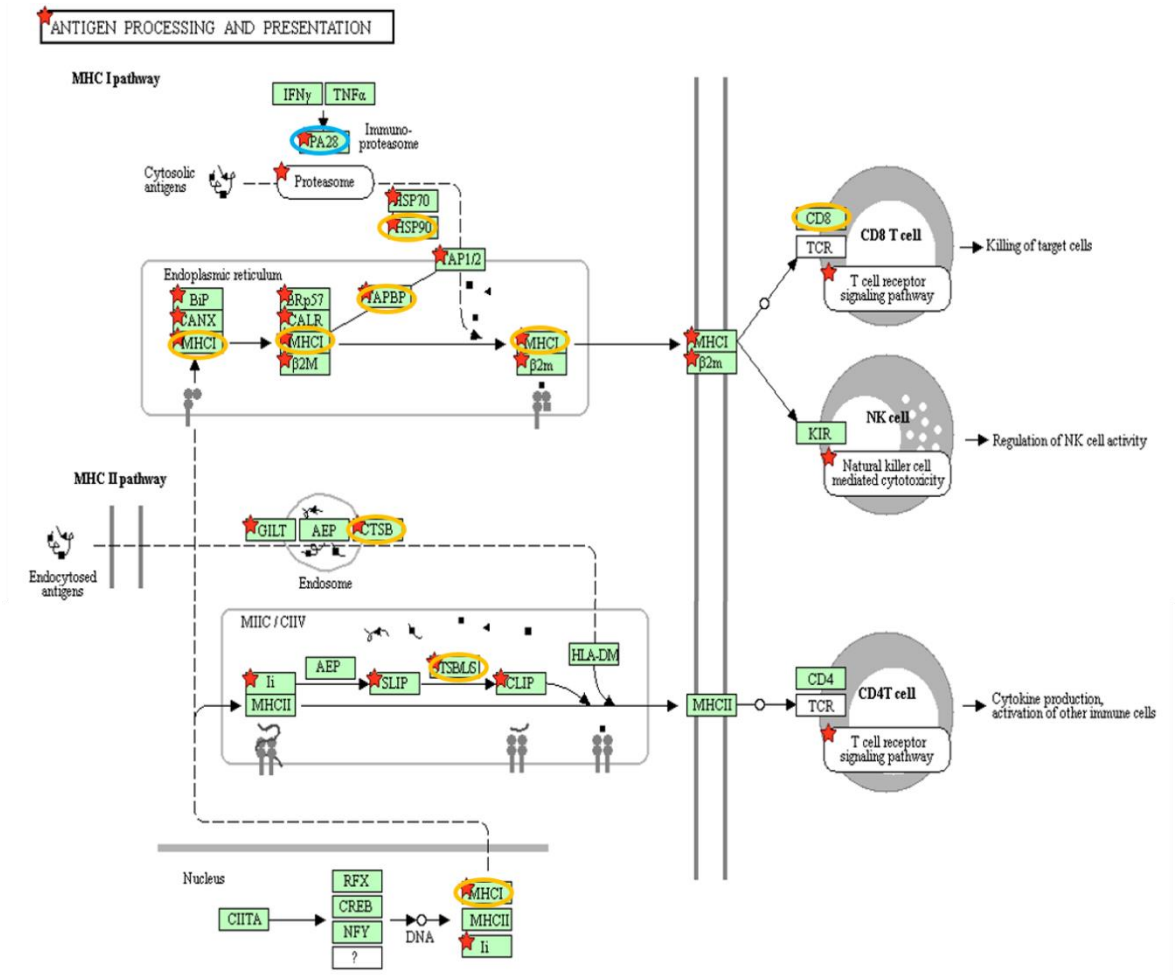

Figure 5.11: Antigen processing and presentation pathway (KEGG) with proteins found in this data.

All proteins identified in this study were analysed on DAVID. The pathways linked to KEGG was chosen and most proteins with statistically degraded proteins p.i. involved in antigen processing and presentation pathway. Red star represented the proteins found in this data. Blue circle represented the significantly degraded proteins in 24 hpi while orange circle represented the significantly degraded proteins in 48 hpi.

Table 5.1: Proteins significantly degraded upon 24 h infection.

Replicates from both uninfected, 24 hpi and 48 hpi THP-1 were grouped and averaged for statistical analysis. Only proteins that had been quantified in all biological replicates were considered for this statistical test. Two-sample t-test was performed on the filtered data and gave rise to 50 differentially degraded proteins (FDR value = 0.05).

Protein names	Gene names	RIA (degradation) Uninfected24h	RIA (degradation) 24hpi	RIA (degradation) Uninfected48h	RIA (degradation) 48hpi	Peptides	Mol. weight [kDa]	Score
Receptor-type tyrosine-protein phosphatase C	PTPRC	0.19	0.82	0.65	0.72	13	147	63
Ras-related protein Rap-1b; Ras-related protein Rap-1A; Ras-related protein Rap-1b-like protein	RAP1B; RAP1A	0.40	0.77	0.56	0.66	8	21	205
26S proteasome non-ATPase regulatory subunit 2	PSMD2	0.45	0.83	0.58	0.66	10	100	28
Glutathione S-transferase omega-1	GSTO1	0.44	0.76	0.51	0.64	7	28	33
Adenine phosphoribosyltransferase	APRT	0.52	0.88	0.81	0.82	6	20	142
Coronin-1A	CORO1A	0.47	0.77	0.62	0.64	9	51	117
Glycine--tRNA ligase	GARS	0.57	0.81	0.62	0.72	11	83	135
Electron transfer flavoprotein subunit beta	ETFB	0.63	0.89	0.90	0.71	6	28	70
Small nuclear ribonucleoprotein Sm D3	SNRPD3	0.66	0.89	0.66	0.92	4	14	39
Ubiquitin-conjugating enzyme E2 L3	UBE2L3	0.61	0.81	0.73	0.54	5	18	53
Programmed cell death 6-interacting protein	PDCD6IP	0.58	0.78	0.58	0.47	14	96	72
Prothymosin alpha;Prothymosin alpha, N-terminally processed;Thymosin alpha-1	PTMA	0.64	0.85	0.71	0.69	6	12	279
Thymosin beta-4; Hematopoietic system regulatory peptide	TMSB4X	0.62	0.82	0.67	0.59	9	5	140

Protein names	Gene names	RIA (degradation) Uninfected24h	RIA (degradation) 24hpi	RIA (degradation) Uninfected48h	RIA (degradation) 48hpi	Peptides	Mol. weight [kDa]	Score
Tubulin beta chain	TUBB	0.69	0.89	0.78	0.78	20	50	155
40S ribosomal protein S7	RPS7	0.64	0.84	0.72	0.79	7	22	129
Plectin	PLEC	0.58	0.74	0.57	0.50	40	532	248
HLA class I histocompatibility antigen, A-2 alpha chain	HLA-A	0.85	0.50	0.35	0.22	10	41	196
HLA class I histocompatibility antigen, B-35 alpha chain	HLA-B	0.17	0.08	0.15	0.17	7	40	142
HLA class I histocompatibility antigen, Cw-15 alpha chain	HLA-C	0.37	0.08	0.25	0.14	4	41	74
Tubulin beta-4B chain	TUBB4B	0.70	0.90	0.80	0.77	21	50	323
Palmitoyl-protein thioesterase 1	PPT1	0.55	0.70	0.46	0.47	8	34	74
Proteasome activator complex subunit 1	PSME1	0.65	0.82	0.70	0.77	10	29	137
Lamin-B1	LMNB1	0.79	0.99	0.94	0.93	25	66	323
Niban-like protein 1	FAM129B	0.59	0.72	0.47	0.51	16	84	170
Tubulin alpha-1C chain;Tubulin alpha-8 chain	TUBA1C; TUBA8	0.72	0.88	0.79	0.79	21	50	323
KH domain-containing, RNA-binding, signal transduction-associated protein 1	KHDRBS1	0.65	0.79	0.65	0.67	5	48	223
Cytoskeleton-associated protein 4	CKAP4	0.75	0.91	0.78	0.76	6	66	96
Apoptosis-associated speck-like protein containing a CARD	PYCARD	0.90	0.88	0.76	0.90	3	22	296
60S ribosomal protein L15	RPL15	0.79	0.84	0.69	0.78	5	24	19
Superoxide dismutase (Mn)	SOD2	0.70	0.73	0.77	0.86	11	25	273
Cytochrome b-c1 complex subunit 7	UQCRB	0.75	0.80	0.64	0.70	3	14	64

Protein names	Gene names	RIA (degradation) Uninfected24h	RIA (degradation) 24hpi	RIA (degradation) Uninfected48h	RIA (degradation) 48hpi	Peptides	Mol. weight [kDa]	Score
Phenylalanine--tRNA ligase beta subunit	FARSB	0.84	0.85	0.79	0.86	5	66	24
Galectin-9	LGALS9	0.82	0.64	0.59	0.63	4	26	65
Fatty acid-binding protein, epidermal	FABP5	0.66	0.77	0.70	0.74	13	15	148
Fumarate hydratase, mitochondrial	FH	0.85	0.89	0.85	0.90	9	55	165
Thioredoxin-related transmembrane protein 1	TMX1	0.80	0.82	0.66	0.69	4	32	15
Vimentin	VIM	0.60	0.68	0.51	0.54	48	54	323
Malate dehydrogenase, mitochondrial	MDH2	0.80	0.84	0.77	0.79	12	36	302
Peroxiredoxin-4	PRDX4	0.85	0.87	0.81	0.81	8	31	138
Cytochrome b-c1 complex subunit 2, mitochondrial	UQCRC2	0.81	0.83	0.75	0.76	8	48	61
Purine nucleoside phosphorylase	PNP	0.76	0.84	0.73	0.72	15	32	216
Fatty acid-binding protein, adipocyte	FABP4	0.59	0.65	0.66	0.64	7	15	323
Calreticulin	CALR	0.86	0.91	0.84	0.82	22	48	323
14-3-3 protein beta/alpha;14-3-3 protein beta/alpha, N-terminally processed	YWHAB	0.85	0.79	0.75	0.72	11	28	323
Glyceraldehyde-3-phosphate dehydrogenase	GAPDH	0.80	0.85	0.73	0.71	17	36	323
L-lactate dehydrogenase B chain	LDHB	0.85	0.93	0.86	0.83	11	37	280
Moesin	MSN	0.73	0.81	0.68	0.65	39	68	323
Peroxiredoxin-2	PRDX2	0.87	0.93	0.88	0.83	7	22	69
Lysine--tRNA ligase	KARS	0.82	0.84	0.73	0.69	9	68	208
Isocitrate dehydrogenase [NADP], mitochondrial	IDH2	0.85	0.93	0.84	0.79	14	51	169

Table 5.2: Proteins significantly degraded upon 48 h infection.

Replicates from both uninfected, 24 hpi and 48 hpi THP-1 were grouped and averaged for statistical analysis. Only proteins that had been quantified in all biological replicates were considered for this statistical test. Two-sample t-test was performed on the filtered data and gave rise to 38 differentially expressed proteins (FDR value = 0.05).

Protein names	Gene names	RIA (degradation) Uninfected24h	RIA (degradation) 24hpi	RIA (degradation) Uninfected48h	RIA (degradation) 48hpi	Peptides	Unique peptides	Mol. weight [kDa]	Score
Electron transfer flavoprotein subunit alpha, mitochondrial	ETFA	0.89	0.88	0.44	0.79	8	8	35	77
Heterogeneous nuclear ribonucleoprotein A0	HNRNPA0	0.75	0.80	0.54	0.78	7	7	31	135
Small nuclear ribonucleoprotein Sm D3	SNRPD3	0.66	0.89	0.66	0.92	4	4	14	39
Annexin A11	ANXA11	0.69	0.72	0.52	0.71	6	6	54	72
Casein kinase II subunit alpha;Casein kinase II subunit alpha 3	CSNK2A1; CSNK2A3	0.72	0.76	0.49	0.65	4	4	45	7
Cytoplasmic FMR1-interacting protein 1	CYFIP1	0.67	0.72	0.58	0.77	9	9	145	20
Hippocalcin-like protein 1; Neuron-specific calcium-binding protein hippocalcin	HPCAL1; HPCA	0.85	0.68	0.45	0.59	7	7	22	69
Glutathione S-transferase omega-1	GSTO1	0.44	0.76	0.51	0.64	7	7	28	33
Polyadenylate-binding protein 1	PABPC1	0.77	0.78	0.59	0.74	8	4	71	127
UDP-glucose:glycoprotein glucosyltransferase 1	UGGT1	0.87	0.85	0.65	0.81	15	14	177	156
Pyridoxal kinase	PDXK	0.80	0.76	0.61	0.76	7	7	35	260
Nodal modulator 1; Nodal modulator 3; Nodal modulator 2	NOMO1; NOMO3; NOMO2	0.68	0.74	0.53	0.66	7	7	134	85
NADH-cytochrome b5 reductase 3; NADH-cytochrome b5 reductase 3 membrane-bound	CYB5R3	0.79	0.82	0.67	0.83	7	7	34	11

Protein names	Gene names	RIA (degradation) Uninfected24h	RIA (degradation) 24hpi	RIA (degradation) Uninfected48h	RIA (degradation) 48hpi	Peptides	Unique peptides	Mol. weight [kDa]	Score
form; NADH-cytochrome b5 reductase 3 soluble form									
60S ribosomal protein L23a	RPL23A	0.71	0.83	0.58	0.71	8	8	18	48
CTP synthase 1	CTPS1	0.81	0.84	0.68	0.83	8	7	67	140
Cystatin-B	CSTB	0.60	0.69	0.53	0.64	6	6	11	147
2-oxoglutarate dehydrogenase, mitochondrial	OGDH	0.75	0.79	0.65	0.78	10	10	116	63
Signal transducer and activator of transcription 1-alpha/beta	STAT1	0.61	0.68	0.49	0.59	4	4	40	52
Choline-phosphate cytidylyltransferase A; Choline-phosphate cytidylyltransferase B	PCYT1A; PCYT1B	0.67	0.71	0.58	0.70	2	2	42	4
Eukaryotic translation initiation factor 6	EIF6	0.72	0.75	0.58	0.70	5	5	27	68
Osteoclast-stimulating factor 1	OSTF1	0.77	0.77	0.63	0.75	3	3	24	81
HLA class I histocompatibility antigen, A-2 alpha chain	HLA-A	0.85	0.50	0.35	0.22	10	41	196	196
HLA class I histocompatibility antigen, B-35 alpha chain	HLA-B	0.17	0.08	0.15	0.17	7	40	142	142
HLA class I histocompatibility antigen, Cw-15 alpha chain	HLA-C	0.37	0.08	0.25	0.14	4	41	74	72
Apoptosis-associated speck-like protein containing a CARD	PYCARD	0.90	0.88	0.76	0.90	3	3	22	296
Superoxide dismutase (Mn)	SOD2	0.70	0.73	0.77	0.86	11	11	25	273
Cytochrome b-c1 complex subunit 7	UQCRB	0.75	0.80	0.64	0.70	3	3	14	64
Phenylalanine--tRNA ligase beta subunit	FARSB	0.84	0.85	0.79	0.86	5	5	66	24

Protein names	Gene names	RIA (degradation) Uninfected24h	RIA (degradation) 24hpi	RIA (degradation) Uninfected48h	RIA (degradation) 48hpi	Peptides	Unique peptides	Mol. weight [kDa]	Score
Galectin-9	LGALS9	0.82	0.64	0.59	0.63	4	4	26	65
Vimentin	VIM	0.60	0.68	0.51	0.54	48	48	54	323
Peroxiredoxin-4	PRDX4	0.85	0.87	0.81	0.81	8	8	31	138
Purine nucleoside phosphorylase	PNP	0.76	0.84	0.73	0.72	15	15	32	216
Glyceraldehyde-3-phosphate dehydrogenase	GAPDH	0.80	0.85	0.73	0.71	17	17	36	323
L-lactate dehydrogenase B chain	LDHB	0.85	0.93	0.86	0.83	11	11	37	280
Moesin	MSN	0.73	0.81	0.68	0.65	39	39	68	323
Peroxiredoxin-2	PRDX2	0.87	0.93	0.88	0.83	7	7	22	69
Lysine--tRNA ligase	KARS	0.82	0.84	0.73	0.69	9	9	68	208
Isocitrate dehydrogenase [NADP], mitochondrial	IDH2	0.85	0.93	0.84	0.79	14	14	51	169

Based on RIA (degradation) values, we plotted graphs for several proteins over the duration of 48 hours of infection. Gamma-interferon-inducible protein 16 and carbonic anhydrase 2 had lower RIA degradation in infected THP-1 (24 hpi and 48 hpi) compared to the uninfected THP-1 (Figure 5.12). Whereas, proteins such as histone H1.5 and histone H4 had no significant differences of RIA degradation in both uninfected and infected THP-1. Heat shock 70 kDa protein and STAT1 had bigger RIA values in infected THP-1 than the uninfected THP-1 (Figure 5.13).

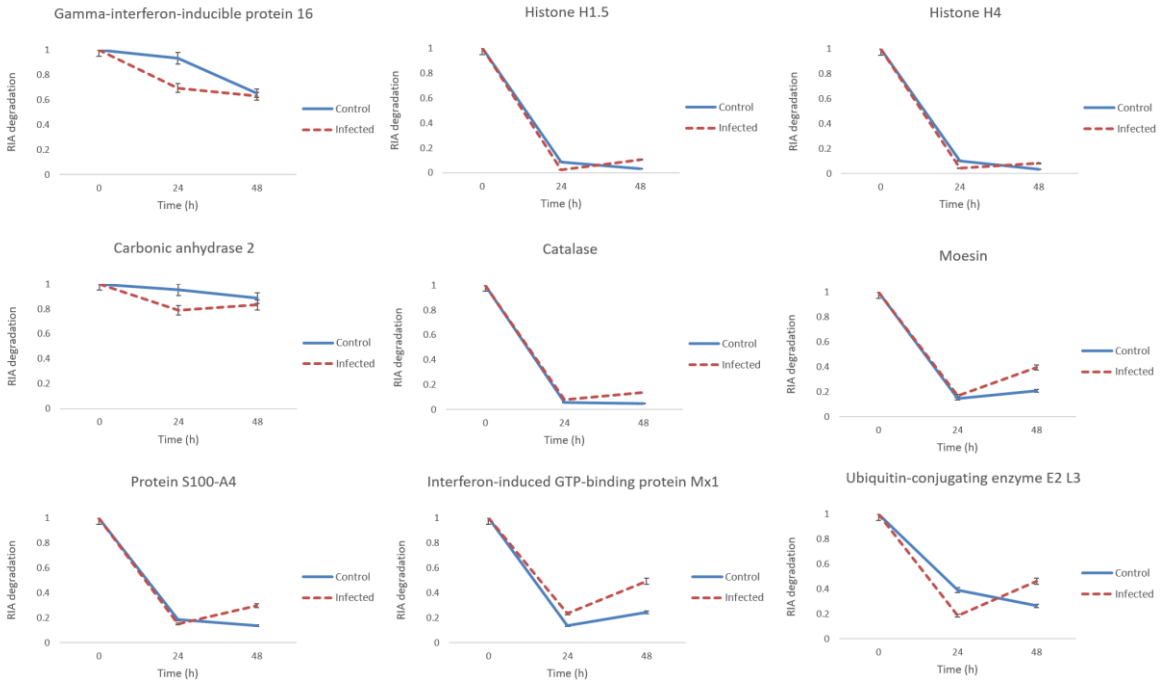

Figure 5.12: Relative isotope abundance (RIA) degradation for several significantly changing proteins.

RIA, *t* for several proteins were calculated and plotted against time of infection. Each point corresponds to the mean values ± SD of three biological replicates.

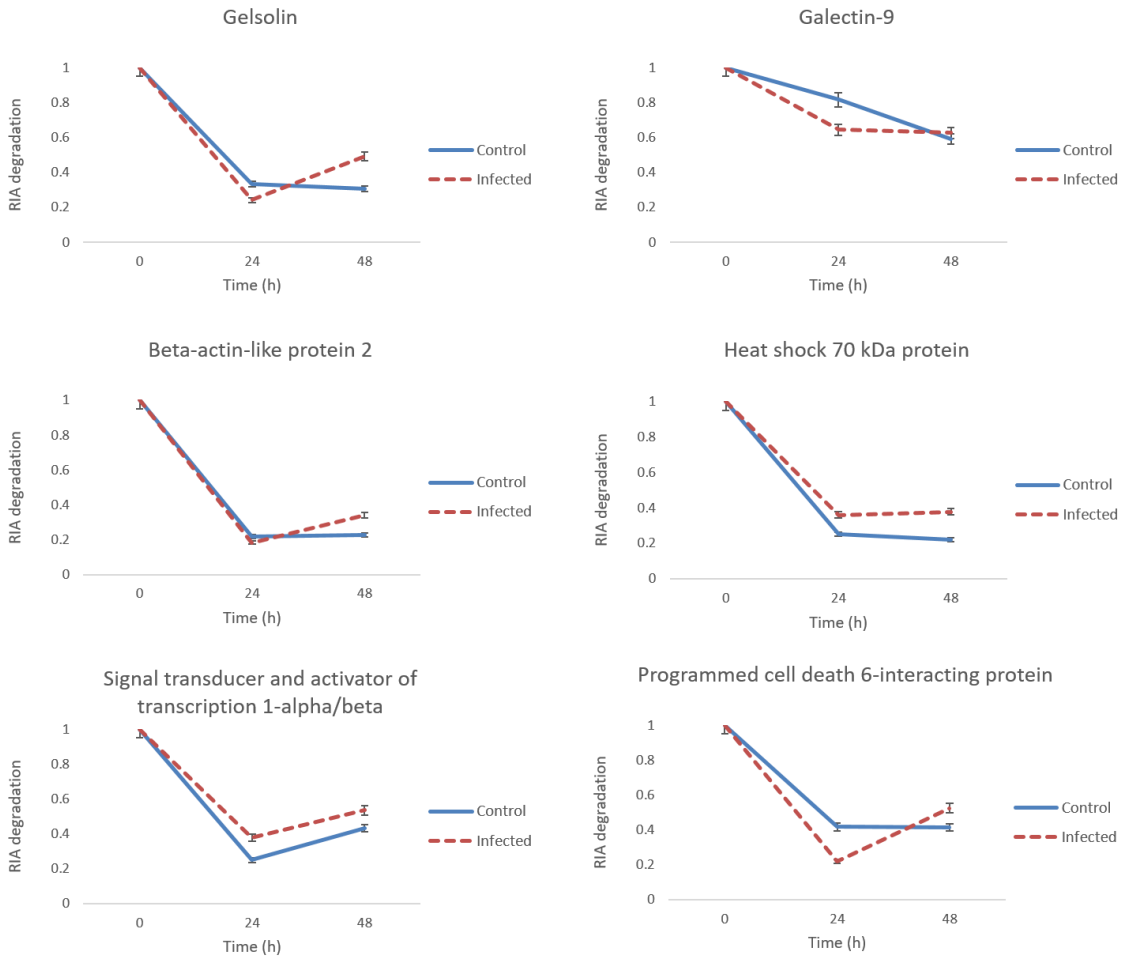

Figure 5.13: Relative isotope abundance (RIA) degradation for several significantly changing proteins.

RIA, t for several proteins were calculated and plotted against time of infection. Each point corresponds to the mean values ± SD of three biological replicates.

Interestingly, HLA complexes showed much lower RIA values in infected cells compared to uninfected cells (Figure 5.14). Furthermore, most metabolic enzymes had almost the same RIA values in uninfected, 24 hpi and 48 hpi THP-1 (Figure 5.15). This clearly showed that proteins with the same function behave similarly in cells.

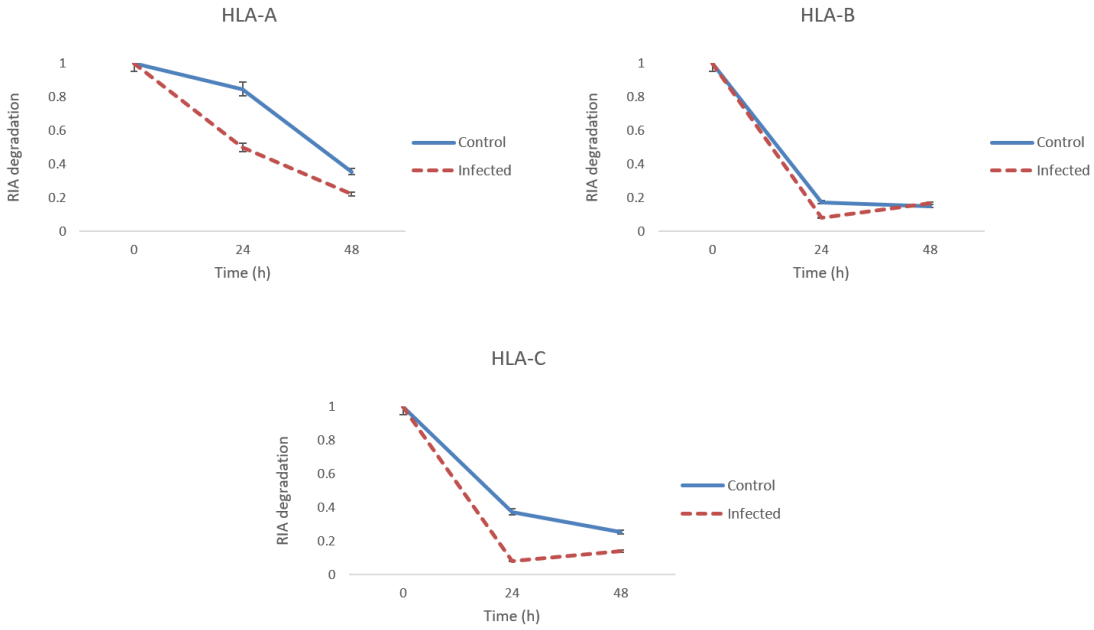

Figure 5.14: Relative isotope abundance (RIA) degradation for proteins involve in antigen processing and presentation.

RIA, t for several proteins were calculated and plotted against time of infection. Each point corresponds to the mean values ± SD of three biological replicates.

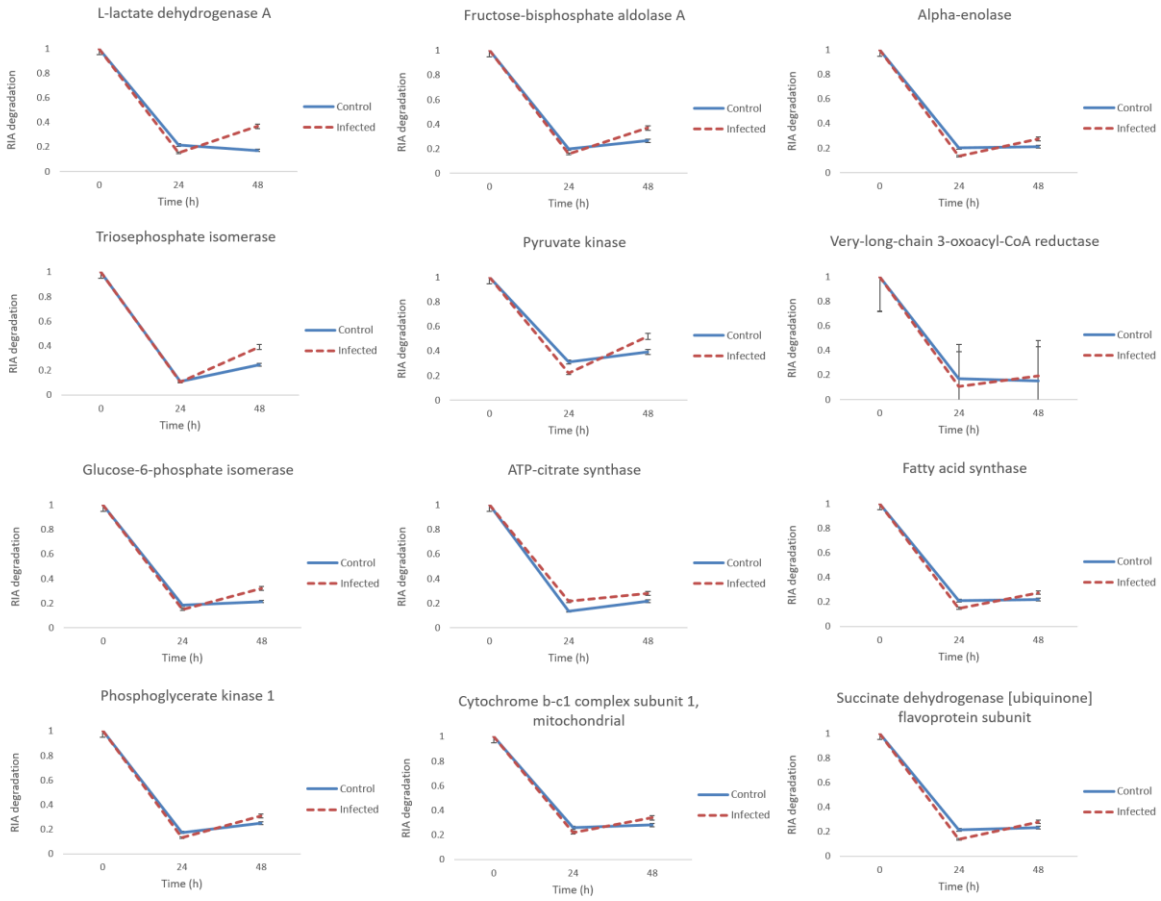

Figure 5.15: Relative isotope abundance (RIA) degradation for proteins involve in metabolic process.

RIA, t for several proteins were calculated and plotted against time of infection. Each point corresponds to the mean values ± SD of three biological replicates.

60S ribosomal proteins and 40S ribosomal proteins such as the ones depicted in Figure 5.16 showed no change in uninfected cell and 24 hpi, but the RIA values in 48 hpi were slightly increased compared to uninfected cells.

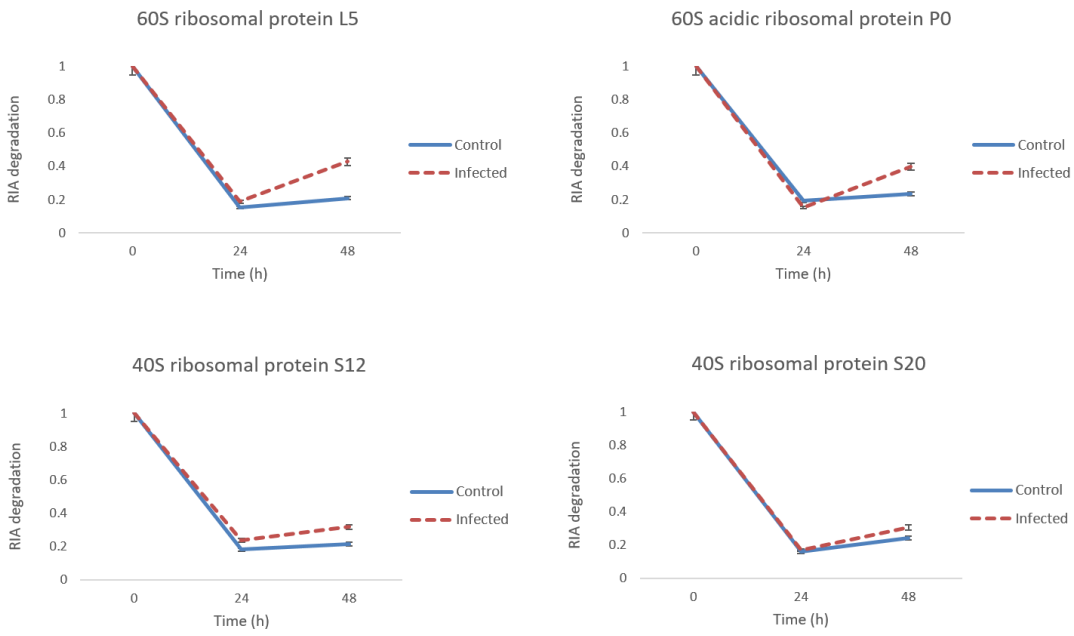

Figure 5.16: Relative isotope abundance (RIA) degradation for proteins involve in translation.
RIA, t for several proteins were calculated and plotted against time of infection. Each point corresponds to the mean values ± SD of three biological replicates.

The RIA, *t* values were then used to derive the degradation rate constant, k_{deg}. Degradation rate constants (k_{deg}) were calculated from the exponential decay formula as RIA = exp (k_{deg}*time). Overall, we observed that most proteins were quite stable and not degrading rapidly. As shown in Figure 5.17, the highest k_{deg} value is 0.04 h^{-1}. The data also indicated that 23.5% of the 400 proteins were degraded at a rate of 4% every hour. The degradation rates were not normally distributed (Figure 5.19). Global analysis of protein degradation revealed that the majority of the proteins were relatively stable as most have relatively low k_{deg} values. The k_{deg} values less than 0.04 h^{-1} reflected proteins slowly decayed.

Examples included ATP-dependent RNA helicase, myosin-IF, succinate dehydrogenase and actin related protein 2/3 complex subunit (Figure 5.20). The lowest k_{deg} value is 0.01 h^{-1}. Slowly degraded proteins with k_{deg} of 0.01 h^{-1} included gamma-interferon-inducible protein 16, gelsolin and galectin-9 (example in Appendix 8.3). Interestingly, several proteins that are implicated in the immune response, such as HLA complexes demonstrated marked differences of degradation rate between infected and uninfected samples (Figure 5.21). HLA complexes had a relatively high degradation rate after infection (90% decayed after 48 h) compared to uninfected.

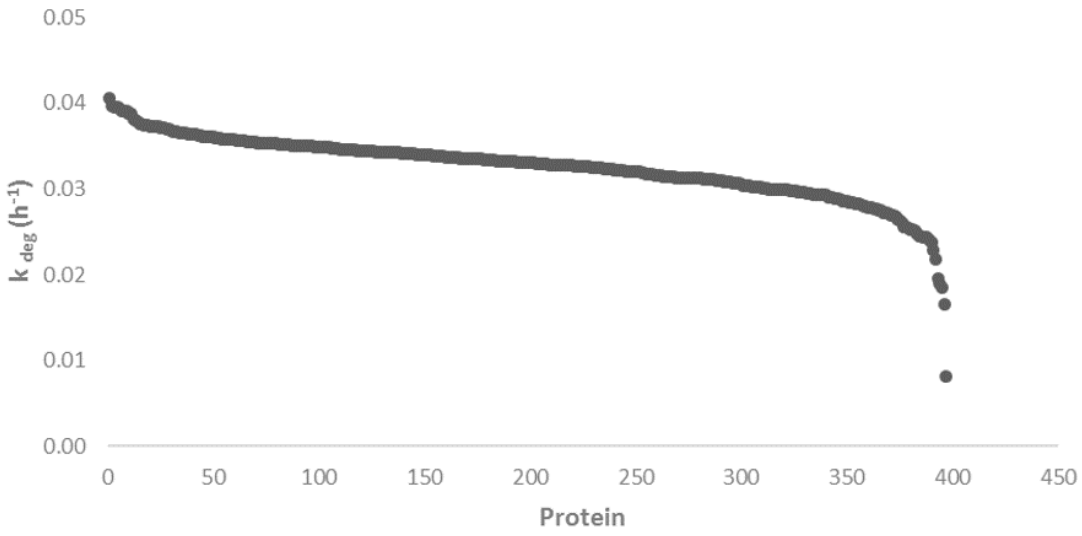

Figure 5.17: Global degradation profile.

The change in relative isotope abundance (RIA) for each protein was assessed. The rate constant k_{deg} for 400 proteins was calculated. Graph showed the distribution of degradation rate constants for 400 proteins.

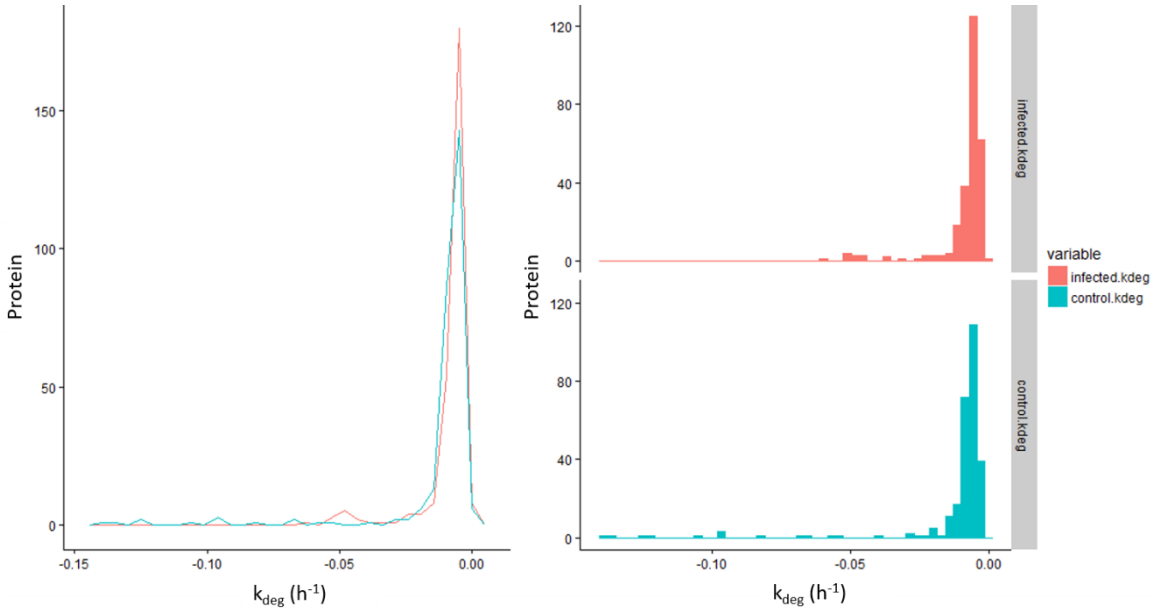

Figure 5.18: Global analysis of protein degradation.

The change in relative isotope abundance (RIA) for each protein was assessed during the unlabelled 'chase' period. The RIA data were fitted to a single exponential decay curve and the degradation rate constant (*kdeg*) was calculated.

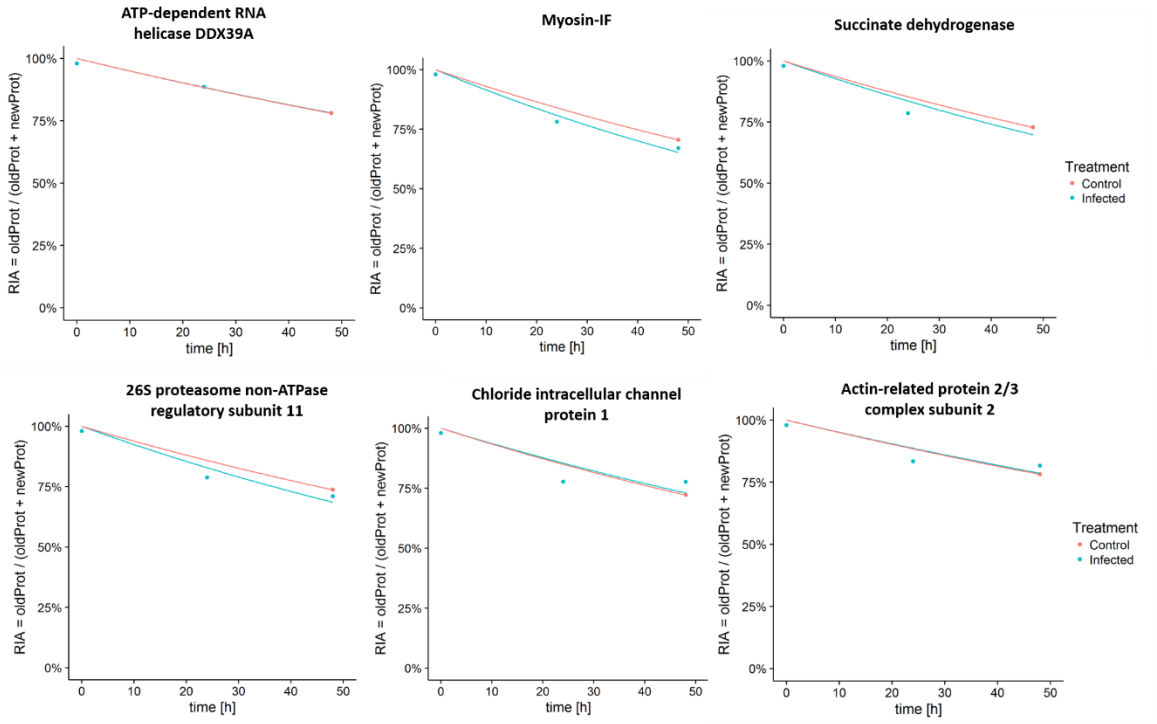

Figure 5.19: Identification of rapidly depleted proteins.

R script was used to generate degradation plot over 48 h between uninfected and infected THP-1.

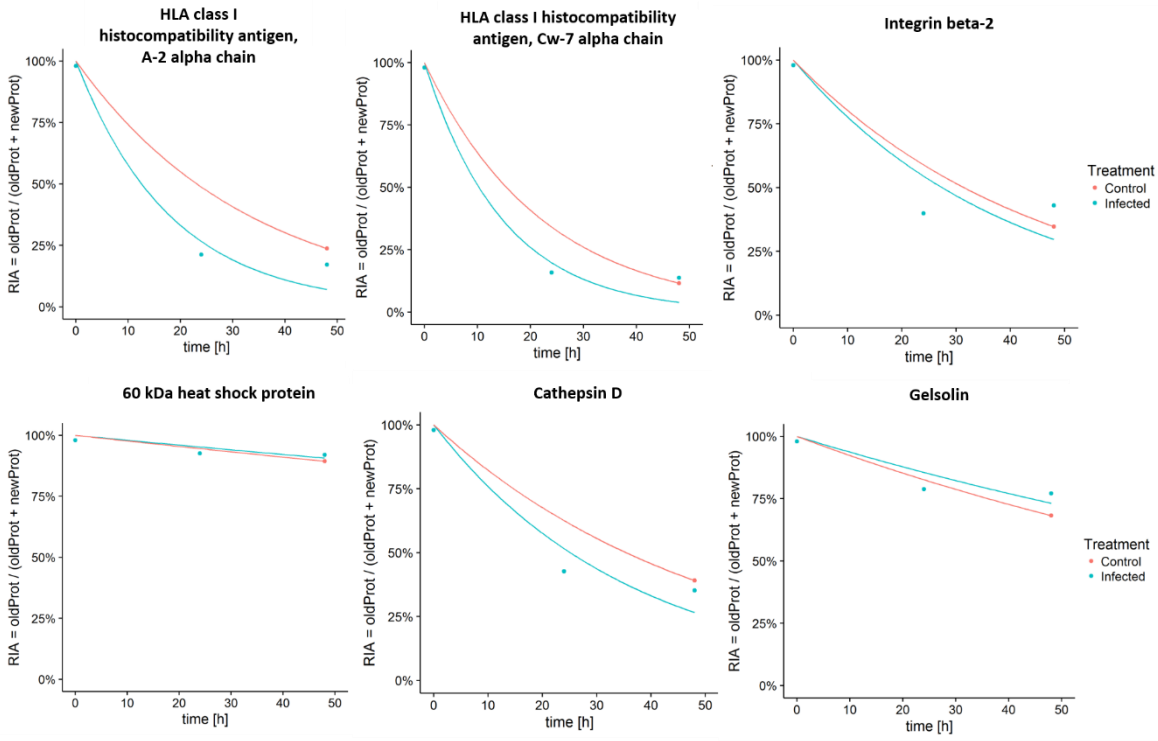

Figure 5.20: Analysis of protein degradation profile.

R script was used to generate degradation plot over 48 h between uninfected and infected data.

Figure 5.21 depicts k_{deg} graphs of several statistically significant proteins that show differences in degradation rate constant between uninfected and infected groups. Proteins involved in glycolysis including lactate dehydrogenase, fructose-bisphosphate aldolase A, fumarate hydratase, and glucose-2-phosphate isomerase had similar k_{deg} in all groups (Figure 5.22 a). Although it has been shown previously that most metabolic enzymes are stable, this graph showed that k_{deg} values were significantly reduced in 48 hpi compared to 24 hpi and uninfected THP-1. HLA complexes also showed similar pattern as metabolic enzymes (Figure 5.22 b). Next, we investigate the k_{deg} value of stress proteins and ribosomal proteins (Figure 5.23 a and b). Some of the stress proteins and ribosomal proteins have quite striking changes in degradation after 48 h of infection as opposed to 24 h of infection.

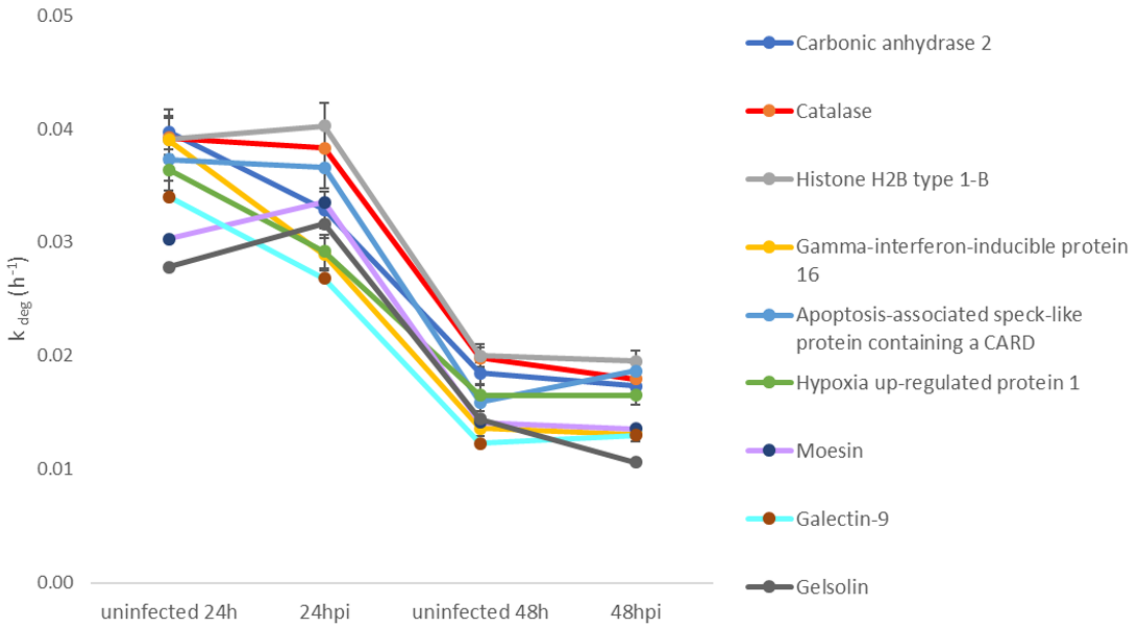

Figure 5.21: The degradation rate constant (k_{deg}) over time for statistically significant proteins.

RIA, t values were used to derive the degradation rate constant for each protein and plotted for uninfected 24h, 24 hpi, uninfected 48h and 48 hpi. Each point corresponds to the mean values ± SD of three biological replicates.

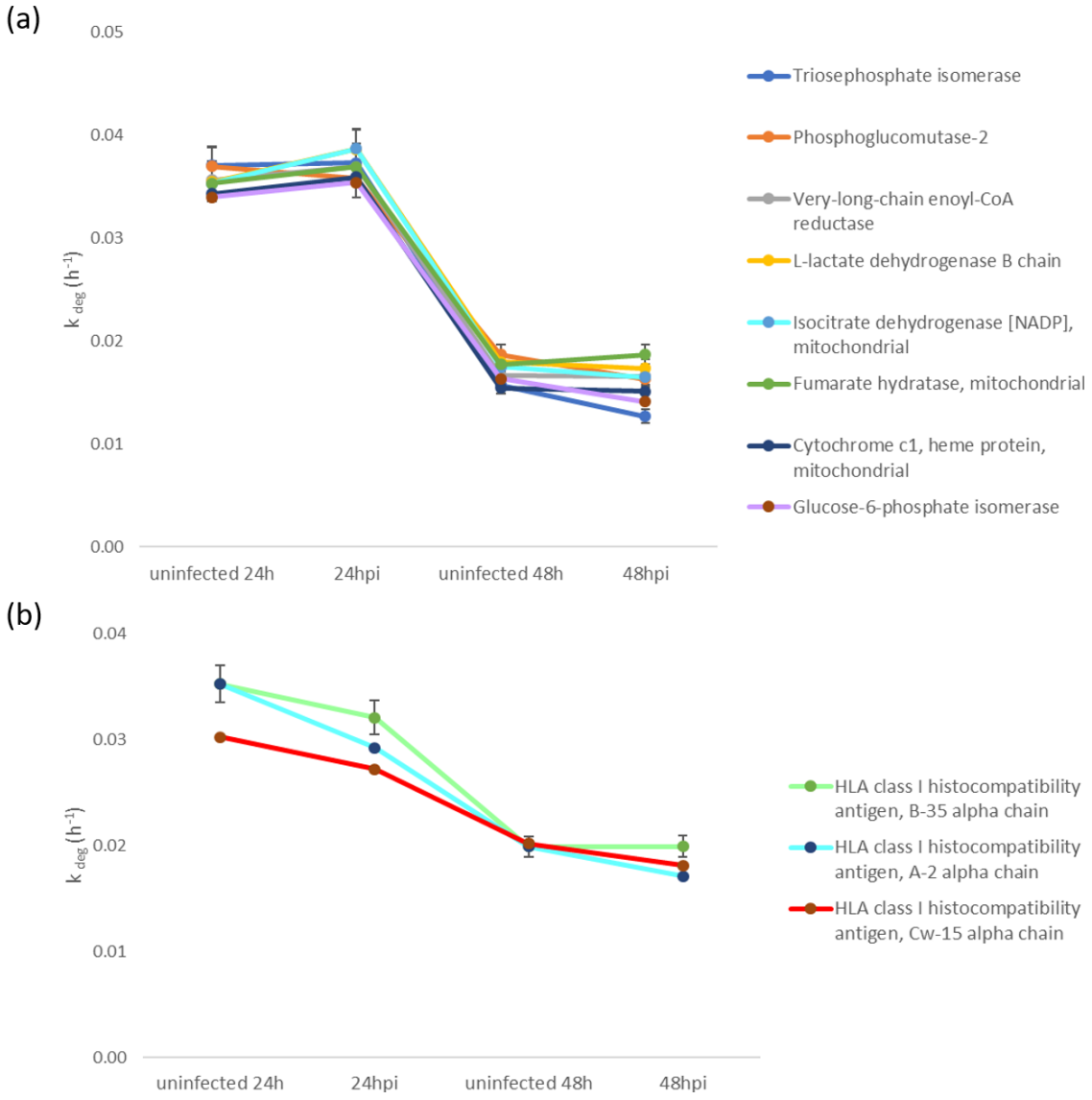

Figure 5.22: The degradation rate constant (k_{deg}) over time for proteins involve in metabolic process and antigen processing and presentation.

RIA, t values were used to derive the degradation rate constant for each protein and plotted for uninfected 24h, 24 hpi, uninfected 48h and 48 hpi. Each point corresponds to the mean values ± SD of three biological replicates.

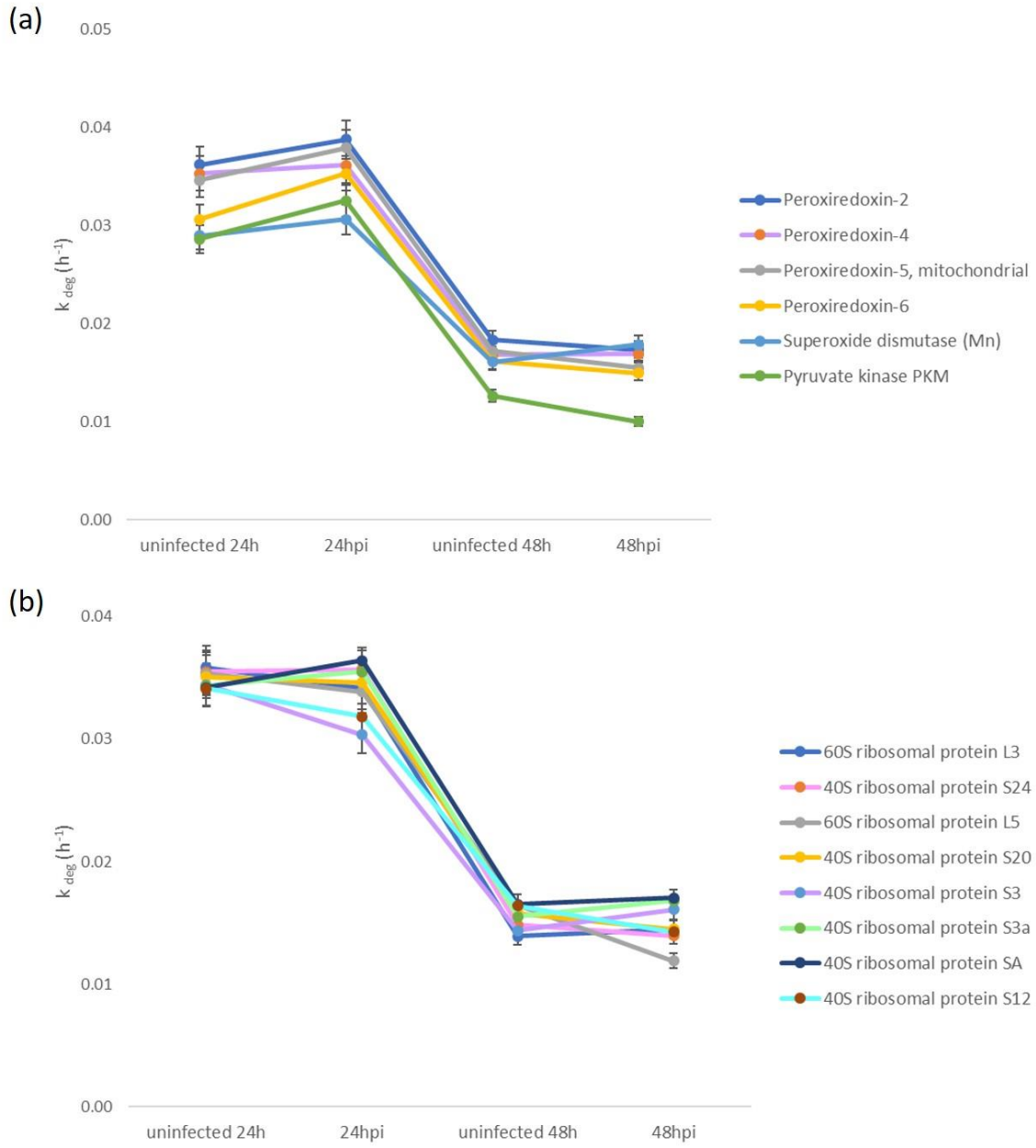

Figure 5.23: The degradation rate constant (k_{deg}) over time for proteins involve in stress response and ribosome.

RIA, t values were used to derive the degradation rate constant for each protein and plotted for uninfected 24h, 24 hpi, uninfected 48h and 48 hpi. Each point corresponds to the mean values ± SD of three biological replicates.

Most proteins in infected samples have k_{deg} differences than the uninfected samples, even more differences in 24 and 48 hpi (Figure 5.24). For example, carbonic anhydrase 2 had k_{deg} of 0.04 h^{-1} in uninfected 24h but slightly increased to 0.03 h^{-1} in 24 hpi. However, the k_{deg} in both uninfected 48h and 48 hpi remained the same (0.02 h^{-1}). Catalase, histones, annexins, and several ribosomal proteins had reduced k_{deg} following 48 h of infection.

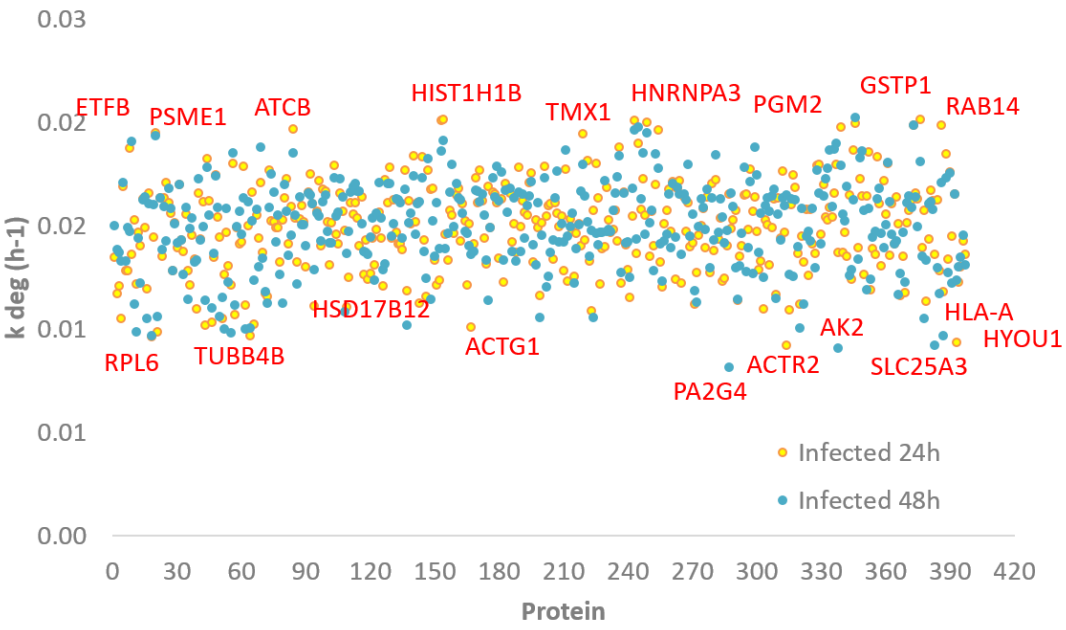

Figure 5.24: The distribution of degradation rate constant (k_{deg}) for 400 proteins in uninfected, 24 hpi and 48 hpi THP-1.

RIA, t values were used to derive the degradation rate constant for each protein and plotted for 24 hpi and 48 hpi. Proteins with high and low k_{deg} were highlighted.

Protein networks of the significantly changing rates of degradation were constructed in the STRING database with interaction confidence > 0.5 and visualized using Cytoscape. Figure 5.25 showed the protein network involving the highly-regulated proteins (p-value < 0.05).

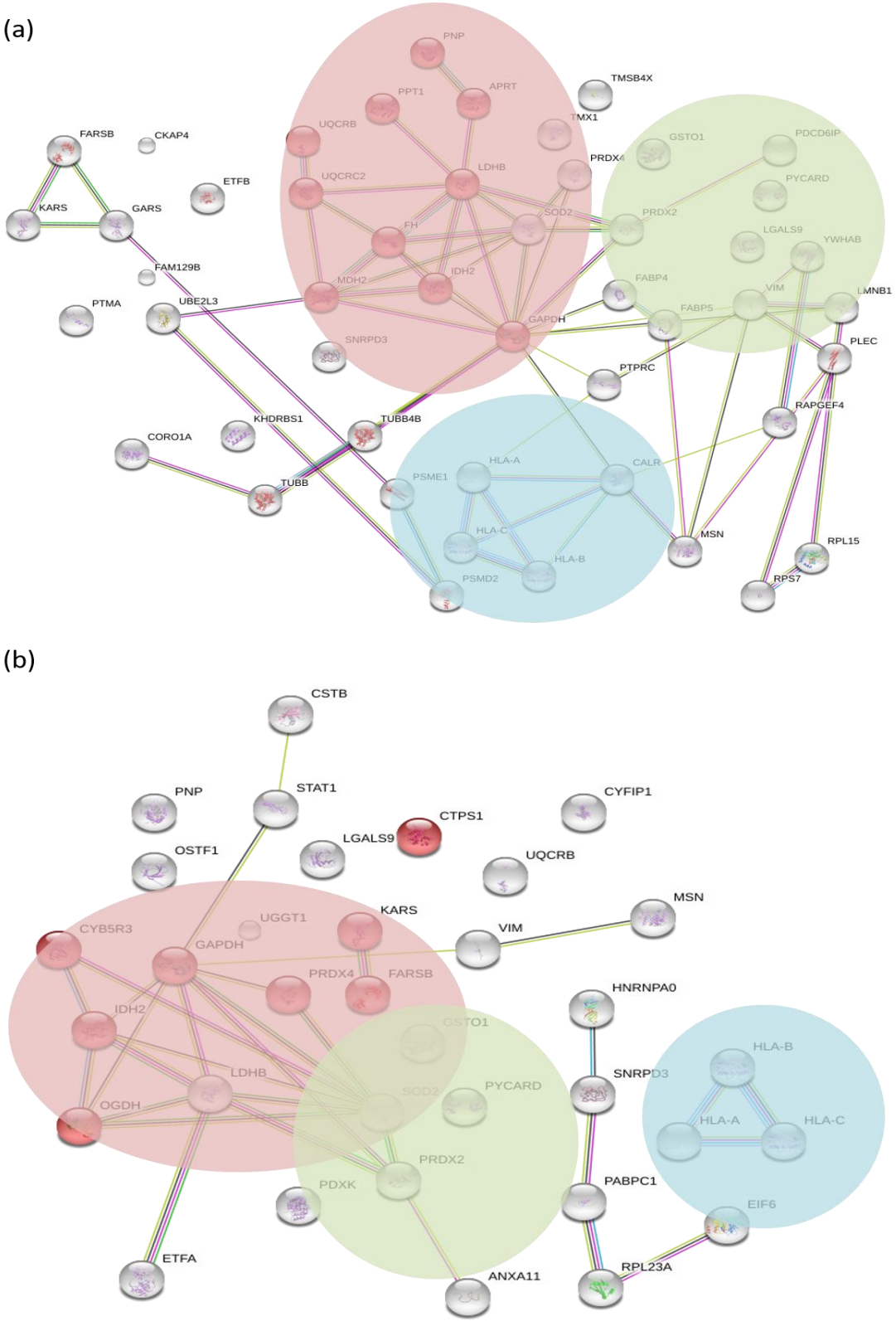

Figure 5.25: Protein network of proteins with significant change in degradation rates (p=0.05).

Significantly degraded proteins were analysed on STRING database to determine the protein-protein interactions between them. (a) Proteins with changes in degradation rate in 24 hpi (b) Proteins with changes in degradation rate in 48 hpi.

5.3.2 Protein turnover of human cell lines THP-1 in response to *L. mexicana* infection

Our workflow permitted us to determine intracellular protein replacement rates (turnover) on a large scale. For this purpose, we measured the half-life of 400 proteins that met the criteria as described in chapter 4, with MOWSE score and ion score of < 0.05. We filtered the data to have L/H values for each group by removing the proteins with missing values. Half-lives were calculated using the formula in section 2.10.6. For the 400 proteins, the mean half-life for uninfected 24 h, 24 hpi, uninfected 48h and 48 hpi were 21.74 h, 20.51 h, 47.39 h and 47.33 h, respectively. Half-lives of proteins in uninfected 24h range from 16.63 to 85.44 h, 16.80 to 30.36 h in 24 hpi, 34.34 to 75.22 h in uninfected 48h, and 34.23 to 85.18 h in 48 hpi (summarized in Table 5.3). All calculations were derived from 3 replicates that have been averaged in Excel spreadsheet. Figure 5.26 illustrate the distribution of protein half-lives in all 4 groups. Interestingly, almost all proteins have relatively increased half-life from 24 to 48 h of infection. These includes 26S proteasome non-ATPase regulatory subunit (19.55 h in 24 hpi to 42.59 h in 48 hpi), several actin-related proteins (2-fold increased from 24 hpi to 48 hpi), 14-3-3 proteins (2-fold increased from 24 hpi to 48 hpi), PNP (19.83 h in 24 hpi to 46 h in 48 hpi), galactokinase (GALK1), fumarate hydratase (FH), ubiquitin-conjugating enzyme E2 N (UBE2N), several subunits of 60S and 40S ribosomal proteins (2-fold increased from 24 hpi to 48 hpi), moesin (MSN), Ras-related protein (RAB1B), calmodulin (CALM1), gamma-interferon-inducible protein 16 (IFI16), cathepsin-B (CTSB), pyruvate kinase (PKM), interferon-induced GTP-binding protein (MX1) and STAT1. Protein with the longest half-life was leukotriene A-4 hydrolase (85.18 h), whereas protein with the shortest half-life was interleukin-8 (16.63 h).

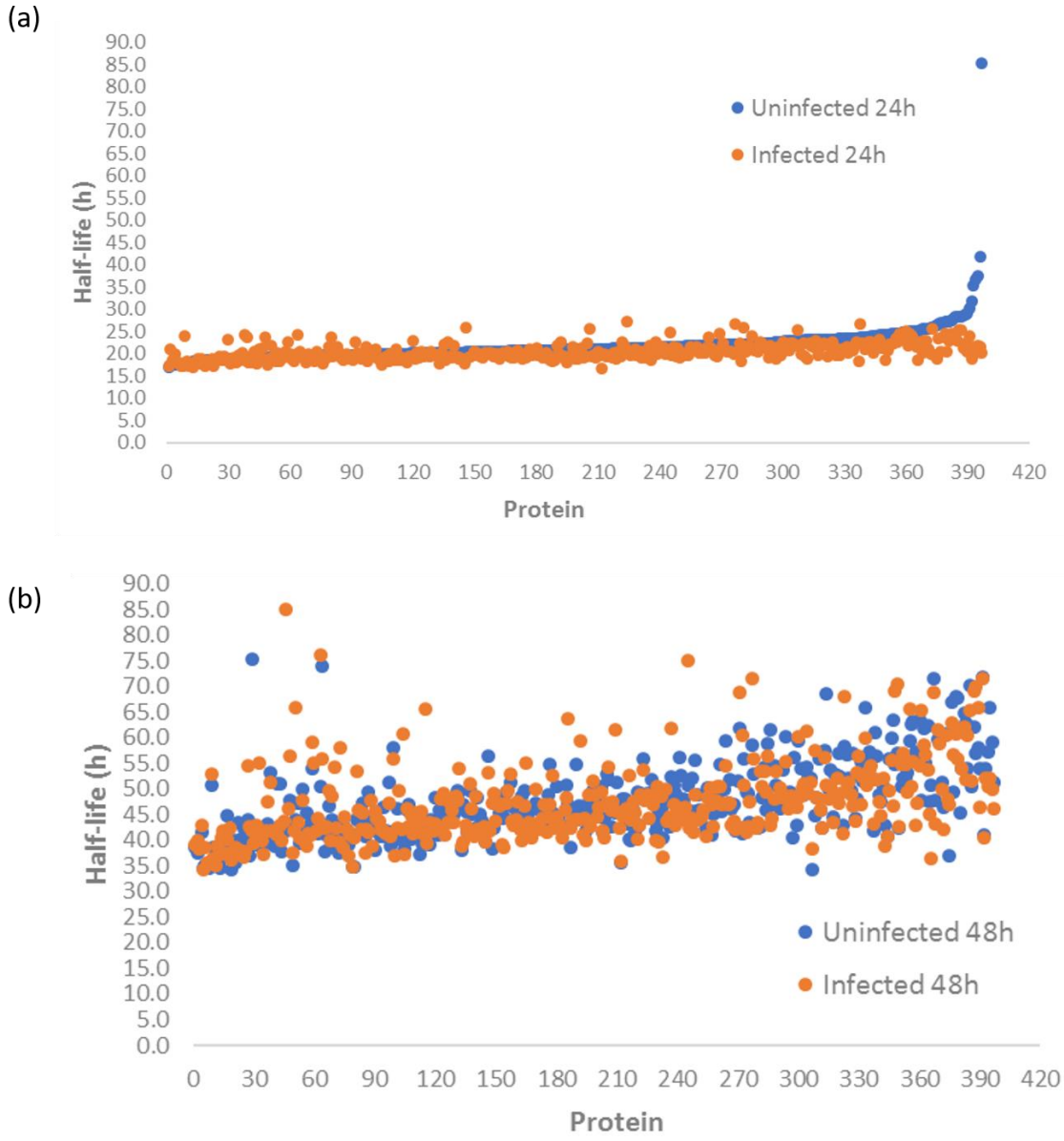

Figure 5.26: Protein turnover distribution.

RIA, t values were used to derive the degradation rate constant for each protein. From the measurements, protein half-lives were determined for all 400 proteins and compared between (a) uninfected 24h and 24 hpi, and (b) uninfected 48h and 48 hpi.

To evaluate the protein half-lives that were only involved in infection groups, triplicates of 24 hpi and 48 hpi were grouped together and averaged. Hierarchical clustering heatmap for these groups was made using a feature in Perseus, revealing altered half-lives of several proteins between 24 and 48 hpi (Figure 5.27). For example, peroxiredoxin 6 (PRDX6) was turnover rapidly after 24 h of *L. mexicana* infection but was turnover slowly after 48 h of infection.

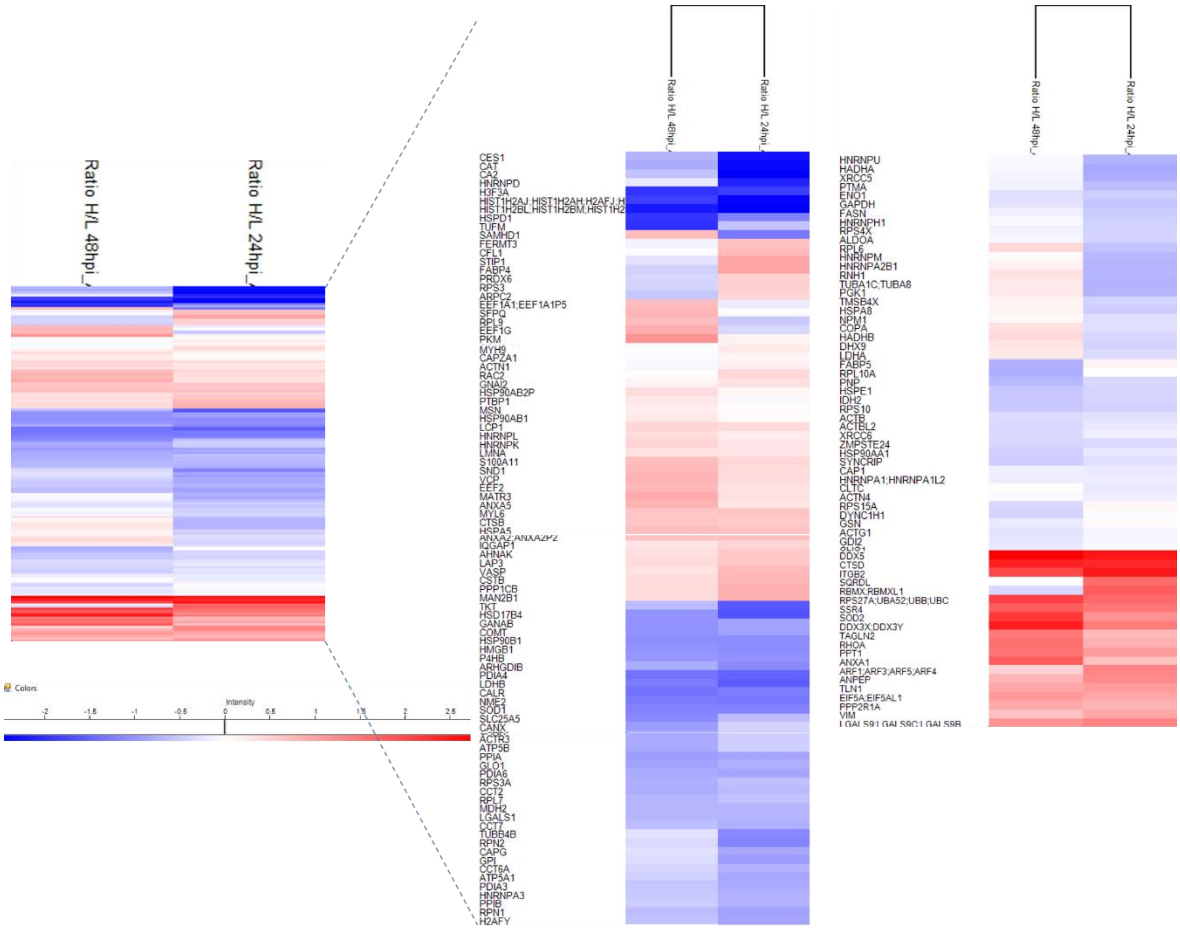

Figure 5.27: Heatmap representation of protein expressions of 24 hpi and 48 hpi.

Triplicates of 24 hpi and 48 hpi were grouped together and averaged. All missing values were filtered out from the data. Heat map showing fold change patterns of several altered genes between 24 hpi and 48 hpi; red = increased half-life, blue = decreased half-life.

The proteins were ranked according to fold change of half-lifes. Of 400 proteins, 368 had more than 2 FC. Gene ontolgy on DAVID demonstrated that 47% of the proteins were involved in metabolic processes, 13% were involved in response to stimulus and 10% were involved in oxidation reduction process. The protein IDs were also uploaded to the PANTHER database to predict gene ontology and pathway association. As observed on the DAVID database, the PANTHER database also reported that the highest number of significantly modulated proteins were associated with metabolic processes (Figure 5.28).

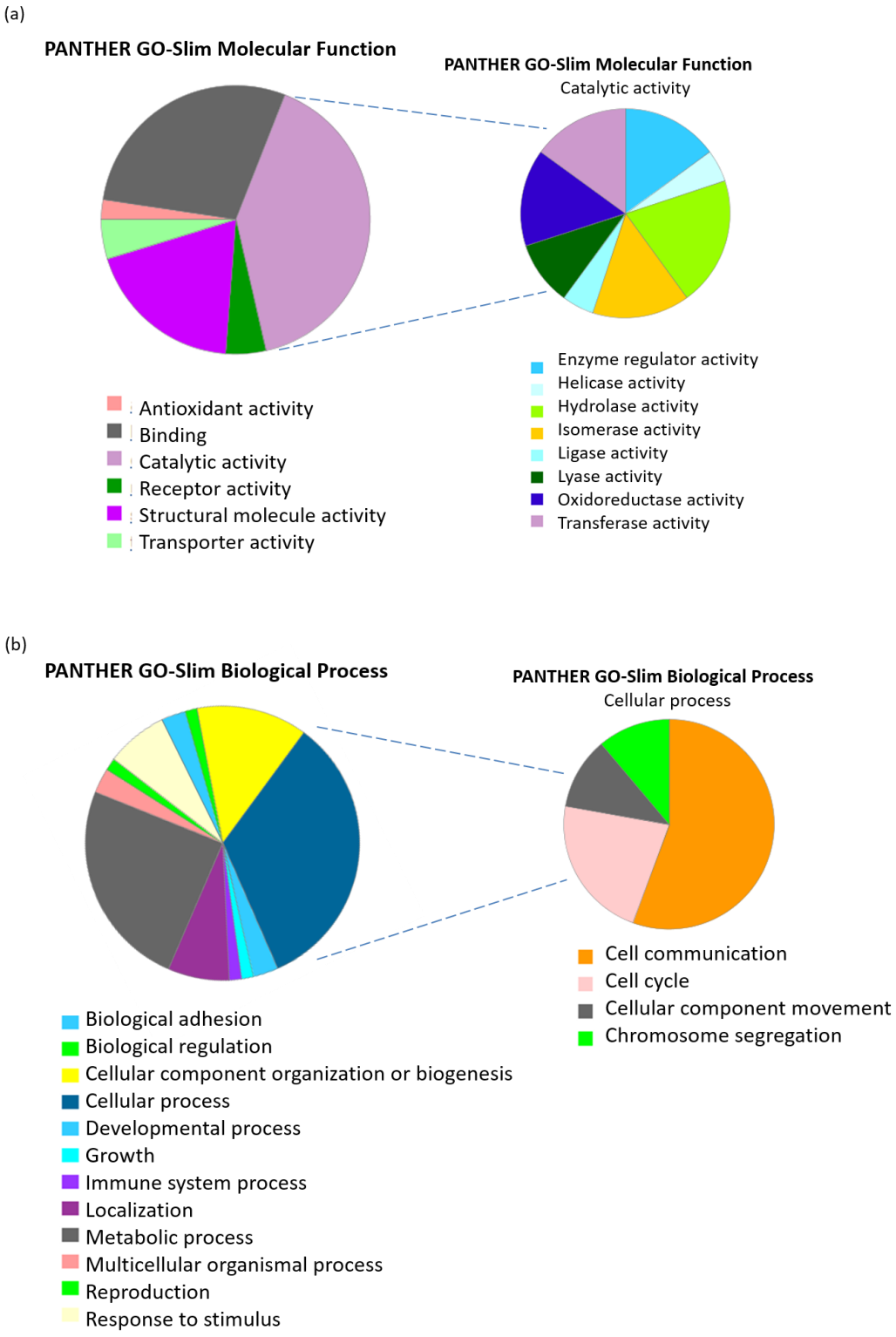

Figure 5.28: Gene ontology performed using PANTHER database on proteins with more than 2-fold change in half-lives upon 24 and 48 h infection.

Conventional data were normalized and those with no quantification report were removed from all samples. The half-lives were ranked according to fold changes between 48 hpi and 24 hpi, selecting only those with more than 2-fold change. The protein Uniprot IDs were uploaded on PANTHER database for functional analyses. (a) Gene ontology of significantly modulated proteins based on molecular function (b) Gene ontology of significantly modulated proteins based on biological process.

Several proteins from Table 4.2 and 4.3 were selected to observe the half-lives in uninfected and infected macrophage. As depicted in Figure 5.29, carbonic anhydrase 2 showed longer half-life after 24 h of infection and kept on increasing following 48 h of infection. Catalase, gamma-interferon-inducible protein 16histone H2B type 1-B and moesin also had similar pattern. Apoptosis-associated speck-like protein and galectin-9 had increased half-lives in the early infection (24 h) but decreased their half-lives after 48 h of infection.

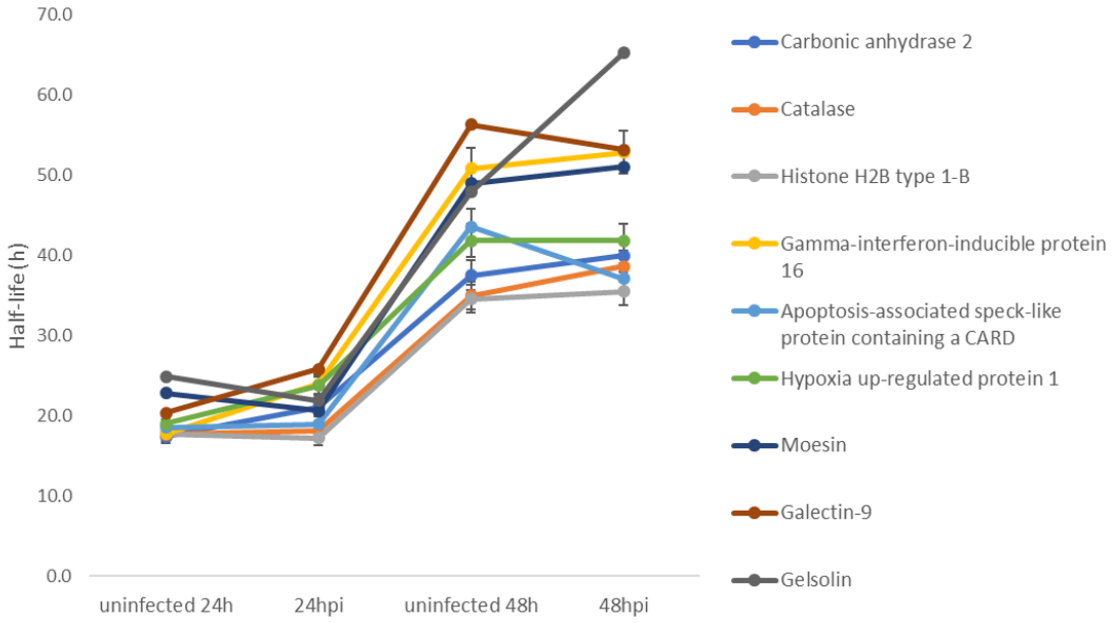

Figure 5.29: Measurement of protein half-lives.

RIA, *t* values were used to derive the degradation rate constant for each protein. From the measurements, protein half-lives were determined for several statistically significant proteins. Each point corresponds to the mean values ± SD of three biological replicates.

Most proteins involved in glycolysis were rapidly turned-over during 24 h infection but they increased their half-lives after 48 h infection (Figure 5.30). Proteins that showed increased half-lives after 48 h infection compared to uninfected and 24 hpi were phosphoglucomutase-2, very-long-chain enoyl-CoA reductase, L-lactate dehydrogenase B chain, isocitrate dehydrogenase [NADP], mitochondrial, fumarate hydratase, mitochondrial, cytochrome c1, heme protein, mitochondrial, and glucose-6-phosphate isomerase (Figure 5.31 a). Phosphoglycerate kinase (PGK) catalyzes the reversible transfer of a phosphate group from 1,3-bisphosphoglycerate (1,3-BPG) to ADP producing 3-phosphoglycerate (3-PG) and ATP (Watson et al. 1982). PGK1 is secreted by tumour cells and overexpression of PGK1 has been associated with angiogenic process (Lay et al. 2000). Alpha-enolase

(ENO1), also known as 2-phospho-D-glycerate hydrolase, is a metalloenzyme involved in the ninth step of glycolysis. ENO1 responsible for the catalysis of the conversion of 2-phosphoglycerate (2-PG) to phosphoenolpyruvate (PEP) (Ji et al. 2016). In addition to its glycolytic function, this multifunctional enzyme also involved in cellular stress, bacterial and fungal infections, auto-antigen activities, the occurrence and metastasis of cancer, parasitic infections, as well as the growth, development and reproduction of organisms (Ji et al. 2016). Another glycolytic protein found to be turnover slowly in our data is pyruvate kinase (PKM). PKM irreversibly catalyzes the last step of glycolysis, where the phosphoryl group of PEP is transferred to ADP to form pyruvate and ATP. This final step of glycolysis is important as the substrates PEP and pyruvate involves in various metabolic process (Valentini et al. 2000).

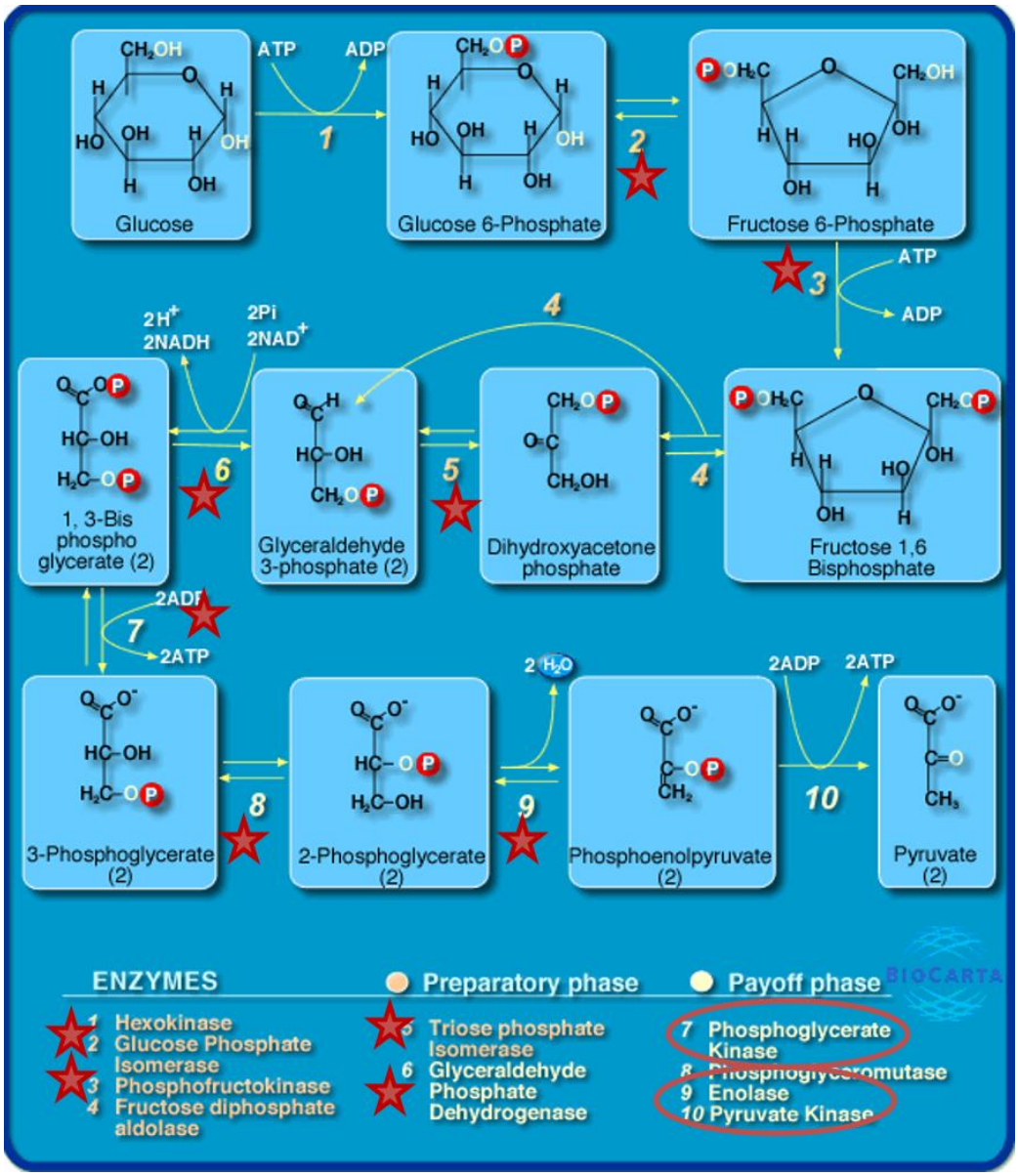

Figure 5.30: Glycolysis pathway showing increased half-lives proteins.

All proteins identified in this study were analysed on DAVID. The pathways linked to BioCarta was chosen and several proteins with increased half-lives were found in glycolysis pathway (red circle): phosphoglycerate kinase, enolase, phosphoglycerate mutase and pyruvate kinase. The red stars represent the remaining proteins found in our data.

HLA complexes showed increased half-lives in infected cells compared to uninfected cells (Figure 5.31 b). They took around 37 h (average) to recover 50% of their proteins following 48 h of infection. This means that after 48 h infection, the proteins are becoming more stable.

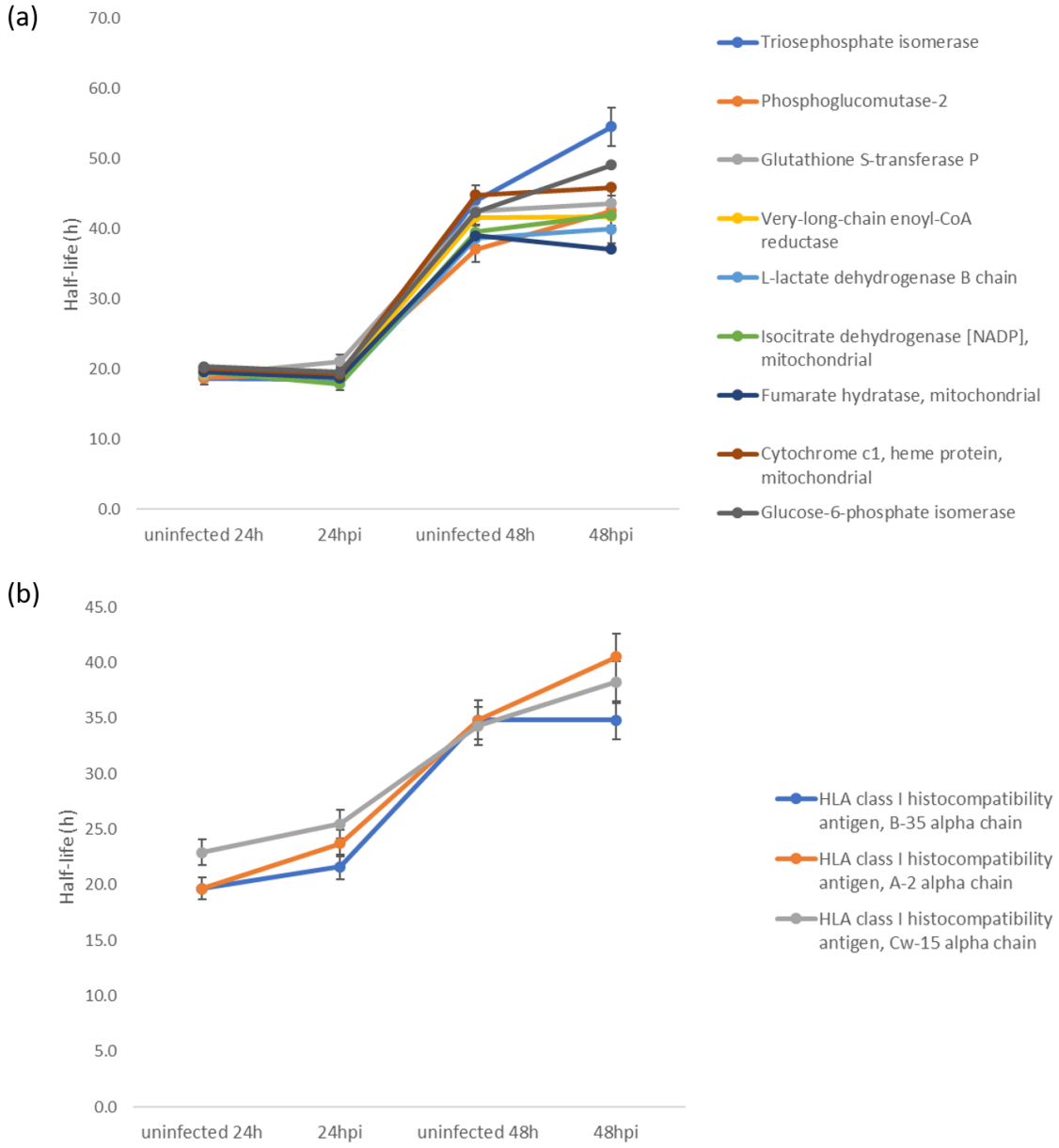

Figure 5.31: Measurement of protein half-lives for metabolic enzymes and proteins involve in antigen processing and presentation.

RIA, t values were used to derive the degradation rate constant for each protein. From the measurements, protein half-lives were determined for several (a) metabolic enzymes, and (b) proteins involve in antigen processing and presentation. Each point corresponds to the mean values ± SD of three biological replicates.

One of the proteins that have significant increased turnover following 48 h infection of THP-1 with *L. mexicana* is peroxiredoxin (PRDX6) which is involved in oxidative stress responses and cellular redox homeostasis (Whitbread et al. 2005) (Figure 5.32 a). In contrast, superoxide dismutase had decreased half-life in 48 hpi, compared to 24 hpi (Figure 5.32 a). From the graph in Figure 5.32 b, it is

apparent that subunits of ribosomal proteins have different half-lives and do not show the same trend.

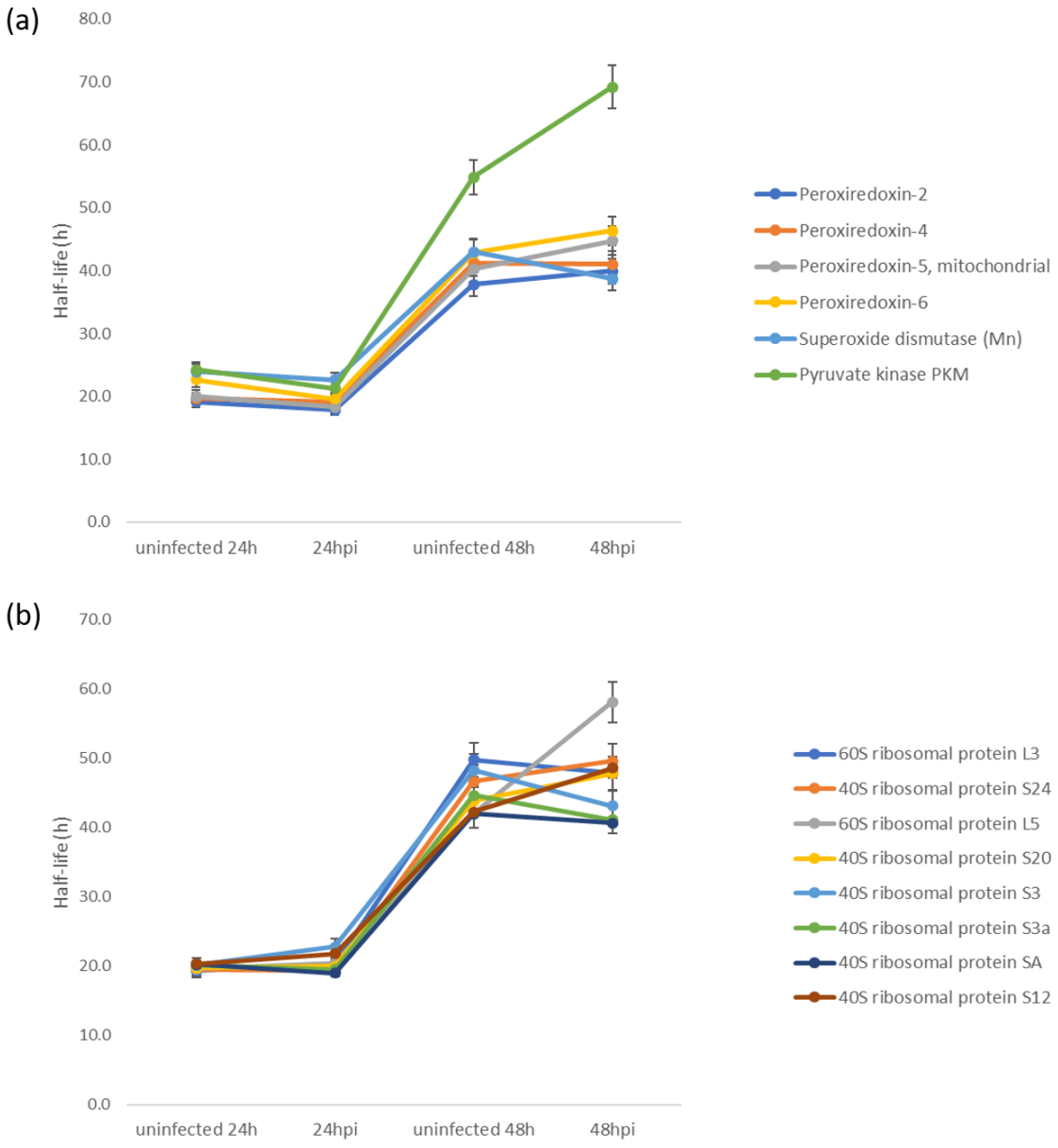

Figure 5.32: Measurement of protein half-lives for proteins involve in stress response and ribosomal pathway.

RIA, t values were used to derive the degradation rate constant for each protein. From the measurements, protein half-lives were determined for several (a) stress proteins, and (b) ribosomal proteins. Each point corresponds to the mean values ± SD of three biological replicates.

Evidently, our 48-h dataset contains more missing values compared to 24-h dataset. This could be due to the gradual loss of H isotopes, replaced by L isotopes, during the chase period. Therefore, to fully understand the modulation and turnover of proteins after 48 h infection, data imputation was applied. Missing

values in the L/H values were imputed by random selection from a normal distribution generated at 1.8 standard deviations, subtracted from the mean, of the total L/H ratios distribution and a width of 0.3 sd (as described in chapter 4). This places the imputed values at the lower limit of the intensity scale, which represents the detection limit of the instrumentation used. The resulting data matrix was exported for further discussion.

Table 5.3: Summary of calculated degradation rate constants and half-lives.

RIA, *t* values were used to derive the degradation rate constant for each protein. From the measurements, protein half-lives were determined.

	Uninfected 24h	***Infected 24h***	***Uninfected 48h***	***Infected 48h***
Mean kdeg (h^{-1})	0.03	0.03	0.01	0.01
Mean half-life (h)	21.74	20.51	47.39	47.33
Lowest kdeg (h^{-1})	0.01	0.02	0.01	0.01
Highest kdeg (h^{-1})	0.04	0.04	0.02	0.02
Lowest half-life (h)	16.63	16.8	34.34	34.23
Highest half-life (h)	84.44	30.36	75.22	85.18

5.4 Discussion

Perturbations such as infection often elicit major changes in gene and protein expression, reflecting the response of host to pathogen or the mechanisms exploited by the pathogen to establish infection. Proteins are continuously synthesized and degraded as cells maintain homoeostasis but challenges such as infection may prompt changes in both protein expression and degradation, leading to different turnover rates (Kristensen et al. 2013). It is difficult to study protein dynamics globally and to accurately measure half-lives. Degradation will, to some extent, effect newly synthesized proteins. Additionally, cell division can influence protein levels through dilution effects (Pratt et al. 2002). Dilution has been reported to affect degradation by 10% in human cancer cells (Eden et al. 2011; Doerr 2011). In non-dividing and slowly dividing cells such as mammalian cells, degradation is more dominant than dilution (Jovanovic et al. 2014). In addition, a study by Doherty et al.(2009) did not find a correlation between degradation rate with MW, pI, GO classification, the presence of stabilizing residues or the presence of PEST sequences.

In this work, we employed pulse-chase SILAC to investigate the changes in host cell proteome after 24 and 48 h of infection with *L. mexicana*. Temporal proteomics encompasses changes in protein dynamics following infection and could give an insight into the physiological response of the host. Over the time-course, the first 24 hours of infection showed transient changes in protein expression. However, the protein expression profiles after 48 h infection reflected a changing dynamic of the host-parasite interaction.

In total, we identified 2104 proteins in control24h (mock-infected), 24 hpi, control48h (mock-infected) and 48 hpi groups (biological replicates, n=3). Evidently, 48 h datasets contain higher number of missing values due to the gradual loss of heavy isotopes over the period. This leaves only 400 significantly modulating proteins (p-value < 0.05) because proteins with missing values were required to be omitted when applying statistical tests in Perseus. Among the proteins that we found to be constantly changing (in terms of degradation and turnover) in 24 hpi and 48 hpi THP-1 were pyruvate kinase (PKM), superoxide dismutase (SOD2), L-lactate dehydrogenase, alpha-enolase, purine nucleoside phosphorylase (PNP), peroxiredoxin-2, succinate dehydrogenase, tubulin beta chain, moesin and plastin-2. More importantly, these proteins also had increased synthesis rates in infected 48 h compared to 24 h infected cells.

Since turnover rate correlates with responsiveness to metabolic changes, proteins with the highest turnover rates might be expected to be regulatory proteins, which are usually low abundance and might be missed in the analysis (Claydon & Beynon 2012). High abundance proteins often have low rates of turnover and they perform more housekeeping roles in the cell (Claydon & Beynon 2012). Turnover can be assessed by monitoring the incorporation or loss of a label into or from the protein pool. Very rapid degradation would reflect high turnover proteins.

A study on ribosomal proteins degradation undertaken by Lam et al. (2007) concluded that ribosomal proteins are highly regulated in cells. They found that the free newly synthesized ribosomal proteins are rapidly degraded in nucleoplasmic compartment. However, when free ribosomal proteins assembled into ribosomal subunits and exported to the cytoplasm they acquire long half-lives (Lam et al. 2007). Of note, only a subset of newly synthesized ribosomal proteins are assembled into ribosomes and exported to the cytoplasm (Lam et al. 2007). It

is known that ribosomal proteins are synthesized in excess to ensure that efficient ribogenesis is never limited by the available supply of protein components (Lam et al. 2007). As apparent in KEGG pathway (Figure 5.8), ribosomal proteins were enriched in our data. In line with this notion, several reports demonstrated that ribosomal proteins were unstable or rapidly degraded (Helbig et al. 2011a; Kristensen et al. 2013; Martin-Perez & Villén 2015). Our degradation data indicated that one of the 60 S ribosomal protein, 60S acidic ribosomal protein, was degraded by 30% in 24 hpi (10% in control) but further degraded up to 60% in 48 hpi (15% in control). This suggested that the half-life of 60S subunit ribosomal proteins is increased in infected cells, which means that this protein was slowly turnover after 48 h infection. Though, Doherty et al. (2009) reported that the ribosome subunits do not turnover at a uniform rate. This is held true for several ribosomal proteins in our data that showed to be more stable in 48 h of infection, including 40S ribosomal protein S12, and 60S ribosomal protein L5. These two proteins, as well as 40S ribosomal protein S24 and 40S ribosomal protein S20 had longer turnover times in 48 hpi compared to uninfected and 24 hpi. Whereas, 40S ribosomal protein S3, 40S ribosomal protein S3a and 60S ribosomal protein L3 had shorter turnover times in 48 hpi compared to other groups. Further exploration of ribosomal subunit turnover is warranted to validate this.

Intriguingly, newly synthesized proteins involved in immune responses, including HLA complexes, were also shown to be very unstable and rapidly degraded. In 24 hpi, HLA complexes degraded up to 75% compared to 50% in control, while in 48 hpi, they were degraded by up to 90% (average half-life 37.88 h). HLA complex is a gene complex encoding the MHC proteins that are responsible for the regulation of the immune system in humans. It has been well-documented that parasitophorous vacuoles of macrophages infected with *L. amazonensis* and *L. mexicana* contain various lysosomal enzymes including proteases, particularly within 48 to 72 h after infection (Antoine et al. 1990; Antoine et al. 1999). In addition, parasitophorous membrane contains MHC class II molecules after stimulation with IFN-γ. Many pathogens residing in parasitophorous vacuole including *L. amazonensis* and *Salmonella* internalized MHC II molecules of their host cells and degrade them to evade immune recognition by inhibiting phagolysosome biogenesis (Antoine et al. 1999; Leao et al. 1995; Mitchell et al. 2004). These molecules were reported to be degraded by parasite cysteine

proteases which are critical for their survival within macrophages (Leao et al. 1995). Furthermore, phagolysosome biogenesis is driven by complex sets of membrane-trafficking events involving soluble N-ethylmaleimide-sensitive factor attachment receptor (SNARE). The *Leishmania* cell surface metalloprotease GP63 (also regulates cysteine peptidase CPB expressions) able to cleave a subset of SNAREs, thereby preventing phagolysosome biogenesis. This in turn inhibits presentation of exogenous *Leishmania* antigens on MHC class I molecules (Matheoud et al. 2013; Jaramillo et al. 2011; Casgrain et al. 2016).

We also observed that several glycolytic proteins were shown to be resistant to degradation with k_{deg} ranges from 0.01 to 0.04 h^{-1}. This observation coincides with reports by Helbig et al. (2011) and Martin-Perez & Villén (2015). Glycolytic enzymes such as Hxk1p and Fba1p and TCA cycle proteins were reported to be very stable proteins (Helbig et al. 2011a). They also reported that proteins with similar function tend to present similar half-lives. Proteins involved in mitochondrial related functions (TCA, oxidative phosphorylation) as well as other energy production pathways were more stable (Martin-Perez & Villén 2015). Having more stable proteins could be one of the many ways for the host cells to conserve energy expenditure and focus on counteracting the infection threat (Schwanhäusser et al. 2011). Trötschel et al. (2013) reported the analysis of protein turnover in bacteria and found that under ideal environmental condition, the bacteria do not require large quantities of protein degradation to sustain optimal growth. Also, long-lived proteins correlates with protein lifespan and damage (Toyama et al. 2013).

Protein with the shortest measured half-life in our data was interleukin-8 (16.63 h). Interleukin-8 is a chemokine produced by macrophage and other cells. It was found to be significantly elevated in *M. tuberculosis*-infected U937 cells and may be critically associated with distinct host responses in tuberculosis (Song et al. 2003). It is not surprising that proteins involve in immune response to have higher turnover.

Another confounding discovery was that most of the proteins studied in our work only slightly increased their half-lives during early infection (the first 24 h) but markedly increased their half-lives during longer exposure to the parasites (48 h infection). These observations suggest that the host can quickly recover their

proteins during early infection but took longer recovery time when the host is exposed to threats for a longer period. Intuitively, we would expect that the half-lives would increase in response to infection. Additionally, about 50% to 60% of the proteins had half-lives longer than the host growth rate (20.4 h).

Many of the proteins reported in our work have been implicated with *Leishmania* infection (as have been discussed in previous chapter). However, interestingly, no report on moesin that can be relate to *Leishmania* infection. This newly synthesized protein was shown to be stable with only 25% degradation rate in 24 hpi and 30% in 48 hpi, thereby being a low turnover protein.

5.5 Summary

It is difficult to understand the complete mechanistic details underpinning proteome dynamics, as it is influenced by many factors including localisation and external perturbation. Furthermore, different species and cell types exhibit different protein turnover rates, whereby smaller mammals have higher turnover than larger mammals (Nagy et al. 1999). Having said that, the determination of degradation rate is one of the essential parameters to understanding the regulation of protein turnover. By corollary, this would be another step toward unravelling the dynamic proteome and correlates with host-pathogen interaction.

Overall, the pulse-chase SILAC combined with MS approach is very useful to investigate protein turnover, as it allows measurement of endogenous proteins expressed at physiological levels in large-scale without the need to use translation inhibitors. This is more favourable because translation inhibitors have been reported to affect protein stability (Belle et al. 2006). Furthermore, we observed a strong positive correlation (Pearson correlation coefficient close to 1) between all data sets, suggesting that they are highly reproducible.

Temporal proteomics data revealed that the cells synthesized a large number of metabolic enzymes in 48 hpi compared to control. From the global perspective, the dominance of metabolic processes makes sense given the high-energy costs associated with protein synthesis. Our study also demonstrates that proteins with roles in infection tend to be rapidly degraded and have shorter half-lives, example

being ribosomal proteins (particularly 60S subunits), proteins involved in immune response and proteolytic proteins.

For this work, we deliberately restricted the degradation analysis to relatively few hundred proteins due to manual calculations of protein turnover and the time-consuming nature of this analysis. Furthermore, the data that we have gathered should be taken as guidelines rather than absolute measurements as turnover rates of individual proteins can change depending on factors including subcellular localisation, cell cycle stage, and PTM (Larance et al. 2013; Larance & Lamond 2015). Nevertheless, this study was able to yield extensive data that provide an insight into changes upon infection at two-time points (24 and 48 h), as well as on the stability of several important proteins. To our knowledge, this is the first report of proteome dynamics in THP-1 in response to *L. mexicana* infection.

Collectively, we found that the rates of protein degradation, although globally low, were increased in 48 h of infection compared to 24 h of infection. Moreover, long-lived protein became longer-lived in response to infection, while short-lived proteins only changed slightly.

CHAPTER 6

6 Concluding remarks

6.1 Comparative proteomic analysis in *L. mexicana* revealed striking differences between promastigote and amastigote stage

The differentiation from promastigote to amastigote form in *Leishmania* species is triggered by several environmental changes including elevation of temperature, decrease of pH in the phagolysosome, exposure to oxygen and nitrogen reactive species, exposure to proteolytic activity as well as nutrition starvation (Besteiro et al. 2007). Thus, it is not surprising that these two life-stages of *Leishmania* have different expressions of proteins and metabolic pathways.

Stable isotope Dimethyl Labelling (DiMe) coupled with MS approach has enabled us to investigate differentially expressed proteins in promastigote and axenic amastigote. We observed many identified putative proteins that were differentially regulated covered a diversity of functions, mainly metabolism, redox process, proteolysis and protein synthesis. Promastigotes rely on glycolysis, gluconeogenesis and oxidative phosphorylation for energy production. In contrast, amastigotes increased fatty acid oxidation as carbon source. Additionally, stress response proteins such as tryparedoxin peroxidase, heat shock proteins, and glutathione peroxidase were found upregulated in promastigotes. Upregulated amastigote proteins included ribosomal proteins, histones, and proteolytic enzymes. The findings reported here indicates that the parasite *Leishmania* undergo a variety of metabolic changes during the differentiation. Our results substantially advance our knowledge on stage-regulated proteome of *Leishmania* and could complement present data.

6.2 Pulse-chase SILAC potential to investigate host-parasite interaction

Most global gene expression investigations performed to date rely on measuring changes in steady-state mRNA levels. However, it is very clear that mRNA

expression does not always correlate with protein expression. Since proteins mediate most biochemical transformations, there is growing interest in studies of gene expression at the protein level. Despite existing data on host cell-*Leishmania* interactions, changes that take place in infected macrophages remain poorly understood. The determination of protein degradation rate is one of the essential parameters for understanding the regulation of protein turnover. By corollary, this would be another step toward unravelling the dynamic proteome and correlating it with host-pathogen interaction.

The pulse-chase SILAC approach presented in this work revealed the changes in proteome dynamics in macrophages upon infection with *Leishmania*. Of note, this is the first report utilising pulse-chase SILAC to investigate the proteome dynamic upon *Leishmania* infection. The primary system used here was the human THP-1 myelomonocytic leukaemia cell line that can be differentiated from monocytes into macrophage-like cells by stimulation with PMA. Our aim was to characterize the factors affecting regulation of protein expression change during infection by measuring the synthesis and degradation rates of proteins, as well as protein half-lives.

Temporal proteomics in two time points (24 and 48 h) revealed a distinct clustering of modulated proteins, based on Gene Ontology. 24 hpi proteins were enriched in cellular process such as cell communication while 48 hpi proteins enriched in metabolic process. During the first 24 h of infection, THP-1 cells appear to respond to invading *L. mexicana* by increasing the production of stress response proteins and apoptotic proteins (based on increasing RIA synthesis). Additionally, proteins involve in cell communication, cell growth, phagocytosis and cell cycle such as IL-8, a known chemotactic factor, TNF-α-induced protein, apoptosis regulator BAX, caspase 3 and STAT1 were also had increased synthesis. Our data also suggest that *L. mexicana* might modulate the host to induce M2 type of macrophage activation due to the increased synthesis of IL-10 and TNF-α. Furthermore, the parasite may have used the increasing apoptosis to their advantage. It is known that several pathogens modulate apoptotic machinery to replicate inside the macrophage and hide without triggering host's immune response (Bruchhaus et al. 2007; Getti et al. 2008).

Another key finding during the 24 hpi were protein synthesis of several glycolytic enzymes was lower than the uninfected cells. Instead, the synthesis of proteins involve in oxidative phosphorylation was increasing. TNF-α-IP8 has been shown to inhibit the production of nitric oxide which resulted in the increasing of oxidative phosphorylation (Moreira et al. 2015). Interesting, we found the opposite trends for these proteins in 48 hpi. Several glycolytic enzymes had higher synthesis rate compared to uninfected while oxidative phosphorylation proteins had decreased synthesis in 48 hpi. We hypothesized that this could be correlated with the time taken for promastigotes to differentiate to amastigotes. Further, our degradation data revealed that these glycolytic proteins and oxidative phosphorylation proteins were stable and have long half-lives. These findings were similar to the report by Helbig et al. (2011) and Martin-Perez & Villén (2015). Host cells might trying to conserve energy expenditure and focus on counteracting the infection threat by having more stable proteins (Schwanhäusser et al. 2011).

Among the proteins that we found to be significantly changing in 24 hpi and 48 hpi THP-1 were PKM, SOD2, LDHA, PNP, tubulin beta chain, moesin and 14-3-3 protein. PKM, SOD2, PNP, tubulin beta chain and moesin had lower synthesis in 24 hpi compared to uninfected but increased synthesis in 48 hpi. Except PKM and SOD2 which were rapidly degraded proteins, the rest of the proteins were relatively stable in uninfected and infected groups. On the other hand, LDHA had higher synthesis in 24 hpi but was slowly synthesized in 48 hpi, while 14-3-3 protein had increased translation in both 24 and 48 hpi. Unlike LDHA, 14-3-3 was rapidly degraded upon infection. Remarkably, 14-3-3 has been found to be inhibit the activity of pro-apoptotic member of Bcl-2 family in macrophage infected with *L. donovani* (Gupta et al. 2016).

Taking all of this together, pulse-chase SILAC coupled with high resolution mass spectrometry reveals as a promising approach to investigate global degradation profile and ultimately protein turnover. Comparative studies of proteome dynamics may contribute to elucidation of the host-pathogen relationship.

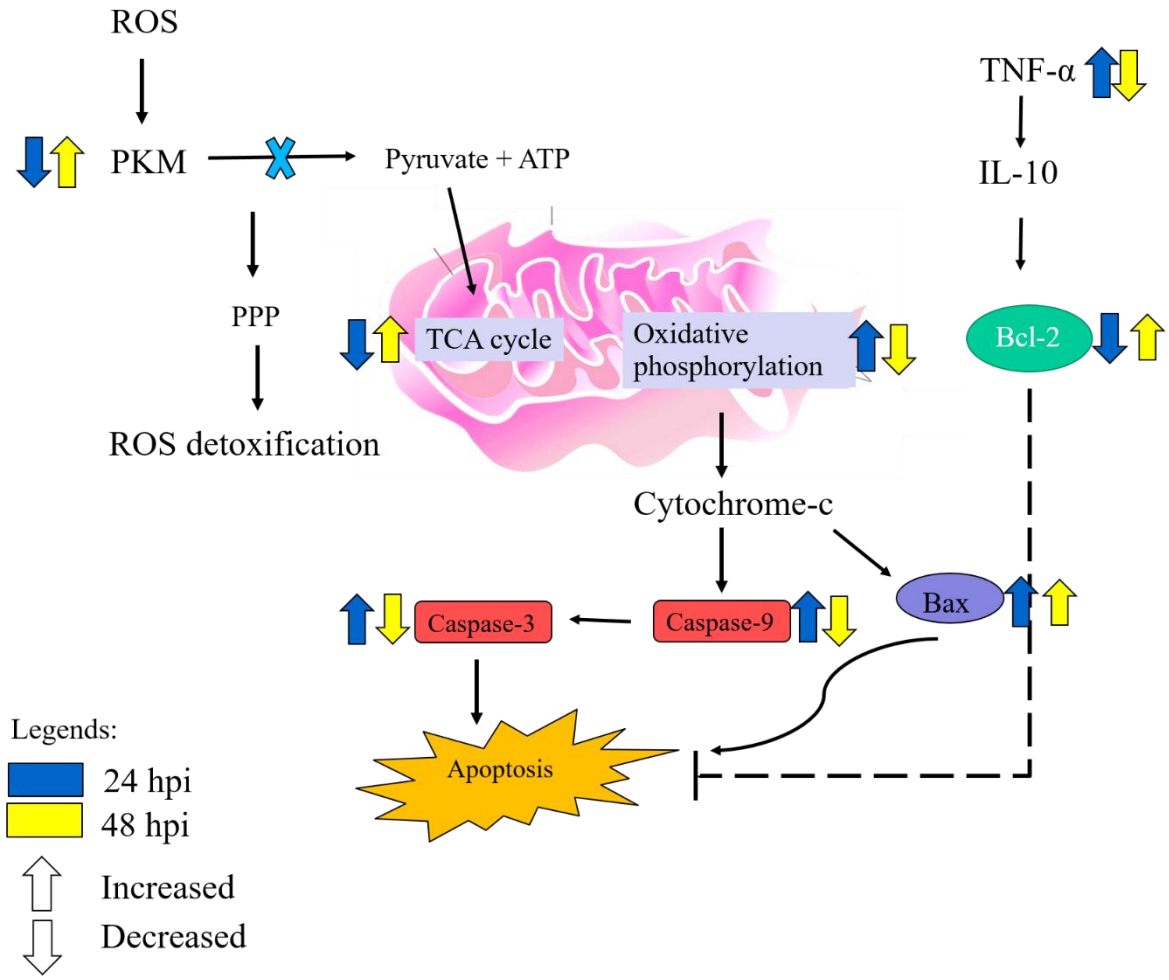

Figure 6.1: Illustration of several proteins expression in 24 and 48 hpi.

Following 24 h infection, PKM which catalyses the final step in glycolysis to produce pyruvate and ATP was decreased. The decreased of PKM prevents production of pyruvate but instead used the glucose flux for PPP, resulted in ROS detoxification. In 48 hpi, PKM was increased. Cytochrome c that was released by mitochondria activates caspase-9 which activates caspase-3 and induces apoptosis. Activation of TNF-α induced IL-10 which reduced expression of Bcl-2 (pro-apoptotic). Bax also induces apoptosis.

6.3 Drug targets

Many of *Leishmania* virulence factors have been reported (Diniz Atayde et al. 2016). Proteins such as GP63, cysteine peptidases and peroxiredoxins have the potential as molecular targets to develop new treatment approaches or as prognostic markers. Evidently, numerous macrophage proteins are known to be targeted by GP63, including PTP-1B, NF-κB, STAT1, and AP1. GP63 causes rapid cleavage and activation of three host phosphatases: SHP-1, PTP1B, and TCPTP, thereby attenuating the innate immune response against the parasite (Yao et al. 2003; Isnard et al. 2012; Olivier et al. 2012). Moreover, parasite could evade the

host complement-mediated lysis as well as parasite binding and phagocytosis by modulating host signalling pathways through GP63 (Isnard et al. 2012). GP63 degrades components of extra-cellular matrix (ECM) such as fibronectin to facilitate the migration of promastigotes (Mcgwire et al. 2003). Furthermore, proteins downregulated upon infection might be substrates for proteases released by *Leishmania*. Our observations detected rapid degradation of MHC molecules such as HLA (by up to 90% after 48 h infection). As it is well-established that *Leishmania* cysteine proteases degrade MHC molecules, these could be further evaluated as drug target (Leao et al. 1995).

Intracellular degradation is tightly regulated and plays major roles in many pathways including cell cycle, metabolism, antigen presentation and quality control. Many proteins are degraded through proteasome-mediated degradation pathway (Bedford et al. 2011). Hence, substrates for this pathway would be an ideal platform for drug targeting.

Many of the proteins discussed in this thesis have previously been implicated in a host response to intracellular pathogens. Such example was Bcl-2 that has been shown to accelerate *L. donovani* clearance when inhibited, therefore have anti-leishmanial potential (Pandey et al. 2016). However, some proteins, including 14-3-3 and moesin, have not been reported to be associated with *Leishmania* infection. Given that these proteins have a multitude of important functions in cells and they both have been significantly changing in 24 and 48 hpi data, these would be a novel target for further investigation.

6.4 Future suggestions

The pcSILAC approach generates data that might permit the inference of protein synthesis profiles and protein turnover profiles. Analysis could be extended to include measuring the rate of heavy isotope incorporation as well as the loss of heavy label at various time points prior to and after perturbation in order to get robust synthesis and degradation profiles. Having this together with the synthesis and degradation profiles generated in this study would enable calculation of the relative low and high turnover. This is because low turnover proteins might not incorporate the label whereas high turnover proteins might undergo extensive

replacement. Thus, having more time-points with shorter intervals could cover both low and high turnover proteins (Claydon & Beynon 2012).

For specific proteins that show interesting difference in modulation between uninfected and infected cells, live-cell fluorescence imaging could enable measurement of the dynamics of specific proteins, in real time, in living cells. For validation, genetic perturbation (knock down or knock out) of interesting proteins would offer more information on the physiology of macrophages infected with *Leishmania*.

Protein degradation is controlled by different factors such as subcellular localisation and PTMs (Fischer et al. 2012). For example, many nuclear proteins in rat tissues have low turnover and have longer life span (Toyama et al. 2013). Therefore, combining subcellular fractionation with protein turnover analysis would greatly increase the information gained compared with the analysis of total cell lysates. Ultimately, multidimensional analysis of the infected macrophage proteome, including studies of isoform expression, PTMs, and cell interactions (Figure 6.1) will substantially increase our understanding of the complex host-pathogen relationship.

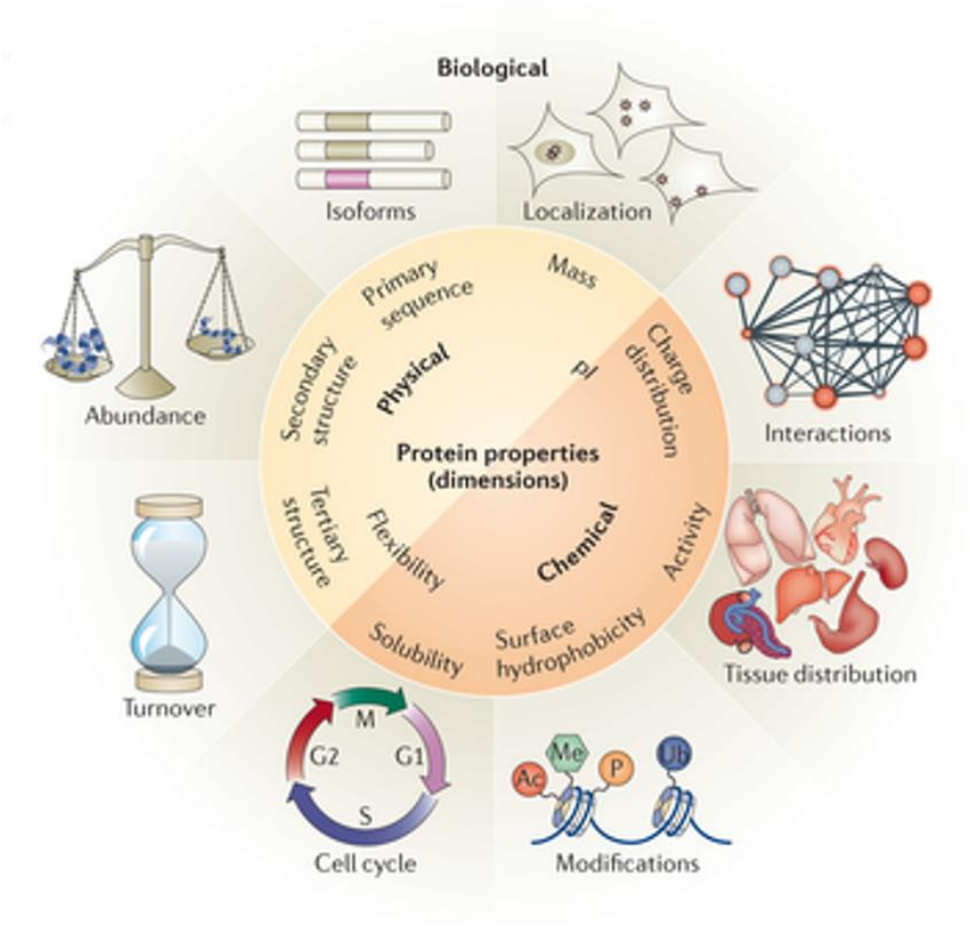

Figure 6.2: Multidimensional proteome analysis of cells.

Proteins can have many different properties (dimensions) that are either largely physically (yellow shaded area), chemically (orange shaded area) or biologically (beige shaded area) relevant. Shown in this figure are some of the properties that are most important for cell biology research and those that need to be taken into consideration when developing new separation methods for multidimensional analysis. Adapted from Larance & Lamond (2015).

Consequently, it would be ideal to link proteomics data with metabolomics data to obtain insight into the metabolic architecture of a cell or organism in response to infection at unprecedented depth and specificity.

7 References

Aitken, A. et al., 2002. Specificity of 14-3-3 isoform dimer interactions and phosphorylation. *Biochemical Society transactions*, 30(4), pp.351–360.

Akopyants, N.S. et al., 2009. Demonstration of genetic exchange during cyclical development of *Leishmania* in the sand fly vector. *Science*, 324(5924), pp.265–268.

Alcolea, P.J. et al., 2016. In vitro infectivity and differential gene expression of Leishmania infantum metacyclic promastigotes: negative selection with peanut agglutinin in culture versus isolation from the stomodeal valve of Phlebotomus perniciosus. *BMC genomics*, 17(1), p.375. Available at: http://bmcgenomics.biomedcentral.com/articles/10.1186/s12864-016-2672-8.

Alvar, J. et al., 2012. Leishmaniasis worldwide and global estimates of its incidence. *PLoS ONE*, 7(5).

Alves, L.C. et al., 2001. Identification of peptides inhibitory to recombinant cysteine proteinase, CPB, of *Leishmania mexicana*. *Molecular and biochemical parasitology*, 114(1), pp.81–8. Available at: http://www.ncbi.nlm.nih.gov/pubmed/11356516.

Anastasiou, D. et al., 2012. Inhibition of pyruvate kinase M2 by reactive oxygen species contributes to cellular antioxidant responses. *Science*, 334(6060), pp.1278–1283.

Andersen, J.S. et al., 2005. Nucleolar proteome dynamics. *Nature*, 433(January), pp.77–83.

Anderson, C.F. & Mosser, D.M., 2002. A novel phenotype for an activated macrophage: the type 2 activated macrophage. *Journal of leukocyte biology*, 72(July), pp.101–106.

Andersson, I. et al., 2004. Human MxA Protein Inhibits the Replication of Crimean-Congo Hemorrhagic Fever Virus Human MxA Protein Inhibits the Replication of Crimean-Congo Hemorrhagic Fever Virus. *Journal of virology*, 78(8), pp.4323–4329.

Antoine, J. et al., 1990. Parasitophorous Vacuoles of *Leishmania amazonensis*-Infected Macrophages Maintain an Acidic pH. *Infection and Immunity*, 58(3), pp.779–787.

Antoine, J.-C. et al., 2004. *Leishmania spp.*: on the interactions they establish with antigen-presenting cells of their mammalian hosts. *Advances in parasitology*, 58(4), pp.1–68. Available at: http://www.ncbi.nlm.nih.gov/pubmed/15603761 [Accessed July 2, 2013].

Antoine, J.C. et al., 1999. H-2M molecules, like MHC class II molecules, are targeted to parasitophorous vacuoles of *Leishmania*-infected macrophages and internalized by amastigotes of *L. amazonensis* and *L. mexicana*. *Journal of cell science*, 112 (Pt 1, pp.2559–2570.

Argueta-donohué, J., Wilkins-rodríguez, A. a & Aguirre-, M., 2015. Differential phagocytosis of *Leishmania* promastigotes and amastigotes by monocyte-derived dendritic cells Running title : L . mexicana phagocytosis by DC. *Microbiology and Immunology*, pp.1–34.

Aste-Amezaga, M. et al., 1998. Molecular Mechanisms of the Induction of IL-12 and Its Inhibition by IL-10. *Journal of Immunology*, 160(12), pp.5963–5944.

Auwerx, J., 1991. The human leukemia cell line, THP-1: A multifacetted model for the study of monocyte-macrophage differentiation. *Experientia*, 47, pp.22–31.

Awasthi, A. et al., 2004. Immune response to *Leishmania* infection. *Indian J Med Res*, (119), pp.238–258.

Bantscheff, M. et al., 2007. Quantitative mass spectrometry in proteomics: a critical review. *Analytical and bioanalytical chemistry*, 389(4), pp.1017–31. Available at: http://www.ncbi.nlm.nih.gov/pubmed/17668192 [Accessed May 30, 2014].

Bates, P.A., 1993. Axenic culture of *Leishmania* Amastigotes. *Parasitology Today*, 9(4), pp.143–146.

Bates, P.A., 1994. Complete developmental cycle of *Leishmania mexicana* in axenic culture. *Parasitology*, 108(June 1993), pp.1–9.

Bates, P.A. et al., 2015. Recent advances in phlebotomine sand fly research related to leishmaniasis control. *Parasites & vectors*, 8, p.131. Available at: http://www.pubmedcentral.nih.gov/articlerender.fcgi?artid=4352286&tool=pmcentrez&rendertype=abstract.

Bates, P.A., 2007. Transmission of *Leishmania* metacyclic promastigotes by phlebotomine sand flies. *International journal for parasitology*, 37(10), pp.1097–106. Available at: http://www.sciencedirect.com/science/article/pii/S0020751907001269 [Accessed October 20, 2015].

Bates, P.A. & Tetley, L., 1993. *Leishmania mexicana*: induction of metacyclogenesis by cultivation of promastigotes at acidic pH. *Experimental parasitology*, 76, pp.412–423.

Bates, P.A et al., 1992. Axenic cultivation and characterization of *Leishmania mexicana* amastigote-like forms. *Parasitology*, 105 (Pt 2(November 1992), pp.193–202.

Bedford, L. et al., 2011. Ubiquitin-like protein conjugation and the ubiquitin-proteasome system as drug targets. *Nature reviews. Drug discovery*, 10(1), pp.29–46. Available at: http://dx.doi.org/10.1038/nrd3321.

Belle, A. et al., 2006. Quantification of protein half-lives in the budding yeast proteome. *Proceedings of the National Academy of Sciences of the United States of America*, 103(35), pp.13004–9. Available at: http://www.pubmedcentral.nih.gov/articlerender.fcgi?artid=1550773&tool=pmcentrez&rendertype=abstract.

Benjamini, Y. & Hochberg, Y., 1995. Controlling the false discovery rate: a practical and powerful approach to multiple testing. *Journal of the Royal Statistical Society B*, 57(1), pp.289–300. Available at: http://www.stat.purdue.edu/~doerge/BIOINFORM.D/FALL06/Benjamini and Y FDR.pdf%5Cnhttp://engr.case.edu/ray_soumya/mlrg/controlling_fdr_benjamini95.pdf.

Bente, M. et al., 2003. Developmentally induced changes of the proteome in the protozoan parasite *Leishmania donovani*. *Proteomics*, 3(9), pp.1811–1829.

Besteiro, S. et al., 2007. Protein turnover and differentiation in *Leishmania*. *International journal for parasitology*, 37(10), pp.1063–75. Available at: http://www.pubmedcentral.nih.gov/articlerender.fcgi?artid=2244715&tool=pmcentrez&rendertype=abstract [Accessed March 6, 2013].

Beynon, R.J., 2005. The dynamics of the proteome: Strategies for measuring protein turnover on a proteome-wide scale. *Briefings in Functional Genomics and Proteomics*, 3(4), pp.382–390.

Bhattacharya, P. et al., 2010. Arabinosylated Lipoarabinomannan–Mediated Protection in Visceral Leishmaniasis through Up-Regulation of Toll-Like Receptor 2 Signaling: An Immunoprophylactic Approach. *The Journal of Infectious Diseases*, 202(1), pp.145–155. Available at: http://www.scopus.com/inward/record.url?eid=2-s2.0-77953710258&partnerID=tZOtx3y1.

Bhaumik, S. et al., 2009. KMP-11 DNA immunization significantly protects against *L. donovani* infection but requires exogenous IL-12 as an adjuvant for comparable protection against *L. major*. *Vaccine*, 27(9), pp.1306–1316.

Biyani, N. & Madhubala, R., 2012. Quantitative proteomic profiling of the promastigotes and the intracellular amastigotes of *Leishmania donovani* isolates identifies novel proteins having a role in *Leishmania* differentiation and intracellular survival. *BBA - Proteins and Proteomics*, 1824(12), pp.1342–1350. Available at: http://dx.doi.org/10.1016/j.bbapap.2012.07.010.

Blanchette, J. et al., 2009. Regulation of macrophage nitric oxide production by the protein tyrosine phosphatase Src homology 2 domain phosphotyrosine phosphatase 1 (SHP-1). *Immunology*, 127(1), pp.123–133.

Boersema, P.J. et al., 2009. Multiplex peptide stable isotope dimethyl labeling for quantitative proteomics. *Nature protocols*, 4(4), pp.484–94. Available at: http://www.ncbi.nlm.nih.gov/pubmed/19300442 [Accessed May 27, 2013].

Boitz, J.M. et al., 2017. Arginase Is Essential for Survival of *Leishmania donovani* Promastigotes but not intracellular amastigotes. *Infection and immunity*, 85(1), pp.1–14.

Bojkowska, K. et al., 2011. Measuring in vivo protein half-life. *Chemistry and Biology*, 18(6), pp.805–815. Available at: http://dx.doi.org/10.1016/j.chembiol.2011.03.014.

Bresciani, G., da Cruz, I.B.M. & Gonzalez-Gallego, J., 2015. Manganese superoxide dismutase and oxidative stress modulation., *Advances In Clinical Chemistry*, 68:87-130

Brooks, D.R. et al., 2000. Processing and trafficking of cysteine proteases in *Leishmania mexicana*. *Journal of cell science*, 113 (Pt 2, pp.4035–4041.

Brotherton, M.C. et al., 2010. Analysis of stage-specific expression of basic proteins in *Leishmania infantum*. *Journal of Proteome Research*, 9(8), pp.3842–3853.

Bruchhaus, I. et al., 2007. Protozoan parasites: programmed cell death as a mechanism of parasitism. *Trends in Parasitology*, 23(8), pp.376–383.

Bunner, A.E. & Williamson, J.R., 2009. Stable isotope pulse-chase monitored by quantitative mass spectrometry applied to *E. coli* 30S ribosome assembly kinetics. *Methods*, 49(2), pp.136–141. Available at: http://dx.doi.org/10.1016/j.ymeth.2009.06.002.

Burchmore, R.J. & Hart, D.T., 1995. Glucose transport in amastigotes and promastigotes of *Leishmania mexicana mexicana*. *Molecular and biochemical parasitology*, 74(1), pp.77–86. Available at: http://www.ncbi.nlm.nih.gov/pubmed/8719247.

Burchmore, R.J. & Landfear, S.M., 1998. Differential regulation of multiple glucose transporter genes in *Leishmania mexicana*. *The Journal of biological chemistry*, 273(44), pp.29118–29126.

Burchmore, R.J.S. & Barrett, M.P., 2001. Life in vacuoles – nutrient acquisition by *Leishmania* amastigotes. *International Journal for Parasitology*, 31, pp.1311–1320.

Butter, F. et al., 2013. Comparative proteomics of two life cycle stages of stable isotope-labeled *Trypanosoma brucei* reveals novel components of the parasite's host adaptation machinery. *Molecular & cellular proteomics : MCP*, 12(1), pp.172–9. Available at: http://www.pubmedcentral.nih.gov/articlerender.fcgi?artid=3536898&tool=

pmcentrez&rendertype=abstract [Accessed August 21, 2013].

Cameron, M.M. et al., 1995. Sugar meal sources for the phlebotomine sandfly *Lutzomyia longipalpis* in Ceará State, Brazil. *Medical and veterinary entomology*, 9, pp.263–272.

Cameron, P. et al., 2004. Inhibition of Lipopolysaccharide-Induced Macrophage IL-12 Production by *Leishmania mexicana* amastigotes: The Role of Cysteine Peptidases and the NF-kB signaling pathway. *Journal of immunology*, 173, pp.3297–3304.

Carson, C. et al., 2010. Comparison of Leishmania OligoC-TesT PCR with conventional and real-time PCR for diagnosis of canine *Leishmania* infection. *Journal of Clinical Microbiology*, 48(9), pp.3325–3330.

de Carvalho Vivarini, Á. et al., 2011. Human cutaneous leishmaniasis: interferon-dependent expression of double-stranded RNA-dependent protein kinase (PKR) via TLR2. *The FASEB Journal* , 25(12), pp.4162–4173. Available at: http://www.fasebj.org/content/25/12/4162.abstract.

Casgrain, P.-A. et al., 2016. Cysteine Peptidase B Regulates *Leishmania mexicana* Virulence through the Modulation of GP63 Expression. *PLOS Pathogens*, 12(5), p.e1005658. Available at: http://dx.plos.org/10.1371/journal.ppat.1005658.

Chahrour, O., Cobice, D. & Malone, J., 2015. Stable isotope labelling methods in mass spectrometry-based quantitative proteomics. *Journal of Pharmaceutical and Biomedical Analysis*, 113, pp.2–20. Available at: http://dx.doi.org/10.1016/j.jpba.2015.04.013.

Chakraborty, A. & Regnier, F.E., 2002. Global internal standard technology for comparative proteomics. *Journal of Chromatography A*, 949(1–2), pp.173–184.

Chakravarty, J. et al., 2011. A clinical trial to evaluate the safety and immunogenicity of the LEISH-F1+MPL-SE vaccine for use in the prevention of visceral leishmaniasis. *Vaccine*, 29(19), pp.3531–3537. Available at: http://dx.doi.org/10.1016/j.vaccine.2011.02.096.

Chanput, W., Mes, J.J. & Wichers, H.J., 2014. THP-1 cell line: An in vitro cell model for immune modulation approach. *International Immunopharmacology*, 23(1), pp.37–45. Available at: http://dx.doi.org/10.1016/j.intimp.2014.08.002.

Chawla, A., 2010. Control of macrophage activation and function by PPARs. *Circulation research*, 106(10), pp.1559–69. Available at: http://www.pubmedcentral.nih.gov/articlerender.fcgi?artid=2897247&tool=pmcentrez&rendertype=abstract [Accessed May 23, 2013].

Chenau, J. et al., 2008. Peptides OFFGEL electrophoresis : a suitable pre-

analytical step for complex eukaryotic samples fractionation compatible with quantitative iTRAQ labeling. *Proteome science*, 8(6), pp.1–8.

Chou, C.J., Affolter, M. & Kussmann, M., 2012. A nutrigenomics view of protein intake: Macronutrient, bioactive peptides, and protein turnover. 1st ed., Elsevier Inc. Available at: http://dx.doi.org/10.1016/B978-0-12-398397-8.00003-4.

Christiano, R. et al., 2014. Global Proteome Turnover Analyses of the Yeasts *S.cerevisiae* and *S.pombe*. *Cell Reports*, 9(5), pp.1959–1966.

Claydon, A.J. & Beynon, R., 2012. Proteome Dynamics: Revisiting Turnover with a Global Perspective. *Molecular & Cellular Proteomics*, 11(12), pp.1551–1565. Available at: http://www.ncbi.nlm.nih.gov/pubmed/23125033%5Cnhttp://www.mcponline.org/cgi/doi/10.1074/mcp.O112.022186.

Coleman, M. et al., 2015. DDT-based indoor residual spraying suboptimal for visceral leishmaniasis elimination in India. *Proceedings of the National Academy of Sciences of the United States of America*, 112(28), pp.8573–8. Available at: http://www.pubmedcentral.nih.gov/articlerender.fcgi?artid=4507214&tool=pmcentrez&rendertype=abstract.

Contreras, I. et al., 2010. *Leishmania*-induced inactivation of the macrophage transcription Factor AP-1 Is Mediated by the Parasite Metalloprotease GP63. *PLoS Pathogens*, 6(10).

Cory, S. & Adams, J.M., 2002. The Bcl2 family: regulators of the cellular life-or-death switch. *Nature Reviews Cancer*, 2(9), pp.647–656. Available at: http://www.nature.com.gate1.inist.fr/nrc/journal/v2/n9/full/nrc883.html%5Cnhttp://www.nature.com.gate1.inist.fr/nrc/journal/v2/n9/pdf/nrc883.pdf.

Cox, J. et al., 2009. A practical guide to the MaxQuant computational platform for SILAC-based quantitative proteomics. *Nature protocols*, 4(5), pp.698–705. Available at: http://www.ncbi.nlm.nih.gov/pubmed/19373234 [Accessed May 25, 2014].

Cox, J. et al., 2014. Accurate Proteome-wide Label-free Quantification by Delayed Normalization and Maximal Peptide Ratio Extraction, Termed MaxLFQ. *Molecular & Cellular Proteomics*, 13(9), pp.2513–2526. Available at: http://www.mcponline.org/cgi/doi/10.1074/mcp.M113.031591.

Cox, J. et al., 2011. Andromeda: A peptide search engine integrated into the MaxQuant environment. *Journal of Proteome Research*, 10(4), pp.1794–1805.

Cox, J. & Mann, M., 2008. MaxQuant enables high peptide identification rates, individualized p.p.b.-range mass accuracies and proteome-wide protein quantification. *Nature biotechnology*, 26(12), pp.1367–72. Available at:

http://www.ncbi.nlm.nih.gov/pubmed/19029910 [Accessed January 21, 2014].

Cox, J. & Mann, M., 2011. Quantitative, high-resolution proteomics for data-driven systems biology. *Annual review of biochemistry*, 80, pp.273–299.

Cuvillier, A. et al., 2003. Abortive infection of *Lutzomyia longipalpis* insect vectors by aflagellated LdARL-3A-Q70L overexpressing *Leishmania* amazonensis parasites. *Cellular Microbiology*, 5(10), pp.717–728.

Cuvillier, a et al., 2000. LdARL-3A, a Leishmania promastigote-specific ADP-ribosylation factor-like protein, is essential for flagellum integrity. *Journal of cell science*, 113 (Pt 1(July), pp.2065–2074.

Daigneault, M. et al., 2010. The identification of markers of macrophage differentiation in PMA-stimulated THP-1 cells and monocyte-derived macrophages. *PloS one*, 5(1), p.e8668. Available at: http://www.pubmedcentral.nih.gov/articlerender.fcgi?artid=2800192&tool=pmcentrez&rendertype=abstract [Accessed March 24, 2014].

DaMata, J.P. et al., 2015. Distinct macrophage fates after in vitro infection with different species of *Leishmania*: Induction of apoptosis by *Leishmania (Leishmania) amazonensis*, but not by *Leishmania (Viannia) guyanensis*. *PLoS ONE*, 10(10).

Daneshvar, H. et al., 2012. Comparative proteomics profiling of a gentamicin-attenuated *Leishmania infantum* cell line identifies key changes in parasite thiol-redox metabolism. *Journal of proteomics*, 75(5), pp.1463–71. Available at: http://www.ncbi.nlm.nih.gov/pubmed/22154982 [Accessed April 15, 2013].

Debarba, J.A. et al., 2015. Identification of Newly Synthesized Proteins by *Echinococcus* granulosus Protoscoleces upon Induction of Strobilation. *PLoS Neglected Tropical Diseases*, 9(9), pp.1–18.

Debrabant, A. et al., 2004. Generation of Leishmania donovani axenic amastigotes: their growth and biological characteristics. *International journal for parasitology*, 34(2), pp.205–17. Available at: http://www.ncbi.nlm.nih.gov/pubmed/15037106 [Accessed September 3, 2013].

Defacque, H. et al., 2000. Involvement of ezrin/moesin in de novo actin assembly on phagosomal membranes. *The EMBO journal*, 19(2), pp.199–212. Available at: http://www.pubmedcentral.nih.gov/articlerender.fcgi?artid=305554&tool=pmcentrez&rendertype=abstract.

Delahunty, C. & Yates, J.R., 2005. Protein identification using 2D-LC-MS/MS. *Methods*, 35(3 SPEC.ISS.), pp.248–255.

Denise, H. et al., 2006. Studies on the CPA cysteine peptidase in the *Leishmania infantum* genome strain JPCM5. *BMC molecular biology*, 7, p.42. Available at: http://www.pubmedcentral.nih.gov/articlerender.fcgi?artid=1657026&tool=pmcentrez&rendertype=abstract [Accessed April 22, 2013].

Dinarello, C.A., 2009. Immunological and inflammatory functions of the interleukin-1 family. *Annual Review of Immunology*, 27, pp.519–50. Available at: http://www.ncbi.nlm.nih.gov/pubmed/19302047.

Dinarello, C.A., 2011. Interleukin-1 in the pathogenesis and treatment of inflammatory diseases. *Blood*, 117(14), pp.3720–3732.

Dinasarapu, A.R. et al., 2013. A combined omics study on activated macrophages - Enhanced role of STATs in apoptosis, immunity and lipid metabolism. *Bioinformatics*, 29(21), pp.2735–2743.

Diniz Atayde, V. et al., 2016. *Leishmania* exosomes and other virulence factors: Impact on innate immune response and macrophage functions. *Cellular Immunology*. Available at: http://dx.doi.org/10.1016/j.cellimm.2016.07.013.

Diro, E. et al., 2014. High Parasitological Failure Rate of Visceral Leishmaniasis to Sodium Stibogluconate among HIV Co-infected Adults in Ethiopia. *PLoS Neglected Tropical Diseases*, 8(5), pp.14–17.

Dixit, N. & Simon, S.I., 2012. Chemokines, selectins and intracellular calcium flux: Temporal and spatial cues for leukocyte arrest. *Frontiers in Immunology*, 3(JUL), pp.1–9.

Doerr, A., 2011. A day in the half-life of a protein. *Nature methods*, 8(3), p.201. Available at: http://dx.doi.org/10.1038/nmeth0311-201.

Doherty, M.K. et al., 2005. Proteome dynamics in complex organisms: Using stable isotopes to monitor individual protein turnover rates. *Proteomics*, 5(2), pp.522–533.

Doherty, M.K. et al., 2009. Turnover of the human proteome: Determination of protein intracellular stability by dynamic SILAC. *Journal of Proteome Research*, 8(1), pp.104–112.

Donders, A.R.T. et al., 2006. Review: A gentle introduction to imputation of missing values. *Journal of Clinical Epidemiology*, 59(10), pp.1087–1091.

Dostálová, A. et al., 2011. The midgut transcriptome of Phlebotomus (Larroussius) perniciosus, a vector of *Leishmania infantum*: comparison of sugar fed and blood fed sand flies. *BMC genomics*, 12(1), p.223. Available at: http://www.biomedcentral.com/1471-2164/12/223.

Doulias, P. et al., 2014. Nitric oxide regulates mitochondrial Fatty Acid

metabolism through reversible. *Science Signal*, 6(256), p.23281369.

Doyle, A.G. et al., 1994. Interleukin-13 alters the activation state of murine macrophages in vitro: comparison with interleukin-4 and interferon-gamma. *European Journal of Immunology*, 24(6), pp.1441–1445.

Eden, E. et al., 2011. Proteome Half-Life Dynamics in Living Human Cells. *Science*, 331(6018), pp.764–768. Available at: http://www.ncbi.nlm.nih.gov/pubmed/21233346.

Ehrchen, J.M. et al., 2010. Keratinocytes determine Th1 immunity during early experimental leishmaniasis. *PLoS pathogens*, 6(4), p.e1000871. Available at: http://www.pubmedcentral.nih.gov/articlerender.fcgi?artid=2861693&tool=pmcentrez&rendertype=abstract.

Eichelbaum, K. & Krijgsveld, J., 2014. Rapid temporal dynamics of transcription, protein synthesis, and secretion during macrophage activation. *Molecular & cellular proteomics : MCP*, 13(3), pp.792–810. Available at: http://www.ncbi.nlm.nih.gov/pubmed/24396086.

Eriksson, S. et al., 2003. Unravelling the biology of macrophage infection by gene expression profiling of intracellular *Salmonella enterica*. *Molecular Microbiology*, 47(1), pp.103–118.

ESCALONA-MONTAÑO, A.R. et al., 2016. *Leishmania mexicana*: promastigotes and amastigotes secrete protein phosphatases and this correlates with the production of inflammatory cytokines in macrophages. *Parasitology*, pp.1–12. Available at: http://www.journals.cambridge.org/abstract_S0031182016000949.

El Fakhry, Y., Ouellette, M. & Papadopoulou, B., 2002. A proteomic approach to identify developmentally regulated proteins in *Leishmania infantum*. *Proteomics*, 2(8), pp.1007–17. Available at: http://www.ncbi.nlm.nih.gov/pubmed/12203896.

Fettucciari, K. et al., 2015. Macrophage induced gelsolin in response to Group B *Streptococcus* (GBS) infection. *Cellular Microbiology*, 17(1), pp.79–104.

Fierro-Monti, I. et al., 2013. A Novel Pulse-Chase SILAC Strategy Measures Changes in Protein Decay and Synthesis Rates Induced by Perturbation of Proteostasis with an Hsp90 Inhibitor. *PloS one*, 8(11), p.e80423. Available at: http://www.pubmedcentral.nih.gov/articlerender.fcgi?artid=3842330&tool=pmcentrez&rendertype=abstract [Accessed January 9, 2014].

Fischer, F., Hamann, A. & Osiewacz, H.D., 2012. Mitochondrial quality control : an integrated network of pathways. *Trends in Biochemical Sciences*, 37(7), pp.284–292. Available at: http://dx.doi.org/10.1016/j.tibs.2012.02.004.

Fischer, S.F. & Häcker, G., 2003. Characterization of Antiapoptotic Activities of

Chlamydia pneumoniae in Infected Cells. *Annals of the New York Academy of Sciences*, 1010(11), pp.565–567.

Flandin, J.F., Chano, F. & Descoteaux, A., 2006. RNA interference reveals a role for TLR2 and TLR3 in the recognition of *Leishmania donovani* promastigotes by interferon-γ-primed macrophages. *European Journal of Immunology*, 36(2), pp.411–420.

Forestier, C.-L., Gao, Q. & Boons, G.-J., 2014. *Leishmania* lipophosphoglycan: how to establish structure-activity relationships for this highly complex and multifunctional glycoconjugate? *Frontiers in cellular and infection microbiology*, 4(January), p.193. Available at: http://www.pubmedcentral.nih.gov/articlerender.fcgi?artid=4301024&tool=pmcentrez&rendertype=abstract.

Freitas, E.O. et al., 2015. Immucillins impair *Leishmania (L.) infantum chagasi* and *Leishmania (L.) amazonensis* multiplication In Vitro. *PLoS ONE*, 10(4), pp.1–18.

Fu, H., Subramanian, R.R. & Masters, S.C., 2000. 14-3-3 Proteins : Structure , Function , and Regulation. *Annual Review Pharmacology Toxicology*, 40, pp.617–647.

Fujii, S.I. et al., 2001. Interleukin-10 promotes the maintenance of antitumor CD8 + T-cell effector function in situ. *Blood*, 98(7), pp.2143–2151.

Gebre-Hiwot, A. et al., 1992. An in vitro model for screening antileishmanial drugs: the human leukaemia monocyte cell line, THP-1. *Acta Tropica*, 51(3–4), pp.237–245.

Geiger, T. et al., 2012. Comparative proteomic analysis of eleven common cell lines reveals ubiquitous but varying expression of most proteins. *Molecular & cellular proteomics : MCP*, 11(3), p.M111.014050. Available at: http://www.pubmedcentral.nih.gov/articlerender.fcgi?artid=3316730&tool=pmcentrez&rendertype=abstract [Accessed August 8, 2013].

Geiger, T. et al., 2011. Use of stable isotope labeling by amino acids in cell culture as a spike-in standard in quantitative proteomics. *Nature protocols*, 6(2), pp.147–57. Available at: http://www.ncbi.nlm.nih.gov/pubmed/21293456 [Accessed May 26, 2014].

Gerber, J.S. & Mosser, D.M., 2001. Reversing Lipopolysaccharide Toxicity by Ligating the Macrophage Fcγ Receptors. *The Journal of Immunology*, 166(11), p.6861 LP-6868. Available at: http://www.jimmunol.org/content/166/11/6861.abstract.

Getti, G.T., Cheke, R. a & Humber, D.P., 2008. Induction of apoptosis in host cells: a survival mechanism for *Leishmania* parasites? *Parasitology*, 135(12), pp.1391–9. Available at: http://www.ncbi.nlm.nih.gov/pubmed/18775094.

Gillespie, P. et al., 2016. Status of vaccine research and development of vaccines for leishmaniasis. *Vaccine*, 34(26), pp.2992–2995. Available at: http://dx.doi.org/10.1016/j.vaccine.2015.12.071.

Giudice, A. et al., 2012. Macrophages participate in host protection and the disease pathology associated with *Leishmania braziliensis* infection. *BMC infectious diseases*, 12(1), p.75. Available at: http://www.pubmedcentral.nih.gov/articlerender.fcgi?artid=3373377&tool=pmcentrez&rendertype=abstract [Accessed April 16, 2013].

Gluenz, E., Ginger, M.L. & McKean, P.G., 2010. Flagellum assembly and function during the *Leishmania* life cycle. *Current Opinion in Microbiology*, 13(4), pp.473–479. Available at: http://dx.doi.org/10.1016/j.mib.2010.05.008.

Gobert, A.P. et al., 2001. *Helicobacter pylori* arginase inhibits nitric oxide production by eukaryotic cells: a strategy for bacterial survival. *Proceedings of the National Academy of Sciences of the United States of America*, 98(24), pp.13844–9. Available at: http://www.ncbi.nlm.nih.gov/pubmed/11717441%5Cnhttp://www.pubmedcentral.nih.gov/articlerender.fcgi?artid=PMC61129.

Gordon, S., 2007. The macrophage: past, present and future. *European journal of immunology*, 37 Suppl 1, pp.S9-17. Available at: http://www.ncbi.nlm.nih.gov/pubmed/17972350 [Accessed July 30, 2013].

Gossage, S.M., Rogers, M.E. & Bates, P.A., 2010. Two separate growth phases during the development of *Leishmania* in sand flies : implications for understanding the life cycle. , 33(10), pp.1027–1034.

Gronborg, M., 2005. Biomarker Discovery from Pancreatic Cancer Secretome Using a Differential Proteomic Approach. *Molecular & Cellular Proteomics*, 5(1), pp.157–171. Available at: http://www.mcponline.org/cgi/doi/10.1074/mcp.M500178-MCP200.

Guerfali, F.Z. et al., 2008. Simultaneous gene expression profiling in human macrophages infected with Leishmania major parasites using SAGE. *BMC genomics*, 9(i), p.238.

Guerin, P.J. et al., 2002. Visceral leishmaniasis: current status of control, diagnosis, and treatment, and a proposed research and development agenda. *The Lancet. Infectious diseases*, 2(8), pp.494–501. Available at: http://www.ncbi.nlm.nih.gov/pubmed/12150849.

Gupta, G., Oghumu, S. & Satoskar, A.R., 2014. Mechanisms of Immune Evasion in Leishmaniasis. *Advances in applied microbiology*, 82, pp.1–23.

Gupta, G., Oghumu, S. & Satoskar, A.R., 2013. *Mechanisms of immune evasion in leishmaniasis.*, Elsevier. Available at: http://www.ncbi.nlm.nih.gov/pubmed/23415155 [Accessed July 2, 2013].

Gupta, N., Goyal, N. & Rastogi, a K., 2001. In vitro cultivation and characterization of axenic amastigotes of *Leishmania*. *Trends in parasitology*, 17(3), pp.150–3. Available at: http://www.ncbi.nlm.nih.gov/pubmed/11286801.

Gupta, P. et al., 2016. *Leishmania donovani* inhibits macrophage apoptosis and pro-inflammatory response through AKT-mediated regulation of ß-catenin and FOXO-1. *Cell Death and Differentiation*, 23(11), pp.1815–1826. Available at: http://www.nature.com/doifinder/10.1038/cdd.2016.101.

Guthrie, L.A. et al., 1984. Priming of neutrophils for enhanced release of oxygen metabolites by bacterial lipopolysaccharide. Evidence for increased activity of the superoxide-producing enzyme. *The Journal of experimental medicine*, 160(6), pp.1656–71. Available at: http://www.pubmedcentral.nih.gov/articlerender.fcgi?artid=2187529&tool=pmcentrez&rendertype=abstract.

Hailu, A. et al., 2005. Visceral leishmaniasis: new health tools are needed. *PLoS medicine*, 2(7), pp.0590–0594. Available at: http://www.pubmedcentral.nih.gov/articlerender.fcgi?artid=1181879&tool=pmcentrez&rendertype=abstract [Accessed March 26, 2013].

Helbig, A.O. et al., 2011. The diversity of protein turnover and abundance under nitrogen-limited steady-state conditions in *Saccharomyces cerevisiae*. *Molecular bioSystems*, (March), pp.3316–3326. Available at: http://www.ncbi.nlm.nih.gov/pubmed/21984188.

Hervey IV, W.J., Strader, M.B. & Hurst, G.B., 2007. Comparison of digestion protocols for microgram quantities of enriched protein samples. *Journal of Proteome Research*, 6(8), pp.3054–3061.

Hesse, M. et al., 2001. Differential Regulation of Nitric Oxide Synthase-2 and Arginase-1 by Type 1/Type 2 Cytokines In Vivo: Granulomatous Pathology Is Shaped by the Pattern of L-Arginine Metabolism. *The Journal of Immunology*, 167(11), pp.6533–6544. Available at: http://www.jimmunol.org/content/167/11/6533.full.

Hinkson, I. V. & Elias, J.E., 2011. The dynamic state of protein turnover: It's about time. *Trends in Cell Biology*, 21(5), pp.293–303. Available at: http://dx.doi.org/10.1016/j.tcb.2011.02.002.

Hirata, T. et al., 2012. Moesin-deficient mice reveal a non-redundant role for moesin in lymphocyte homeostasis. *International Immunology*, 24(11), pp.705–717.

Hockenbery, D. et al., 1990. Bcl-2 is an inner mitochondrial membrane protein that blocks programmed cell death. *Nature*, 348, pp.334–336.

Hoedt, E. et al., 2014. SILAC-based proteomic profiling of the human MDA-MB-231 metastatic breast cancer cell line in response to the two antitumoral

lactoferrin isoforms: The secreted lactoferrin and the intracellular delta-lactoferrin. *PLoS ONE*, 9(8).

Holzer, T.R., McMaster, W.R. & Forney, J.D., 2006. Expression profiling by whole-genome interspecies microarray hybridization reveals differential gene expression in procyclic promastigotes, lesion-derived amastigotes, and axenic amastigotes in *Leishmania mexicana*. *Molecular and Biochemical Parasitology*, 146(2), pp.198–218.

Horvatić, A. et al., 2016. High-throughput proteomics and fight against pathogens. *Mol. BioSyst.*, 12, pp.2373–2384. Available at: http://pubs.rsc.org/en/Content/ArticleLanding/2016/MB/C6MB00223D.

Hotez, P.J., 2014. Leishmaniasis: the neglected disease of war, conflict, and human misery. *Huffington post*. Available at: http://www.huffingtonpost.com/peter-hotez-md-phd/leishmaniasis-the-neglect_b_4847618.html.

Hsu, J.-L. et al., 2003. Stable-isotope dimethyl labeling for quantitative proteomics. *Analytical Chemistry*, 75(24), pp.6843–6852. Available at: http://www.ncbi.nlm.nih.gov/pubmed/14670044.

Hsu, J.-L., Chen, S.-H. & Chen, S.-H., 2016. Stable isotope dimethyl labelling for quantitative proteomics and beyond. *Philosophical Transactions of the Royal Society of London A: Mathematical, Physical and Engineering Sciences*, 374(2079).

Huang, D.W., Lempicki, R. a & Sherman, B.T., 2009. Systematic and integrative analysis of large gene lists using DAVID bioinformatics resources. *Nature Protocols*, 4(1), pp.44–57.

Huynh, C., Sacks, D.L. & Andrews, N.W., 2006. A *Leishmania amazonensis* ZIP family iron transporter is essential for parasite replication within macrophage phagolysosomes. *The Journal of experimental medicine*, 203(10), pp.2363–75. Available at: http://www.pubmedcentral.nih.gov/articlerender.fcgi?artid=2118100&tool=pmcentrez&rendertype=abstract.

Ibarrola, N. et al., 2003. A proteomic approach for quantitation of phosphorylation using stable isotope labeling in cell culture. *Analytical chemistry*, 75(22), pp.6043–9. Available at: http://www.ncbi.nlm.nih.gov/pubmed/14615979.

Inbar, E. et al., 2013. The Mating Competence of Geographically Diverse *Leishmania major* Strains in Their Natural and Unnatural Sand Fly Vectors. *PLoS genetics*, 9(7), p.e1003672. Available at: http://www.pubmedcentral.nih.gov/articlerender.fcgi?artid=3723561&tool=pmcentrez&rendertype=abstract [Accessed August 19, 2013].

Iontcheva, I. et al., 2004. Role for Moesin in Lipopolysaccharide-Stimulated Signal Transduction. *Infection and Immunity*, 72(4), pp.2312–2320.

Isnard, A. et al., 2015. Impact of *Leishmania* Infection on Host Macrophage Nuclear Physiology and Nucleopore Complex Integrity. *PLoS Pathogens*, 11(3), pp.1–26.

Isnard, A., Shio, M.T. & Olivier, M., 2012. Impact of *Leishmania* metalloprotease GP63 on macrophage signaling. *Frontiers in cellular and infection microbiology*, 2, p.72. Available at: http://www.pubmedcentral.nih.gov/articlerender.fcgi?artid=3417651&tool=pmcentrez&rendertype=abstract [Accessed March 4, 2013].

Jain, S.K. et al., 2012. A parasite rescue and transformation assay for antileishmanial screening against intracellular Leishmania donovani amastigotes in THP1 human acute monocytic leukemia cell line. *Journal of visualized experiments : JoVE*, (70), pp.1–14. Available at: http://www.pubmedcentral.nih.gov/articlerender.fcgi?artid=3577863&tool=pmcentrez&rendertype=abstract [Accessed March 28, 2014].

Jang, S.W. et al., 2009. Interaction of Akt-phosphorylated SRPK2 with 14-3-3 mediates cell cycle and cell death in neurons. *Journal of Biological Chemistry*, 284(36), pp.24512–24525.

Jaramillo, M. et al., 2011. Leishmania repression of host translation through mTOR cleavage is required for parasite survival and infection. *Cell Host and Microbe*, 9(4), pp.331–341.

Jayakumar, A. et al., 2008. Leishmania major infection activates NF-κB and interferon regulatory factors 1 and 8 in human dendritic cells. *Infection and Immunity*, 76(5), pp.2138–2148.

Jensen, R.E. & Englund, P.T., 2012. Network news: the replication of kinetoplast DNA. *Annual Review of Microbiology*, 66, pp.473–491. Available at: http://www.ncbi.nlm.nih.gov/pubmed/22994497%5Cnhttp://www.annualreviews.org/doi/pdf/10.1146/annurev-micro-092611-150057.

Ji, H. et al., 2016. Progress in the biological function of alpha-enolase. *Animal Nutrition*, 2(1), pp.12–17. Available at: http://www.sciencedirect.com/science/article/pii/S2405654515300755.

Joshi, P.B. et al., 1998. Targeted gene deletion of *Leishmania major* genes encoding developmental stage-specific leishmanolysin (GP63). *Molecular Microbiology*, 27(3), pp.519–530.

Jovanovic, M. et al., 2014. Dynamic profiling of the protein life cycle in response to pathogens. *Science*, 347(6222), pp.664–667. Available at: http://www.sciencemag.org/content/347/6222/664.full.

Kang, J.H. et al., 2006. Proteome analysis of human monocytic THP-1 cells primed with oxidized low-density lipoproteins. *Proteomics*, 6(4), pp.1261–73. Available at: http://www.ncbi.nlm.nih.gov/pubmed/16402358 [Accessed June 10, 2014].

Karpievitch, Y. V, Dabney, A.R. & Smith, R.D., 2012. Normalization and missing value imputation for label-free LC-MS analysis. *BMC bioinformatics*, 13 Suppl 1(Suppl 16), p.S5. Available at: http://www.pubmedcentral.nih.gov/articlerender.fcgi?artid=3489534&tool=pmcentrez&rendertype=abstract.

Karsan, A., Yee, E. & Harlan, J.M., 1996. Endothelial cell death induced by tumor necrosis factor-alpha is inhibited by the Bcl-2 family member, A1. *Journal of Biological Chemistry*, 271(44), pp.27201–27204.

Kavoosi, G., Ardestani, S.K. & Kariminia, A., 2009. The involvement of TLR2 in cytokine and reactive oxygen species (ROS) production by PBMCs in response to Leishmania major phosphoglycans (PGs). *Parasitology*, 136(10), pp.1193–1199.

Kaye, P. & Scott, P., 2011. Leishmaniasis: complexity at the host-pathogen interface. *Nature reviews. Microbiology*, 9(8), pp.604–615. Available at: http://dx.doi.org/10.1038/nrmicro2608.

Kelly, B. & O'Neill, L.A., 2015a. Metabolic reprogramming in macrophages and dendritic cells in innate immunity. *Cell research*, 25(7), pp.771–84. Available at: http://dx.doi.org/10.1038/cr.2015.68%5Cnhttp://www.pubmedcentral.nih.gov/articlerender.fcgi?artid=4493277&tool=pmcentrez&rendertype=abstract.

Kelly, B. & O'Neill, L.A., 2015b. Metabolic reprogramming in macrophages and dendritic cells in innate immunity. *Cell research*, 25(7), pp.771–84.

Kenneth, M., Travers, P. & Walport, M., 2017. Innate Immunity : The First Lines of Defense. In *Janeway's Immunobiology*. pp. 37–73.

Killick-Kendrick, R., 1999. The biology and control of Phlebotomine sand flies. *Clinics in Dermatology*, 17(3), pp.279–289.

Kim, H.S. & Lee, M.S., 2007. STAT1 as a key modulator of cell death. *Cellular Signalling*, 19(3), pp.454–465.

Kito, K. & Ito, T., 2008. Mass spectrometry-based approaches toward absolute quantitative proteomics. *Current genomics*, 9(4), pp.263–74. Available at: http://www.ncbi.nlm.nih.gov/pubmed/19452043%5Cnhttp://www.pubmedcentral.nih.gov/articlerender.fcgi?artid=PMC2682933.

Klegeris, A. et al., 2008. Prolyl endopeptidase is revealed following SILAC analysis to be a novel mediator of human microglial and THP-1 cell neurotoxicity. *Glia*, 56(6), pp.675–85. Available at: http://www.ncbi.nlm.nih.gov/pubmed/18293395 [Accessed August 21, 2013].

Kotaka, M. et al., 2005. Structural studies of glucose-6-phosphate and NADP+ binding to human glucose-6-phosphate dehydrogenase. *Acta Crystallographica Section D: Biological Crystallography*, 61(5), pp.495–504.

Koya, R.C. et al., 2000. Gelsolin inhibits apoptosis by blocking mitochondrial membrane potential loss and cytochrome c release. *Journal of Biological Chemistry*, 275(20), pp.15343–15349.

Koziel, J. et al., 2009. Phagocytosis of *Staphylococcus aureus* by macrophages exerts cytoprotective effects manifested by the upregulation of antiapoptotic factors. *PLoS ONE*, 4(4).

Kramer, P.R. & Wray, S., 2002. 17-Beta-estradiol regulates expression of genes that function in macrophage activation and cholesterol homeostasis. *J Steroid Biochem Mol Biol.*, 81(3), pp.203–16.

Kristensen, A.R., Gsponer, J. & Foster, L.J., 2013. Protein synthesis rate is the predominant regulator of protein expression during differentiation. *Molecular systems biology*, 9(689), p.689. Available at: http://www.pubmedcentral.nih.gov/articlerender.fcgi?artid=3792347&tool=pmcentrez&rendertype=abstract.

Kristensen, L.P. et al., 2012. Temporal profiling and pulsed SILAC labeling identify novel secreted proteins during ex vivo osteoblast differentiation of human stromal stem cells. *Molecular & Cellular Proteomics*, 11(10), pp.989–1007.

Kropf, P. et al., 2005. Arginase and polyamine synthesis are key factors in the regulation of experimental leishmaniasis in vivo. *FASEB journal : official publication of the Federation of American Societies for Experimental Biology*, 19(8), pp.1000–2. Available at: http://www.ncbi.nlm.nih.gov/pubmed/15811879 [Accessed May 26, 2013].

Kwiatkowski, D.J., 1999. Functions of gelsolin : motility , signaling , apoptosis , cancer. *Current Opinion in Cell Biology*, 11, pp.103–108.

Lam, Y.W. et al., 2007. Analysis of Nucleolar Protein Dynamics Reveals the Nuclear Degradation of Ribosomal Proteins. *Current Biology*, 17(9), pp.749–760. Available at: http://dx.doi.org/10.1016/j.cub.2007.03.064.

Lamour, S.D. et al., 2012. Metabolic characterization of *Leishmania major* infection in activated and nonactivated macrophages. *Journal of proteome research*, 11(8), pp.4211–22. Available at: http://www.pubmedcentral.nih.gov/articlerender.fcgi?artid=3411194&tool=pmcentrez&rendertype=abstract.

Larance, M. et al., 2013. Global Subcellular Characterization of Protein Degradation Using Quantitative Proteomics. *Molecular & Cellular Proteomics*, 12(3), pp.638–650. Available at: http://www.mcponline.org/content/12/3/638.abstract.

Larance, M. & Lamond, A.I., 2015. Multidimensional proteomics for cell biology. *Nature Publishing Group*, 16(5), pp.269–280. Available at: http://dx.doi.org/10.1038/nrm3970.

Lauber, K. et al., 2003. Apoptotic Cells Induce Migration of Phagocytes via Caspase-3-Mediated Release of a Lipid Attraction Signal. *Cell*, 113, pp.717–730.

Laurenti, M.D. et al., 2004. The role of complement in the early phase of *Leishmania (Leishmania) amazonensis* infection in BALB/c mice. *Brazilian journal of medical and biological research*, 37(3), pp.427–34. Available at: http://www.ncbi.nlm.nih.gov/pubmed/15060713.

Lay, a J. et al., 2000. Phosphoglycerate kinase acts in tumour angiogenesis as a disulphide reductase. *Nature*, 408(6814), pp.869–873.

Lazar, C. et al., 2016. Accounting for the Multiple Natures of Missing Values in Label-Free Quantitative Proteomics Data Sets to Compare Imputation Strategies. *Journal of Proteome Research*, 15(4), pp.1116–1125.

Leao, S.D.S. et al., 1995. Intracellular *Leishmania amazonensis* amastigotes internalize and degrade MHC class II molecules of their host cells. *Journal of Cell Science*, 3231, pp.3219–3231.

Leifso, K. et al., 2007. Genomic and proteomic expression analysis of *Leishmania* promastigote and amastigote life stages: the *Leishmania* genome is constitutively expressed. *Molecular and biochemical parasitology*, 152(1), pp.35–46. Available at: http://www.ncbi.nlm.nih.gov/pubmed/17188763 [Accessed August 6, 2013].

Li, C. et al., 2012. Quantitative proteomic strategies for the identification of microRNA targets. *Expert review of proteomics*, 9(5), pp.549–59. Available at: http://www.ncbi.nlm.nih.gov/pubmed/23194271.

Li, G.-W. et al., 2015. Quantifying absolute protein synthesis rates reveals principles underlying allocation of cellular resources. *Cell*, 157(3), pp.624–635.

Liaud, M.F. et al., 2000. Compartment-specific isoforms of TPI and GAPDH are imported into diatom mitochondria as a fusion protein: evidence in favor of a mitochondrial origin of the eukaryotic glycolytic pathway. *Molecular Biology and Evolution*, 17(2), pp.213–223. Available at: http://www.ncbi.nlm.nih.gov/pubmed/10677844.

Liévin-Le Moal, V. & Loiseau, P.M., 2016. *Leishmania* hijacking of the macrophage intracellular compartments. *FEBS Journal*, 283(4), pp.598–607.

Lill, J., 2003. Proteomic tools for quantitation by mass spectrometry. *Mass Spectrometry Reviews*, 22(3), pp.182–194.

Lithgow, T., 2000. Targeting of proteins to mitochondria. *FEBS Letters*, 476(1–2), pp.22–26.

Liu, D. & Uzonna, J.E., 2012. The early interaction of *Leishmania* with macrophages and dendritic cells and its influence on the host immune response. *Frontiers in cellular and infection microbiology*, 2(June), p.83. Available at: http://www.pubmedcentral.nih.gov/articlerender.fcgi?artid=3417671&tool=pmcentrez&rendertype=abstract [Accessed March 4, 2013].

Liu, K.T. et al., 2016. Serum galectin-9 and galectin-3-binding protein in acute dengue virus infection. *International Journal of Molecular Sciences*, 17(6).

Lockwood, D.N.J. & Sundar, S., 2006. Serological tests for visceral leishmaniasis. *BMJ (Clinical research ed.)*, 333(7571), pp.711–712.

Lynn, M.A., Marr, A.K. & McMaster, W.R., 2013. Differential quantitative proteomic profiling of *Leishmania infantum* and *Leishmania mexicana* density gradient separated membranous fractions. *Journal of Proteomics*, 82, pp.179–192. Available at: http://dx.doi.org/10.1016/j.jprot.2013.02.010.

Mann, M., 2014. Fifteen Years of Stable Isotope Labeling by Amino Acids in Cell Culture (SILAC), Available at: http://link.springer.com/10.1007/978-1-60327-064-9_9%5Cnhttp://link.springer.com/protocol/10.1007/978-1-4939-1142-4_1.

Mann, M., 2006. Functional and quantitative proteomics using SILAC. *Nature reviews. Molecular cell biology*, 7(12), pp.952–8. Available at: http://www.ncbi.nlm.nih.gov/pubmed/17139335.

Maroli, M. et al., 2001. Evidence for an impact on the incidence of canine leishmaniasis by the mass use of deltamethrin-impregnated dog collars in southern Italy. *Medical and Veterinary Entomology*, 15(4), pp.358–363.

Martin-Perez, M. & Villén, J., 2015. Feasibility of Protein Turnover Studies in Prototroph *Saccharomyces cerevisiae* Strains. *Analytical Chemistry*, 87(7), pp.4008–4014.

Martinez, F.O., Helming, L. & Gordon, S., 2009. Alternative Activation of Macrophages: An Immunologic Functional Perspective. *Annual Review of Immunology*, 27(1), pp.451–483. Available at: http://www.annualreviews.org/doi/10.1146/annurev.immunol.021908.132532.

Maslov, D.A. et al., 2013. Diversity and phylogeny of insect trypanosomatids: All that is hidden shall be revealed. *Trends in Parasitology*, 29(1), pp.43–52.

Matallana-Surget, S., Leroy, B. & Wattiez, R., 2010. Shotgun proteomics: concept, key points and data mining. *Expert review of proteomics*, 7(1), pp.5–7.

Available at: http://www.ncbi.nlm.nih.gov/pubmed/20121468.

Matheoud, D. et al., 2013. *Leishmania* evades host immunity by inhibiting antigen cross-presentation through direct cleavage of the SNARE VAMP8. *Cell Host and Microbe*, 14(1), pp.15–25.

Matthews, L. et al., 2009. Reactome knowledgebase of human biological pathways and processes. *Nucleic Acids Research*, 37(SUPPL. 1), pp.619–622.

Mazur, A.J. et al., 2016. Gelsolin interacts with LamR, hnRNP U, nestin, Arp3 and α-tubulin in human melanoma cells as revealed by immunoprecipitation and mass spectrometry. *European Journal of Cell Biology*, 95(1), pp.26–41. Available at: http://dx.doi.org/10.1016/j.ejcb.2015.11.001.

Mcconville, M.J. et al., 2002. Secretory Pathway of Trypanosomatid Parasites. *Microbiol. Mol. Biol. Rev.*, 66(1), pp.122–154.

McConville, M.J. et al., 2015. *Leishmania* carbon metabolism in the macrophage phagolysosome- feast or famine? *F1000Research*, 4(F1000 Faculty Rev), p.938. Available at: http://www.pubmedcentral.nih.gov/articlerender.fcgi?artid=4648189&tool=pmcentrez&rendertype=abstract.

McConville, M.J. et al., 2007. Living in a phagolysosome; metabolism of *Leishmania* amastigotes. *Trends in Parasitology*, 23(8), pp.368–375.

McConville, M.J. & Handman, E., 2007. The molecular basis of *Leishmania* pathogenesis. *International journal for parasitology*, 37(10), pp.1047–51. Available at: http://www.ncbi.nlm.nih.gov/pubmed/17629957 [Accessed January 22, 2014].

McConville, M.J. & Naderer, T., 2011. Metabolic pathways required for the intracellular survival of *Leishmania*. *Annual review of microbiology*, 65, pp.543–61. Available at: http://www.annualreviews.org/doi/full/10.1146/annurev-micro-090110-102913.

Mcgwire, B.S., Chang, K. & Engman, D.M., 2003. Migration through the Extracellular Matrix by the Parasitic Protozoan *Leishmania* Is Enhanced by Surface Metalloprotease gp63. *Infection and Immunity*, 71(2), pp.1008–1010.

Mehta, S.R. et al., 2011. Flow Cytometric Screening for Anti-Leishmanials in a Human Macrophage Cell Line. *Exp Parasitol*, 126(4), pp.617–620.

Meier, C.L., Svensson, M. & Kaye, P.M., 2003. *Leishmania*-induced inhibition of macrophage antigen presentation analyzed at the single-cell level. *Journal of immunology (Baltimore, Md. : 1950)*, 171(12), pp.6706–13. Available at: http://www.ncbi.nlm.nih.gov/pubmed/14662874.

de Menezes, J.., Saraiva, E.M. & da Rocha-Azevedo, B., 2016. The site of the bite: *Leishmania* interaction with macrophages, neutrophils and the extracellular matrix in the dermis. *Parasites & vectors*, 9(264), pp.1–8. Available at: http://download.springer.com/static/pdf/509/art%3A10.1186%2Fs13071-016-1540-3.pdf?originUrl=http://parasitesandvectors.biomedcentral.com/article/10.1186/s13071-016-1540-3&token2=exp=1462793074~acl=/static/pdf/509/art%25253A10.1186%25.

Menezes, J.P.B. et al., 2013. Proteomic analysis reveals differentially expressed proteins in macrophages infected with Leishmania amazonensis or *Leishmania major*. *Microbes and infection / Institut Pasteur*, pp.1–13. Available at: http://www.ncbi.nlm.nih.gov/pubmed/23628411 [Accessed May 29, 2013].

Metzdorf, P.I. et al., 2017. Molecular characterization of *Leishmania infantum* in domestic cats in a region of Brazil endemic for human and canine visceral leishmaniasis. *Acta Tropica*, 166, pp.121–125. Available at: http://dx.doi.org/10.1016/j.actatropica.2016.11.013.

Michels, P.A.M. et al., 2006. Metabolic functions of glycosomes in trypanosomatids. *Biochimica et Biophysica Acta - Molecular Cell Research*, 1763(12), pp.1463–1477.

Millar, J.A. et al., 2015. *Coxiella burnetii* and *Leishmania mexicana* residing within similar parasitophorous vacuoles elicit disparate host responses. *Frontiers in microbiology*, 6(August), p.794. Available at: http://journal.frontiersin.org/article/10.3389/fmicb.2015.00794/abstract.

Mirza, S.P., 2012. Quantitative mass spectrometry-based approaches in cardiovascular research. *Circulation: Cardiovascular Genetics*, 5(4), pp.1–8.

Mitchell, E.K. et al., 2004. Inhibition of cell surface MHC class II expression by *Salmonella*. *European journal of immunology*, 34, pp.2559–2567.

Mohapatra, S., 2014. Drug resistance in leishmaniasis: Newer developments. *Tropical parasitology*, 4(1), pp.4–9. Available at: http://www.pubmedcentral.nih.gov/articlerender.fcgi?artid=3992802&tool=pmcentrez&rendertype=abstract.

Monroy, F.., 2012. *Toxoplasma gondii*: Effect of infection on expression of 14-3-3 proteins in human epithelial cells. *Experiment*, 100(2), pp.130–134.

Monzote, L., 2009. Current Treatment of Leishmaniasis : A Review. *The Open Antimicrobial Agents Journal*, 1, pp.9–19.

Moore, L.L., Santrich, C. & LeBowitz, J.H., 1996. Stage-specific expression of the *Leishmania mexicana* paraflagellar rod protein PFR-2. *Molecular and Biochemical Parasitology*, 80(2), pp.125–135.

de Morais, C.G.V. et al., 2015. The Dialogue of the Host-Parasite Relationship: *Leishmania* spp. and *Trypanosoma cruzi* Infection. *BioMed Research International*, 2015(August 2016), pp.1–19. Available at: http://www.hindawi.com/journals/bmri/2015/324915/.

Morales, D., Skoulakis, E.C.M. & Acevedo, S.F., 2012. 14-3-3s are potential biomarkers for HIV-related neurodegeneration. *Journal of NeuroVirology*, 18(5), pp.341–353.

Moreira, D. et al., 2015. *Leishmania infantum* Modulates Host Macrophage Mitochondrial Metabolism by Hijacking the SIRT1-AMPK Axis. *PLoS Pathogens*, 11(3), pp.1–24.

Mosser, D.M., 2003. The many faces of macrophage activation. *Journal of leukocyte biology*, 73(February), pp.209–212.

Mosser, D.M. & Edwards, J.P., 2008. Exploring the full spectrum of macrophage activation. *Nature reviews. Immunology*, 8(12), pp.958–69. Available at: http://www.pubmedcentral.nih.gov/articlerender.fcgi?artid=2724991&tool=pmcentrez&rendertype=abstract.

Mosser, D.M. & Zhang, X., 2010. Activation of murine macrophages. *Current Protocol in Immunology*, 16.

Mottram, J.C., Coombs, G.H. & Alexander, J., 2004. Cysteine peptidases as virulence factors of *Leishmania*. *Current opinion in microbiology*, 7(4), pp.375–81. Available at: http://www.ncbi.nlm.nih.gov/pubmed/15358255 [Accessed April 15, 2013].

Mullin, K. a et al., 2001. Regulated degradation of an endoplasmic reticulum membrane protein in a tubular lysosome in *Leishmania mexicana*. *Molecular biology of the cell*, 12(August), pp.2364–2377.

Nag, S. et al., 2009. Ca2+ binding by domain 2 plays a critical role in the activation and stabilization of gelsolin. *Proceedings of the National Academy of Sciences of the United States of America*, 106(33), pp.13713–13718. Available at: http://www.pnas.org/cgi/doi/10.1073/pnas.0812374106%5Cnpapers3://publication/doi/10.1073/pnas.0812374106.

Nagill, R. & Kaur, S., 2011. Vaccine candidates for leishmaniasis: A review. *International Immunopharmacology*, 11(10), pp.1464–1488. Available at: http://dx.doi.org/10.1016/j.intimp.2011.05.008.

Nagy, K.A., Girard, I.A. & Brown, T.K., 1999. Energetics of free-ranging mammals, reptiles, and birds. *Annual review of nutrition*, 19, pp.247–77. Available at: http://www.ncbi.nlm.nih.gov/pubmed/10448524.

Nandan, D. et al., 2000. Exploitation of host cell signaling machinery: activation of macrophage phosphotyrosine phosphatases as a novel mechanism of

molecular microbial pathogenesis. *Journal of leukocyte biology*, 67(4), pp.464–470.

Newmeyer, D.D. & Ferguson-Miller, S., 2003. Mitochondria: Releasing power for life and unleashing the machineries of death. *Cell*, 112(4), pp.481–490.

Ng, L.G. et al., 2008. Migratory dermal dendritic cells act as rapid sensors of protozoan parasites. *PLoS pathogens*, 4(11).

Noble, K.E. et al., 1999. Monocytes stimulate expression of the Bcl-2 family member, A1, in endothelial cells and confer protection against apoptosis. *Journal of immunology (Baltimore, Md. : 1950)*, 162(3), pp.1376–83. Available at: http://www.ncbi.nlm.nih.gov/pubmed/9973392.

North, M.J. & Coombs, G.H., 1982. Proteinases Of *Leishmania mexicana* Amastigotes And Promastigotes: Analysis By Gel Electrophoresis. *Molecular and Biochemical Parasitology*, 3, pp.293–300.

Nugent, P.G. et al., 2004. Proteomic analysis of *Leishmania mexicana* differentiation. *Molecular and biochemical parasitology*, 136(1), pp.51–62. Available at: http://www.ncbi.nlm.nih.gov/pubmed/15138067 [Accessed January 22, 2014].

O'Farrell, P.H., 1975. High resolution two-dimensional electrophoresis of proteins. *The Journal of biological chemistry*, 250(10), pp.4007–21. Available at: http://www.pubmedcentral.nih.gov/articlerender.fcgi?artid=2874754&tool=pmcentrez&rendertype=abstract.

Obsil, T. & Obsilova, V., 2011. Structural basis of 14-3-3 protein functions. *Semin Cell Dev Biol*, 22(7), pp.663–672. Available at: http://www.ncbi.nlm.nih.gov/pubmed/21920446.

Odegaard, J.I. & Chawla, A., 2012. Alternative macrophage activation and metabolism. *Annual review of pathology*, 6, pp.275–297.

Ogunkolade, B.W., Colomb-valet, I. & Monjour, L., 1990. Interactions between the human monocytic leukaemia THP-1 cell line and Old and New World species of *Leishmania*. *Acta Tropica*, 47, pp.171–176.

Oliveira, F. et al., 2015. A sand fly salivary protein vaccine shows efficacy against vector-transmitted cutaneous leishmaniasis in nonhuman primates. *Science translational medicine*, 7(290), p.290ra90. Available at: http://stm.sciencemag.org/content/7/290/290ra90.

Olivier, M. et al., 2012. Leishmania virulence factors: Focus on the metalloprotease GP63. *Microbes and Infection*, 14(15), pp.1377–1389. Available at: http://dx.doi.org/10.1016/j.micinf.2012.05.014.

Olivier, M., Gregory, D.J. & Forget, G., 2005. Subversion mechanisms by which *Leishmania* parasites can escape the host immune response: a signaling point of view. *Clinical microbiology reviews*, 18(2), pp.293–305. Available at: http://www.pubmedcentral.nih.gov/articlerender.fcgi?artid=1082797&tool=pmcentrez&rendertype=abstract [Accessed April 22, 2013].

Olliaro, P. et al., 2013. Methodology of Clinical Trials Aimed at Assessing Interventions for Cutaneous Leishmaniasis. *PLoS Neglected Tropical Diseases*, 7(3).

Olsen, J. V. et al., 2006. Global, In Vivo, and Site-Specific Phosphorylation Dynamics in Signaling Networks. *Cell*, 127(3), pp.635–648.

Ong, S. et al., 2002. Stable isotope labeling by amino acids in cell culture , SILAC , as a simple and accurate approach to expression proteomics. *The American Society for Biochemistry and Molecular Biology*.

Ong, S.-E. & Mann, M., 2006. A practical recipe for stable isotope labeling by amino acids in cell culture (SILAC). *Nature protocols*, 1(6), pp.2650–60. Available at: http://www.ncbi.nlm.nih.gov/pubmed/17406521 [Accessed March 3, 2013].

Ong, S.-E. & Mann, M., 2005. Mass spectrometry-based proteomics turns quantitative. *Nature chemical biology*, 1(5), pp.252–62. Available at: http://www.ncbi.nlm.nih.gov/pubmed/16408053.

Opperdoes, F.R. & Coombs, G.H., 2007. Metabolism of *Leishmania*: proven and predicted. *Trends in Parasitology*, 23(4), pp.149–158.

Oryan, A., 2015. Plant-derived compounds in treatment of leishmaniasis. *Iranian Journal of Veterinary Research*, 16(1), pp.1–19.

Oveland, E. et al., 2009. Ligand-induced Flt3-downregulation modulates cell death associated proteins and enhances chemosensitivity to idarubicin in THP-1 acute myeloid leukemia cells. *Leukemia research*, 33(2), pp.276–87. Available at: http://www.ncbi.nlm.nih.gov/pubmed/18691757 [Accessed June 10, 2014].

Paape, D. et al., 2010. Gel free analysis of the proteome of intracellular *Leishmania mexicana*. *Molecular and biochemical parasitology*, 169(2), pp.108–14. Available at: http://www.ncbi.nlm.nih.gov/pubmed/19900490 [Accessed January 22, 2014].

Paape, D. et al., 2008. Transgenic, fluorescent *Leishmania mexicana* allow direct analysis of the proteome of intracellular amastigotes. *Molecular & cellular proteomics : MCP*, 7, pp.1688–1701.

Paape, D. & Aebischer, T., 2011. Contribution of proteomics of *Leishmania spp*. to the understanding of differentiation, drug resistance mechanisms, vaccine

and drug development. *Journal of Proteomics*, 74(9), pp.1614–1624.

de Paiva, R.M.C. et al., 2015. Amastin Knockdown in *Leishmania braziliensis* Affects Parasite-Macrophage Interaction and Results in Impaired Viability of Intracellular Amastigotes. *PLoS Pathogens*, 11(12), pp.1–24.

Pandey, R.K. et al., 2016. *Leishmania donovani*-Induced Increase in Macrophage Bcl-2 Favors Parasite Survival. *Frontiers in Immunology*, 7(October). Available at: http://journal.frontiersin.org/article/10.3389/fimmu.2016.00456/full.

Papadopoulou, B. et al., 2003. Stage-Specific regulation of gene expresion in *Leishmania*. *ASN News*, 69(6), pp.282–288.

Paramchuk, W.J. et al., 1997. Cloning, characterization and overexpression of two iron superoxide dismutase cDNAs from *Leishmania chagasi*: role in pathogenesis. *Molecular and Biochemical Parasitology*, 90(1), pp.203–221. Available at: http://www.sciencedirect.com/science/article/pii/S0166685197001412.

Pelletier, I. et al., 2003. Specific recognition of *Leishmania major* poly-ß-galactosyl epitopes by galectin-9: Possible implication of galectin-9 in interaction between L. major and host cells. *Journal of Biological Chemistry*, 278(25), pp.22223–22230.

Pescher, P. et al., 2011. Quantitative proteome profiling informs on phenotypic traits that adapt *Leishmania donovani* for axenic and intracellular proliferation. *Cellular Microbiology*, 13(7), pp.978–991.

Pförtner, H. et al., 2013. A proteomics workflow for quantitative and time-resolved analysis of adaptation reactions of internalized bacteria. *Methods (San Diego, Calif.)*, 61(3), pp.244–50. Available at: http://www.ncbi.nlm.nih.gov/pubmed/23643866 [Accessed October 2, 2013].

Piechura, H., Oeljeklaus, S. & Warscheid, B., 2012. Quantitative Methods in Proteomics K. Marcus, ed. , 893, pp.201–221. Available at: http://www.springerlink.com/index/10.1007/978-1-61779-885-6 [Accessed August 7, 2013].

Pimienta, G., Chaerkady, R. & Pandey, A., 2009. SILAC for Global Phosphoproteomics Analysis M. de Graauw, ed. *Phospho-Proteomics, Methods and Protocols*, 527, pp.107–116. Available at: http://link.springer.com/10.1007/978-1-60327-834-8 [Accessed January 22, 2014].

Podlipaev, S., 2001. The more insect trypanosomatids under study-the more diverse Trypanosomatidae appears. *International journal for parasitology*, 31(5–6), pp.648–652.

Poortmans, J.R. et al., 2012. Protein turnover, amino acid requirements and recommendations for athletes and active populations. *Brazilian Journal of Medical and Biological Research*, 45(10), pp.875–890.

Pral, E.M.F. et al., 1993. *Leishmania mexicana*: Proteinase Activities and Megasomes in Axenically Cultivated Amastigote-like Forms. *Experimental parasitology*, 77, pp.62–73.

Pratt, J.M. et al., 2002. Dynamics of Protein Turnover, a Missing Dimension in Proteomics. *Molecular & Cellular Proteomics*, 1(8), pp.579–591. Available at: http://www.mcponline.org/cgi/content/abstract/1/8/579.

Price, J.C. et al., 2010. Analysis of proteome dynamics in the mouse brain. *Proceedings of the National Academy of Sciences of the United States of America*, 107(32), pp.14508–14513.

Qualls, J.E. et al., 2013. Sustained generation of nitric oxide and control of mycobacterial infection requires argininosuccinate synthase 1. *Cell Host Microbe*, 12(3), pp.313–323.

Rabhi, I. et al., 2012. Transcriptomic signature of *Leishmania* infected mice macrophages: a metabolic point of view. *PLoS neglected tropical diseases*, 6(8), p.e1763. Available at: http://www.pubmedcentral.nih.gov/articlerender.fcgi?artid=3424254&tool=pmcentrez&rendertype=abstract [Accessed April 13, 2013].

Rauniyar, N. & Yates, J.R., 2014. Isobaric Labeling-Based Relative Quantification in Shotgun Proteomics. *Journal of proteome research*, 13, pp.5293–5309.

Rawlings, J.S., Rosler, K.M. & Harrison, D. a, 2004. The JAK/STAT signaling pathway. *Journal of cell science*, 117(Pt 8), pp.1281–3. Available at: http://www.ncbi.nlm.nih.gov/pubmed/15020666 [Accessed February 28, 2013].

Read, J. et al., 2001. The crystal structure of human phosphoglucose isomerase at 1.6 A resolution: implications for catalytic mechanism, cytokine activity and haemolytic anaemia. *Journal of molecular biology*, 309(2), pp.447–63. Available at: http://www.ncbi.nlm.nih.gov/pubmed/11371164.

Reguera, R.M. et al., 2016. Current status on prevention and treatment of canine leishmaniasis. *Veterinary Parasitology*, 227, pp.98–114. Available at: http://linkinghub.elsevier.com/retrieve/pii/S0304401716302709.

Rezvan, H. & Moafi, M., 2015. An overview on *Leishmania* vaccines: A narrative review article. *Veterinary research forum : an international quarterly journal*, 6(1), pp.1–7. Available at: http://www.pubmedcentral.nih.gov/articlerender.fcgi?artid=4405679&tool=pmcentrez&rendertype=abstract.

Ribeiro-Gomes, F.L. et al., 2004. Macrophage interactions with neutrophils regulate *Leishmania major* infection. *Journal of immunology (Baltimore, Md. : 1950)*, 172(7), pp.4454–62. Available at: http://www.ncbi.nlm.nih.gov/pubmed/15034061.

Rich, P.R., 2003. The molecular machinery of Keilin's respiratory chain. *Biochemical Society transactions*, 31(Pt 6), pp.1095–1105.

Rochette, A. et al., 2008. Genome-wide gene expression profiling analysis of *Leishmania major* and *Leishmania infantum* developmental stages reveals substantial differences between the two species. *BMC genomics*, 9, p.255.

Rodriguez-Contreras, D. & Hamilton, N., 2014. Gluconeogenesis in *Leishmania mexicana*: Contribution of glycerol kinase, phosphoenolpyruvate carboxykinase, and pyruvate phosphate dikinase. *Journal of Biological Chemistry*, 289(47), pp.32989–33000.

Rodriguez, N.E., Chang, H.K. & Wilson, M.E., 2004. Novel Program of Macrophage Gene Expression Induced by Phagocytosis of *Leishmania chagasi*. *Infection and Immunity*, 72(4), pp.2111–2122.

Rolland, S. & Conradt, B., 2006. The role of mitochondria in apoptosis induction in *Caenorhabditis elegans*: more than just innocent bystanders? *Cell death and differentiation*, 13(8), pp.1281–1286.

Rosenzweig, D. et al., 2008. Retooling *Leishmania* metabolism: from sand fly gut to human macrophage. *FASEB journal : official publication of the Federation of American Societies for Experimental Biology*, 22(2), pp.590–602. Available at: http://www.ncbi.nlm.nih.gov/pubmed/17884972 [Accessed August 1, 2013].

Rossi, F. & Zatti, M., 1964. Changes in the metabolic pattern of polymorphonuclear leukocytes during phagocytosis. *Br J Exp Pathol*, 45(5), pp.548–559.

Russell, J.B. & Cook, G.M., 1995. Energetics of Bacterial Growth : Balance of Anabolic and Catabolic Reactions. *Microbiological Reviews*, 59(1), pp.48–62.

Saar, Y. et al., 1998. Characterization of developmentally-regulated activities in axenic amastigotes of *Leishmania donovani*. *Molecular and Biochemical Parasitology*, 95(1), pp.9–20.

Sacks, D. & Noben-Trauth, N., 2002. The immunology of susceptibility and resistance to *Leishmania major* in mice. *Nature reviews. Immunology*, 2(11), pp.845–58. Available at: http://www.ncbi.nlm.nih.gov/pubmed/12415308 [Accessed August 14, 2013].

Sacks, D.L., 1989. Metacyclogenesis in *Leishmania* promastigotes. *Experimental Parasitology*, 69(1), pp.100–103.

Santos, C. sDS et al., 2015. Proteome Profiling of Human Cutaneous Leishmaniasis Lesion. *Journal of Investigative Dermatology*, 135(10), pp.400–410.

Sattarahmady, N. et al., 2016. Gold nanoparticles-based biosensing of *Leishmania major* kDNA genome: Visual and spectrophotometric detections. *Sensors and Actuators B: Chemical*, 235, pp.723–731. Available at: http://linkinghub.elsevier.com/retrieve/pii/S0925400516306979.

Saunders, E.C. et al., 2014. Induction of a Stringent Metabolic Response in Intracellular Stages of *Leishmania mexicana* Leads to Increased Dependence on Mitochondrial Metabolism. *PLoS Pathogens*, 10(1).

Schenten, D. & Medzhitov, R., 2011. The Control of Adaptive Immune Responses by the Innate Immune System 1st ed., Elsevier inc. Available at: http://dx.doi.org/10.1016/B978-0-12-387664-5.00003-0.

Schilling, B. et al., 2012. Platform-independent and Label-free Quantitation of Proteomic Data Using MS1 Extracted Ion Chromatograms in Skyline: Application To Protein Acetylation And Phosphorylation. *Molecular & Cellular Proteomics*, 11(5), pp.202–214. Available at: http://www.pubmedcentral.nih.gov/articlerender.fcgi?artid=3418851&tool=pmcentrez&rendertype=abstract%5Cnhttp://www.mcponline.org/cgi/doi/10.1074/mcp.M112.017707.

Schmidt, F. et al., 2007. Rapid determination of amino acid incorporation by stable isotope labeling with amino acids in cell culture (SILAC). *Rapid communications in mass spectrometry : RCM*, 21, pp.3919–3926.

Schmidt, F. et al., 2010. Time-resolved quantitative proteome profiling of host-pathogen interactions: the response of *Staphylococcus aureus* RN1HG to internalisation by human airway epithelial cells. *Proteomics*, 10(15), pp.2801–11. Available at: http://www.ncbi.nlm.nih.gov/pubmed/20518028 [Accessed January 22, 2014].

Schwanhäusser, B. et al., 2009. Global analysis of cellular protein translation by pulsed SILAC. *Proteomics*, 9(1), pp.205–209.

Schwanhäusser, B. et al., 2008. Widespread changes in protein synthesis induced by microRNAs. *Nature*, 455 (7209), pp.58–63. Available at: http://www.ncbi.nlm.nih.gov/pubmed/18668040%5Cnhttp://www.ncbi.nlm.nih.gov/pubmed/18668040?ordinalpos=&itool=EntrezSystem2.PEntrez.Pubmed.Pubmed_ResultsPanel.SmartSearch&log$=citationsensor.

Schwanhäusser, B., Busse, D. & Li, N., 2011. Global quantification of mammalian gene expression control. *Nature*, 473(7347), pp.337–342. Available at: http://www.ncbi.nlm.nih.gov/entrez/query.fcgi?db=pubmed&cmd=Retrieve&dopt=AbstractPlus&list_uids=21593866%5Cnhttp://www.nature.com/nature/journal/v473/n7347/abs/nature10098.html.

Scott, P. & Novais, F.O., 2016. Cutaneous leishmaniasis : immune responses in

protection and pathogenesis. *Nature Reviews Immunology*, 16, pp.581–592.

Serafim, T.D. et al., 2012. *Leishmania* metacyclogenesis is promoted in the absence of purines. *PLoS neglected tropical diseases*, 6(9), p.e1833. Available at: http://www.pubmedcentral.nih.gov/articlerender.fcgi?artid=3458635&tool=pmcentrez&rendertype=abstract [Accessed July 4, 2014].

Sharma, U. & Singh, S., 2009. Immunobiology of leishmaniasis. *Indian journal of experimental biology*, 47(6), pp.412–23. Available at: http://www.ncbi.nlm.nih.gov/pubmed/19634705.

Shibata, K.I. et al., 1994. Acid phosphatase purified from *Mycoplasma fermentans* has protein tyrosine phosphatase-like activity. *Infection and Immunity*, 62(1), pp.313–315.

Shio, M.T. et al., 2012. Host cell signalling and leishmania mechanisms of evasion. *Journal of tropical medicine*, 2012, p.819512. Available at: http://www.pubmedcentral.nih.gov/articlerender.fcgi?artid=3216306&tool=pmcentrez&rendertype=abstract [Accessed March 9, 2013].

Shweash, M. et al., 2011. *Leishmania mexicana* promastigotes inhibit macrophage IL-12 production via TLR-4 dependent COX-2, iNOS and arginase-1 expression. *Molecular immunology*, 48(15–16), pp.1800–8. Available at: http://www.pubmedcentral.nih.gov/articlerender.fcgi?artid=3173610&tool=pmcentrez&rendertype=abstract [Accessed July 2, 2013].

Simpson, L. et al., 2000. Evolution of RNA editing in trypanosome mitochondria. *Proceedings of the National Academy of Sciences of the United States of America*, 97(13), pp.6986–6993. Available at: http://www.scopus.com/inward/record.url?eid=2-s2.0-0034691061&partnerID=40&md5=849d81049dd195be154f0cb4447cc6fb.

Singh, A.K. et al., 2015. Proteomic-based approach to gain insight into reprogramming of THP-1 cells exposed to *Leishmania donovani* over an early temporal window. *Infection and Immunity*, 83(5), pp.1853–1868.

Song, C. et al., 2003. Interleukin-8 Is Differentially Expressed by Human-Derived Monocytic Cell Line U937 Infected with *Mycobacterium tuberculosis* H37Rv and *Mycobacterium marinum*. *Infection and immunity*, 71(10), pp.5480–5487.

Soufi, B. et al., 2010. Stable Isotope Labeling by Amino Acids in Cell Culture (SILAC) Applied to Quantitative Proteomics of Bacillus subtilis. *Journal of Proteome Research*, 9(7), pp.3638–3646. Available at: http://dx.doi.org/10.1021/pr100150w.

Spitzenberger, F., Graessler, J. & Schroeder, H.E., 2001. Molecular and functional characterization of galectin 9 mRNA isoforms in porcine and human cells and tissue. *Biochimie*, 83(9), pp.851–862.

Stebeck, C.E. et al., 1995. Kinetoplastid membrane protein-11 (KMP-11) is differentially expressed during the life cycle of African trypanosomes and is found in a wide variety of kinetoplastid parasites. *Molecular and Biochemical Parasitology*, 71(1), pp.1–13.

Stevens, J.R. & Gibson, W., 1999. The molecular evolution of trypanosomes. *Parasitology Today*, 15(11), pp.432–437.

Subramanian, A. et al., 2005. Gene set enrichment analysis: a knowledge-based approach for interpreting genome-wide expression profiles. *Proceedings of the National Academy of Sciences of the United States of America*, 102(43), pp.15545–50. Available at: http://www.ncbi.nlm.nih.gov/pubmed/16199517.

Sutterwala, F.S. et al., 1998. Reversal of proinflammatory responses by ligating the macrophage Fcgamma receptor type I. *The Journal of experimental medicine*, 188(1), pp.217–22. Available at: http://www.pubmedcentral.nih.gov/articlerender.fcgi?artid=2525554&tool=pmcentrez&rendertype=abstract.

Sutterwala, F.S. et al., 1997. Selective Suppression of Interleukin-12 Induction after Macrophage Receptor Ligation. *J. Exp. Med.*, 185(11), pp.1977–1985.

Szanto, A. et al., 2010. STAT6 transcription factor is a facilitator of the nuclear receptor PPAR-regulated gene expression in macrophages and dendritic cells. *Immunity*, 33(5), pp.699–712. Available at: http://dx.doi.org/10.1016/j.immuni.2010.11.009.

T, W. et al., 2016. Macrophage Models for Tuberculosis Studies. *Air & Water Borne Diseases*, 2016(1), pp.3–8.

Teixeira, M.J. et al., 2006. Chemokines in host-parasite interactions in leishmaniasis. *Trends in parasitology*, 22(1), pp.32–40. Available at: http://www.ncbi.nlm.nih.gov/pubmed/16310413 [Accessed March 22, 2013].

Teo, Z.P. & Hughes, D., 2003. The Role of Macrophages in Apoptosis : Initiator , Regulator , Scavenger. *Reviews in Undergraduate Research*, 2, pp.7–11.

Thelen., J., 2007. Introduction to Proteomics: a Brief Historical Perspective on Contemporary Approaches. *Plant Proteomics*, pp.1–5.

Thiede, B. et al., 2013. High resolution quantitative proteomics of HeLa cells protein species using stable isotope labeling with amino acids in cell culture (SILAC), two-dimensional gel electrophoresis (2DE) and nano-liquid chromatograpohy coupled to an LTQ-OrbitrapMass spectrom. *Molecular & cellular proteomics : MCP*, 12(2), pp.529–38. Available at: http://www.pubmedcentral.nih.gov/articlerender.fcgi?artid=3567871&tool=pmcentrez&rendertype=abstract.

Toyama, B.H. et al., 2013. Identification of long-lived proteins reveals exceptional stability of essential cellular structures. *Cell*, 154(5), pp.971–982. Available at: http://dx.doi.org/10.1016/j.cell.2013.07.037.

Tran, K.D. et al., 2013. KHARON1 mediates flagellar targeting of a glucose transporter in *Leishmania mexicana* and is critical for viability of infectious intracellular amastigotes. *Journal of Biological Chemistry*, 288(31), pp.22721–22733.

Trötschel, C., Albaum, S.P. & Poetsch, A., 2013. Proteome turnover in bacteria: Current status for *Corynebacterium glutamicum* and related bacteria. *Microbial Biotechnology*, 6(6), pp.708–719.

Tsuchiya, S. et al., 1982. Induction of Maturation in Cultured Human Monocytic Leukemia Cells by a Phorbol Diester1. *Cancer Research*, 42, pp.1530–1536.

Turco, S.J. & Descoteaux, A., 1992. The lipophosphoglycan of *Leishmania* parasites. *Annu. Rev. Microbiol*, 46, pp.65–94.

Tyanova, S., Temu, T., Sinitcyn, P., et al., 2016. The Perseus computational platform for comprehensive analysis of (prote)omics data. *Nature Methods*, (June). Available at: http://www.nature.com/doifinder/10.1038/nmeth.3901.

Tyanova, S., Temu, T. & Cox, J., 2016. The MaxQuant computational platform for mass spectrometry-based shotgun proteomics. *Nature protocols*, 11(12), pp.2301–2319. Available at: http://dx.doi.org/10.1038/nprot.2016.136%5Cnhttp://www.nature.com/doifinder/10.1038/nprot.2016.136%5Cnhttp://www.ncbi.nlm.nih.gov/pubmed/27809316.

Tzivion, G. & Avruch, J., 2002. 14-3-3 Proteins: Active cofactors in cellular regulation by serine/threonine phosphorylation. *Journal of Biological Chemistry*, 277(5), pp.3061–3064.

Unlu, M., Morgan, M.E. & Minden, J.S., 1997. Difference gel electrophoresis: a single gel method for detecting changes in protein extracts. *Electrophoresis*, 18(11), pp.2071–2077. Available at: http://www.ncbi.nlm.nih.gov/pubmed/9420172.

Urban, P.L., 2016. Quantitative mass spectrometry: an overview. *Philosophical Transactions of the Royal Society A: Mathematical, Physical and Engineering Sciences*, 374(2079), p.20150382. Available at: http://www.ncbi.nlm.nih.gov/pubmed/27644965%5Cnhttp://www.pubmedcentral.nih.gov/articlerender.fcgi?artid=PMC5031646%5Cnhttp://rsta.royalsocietypublishing.org/lookup/doi/10.1098/rsta.2015.0382.

Valentini, G. et al., 2000. The Allosteric Regulation of Pyruvate Kinase. A Site-directed mutagenesis study. *The Journal of biological chemistry*, 275(24), pp.18145–18152.

Vasta, G.R., 2009. Roles of galectins in infection. *Nature reviews. Microbiology*, 7(6), pp.424–38. Available at: http://dx.doi.org/10.1038/nrmicro2146.

Vermelho, A.B. et al., 2010. Biological Roles of Peptidases in Trypanosomatids. , (December 2007), pp.5–23.

Walker, D.M. et al., 2013. Mechanisms of cellular invasion by intracellular parasites. *Cellular and Molecular Life Sciences*, 71(7), pp.1–19.

Walker, J. et al., 2006. Identification of developmentally-regulated proteins in *Leishmania panamensis* by proteome profiling of promastigotes and axenic amastigotes. *Molecular and biochemical parasitology*, 147(1), pp.64–73. Available at: http://www.ncbi.nlm.nih.gov/pubmed/16530278 [Accessed July 1, 2013].

Wallace, F.G., 1966. The trypanosomatid parasites of insects and arthropods. *Exp Parasitol*, 18, pp.124–193.

Warburg, B.Y.O., Wind, F. & Negelein, E., 1926. The metabolism of tumors in the body. *The Journal of General Physiology*, 8, pp.519–530.

Watson, H.C. et al., 1982. Sequence and structure of yeast phosphoglycerate kinase. *The EMBO journal*, 1(12), pp.1635–40. Available at: http://www.pubmedcentral.nih.gov/articlerender.fcgi?artid=553262&tool=pmcentrez&rendertype=abstract.

Whitbread, A.K. et al., 2005. Characterization of the omega class of glutathione transferases. *Methods in Enzymology*, 401(5), pp.78–99.

Wiberg, H.K. et al., 2016. Review, Evaluation, and Discussion of the Challenges of Missing Value Imputation for Mass Spectrometry-Based Label-Free Global Proteomics. *Journal of Proteome Research*, 14(5), pp.1993–2001.

Wiese, M., 2007. *Leishmania* MAP kinases – Familiar proteins in an unusual context. *International Journal for Parasitology*, 37, pp.1053–1062.

Wisniewski, J.R. et al., 2009. Universal sample preparation method for proteome analysis. *Nat Methods*, 6(5), pp.359–362. Available at: http://www.ncbi.nlm.nih.gov/pubmed/19377485.

Wu, Y. et al., 2000. A new developmentally regulated gene family in *Leishmania* amastigotes encoding a homolog of amastin surface proteins. *Molecular and Biochemical Parasitology*, 110(2), pp.345–357.

Yakirevich, E. & Naot, Y., 2000. Cloning of a glucose phosphate isomerase/neuroleukin-like sperm antigen involved in sperm agglutination. *Biology of reproduction*, 62(4), pp.1016–1023.

Yao, C. et al., 2010. Proteomic examination of *Leishmania chagasi* plasma

membrane proteins: contrast between avirulent and virulent (metacyclic) parasite forms. *Proteomics Clinical Application*, 4(1), pp.4–16.

Yao, C., Donelson, J.E. & Wilson, M.E., 2003. The major surface protease (MSP or GP63) of *Leishmania sp*. Biosynthesis, regulation of expression, and function. *Molecular and Biochemical Parasitology*, 132(1), pp.1–16.

van Zandbergen, G. et al., 2004. Cutting edge: neutrophil granulocyte serves as a vector for *Leishmania* entry into macrophages. *Journal of immunology (Baltimore, Md. : 1950)*, 173(11), pp.6521–5. Available at: http://www.ncbi.nlm.nih.gov/pubmed/15557140.

Van Zandbergen, G. et al., 2002. Leishmania promastigotes release a granulocyte chemotactic factor and induce interleukin-8 release but inhibit gamma interferon-inducible protein 10 production by neutrophil granulocytes. *Infection and Immunity*, 70(8), pp.4177–4184.

Zanivan, S. et al., 2013. In vivo SILAC-based proteomics reveals phosphoproteome changes during mouse skin carcinogenesis. *Cell reports*, 3(2), pp.552–66. Available at: http://www.ncbi.nlm.nih.gov/pubmed/23375375 [Accessed May 27, 2014].

Zanivan, S., Kruger, M. & Mann, M., 2012. In Vivo Quantitative Proteomics: The SILAC Mouse. *Methods in Molecular Biology*, 757(4), pp.435–450. Available at: http://link.springer.com/10.1007/978-1-61779-166-6.

Zawawi, K.H. et al., 2010. Moesin-induced signaling in response to lipopolysaccharide in macrophages. *Journal of Periodontal Research*, 45(5), pp.589–601.

Zha, J. et al., 1996. Serine phosphorylation of death agonist BAD in response to survival factor results in binding to 14-3-3 not BCL-X(L). *Cell*, 87(4), pp.619–628.

Zhang, G. & Neubert, T.A., 2009. Use of Stable Isotope Labeling by Amino Acids in Cell Culture for Phosphotyrosine protein Identification and Quantitation. *Methods in Molecular Biology*, 527(26), pp.1–11. Available at: http://link.springer.com/10.1007/978-1-60327-834-8.

Zhang, W. et al., 2011. Prediction and characterization of missing proteomic data in *Desulfovibrio vulgaris*. *Comparative and Functional Genomics*, 2011.

Zhang, W.W. & Matlashewski, G., 2001. Characterization of the A2-A2rel gene cluster in *Leishmania donovani*: Involvement of A2 in visceralization during infection. *Molecular Microbiology*, 39(4), pp.935–948.

Zhu, L. et al., 2015. Cellular metabolism and macrophage functional polarization. *International reviews of immunology*, 34(1), pp.82–100. Available at: http://www.ncbi.nlm.nih.gov/pubmed/25340307.

Zilberstein, D., 2015. Proteomic Analysis of Posttranslational Modifications Using iTRAQ in *Leishmania*. In C. Peacock, ed. *Parasite Genomics Protocols*. New York, NY: Springer New York, pp. 261–268. Available at: http://dx.doi.org/10.1007/978-1-4939-1438-8_16.

Zilberstein, D. & Shapira, M., 1994. The role of pH and temperature in the development of *Leishmania* parasites. *Annu. Rev. Microbiol*, 48, pp.448–470.

8 Appendix

8.1 Proteins quantified (upregulated) in *L. mexicana* promastigote

Accession No.	Mascot Score	MW	L/H ratio	Protein name
LmxM.26.0620	28	10695	19.17	10 kDa heat shock protein, putative
LmxM.11.0350	31	29414	6.37	14-3-3 protein, putative
LmxM.36.3210	29	29782	6.37	14-3-3 protein-like protein
LmxM.33.4340	44	25088	4.20	20s proteasome beta 7 subunit, (putative)
LmxM.28.2420	38	41939	1.85	2-oxoglutarate dehydrogenase, E2 component, dihydrolipoamide succinyltransferase, putative
LmxM.30.2250	31	38642	6.77	3,2-trans-enoyl-CoA isomerase, mitochondrial precursor, putative
LmxM.32.1590	19	36460	1.08	3-ketoacyl-CoA reductase, putative
LmxM.30.2310	59	41697	1.48	3'-nucleotidase/nuclease precursor, putative
LmxM.22.1520	36	20201	3.50	40S ribosomal protein L14, putative
LmxM.08_29.1800	66	14858	3.85	40S ribosomal protein S15A, putative
LmxM.26.0880	48	16777	2.04	40S ribosomal protein S16, putative
LmxM.28.2555	61	16398	2.72	40S ribosomal protein S17, putative

Accession No.	Mascot Score	MW	L/H ratio	Protein name
LmxM.36.0930	19	17471	2.72	40S ribosomal protein S18, putative
LmxM.19.0060	28	33009	2.48	40S ribosomal protein S2
LmxM.15.0950	66	24741	1.36	40S ribosomal protein S3, putative
LmxM.26.1630	41	9797	1.33	40S ribosomal protein S33, putative
LmxM.34.0400	38	30245	1.26	40S ribosomal protein S3A, putative
LmxM.13.1220	70	48291	3.28	40S ribosomal protein S4, putative
LmxM.24.2070	36	24729	1.74	40S ribosomal protein S8, putative
LmxM.19.1005	27	72621	2.66	4-coumarate:coa ligase-like protein
LmxM.23.0543	35	117876	3.55	5'-3' exonuclease XRNC, putative
LmxM.30.0010	118	86681	3.29	5-methyltetrahydropteroyltriglutamate--homocysteinemethyltransferase, putative
LmxM.04.0750	32	24940	3.28	60S ribosomal protein L10, putative
LmxM.08_29.2460	85	24900	4.54	60S ribosomal protein L13, putative
LmxM.24.0040	22	19299	2.66	60S ribosomal protein L17, putative
LmxM.18.1400	30	19368	2.38	60S ribosomal protein L34, putative
LmxM.34.1880	75	34065	1.73	60S ribosomal protein L5, putative
LmxM.07.0510	96	34049	1.23	60S ribosomal protein L7a, putative
LmxM.08_29.2510	27	54602	3.68	6-phospho-1-fructokinase, putative
LmxM.34.3340	92	52591	15.06	6-phosphogluconate dehydrogenase, decarboxylating, putative

Accession No.	Mascot Score	MW	L/H ratio	Protein name
LmxM.32.1300	14	71322	5.77	ABC transporter, putative
LmxM.33.0670	21	229070	13.24	ABC transporter-like protein
LmxM.15.0760	22	294095	7.26	ABC1 transporter-like protein
LmxM.18.0510	30	98265	2.20	aconitase, putative
LmxM.04.1230	108	40685	13.21	actin
LmxM.28.2510	38	69757	4.35	acyl-CoA dehydrogenase, putative
LmxM.34.2730	37	44782	2.86	acyl-CoA dehydrogenase, putative
LmxM.26.0140	29	26272	2.58	adenine phosphoribosyltransferase
LmxM.29.0880	71	37766	6.69	adenosine kinase, putative
LmxM.21.1250	25	30073	2.85	adenylate kinase, putative
LmxM.19.0200	70	35520	5.75	ADP,ATP carrier protein 1, mitochondrial precursor, putative
LmxM.19.0210	48	35536	6.70	ADP,ATP carrier protein 1, mitochondrial precursor, putative,ADP/ATP translocase 1, putative
LmxM.30.2790	56	20230	1.88	ADP-ribosylation factor, putative
LmxM.33.2580	21	22616	9.03	ALBA-domain protein 3
LmxM.25.1120	51	54795	4.44	aldehyde dehydrogenase, mitochondrial precursor
LmxM.13.0280	288	61058	14.68	alpha tubulin
LmxM.27.1310	31	78594	2.38	arginyl-tRNA synthetase, putative
LmxM.16.0540	87	35620	1.67	aspartate carbamoyltransferase, putative

Accession No.	Mascot Score	MW	L/H ratio	Protein name
LmxM.21.1770	56	34671	5.11	ATP synthase F1 subunit gamma protein, putative
LmxM.25.1180	120	53265	8.06	ATP synthase subunit beta, mitochondrial
LmxM.29.3600	25	20315	19.92	ATP synthase, epsilon chain, putative
LmxM.05.0510	29	73310	13.82	ATPase alpha subunit, putative
LmxM.05.0500	64	62845	1.90	ATPase alpha subunit, putative
LmxM.25.1170	120	56458	8.06	ATPase beta subunit, putative
LmxM.33.3350	14	59094	2.29	ATPase-like protein
LmxM.11.1220	14	187925	2.18	ATP-binding cassette protein subfamily A, member 2, putative
LmxM.11.1250	14	229693	1.69	ATP-binding cassette protein subfamily A, member 4, putative
LmxM.34.0370	82	46678	3.91	ATP-dependent DEAD-box RNA helicase, putative
LmxM.34.3100	51	101215	3.99	ATP-dependent RNA helicase, putative
LmxM.34.3100	51	101215	3.99	ATP-dependent RNA helicase, putative
LmxM.05.0360	14	66210	16.23	ATP-dependent RNA helicase, putative
LmxM.31.0400	111	68201	10.2	ATP-dependent RNA helicase, putative
LmxM.32.3210	26	98888	8.22	beta prime cop protein, putative
LmxM.08.1230	725	46842	9.29	beta tubulin
LmxM.21.1860	744	50394	11.65	beta tubulin
LmxM.32.0794	690	55687	8.86	beta tubulin

Accession No.	Mascot Score	MW	L/H ratio	Protein name
LmxM.09.0910	87	16814	28.45	calmodulin, putative
LmxM.20.1180	35	104946	2.71	calpain-like cysteine peptidase
LmxM.20.1185	37	73942	3.02	calpain-like cysteine peptidase, putative
LmxM.20.1310	36	15167	5.20	calpain-like cysteine peptidase, putative,calpain-like cysteine peptidase, Clan CA, family C2
LmxM.04.0450	36	89443	3.59	calpain-like cysteine peptidase, putative,cysteine peptidase, Clan CA, family C2, putative
LmxM.32.2540	48	57378	3.63	carboxypeptidase, putative,metallo-peptidase, Clan MA(E), Family M32
LmxM.29.0710	18	62847	3.28	CDC16, putative
LmxM.21.1080	32	34737	2.55	cell division protein kinase 2,cdc2-related kinase
LmxM.22.1410	71	16437	1.08	centrin, putative,Ca2 -binding EF-hand protein
LmxM.34.2980	18	51628	3.69	chaperone protein DNAj, putative
LmxM.31.3270	20	59552	3.55	chaperonin alpha subunit, putative
LmxM.36.2030	331	59903	6.77	chaperonin HSP60, mitochondrial precursor
LmxM.36.2020	322	60610	5.48	chaperonin HSP60, mitochondrial precursor
LmxM.32.1060	19	105907	2.64	chloride channel protein, putative
LmxM.06.0120	24	20535	2.67	cyclophilin
LmxM.34.3230	57	45102	6.70	cystathione gamma lyase, putative
LmxM.08_29.0820	47	38009	1.53	cysteine peptidase C (CPC),CPC cysteine peptidase, Clan CA, family C1, Cathepsin B-like

Accession No.	Mascot Score	MW	L/H ratio	Protein name
LmxM.05.0960	21	76027	4.16	dipeptidyl-peptidase III, putative,metallo-peptidase, Clan M-, Family M49
LmxM.22.1110	21	627131	1.03	dynein heavy chain, cytosolic, putative
LmxM.17.0083	111	23325	22.56	elongation factor 1-alpha
LmxM.17.0080	180	49575	20.27	elongation factor 1-alpha
LmxM.17.0084	62	23439	8.12	elongation factor 1-alpha
LmxM.36.0180	520	94852	6.29	elongation factor 2
LmxM.36.0180	520	94852	6.29	elongation factor 2
LmxM.09.0970	101	46514	6.29	elongation factor-1 gamma
LmxM.14.1160	296	46743	6.90	enolase
LmxM.01.0770	95	51225	3.10	Eukaryotic initiation factor 4A-1
LmxM.14.0660	51	32705	7.40	fatty acid elongase, putative
LmxM.16.0910	24	18262	9.04	flagellar calcium-binding protein, putative
LmxM.36.1260	175	41150	9.68	fructose-1,6-bisphosphate aldolase
LmxM.34.3700	47	25320	6.71	Gim5A protein, putative,glycosomal membrane protein
LmxM.22.0660	23	115396	9.48	glucoamylase-like protein
LmxM.28.1200	107	71919	3.90	glucose-regulated protein 78, putative
LmxM.15.1010	155	115208	4.08	glutamate dehydrogenase
LmxM.28.2910	80	49561	5.41	glutamate dehydrogenase, putative

Accession No.	Mascot Score	MW	L/H ratio	Protein name
LmxM.06.0370	36	42893	1.79	glutamine synthetase, putative
LmxM.29.2980	135	39326	16.81	glyceraldehyde 3-phosphate dehydrogenase, glycosomal
LmxM.19.0710	41	33934	6.14	glycosomal malate dehydrogenase
LmxM.27.1810	189	58742	3.27	glycosomal phosphoenolpyruvate carboxykinase, putative
LmxM.27.1805	144	58770	16.68	glycosomal phosphoenolpyruvate carboxykinase, putative
LmxM.18.0900	18	95809	3.67	glycosyltransferase, putative
LmxM.29.2460	110	69430	8.61	heat shock 70-related protein 1, mitochondrial precursor, putative
LmxM.29.2490	165	72990	8.35	heat shock 70-related protein 1, mitochondrial precursor, putative
LmxM.29.2470	93	37663	8.31	heat shock 70-related protein 1, mitochondrial precursor, putative
LmxM.26.1240	49	71012	2.18	heat shock protein 70-related protein
LmxM.32.0312	293	81035	14.52	heat shock protein 83-1
LmxM.18.1370	40	92808	8.87	heat shock protein, putative
LmxM.28.2770	382	71482	7.68	heat-shock protein hsp70, putative
LmxM.21.0240	87	61385	2.94	hexokinase, putative
LmxM.21.0250	34	52151	2.59	hexokinase, putative
LmxM.08_29.1720	77	14066	4.46	histone H2A, putative
LmxM.17.1220	98	11991	14.82	histone H2B
LmxM.09.1340	188	11957	10.46	histone H2B

Accession No.	Mascot Score	MW	L/H ratio	Protein name
LmxM.19.0030	160	11970	7.88	histone H2B
LmxM.10.0870	69	14848	9.10	histone H3
LmxM.16.0570	101	14838	5.05	histone H3
LmxM.19.0630	43	16601	2.94	histone H3 variant, putative
LmxM.15.0010	89	11436	7.14	histone H4
LmxM.21.0015	21	12023	7.14	histone H4
LmxM.06.0010	46	11436	6.21	histone H4
LmxM.25.2450	87	11485	6.14	histone H4
LmxM.25.2450	87	11485	6.14	histone H4
LmxM.13.0290partial	94	17294	13.07	hypothetical protein
LmxM.08.1171	789	50319	13.06	hypothetical protein
LmxM.02.0440	13	86359	12.97	hypothetical protein
LmxM.28.3030	13	149181	19.92	hypothetical protein
LmxM.19.1160	61	41571	13.41	hypothetical protein, conserved
LmxM.04.0890	29	136979	9.05	hypothetical protein, conserved
LmxM.22.0730	70	47352	7.43	hypothetical protein, conserved
LmxM.36.5850	27	57706	7.24	hypothetical protein, conserved
LmxM.22.0180	35	28357	7.14	hypothetical protein, conserved

Accession No.	Mascot Score	MW	L/H ratio	Protein name
LmxM.09.1010	55	67747	7.12	hypothetical protein, conserved
LmxM.08.1100	24	42412	6.61	hypothetical protein, conserved
LmxM.02.0460	35	32685	6.48	hypothetical protein, conserved
LmxM.18.0240	17	43943	6.40	hypothetical protein, conserved
LmxM.18.0390	14	181357	6.40	hypothetical protein, conserved
LmxM.18.0110	15	164316	6.09	hypothetical protein, conserved
LmxM.33.1520	123	14372	5.91	hypothetical protein, conserved
LmxM.32.3090	16	159229	5.58	hypothetical protein, conserved
LmxM.08_29.2680	13	121186	5.08	hypothetical protein, conserved
LmxM.07.0920	14	243484	4.53	hypothetical protein, conserved
LmxM.33.0190	36	56463	4.47	hypothetical protein, conserved
LmxM.14.0190	41	22472	4.07	hypothetical protein, conserved
LmxM.25.2010	83	30664	3.97	hypothetical protein, conserved
LmxM.32.2440	92	56640	3.83	hypothetical protein, conserved
LmxM.18.1250	18	83076	3.70	hypothetical protein, conserved
LmxM.18.1360	17	108396	3.70	hypothetical protein, conserved
LmxM.27.0650	46	19702	3.70	hypothetical protein, conserved
LmxM.26.2000	26	39646	3.55	hypothetical protein, conserved

Accession No.	Mascot Score	MW	L/H ratio	Protein name
LmxM.26.1960	72	90388	3.38	hypothetical protein, conserved
LmxM.15.1340	23	39975	3.17	hypothetical protein, conserved
LmxM.19.0020	24	40574	3.01	hypothetical protein, conserved
LmxM.23.1580	64	17008	2.88	hypothetical protein, conserved
LmxM.34.3720	48	50938	2.80	hypothetical protein, conserved
LmxM.29.1870	24	135476	2.72	hypothetical protein, conserved
LmxM.17.0870	41	48831	2.55	hypothetical protein, conserved
LmxM.18.0820	32	292990	2.53	hypothetical protein, conserved
LmxM.18.0930	21	94529	2.53	hypothetical protein, conserved
LmxM.36.0740	20	61499	2.53	hypothetical protein, conserved
LmxM.18.0940	14	139924	2.34	hypothetical protein, conserved
LmxM.18.1250	18	83076	2.34	hypothetical protein, conserved
LmxM.21.0430	53	47692	2.23	hypothetical protein, conserved
LmxM.21.1567	19	38082	2.18	hypothetical protein, conserved
LmxM.22.1100	22	240267	2.18	hypothetical protein, conserved
LmxM.24.0140	14	43131	2.18	hypothetical protein, conserved
LmxM.17.0010	53	88600	2.17	hypothetical protein, conserved
LmxM.36.5910	60	41601	1.93	hypothetical protein, conserved

Accession No.	Mascot Score	MW	L/H ratio	Protein name
LmxM.36.5250	26	373769	1.79	hypothetical protein, conserved
LmxM.09.0190	15	14523	1.77	hypothetical protein, conserved
LmxM.26.0740	15	91756	1.66	hypothetical protein, conserved
LmxM.31.1800	18	25409	1.61	hypothetical protein, conserved
LmxM.36.5160	22	65802	1.60	hypothetical protein, conserved
LmxM.36.1500	18	97331	1.32	hypothetical protein, conserved
LmxM.17.1270	16	36860	1.16	hypothetical protein, conserved
LmxM.36.1520	35	57171	1.13	hypothetical protein, conserved
LmxM.31.2850	20	70575	1.01	hypothetical protein, conserved
LmxM.24.1470	26	306493	14.8	hypothetical protein, conserved
LmxM.24.0260	17	357925	9.93	hypothetical protein, conserved
LmxM.04.0740	16	82689	9.15	hypothetical protein, conserved
LmxM.04.0050	29	58805	9.05	hypothetical protein, conserved
LmxM.24.1580	19	42904	8.40	hypothetical protein, conserved
LmxM.01.0430	25	82297	8.34	hypothetical protein, conserved
LmxM.24.1910	28	13591	8.29	hypothetical protein, conserved
LmxM.13.0450	76	13372	8.07	hypothetical protein, conserved
LmxM.17.0100	14	71022	7.43	hypothetical protein, conserved

Accession No.	Mascot Score	MW	L/H ratio	Protein name
LmxM.14.1440	24	109459	2.49	hypothetical protein, conserved
LmxM.23.1020	132	12671	7.22	hypothetical protein, unknown function
LmxM.02.0550	74	17721	6.75	hypothetical protein, unknown function
LmxM.29.2060	22	104057	1.46	hypothetical protein, unknown function
LmxM.22.1460	30	23264	11.05	i/6 autoantigen-like protein
LmxM.24.1500	58	31472	7.13	IgE-dependent histamine-releasing factor, putative
LmxM.19.1560	27	56102	7.34	inosine-5'-monophosphate dehydrogenase
LmxM.08.0200	15	71576	12.54	Inositol phosphosphingolipids phospholipase C
LmxM.31.1830	107	23527	8.39	iron superoxide dismutase, putative
LmxM.31.1820	124	21994	8.66	iron superoxide dismutase, putative
LmxM.10.0290	56	48772	8.53	isocitrate dehydrogenase [NADP], mitochondrial precursor, putative
LmxM.34.2220	53	11201	55.37	kinetoplastid membrane protein-11
LmxM.34.2210	60	11271	13.99	kinetoplastid membrane protein-11
LmxM.33.0160	62	34272	1.61	malate dehydrogenase, putative
LmxM.24.0761	60	62922	2.48	malic enzyme
LmxM.23.0110	81	41849	6.92	mannose-1-phosphate guanyltransferase
LmxM.05.0380	81	89588	25.37	microtubule-associated protein, putative
LmxM.14.0920	20	170228	1.52	mitochondrial DNA polymerase I protein C, putative

Accession No.	Mascot Score	MW	L/H ratio	Protein name
LmxM.34.1380	23	55120	1.76	mitochondrial processing peptidase, beta subunit, putative,metallo-peptidase, Clan ME, Family M16
LmxM.30.3035	26	37629	7.09	mu-adaptin 4, putative (pseudogene)
LmxM.19.0190	72	18454	6.22	multiprotein-bridging factor 1, putative
LmxM.23.0360	60	39199	4.08	NADP-dependent alcohol dehydrogenase, putative
LmxM.13.1210	36	55108	3.06	nucleobase transporter
LmxM.31.2950	68	16891	22.67	nucleoside diphosphate kinase b
LmxM.36.1940	182	54565	5.18	nucleoside transporter 1, putative
LmxM.16.0550	128	50003	4.25	orotidine-5-phosphate decarboxylase/orotate phosphoribosyltransferase, putative,OMPDCase-OPRTase, putative
LmxM.05.0040	20	68912	13.4	paraflagellar rod component par4, putative
LmxM.08_29.1750	33	69389	4.80	paraflagellar rod protein 1D, putative
LmxM.16.1430	69	76580	9.46	paraflagellar rod protein 2C
LmxM.16.1425partial	39	23043	7.99	paraflagellar rod protein 2C
LmxM.02.0740	34	76921	1.31	peptidyl dipeptidase, putative,metallo-peptidase, Clan MA(E), Family M3
LmxM.23.0040	107	25585	3.50	peroxidoxin,tryparedoxin peroxidase
LmxM.26.2400	24	25213	3.50	peroxisomal membrane protein 4, putative
LmxM.33.0990	30	147839	3.50	p-glycoprotein
LmxM.27.1807	125	38018	5.21	Phosphoenolpyruvate carboxykinase [ATP], glycosomal
LmxM.20.0100	47	51986	14.48	phosphoglycerate kinase C, glycosomal

Accession No.	Mascot Score	MW	L/H ratio	Protein name
LmxM.09.0891	114	14962	14.8	polyubiquitin, putative
LmxM.36.3530partial	83	8917	9.31	polyubiquitin, putative
LmxM.36.1635	70	15594	9.31	poly-zinc finger protein 2, putative
LmxM.24.0380	36	105916	9.31	ppg3-related protein-like protein
LmxM.36.1600	22	29851	2.83	proteasome alpha 1 subunit, putative
LmxM.12.0030	77	30881	8.33	proteasome beta-1 subunit, putative
LmxM.36.6940	36	52611	5.02	protein disulfide isomerase
LmxM.36.5090	14	31193	5.03	protein kinase ck2 regulatory subunit, putative
LmxM.06.0640	14	321148	5.02	protein kinase, putative
LmxM.08.0660	15	148179	4.08	protein kinase, putative
LmxM.09.0400	15	49300	4.08	protein kinase, putative
LmxM.28.3000	14	43321	3.84	protein kinase, putative
LmxM.28.1760	15	174421	3.74	protein kinase, putative
LmxM.32.2070	13	109815	3.74	protein kinase, putative
LmxM.27.2470	35	62067	1.94	protein kinase, putative
LmxM.20.0770	16	419591	1.65	protein kinase, putative
LmxM.15.1200	15	289447	1.78	protein kinase, putative
LmxM.19.0590	13	159845	1.78	protein kinase, putative

Accession No.	Mascot Score	MW	L/H ratio	Protein name
LmxM.25.1520	21	101474	1.65	protein kinase, putative
LmxM.05.0280	49	25210	1.35	protein tyrosine phosphatase, putative
LmxM.25.1710	92	38476	3.05	pyruvate dehydrogenase E1 beta subunit, putative
LmxM.18.1380	27	43156	2.84	pyruvate dehydrogenase E1 component alpha subunit, putative
LmxM.34.0020	24	29143	3.00	pyruvate kinase
LmxM.34.0030	23	54842	4.16	pyruvate kinase, putative
LmxM.11.1000	55	101685	2.26	pyruvate phosphate dikinase, putative
LmxM.17.0191	22	154125	5.11	receptor-type adenylate cyclase a
LmxM.36.3180	16	153406	1.94	receptor-type adenylate cyclase a-like protein
LmxM.33.2820	54	72033	3.84	regulatory subunit of protein kinase a-like protein
LmxM.08_29.1070	30	41195	1.50	ribosomal protein L1a, putative
LmxM.03.0250	25	9619	3.75	ribosomal protein L38, putative
LmxM.25.0490	58	19915	1.55	RNA-binding protein, putative, UPB1
LmxM.36.3910	71	48525	7.38	S-adenosylhomocysteine hydrolase
LmxM.23.1200	15	54903	10.54	S-adenosyl-methyltransferase mraW-like protein
LmxM.20.1680	14	141265	9.33	separin, putative
LmxM.11.0100	67	53671	3.40	seryl-tRNA synthetase, putative
LmxM.11.0100	30	53671	5.29	seryl-tRNA synthetase, putative

Accession No.	Mascot Score	MW	L/H ratio	Protein name
LmxM.10.0910	39	23629	3.09	small GTP-binding protein Rab11, putative,Rab11 GTPase, putative
LmxM.10.0910	39	23629	3.09	small GTP-binding protein Rab11, putative,Rab11 GTPase, putative
LmxM.14.0850	53	13055	9.85	small myristoylated protein-3, putative
LmxM.11.0050	43	108666	34.46	SNF2/RAD54 related DNA helicase, putative
LmxM.23.0650	16	24363	5.07	spliceosomal U5 snRNP-specific protein, putative,DIM-like protein, putative
LmxM.36.0070	47	29244	2.53	stress-inducible protein STI1 homolog
LmxM.36.2950	87	44526	12.39	succinyl-CoA ligase [GDP-forming] beta-chain, putative
LmxM.25.2130	42	31175	10.54	succinyl-CoA synthetase alpha subunit, putative
LmxM.25.2140	35	31209	10.54	succinyl-CoA synthetase alpha subunit, putative
LmxM.32.2340	142	53127	1.60	succinyl-coA:3-ketoacid-coenzyme A transferase, mitochondrial precursor, putative
LmxM.08_29.0070	14	30016	1.32	syntaxin, putative
LmxM.21.1090	27	60294	1.74	T-complex protein 1, delta subunit, putative
LmxM.23.1220	17	60877	1.91	T-complex protein 1, gamma subunit, putative
LmxM.36.6910	69	58716	3.50	T-complex protein 1, theta subunit, putative
LmxM.36.3930	33	159222	2.44	telomerase reverse transcriptase, putative
LmxM.24.2280	16	92641	5.21	TFIIH basal transcription factor complex helicase subunit, putative,RAD3/XPD protein, putative,DNA excision repair protein, putative
LmxM.26.1570	26	77680	2.28	thimet oligopeptidase, putative,metallo-peptidase, Clan MA(E), Family M3

Accession No.	Mascot Score	MW	L/H ratio	Protein name
LmxM.03.0450	24	167515	10.55	TLD domain protein, conserved
LmxM.16.0760	94	37238	7.39	transaldolase, putative
LmxM.24.2060	63	72496	5.18	transketolase, putative
LmxM.36.1430	48	22940	8.00	translation elongation factor 1-beta, putative
LmxM.33.0840	57	34278	6.34	translation elongation factor 1-beta, putative
LmxM.22.1240	16	86462	6.34	translation initiation factor IF-2, putative
LmxM.08_29.0680	37	81217	1.86	Triple RNA binding domain protein 3
LmxM.05.0350	33	53710	5.18	trypanothione reductase
LmxM.15.1040	160	22557	5.44	tryparedoxin peroxidase
LmxM.15.1160	184	22538	1.15	tryparedoxin peroxidase
LmxM.15.1160	184	22538	15.92	tryparedoxin peroxidase
LmxM.08_29.1160	95	16739	9.43	tryparedoxin
LmxM.31.2930	13	57104	11	tubulin-tyrosine ligase-like protein
LmxM.26.0800	58	20601	1.38	type II (glutathione peroxidase-like) tryparedoxin peroxidase
LmxM.09.0420	18	105747	9.31	tyrosine phosphatase, putative
LmxM.34.3060	23	127523	1.77	ubiquitin-activating enzyme e1, putative
LmxM.13.1580	22	16194	2.74	ubiquitin-conjugating enzyme-like protein
LmxM.30.1900	138	14958	9.93	ubiquitin-fusion protein

Accession No.	Mascot Score	MW	L/H ratio	Protein name
LmxM.36.1620	70	21349	10.72	universal minicircle sequence binding protein
LmxM.36.1610	61	13441	19.93	universal minicircle sequence binding protein, putative
LmxM.13.0300	86	32748	5.05	unspecified product
LmxM.03.0770	24	58387	5.00	unspecified product
LmxM.03.0350	38	148740	5.00	unspecified product
LmxM.04.0350	37	229064	3.80	unspecified product
LmxM.08.1040b	33	39253	3.13	unspecified product
LmxM.30.0440	30	80817	2.09	unspecified product
LmxM.16.1010partial	19	102411	2.09	unspecified product
LmxM.08.1040	34	55540	2.09	unspecified product
LmxM.30.0440b	33	49733	1.37	unspecified product
LmxM.04.0760	32	29836	1.33	unspecified product
LmxM.29.1280	17	159199	16.23	vacuolar assembly protein vps41, putative
LmxM.33.3670	14	68282	15.43	vacuolar ATP synthase catalytic subunit A, putative
LmxM.28.2430	20	55837	12.31	vacuolar ATP synthase subunit b, putative
LmxM.36.2230	15	62870	3.35	vacuolar protein sorting-associated protein 45- like protein
LmxM.25.2180	14	67310	3.09	vacuolar protein sorting-like protein
LmxM.21.0470	32	112525	30.15	vacuolar sorting-associated-like protein

Accession No.	Mascot Score	MW	L/H ratio	Protein name
LmxM.30.1220	91	84295	3.96	vacuolar-type proton translocating pyrophosphatase 1, putative

8.2 Proteins quantified (upregulated) in *L. mexicana* amastigote

Accession No.	Mascot Score	MW	L/H ratio	Protein name
LmxM.36.3210	40	29782	0.003	14-3-3 protein-like protein
LmxM.36.6650	39	61118	0.30	2,3-bisphosphoglycerate-independent phosphoglycerate mutase
LmxM.32.0830	40	79396	0.12	2,4-dienoyl-coa reductase fadh1, putative
LmxM.29.0180	31	31406	0.47	2-hydroxy-3-oxopropionate reductase, putative
LmxM.23.0690	29	47855	0.26	3-ketoacyl-CoA thiolase-like protein
LmxM.30.2300	14	47149	0.09	3'-nucleotidase/nuclease, putative
LmxM.13.0570	25	15810	0.82	40S ribosomal protein S12, putative
LmxM.22.0420	22	17424	0.99	40S ribosomal protein S15, putative
LmxM.08_29.2860	60	18313	0.51	40S ribosomal protein S19-like protein
LmxM.21.1780	48	28302	0.97	40S ribosomal protein S6, putative
LmxM.07.0680	15	22257	0.78	40S ribosomal protein S9, putative
LmxM.36.5010	37	27837	0.85	40S ribosomal protein SA, putative
LmxM.19.0995	19	69384	0.63	4-coumarate:coa ligase-like protein
LmxM.19.0985	19	70689	0.63	4-coumarate:coa ligase-like protein

Accession No.	Mascot Score	MW	L/H ratio	Protein name
LmxM.29.0750	38	20885	0.37	4-methyl-5(beta-hydroxyethyl)-thiazole monophosphate synthesis protein, putative
LmxM.15.1203	37	11050	0.99	60S acidic ribosomal protein P2
LmxM.04.0470	19	21675	0.85	60S ribosomal protein L11 (L5, L16)
LmxM.15.0200	20	25733	0.35	60S ribosomal protein L13a, putative
LmxM.36.4510	16	22193	0.88	60S ribosomal protein L18, putative
LmxM.13.0560	16	22207	0.82	60S ribosomal protein L18, putative
LmxM.16.0460	60	18098	0.85	60S ribosomal protein L21, putative
LmxM.34.3790	17	15118	0.28	60S ribosomal protein L23, putative
LmxM.06.0570	20	16286	0.43	60S ribosomal protein L23a, putative
LmxM.34.3760	32	16231	0.26	60S ribosomal protein L27A/L29, putative
LmxM.34.0240	18	11603	0.26	60S ribosomal protein L30
LmxM.21.0730	16	11976	0.99	60S Ribosomal protein L36, putative
LmxM.32.1955	21	10114	0.26	60S ribosomal protein L37
LmxM.32.1955	22	10114	0.25	60S ribosomal protein L37
LmxM.07.0500	60	29857	0.33	60S ribosomal protein L7a, putative
LmxM.34.3340	40	52591	0.34	6-phosphogluconate dehydrogenase, decarboxylating, putative
LmxM.26.2700	16	28690	0.29	6-phosphogluconolactonase
LmxM.03.0160	18	82808	0.30	ABC transporter protein, putative

Accession No.	Mascot Score	MW	L/H ratio	Protein name
LmxM.08_29.0620	16	208833	0.25	ABC transporter, putative
LmxM.25.0530	21	72376	0.23	ABC transporter, putative
LmxM.11.1270	19	202022	0.08	ABC transporter, putative
LmxM.06.0880	53	45641	0.22	acyl-coenzyme a dehydrogenase, putative
LmxM.11.0990	18	109251	0.32	adaptin-related protein-like protein
LmxM.13.1190	22	79189	0.25	adenylosuccinate synthetase, putative
LmxM.29.2900	18	64615	0.47	aldehyde dehydrogenase, putative
LmxM.34.0970	14	41987	0.25	aldose 1-epimerase, putative
LmxM.34.0980	14	42527	0.25	aldose 1-epimerase-like protein
LmxM.34.2350	26	54601	0.26	aminopeptidase P, putative
LmxM.11.0620	43	29787	0.69	aminopeptidase, putative
LmxM.11.0630	60	57922	0.49	aminopeptidase, putative,metallo-peptidase, Clan MF, Family M17
LmxM.34.1480	68	36572	0.44	arginase
LmxM.21.0895	24	70413	0.4	aspartyl-tRNA synthetase, putative
LmxM.07.0340	36	46871	0.78	ATP-dependent DEAD/H RNA helicase, putative
LmxM.31.1500	24	78552	0.59	ATP-dependent zinc metallopeptidase, putative,metallo-peptidase, Clan MA(E), Family M41
LmxM.30.1070	79	28760	0.75	biotin/lipoate protein ligase-like protein
LmxM.21.0120	23	182271	0.19	calpain, putative,cysteine peptidase, Clan CA, family C2, putative

Accession No.	Mascot Score	MW	L/H ratio	Protein name
LmxM.20.1300	30	14952	0.32	calpain-like cysteine peptidase, putative,calpain-like cysteine peptidase, Clan CA, family C2
LmxM.27.0490	16	271511	0.01	calpain-like cysteine peptidase, putative,cysteine peptidase, Clan CA, family C2, putative
LmxM.27.0500	23	656104	0.95	calpain-like cysteine peptidase, putative,cysteine peptidase, Clan CA, family C2, putative
LmxM.31.0970	19	202700	0.55	calpain-like cysteine peptidase, putative,cysteine peptidase, Clan CA, family C2, putative
LmxM.27.0510	18	492173	0.37	calpain-like cysteine peptidase, putative,cysteine peptidase, Clan CA, family C2, putative
LmxM.13.0090	14	57670	0.48	carboxypeptidase, putative,metallo-peptidase, Clan MA(E), family 32
LmxM.14.0180	16	54210	0.05	carboxypeptidase, putative,metallo-peptidase, Clan MA(E), Family M32
LmxM.08_29.1310	51	68933	0.92	carnitine/choline acetyltransferase, putative
LmxM.08.1070	34	49006	0.54	cathepsin L-like protease, putative
LmxM.08.1060	109	40038	0.41	cathepsin L-like protease, putative
LmxM.18.1430	14	123328	0.09	chaperone DNAJ protein, putative
LmxM.13.1660	25	59246	0.35	chaperonin TCP20, putative
LmxM.18.0670	37	50618	0.22	citrate synthase, putative
LmxM.08_29.1230	17	204893	0.53	COPII coat assembly protein sec16, putative (fragment)
LmxM.25.0910	31	19010	0.74	cyclophilin a
LmxM.19.1420	27	39177	0.18	cysteine peptidase A (CBA)
LmxM.36.3590	36	35738	0.11	cysteine synthase, putative
LmxM.26.1710	50	22372	0.96	cytochrome c oxidase subunit V, putative

Accession No.	Mascot Score	MW	L/H ratio	Protein name
LmxM.25.1130	29	19033	0.23	cytochrome c oxidase VII, putative
LmxM.16.1310	83	12272	0.57	cytochrome c, putative
LmxM.28.1530	16	44296	0.29	DEAD box RNA helicase, putative
LmxM.31.1400	34	187137	0.33	DEAD/DEAH box helicase-like protein, putative
LmxM.03.0200	40	60113	0.86	delta-1-pyrroline-5-carboxylate dehydrogenase, putative
LmxM.21.0550	83	40435	0.27	dihydrolipoamide acetyltransferase precursor like protein
LmxM.31.3310	39	51083	0.60	dihydrolipoamide dehydrogenase, putative
LmxM.30.1610	27	29549	0.15	diphthine synthase-like protein
LmxM.24.1080	20	49408	0.57	DNAJ domain protein, putative
LmxM.13.1650	14	533823	0.04	dynein heavy chain, putative
LmxM.26.1020	15	460992	0.20	dynein heavy chain, putative
LmxM.07.0600	46	63739	0.11	electron transfer flavoprotein-ubiquinone oxidoreductase, putative
LmxM.36.0180	53	94852	0.95	elongation factor 2
LmxM.03.0980	33	47335	0.77	elongation initiation factor 2 alpha subunit, putative
LmxM.10.0610	39	54975	0.06	endonuclease G, putative
LmxM.23.0200	73	17122	0.65	endoribonuclease L-PSP (pb5), putative
LmxM.16.0140	15	18681	0.31	eukaryotic translation initiation factor 1A, putative
LmxM.18.1660	26	79380	0.97	gamma-glutamylcysteine synthetase, putative

Accession No.	Mascot Score	MW	L/H ratio	Protein name
LmxM.28.2260	91	24525	0.37	glycosomal membrane protein, putative
LmxM.10.0390	29	64893	0.03	GP63, leishmanolysin
LmxM.10.0470	15	64758	0.77	GP63, leishmanolysin
LmxM.08_29.2200	31	77363	0.88	GTP-binding protein, putative
LmxM.08_29.0090	28	21128	0.16	GTP-binding protein-like protein
LmxM.27.2400	16	44223	0.61	heat shock protein DNAJ, putative
LmxM.21.0920	41	13938	0.61	histone H2A, putative
LmxM.06.0010	99	11436	0.53	histone H4
LmxM.19.0290	34	145648	0.97	hypothetical protein, conserved
LmxM.27.0700	15	49137	0.97	hypothetical protein, conserved
LmxM.34.1870	16	78271	0.94	hypothetical protein, conserved
LmxM.14.0790	20	451832	0.80	hypothetical protein, conserved
LmxM.04.0240	27	32118	0.79	hypothetical protein, conserved
LmxM.28.0430	14	45789	0.77	hypothetical protein, conserved
LmxM.23.0310	22	141146	0.76	hypothetical protein, conserved
LmxM.30.0620	19	89087	0.68	hypothetical protein, conserved
LmxM.16.0670	23	70935	0.64	hypothetical protein, conserved
LmxM.36.3500	23	88979	0.62	hypothetical protein, conserved

Accession No.	Mascot Score	MW	L/H ratio	Protein name
LmxM.17.0910	17	54951	0.59	hypothetical protein, conserved
LmxM.36.1570	16	53016	0.58	hypothetical protein, conserved
LmxM.17.1450	28	55199	0.53	hypothetical protein, conserved
LmxM.02.0450	53	30392	0.49	hypothetical protein, conserved
LmxM.02.0700	22	106856	0.42	hypothetical protein, conserved
LmxM.02.0130	18	26777	0.41	hypothetical protein, conserved
LmxM.03.0480	25	112548	0.41	hypothetical protein, conserved
LmxM.03.0530	22	220559	0.41	hypothetical protein, conserved
LmxM.03.0550	17	144069	0.39	hypothetical protein, conserved
LmxM.03.0690	55	232774	0.39	hypothetical protein, conserved
LmxM.20.1710	17	65912	0.36	hypothetical protein, conserved
LmxM.25.0110	33	54063	0.35	hypothetical protein, conserved
LmxM.33.4080	14	30096	0.31	hypothetical protein, conserved
LmxM.32.2510	14	75441	0.28	hypothetical protein, conserved
LmxM.24.1120	19	97608	0.26	hypothetical protein, conserved
LmxM.30.1240	14	135840	0.21	hypothetical protein, conserved
LmxM.31.3930	14	459570	0.16	hypothetical protein, conserved
LmxM.30.0460	20	79485	0.15	hypothetical protein, conserved

Accession No.	Mascot Score	MW	L/H ratio	Protein name
LmxM.30.2040	18	53381	0.15	hypothetical protein, conserved
LmxM.32.2280	28	109548	0.15	hypothetical protein, conserved
LmxM.32.2660	15	124536	0.15	hypothetical protein, conserved
LmxM.33.2620	17	76235	0.15	hypothetical protein, conserved
LmxM.08.0130	14	122717	0.13	hypothetical protein, conserved
LmxM.31.3570	20	132687	0.03	hypothetical protein, conserved
LmxM.34.3730	34	97046	0.02	hypothetical protein, conserved
LmxM.34.4320	15	60949	0.02	hypothetical protein, conserved
LmxM.34.4380	22	58147	0.02	hypothetical protein, conserved
LmxM.34.4470	29	21880	0.02	hypothetical protein, conserved
LmxM.34.4690	70	34780	0.02	hypothetical protein, conserved
LmxM.34.4940	45	23700	0.02	hypothetical protein, conserved
LmxM.34.4950	16	107500	0.02	hypothetical protein, conserved
LmxM.34.5090	15	66283	0.02	hypothetical protein, conserved
LmxM.34.5390	14	741481	0.02	hypothetical protein, conserved
LmxM.34.0570	13	227054	0.02	hypothetical protein, conserved
LmxM.34.0670	17	459091	0.02	hypothetical protein, conserved
LmxM.34.0140	21	14494	0.02	hypothetical protein, conserved

Accession No.	Mascot Score	MW	L/H ratio	Protein name
LmxM.34.0850	16	59337	0.02	hypothetical protein, conserved
LmxM.34.0170	18	38247	0.02	hypothetical protein, conserved
LmxM.34.0190	19	27523	0.02	hypothetical protein, conserved
LmxM.34.1090	19	115007	0.02	hypothetical protein, conserved
LmxM.34.1100	15	71362	0.02	hypothetical protein, conserved
LmxM.34.1490	30	30713	0.02	hypothetical protein, conserved
LmxM.34.1620	30	214290	0.02	hypothetical protein, conserved
LmxM.06.0720	22	180297	0.02	hypothetical protein, conserved
LmxM.07.0320	28	111116	0.02	hypothetical protein, conserved
LmxM.08_29.1010	28	37752	0.02	hypothetical protein, conserved
LmxM.14.0090	13	41747	0.02	hypothetical protein, conserved
LmxM.16.0270	33	110528	0.02	hypothetical protein, conserved
LmxM.17.1260	22	47491	0.02	hypothetical protein, conserved
LmxM.13.1470	30	597321	0.01	hypothetical protein, conserved
LmxM.33.0060	31	116356	0.19	hypothetical protein, conserved
LmxM.04.0600	19	318310	0.99	hypothetical protein, unknown function
LmxM.02.0470	18	298701	0.85	hypothetical protein, unknown function
LmxM.30.2410	14	22054	0.30	hypothetical protein, unknown function

Accession No.	Mascot Score	MW	L/H ratio	Protein name
LmxM.21.0845	26	23712	0.22	hypoxanthine-guanine phosphoribosyltransferase
LmxM.14.0930	17	91851	0.11	immunodominant antigen, putative,tc40 antigen-like
LmxM.27.0930	47	44804	0.5	isovaleryl-coA dehydrogenase, putative
LmxM.14.1110	20	254630	0.35	kinesin K39, putative
LmxM.14.1100	20	536483	0.07	kinesin K39, putative
LmxM.11.0870	29	149571	0.28	kinesin, putative
LmxM.19.0680	28	126327	0.25	kinesin, putative
LmxM.29.3060	18	134218	0.03	kinesin, putative
LmxM.21.1040	15	231910	0.22	kinesin, putative
LmxM.09.0800	17	156380	0.01	kinetoplast-associated protein-like protein
LmxM.01.0530	14	171151	0.03	long-chain-fatty-acid-CoA ligase, putative
LmxM.28.0570	20	62419	0.2	major surface protease gp63, putative,leishmanolysin, putative
LmxM.33.0140	66	33945	0.34	malate dehydrogenase
LmxM.13.0130	17	80921	0.01	MCAK-like kinesin, putative
LmxM.15.1290	15	139453	0.11	mitochondrial DNA topoisomerase II
LmxM.13.0870	49	58057	0.77	mitochondrial processing peptidase alpha subunit, putative,metallo-peptidase, Clan ME, Family M16
LmxM.23.0830	15	167118	0.02	Na/H antiporter-like protein
LmxM.13.1060	28	34818	0.95	NADH-cytochrome b5 reductase, putative

Accession No.	Mascot Score	MW	L/H ratio	Protein name
LmxM.10.0850	21	14006	0.78	nuclear transport factor 2, putative,ntf2-like
LmxM.19.0440	22	39915	0.44	nucleosome assembly protein, putative
LmxM.36.4170	32	36526	0.05	oxidoreductase, putative
LmxM.28.0940	13	107180	0.19	oxidoreductase-like protein
LmxM.28.1240	17	73373	0.59	p450 reductase, putative
LmxM.19.1530	25	48145	0.55	peptidylprolyl isomerase-like protein
LmxM.30.1280	15	169323	0.06	p-glycoprotein e, putative
LmxM.05.0720	25	146524	0.22	phosphatase-like protein
LmxM.20.1120	20	360565	0.07	phosphatidylinositol 3-kinase, putative
LmxM.02.0120	16	531677	0.04	phosphatidylinositol 3-kinase-like protein
LmxM.08_29.2600	21	56002	0.33	poly(A) polymerase, putative
LmxM.05.1200	16	15291	0.54	prefoldin subunit, putative
LmxM.24.1100	24	137307	0.23	pre-mRNA splicing factor, putative
LmxM.26.1610	19	64033	0.74	proline oxidase, mitochondrial precursor-like protein
LmxM.06.0140	30	28120	0.26	proteasome beta 6 subunit, putative,20S proteasome beta 6 subunit, putative
LmxM.06.1050	30	15144	0.63	protein disulfide isomerase
LmxM.25.1340	18	112450	0.02	protein transport protein Sec24C, putative
LmxM.18.1520	49	108528	0.13	P-type H -ATPase, putative

Accession No.	Mascot Score	MW	L/H ratio	Protein name
LmxM.32.1150	18	92908	0.07	pumilio protein, putative
LmxM.29.1250	29	33288	0.74	Pyridoxal kinase, putative
LmxM.18.0890	35	24345	0.55	rab7 GTP binding protein, putative
LmxM.08_29.2160	17	50458	0.69	rab-GDP dissociation inhibitor, putative
LmxM.15.0275	18	21629	0.77	ribonucleoprotein p18, mitochondrial precursor, putative
LmxM.22.1290	22	44723	0.23	ribonucleoside-diphosphate reductase small chain, putative
LmxM.08.0510	13	94211	0.87	ribose-phosphate pyrophosphokinase, putative
LmxM.10.0070	32	16584	0.45	ribosomal protein l35a, putative
LmxM.31.0750	38	25291	0.44	RNA binding protein, putative
LmxM.28.0160	17	22305	0.13	RNA binding protein, putative
LmxM.25.0620	13	183241	0.09	RNA polymerase I second largest subunit, putative
LmxM.34.1120	17	24599	0.02	Selenoprotein T, putative
LmxM.14.1320	15	50854	0.24	serine hydroxymethyltransferase, putative
LmxM.08_29.2570	23	56555	0.22	serine/threonine-protein kinase, putative,protein kinase, putative
LmxM.08_29.1330	23	63331	0.13	serine/threonine-protein kinase, putative,protein kinase, putative
LmxM.07.0870	14	41829	0.33	splicing factor ptsr1-like protein
LmxM.15.0990	15	22905	0.445	succinate dehydrogenase, putative
LmxM.26.1550	17	80272	0.42	trifunctional enzyme alpha subunit, mitochondrial precursor-like protein

Accession No.	Mascot Score	MW	L/H ratio	Protein name
LmxM.24.0850	59	27265	0.99	triosephosphate isomerase
LmxM.36.1660	14	76635	0.99	tRNA pseudouridine synthase A, putative
LmxM.19.1020	19	58386	0.02	tRNA pseudouridine synthase A-like protein
LmxM.11.0400	19	122147	0.99	tubulin-tyrsoine ligase-like protein
LmxM.24.0420	15	34761	0.24	ubiquitin carboxyl-terminal hydrolase, putative,cysteine peptidase, Clan CA, family C12, putative
LmxM.07.0280	21	670620	0.11	ubiquitin-protein ligase-like, putative
LmxM.08_29.0780	34	67343	0.03	U-box domain protein, putative
LmxM.08.1030a	109	58965	0.41	unspecified product
LmxM.08.1070partial	109	41406	0.41	unspecified product
LmxM.10.0483	15	98541	0.41	unspecified product
LmxM.10.0935	20	93116	0.41	unspecified product
LmxM.21.1290	13	28572	0.33	vesicule-associated membrane protein, putative
LmxM.17.0735	22	35345	0.17	ysine decarboxylase-like protein

8.3 Protein degradation rate constant (k_{deg}) and half-lives of uninfected and infected THP-1 (top 50)

Protein names	ln (kdeg) Control24h	Half-life Control24h	ln (kdeg) 24hpi	Half-life 24 hpi	ln (kdeg) control48h	Half-life control48h	ln (kdeg) 48 hpi	Half-life 48 hpi	Unique peptides	Score
Leukotriene A-4 hydrolase	0.04	19.19	0.04	18.96	0.02	41.87	0.01	85.18	9	55
Heat shock protein 105 kDa	0.04	19.47	0.03	19.88	0.01	50.45	0.01	76.16	12	128
Splicing factor U2AF 65 kDa subunit	0.03	21.61	0.03	24.79	0.01	50.78	0.01	75.01	8	80
Palmitoyl-protein thioesterase 1	0.02	30.24	0.03	23.91	0.01	71.82	0.01	71.53	8	74
Signal transducer and activator of transcription 1-alpha/beta	0.03	22.17	0.03	26.77	0.01	58.63	0.01	71.47	8	21
Ras-related protein Rab-7a	0.03	24.25	0.03	21.43	0.01	56.98	0.01	70.57	11	312
Programmed cell death 6-interacting protein	0.02	28.52	0.03	21.31	0.01	56.92	0.01	70.04	14	72
Pyruvate kinase PKM	0.03	24.22	0.03	21.29	0.01	54.84	0.01	69.23	32	323
Talin-1	0.02	28.39	0.03	25.28	0.01	62.01	0.01	69.13	45	323
F-actin-capping protein subunit alpha-2	0.03	22.15	0.03	22.35	0.01	61.87	0.01	68.88	5	39
Splicing factor 3B subunit 1	0.03	25.44	0.03	22.74	0.01	71.44	0.01	68.78	12	141
Neuroblast differentiation-associated protein AHNAK	0.03	23.27	0.03	21.61	0.01	58.39	0.01	68.01	45	122
Interleukin-8;MDNCF-a;Interleukin-8;IL-8(5-77);IL-8(6-77);IL-8(7-77);IL-8(8-77);IL-8(9-77)	0.04	16.63	0.02	30.36	0.01	66.53	0.01	66.53	1	3
Plectin	0.02	28.81	0.03	22.47	0.01	58.04	0.01	65.99	40	248
Interferon-induced GTP-binding protein Mx1;Interferon-induced GTP-binding protein Mx1, N-terminally processed	0.04	19.28	0.03	21.76	0.02	43.95	0.01	65.76	4	58
Cell division control protein 42 homolog	0.03	24.56	0.03	23.39	0.01	59.48	0.01	65.58	5	141
T-complex protein 1 subunit epsilon	0.03	20.08	0.04	19.26	0.02	44.00	0.01	65.53	16	193
Niban-like protein 1	0.02	28.26	0.03	22.99	0.01	70.26	0.01	65.33	16	170
Gelsolin	0.03	24.92	0.03	21.89	0.01	47.92	0.01	65.23	10	323
Heat shock 70 kDa protein 4	0.03	20.84	0.04	19.17	0.01	46.90	0.01	63.83	15	323

Protein names	ln (kdeg) Control24h	Half-life Control24h	ln (kdeg) 24hpi	Half-life 24 hpi	ln (kdeg) control48h	Half-life control48h	ln (kdeg) 48 hpi	Half-life 48 hpi	Unique peptides	Score
Transforming protein RhoA	0.03	26.66	0.03	23.34	0.01	67.00	0.01	62.95	2	80
Vimentin	0.03	27.62	0.03	24.44	0.01	64.80	0.01	62.10	41	323
Ubiquitin-conjugating enzyme E2 L3	0.03	27.36	0.03	20.43	0.02	45.30	0.01	61.89	5	53
Alpha-soluble NSF attachment protein	0.03	21.45	0.03	21.70	0.01	52.33	0.01	61.77	5	80
Myosin light polypeptide 6	0.03	25.53	0.03	22.97	0.01	59.79	0.01	61.62	9	248
Lysosome-associated membrane glycoprotein 2	0.03	21.11	0.04	19.06	0.02	45.31	0.01	61.43	3	36
LIM and SH3 domain protein 1	0.03	22.87	0.03	22.41	0.01	54.37	0.01	61.26	7	12
Dolichyl-diphosphooligosaccharide--protein glycosyltransferase 48 kDa subunit	0.03	19.92	0.04	18.80	0.02	40.98	0.01	60.87	10	182
Lysosomal alpha-mannosidase;Lysosomal alpha-mannosidase A peptide;Lysosomal alpha-mannosidase B peptide;Lysosomal alpha-mannosidase C peptide;Lysosomal alpha-mannosidase D peptide;Lysosomal alpha-mannosidase E peptide	0.03	27.08	0.03	23.63	0.01	67.91	0.01	60.66	12	214
Prosaposin;Saposin-A;Saposin-B-Val;Saposin-B;Saposin-C;Saposin-D	0.03	25.94	0.03	25.67	0.01	60.74	0.01	60.60	6	201
Cathepsin B;Cathepsin B light chain;Cathepsin B heavy chain	0.02	28.22	0.03	24.17	0.01	53.97	0.01	60.50	7	309
Dihydropyrimidinase-related protein 2	0.03	22.15	0.03	20.71	0.02	41.31	0.01	60.49	10	174
Guanine nucleotide-binding protein subunit beta-2-like 1;Guanine nucleotide-binding protein subunit beta-2-like 1, N-terminally processed	0.03	22.66	0.03	22.66	0.01	59.41	0.01	60.17	8	284
RNA-binding protein FUS	0.03	23.53	0.03	20.69	0.01	65.98	0.01	60.03	5	33
Vesicle-fusing ATPase	0.03	20.90	0.03	22.58	0.02	45.83	0.01	59.42	8	83
Ras-related protein Rab-14	0.04	19.38	0.03	22.69	0.01	53.91	0.01	59.19	7	90
Serine/threonine-protein phosphatase 2A 65 kDa regulatory subunit A alpha isoform	0.03	25.62	0.03	23.02	0.01	59.12	0.01	58.73	12	189
Tropomyosin alpha-4 chain	0.03	24.96	0.03	24.46	0.01	61.88	0.01	58.51	8	118
60S ribosomal protein L5	0.04	19.62	0.03	20.48	0.02	42.06	0.01	58.14	8	68
Heat shock 70 kDa protein 6;Putative heat shock 70 kDa protein 7	0.03	22.98	0.03	21.91	0.02	44.76	0.01	57.54	1	11
14-3-3 protein zeta/delta	0.03	24.41	0.03	22.19	0.01	52.19	0.01	56.94	11	323
Thymosin beta-4;Hematopoietic system regulatory peptide	0.03	27.04	0.03	20.41	0.01	49.39	0.01	56.71	7	140

Protein names	ln (kdeg) Control24h	Half-life Control24h	ln (kdeg) 24hpi	Half-life 24 hpi	ln (kdeg) control48h	Half-life control48h	ln (kdeg) 48 hpi	Half-life 48 hpi	Unique peptides	Score
Heterogeneous nuclear ribonucleoprotein D-like	0.03	25.02	0.03	23.94	0.01	55.10	0.01	56.67	5	219
Serine/arginine-rich splicing factor 1	0.04	19.21	0.03	23.80	0.01	47.79	0.01	56.55	6	51
Ras-related protein Rab-2A;Ras-related protein Rab-2B	0.03	22.24	0.03	24.08	0.01	58.87	0.01	56.44	9	37
Chloride intracellular channel protein 1	0.03	23.44	0.03	20.71	0.01	52.95	0.01	56.43	14	323
Poly(rC)-binding protein 1	0.03	23.12	0.03	22.50	0.01	57.53	0.01	56.20	6	43
Annexin A5	0.03	22.18	0.03	20.49	0.01	52.81	0.01	56.02	17	323
Hippocalcin-like protein 1;Neuron-specific calcium-binding protein hippocalcin	0.04	19.48	0.03	24.38	0.01	73.98	0.01	55.95	7	69
Pleckstrin	0.03	27.30	0.03	24.43	0.01	67.63	0.01	55.95	4	52

8.4 Protein degradation profiles of several proteins.

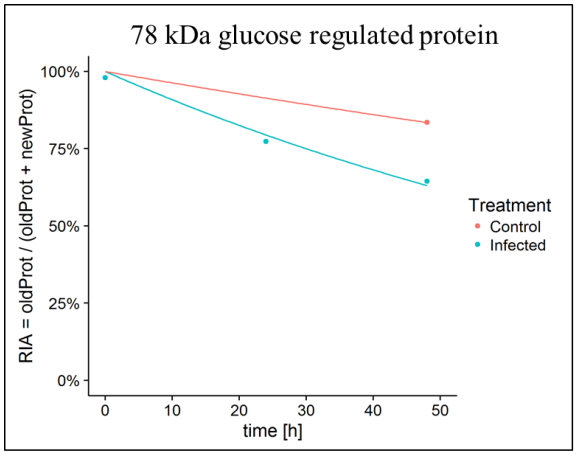

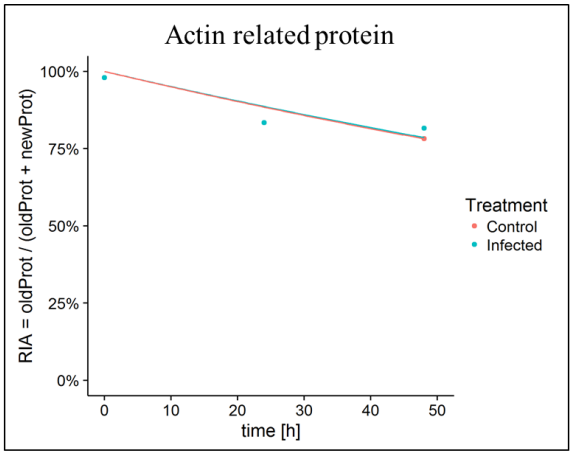

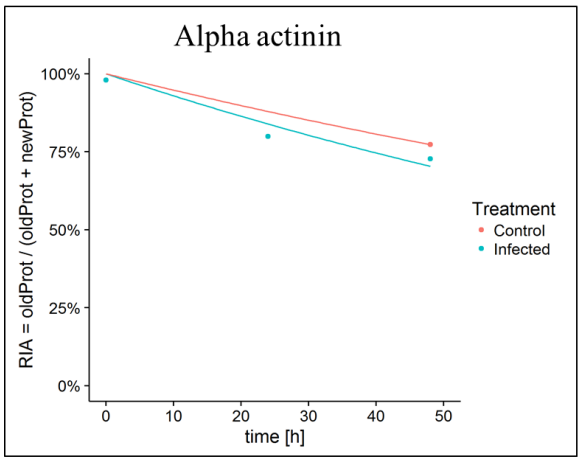

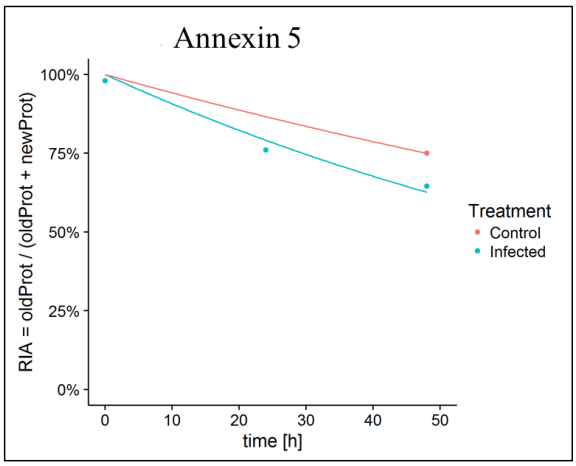

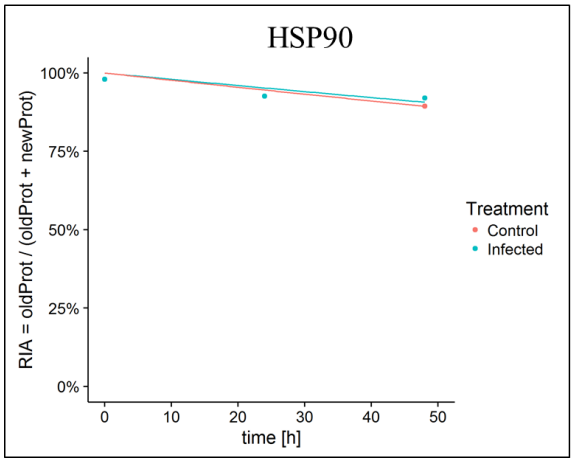

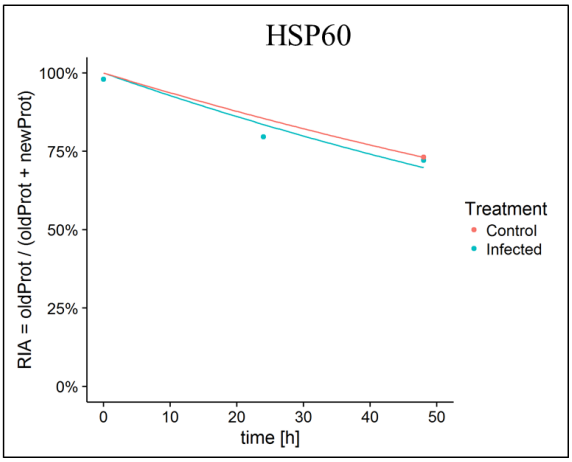

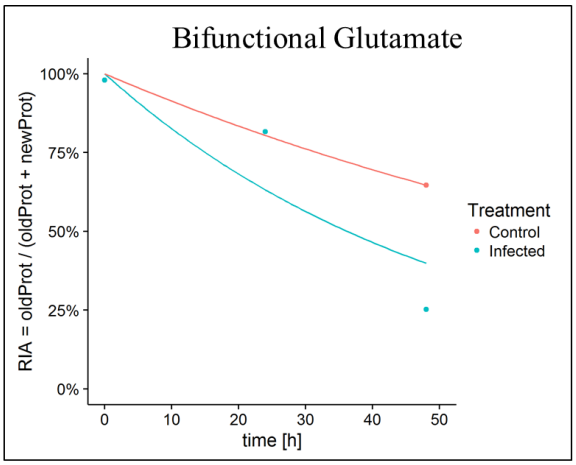
Bifunctional Glutamate
RIA = oldProt / (oldProt + newProt)
100%
75%
50%
25%
0%
0
10
20
30
40
50
time [h]
Treatment
Control
Infected

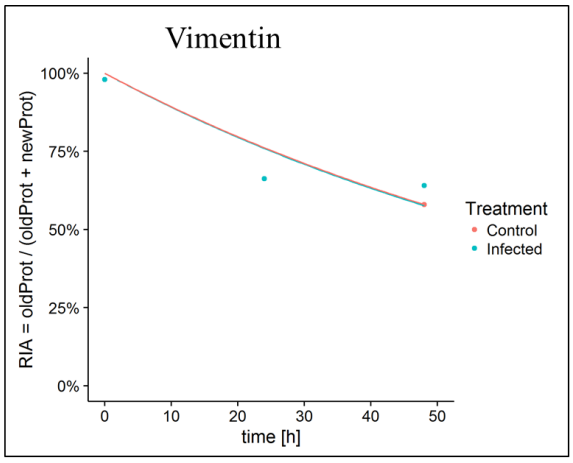
Vimentin
RIA = oldProt / (oldProt + newProt)
100%
75%
50%
25%
0%
0
10
20
30
40
50
time [h]
Treatment
Control
Infected

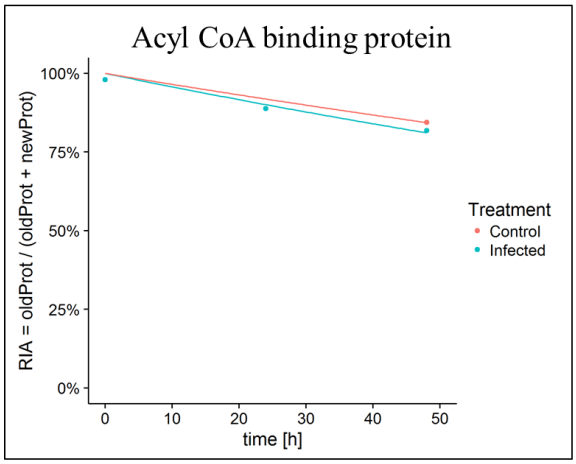
Acyl CoA binding protein
RIA = oldProt / (oldProt + newProt)
100%
75%
50%
25%
0%
0
10
20
30
40
50
time [h]
Treatment
Control
Infected

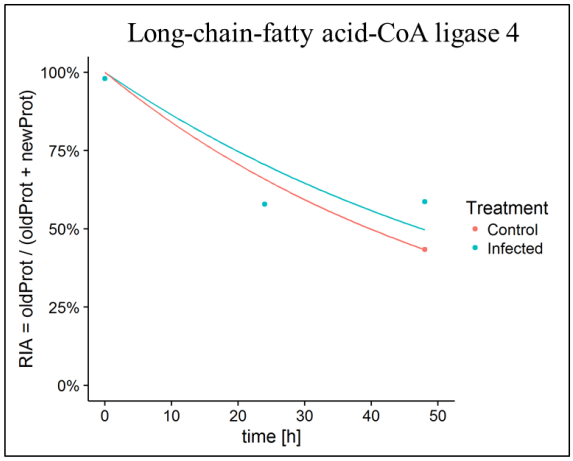
Long-chain-fatty acid-CoA ligase 4
RIA = oldProt / (oldProt + newProt)
100%
75%
50%
25%
0%
0
10
20
30
40
50
time [h]
Treatment
Control
Infected

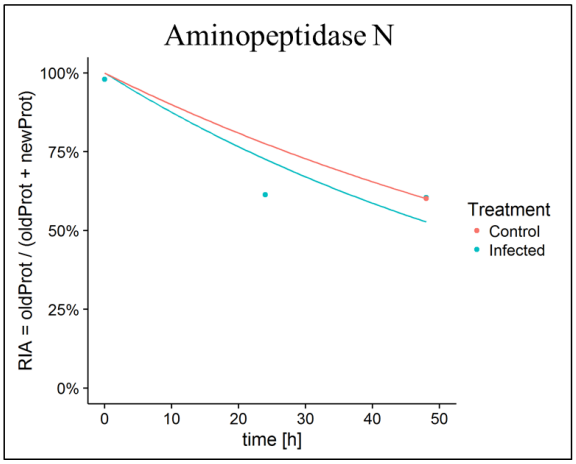
Aminopeptidase N
RIA = oldProt / (oldProt + newProt)
100%
75%
50%
25%
0%
0
10
20
30
40
50
time [h]
Treatment
Control
Infected

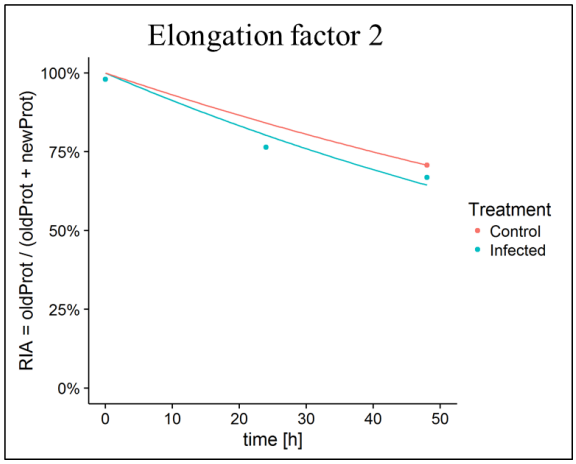
Elongation factor 2
RIA = oldProt / (oldProt + newProt)
100%
75%
50%
25%
0%
0
10
20
30
40
50
time [h]
Treatment
Control
Infected

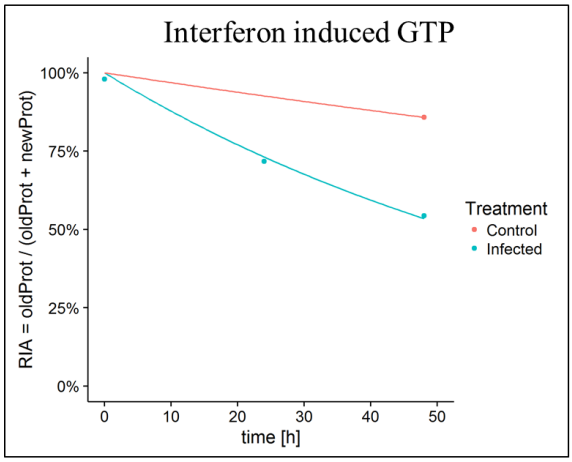
Interferon induced GTP
RIA = oldProt / (oldProt + newProt)
100%
75%
50%
25%
0%
0
10
20
30
40
50
time [h]
Treatment
Control
Infected

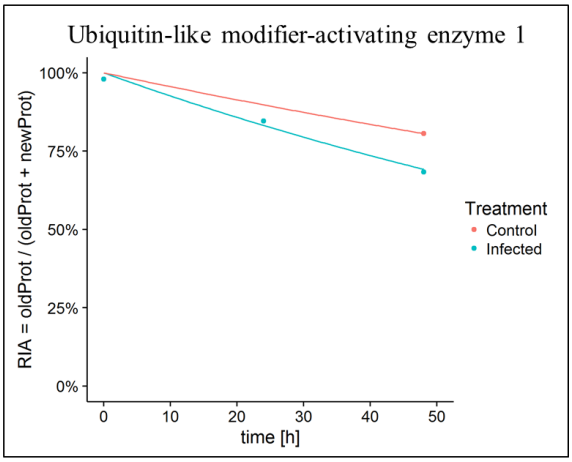
Ubiquitin-like modifier-activating enzyme 1
RIA = oldProt / (oldProt + newProt)
100%
75%
50%
25%
0%
0
10
20
30
40
50
time [h]
Treatment
Control
Infected

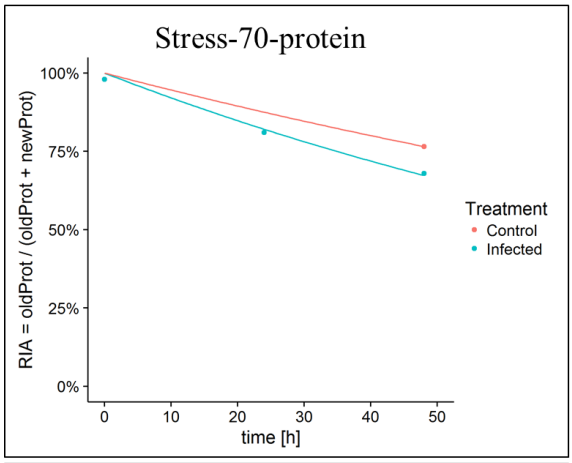
Stress-70-protein
RIA = oldProt / (oldProt + newProt)
100%
75%
50%
25%
0%
0
10
20
30
40
50
time [h]
Treatment
Control
Infected

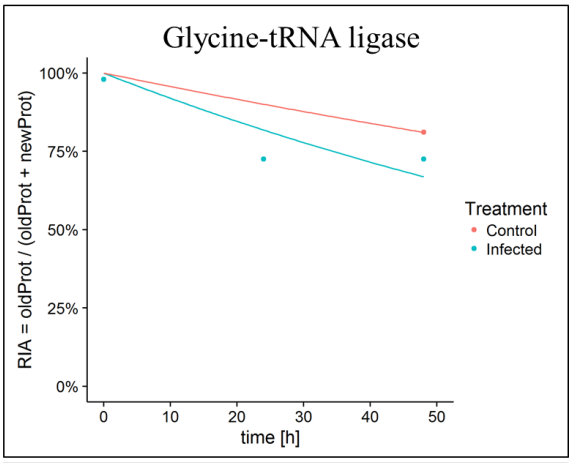
Glycine-tRNA ligase
RIA = oldProt / (oldProt + newProt)
100%
75%
50%
25%
0%
0
10
20
30
40
50
time [h]
Treatment
Control
Infected

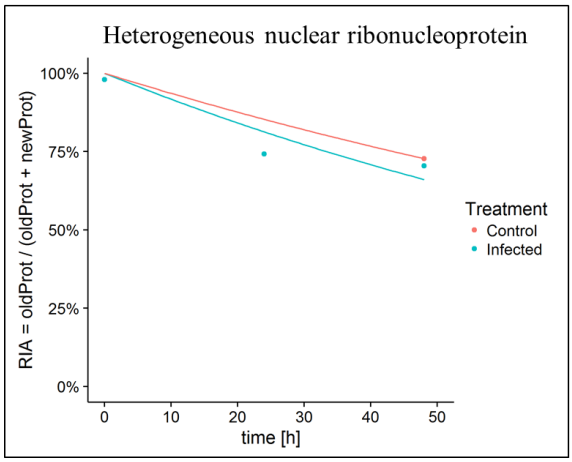
Heterogeneous nuclear ribonucleoprotein
RIA = oldProt / (oldProt + newProt)
100%
75%
50%
25%
0%
0
10
20
30
40
50
time [h]
Treatment
Control
Infected

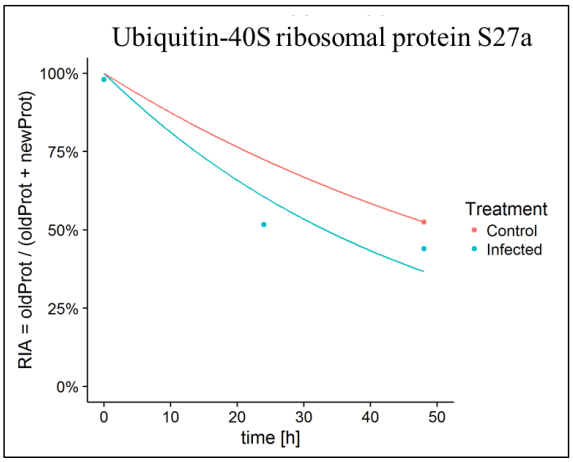
Ubiquitin-40S ribosomal protein S27a
RIA = oldProt / (oldProt + newProt)
100%
75%
50%
25%
0%
0
10
20
30
40
50
time [h]
Treatment
Control
Infected

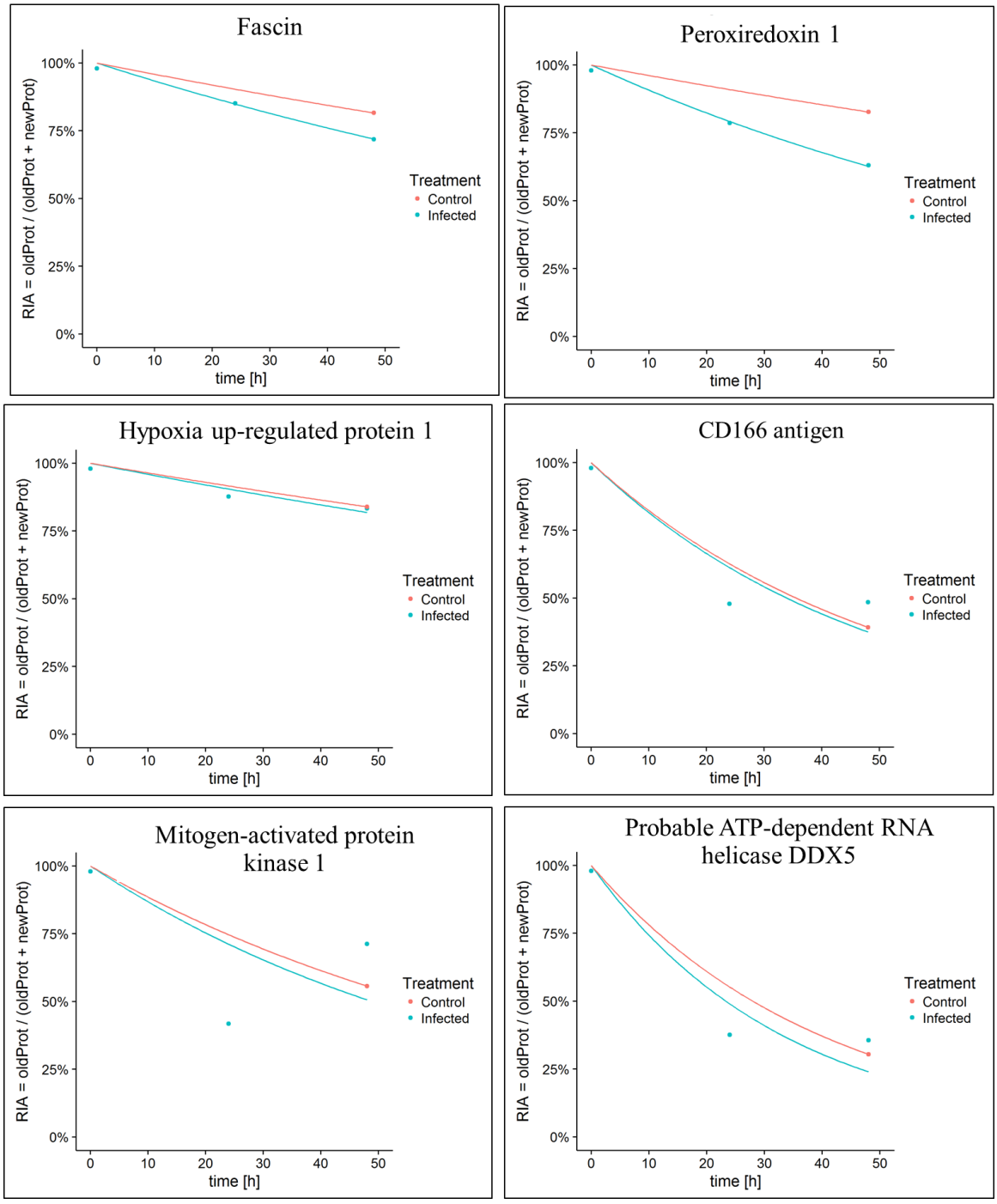

Fig. 8.1: An R script was used to calculate and plot protein degradation of several newly synthesized proteins (n = 3 biological replicates).